UNIVERSITY OF SOUTHAMPTON
FACULTY OF PHYSICAL AND APPLIED SCIENCES
PHYSICS AND ASTRONOMY

THE REXCESS CLUSTER SAMPLE IN RADIO WAVELENGTH

by

Susanne Roswitha Heidenreich

Thesis for the degree of Doctor of Philosophy
May 27, 2019

UNIVERSITY OF SOUTHAMPTON

ABSTRACT

FACULTY OF PHYSICAL AND APPLIED SCIENCES

PHYSICS AND ASTRONOMY

Doctor of Philosophy

THE REXCESS CLUSTER SAMPLE IN RADIO WAVELENGTH

by Susanne Roswitha Heidenreich

ABSTRACT

Galaxy clusters are the largest gravitationally bound structures in the universe. Their examination provides valuable information about how the universe evolved and still evolves today.

It is important to gain greater understanding in the relation between x-ray and radio observations in order to get a deeper comprehension of the astrophysical processes underlying the observed results. The REXCESS sample is constructed in a way to make it representative for the local universe, so conclusions drawn from it can be easily extrapolated to the local cluster population as a whole. The lack of radio data for this important sample is closed with this work. It covers the medium-low part of the radio spectrum and supports the hypothesis that clusters with a bright central galaxy are more likely to have a central radio source associated with it. It additionally finds that bright x-ray sources doe not always have radio counterparts, at least not at this frequency range.

These results impact the highly active research field of galaxy clusters by implying that radio observations play a valuable part in any multi-wavelength observation of galaxy clusters.

There are certainly a lot more research needed to confirm the findings of this thesis and in order to extend the knowledge to even lower frequencies.

CONTENTS

LIST OF TABLES

LIST OF FIGURES

Declaration

I, Susanne Roswitha Heidenreich , declare that the thesis entitled *THE REXCESS CLUSTER SAMPLE IN RADIO WAVELENGTH* and the work presented in the thesis are both my own, and have been generated by me as a result of my own original research. I confirm that:

- this work was done wholly or mainly while in candidature for a research degree at this University;
- where any part of this thesis has previously been submitted for a degree or any other qualification at this University or any other institution, this has been clearly stated;
- where I have consulted the published work of others, this is always clearly attributed;
- where I have quoted from the work of others, the source is always given. With the exception of such quotations, this thesis is entirely my own work;
- I have acknowledged all main sources of help;
- where the thesis is based on work done by myself jointly with others, I have made clear exactly what was done by others and what I have contributed myself;

Susanne Roswitha Heidenreich , May 27, 2019

ACKNOWLEDGEMENTS

Without the support of the following people this thesis would never have got completed. I am so thankful for their continuing support. Thank you all for believing in me, even when I didn't believe in myself. I can never feed you with enough cakes and cookies for that.

First of all I want to thank my family. My parents Ingrid and Karl-Heinz gave me all the support they possible could to make sure I was able to finish my thesis, despite all health issues and odds. I also want to thank my sister Ramona for her support and understanding.
I also want to thank Judith Croston for her supervision and support throughout the years. She guided me through the steep learning curve of radio astronomy software and all the small and larger obstacles that were along the science route.
I also want to thank Simon Harris for his always open door whenever I had issues with my laptop or desktop PC.
I want to thank my good friend Andrea Dieball for the amazing tea breaks and her support whenever I needed somebody to talk to.
A special thanks goes to my friends Claudia Mader, Eva Strebl, Sandra Vahle, Elke Pfister, Mahmut Güzel, Ludger Konzag, Konrad Gerngross and Alfred Schöne for their support and help. They provided me with motivational posters, made sure I never forgot to laugh and fought all doubts and thoughts of quitting. I could always count on them. I also want to thank all my collegues at Siemens EM TS LTS FACTS C&P for their support along the final writing process and to Manuel Steger and Ralph Morgenstern for their understanding whenever I had to change my working days with short notice. I also want to mention the help and support I received from the ladies at untamed tresses.
Whenever I felt I need someone who understands my worries I found someone I could talk to or write with.
And I also want to thank the Lord for guiding me my whole life by proving advice on a spiritual level. Sometimes it was hard and I was not sure if I would be able to handle all that, but then it all worked out somehow.
Special thanks to all members of the RECXESS collaboration for their support and patience.

Susanne Roswtiha Heidenreich , May 27, 2019

> If you take a galaxy and try to make it bigger, it becomes a cluster of galaxies, not a galaxy. If you try to make it smaller than that, it seems to blow itself apart.
>
> JEREMIAH P. OSTRIKER

To Ingrid and Karl-Heinz Heidenreich

Learn from yesterday, live for today, hope for tomorrow. The important thing is not to stop questioning.

ALBERT EINSTEIN (1879 – 1955)

Natural science, does not simply describe and explain nature; it is part of the interplay between nature and ourselves.

WERNER HEISENBERG (1901 – 1976)

There are at least as many galaxies in our observable universe as there are stars in our galaxy.

M. REES (1942 - PRESENT)

1 Introduction

1.1 Motivation

With the planning of the Square Kilometre Array (SKA) to be build in the near future radio astronomy made a step towards an even brighter future. The SKA is meant to look back until the time of the cosmic dawn, detecting faint proto-galaxies and the switching off of the 21 cm line by the so-called reionisation. This is caused by the light emitted from those proto-galaxies and their stars, formed by gravitational instabilities. The emitted photons ionised the gas surrounding them and thus switching off the 21cm line of neutral hydrogen. SKA (2018)

Currently there are quite a few radio telescope arrays already working and enable us to get a deeper understanding of what is happening in the radio universe. It is worth mentioning that the development of faster data transmission had its impact on how radio telescopes are build. For example the LOFAR telescope, build across Europe, was only possible because glass fibre cables are available now.

Another important telescope is the GMRT in Pune, India, with its recent refurbishment. This is the one which recorded most of the observations necessary to collect the data used throughout this thesis.

Another important instrument is the construction of samples of galaxies. If this is

done carefully, the results drawn from these samples can be extrapolated to larger populations of similar objects. The REXCESS Sample Böhringer *et al.* (2007) is such a sample of carefully selected objects and the one that gives the base of the galaxies observed with the GMRT in order to draw conclusions from. It also is the sample that was used to select the galaxies, which were examined for this thesis. How this sample was constructed and more detailed information about the individual sources and there properties can be found in the later chapters.
The main goal of this work is to determine what the radio properties of the REXCESS clusters are and if they are related to other observed properties.
The in depth evaluation of the relations between these observables and how they correlate to each other is not discussed in this thesis as this would easily fill another one. This work focuses on a selection of clusters from the REXCESS sample and its observed properties at the 610MHz and 240MHz wavelength. This rather narrow topic selection was made in order to be able to give a good amount of detail about the individual sources, while still have a large enough quantity to draw some conclusions from statistical evaluation.

1.2 Research Questions and Goals of this thesis

The research questions arising from this context are:

- What properties at the two observed wavelengths do the clusters have?
  Each cluster underwent an in-depth flagging and calibration process, described later in detail, in order to assure that the described properties are valid in respect to uncertainties and error propagation. The total flux and noise levels were recorded as well as how well the calibration process compared to the theoretical noise level.

- How do the radio point sources coincide with detected optical sources?
  This question is answered by doing overlays of optical and radio maps and identifying the which optical and radio sources coincide. For the optical data the positions of known cluster members were provided by the REXCESS collaboration. A detailed optical analysis is going to be published soon.

- How do the radio observations compare to the X-Ray observations?
  This is also done by using overlays. The X-Ray data was provided by Judith Croston and the REXCESS collaboration. For this question there are overlays

with the point source removed X-Ray Images as well as with the X-Ray point sources to evaluate if there is any correlation.

1.3 Summary of Thesis

In order to answer these questions the first step was to carefully calibrate the radio data, apply the corrections and flag the bad data points in order to get the most valid maps possible.
To produce the maps the CASA software war chosen. At this time this software provided the most intuitive way to calibrate the data and it had a build-in task for the GMRT, which simplified the importing and made this step even more consistent. The first step was identifying and calibrating the flux calibrator. This was all half-automated by using a python script, which can be found in the appendix. The next step was calibrating the phase calibrator and finally the source was calibrated and imaged. This process is described in detail in a later chapter. Once all sources were calibrated, a source extraction tool was used to get accurate source positions and fluxes. Having collected all this data made it possible to check what their properties are and if their positions coincide with optical or X-Ray sources.
In the following chapters a theoretical overview of the topic and the key concepts is given as well as a definition of what a galaxy is, what a galaxy cluster is. The first section focuses on radio astronomy, from its beginnings to its current state. This is followed by a brief summary of the theory regarding observational properties and the types of environment radio galaxies can be found in.This chapter closes on the theory of radio emission mechanisms.
The next chapter gives a brief introduction of radio interferometry and the telescope used to obtain the data. It further describes the detailed calibration, reduction and imaging process the data underwent in order to produce valid radio maps. It also describes the source extraction process and how the data was analysed in order to obtain the scientific results.
The fourth chapter focuses on the individual sources observed at 610MHz. It provides the observational properties as well as it compares them to data from previous radio surveys. It also provides the position of the sources and the observed clusters.
In the fifth chapter some of the sources provided good enough data to be also calibrated at the 240MHz frequency. Which led to comparison of these with the data from the previous chapter and it made it possible to calculate the spectral indices.
The next chapter constructs some subsamples and compares the maps with the X-

Ray point sources.

The final chapter focuses on some conclusions and future work to be done.

In the following chapter the theoretical background is provided in order to be able to understand and reflect on the methods and conclusions drawn from the data.

Somewhere, something incredible is waiting to be known.

CARL SAGAN(1934 - 1996)

2

Introduction - Radio Galaxies, Radio Astronomy and Radio Emission

This chapter gives an overview about Radio galaxies, their observational properties and their environment, which is the main focus of this thesis. It gives a brief introduction to radio astronomy as well.

2.1 Radio Astronomy - A brief history

The scientific content of this thesis is mainly based on radio data, reduced and analysed by the author. This chapter gives a brief overview of the history of radio observations and discusses the science of radio interferometry as well as the telescopes used to obtain the data.
In 1932 Karl Jansky detected radio waves from space. He did not search for them he detected them while doing interferometry experiments for the Bell Laboratories. He identified three different sources for interference for communication, which he noted to be either local thunderstorms, or distant thunderstorms or a mysterious signal from space occurring 4 minutes later every day. The source of the signal was fixed with respect to the stars, which allowed him to locate it as the same direction

as the centre of our galaxy, the Milky Way. The Second World War interrupted further investigations in Radio astronomy, but the amateur astronomer Grote Reber, 1937 build his own steerable parabolic reflector dish, 9.5m in diameterJansky (1933) Hey (1984). This was the first radio telescope ever build. He had no luck in detecting the 9cm and 33cm wavelength, but he was successful detecting the 1.9m wavelength and made the first radio map of the milky way Hey (1984). In Fig. 2.1 the telescope can be seen.

In 1942 radio emission from the sun was detected and shortly after it was suggested to search for spectral lines in the radio emission. Van de Hulst proposed the existence of the 21-cm line of neutral hydrogen. It was first observed in 1951. The crab nebula was the first cosmic radio source associated with an optical counterpart.Hey (1984)

Radio galaxies were discovered in the 1950s. Jennison and Das Gupta 1953 discovered radio galaxies with their double lobe structure. That double structure is formed by two particle jets, which originate close to the central black hole of the active galactic nucleus(AGN)of the host galaxy. Jennison & Das Gupta (1953) As time progressed the telescopes got larger and were, with the advent of computers able to calculate the Fourier Transform inversion, supplemented by large interfer-

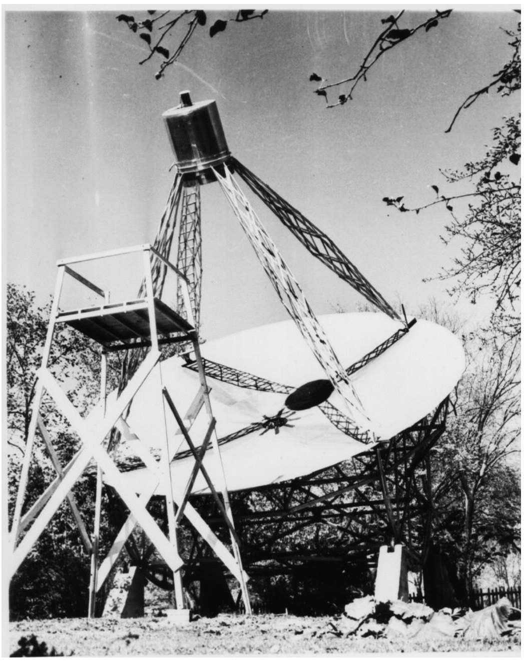

Figure 2.1: The radio telescope amateur astronomer Grote Reber built 1937 in his backyard. Image courtesy of NRAO

Image Credit NRAO

ometre telescope arrays. In the nearer past the interferometres became more and more important as they can provide the long baselines necessary for high spatial resolution.
For the observations the GMRT, a Y-Shaped interferometre telescope in Pune, India was used. More details about this telescope are given at the beginning of the next chapter.

2.2 Galaxies

”Galaxies are the building blocks of the Universe: standing like islands in space, each is made up of many hundreds of millions of stars in which the chemical elements are made, around which planets form, and where on at least one of those planets intelligent life has emerged.” Gribbin (2008)The hierarchical galaxy formation model suggests that the merging of halos from high redshift caused peaks at which galaxies form. The word galaxy itself comes from greek *galaxias* Milky Way. It was first used because our own galaxy forms the Milky Way on the sky.
Galaxies can be detected in many different parts of the electromagnetic spectrum, all the way from radio up to γ -Rays. Today we know many different forms of galaxies. One of them are Radio galaxies, detected by their Radio emission. But most galaxies are still detected by their thermal emission of their stars in the optical waveband. Even though all galaxies emit a wide range of wavelengths, the main concern in this thesis is their radio emission.

Having defined what galaxies are, the next logical step is to have a closer look at their observational properties.

2.3 Observational properties of radio galaxies

Radio galaxies come with different features, the common ones are core, jets, lobes and hotspots.

core

The majority of radio galaxies have a typical unresolved core. This core structure usually coincide with the optical host galaxy.

jets

Radio jets originate from the central region of the active galactic nuclei (AGN) and have rather steep spectra. These beams transport energy to the outer regions of radio galaxies and can extend to several kpc. Depending on the particular radio galaxy, one or two jets can be detected. Bridle & Perley (1984)

lobes

Lobes are larger regions of radio emission, typically observed at two opposite sites of the central source

hotspots

Hotspots are small regions of high radio luminosity at the outer egde of radio lobes. Bridle *et al.* (1994)

2.4 Groups and Clusters of Galaxies

Back in the 18th century Messier and Herschel both realised that galaxies, which were called nebulae at the time, tend to cluster Messier (1781)Herschel (1785). It was Hubble, who proves in the mid 1920's that these nebulae were extragalactic and formed massive and complex systems in the universe Hubble (1925),Hubble (1926). In the late 1950's two important cluster catalogues were published, the Catalogue of Galaxies and Clusters of Galaxies by Herzog et al. Herzog, Wild & Zwicky (1957) and The distribution of rich clusters of galaxies by Abell Abell (1958). Abell's catalogue is still used today.
the redshift measurements of the cluster members revealed their three-dimensional structure and the filaments connecting the individual clusters and voids. The information provided by these catalogues enabled astronomers to examine the cluster population and lead to the discovery that clusters are the largest gravitationally bound objects in the universe with masses up to a few $10^1 5$ solar masses.
In the early 1930's Zwicky used the virial theorem and velocity dispersion measurements to estimate the mass of the coma cluster. This exceeded the mass of all stars of the cluster combined significantly, so he proposed the existance of unseen dark matter Zwicky (1933). Groups of galaxies are smaller than clusters and usually contain no more than 50 galaxies.

2.5 Radio Emission Mechanisms

Radio emission emerges mainly from two emission processes, the synchrotron radiation and the bremsstrahlung (free - free radiation). Blandford & Konigl (1979) Longair (2001) The following paragraph explains the physical processes leading to bremsstrahlung

Electrons and ions are common particles in the central regions of radio galaxies. Bremsstrahlung results from the photons emitted by the electrons as it gets accelerated and decelerated by nearby ions.
Imagine a single electron being accelerated by a nearby ion. While being accelerated the electron gains kinetic energy, which is then released as a photon.
In the centre of radio galaxies there is thought to be hot and dense plasma where the origin of thermal bremsstrahlung is postulated. Non-thermal, relativistic bremsstrahlung occurs when relativistic charged particles interact with the plasma of the central region. In most cases the energy distribution of these relativistic electrons follows a power law.
In the case of synchrotron radiation the electron emitting the radiation spiral in the magnetic field thought to be produced by the nucleus.
Whenever an electron enters the magnetic field it starts spiraling and hence experiencing a centripetal acceleration. This forces the electron to emit cyclotron radiation. If these electrons are highly relativistic, their radiation is trapped inside a narrow cone shaped region, with the opening angle and the energy of the electrons being proportional to each other.Longair (2001) There are two reasons why the observer sees such a strong signal from the synchrotron electrons. the multiplication of the emission power with the Lorentz factor squared γ^2, being the first one and the beaming, which turns the slow sinosoidal variations into sharp pulses, being the second one. The frequencies within such a pulse is higher and is the observed frequency, proportional to $\gamma^2$and the gyro frequency.
In order to obtain the spectrum of the emitted synchrotron radiation, integration over the energy distribution of the emitting electrons is required.
In general compact sources are more likely to have a flat spectrum because of the complex source structure the optical thickness and thinness of the individual substructures vary. As every present electron will have critical frequencies, the superposition causes the spectrum to flatten. At higher frequencies the spectrum gets steeper, caused by the depletion of high energy electrons. This happens as the emitted power is proportional to the energy squared.

Data is a precious thing and will last longer than the systems themselves.

T. BERNERS-LEE (1955 - PRESENT)

3 Data calibration, Reduction and Analysis

This chapter describes in detail how the data reduction and calibration was carried out and the software used to obtain the scientific results.It also gives a brief overview on radio interferometry. The script used containing all specific parameters is in Appendix A. At the beginning the radio interferometry gets a closer examination.

3.1 Radio Interferometry

The spacial angular resolution of a telescope is proportional to the wavelength over the diameter of the telescope. It is well known that radio emission have a the lowest frequency in the electromagnetic spectrum and therefore the longest wavelength. So, if the 300m single dish radio telescope in Arecibo, Puerto Rico observes at 3cm wavelength the spacial resolution is around 20”. To give this number a reference, the optical Faulkes Telescope, Hawaii observes at 0.5” spacial resolution, limited by atmospheric disturbances. This means to get a similar resolution at radio wavelengths a aperture of 100km would be necessary, which is neither engineering-wise nor financially an option. This issue was solved by Ryle and Vonberg in the late

1940's.Ryle & Vonberg (1948) They used two antennae and combined their signals. This process, known as aperture synthesis, synthesises a beam with the angular resolution of a single dish of the diameter equalling the distance of the two antennae. Ryle & Hewish (1960) By using a correlator to multiply the one signal with the complex conjugate of the other the signal is amplified while averaging out the noise.

In radio interferometry a baseline is the distance between two antennae. As modern interferometers consist of multiple antennae, there are a lot of baselines of varying length and consequently resolving different spacial features. While the long baselines give the highest resolution, the short baselines give greater sensitivity for the extended features of the observed object.

The *uv* plane of a interferometer describes the spacial distribution of antennae in the North-South(v) and East-West (u) direction as seen by the source. The rotation of the Earth moves the antennae relative to the source and therefore the projection, which is the *uv* plane, varies with hour angle. Modern interferometers, like the GMRT discussed in the next section aim to give a full coverage of the *uv* plane.

Giant Metrewave Radio Telescope

The Giant Metrewave Radio Telescope (GMRT) is located about 80 km north of Pune and 10km east of Narayangoan town on the Pune-Nasik Highway. This location has the benefit of low man-made radio noise, good infrastructure, and a latitude that ensures a reasonable quiet ionosphere. Its configuration is divided in two parts, the more or less random compact array, consisting of 14 antennae,which are scattered in a region of approximately 1 square kilometre and a "Y"-shaped part, consisting of 16 antennae, which gives interferometric baselines up to about 25 km. This means there are 435 possible antennae pairs. The array has working frequencies of 50, 153, 233, 610 and 1420 MHz. For this thesis the bands 610 MHz and 233 MHz were used. The angular resolution of the GMRT varies from 60 arcsec for low frequencies to 2 arcsec for 1.4 GHz. Operational since 2002 the GMRT was one of the first interferometers that was able to map radio emission at these frequencies at high resolution. Its antennae are made using the 'SMART' concept (Stretch Mesh Attached to Rope Trusses), which made the telesope a low cost one. The dishes have a diameter of 45m each and are placed on concrete towers 15m high.

3.2 Data Calibration and Reduction

To start with the data was stored in fits-format files both side-bands separately. FITS is the acronym for **F**lexible **I**mage **T**ransport **S**ystem, which describes a system that is used for telescope data. One observation was in one file and there were one for 240MHz and 610Mhz each. Most raw data files contained more than one target source which shared the flux calibrator but had their individual phase calibrators. The calibration process itself was automated using a python based script that paused where manual checking was necessary. The calibration package used was the **C**ommon **A**stronomy **S**oftware **A**pplications package CASA (`casa.nrao.edu`) and the RFI-software developed by A. Offringa AO-Flagger(`www.astro.rug.nl/rfi-software/`). Calibrating the data is essential in order to have a base for comparing data from different observations and telescopes.

3.2.1 Initial flagging and calibration of the bandpass and flux calibrator

The very first step was to import the data into CASA. This was done by using the command *importgmrt*, as the data was collected using the **G**iant **M**etrewave **R**adio **T**elescope in Pune, India. This import-task is specifically designed for converting a GMRT fits file into a CASA measurement set. As there were no flagfiles available the standard parameters were used. Importing the data is necessary to alter

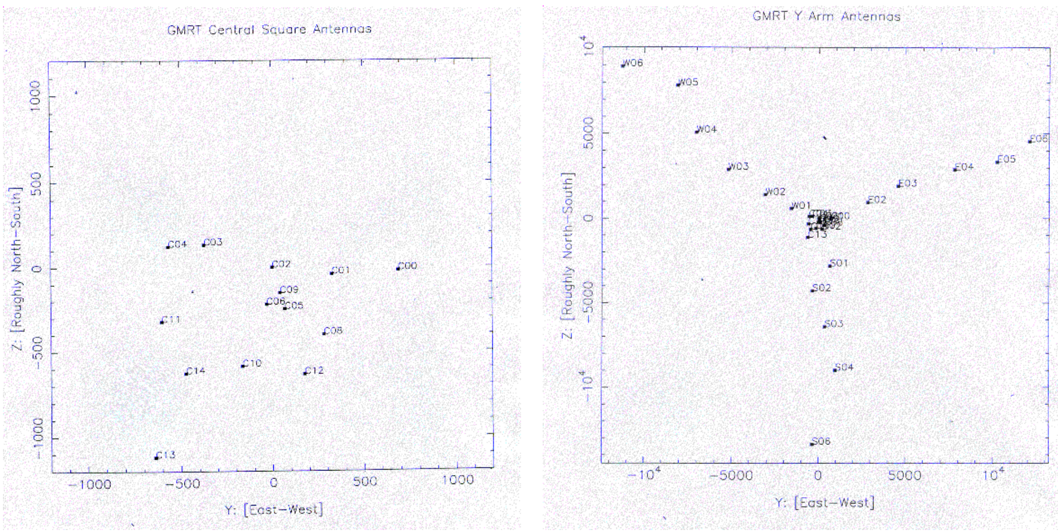

(a) central region of GMRT Telescope **(b)** whole array

Figure 3.1: The geometrical layout of the GMRT, Pune, India image courtesy: http://gmrt.ncra.tifr.res.in

and calibrate the data, as CASA uses its own file system were the data files are in form of measurement sets. After importing the data the task *listobs* was used to get an overview of the available data in this dataset. It lists all observed sources, the specific times of observations and the antennae used with there exact position. This tool was used to identify the flux as well as the phase calibrators and the sources in that particular dataset. The flux calibrator is usually easily identified as it is the one which is observed at the begin of the observation only, for very long observations it is observed a second time in the middle and a third time at the end. The phase calibrator is also easily identified as the observation switches between it and the target source. This is vital as the atmosphere changes constantly as does the phase. This information was then entered into the python script. This information also gives a first rough idea of how long the observation time in the final map will be. After starting the python script using *execfile* it was running half-automated. It first flags the low-flux channels at both ends of the bandwidth, then splitting the flux and phase calibrator of one of the sources of the measurement set in order to calibrate one source after the other.
In order to save time and make the calibration process more efficient the flux calibration is then used for all other sources in that dataset. So it is crucial to save all the individual steps which is done by the script. After splitting them into individual measurement sets with one source in each of them, the AO flagger with very generous parameter settings was executed on the file containing the flux calibrator only. Fig. 3.2 The generous settings are required to only exclude really high-flux **R**adio **F**requency **I**nterference as only this type is easily identified at this stage of the calibration. Lower level RFI will be missed by that and only becomes clear after more calibration is done. For this first level it is not required to have it removed and removing of low-level RFI would lead to removal of good data, which might be misidentified as low-level RFI. This is prevented by using generous parameters for this first flagging.

After saving the measurement set at this stage in a fits-file, the phase calibrator and source were combined which the flux calibrator using *concat* to obtain a single measurement set again. As the following flux calibration should be applied to all sources in the given observation After choosing a channel that seems to be free from RFI, one calibration circle was executed with this channel only. This step provides a first rough calibration of flux levels which helps the following calibration run making it more accurate. Choosing the channel is done by visual inspection. One calibration circle for the flux calibrator starts with the task *setjy*, which calibrates the amplitude

with respect to a given flux calibrator or a value specified. Whenever a flux calibrator function was available it was used. Using the flux calibrator function ensured that the most accurate flux was known to calibrate. The task *bandpass* performed directly after to determine the amplitude and phase as a function of frequency for each spectral window with more than one channel. Bandpass calibration is done to correct for variations across the frequency range. These variations might be introduced by differences in the light path causes by e.g. filters or reflections. The bandpass calibrating source should be a well-known point source, so usually it is the same source as the flux calibrator which should also have those properties. It is important to check after each calibration step if the calculated values are sensible. An easy and quick, but nevertheless reliable way of doing so is to plot the values onto a graph. At this step the most useful graph is to plot antenna vs. amplitude, there should be no points completely off the group with most points. Fig. 3.3
After checking the values with the *plotcal* plotting tool, the gains calibration was done using *gaincal*. This task includes the bandpass calibration on the fly to get a calibration table, which is again checked for being sensible and finally applied using *applycal*. Fig. 3.4
Gains calibration is important to level the flux from each antenna with respect to the other antennae. Each baseline has its very own gain, which is reflected in the visibility of this given baseline. In practice the observed calibrator is used to estimate

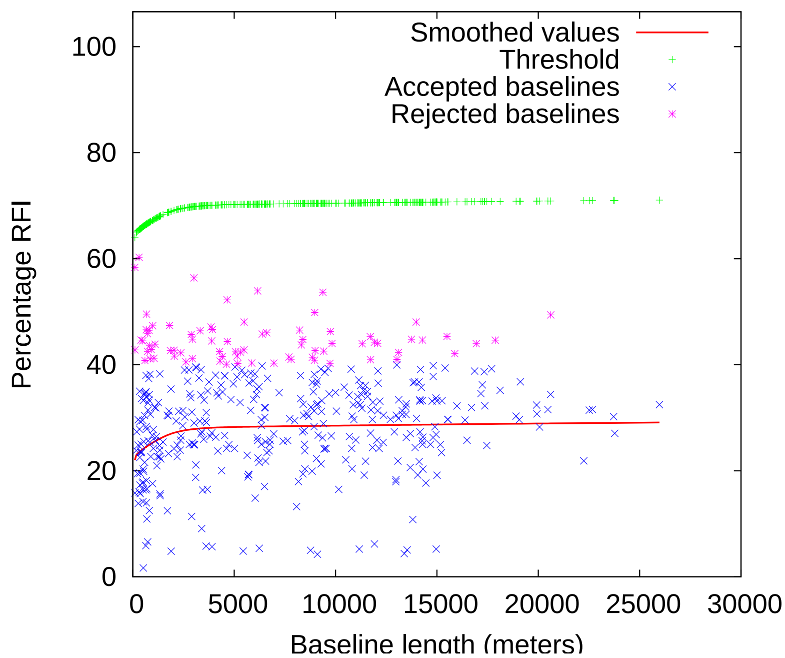

Figure 3.2: The flux calibrator 3C48 with all bad baselines marked for removal

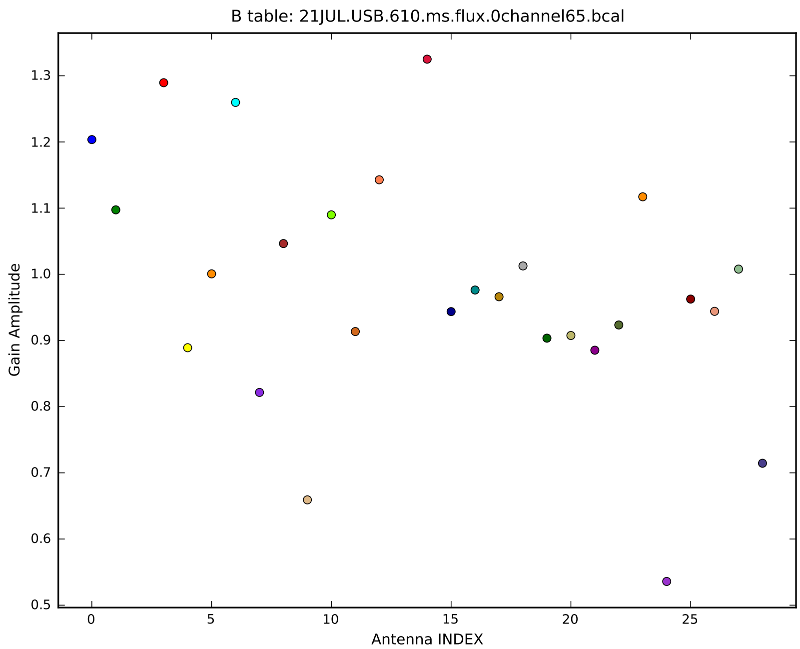

Figure 3.3: The flux calibrator 3C48 checked at channel 65 for bandpass calibration issues

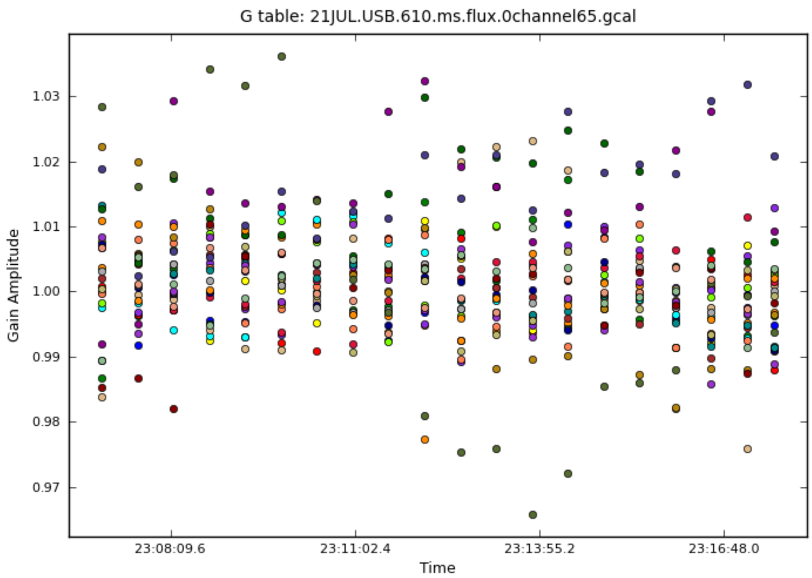

Figure 3.4: The flux calibrator 3C48 gain calibration checked at channel 65

the gains of the antennae and baselines. The gain itself consists of a set of individual measures, which include not only the instrumental part, but also atmospheric offsets and contributions. The flux calibrator calibration circle is completed by saving the outcome in fits-files using *exportuvfits*. This calibration circle is directly followed by another one using all channels. Fig. 3.5

Having finished the rough calibration of the flux calibrator the *split*task was used again to separate, source, flux and phase calibrator in three measurement sets for flagging. At this stage only the flux calibrator is flagged. Constantly improving the accuracy of the flux calibrator measurement set improves the parameters gained from it and therefore improves the quality of the target source as well as the phase calibrator. Flagging is carried out through the whole calibration process with the same parameters from this point onwards using the AO-Flagger. The parameters used were the default ones apart from the one specifying to make a plot of the data as well. Fig. 3.6

After flagging the flux calibrator the files were again concatenated to continue with the calibration, a set of fits-files was produced to save the progress up to this point. Another flux calibrator calibration circle was done with carefully checking everything in order to have the best quality data available for further calibration.Fig. 3.7

Saving the outcomes of this calibration finishes the flux and bandpass calibration. For multiple sources this whole process was carried out once and then applied to all sources and phase calibrators.

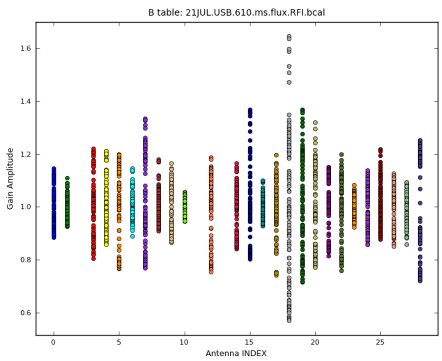

(a) Bandpass calibration table

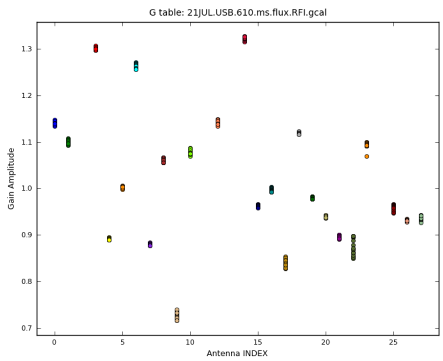

(b) Gains calibration table

Figure 3.5: A rough bandpass and gains calibration including some low level RFI.

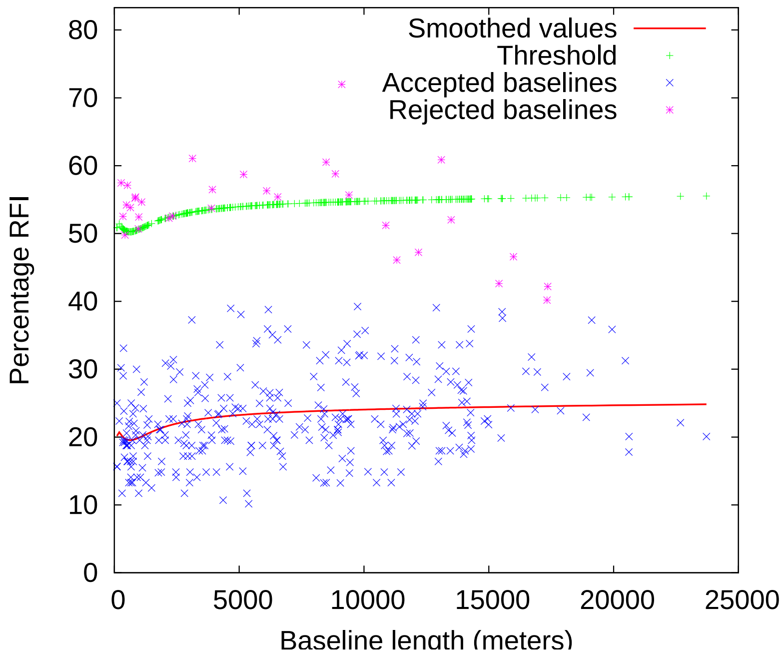

Figure 3.6: The flux calibrator 3C48 being prepared for the second flagging with AO-flagger

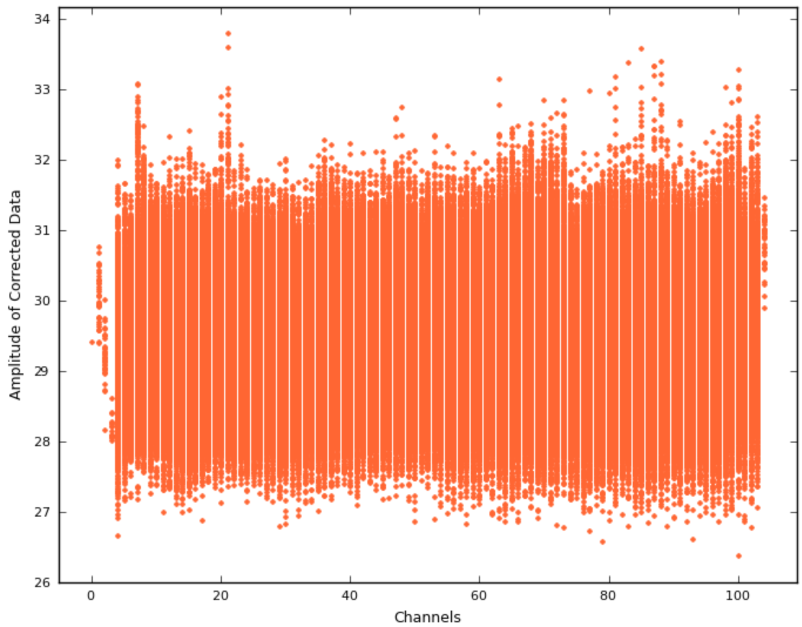

Figure 3.7: The flux calibrator 3C48 after second flagging with AO-flagger

3.2.2 Phase Calibration

The second section of calibration is the phase calibration. It is done for each source and calibrator pair individually. Phase calibration is used to catch instrumental and atmospheric changes resulting in phase rotation. Phase errors cause a loss of sensitivity by decorrelating and degrade the quality of the final image. This is introduced by scattering of the flux. For a phase calibrator the 'ideal' phase (without any contribution from the instruments) is zero. Therefore tracking the change in phase for this one allows us to calculate the offset from the 'ideal' case and calibrate the target source with this information accordingly. The first step in this section is using the previously flux and bandpass calibrated data and the CASA task *gaincal*. The parameter *gaintable*, which identifies the calibration table applied as well, was changed to the table produced in the final bandpass calibration and the the parameter *gainfield* was changed to the field name of the bandpass calibrator in order to specify this already calibrated field and apply those calibrations to the phase calibrator field. The next step used the table created by *gaincal* and rescaled it to the appropriate flux scale. In order to do this, the task *fluxscale* was given the flux calibrator as reference. This step ensures the appropriate flux is assigned to both the phase calibrator and the target source.
Applycal applied all the calibrations carried out during this procedure to the source and phase calibrator fields. In between each step the calibration tables were checked for being reasonable using the task *plotcal*. Fig. 3.8 All the calibration tables should look rather smooth now, without any major jumps. The data was exported to a fits-file to save the progress. After this first rough calibration the AO-flagger was used again to exclude RFI from the phase calibrator data. Another check with *plotms*

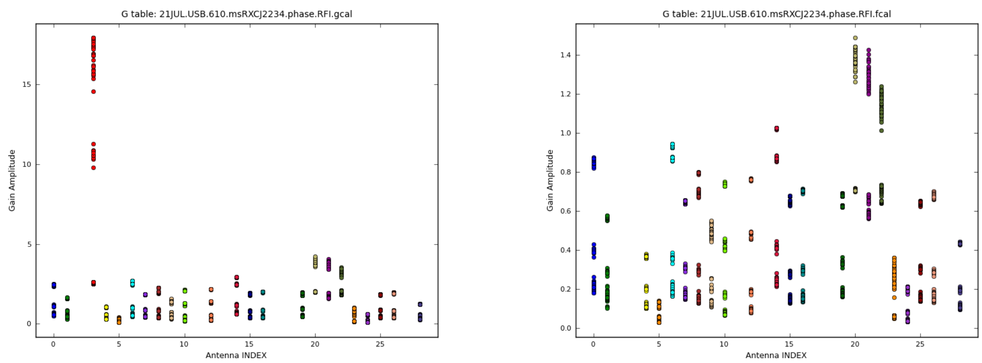

(a) Gains calibration table

(b) Flux calibration table

Figure 3.8: Phase calibration tables before flagging the phase calibrator

was included to catch RFI missed by the flagger. Fig. 3.9
Another fits-file was produced with *exportuvfits* before continuing with the calibration process. Another complete phase calibration set was carried out and applied to the source and phase calibrator. This step was saved again by exporting a fits-file, after inspection with *plotms*. Fig.**??**

3.2.3 Source flagging and reduction

In order to get the target source RFI free, it was again split from the phase and flux calibrators and automatically flagged using the AO-flagger and after this checked by using *plotms* for eventually missed RFI. Fig. 3.11
Saving the measurement set to a fits-file and concatenating it with the calibrator files to average the data in order to reduce the data size was the next step. Averag-

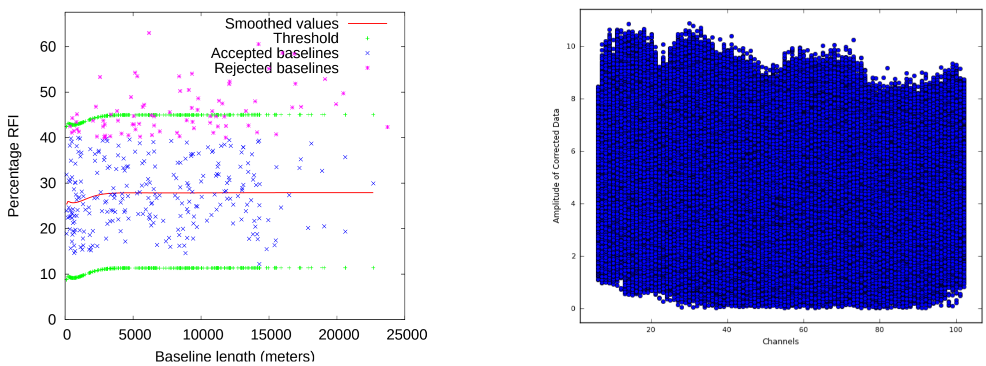

(a) rejected baselines **(b)** Flux calibration table

Figure 3.9: The phase calibrator 2219-279 after flagging with AO-flagger

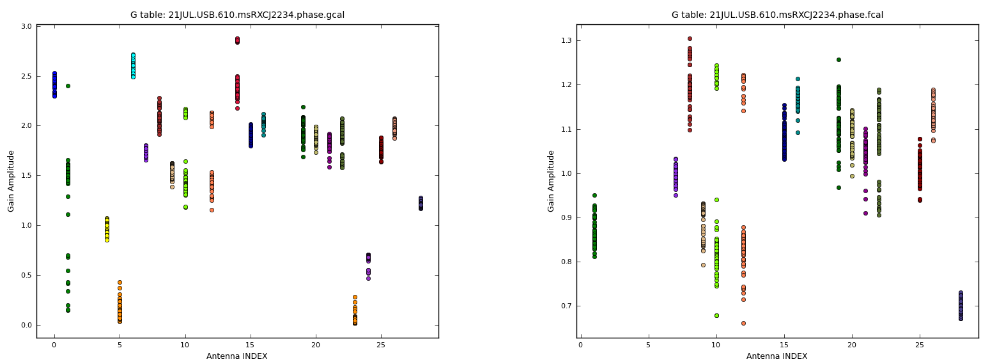

(a) phase calibration gains calibration table **(b)** Flux calibration table

Figure 3.10: The phase calibration tables after flagging the phase calibrator with AO-flagger

ing was done using the task *split* again, but this time the *width* parameter was set to a value which is a divisor of the number of channels left after flagging. The number of channels to be left with after averaging was chosen to be 8 for all observations, to ensure enough channels were left and all resulting channels are of the same width. The averaged source measurement sets were saved to fits-files and split into individual source measurement files to execute a final run of the AO-flagger on the target source. After this a final complete calibration run was done to get the best possible data for the imaging step. Fig. 3.12

3.2.4 Imaging

In order to get the imaging done the target source was separated from the other sources observed. The clean algorithm was used. CASA uses the task *clean* with the parameters *gridmode* 'widefield' and 90 w-planes. The number of these planes where calculated before imaging. For all images Briggs-weighting was used. The robustness parameter was set to 0.5. The final image produces was viewed in CASA Viewer and exported as image as well as uv-data-set.

3.2.5 Self-Calibration

The self-calibration process was only carried out, if there were enough point sources of high enough flux. Otherwise the self calibration process made the rms to noise level either worse or did not improve it at all. If the self-calibration process was applied the following steps were carried out. The first step is the gains calibration carried out and applied to the source. After carefully checking the uv-data the imaging process using *clean* was started. A cellsize of 1 arcsecond was used. A

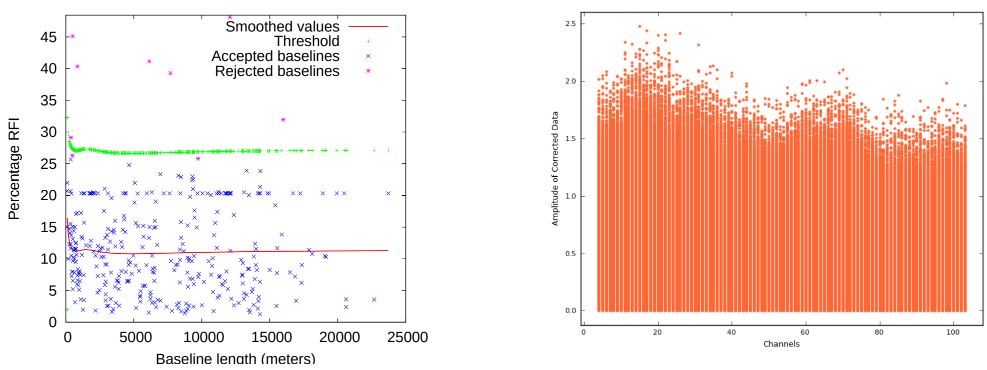

(a) rejected baselines **(b)** source after flagging

Figure 3.11: The source RXCJ2234 after flagging with AO-flagger

theshold of 0.0001 mJy was chosen while the number of iterations was set to 10000. Fig. 3.13 A soon as the rms level increased or there was no further improvement the self-calibration was stopped. Fig. 3.14

3.2.6 Pybdsm - Source extraction

The PyBDSM software provided by ASTRON, Netherlands was used to extract the sources and their position from the radio maps created. A process taking care of maps with artefacts was used in order to detect all sources, but not the artefacts as false positives.

The software is particularly labeled to work with CASA, which was used to calibrate the maps in the first plase.

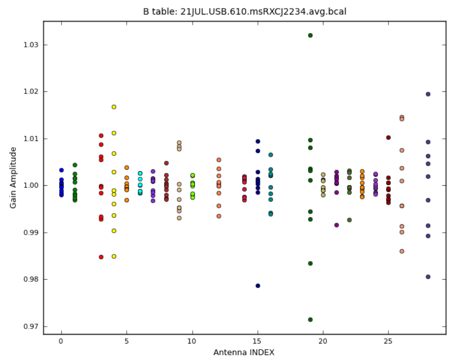

(a) averaged bandpass calibration table table

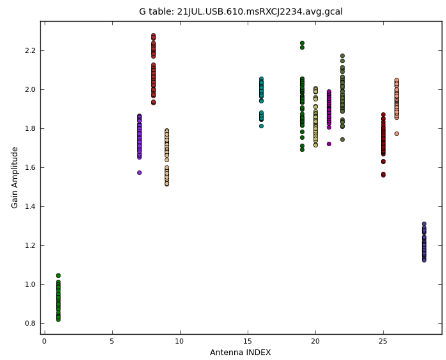

(b) averaged gains calibration table

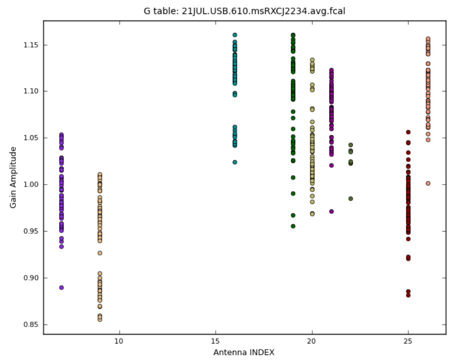

(c) averaged flux calibration table

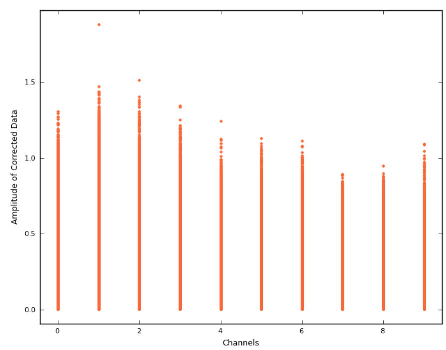

(d) source data after averaging and final calibration

Figure 3.12: The final calibration

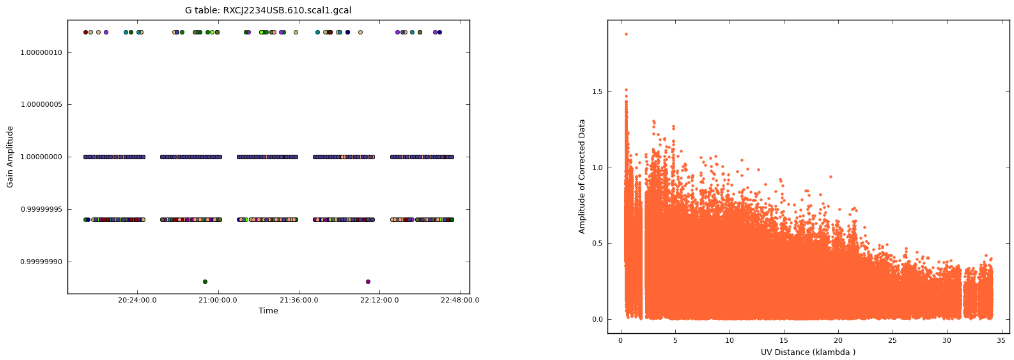

(a) self-calibration gains calibration table **(b)** source after self-calibration run

Figure 3.13: Self-calibration

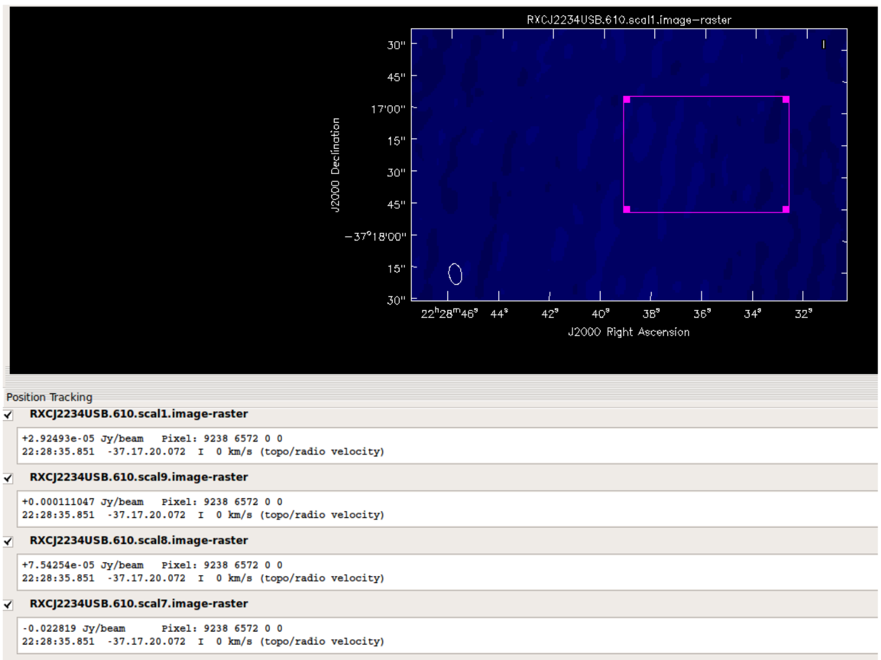

Figure 3.14: The various iterations of the self-calibration process. The bottom panel shows the signal in Jy/beam for all three images at the same position

Equipped with his five senses, man explores the universe around him and calls the adventure Science.

E. HUBBLE (1889 - 1953)

4 Individual sources at 610MHz

This chapter discusses the observations, data quality and optical cross-identification of the 28 REXCESS clusters, observed at 610 MHz. It lists observational properties of the radio sources and compares them with data from previous radio surveys.

4.1 The Representative XMM-Newton Cluster Structure Survey (REXCESS)

The **Re**presentative **X**MM-Newton Cluster **S**tructure **S**urvey is based on the REFLEX survey catalogue, which itself is based on the ROSAT All-Sky Survey. The ROSAT All-Sky Survey is a highly complete flux limited cluster sample covering 4.24 ster in the southern extragalactic sky.

4.1.1 Construction of the sample

REXCESS is restricted to the local universe, only clusters with a redshift of 0.2 or less are included. The second selection criterion is X-ray luminosity, which ensures no preference for any morphology is incorporated into the sample. The sample selection is made so a close to homogeneous coverage of X-ray luminosity range is given, this includes the most massive clusters as well as poor systems. Another selection criterion is a good global characterisation to detect cluster emissions out to the characteristic radius R_{500}. R_{500} is the radius at which the mean cluster density drops below 500 times the critical density of the universe. Another selection criterion was to choose the distances to the objects in such a way, that the field-of-view, angular resolution and photon collection power of the XMM-Newton observatory. Further detail of the selection criteria and how the sample was constructed are published in Böhringer *et al.* (2007). All these criteria ensure a galaxy cluster sample purely selected on basis of their X-ray luminosity in nearby redshift shells. This results in a sample that is representative of an unbiased X-ray luminosity or flux selected subset of the galaxy cluster population in the local universe. Böhringer *et al.* (2007)

4.1.2 Motivation

The member clusters of REXCESS are observed in X-ray and optical wavelengths, but they are not yet observed in the radio part of the electromagnetic spectrum, observing them at 610 MHz provides a perfect opportunity to find radio sources associated with the clusters as well as their influence on the cluster as a whole. This chapter answers the questions about the abundance of radio sources in this area of the sky and if they are associated with the cluster.

4.2 Observational Details

In this section the observational details of the used data are discussed.

All the data was taken using the **G**iant **M**etre **W**ave **T**elescope (GMRT) in Pune, India. Of the 128 original channels 16 were excluded and the remaining central 112 channels were averaged to a total of 13 channels. The channel width was 125 kHz and the total bandwidth was 16MHz. The total observation time was not the same for all sources and varied between 3 hours and 7 hours. This variation was caused by source position, sources that are located far south are not at a high enough elevation for a long enough time to observe them. All calibration was done using CASA and the AO Flagger. Wide-field imaging was adopted in each data reduction step.

Table 4.1 lists the resolution, and observational properties of the individual observations. It additionally lists the time of the observation and the observer.

The following section concentrates on the data quality of theses observations.

Cluster records	Data	Observed Date from	Observed Date to	Observed from	Observed to	# Channels	Frame	Total Bandwidth (kHz)	resolution	
RXCJ0003.8+0203	230150	04.12.2008	04.12.2008	15:44:25.0	19:01:33.0	11	T0P0	6875.0	8.1″	× 6.1″
RXCJ0006.0−3443	168831	20.07.2007	21.07.2007	23:29:02.3	02:13:10.5	11	T0P0	6875.0	9.9″	× 7.2″
RXCJ0020.7−2542	242295	04.12.2008	04.12.2008	11:50:22.5	15:17:34.4	11	T0P0	6875.0	8.1″	× 7.1″
RXCJ0049.4−2931	577680	06.12.2008	06.12.2008	14:25:44.0	18:33:28.7	11	T0P0	6875.0	8.5″	× 5.3″
RXCJ0211.4−4017	237389	21.07.2007	22.07.2007	02:21:50.6	02:06:42.6	32	T0P0	16000.0	8.5″	× 5.3″
RXCJ0225.1−2928	260130	20.07.2008	21.07.2008	23:35:46.5	03:34:51.1	26	T0P0	16000.1	9.3″	× 6.4″
RXCJ0345.7−4112	172956	22.07.2007	22.07.2007	02:17:03.4	04:57:33.5	11	T0P0	5500.0	15.8″	× 11.4″
RXCJ0547.6−3152	213570	23.07.2007	23.07.2007	04:50:59.3	08:23:46.8	11	T0P0	6875.0	9.2″	× 6.1″
RXCJ0605.8−3518	196504	22.07.2007	22.07.2007	05:13:13.0	08:15:48.6	32	T0P0	16000.0	10.5″	× 7.1″
RXCJ0821.8+0112	255780	21.07.2008	21.07.2008	04:00:01.0	08:03:33.9	11	T0P0	6875.1	9.4″	× 5.0″
RXCJ0956.4−1004	298410	05.12.2008	06.12.2008	19:50:02.8	00:14:34.1	11	T0P0	6875.0	7.3″	× 5.4″
RXCJ0958.3−1103	240990	04.12.2008	04.12.2008	20:08:22.7	23:52:21.3	64	T0P0	16000.0	7.1″	× 5.1″
RXCJ1044.5−0704	289710	05.12.2008	05.12.2008	00:47:59.9	04:56:51.7	64	T0P0	16000.0	14.7″	× 4.6″
RXCJ1141.4−1216	264915	06.12.2008	06.12.2008	00:50:55.1	04:44:24.1	32	T0P0	16000.0	7.4″	× 5.6″
RXCJ1236.7−3354	282366	22.07.2007	23.07.2007	08:27:16.4	12:46:03.8	32	T0P0	16000.0	16.6″	× 5.1″
RXCJ1302.8−0230									5.6″	× 4.9″
RXCJ1311.4−0120	233595	21.07.2008	21.07.2008	08:50:15.7	12:33:07.2	11	T0P0	6875.1	6.5″	× 4.8″
RXCJ1516.3+0005									4.7″	× 4.2″
RXCJ1516.5−0056	524610	21.07.2008	21.07.2008	13:01:38.5	17:04:21.1	11	T0P0	6875.1	6.6″	× 5.0″
RXCJ2014.8−2430	290580	21.07.2008	21.07.2008	17:31:45.3	21:49:50.6	11	T0P0	6875.1	7.9″	× 6.9″
RXCJ2023.0−2056									5.6″	× 4.2″
RXCJ2048.1−1750	290580	06.12.2008	06.12.2008	09:19:16.2	13:30:22.1	11	T0P0	6875.0	6.3″	× 5.3″
RXCJ2149.1−3041	260793	19.07.2007	19.07.2007	17:58:58.5	22:18:11.0	11	T0P0	6875.0	16.9″	× 6.8″
RXCJ2152.2−1942	240990	20.07.2008	20.07.2008	19:38:05.9	23:11:26.9	11	T0P0	6875.1	8.6″	× 6.4″
RXCJ2157.4−0747									7.1″	× 5.6″
RXCJ2217.7−3543									14.8″	× 11.9″
RXCJ2218.6−3853	287448	22.07.2007	22.07.2007	18:23:12.4	22:47:43.6	11	T0P0	6875.0	14.0″	× 9.6″
RXCJ2234.5−3744	213408	20.07.2007	20.07.2007	19:26:19.6	23:00:31.0	11	T0P0	6875.0	11.6″	× 6.3″

Table 4.1: Resolution and observational details

4.3 Data Quality Summary

This section gives an overview of the data quality of all 28 cluster observation in general.

9 maps have a measured RMS to theoretical noise factor of less than 2, 13, have it between 2 and 3 and 7 have one higher than 3, with 3 of them between 3 and 4. Table 4.2 shows this in detail as well as the time spend on each source. Table 4.3shows the positions the GMRT was pointing at. All coordinates are J2000. The rms of the SUMSS is given with 1mJy/beam and it was executed at 843MHz. The NVSS has a RMS of 0.45mJy/beam and is observed at 1.4GHz. So for most of the maps the RMS is approximately one power of ten lower compared to those surveys. But the resolution is better as is the sensitivity.

After this discussion of the overall data quality, the next section is focused on the individual radio maps.

4.4 Individual clusters

In this section I discuss the properties of the individual radio maps, summarising the detected source population, comparing with previous radio surveys and discussing optical cross-identification.

Observed source	antennae used	Integration time	theoretical noise (Jy)	measured noise (Jy)	measured x times higher than theoretical	dynamic range
RXCJ0003.8+0203	19	02:26:31	7.27E-005	1.32E-004	1.82	513
RXCJ0006.0−3443	19	02:13:06	7.62E-005	1.23E-004	1.61	873
RXCJ0020.7−2542	18	02:34:21	7.48E-005	2.79E-004	3.72	640
RXCJ0049.4−2931	24	03:04:00	5.10E-005	1.63E-004	3.18	2729
RXCJ0211.4−4017	23	02:53:39	5.49E-005	1.67E-004	3.04	900
RXCJ0225.1−2928	21	02:45:32	6.17E-005	9.93E-005	1.61	714
RXCJ0345.7−4112	19	01:57:26	8.12E-005	1.80E-004	2.22	128
RXCJ0547.6−3152	25	02:35:46	5.32E-005	1.59E-004	2.98	1727
RXCJ0605.8−3518	20	02:13:22	7.23E-005	3.96E-004	5.49	5308
RXCJ0821.8+0112	22	02:42:44	5.93E-005	9.78E-005	1.65	1434
RXCJ0956.4−1004	23	03:09:52	5.25E-005	8.47E-005	1.61	1085
RXCJ0958.3−1103	24	02:33:31	5.59E-005	8.67E-005	1.55	1177
RXCJ1044.5−0704	19	03:05:40	6.46E-005	1.18E-004	1.83	344
RXCJ1141.4−1216	23	02:48:37	5.57E-005	1.52E-004	2.72	1266
RXCJ1236.7−3354	25	03:24:08	4.65E-005	2.45E-004	5.26	343
RXCJ1302.8−0230	26	02:53:05	4.85E-005	9.78E-005	2.02	1386
RXCJ1311.4−0120	24	02:28:29	5.68E-005	1.20E-004	2.12	279
RXCJ1516.3+0005	26	02:51:58	4.87E-005	1.13E-004	2.33	1289
RXCJ1516.5−0056	24	02:46:56	5.36E-005	9.27E-005	1.73	277
RXCJ2014.8−2430	23	03:05:07	5.31E-005	1.46E-004	2.74	1711
RXCJ2023.0−2056	24	02:19:15	5.87E-005	1.28E-004	2.18	346
RXCJ2048.1−1750	24	03:05:07	5.09E-005	1.07E-004	2.11	617
RXCJ2149.1−3041	14	03:25:31	8.41E-005	2.40E-004	2.86	215
RXCJ2152.2−1942	22	02:33:31	6.11E-005	7.65E-004	12.53	3011
RXCJ2157.4−0747	24	03:05:23	5.08E-005	1.20E-004	2.36	413
RXCJ2217.7−3543	12	02:57:50	1.06E-004	2.01E-004	1.89	1321
RXCJ2218.6−3853	25	03:15:11	4.75E-005	2.97E-004	6.25	838
RXCJ2234.5−3744	19	02:48:03	6.79E-005	1.64E-004	2.41	660

Table 4.2: Observation properties for all clusters

source	RA	DEC	4MPc radius in deg	R_{500}	redshift z	angular scale in kpc
RXCJ0003.8+0203	00:03:50.60620	+02:03:48.0404	0.64634	0.14166	0.0924	0.58171
RXCJ0006.0−3443	00:06:03.00404	-34:43:26.9735	0.53414	0.14145	0.1832	0.48073
RXCJ0020.7−2542	00:20:42.80608	-25:42.36.9598	0.44760	0.11697	0.1410	0.40284
RXCJ0049.4−2931	00:49:24.00587	-29:31:27.9605	0.56114	0.11332	0.1198	0.50503
RXCJ0211.4−4017	02:11:25.50326	-40:17:11.9777	0.59823	0.10245	0.1008	0.53840
RXCJ0225.1−2928	02:25:10.50528	-29:28:25.9676	0.95259	0.16525	0.0604	0.85734
RXCJ0345.7−4112	03:45:45.70278	-41:12:26.9853	0.95406	0.	0.0603	0.85865
RXCJ0547.6−3152	05:47:38.20297	-31:52:30.9986	0.42905	0.12160	0.1483	0.40723
RXCJ0605.8−3518	06:05:52.80282	-35:18:02.0007	0.45248	0.11831	0.1483	0.40723
RXCJ0821.8+0112	08:21:51.70622	+01:12:41.9766	0.71802	0.13569	0.0822	0.64622
RXCJ0956.4−1004	09:56:26.40595	-10:04:12.0347	0.39599	NA	0.1634	0.35640
RXCJ0958.3−1103	09:58:22.11399	-11:03:35.0822	0.38918	0.10483	0.1669	0.35026
RXCJ1044.5−0704	10:44:33.01436	-07:04:22.0901	0.46671	0.10873	0.1342	0.42003
RXCJ1141.4−1216	11:41:24.30615	-12:16:20.0403	0.53414	0.11821	0.1195	0.48073
RXCJ1236.7−3354	12:36:44.70426	-33:54:10.0262	0.73923	0.13925	0.0796	0.66532
RXCJ1302.8−0230	13:02:50.70621	-02:30:22.0387	0.69885	0.14712	0.0847	0.62896
RXCJ1311.4−0120	13:11:30.00619	-01:20:07.0383	0.36096	0.11904	0.1832	0.32486
RXCJ1516.3+0005	15:16:19.20617	+00:05:51.9737	0.52077	0.12888	0.1181	0.46870
RXCJ1516.5−0056	15:16:34.00621	-00:56:56.0263	0.51437	0.11921	0.1198	0.46294
RXCJ2014.8−2430	20:14:49.70719	-24:30:29.9777	0.41625	0.12022	0.1612	0.37463
RXCJ2023.0−2056	20:23:01.60701	-20:56:54.9765	1,01536	0.18771	0.0546	0.91382
RXCJ2048.1−1750	20:48:10.60684	-17:50:37.9729	0.40287	0.10857	0.1475	0.38790
RXCJ2149.1−3041	21:49:07.40463	-30:41:54.9777	0.51963	0.11518	0.1184	0.46768
RXCJ2152.2−1942	21:52:14.20668	-19:42:19.9658	0.62295	NA	0.0963	0.56066
RXCJ2157.4−0747	21:57:25.80639	-07:47:40.9652	0.99080	0.18615	0.0579	0.89172
RXCJ2217.7−3543	22:17:43.30462	-35:43:33.9761	0.42833	0.10950	0.1486	0.38551
RXCJ2218.6−3853	22:18:40.20468	-38:53:50.9760	0.44733	0.12638	0.1411	0.40261
RXCJ2234.5−3744	22:34:31.00457	-37:44:05.9753	0.42265	0.13548	0.1510	0.38039

Table 4.3: Positions of pointing centre and 4 MPc radius in degrees and R_{500} in degrees it also provides the redshift of the cluster and its angular scale.

4.4.1 RXCJ0003.8+0203

This cluster, which is pictured in Fig. 4.1 is also known as Abell 2700 (Abell (1958), Abell *et al.* (1989)), and is situated at $z = 0.0924$, which corresponds to an angular scale of 1 arcsec = 0.58171 kpc.

There are **178** sources detected at $> 5\sigma$ level within 4 Mpc of the cluster centre. The central bright source is an extended double source. Of the 178 detected sources, **nine** are extended.The only extended source within R_{500} is the bright central galaxy. Minor artefacts are present around the brighter sources, and there is one RFI stripe near the centre of the field, which we were unable to remove. Fig. 4.1 shows the RMS structure in a typical region, indicating that it is smooth as expected away from the stripe. The overall RMS structure is shown in Fig. 4.1. Fig. 4.2 shows the contours from the NVSS overlaid on the GMRT map, demonstrating that only the central bright of the tabulated sources was detected in that survey. This source and all additionally detected radio sources are listed in 4.4. The optical galaxies in the central region of R_{500} which are associated with the cluster are indicated in Fig. 4.2 as green circles. It is shown that only 2 of the optical sources have radio counterparts. The additional radio sources lack an optical cross-identification, possibly caused by either the faintness of the optical source or a non determined associated redshift, making it impossible to determine if it is associated with the cluster. All known positions of optical sources are provided in Tab. B.1. The redshift range used to identify cluster members was $0.075 - 0.105$, chosen according to Yee (1996). The cluster has a mass of $M_{500} = 2.1 \times 10^{14} M_{\odot}$ Pratt et al. (2010) and has a medium central entropy Pratt et al. (2010).

There is **two** newly confirmed radio source associated with the cluster and **16** new cluster member candidates. Further research is needed to verify if a cluster membership is given for these candidates.

Source ID	RA	Δ RA	DEC	Δ DEC	total flux	Δ total flux	Peak flux	Δ Peak flux	optical cross-ID	cluster member	comments
0	00:04:22	0.00013	02:02:49	0.000057	0.001535	0.000305	0.001614	0.000167	✗	?	
1	00:04:14	0.000143	02:05:17	0.000154	0.001625	0.000259	0.001123	0.000168	✗	?	
2	00:04:07	0.000206	01:57:03	0.000119	0.001257	0.000301	0.001051	0.000182	✗	?	
3	00:03:58	0.000078	02:00:44	0.000048	0.002207	0.000282	0.002195	0.000161	✗	?	
4	00:03:52	0.000228	02:00:22	0.000345	0.004281	0.000321	0.00141	0.000248	✗	?	
5	00:03:52	0.000289	02:04:21	0.000321	0.005079	0.000364	0.001467	0.00029	✗	?	ext.
6	00:03:52	0.00027	02:04:35	0.000347	0.010588	0.000291	0.001878	0.000249	✗	?	
8	00:03:51	0.000201	02:04:34	0.000202	0.004298	0.000429	0.00192	0.000311	✗	?	
10	00:03:50	0.000051	02:03:60	0.00003	0.029397	0.000641	0.012193	0.000285	✔	✔	BCG
10	00:03:50	0.0002	02:04:12	0.000146	0.001471	0.000493	0.00144	0.000283			
11	00:03:49	0.000296	02:03:38	0.000146	0.004308	0.000382	0.001752	0.000281	✗	?	
12	00:03:48	0.000174	02:03:14	0.000276	0.002479	0.000394	0.001376	0.00027	✗	?	
13	00:03:44	0.000187	01:57:33	0.000169	0.001416	0.000276	0.00099	0.000178	✗	?	
14	00:03:33	0.000232	02:00:49	0.000101	0.001029	0.000352	0.00105	0.000196	✗	?	
15	00:03:32	0.000035	02:00:40	0.00002	0.006613	0.000349	0.006461	0.0002	✗	?	
16	00:03:28	0.000194	02:06:60	0.00023	0.003781	0.000219	0.001303	0.000167	✔	✔	

Table 4.4: Positions of radio sources within R_{500} radius of the pointing centre of cluster RXCJ0003.8+0203

4.4.2 RXCJ0006.0−3443

This cluster, shown in Fig. 4.3, is also known as Abell 2721 [Abell (1958), Abell *et al.* (1989)] and is located at $z = 0.1832$, which corresponds to an angular scale of 1 arcsec = 0.48073 kpc.

127 sources are detected at $> 5\sigma$ level within 4 Mpc of the cluster centre. These are tabulated in Table C.1.There is no central bright source detected at this sensitivity. Of the 127 detected sources, **four** are extended and none of them is located within a R_{500} radius. Minor artefacts are present around the brighter sources. Fig. 4.3 indicates the RMS to be as smooth as expected in the overall map. Fig. 4.4 shows the contours from the SUMSS overlaid on the GMRT map, demonstrating that only the three brightest sources were detected in that survey. These sources and all additional sources are listed in Tab. 4.5 There are no optical galaxies in the central region of R_{500} associated with the cluster as indicated in Fig. 4.4 by the green circles the ones not associated are indicated by red circles. It is shown that no radio sources have a optical counterpart. The additional radio sources lack an optical cross-identification, possibly caused by either the faintness of the optical source or no associated redshift, making it impossible to determine if it is associated with the cluster. All known optical sources are provided in Tab. B.2. The redshift range used to identify cluster members was 0.095−0.125, chosen according to Yee (1996).The cluster has a mass of $M_{500} = 4.0 \times 10^{14} M_{\odot}$ Pratt et al. (2010) and has a medium to high central entropy Pratt et al. (2010) and is classified as a disturbed cluster Pratt et al. (2010).

There are **no** newly confirmed radio sources associated with the cluster and **13** new cluster member candidates. Further research is needed to verify if a cluster membership is given for these candidates.

Source ID	RA	Δ RA	DEC	Δ DEC	total flux	Δ total flux	Peak flux	Δ Peak flux	optical cross-ID	cluster member	comments
0	00:06:44	0.000215	-34:44:41	0.000215	0.002961	0.000563	0.002049	0.000364	✗	?	
0	00:06:44	0.000215	-34:44:29	0.000414	0.001271	0.000586	0.001196	0.000337	✗	?	
1	00:06:42	0.000153	-34:48:12	0.000202	0.001604	0.000624	0.001829	0.000343	✗	?	
2	00:06:41	0.000005	-34:50:27	0.000008	0.100146	0.00114	0.103272	0.000641	✗	?	
3	00:06:41	0.00005	-34:50:51	0.00014	0.005557	0.001033	0.006231	0.000546	✗	?	
4	00:06:40	0.0002	-34:49:39	0.000149	0.006353	0.00084	0.004033	0.000556	✗	?	
4	00:06:40	0.000079	-34:49:28	0.000231	0.002666	0.000912	0.003176	0.00047	✗	?	
4	00:06:39	0.0002	-34:49:25	0.000248	0.001684	0.000911	0.002061	0.000484	✗	?	
5	00:06:33	0.000051	-34:46:34	0.000101	0.003146	0.000542	0.003801	0.000283	✗	?	
6	00:06:18	0.000052	-34:41:35	0.000134	0.00325	0.000435	0.003088	0.000245	✗	?	
7	00:06:15	0.00002	-34:47:30	0.00002	0.064745	0.000944	0.031518	0.000399	✗	?	
8	00:05:54	0.000009	-34:44:33	0.000014	0.055758	0.000695	0.04569	0.000419	✗	?	
10	00:05:38	0.000117	-34:48:51	0.000123	0.00639	0.000374	0.003222	0.000263	✗	?	

Table 4.5: Positions of radio sources within R_{500} radius of the pointing centre of cluster RXCJ0006.0−3443

4.4.3 RXCJ0020.7−2542

Fig. 4.5 shows this cluster, also known as A0022 [Abell (1958), Abell *et al.* (1989)], situated at $z = 0.1410$, corresponding to an angular scale of 1 arcsec = 0.40284 kpc. **37** sources are detected at $> 5\sigma$ level within 4 Mpc of the cluster centre. These are tabulated in Table C.2.Of the 37 detected sources, **seven** are double sources and **three** are extended.The are no extended sources within R_{500}. Self calibration was not able to improve this radio map. There is a smooth background present throughout the whole map, which is shown in Fig. 4.5. Fig.4.6 shows the contours from the NVSS overlaid on the GMRT map, demonstrating that only the two bright sources were detected in that survey. These source and all additionally detected radio sources are listed in Tab. 4.6. The optical galaxies in the central region of R_{500} which are associated with the cluster are indicated in Fig. 4.5 as green circles the ones not associated are red. It is shown that only the central bright source has an optical counterpart. The additional radio sources are lacking an optical counterpart, possibly caused by the faintness of the optical source or no associated redshift, making it impossible to determine the cluster membership.All known positions of optical sources are given in Tab. B.3. The redshift range used to identify cluster members was 0.125−0.155, chosen according to Yee (1996). The cluster has a mass of $M_{500} = 3.8 \times 10^{14} M_{\odot}$ Pratt et al. (2010) and has a medium to high central entropy Pratt et al. (2010).
There is **one** newly confirmed radio source associated with the cluster and **one** new cluster member candidates. Further research is needed to verify if a cluster membership is given for these candidates.

4.4.4 RXCJ0049.4−2931

This cluster is known as S0084 (Abell *et al.* (1989)), and is situated at $z = 0.1198$, corresponding to an angular scale of 1 arcsec = 0.50503 kpc. It is shown in Fig. 4.8 **109** sources are detected at $> 5\sigma$ level within 4 Mpc of the cluster centre. These are tabulated in Table C.3. Of the 109 detected sources, **two** extended.The are no extended sources within R_{500}. Minor artefacts are present around the brighter sources, and there is a smooth background as expected away from brighter sources,

Source ID	RA	Δ RA	DEC	Δ DEC	total flux	Δ total flux	Peak flux	Δ Peak flux	optical cross-ID	cluster member	comments
0	00:20:48	0.000016	-25:44:38	0.000016	0.051927	0.001611	0.05218	0.000925	✗	?	
1	00:20:43	0.00003	-25:42:38	0.000034	0.059145	0.001438	0.035786	0.000965	✔	✔	BCG

Table 4.6: Positions of radio sources within R_{500} radius of the pointing centre of cluster RXCJ0020.7−2542

as Fig. 4.7 indicates. Fig. 4.8 shows the contours from the NVSS overlaid on the GMRT map, demonstrating that only two sources were detected in that survey. The optical galaxies in the central region of R_{500} which are associated with the cluster are indicated in Fig. 4.8 as green circles the ones not associated are red. It is shown that no source has an optical counterpart. The additional radio sources lack an optical cross-identification, possibly caused by the faintness of the optical source or lack of determined redshift, making it impossible to determine if it is associated with the cluster. All known positions of optical sources are provided in Tab. B.4. The redshift range used to identify cluster members was 0.085−0.115, chosen according to Yee (1996). The cluster has a mass of $M_{500} = 1,6 \times 10^{14} M_{\odot}$ Pratt et al. (2010) and has a low central entropy Pratt et al. (2010).
There is **no** newly confirmed radio source associated with the cluster and **no** new cluster member candidates. Further research is needed to verify if a cluster membership is given for these candidates.

4.4.5 RXCJ0211.4−4017

This cluster, shown in Fig. 4.9, is also known as Abell 2984 (Abell (1958), Abell *et al.* (1989)), and is situated at $z = 0.1008$, which corresponds to an angular scale of 1 arcsec = 0.53840 kpc.
42 sources are detected at $> 5\sigma$ level within 4 Mpc of the cluster centre. These are tabulated in Table C.4. Of the 42 detected sources, **one** is a double sources and **three** are extended.The is **one** extended source within R_{500}. Minor artefacts are present around the bright central source. The overall smooth RMS structure is shown in Fig. 4.9.Most sources show a slight elongation in two perpendicular directions indicating some leftover structure from the dirty beam, which we were not able to remove. Fig. 4.10 shows the contours from the SUMSS overlaid on the GMRT map, demonstrating that only the central bright source was detected in that survey. This source and all additionally detected radio sources are listed in **??**. The optical galaxies in the central region of R_{500} which are associated with the cluster are indicated in Fig. 4.10 as green circles. The central bright extended radio source is the only one with an optical counterpart. All optical identified galaxies are tabulated in Tab. B.5. The redshift range used to identify cluster members was 0.085−0.115, chosen according to Yee (1996). The cluster has a mass of $M_{500} = 2.1 \times 10^{14} M_{\odot}$ Pratt et al. (2010) and has a low central entropy Pratt et al. (2010). Although the cluster was classified as a non-cool core by its central gas density and central cooling time Pratt *et al.* (2009) it is classified as a cool core cluster by Haarsma et al.

(2010).
There is **one** newly confirmed radio source associated with the cluster and **one** new cluster member candidates. Further research is needed to verify if a cluster membership is given for this candidate.

4.4.6 RXCJ0225.1−2928

This cluster, situated at $z = 0.0604$, corresponding to an angular scale of 1 arcsec = 0.85734 kpc, is shown in Fig. 4.11.
189 sources are detected at $> 5\sigma$ level within 4 Mpc of the cluster centre. These are tabulated in Table C.5. Of the 189 detected sources, **one** is a double sources and **five** are extended.The is **one** extended source within R_{500}. Minor artefacts are present around the bright sources. The overall smooth RMS structure is shown in Fig. 4.11. The source within 200kpc of the centre might be real, even though it was not included as a real source due to the chosen conservative detection limit. Fig. 4.12 shows the contours from the NVSS overlaid on the GMRT map, demonstrating that only the brightest sources were detected in that survey. These sources and all additionally detected radio sources are listed in Tab. 4.8. The optical galaxies in the central region of R_{500} which are associated with the cluster are indicated in Fig. 4.12 as green circles. There are no radio sources with an optical counterpart. All optical identified galaxies are tabulated in Tab. B.6. The redshift range used to identify cluster members was 0.045−0.075, chosen according to Yee (1996). The cluster has a mass of $M_{500} = 2.5 \times 10^{14} M_{\odot}$ Pratt et al. (2010) and has a low to medium central entropy Pratt et al. (2010). It is classified as a disturbed cluster Pratt et al. (2010). This cluster shows one of the lowest core gas densities in the REXCESS sample and is among the clusters possessing multiple galaxies of similar brightness Haarsma et al. (2010).This cluster is also a candidate for a radio relic **?**.
There are **no** newly confirmed radio sources associated with the cluster and **19** new cluster member candidates. Further research is needed to verify if a cluster membership is given for these candidates.

Source ID	RA	Δ RA	DEC	Δ DEC	total flux	Δ total flux	Peak flux	Δ Peak flux	optical cross-ID	cluster member	comments
0	02:11:25	0.000169	-40:17:24	0.000277	0.335445	0.024343	0.150502	0.017478	✔	✔	BCG
1	02:11:21	0.000251	-40:15:46	0.000275	0.010346	0.002689	0.009097	0.001557	✗	?	

Table 4.7: Positions of radio sources within R_{500} radius of the pointing centre of cluster RXCJ0211.4−4017

4.4.7 RXCJ0345.7−4112

The cluster shown in Fig. 4.13, is also known as S0384 (Abell *et al.* (1989)) and is located at $z = 0.0603$, which corresponds to an angular scale of 1 arcsec = 0.85865 kpc.
14 sources are detected at $> 5\sigma$ level within 4 Mpc of the cluster centre. These are tabulated in Table C.6.Of the 14 detected sources, **eight** ones are double sources and **five** are extended.The are **two** extended sources and **two** double sources within R_{500}. Minor artefacts are present around the brighter sources. Fig. 4.13 indicates the RMS to be as smooth as expected in the overall map. Most sources show a slight elongation in the same direction indicating some leftover structure from the dirty beam, which we were not able to remove. Fig. 4.14 shows the contours from the SUMSS overlaid on the GMRT map, demonstrating that only the brightest sources were detected in that These sources and all additionally detected radio sources are listed in Tab. 4.9. The optical galaxies in the central region of R_{500} which are associated with the cluster are indicated in Fig. 4.14 as green circles. Only the central bright radio source has an optical counterpart. All optical identified galaxies are tabulated in Tab. B.7. The redshift range used to identify cluster members was 0.045−0.075, chosen according to Yee (1996). The cluster has a mass of $M_{500} = 2.3 \times 10^{14} M_{\odot}$ Pratt et al. (2010) and has a very low central entropy Pratt et al. (2010). It is classified as a cool core cluster. Pratt et al. (2010).
There is **one** newly confirmed radio source associated with the cluster and **six** new cluster member candidates. Further research is needed to verify if a cluster membership is given for these candidates.

Source ID	RA	Δ RA	DEC	Δ DEC	total flux	Δ total flux	Peak flux	Δ Peak flux	optical cross-ID	cluster member	comments
0	02:25:55	0.00015	-29:19:23	0.0002	0.001651	0.00028	0.001192	0.000177	✗	?	
1	02:25:52	0.000299	-29:36:15	0.000234	0.003845	0.000402	0.001595	0.000297	✗	?	
2	02:25:51	0.000094	-29:24:11	0.000074	0.001975	0.000339	0.002202	0.000182	✗	?	
3	02:25:37	0.000037	-29:26:19	0.000036	0.006846	0.000416	0.006668	0.000237	✗	?	
4	02:25:28	0.000207	-29:32:38	0.000181	0.001779	0.000357	0.001329	0.000223	✗	?	
5	02:25:23	0.000024	-29:30:27	0.000024	0.014491	0.000529	0.013468	0.000307	✗	?	
5	02:25:23	0.000156	-29:30:39	0.000128	0.001004	0.000549	0.001576	0.000258	✗	?	
6	02:25:09	0.00014	-29:27:44	0.000244	0.010628	0.000542	0.003645	0.000415	✗	?	
7	02:25:07	0.000309	-29:31:25	0.000144	0.003623	0.000274	0.001654	0.00019	✗	?	
8	02:25:06	0.000176	-29:19:04	0.00012	0.001095	0.000295	0.001134	0.000163	✗	?	
9	02:24:50	0.000043	-29:37:49	0.000036	0.005335	0.000387	0.005598	0.000214	✗	?	
10	02:24:43	0.000123	-29:37:43	0.000105	0.002414	0.000404	0.002145	0.000241	✗	?	
11	02:24:42	0.000007	-29:34:17	0.000006	0.075696	0.000763	0.070395	0.000444	✗	?	
11	02:24:42	0.00006	-29:34:29	0.000047	0.003381	0.000793	0.005722	0.000359	✗	?	
11	02:24:43	0.000085	-29:34:10	0.000042	0.018852	0.000681	0.01002	0.000469	✗	?	ext.
12	02:24:43	0.000208	-29:33:53	0.000125	0.001812	0.000635	0.001941	0.000354	✗	?	
13	02:24:42	0.000258	-29:34:43	0.000077	0.007509	0.000629	0.004392	0.000394	✗	?	
14	02:24:42	0.000419	-29:30:57	0.00015	0.002688	0.000331	0.001267	0.000232	✗	?	
15	02:24:33	0.000219	-29:23:04	0.00024	0.001948	0.000356	0.00124	0.000235	✗	?	

Table 4.8: Positions of radio sources within R_{500} radius of the pointing centre of cluster RXCJ0225.1−2928

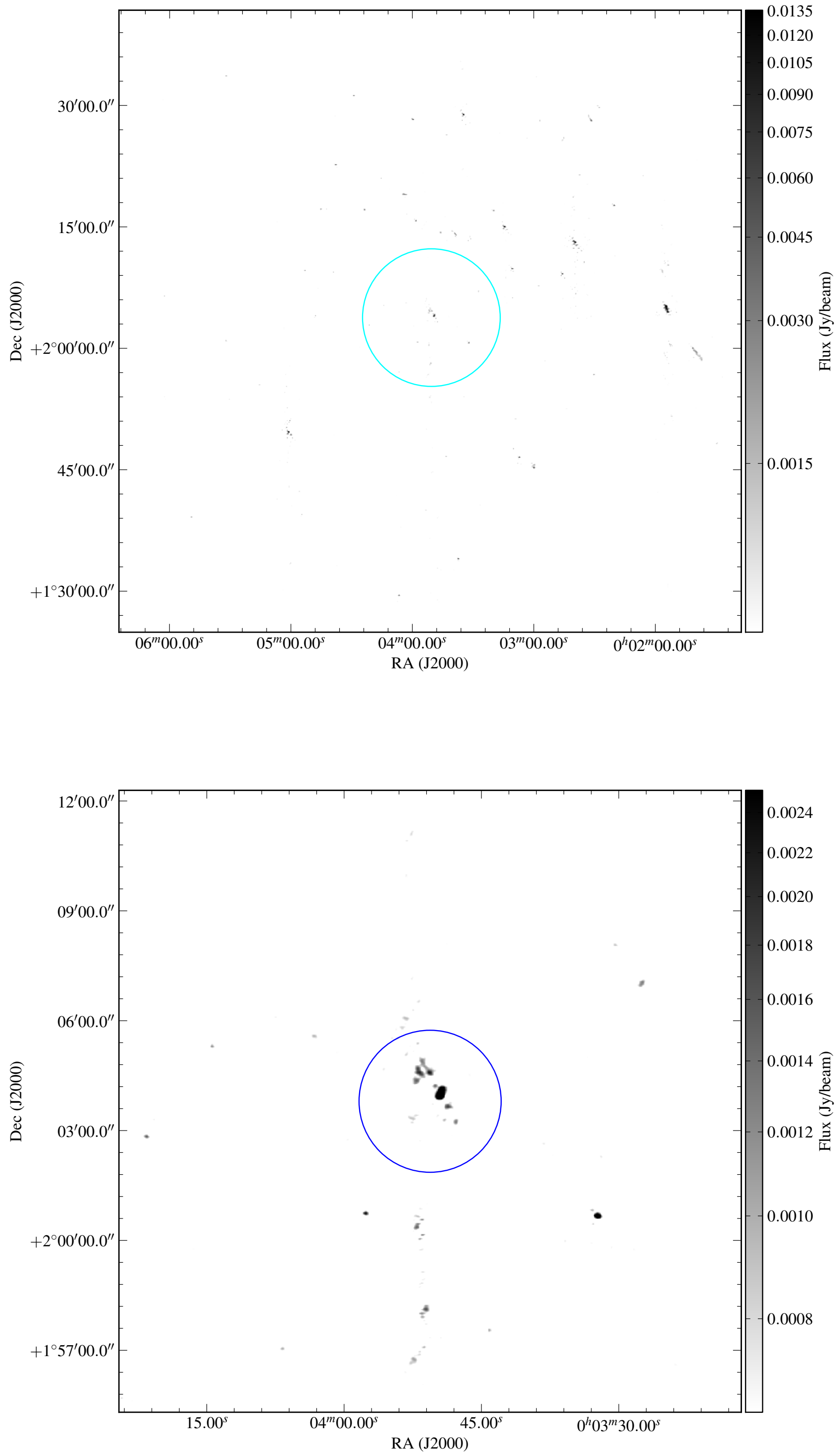

Figure 4.1: 610-MHz GMRT maps of RXCJ0003.8+0203.Top : overview of a region 4 Mpc $\times$ 4 Mpc centred on the cluster, R_{500} being indicated by the circle; bottom: central region of the cluster ($R_{500} \times R_{500}$)the circle indicates a region of radius 200kpc around the centre.

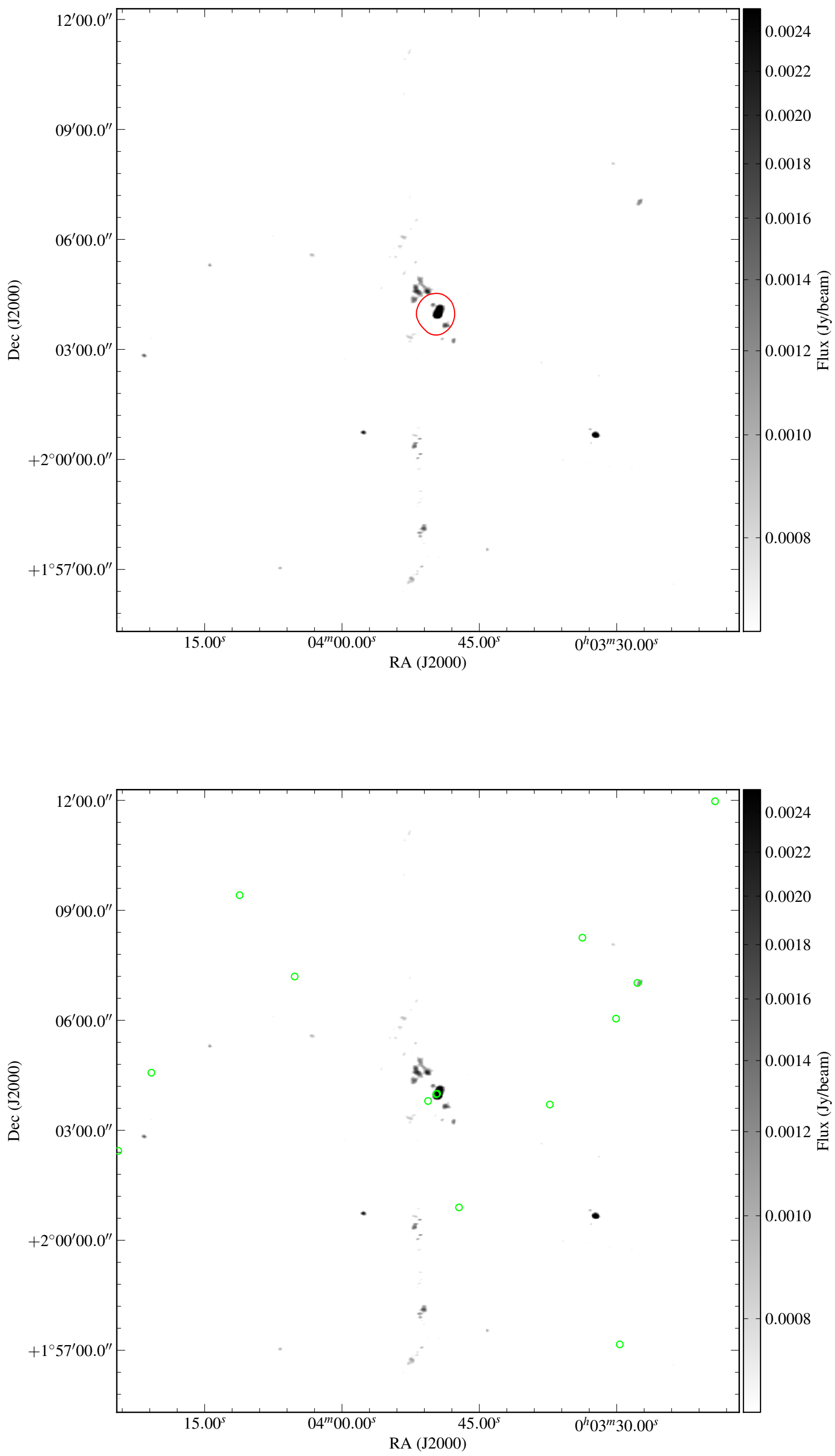

Figure 4.2: 610-MHz GMRT maps of RXCJ0003.8+0203. central region of the cluster ($R_{500} \times R_{500}$)Top: contours from NVSS overlaid; bottom: positions of known cluster member galaxies overlaid in green.

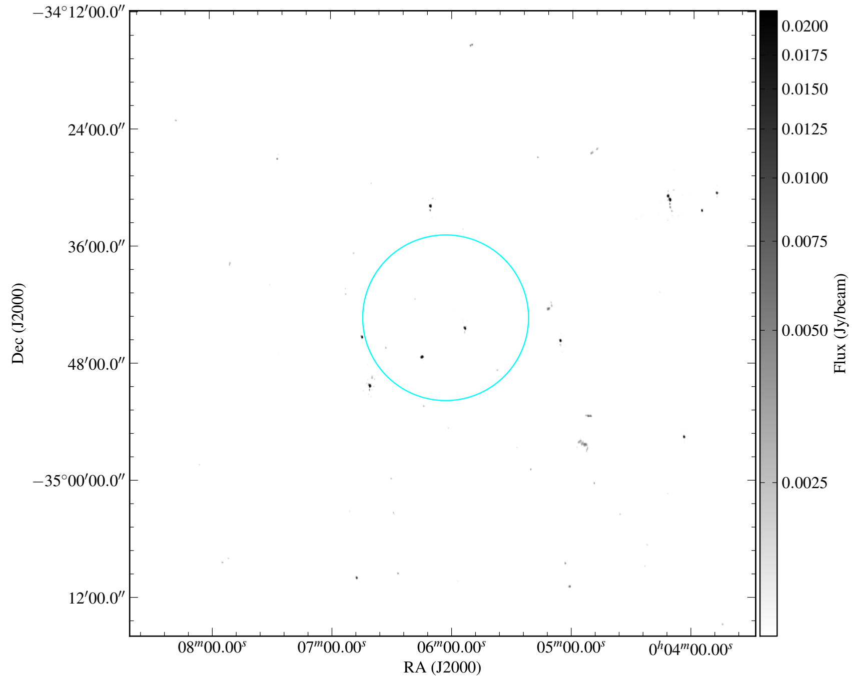

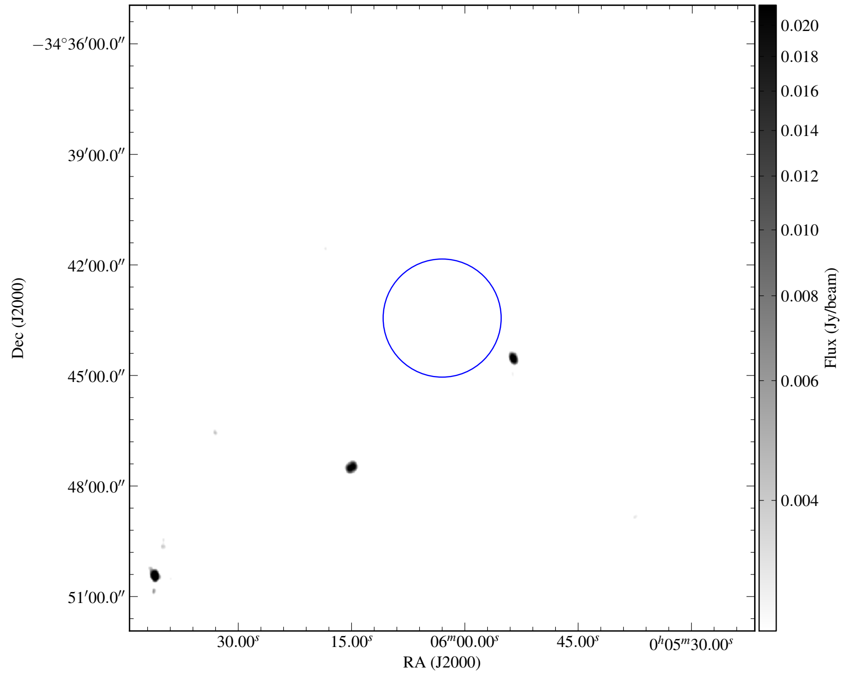

Figure 4.3: 610-MHz GMRT maps of RXCJ0006.0−3443.Top : overview of a region 4 Mpc × 4 Mpc centred on the cluster, R_{500} being indicated by the circle; bottom: central region of the cluster ($R_{500} \times R_{500}$)the circle indicates a region of radius 200kpc around the centre.

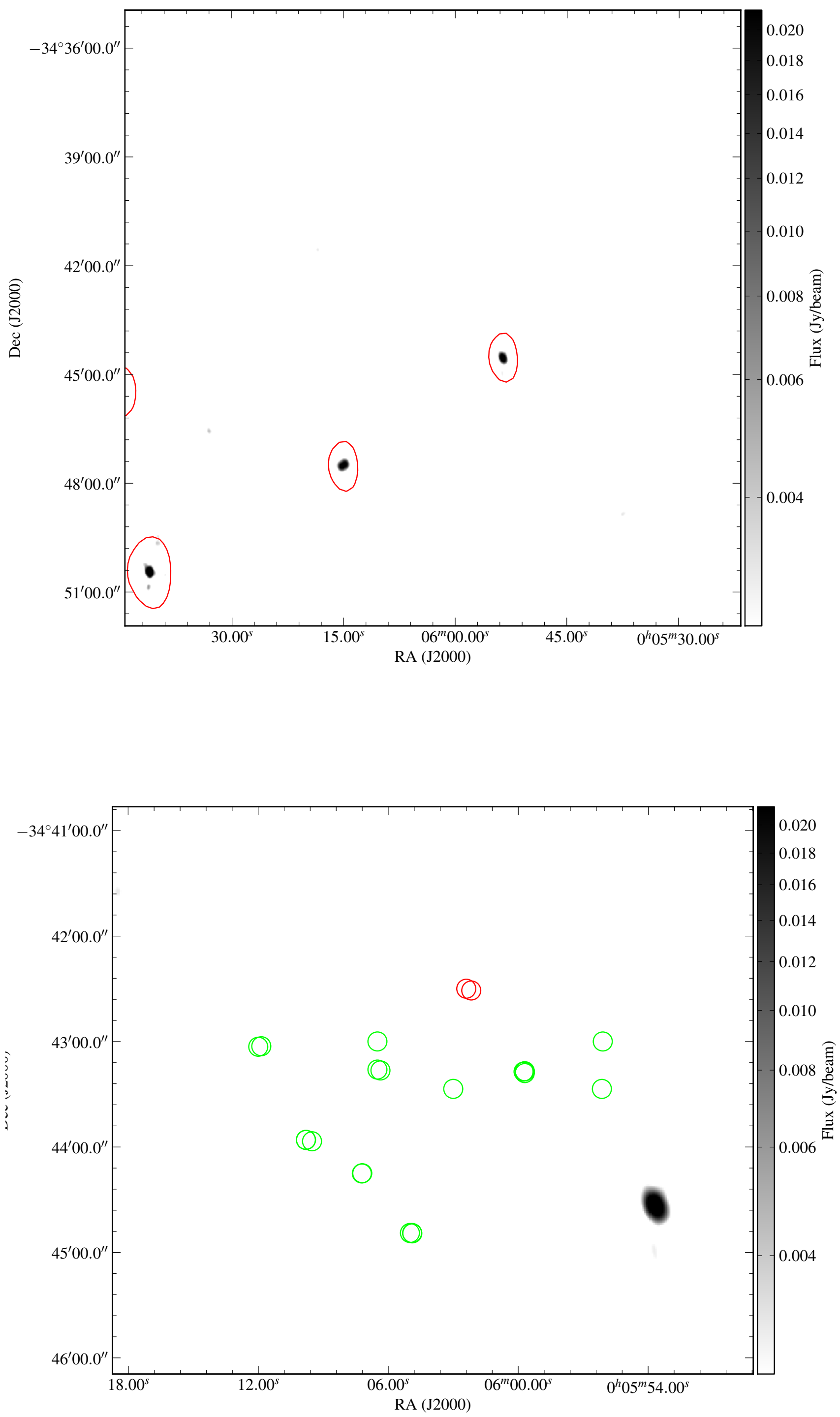

Figure 4.4: 610-MHz GMRT maps of RXCJ0006.0−3443. central region of the cluster ($R_{500} \times R_{500}$); top: contours from SUMSS overlaid; bottom: positions of known cluster member galaxies overlaid in green and known background or foreground sources indicated by red circles.

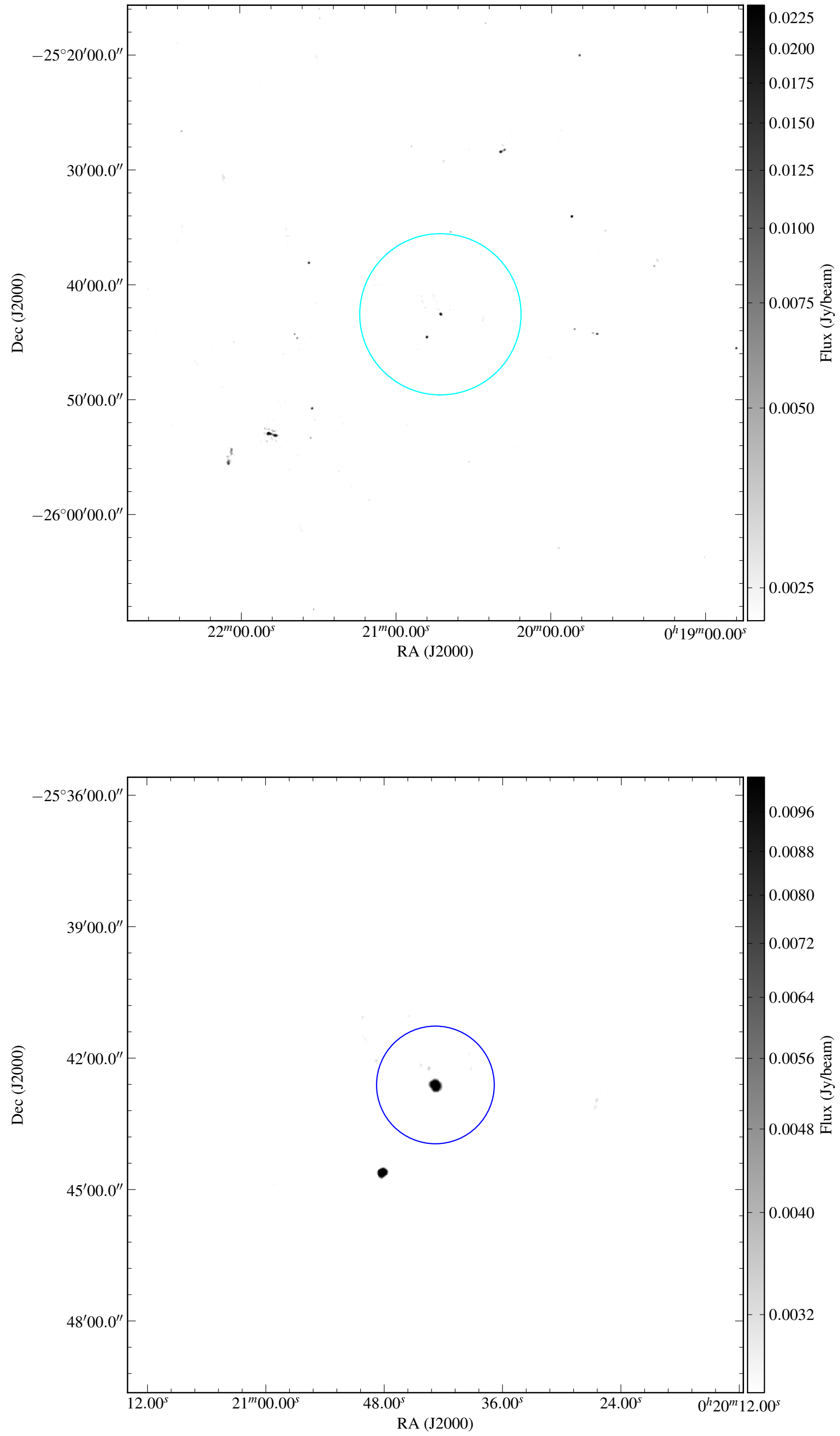

Figure 4.5: 610-MHz GMRT maps of RXCJ0020.7−2542. Top: overview of a region 4 Mpc $\times$ 4 Mpc centred on the cluster, R_{500} being indicated by the circle; bottom: central region of the cluster ($R_{500} \times R_{500}$)the circle indicates a region of radius 200kpc around the centre.

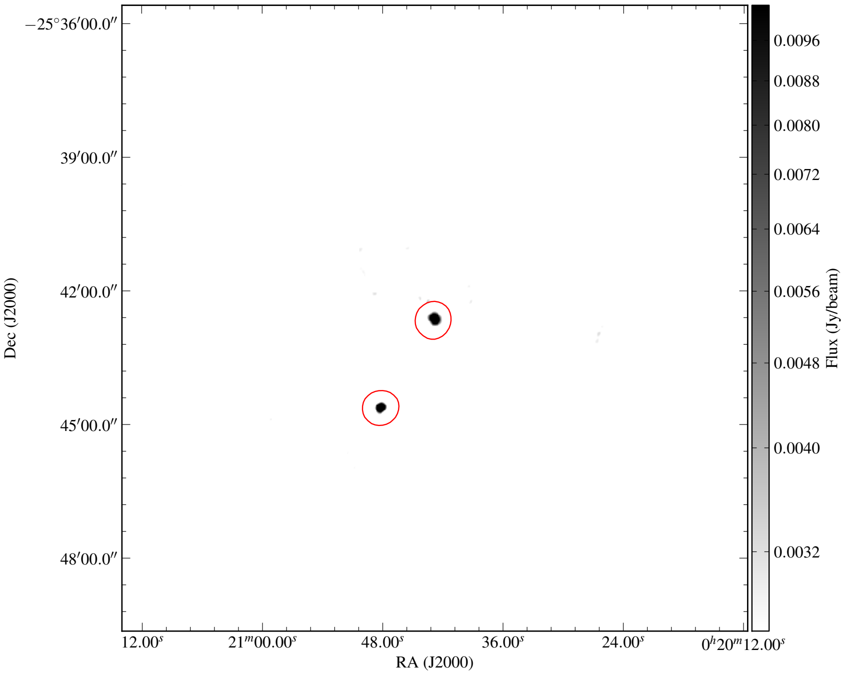

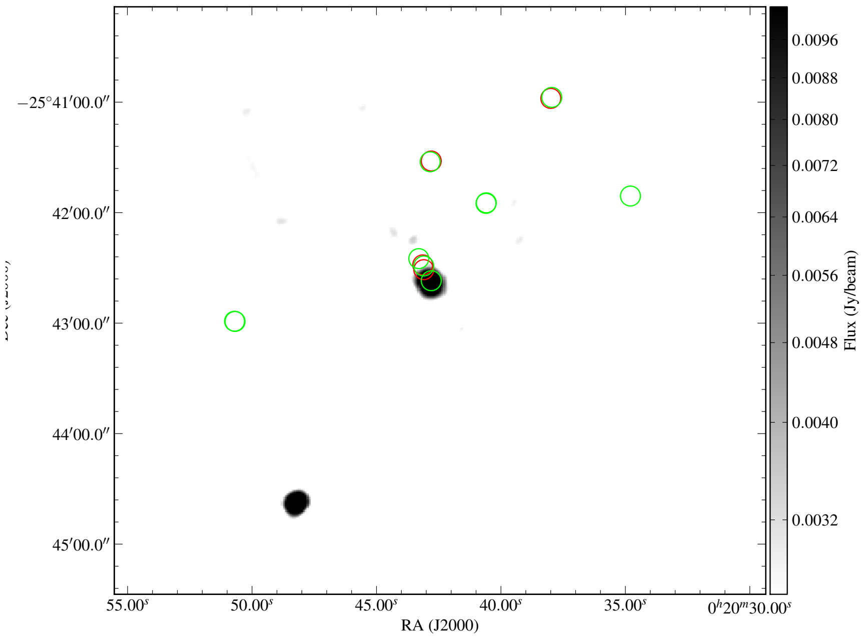

Figure 4.6: 610-MHz GMRT maps of RXCJ0020.7−2542. central region of the cluster ($R_{500} \times R_{500}$); top: contours from NVSS overlaid; bottom: positions of known cluster member galaxies overlaid in green and known background or foreground sources indicated by red circles.

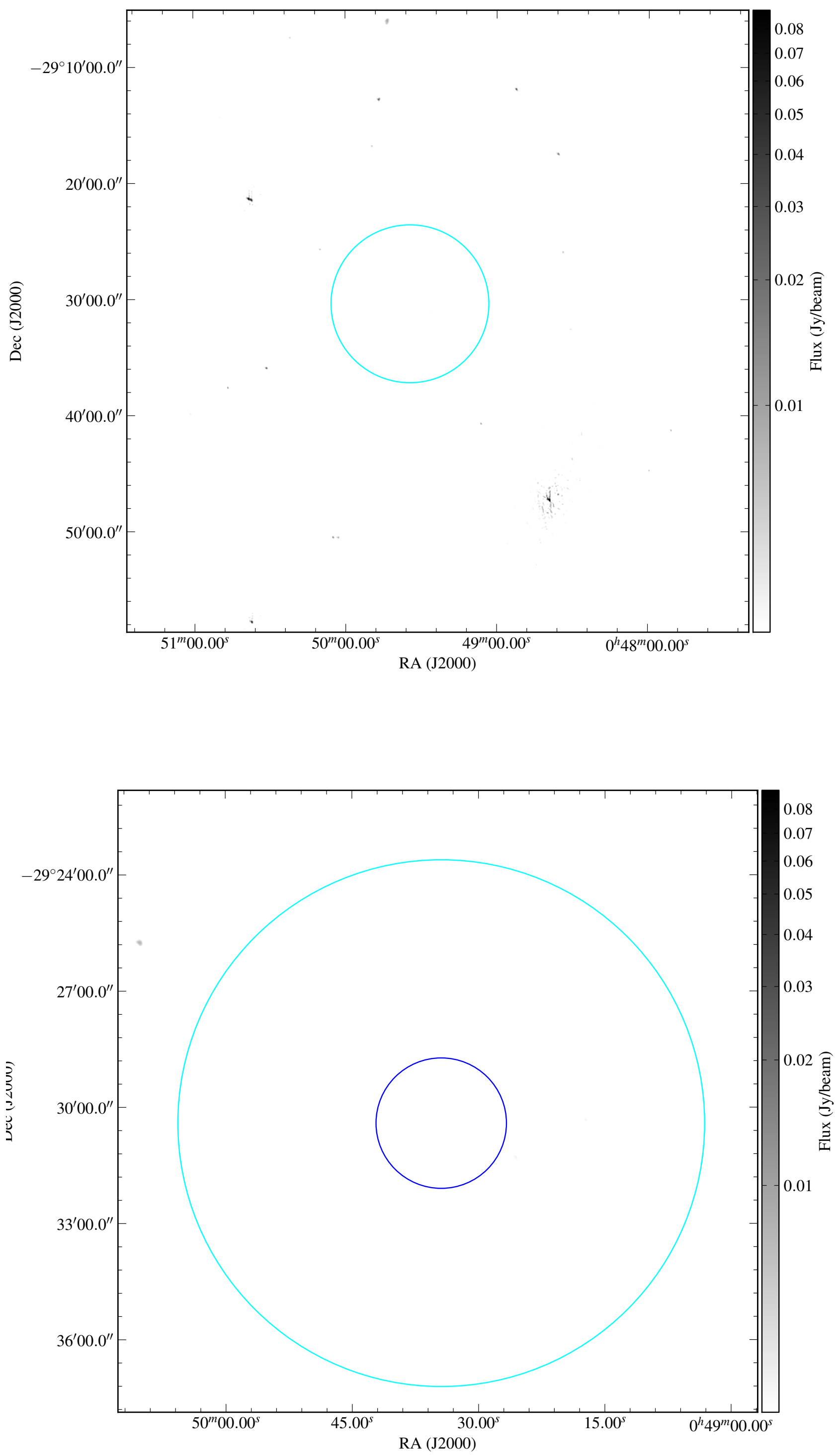

Figure 4.7: 610-MHz GMRT maps of RXCJ0049.4−2931.Top: overview of a region 4 Mpc $\times$ 4 Mpc centred on the cluster, R_{500} being indicated by the light clue circle; bottom: central region of the cluster ($R_{500} \times R_{500}$)the dark blue circle indicates a region of radius 200kpc around the centre.

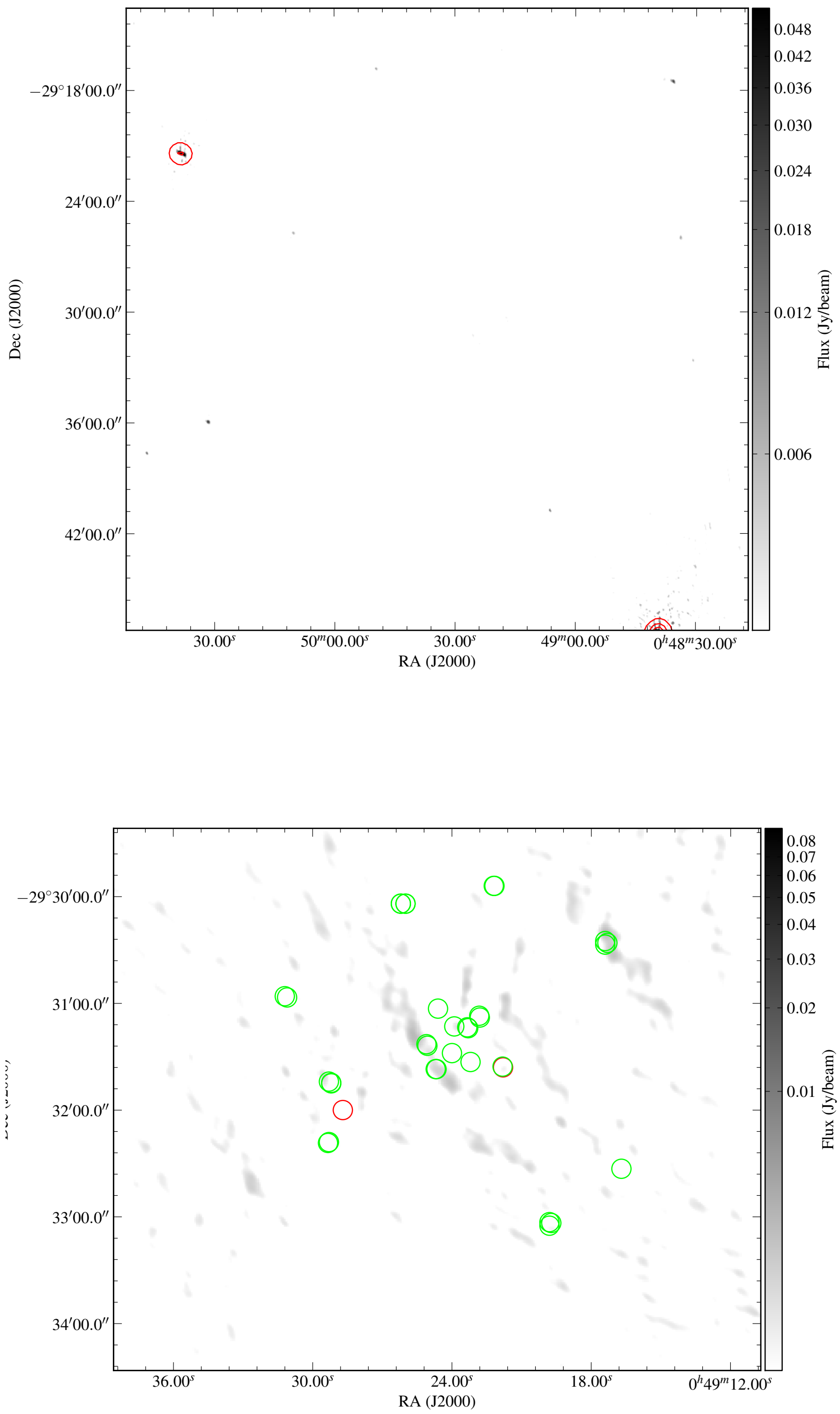

Figure 4.8: 610-MHz GMRT maps of RXCJ0049.4−2931.central region of the cluster ($R_{500} \times R_{500}$); top: contours from NVSS overlaid; bottom: positions of known cluster member galaxies overlaid in green and known background or foreground sources indicated by red circles.

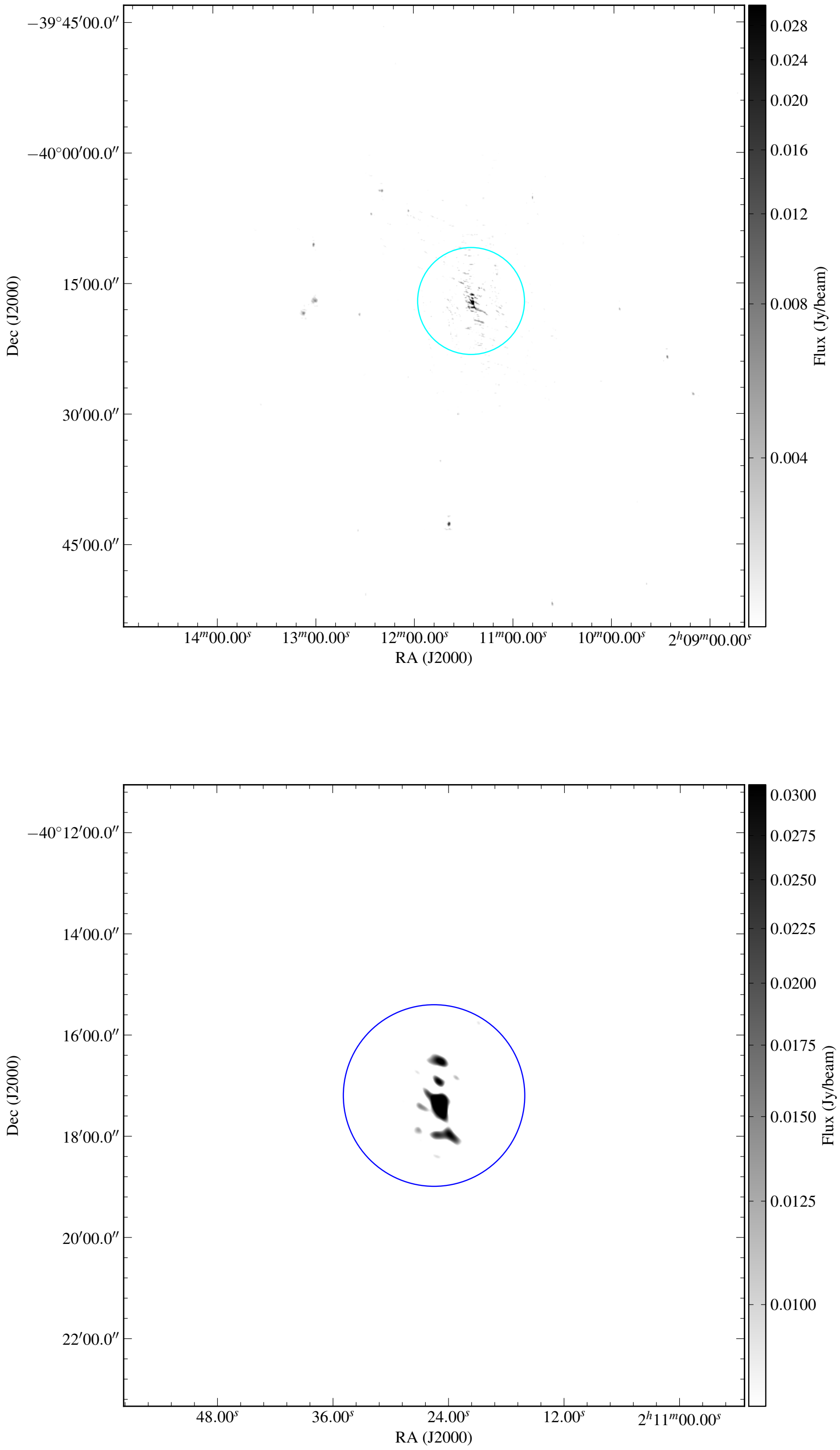

Figure 4.9: 610-MHz GMRT maps of RXCJ0211.4−4017.Top: overview of a region 4 Mpc $\times$ 4 Mpc centred on the cluster, R_{500} being indicated by the circle; bottom: central region of the cluster ($R_{500} \times R_{500}$)the circle indicates a region of radius 200kpc around the centre.

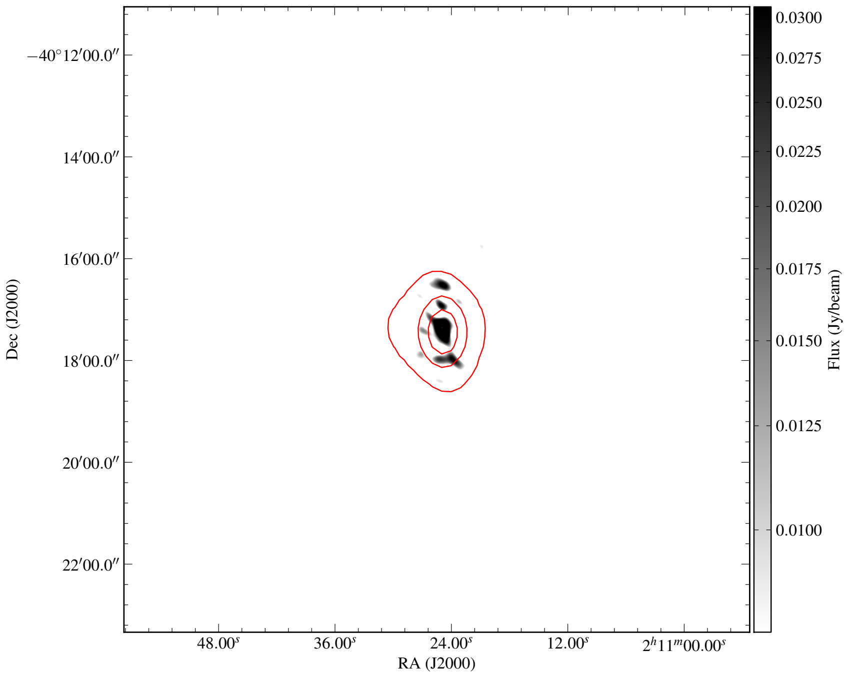

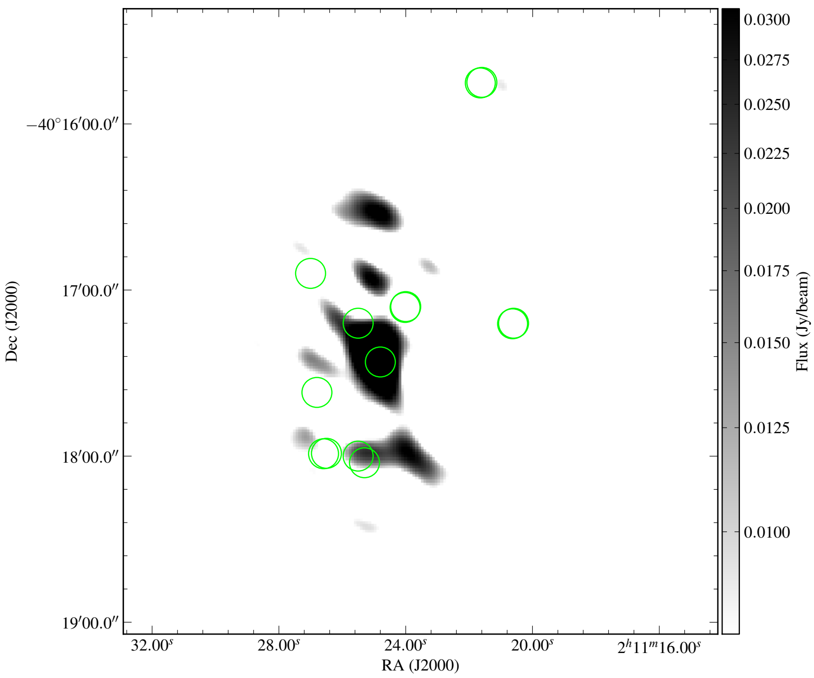

Figure 4.10: 610-MHz GMRT maps of RXCJ0211.4−4017.central region of the cluster ($R_{500} \times R_{500}$); top: contours from SUMSS overlaid; bottom: positions of known cluster member galaxies overlaid in green.

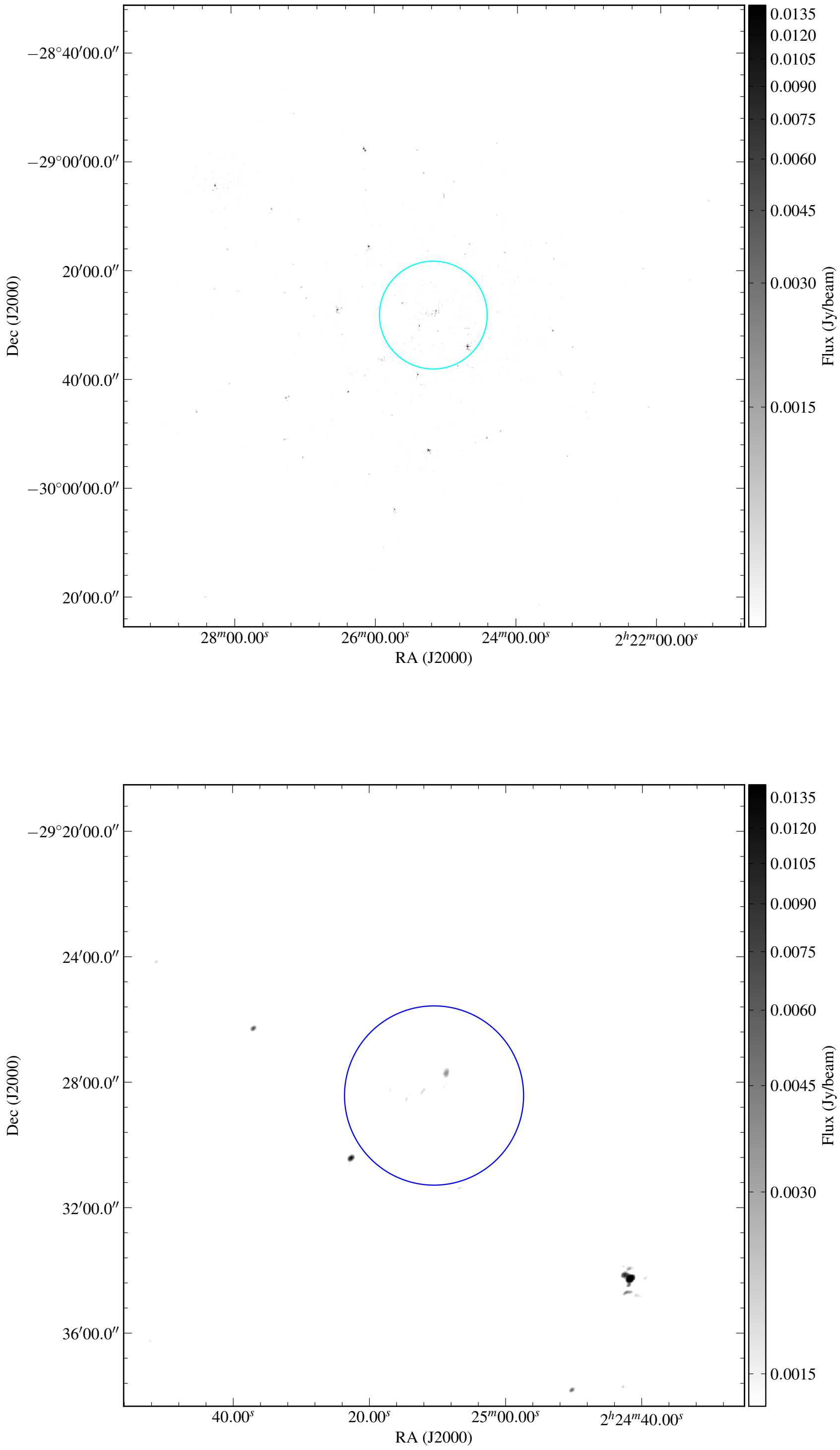

Figure 4.11: 610-MHz GMRT maps of RXCJ0225.1−2928.Top: overview of a region 4 Mpc $\times$ 4 Mpc centred on the cluster, R_{500} being indicated by the circle; bottom: central region of the cluster ($R_{500} \times R_{500}$)the circle indicates a region of radius 200kpc around the centre.

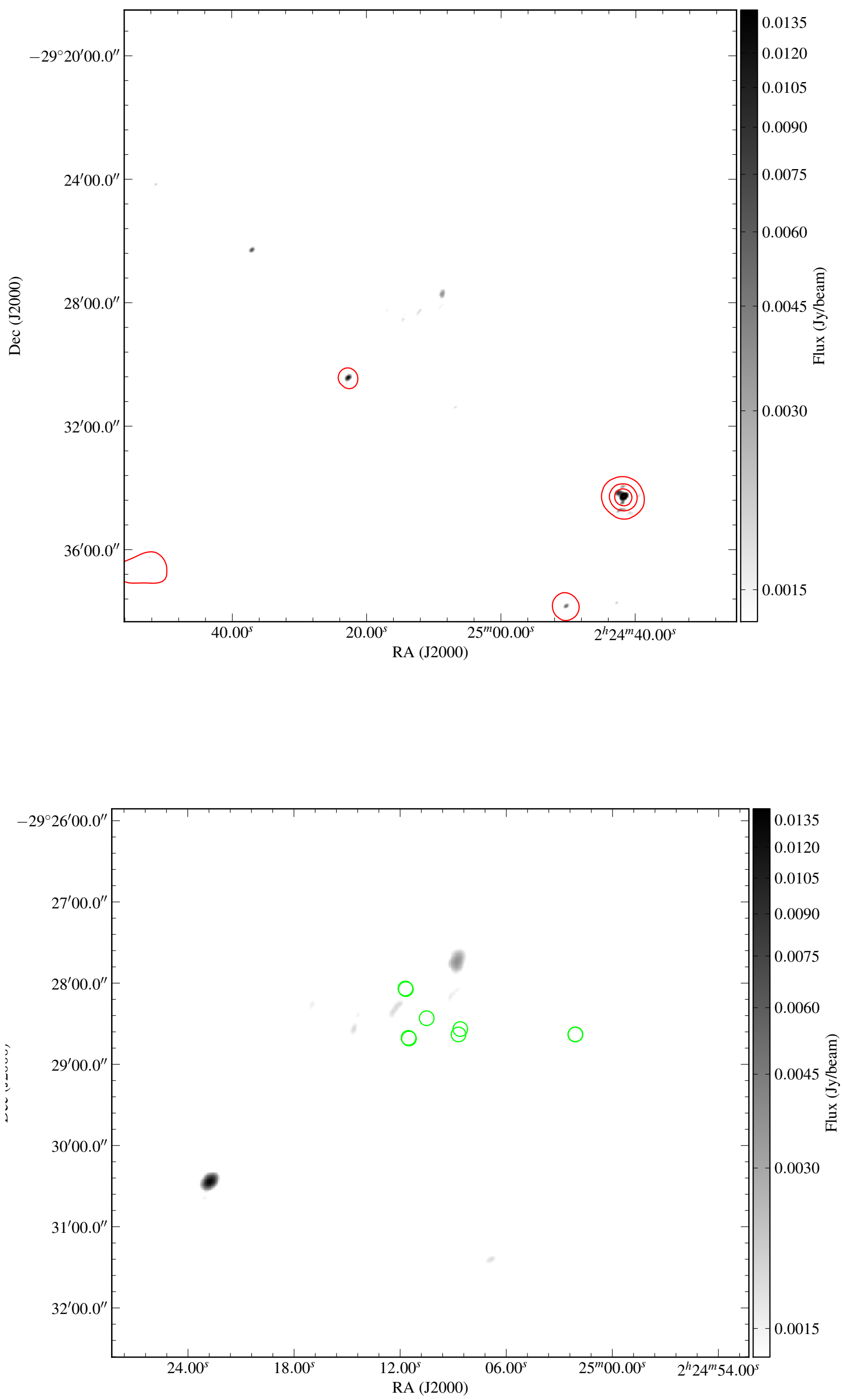

Figure 4.12: 610-MHz GMRT maps of RXCJ0225.1−2928. central region of the cluster ($R_{500} \times R_{500}$)the circle indicates a region of radius 200kpc around the centre; Top: contours from NVSS overlaid; bottom: positions of known cluster member galaxies overlaid in green.

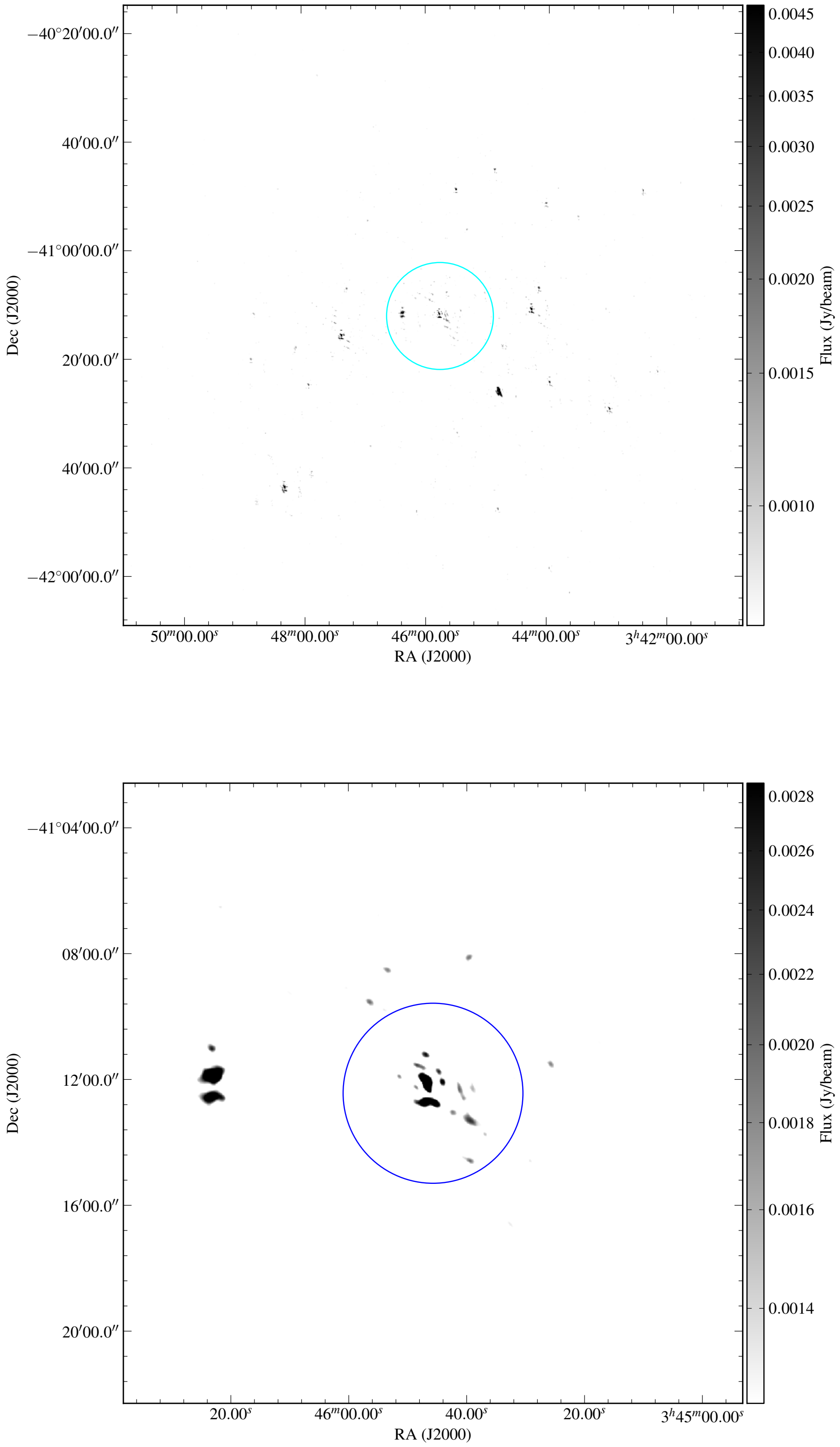

Figure 4.13: 610-MHz GMRT maps of RXCJ0345.7−4112.Top: overview of a region 4 Mpc × 4 Mpc centred on the cluster, R_{500} being indicated by the circle; bottom: central region of the cluster ($R_{500} \times R_{500}$)the circle indicates a region of radius 200kpc around the centre.

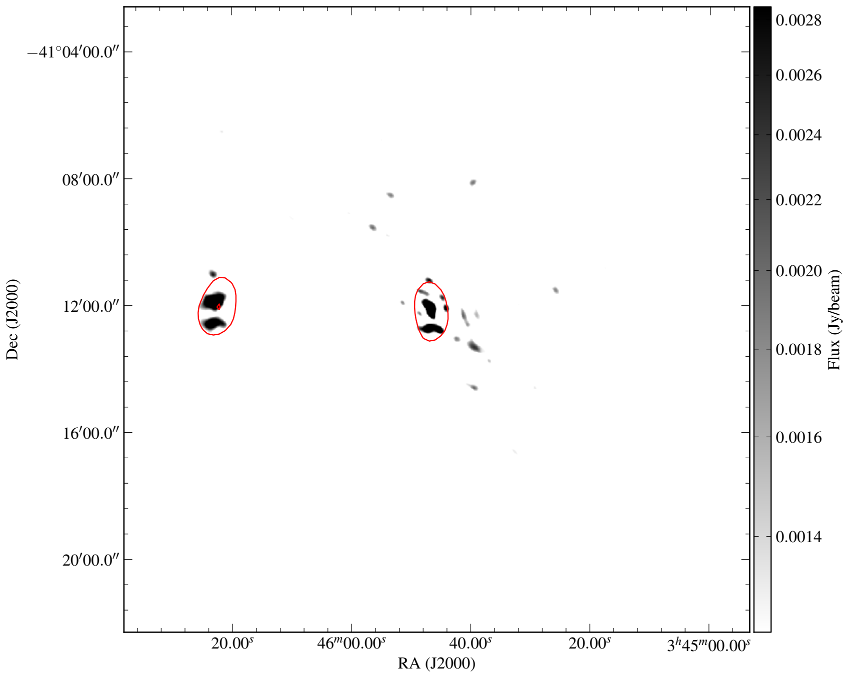

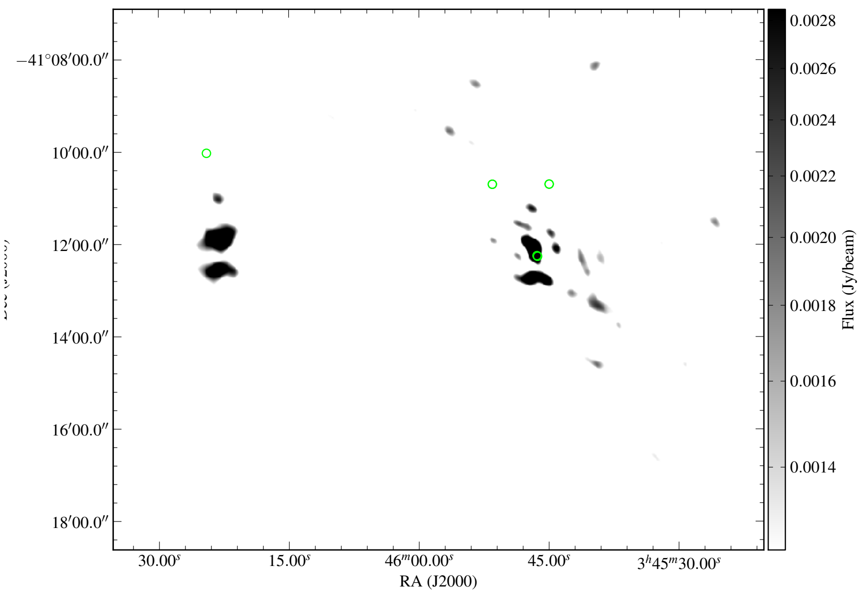

Figure 4.14: 610-MHz GMRT maps of RXCJ0345.7−4112. central region of the cluster ($R_{500} \times R_{500}$); top: contours from SUMSS overlaid; bottom: positions of known cluster member galaxies overlaid in green.

4.4.8 RXCJ0547.6−3152

Fig. 4.15shows the cluster known as A3364 (Abell (1958), Abell *et al.* (1989)), an situated at $z = 0.1483$, corresponding to an angular scale of 1 arcsec = 0.40723 kpc. **90** sources are detected at $> 5\sigma$ level within 4 Mpc of the cluster centre. These are tabulated in Table C.7.Of the 90 detected sources, **three** are double sources and **ten** are extended.The is one extended source within R_{500}. Minor artefacts are present around the brighter sources and there is a smooth background present throughout the whole map, which is shown in Fig. 4.15. In this map all sources are slightly elongated diagonally, indicating some leftover dirty beam structure, which we were not able to remove. Fig. 4.16 shows the contours from the NVSS overlaid on the GMRT map, demonstrating that only the central bright source was detected in that survey. These sources and all additionally detected radio sources are listed in Tab. 4.10. The optical galaxies in the central region of R_{500} which are associated with the cluster are indicated in Fig. 4.16 as green circles the ones not associated are indicated by red circles. It is shown that only the central bright source has an optical counterpart, but it is not clear whether it is associated with the cluster, as there is another source at a different redshift at the same position. The additional radio sources lack an optical cross-identification, possibly caused by the faintness of the optical source or no known information about redshift, making it impossible to determine if it is associated with the cluster. All known positions of optical galaxies are provided in Tab. B.8. The redshift range used to identify cluster members was 0.125−0.155, chosen according to Yee (1996). The cluster has a mass of $M_{500} = 6.0 \times 10^{14} M_{\odot}$ Pratt et al. (2010) and has a medium central entropy Pratt et al. (2010). There are **no** newly confirmed radio sources associated with the cluster and **no** new cluster member candidates. Further research is needed to verify if a cluster membership is given for these candidates.

Source ID	RA	Δ RA	DEC	Δ DEC	total flux	Δ total flux	Peak flux	Δ Peak flux	optical cross-ID	cluster member	comments
0	03:46:23	0.000244	-41:11:54	0.00016	0.031828	0.001045	0.010989	0.000802	✗	?	
1	03:46:23	0.000652	-41:12:34	0.000291	0.020363	0.000799	0.004912	0.000653	✗	?	
2	03:46:23	0.000389	-41:11:02	0.000421	0.004533	0.00055	0.002402	0.000377	✗	?	
3	03:46:22	0.000471	-41:06:33	0.000454	0.002241	0.000396	0.001287	0.000269	✗	?	
6	03:45:47	0.000404	-41:11:15	0.000277	0.002768	0.000901	0.002784	0.0005	✔	✔	BCG
7	03:45:40	0.000435	-41:08:09	0.000389	0.003248	0.000551	0.001931	0.000371	✗	?	
8	03:45:26	0.000373	-41:11:33	0.000425	0.003055	0.000466	0.001846	0.000308	✗	?	

Table 4.9: Positions of radio sources within R_{500} radius of the pointing centre of cluster RXCJ0345.7−4112

Source ID	RA	Δ RA	DEC	Δ DEC	total flux	Δ total flux	Peak flux	Δ Peak flux	optical cross-ID	cluster member	comments
0	05:47:38	0.000078	-31:52:25	0.000132	0.023835	0.00174	0.013861	0.00117	✔	✗	BCG

Table 4.10: Positions of radio sources within R_{500} radius of the pointing centre of cluster RXCJ0547.6−3152

4.4.9 RXCJ0605.8−3518

This cluster is known as A3378 (Abell (1958), Abell *et al.* (1989)), an is situated at $z = 0.1393$, corresponding to an angular scale of 1 arcsec = 0.40723 kpc is shown in Fig. 4.17.

18 sources are detected at $> 5\sigma$ level within 4 Mpc of the cluster centre. These are tabulated in Table C.8.Of the 18 detected sources, **1** is a double source and none are extended. There is a smooth background present throughout the whole map, which is shown in Fig. 4.17. Fig. 4.18 shows the contours from the SUMSS overlaid on the GMRT map, demonstrating that only the central bright source was detected in that survey. These sources and all additionally detected radio sources are listed in Tab. 4.11. The optical galaxies in the central region of R_{500} which are associated with the cluster are indicated in Fig. 4.18 as green circles. It is shown that only the central bright source has an optical counterpart associated with the cluster. The additional radio sources present lack an optical cross-identification, possibly caused by the faintness of the optical source or no associated redshift, making it impossible to determine if it is associated with the cluster. All known positions of optical galaxies are given in Tab. B.8. The redshift range used to identify cluster members was 0.115−0.145, chosen according to Yee (1996). The cluster has a mass of $M_{500} = 4.9 \times 10^{14} M_{\odot}$ Pratt et al. (2010) and has a very low central entropy Pratt et al. (2010). It is classified as a cool core cluster Pratt et al. (2010). Hogan *et al.* (2015a) and Murphy*et al.* (2010) suggest there is an active core present with a significant activity at higher frequencies.

There is **one** newly confirmed radio source associated with the cluster and **one** new cluster member candidates. Further research is needed to verify if a cluster membership is given for this candidate.

4.4.10 RXCJ0821.8+0112

This cluster, shown in Fig. 4.19, is also known as Abell 0653 (Abell (1958), Abell *et al.* (1989)), and is situated at $z = 0.0822$, which corresponds to an angular scale of 1 arcsec = 0.64622 kpc.

132 sources are detected at $> 5\sigma$ level within 4 Mpc of the cluster centre. These are

Source ID	RA	Δ RA	DEC	Δ DEC	total flux	Δ total flux	Peak flux	Δ Peak flux	optical cross-ID	cluster member	comments
0	06:06:25	0.000022	-35:17:10	0.000028	0.054699	0.002108	0.054857	0.001189	✗	?	
1	06:05:53	0.000002	-35:18:02	0.000002	2.186014	0.008317	2.095744	0.003403	✔	✔	BCG

Table 4.11: Positions of radio sources within R_{500} radius of the pointing centre of cluster RXCJ0605.8−3518

tabulated in Table C.9.Of the 132 detected sources, **three** are double sources and **three** are extended.The is **one** extended source and **three** double sources within R_{500}. Minor artefacts are present around the brighter sources. Fig. 4.19 shows the typical RMS structure, indicating that it is smooth as expected. Fig. 4.20 shows the contours from the NVSS overlaid on the GMRT map, demonstrating that only the two bright sources were detected in that survey. These sources and all additionally detected radio sources are listed in Tab. 4.12. The optical galaxies in the central region of R_{500} which are associated with the cluster are indicated in Fig. 4.19 as green circles the ones not associated are indicated by red circles. There are no radio sources with optical counterparts. All other radio sources present lack an optical cross-identification, possibly caused by either the faintness of the optical source or no associated redshift, making it impossible to determine if it is associated with the cluster. All known optical galaxy positions are listed in Tab. B.10. The redshift range used to identify cluster members was $0.065-0.095$, chosen according to Yee (1996). The cluster has a mass of $M_{500} = 2.8 \times 10^{14} M_{\odot}$ Pratt et al. (2010).
There is **one** newly confirmed radio source associated with the cluster and **13** new cluster member candidates. Further research is needed to verify if a cluster membership is given for these candidates.

4.4.11 RXCJ0956.4−1004

This cluster, pictured in Fig. 4.21 is also known as Abell 0901 (Abell (1958), Abell *et al.* (1989)), and is situated at $z = 0.1634$, which corresponds to an angular scale of 1 arcsec = 0.35640 kpc.
125 sources are detected at $> 5\sigma$ level within 4 Mpc of the cluster centre. These are tabulated in Table C.10.Of the 125 detected sources, **three** sources are extended.The is **one** extended source within R_{500}. Minor diagonal artefacts are present around the brighter sources. Fig. 4.21 shows the typical RMS structure, indicating

Source ID	RA	Δ RA	DEC	Δ DEC	total flux	Δ total flux	Peak flux	Δ Peak flux	optical cross-ID	cluster member	comments
0	08:22:11	0.000137	01:15:07	0.000104	0.001876	0.000359	0.00177	0.000202	✗	?	
1	08:22:08	0.000053	01:18:56	0.000036	0.011082	0.000443	0.007198	0.000288	✗	?	double
1	08:22:06	0.000146	01:18:59	0.000136	0.005029	0.000421	0.002539	0.000295	✗	?	
2	08:22:01	0.000169	01:12:15	0.000093	0.004724	0.00042	0.002648	0.000283	✗	?	double
3	08:21:60	0.000162	01:12:14	0.000107	0.00426	0.000445	0.002741	0.000284	✗	?	
4	08:21:60	0.000009	01:10:55	0.000013	0.049081	0.000736	0.031561	0.000315	✗	?	
7	08:21:53	0.000165	01:16:19	0.000072	0.003157	0.00048	0.00264	0.000279	✗	?	
8	08:21:40	0.000161	01:15:45	0.000076	0.00225	0.000381	0.001976	0.000219	✗	?	
9	08:21:37	0.000243	01:17:36	0.00018	0.001175	0.000362	0.001075	0.000204	✗	?	
10	08:21:36	0.000131	01:05:10	0.00014	0.002023	0.0005	0.00235	0.000237	✗	?	
12	08:21:34	0.000187	01:12:09	0.000159	0.002691	0.000469	0.001839	0.00030	✗	?	double
14	08:21:33	0.000139	01:12:02	0.00022	0.002489	0.000486	0.001919	0.000292	✗	?	
13	08:21:34	0.000116	01:06:18	0.000107	0.004434	0.00056	0.003417	0.000341	✗	?	

Table 4.12: Positions of radio sources within R_{500} radius of the pointing centre of cluster RXCJ0821.8+0112

that it is smooth as expected away from the sources. Fig. 4.22 shows the contours from the NVSS overlaid on the GMRT map, demonstrating that only the two bright sources were detected in that survey. These sources and all additionally detected radio sources are listed in Tab. **??**. The optical galaxies in the central region of R_{500} which are associated with the cluster are indicated in Fig. 4.22 as green circles the ones not associated are drawn in red. It is shown that no radio radio source has an optical counterpart. All additional radio sources present lack an optical cross-identification, possibly caused by the faintness of the optical source or no associated redshift, making it impossible to determine if it is associated with the cluster. All known positions of optical galaxies are listed in Tab. B.11. The redshift range used to identify cluster members was 0.145−0.175, chosen according to Yee (1996).
There is **one** newly confirmed radio source associated with the cluster and **54** new cluster member candidates. Further research is needed to verify if a cluster membership is given for these candidates.

4.4.12 RXCJ0958.3−1103

Fig. 4.23 shows the cluster known as A0907 (Abell (1958), Abell *et al.* (1989)), and situated at $z = 0.1669$, corresponding to an angular scale of 1 arcsec = 0.35026 kpc. **92** sources are detected at $> 5\sigma$ level within 4 Mpc of the cluster centre. These are tabulated in Table C.11. Of the 92 detected sources, **one** is a double source and **two** are extended.The is **one** extended source within R_{500}. Minor artefacts are present around the brighter sources with a smooth background, as expected, away from the sources as shown in Fig. 4.23. Fig. 4.24 shows the contours from the NVSS overlaid on the GMRT map, demonstrating that only three bright sources were detected in that survey. These sources and all additionally detected radio sources are listed in Tab. 4.14. The optical galaxies in the central region of R_{500} which are associated with the cluster are indicated in Fig. 4.24 as green circles the ones not associated are indicated by red circles. It is shown that only the central bright source has an optical counterpart. All additional radio sources present are lacking an optical cross-identification, possibly caused by the faintness of the optical source or no associated redshift, making it impossible to determine if it is associated with the cluster. All known optical galaxy positions were not indicated in Fig. 4.23 and tabulated in Tab. B.12. The redshift range used to identify cluster members was 0.145−0.175, chosen according toYee (1996). The cluster has a mass of $M_{500} = 6.0 \times 10^{14} M_{\odot}$ Pratt et al. (2010) and has a low central entropy Pratt et al. (2010). It is classified as a cool core cluster Pratt et al. (2010).

There is **one** newly confirmed radio source associated with the cluster and **nine** new cluster member candidates. Further research is needed to verify if a cluster membership is given for these candidates.

4.4.13 RXCJ1044.5−0704

This cluster, shown inFig. 4.25, is known as A1084 (Abell (1958), Abell *et al.* (1989)), an is situated at $z = 0.1342$, corresponding to an angular scale of 1 arcsec = 0.42003 kpc.
78 sources are detected at $> 5\sigma$ level within 4 Mpc of the cluster centre. These are tabulated in Table C.12.Of the 78 detected sources, **five** are double sources and **four** are extended.The are no extended sources within R_{500}. Minor artefacts are present around the brighter sources and there is a smooth background present away from the sources as expected, which is shown in Fig. 4.25. As indicated by the shape of all sources there are major phase artefacts present, which we were unable to remove. This map was excluded from all morphological studies, due to these phase calibration issues. Fig. 4.26 shows the contours from the NVSS overlaid on the GMRT map, demonstrating that four sources were detected in that survey. These sources and all additionally detected radio sources are listed in Tab. 4.15. The optical galaxies in the central region of R_{500} which are associated with the cluster are indicated in Fig. 4.26 as green circles the ones not associated are indicated by red ones. It is shown that only the central bright source has an optical counterpart. All additional radio sources present lack an optical cross-identification, possibly caused by the faintness of the optical source or no associated redshift, making it impossible to determine if it is associated with the cluster. All known optical galaxy positions are listed in Tab. B.13. The redshift range used to identify cluster members was 0.115−0.145, chosen according to Yee (1996). The cluster has a mass of $M_{500} = 3.6 \times 10^{14} M_{\odot}$ Pratt et al. (2010) and is classified as a cool core cluster Pratt et al. (2010). This cluster is not detected in the VLSS Cohan *et al.* (2007), the source is core-dominated Hogan *et al.* (2015b). The spectrum of this cluster is fitted by a Power-like component Hogan *et al.* (2015b). This cluster is unresolved in the L- and C-bands.Hogan *et al.* (2015a)
There is **one** newly confirmed radio source associated with the cluster and **five** new cluster member candidates. Further research is needed to verify if a cluster membership is given for these candidates.

Source ID	RA	Δ RA	DEC	Δ DEC	total flux	Δ total flux	Peak flux	Δ Peak flux	optical cross-ID	cluster member	comments
1	09:57:13	0.00021	-10:15:08	0.000214	0.001371	0.00021	0.000716	0.000147	✗	?	
3	09:57:09	0.000186	-09:53:16	0.00008	0.004855	0.000236	0.001849	0.000175	✗	?	
4	09:57:08	0.000253	-10:13:55	0.000332	0.002517	0.000193	0.000744	0.000153	✗	?	
5	09:57:05	0.000026	-10:03:19	0.000014	0.006507	0.000246	0.005911	0.000144	✗	?	
6	09:57:03	0.000152	-09:58:16	0.000078	0.001379	0.000274	0.001236	0.000159	✗	?	
7	09:57:01	0.000372	-09:58:58	0.000137	0.002094	0.000201	0.000805	0.000149	✗	?	
7	09:57:00	0.000212	-09:58:56	0.000594	0.000419	0.000245	0.000343	0.000145	✗	?	
8	09:57:01	0.000178	-10:05:38	0.000086	0.000739	0.000274	0.000847	0.000147	✗	?	
9	09:56:54	0.000103	-10:02:18	0.000117	0.001511	0.000268	0.001264	0.000163	✗	?	
10	09:56:54	0.000011	-10:01:46	0.000024	0.008437	0.000378	0.00733	0.000156	✗	?	
11	09:56:52	0.000137	-10:00:30	0.00011	0.002865	0.000234	0.001474	0.000163	✗	?	
12	09:56:52	0.000122	-09:52:54	0.00008	0.001168	0.000272	0.001174	0.000156	✗	?	
13	09:56:51	0.000281	-10:10:22	0.000272	0.003312	0.000175	0.000794	0.000143	✗	?	
14	09:56:47	0.000181	-10:01:39	0.000105	0.000792	0.000305	0.000887	0.000165	✗	?	
15	09:56:44	0.000028	-09:55:43	0.00002	0.010589	0.000281	0.007165	0.000182	✗	?	
16	09:56:40	0.00025	-09:53:01	0.000087	0.001099	0.000321	0.001003	0.000182	✗	?	
17	09:56:40	0.000037	-10:10:22	0.000022	0.004291	0.000266	0.004125	0.000154	✗	?	
18	09:56:37	0.000123	-10:07:52	0.000072	0.000764	0.000264	0.000984	0.000137	✗	?	
19	09:56:35	0.000205	-09:53:29	0.0001	0.001472	0.000307	0.001139	0.000188	✗	?	
20	09:56:29	0.000236	-10:11:32	0.000133	0.001594	0.000315	0.001074	0.000203	✗	?	
21	09:56:28	0.000003	-09:57:19	0.000004	0.149655	0.001072	0.090002	0.000291	✗	?	ext.
23	09:56:27	0.000281	-10:05:52	0.000167	0.002714	0.000649	0.001927	0.000405	✗	?	
23	09:56:27	0.000288	-10:05:56	0.000137	0.002513	0.000659	0.001826	0.000413	✗	?	
24	09:56:27	0.000198	-10:04:49	0.000125	0.004001	0.000742	0.00274	0.000479	✗	?	
24	09:56:27	0.000223	-10:04:55	0.00013	0.001953	0.000783	0.001957	0.000446	✗	?	double
26	09:56:27	0.000258	-10:04:36	0.000247	0.005525	0.000679	0.002396	0.000494	✗	?	
25	09:56:27	0.000221	-09:57:43	0.000145	0.002696	0.000396	0.00152	0.00027	✗	?	double
27	09:56:27	0.000214	-09:58:04	0.000204	0.003812	0.000314	0.001527	0.000232	✗	?	
28	09:56:26	0.000335	-10:06:48	0.000228	0.005512	0.000533	0.002065	0.000398	✗	?	
29	09:56:26	0.000292	-10:07:29	0.000233	0.004792	0.00058	0.002084	0.000419	✗	?	
30	09:56:24	0.000232	-10:12:12	0.000257	0.004757	0.000448	0.001749	0.00034	✗	?	
30	09:56:23	0.00051	-10:12:21	0.000254	0.002737	0.000452	0.001095	0.000334	✗	?	
31	09:56:23	0.000007	-09:55:15	0.000013	0.018076	0.000491	0.016327	0.000201	✗	?	
32	09:56:19	0.000094	-09:55:59	0.000067	0.002632	0.000269	0.001907	0.000171	✗	?	
33	09:56:17	0.000168	-09:54:32	0.000092	0.00128	0.00029	0.001113	0.000173	✗	?	
35	09:56:14	0.000024	-09:53:02	0.000032	0.029109	0.000346	0.009349	0.000183	✗	?	
36	09:56:11	0.000174	-09:55:21	0.000125	0.000966	0.00025	0.000831	0.000151	✗	?	
37	09:56:08	0.000175	-09:54:08	0.00007	0.002021	0.00026	0.001387	0.000164	✗	?	
38	09:56:03	0.000091	-10:07:42	0.000038	0.003044	0.000277	0.002416	0.000168	✗	?	
39	09:56:03	0.000127	-10:02:35	0.000168	0.001012	0.000273	0.000912	0.000161	✗	?	
40	09:56:02	0.000303	-10:15:42	0.000252	0.005546	0.000183	0.000998	0.000157	✗	?	
41	09:56:00	0.000212	-10:06:17	0.000106	0.000937	0.000282	0.000858	0.000165	✗	?	
42	09:55:58	0.00009	-10:06:22	0.000056	0.002095	0.000283	0.001866	0.000168	✗	?	
43	09:55:57	0.000004	-09:59:03	0.000007	0.035353	0.000577	0.030881	0.000202	✗	?	
45	09:55:54	0.000022	-09:53:60	0.00002	0.0162	0.000376	0.009362	0.000172	✗	?	double
46	09:55:54	0.000133	-09:53:20	0.000091	0.00345	0.000257	0.001734	0.000181	✗	?	
46	09:55:54	0.000168	-09:53:28	0.000084	0.001025	0.00029	0.00103	0.000164	✗	?	
47	09:55:50	0.00016	-09:58:11	0.000065	0.002564	0.000222	0.001457	0.000149	✗	?	
48	09:55:42	0.000179	-10:14:54	0.000085	0.005668	0.000191	0.001679	0.00015	✗	?	
48	09:55:42	0.000136	-10:15:02	0.000085	0.001957	0.000244	0.001349	0.000157	✗	?	
49	09:55:40	0.00017	-10:10:28	0.000117	0.001981	0.000246	0.001155	0.000167	✗	?	
50	09:55:39	0.000164	-10:10:21	0.000095	0.006346	0.000206	0.001829	0.000164	✗	?	
50	09:55:38	0.000157	-10:10:17	0.000161	0.003612	0.000227	0.001331	0.000173	✗	?	
51	09:55:38	0.000112	-10:09:34	0.00011	0.002395	0.000291	0.001577	0.000191	✗	?	

Table 4.13: Positions of radio sources within R_{500} radius of the pointing centre of cluster RXCJ0956.4−1004

Source ID	RA	Δ RA	DEC	Δ DEC	total flux	Δ total flux	Peak flux	Δ Peak flux	optical cross-ID	cluster member	comments
1	09:58:40	0.000043	-11:04:57	0.000037	0.003737	0.000376	0.003968	0.000209	✗	?	
2	09:58:34	0.000087	-11:02:13	0.000064	0.017053	0.000494	0.006584	0.000367	✗	?	
3	09:58:34	0.000143	-11:01:47	0.000278	0.009225	0.000501	0.003403	0.000363	✗	?	
4	09:58:34	0.000099	-11:01:23	0.000181	0.002392	0.000523	0.001964	0.000315	✗	?	
5	09:58:31	0.000313	-11:06:48	0.000207	0.001937	0.000289	0.00097	0.0002	✗	?	
6	09:58:31	0.000149	-10:57:31	0.000153	0.001545	0.000491	0.00153	0.000276	✗	?	
7	09:58:30	0.000047	-11:05:54	0.000033	0.010746	0.000499	0.007279	0.000323	✗	?	
8	09:58:25	0.000186	-11:01:34	0.000299	0.007524	0.000645	0.002753	0.000485	✗	?	
9	09:58:22	0.000008	-11:03:35	0.00001	0.127187	0.001734	0.101351	0.001062	✔	✔	BCG
11	09:58:21	0.000295	-11:03:59	0.000083	0.011107	0.001294	0.003212	0.000601	✗	?	

Table 4.14: Positions of radio sources within R_{500} radius of the pointing centre of cluster RXCJ0958.3−1103

Source ID	RA	Δ RA	DEC	Δ DEC	total flux	Δ total flux	Peak flux	Δ Peak flux	optical cross-ID	cluster member	comments
0	10:44:55	0.000178	-06:58:29	0.000088	0.005962	0.00057	0.004777	0.000307	✗	?	double
1	10:44:54	0.000036	-06:58:10	0.000066	0.013808	0.000998	0.012838	0.000427	✗	?	
2	10:44:47	0.000119	-07:07:10	0.000068	0.006996	0.000419	0.00509	0.000241	✗	?	
5	10:44:33	0.00005	-07:04:06	0.0001	0.030306	0.001702	0.022564	0.000827	✔	✔	BCG
8	10:44:21	0.000027	-06:59:17	0.000015	0.036973	0.00085	0.038777	0.00039	✗	?	

Table 4.15: Positions of radio sources within R_{500} radius of the pointing centre of cluster RXCJ1044.5−0704

4.4.14 RXCJ1141.4−1216

The cluster,also known as Abell 1348 (Abell (1958), Abell *et al.* (1989)), and situated at $z = 0.1195$, which corresponds to an angular scale of 1 arcsec = 0.48073 kpc. is shown in Fig. 4.27.
14 sources are detected at $> 5\sigma$ level within 4 Mpc of the cluster centre. These are tabulated in Table C.13.Of the 14 detected sources, **two** are double sources and **three** are extended.The are no extended sources within R_{500}. One of the extended sources shows the same morphology as a typical FR type I galaxy. Minor artefacts are present around the brighter sources. Fig. 4.27 shows the typical RMS structure, indicating that it is smooth as expected. There might have been minor issues with the removing of the dirty beam, as all central sources are slightly elongated. We were unable to remove these elongations. Fig. 4.28 shows the contours from the NVSS overlaid on the GMRT map, demonstrating that three sources were detected in that survey. These sources and all additionally detected radio sources are listed in Tab. 4.16. The optical galaxies in the central region of R_{500} which are associated with the cluster are indicated in Fig. 4.28 as green circles the ones not associated are red. It is shown that only the central bright source has an optical counterpart. All additional radio sources present lack an optical counterpart, possibly caused by the faintness of the optical source or no associated redshift, making it impossible to determine if it is associated with the cluster. All known optical galaxy positions are provided in Tab. B.14. The redshift range used to identify cluster members was 0.095−0.125, chosen according to Yee (1996). The cluster has a mass of $M_{500} = 2.3 \times 10^{14} M_{\odot}$ Pratt et al. (2010) and has a very low central entropy Pratt et al. (2010). It is classified as a cool core cluster Pratt et al. (2010). This cluster shows the highest variability when sampled at 15GHz Hogan *et al.* (2015b). The spectrum of this cluster is fitted by two different components, a GPS-like component, below 1 GHz and a Power-like component above 1 GHz Hogan *et al.* (2015b).The cluster is core dominated as verified by VLBA imaging **?**
There are **no** newly confirmed radio sources associated with the cluster and **eight** new cluster member candidates. Further research is needed to verify if a cluster membership is given for these candidates.

4.4.15 RXCJ1236.7−3354

This cluster, shown in Fig. 4.29, is also known as S0384 (Abell *et al.* (1989)) and is located at $z = 0.0796$, which corresponds to an angular scale of 1 arcsec = 0.66532

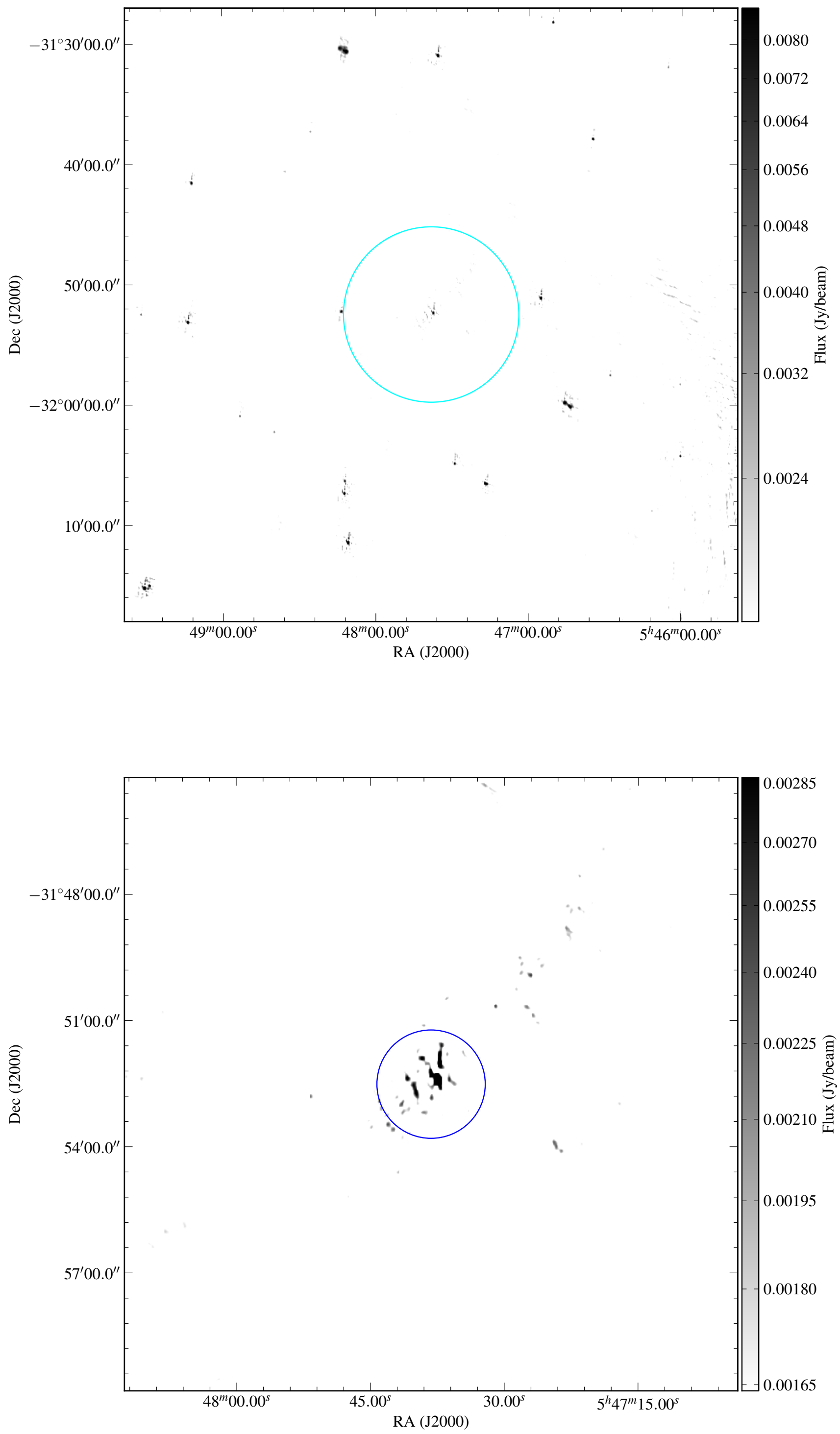

Figure 4.15: 610-MHz GMRT maps of RXCJ0547.6−3152.Top: overview of a region 4 Mpc × 4 Mpc centred on the cluster, R_{500} being indicated by the circle; bottom: central region of the cluster ($R_{500} \times R_{500}$)the circle indicates a region of radius 200kpc around the centre.

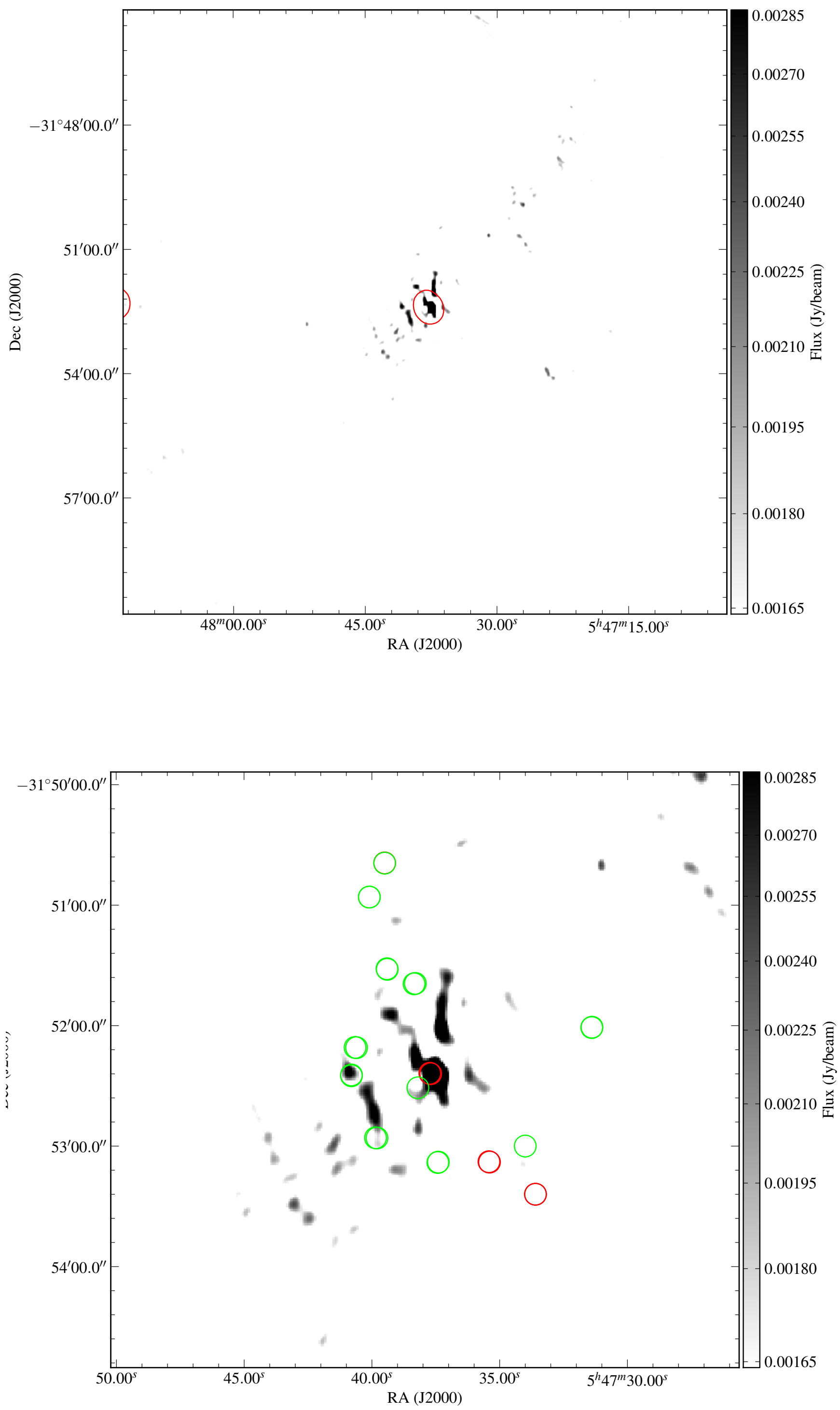

Figure 4.16: 610-MHz GMRT maps of RXCJ0547.6−3152.central region of the cluster ($R_{500} \times R_{500}$); top: contours from NVSS overlaid; bottom: positions of known cluster member galaxies overlaid in green and known background or foreground sources indicated by red circles.

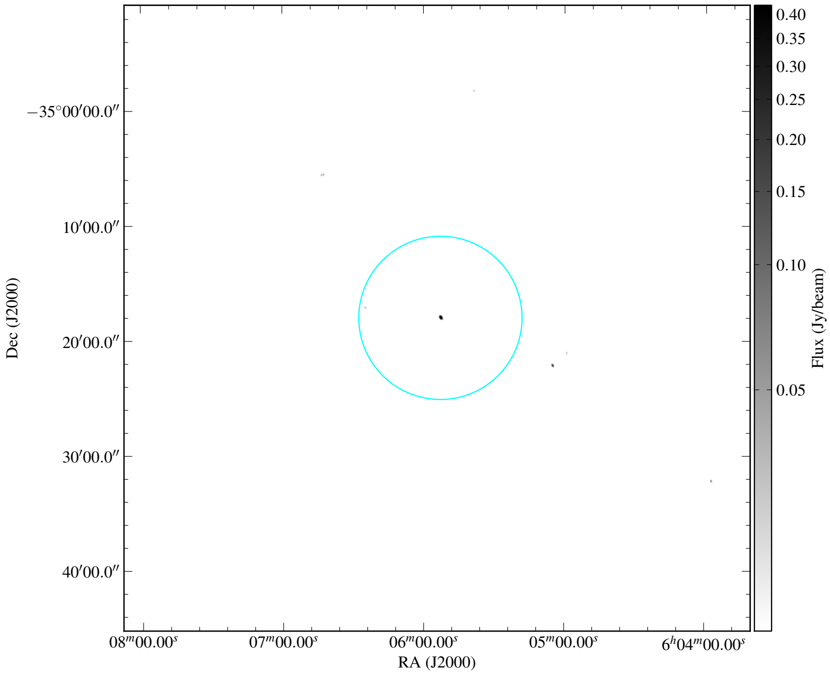

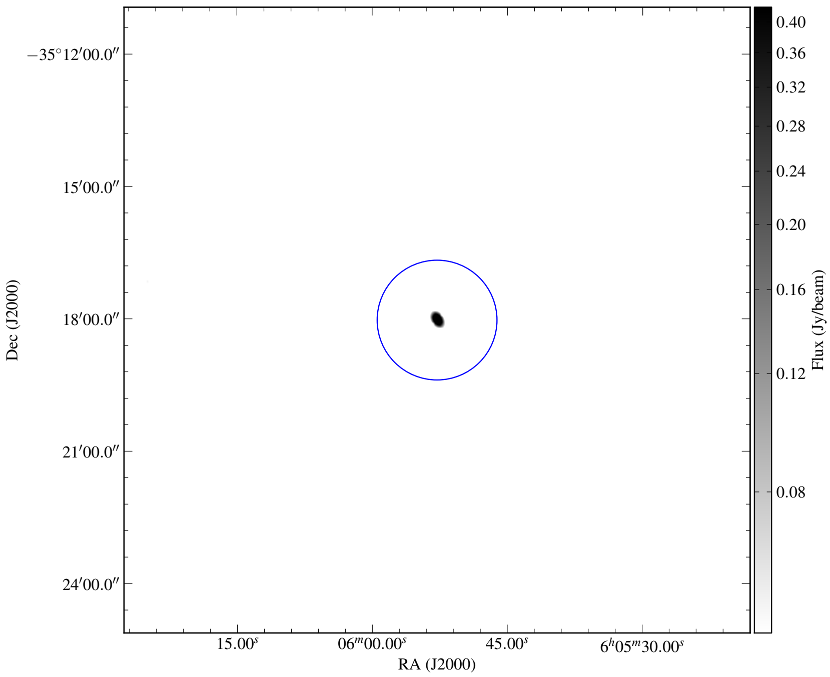

Figure 4.17: 610-MHz GMRT maps of RXCJ0605.8−3518.Top: overview of a region 4 Mpc × 4 Mpc centred on the cluster, R_{500} being indicated by the circle; bottom: central region of the cluster ($R_{500} \times R_{500}$)the circle indicates a region of radius 200kpc around the centre.

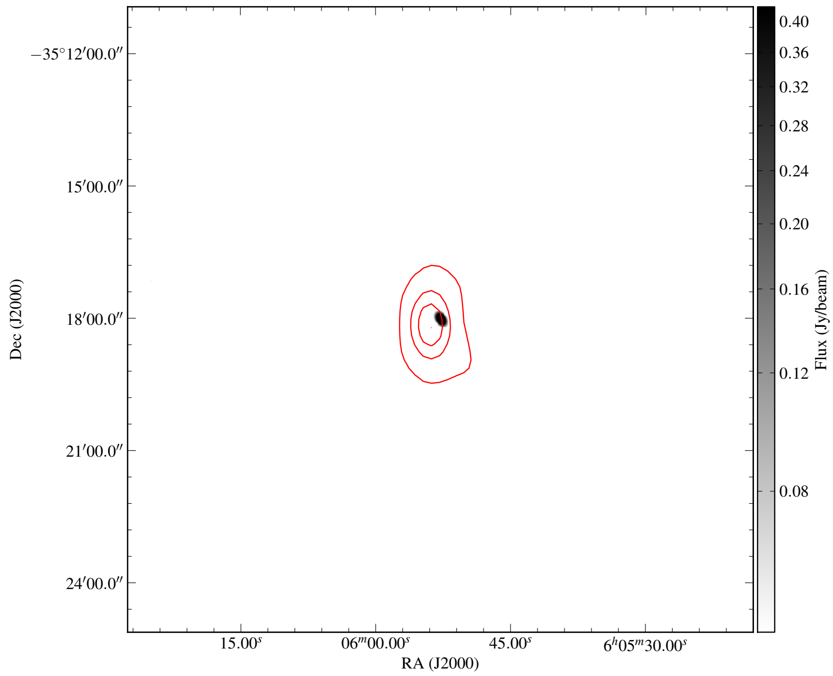

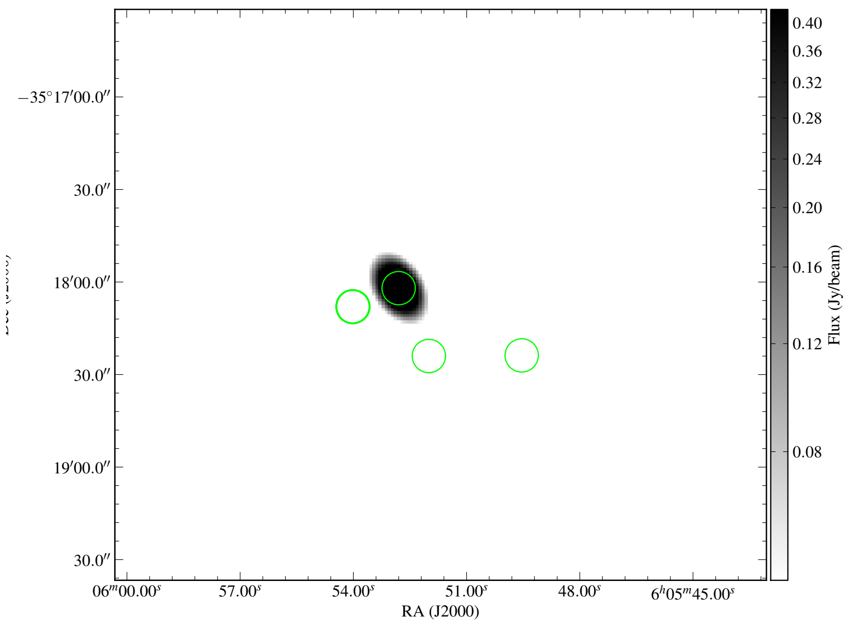

Figure 4.18: 610-MHz GMRT maps of RXCJ0605.8−3518. central region of the cluster ($R_{500} \times R_{500}$); top: contours from SUMSS overlaid; bottom: positions of known cluster member galaxies overlaid in green.

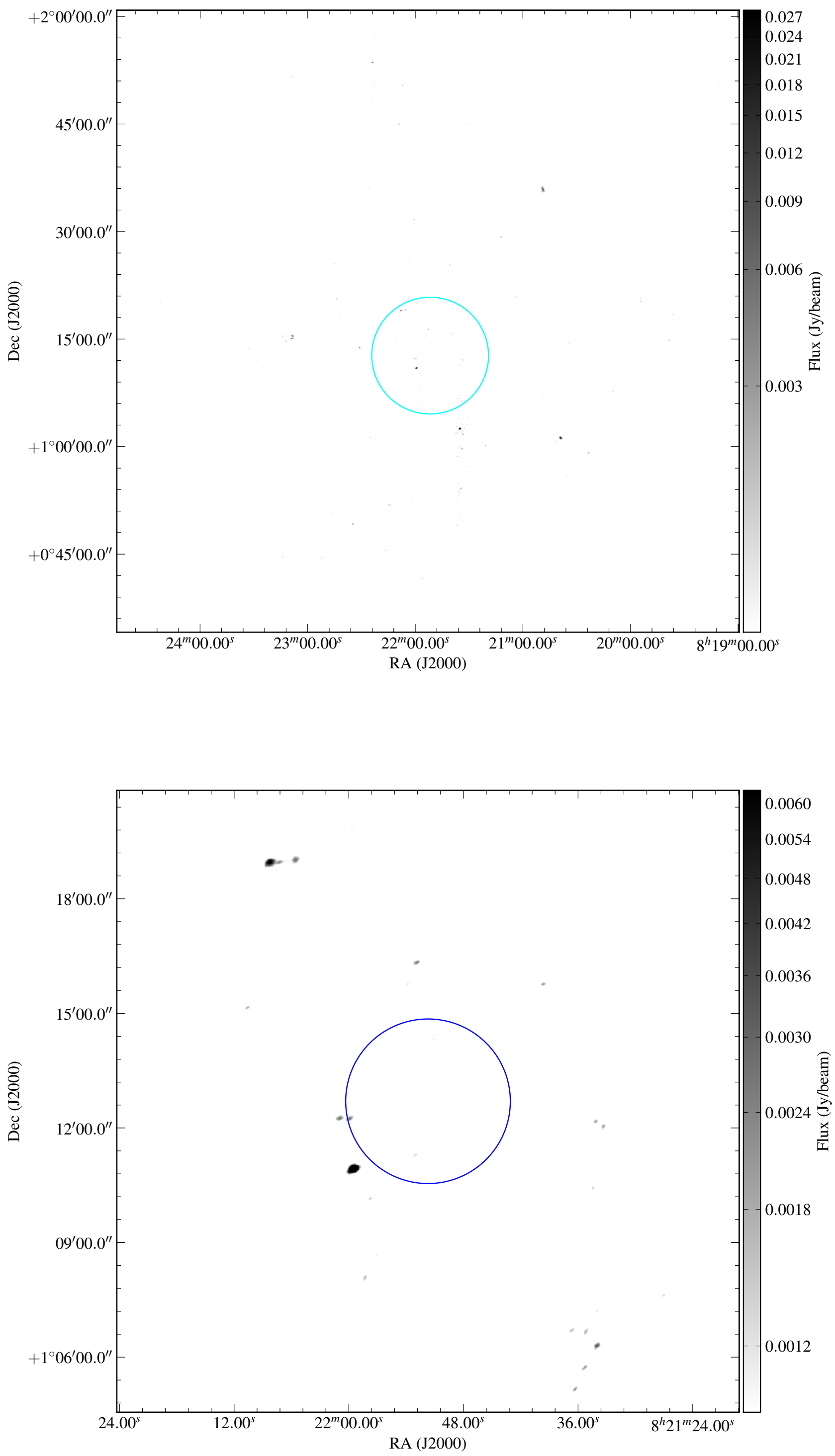

Figure 4.19: 610-MHz GMRT maps of RXCJ0821.8+0112.Top: overview of a region 4 Mpc $\times$ 4 Mpc centred on the cluster, R_{500} being indicated by the circle; bottom: central region of the cluster ($R_{500} \times R_{500}$)the circle indicates a region of radius 200kpc around the centre.

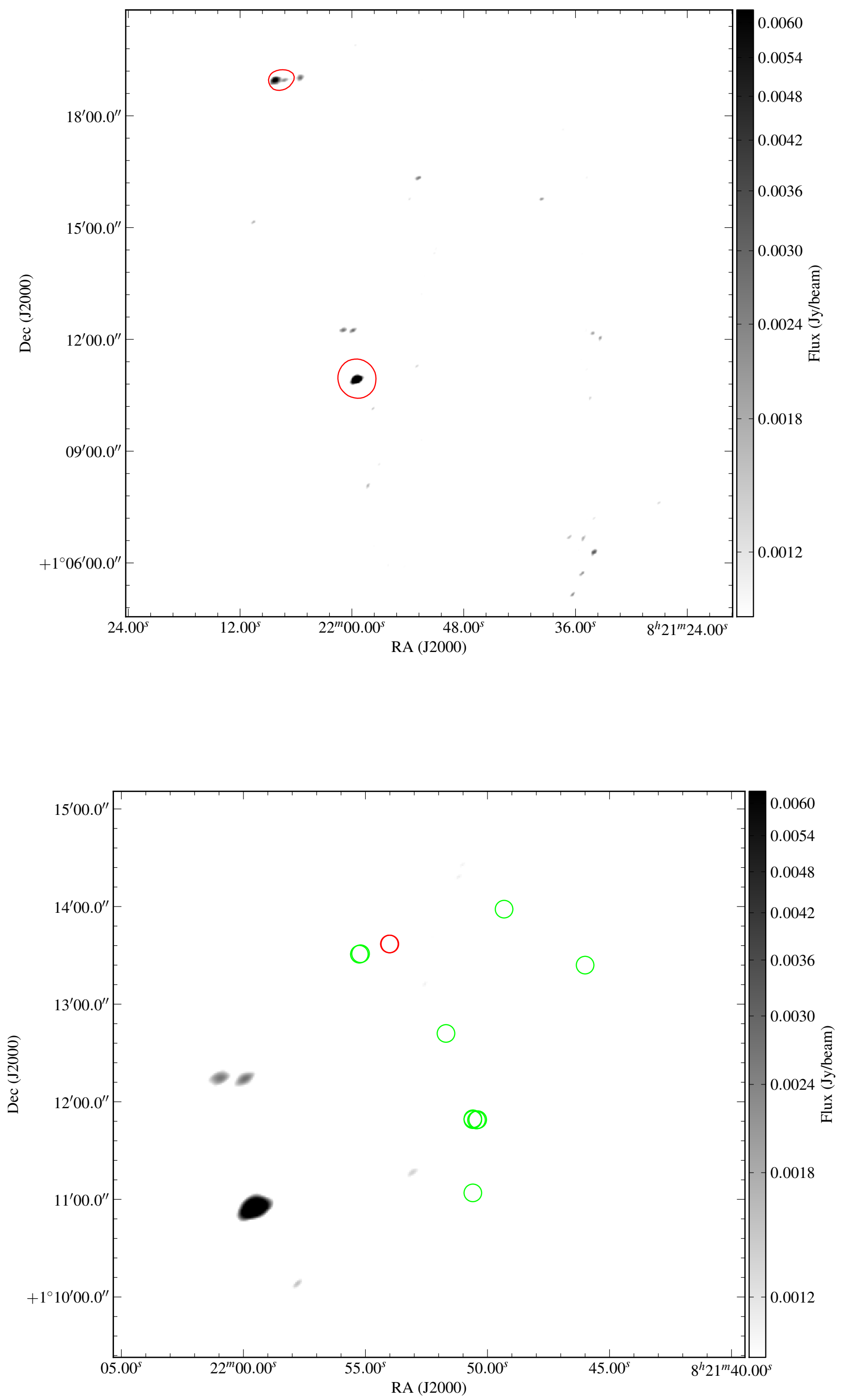

Figure 4.20: 610-MHz GMRT maps of RXCJ0821.8+0112. central region of the cluster ($R_{500} \times R_{500}$); top: contours from NVSS overlaid; bottom: positions of known cluster member galaxies overlaid in green and known background or foreground sources indicated by red circles.

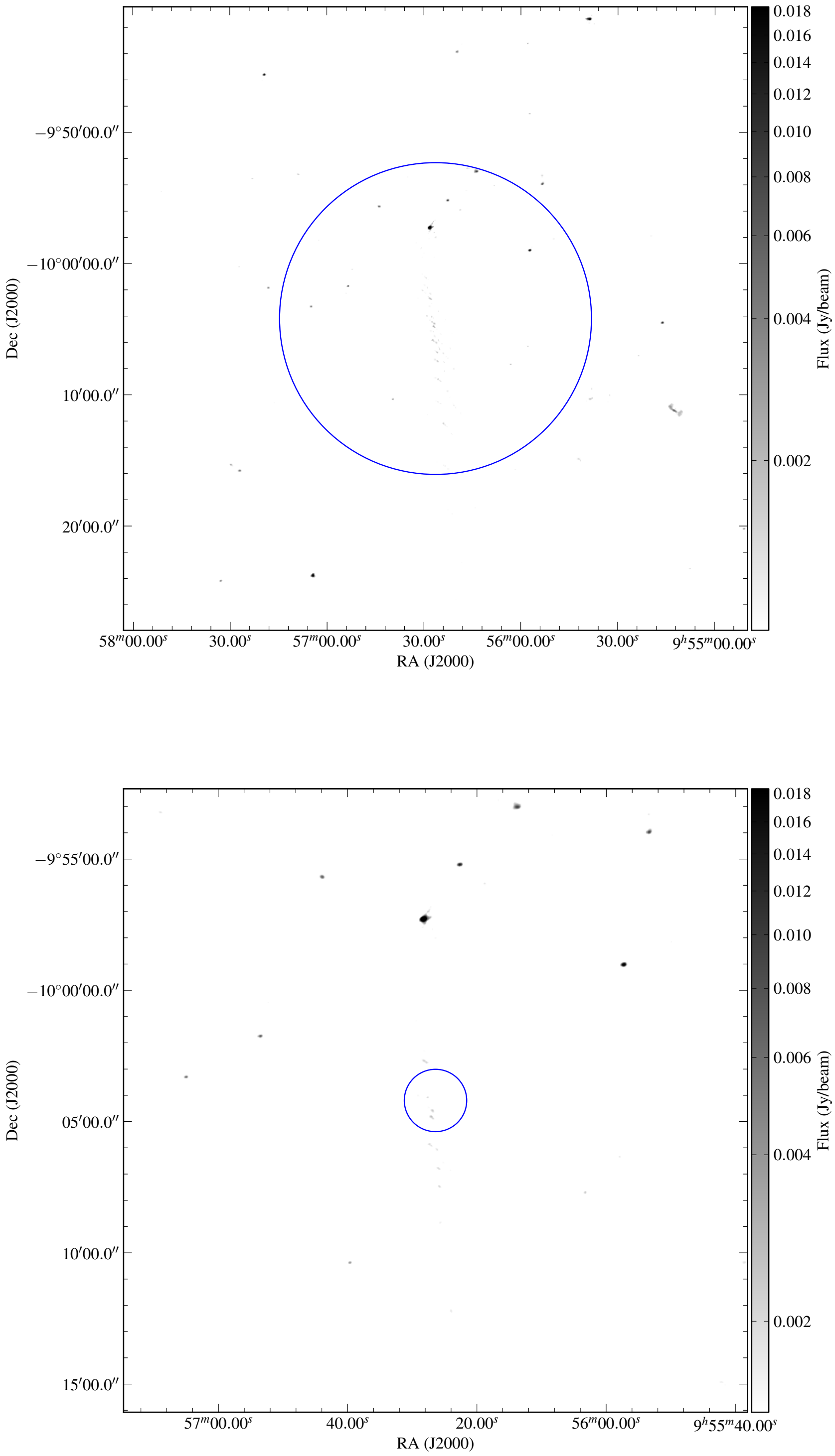

Figure 4.21: 610-MHz GMRT maps of RXCJ0956.4−1004. Top: overview of a region 4 Mpc × 4 Mpc centred on the cluster; bottom: central region of the cluster (2 Mpc × 2 Mpc)the circle indicates a region of radius 200kpc around the centre.

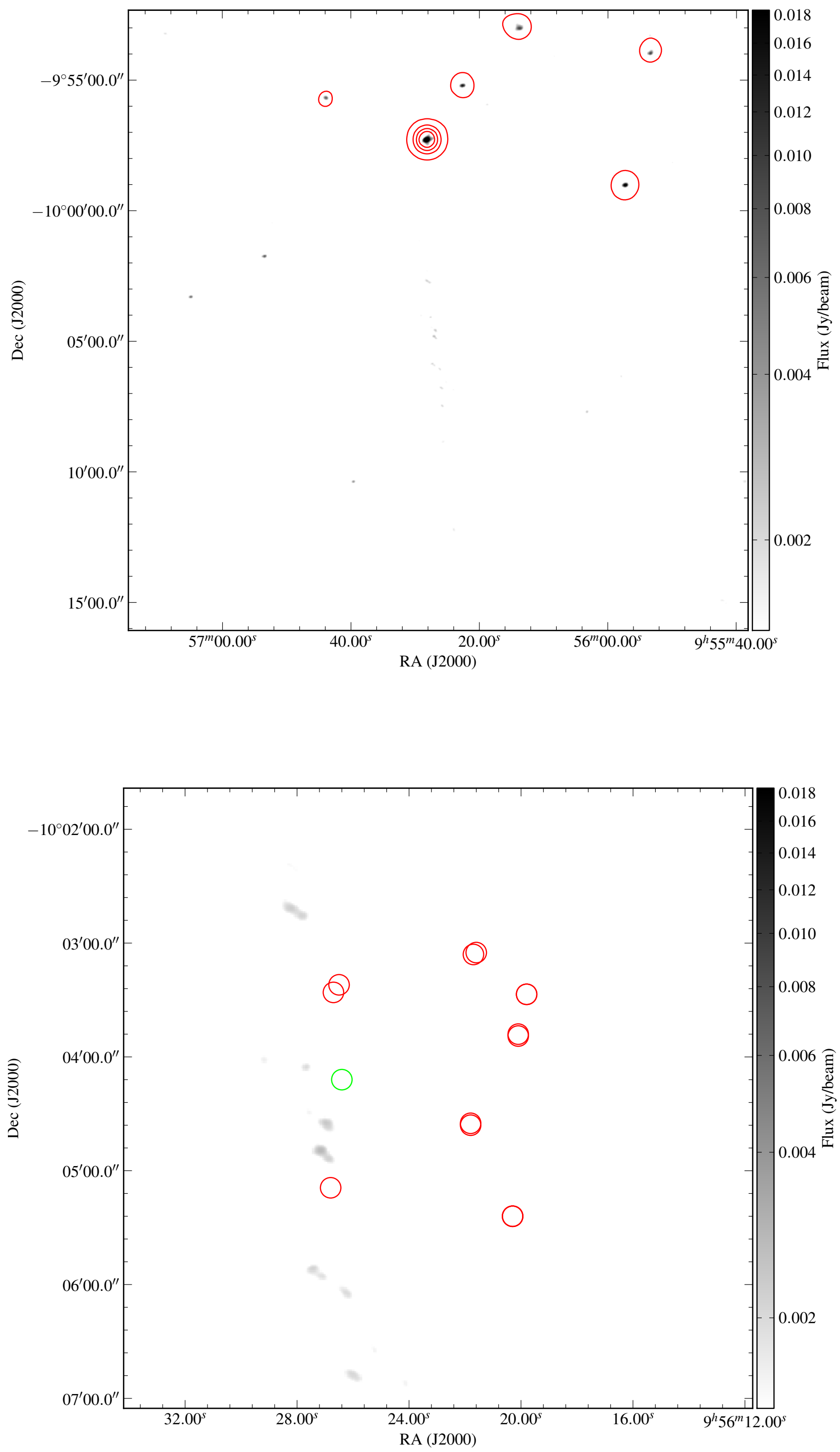

Figure 4.22: 610-MHz GMRT maps of RXCJ0956.4−1004. central region of the cluster (2 Mpc $\times$ 2 Mpc); top: contours from NVSS overlaid; bottom: positions of known cluster member galaxies overlaid in green and known background or foreground sources indicated by red circles.

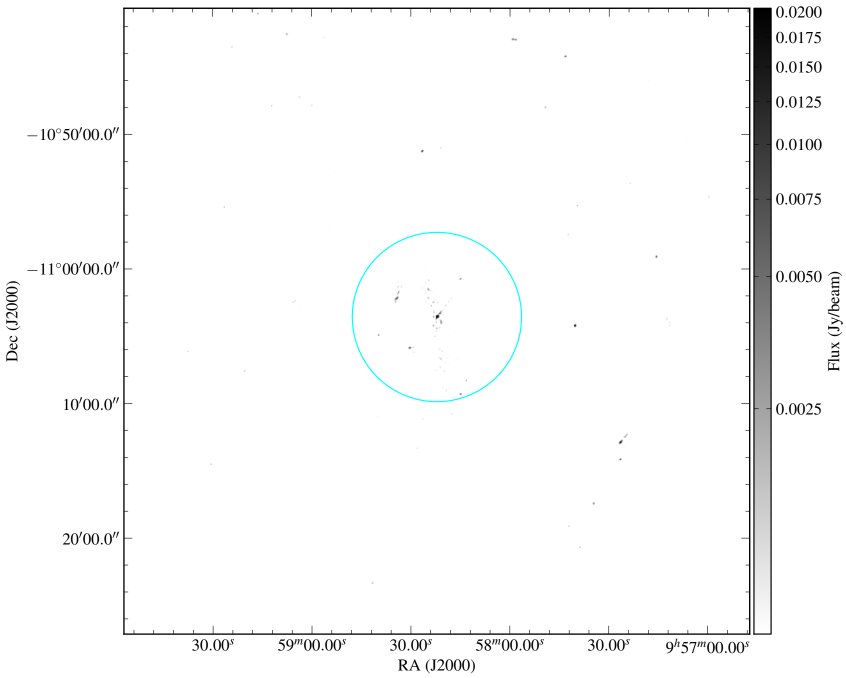

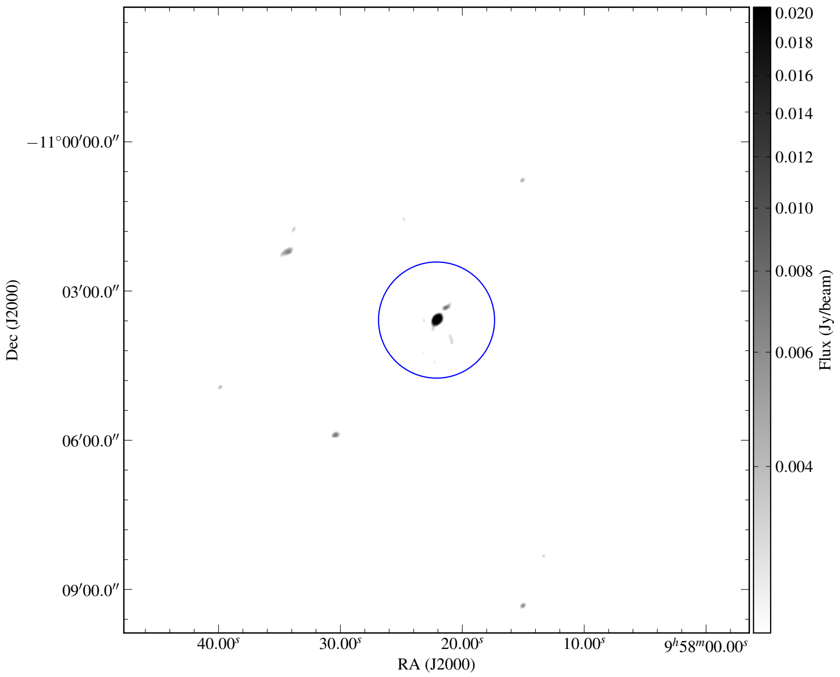

Figure 4.23: 610-MHz GMRT maps of RXCJ0958.3−1103. Top: overview of a region 4 Mpc $\times$ 4 Mpc centred on the cluster, R_{500} being indicated by the circle; bottom: central region of the cluster ($R_{500} \times R_{500}$)the circle indicates a region of radius 200kpc around the centre.

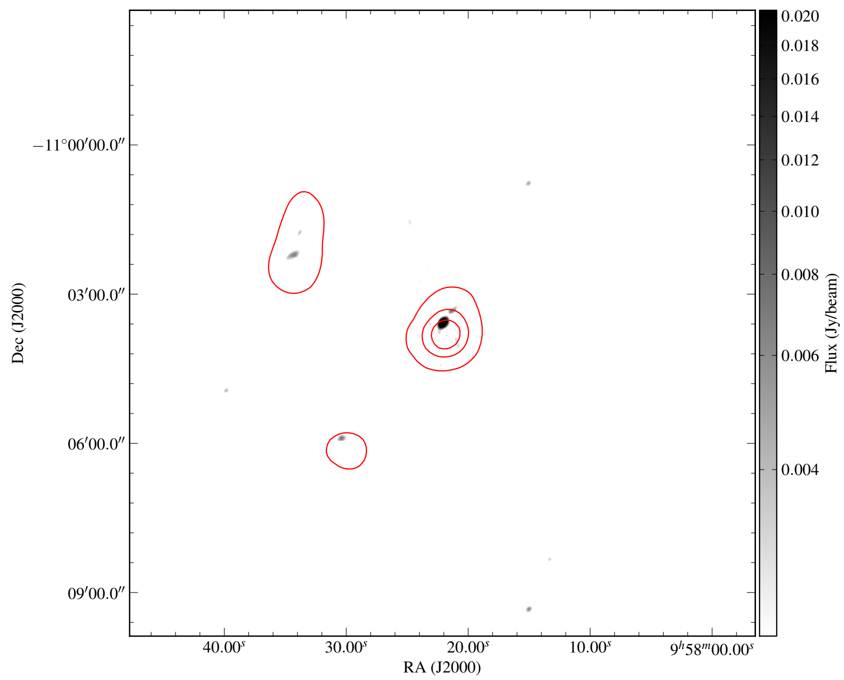

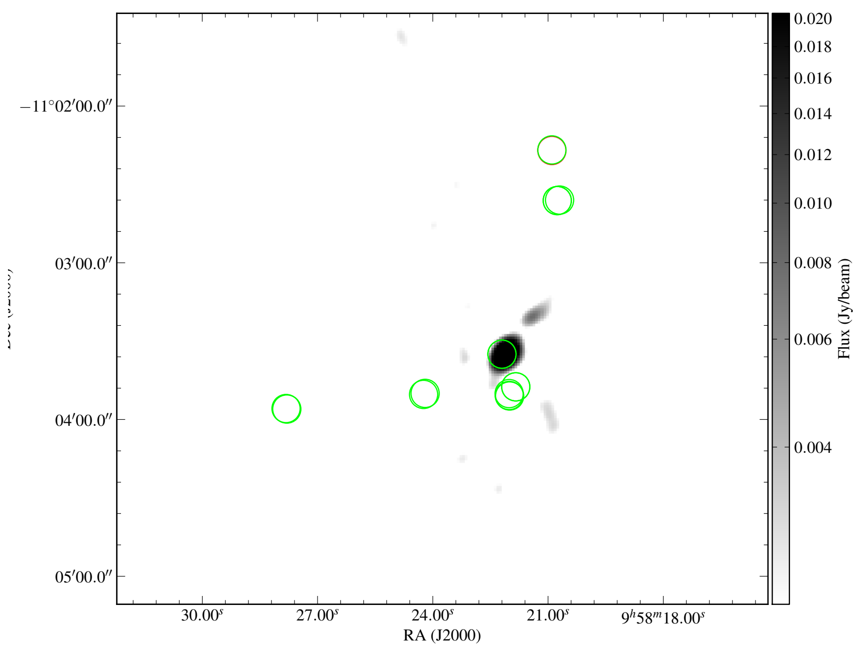

Figure 4.24: 610-MHz GMRT maps of RXCJ0958.3−1103. central region of the cluster ($R_{500} \times R_{500}$); top: contours from NVSS overlaid; bottom: positions of known cluster member galaxies overlaid in green and known background or foreground sources indicated by red circles.

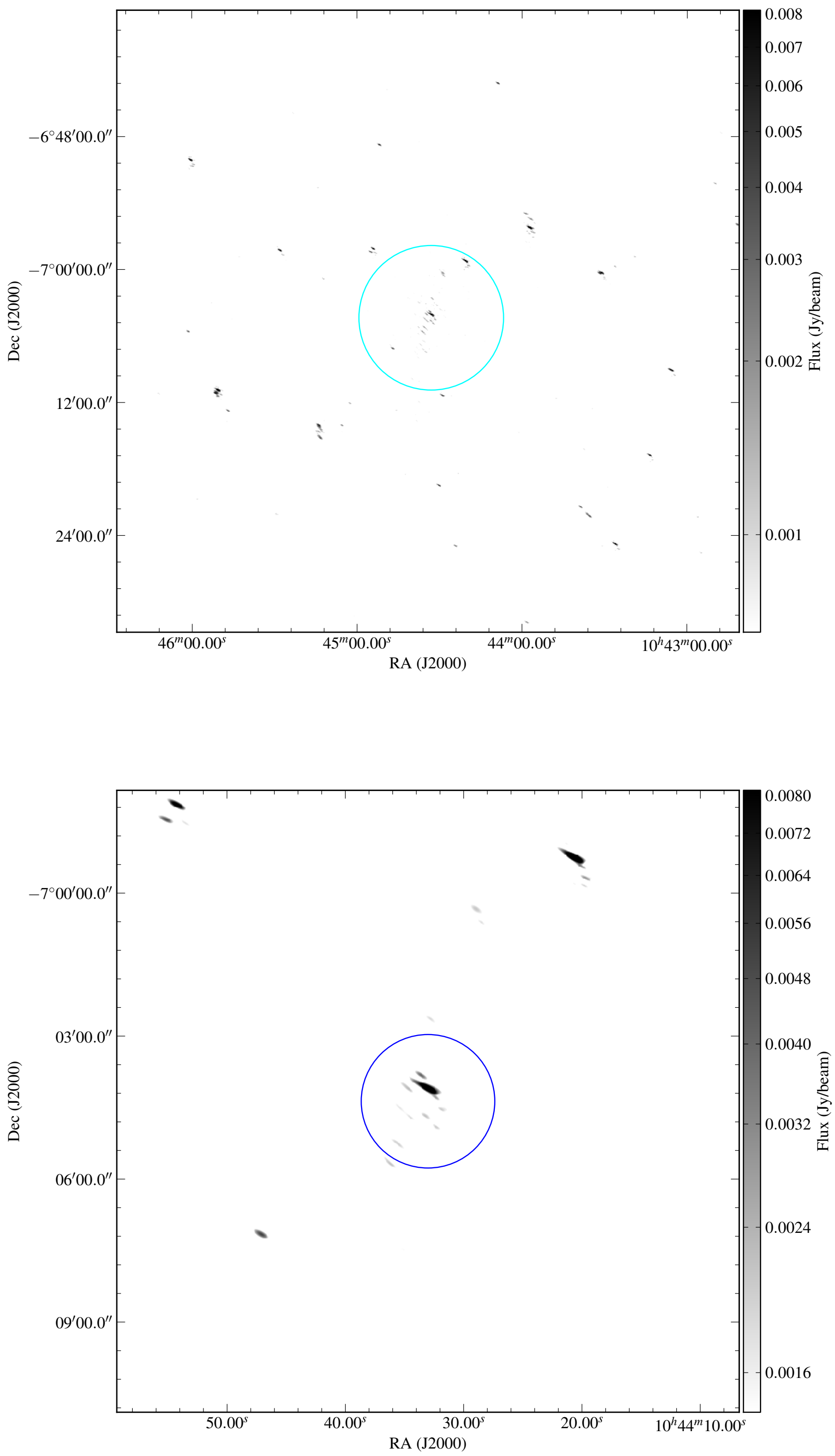

Figure 4.25: 610-MHz GMRT maps of RXCJ1044.5−0704. Top: overview of a region 4 Mpc × 4 Mpc centred on the cluster, R_{500} being indicated by the circle; bottom: central region of the cluster ($R_{500} \times R_{500}$)the circle indicates a region of radius 200kpc around the centre.

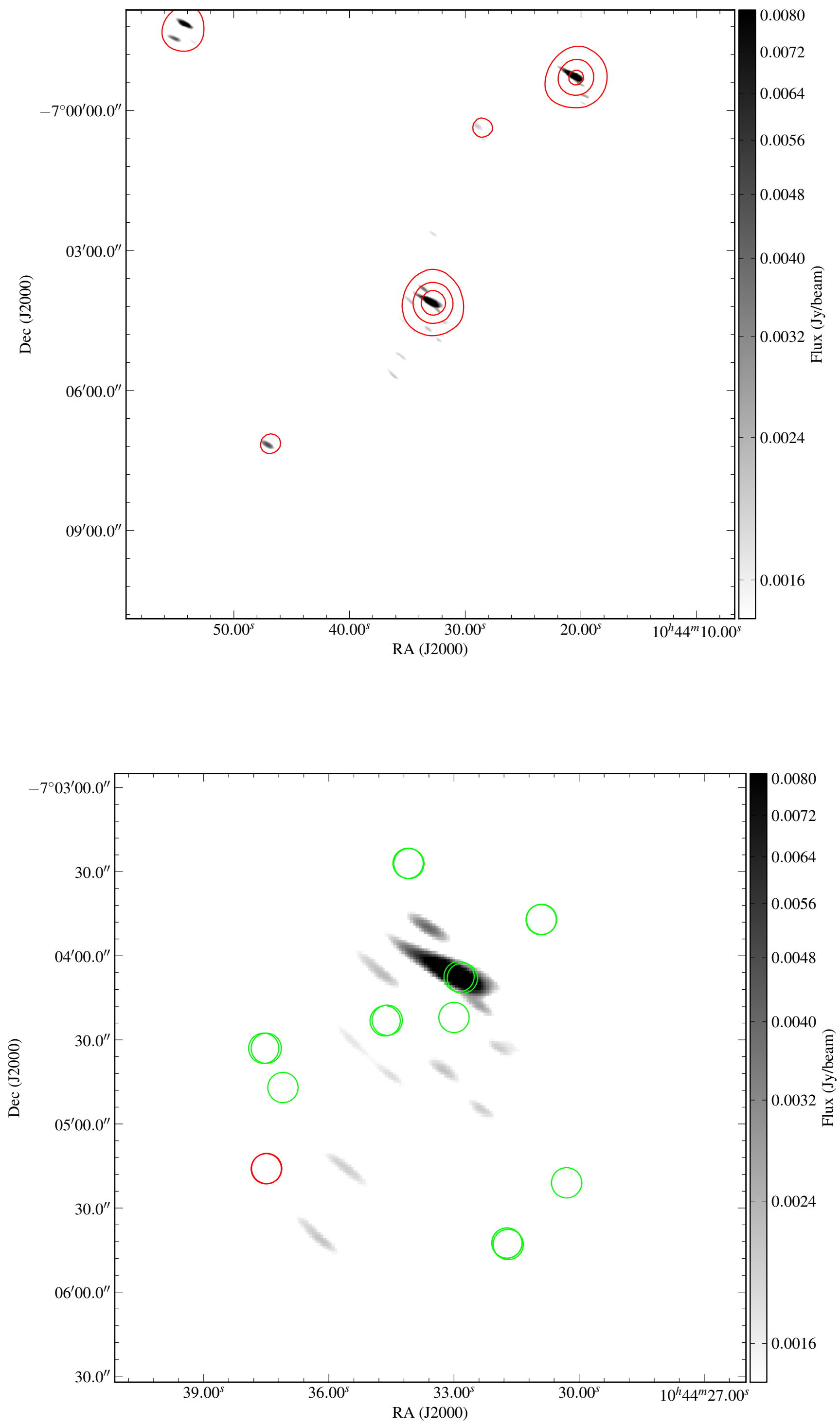

Figure 4.26: 610-MHz GMRT maps of RXCJ1044.5−0704. central region of the cluster ($R_{500} \times R_{500}$); top: contours from NVSS overlaid; bottom: positions of known cluster member galaxies overlaid in green and known background or foreground sources indicated by red circles.

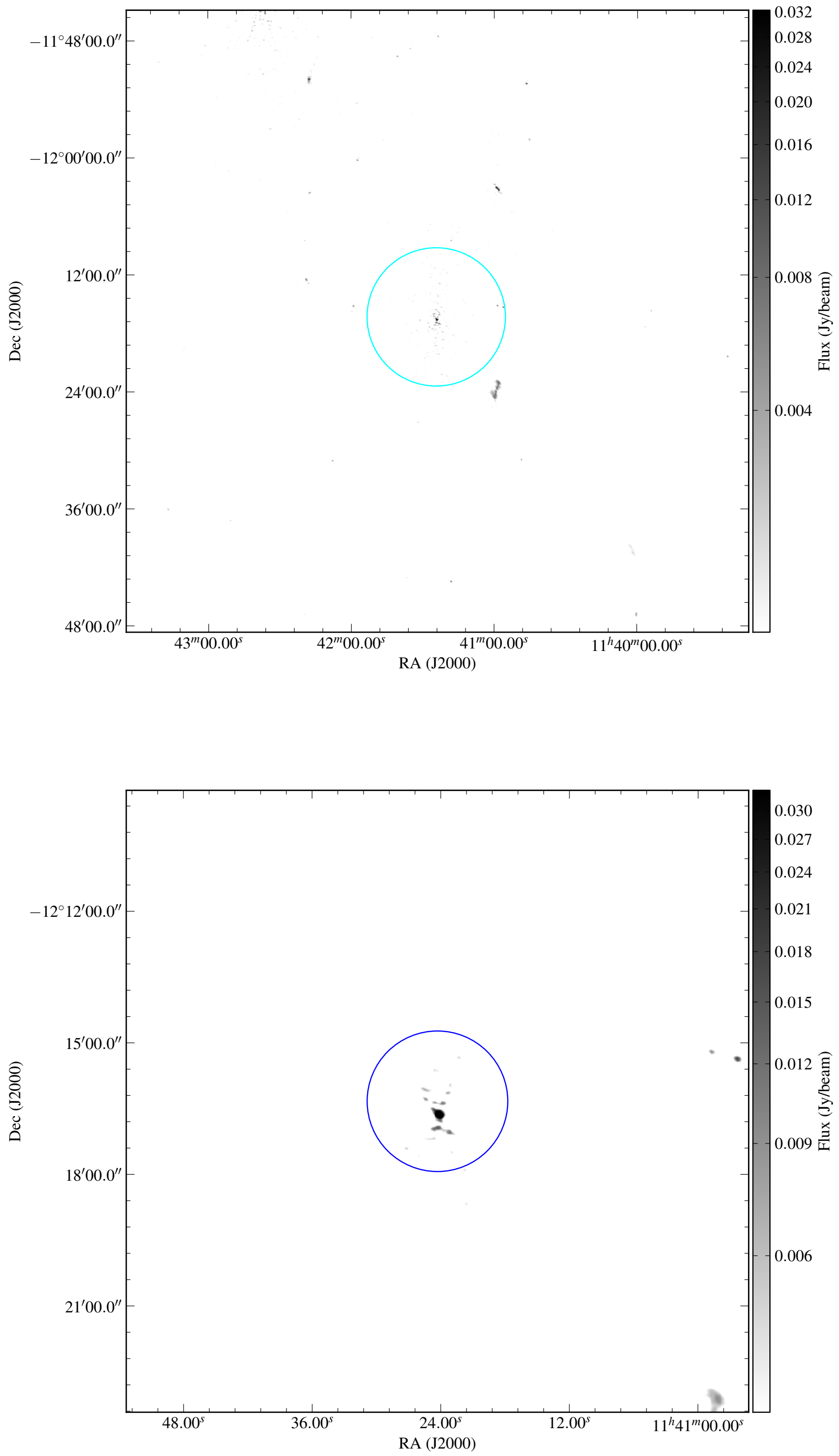

Figure 4.27: 610-MHz GMRT maps of RXCJ1141.4−1216. Top: overview of a region 4 Mpc × 4 Mpc centred on the cluster, R_{500} being indicated by the circle; bottom: central region of the cluster ($R_{500} \times R_{500}$)the circle indicates a region of radius 200kpc around the centre.

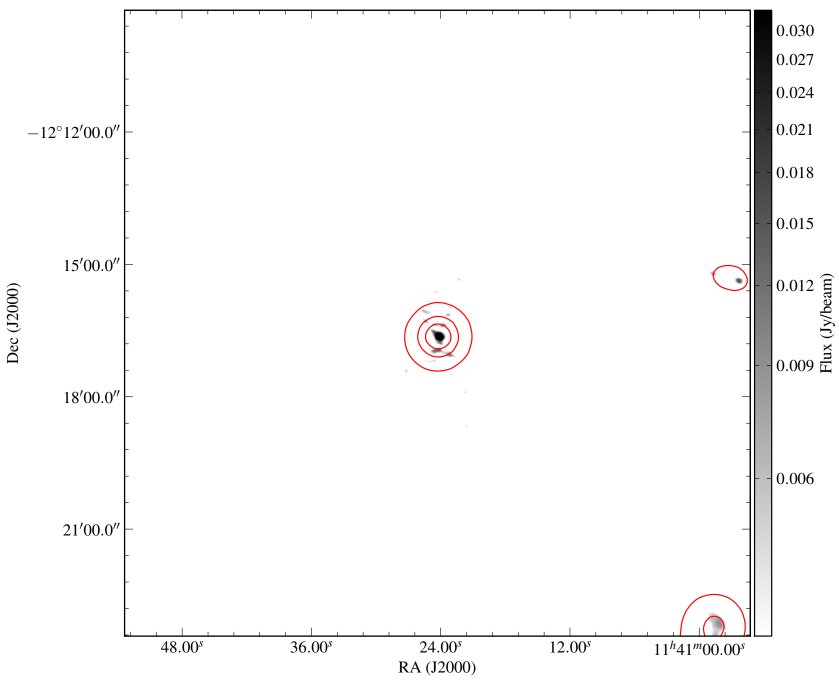

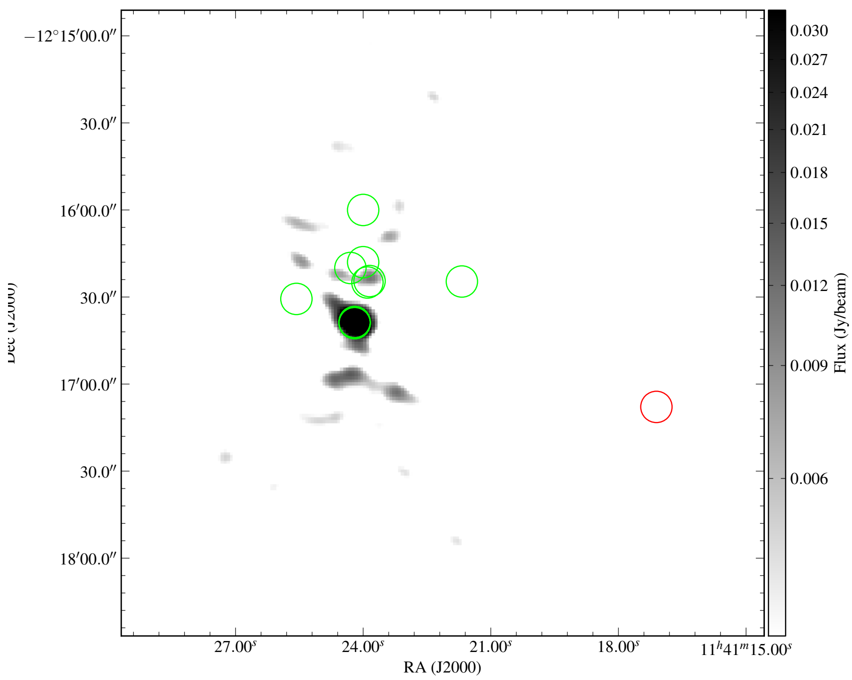

Figure 4.28: 610-MHz GMRT maps of RXCJ1141.4−1216. central region of the cluster ($R_{500} \times R_{500}$); top: contours from NVSS overlaid; bottom: positions of known cluster member galaxies overlaid in green and known background or foreground sources indicated by red circles.

kpc.
61 sources are detected at $> 5\sigma$ level within 4 Mpc of the cluster centre. These are tabulated in Table C.14.Of the 61 detected sources, **seven** are extended.There are three extended source within R_{500} is the bright central galaxy.The central bright source is an extended double source. Minor artefacts are present around the brighter source sand there is one RFI stripe near the centre of the field, which we were unable to remove. Fig. 4.29 shows the RMS structure, indicating that it is smooth as expected away from the stripe. Fig. 4.30 shows the contours from the SUMSS overlaid on the GMRT map, demonstrating that three sources were detected in that survey, the bright central source was not detected by NVSS. These sources and all additionally detected radio sources are listed in Tab. 4.17. The optical galaxies in the central region of R_{500} which are associated with the cluster are indicated in Fig. 4.30 as green circles. It is shown that no radio sources have optical counterparts. All radio sources present lack an optical counterpart, possibly caused by the faintness of the optical source orno associated redshift, making it impossible to determine if it is associated with the cluster. All known optical galaxy positions are listed in Tab. B.15. The redshift range used to identify cluster members was $0.055-0.085$, chosen according to Yee (1996). The cluster has a mass of $M_{500} = 1.3 \times 10^{14} M_{\odot}$ Pratt et al. (2010) and has a low central entropy Pratt et al. (2010). It is one of the least massive clusters in the REXCESS sample.
There are **no** newly confirmed radio sources associated with the cluster and **seven** new cluster member candidates. Further research is needed to verify if a cluster membership is given for these candidates.

Source ID	RA	Δ RA	DEC	Δ DEC	total flux	Δ total flux	Peak flux	Δ Peak flux	optical cross-ID	cluster member	comments
0	11:41:35	0.000101	-12:18:03	0.00014	0.002659	0.000853	0.00291	0.000475	✗	?	
1	11:41:27	0.000116	-12:17:25	0.000125	0.004961	0.0014	0.00505	0.000804	✗	?	
2	11:41:24	0.000022	-12:16:39	0.000017	0.157953	0.006608	0.153916	0.003823	✔	✔	BCG
3	11:41:22	0.000094	-12:15:21	0.000072	0.003771	0.001098	0.005062	0.000553	✗	?	
4	11:41:22	0.000165	-12:17:54	0.000125	0.004768	0.001149	0.004379	0.000659	✗	?	
4	11:41:21	0.000094	-12:17:58	0.000188	0.001018	0.00118	0.002061	0.000509	✗	?	
5	11:41:22	0.000226	-12:18:41	0.000138	0.005109	0.001269	0.004452	0.000719	✗	?	
6	11:40:59	0.000062	-12:15:13	0.000042	0.010175	0.001013	0.009566	0.000588	✗	?	} double
7	11:40:56	0.000041	-12:15:23	0.000031	0.018728	0.001369	0.018119	0.000791	✗	?	

Table 4.16: Positions of radio sources within R_{500} radius of the pointing centre of cluster RXCJ1141.4−1216

Source ID	RA	Δ RA	DEC	Δ DEC	total flux	Δ total flux	Peak flux	Δ Peak flux	optical cross-ID	cluster member	comments
0	12:37:19	0.000282	-33:49:37	0.000218	0.002339	0.000443	0.002246	0.000207	✗	?	
1	12:36:45	0.000033	-33:45:36	0.000027	0.018801	0.000446	0.017782	0.000217	✗	?	
2	12:36:43	0.000452	-33:56:50	0.000634	0.005665	0.00031	0.001209	0.000259	✗	?	
3	12:36:41	0.000216	-33:55:05	0.000233	0.014475	0.000306	0.002891	0.000259	✗	?	
4	12:36:38	0.000423	-33:55:19	0.000404	0.005374	0.000342	0.001495	0.000273	✗	?	
5	12:36:38	0.000353	-33:55:58	0.000373	0.01092	0.000287	0.001819	0.000248	✗	?	
7	12:36:10	0.000063	-33:52:12	0.000051	0.009797	0.000447	0.009348	0.000216	✗	?	

Table 4.17: Positions of radio sources within R_{500} radius of the pointing centre of cluster RXCJ1236.7−3354

4.4.16 RXCJ1302.8−0230

Fig. 4.31 shows the cluster also known as Abell 1663 (Abell (1958), Abell *et al.* (1989)), and situated at $z = 0.0847$, which corresponds to an angular scale of 1 arcsec = 0.62896 kpc.
421 sources are detected at $> 5\sigma$ level within 4 Mpc of the cluster centre. These are tabulated in Table C.15. Of the 421 detected sources, **one** is an extended double bright source, the bright central galaxy. Minor artefacts are present around the brighter sources. Fig. 4.31 shows the typical RMS structure, indicating that it is smooth as expected. In this map especially the fainter sources aroung the central bright source show some elongation in the same direction, indicating some leftover dirty beam structure, which we were not able to remove. Fig. 4.32 shows the contours from the NVSS overlaid on the GMRT map, demonstrating that two sources were detected in that survey. These sources and all additionally detected radio sources are listed in Tab. 4.18. The optical galaxies in the central region of R_{500} which are associated with the cluster are indicated in Fig. 4.32 as green circles the ones not associated are indicated by red circles. It is shown that only the central bright source has an optical counterpart. All other radio sources present lack an optical cross-identification, possibly caused by the faintness of the optical source or no associated redshift, makin it impossible to determine if it is associated with the cluster. All known optical galaxy positions are provided in Tab. B.16. The redshift range used to identify cluster members was $0.065-0.095$ chosen according to Yee (1996). The cluster has a mass of $M_{500} = 3.5 \times 10^{14} M_{\odot}$ Pratt et al. (2010) and has a medium central entropy Pratt et al. (2010). The cluster has a mass of $M_{500} = 2.1 \times 10^{14} M_{\odot}$ Pratt et al. (2010) and has a lot to medium central entropy Pratt et al. (2010). It is classified as a cool core cluster as well as a disturbed cluster Pratt et al. (2010). This galaxy is thought to have internal galactic dust Haarsma et al. (2010).
There are **no** newly confirmed radio sources associated with the cluster and **four** new cluster member candidates. Further research is needed to verify if a cluster membership is given for these candidates.

Source ID	RA	Δ RA	DEC	Δ DEC	total flux	Δ total flux	Peak flux	Δ Peak flux	optical cross-ID	cluster member	comments
0	13:02:53	0.000053	-02:30:53	0.000035	0.069922	0.001366	0.025382	0.001036	✔	✔	BCG
0	13:02:53	0.000083	-02:31:07	0.000069	0.045747	0.001334	0.014892	0.001037			
2	13:02:51	0.000153	-02:30:14	0.000263	0.009281	0.001232	0.004558	0.000854	✗	?	
3	13:02:51	0.000237	-02:35:49	0.000378	0.018036	0.000597	0.002911	0.000518	✗	?	
4	13:02:21	0.00014	-02:28:54	0.000112	0.002993	0.000691	0.00239	0.000427	✗	?	
5	13:02:20	0.000269	-02:28:20	0.000383	0.010481	0.000422	0.001775	0.000364	✗	?	

Table 4.18: Positions of radio sources within R_{500} radius of the pointing centre of cluster RXCJ1302.8−0230

4.4.17 RXCJ1311.4−0120

This cluster, pictured in Fig. 4.33, is also known as Abell 1689 (Abell (1958), Abell *et al.* (1989)), and is situated at $z = 0.1832$, which corresponds to an angular scale of 1 arcsec = 0.32486 kpc.
113 sources are detected at $> 5\sigma$ level within 4 Mpc of the cluster centre. These are tabulated in Table C.16. Minor artefacts are present around the brighter sources. Fig. 4.33 shows the typical RMS structure, indicating that it is smooth as expected. Fig. 4.34 shows the contours from the NVSS overlaid on the GMRT map, demonstrating that only the central bright source was detected in that These sources and all additionally detected radio sources are listed in Tab. 4.19. Of the 113 detected sources, **two** are double sources. The optical galaxies in the central region of R_{500} which are associated with the cluster are indicated in Fig. 4.34 as green circles the ones not associated are red. It is shown that none of the radio sources has an optical counterpart, possibly caused by the faintness of the optical source or no associated redshift, making it impossible to determine if it is associated with the cluster. All known optical galaxy positions are listed in Tab. B.17. The redshift range used to identify cluster members was 0.165−0.195 chosen according to Yee (1996). The cluster has a mass of $M_{500} = 8.7 \times 10^{14} M_{\odot}$ Pratt et al. (2010) and has a low central entropy Pratt et al. (2010). It is the most massive cluster in the REXCESS sample and classified as a cool core cluster Pratt et al. (2010).
There are **no** newly confirmed radio sources associated with the cluster and **seven** new cluster member candidates. Further research is needed to verify if a cluster membership is given for these candidates.

4.4.18 RXCJ1516.3+0005

This cluster is known as A2050 (Abell (1958), Abell *et al.* (1989)), an is situated at $z = 0.1181$, corresponding to an angular scale of 1 arcsec = 0.46870 kpc.
255 sources are detected at $> 5\sigma$ level within 4 Mpc of the cluster centre. These are tabulated in Table C.17.Of the 255 detected sources, **one** is extended.

Source ID	RA	Δ RA	DEC	Δ DEC	total flux	Δ total flux	Peak flux	Δ Peak flux	optical cross-ID	cluster member	comments
0	13:11:44	0.000155	-01:19:20	0.000169	0.013744	0.000463	0.003398	0.000377	✗	?	
1	13:11:43	0.000174	-01:24:02	0.000109	0.003405	0.000684	0.002751	0.000402	✗	?	
2	13:11:42	0.000028	-01:23:44	0.000024	0.011314	0.000693	0.011081	0.000397	✗	?	
2	13:11:42	0.000243	-01:23:52	0.000154	0.002057	0.000674	0.001752	0.000394	✗	?	
3	13:11:32	0.000034	-01:19:30	0.000027	0.097801	0.001532	0.024261	0.000503	✗	?	ext.
4	13:11:30	0.000037	-01:20:28	0.000029	0.0147	0.000845	0.011908	0.000518	✗	?	double
5	13:11:30	0.000151	-01:20:13	0.000083	0.004378	0.000818	0.003569	0.000489	✗	?	

Table 4.19: Positions of radio sources within R_{500} radius of the pointing centre of cluster RXCJ1311.4−0120

There is one RFI stripe present, caused by a bright source, just outside R_{500} which we were unable to remove, Fig. 4.35 shows the RMS structure in a typical region, indicating that it is smooth as expected away from the stripe.

Fig. 4.36 shows the contours from the NVSS overlaid on the GMRT map, demonstrating that only the bright source just outside of R_{500} was detected in that survey. This source and all additionally detected radio sources are listed in Tab. **??**.
The optical galaxies in the central region of R_{500} which are associated with the cluster are indicated in Fig. 4.36 as green circles. It is shown that no radio source has an optical counterpart. Additional radio sources present lack an optical cross-identification, possibly caused by the faintness of the optical source or no associated redshift, making it impossible to determine if it is associated with the cluster. All known positions of optical galaxies are provided by Tab. B.17.
The redshift range used to identify cluster members was 0.095−0.125 chosen according to Yee (1996). The cluster has a mass of $M_{500} = 3.3 \times 10^{14} M_{\odot}$ Pratt et al. (2010) and has a low to medium central entropy Pratt et al. (2010).
There are **no** newly confirmed radio sources associated with the cluster and **nine** new cluster member candidates.
Further research is needed to verify if a cluster membership is given for these candidates.

4.4.19 RXCJ1516.5−0056

This cluster is also known as Abell 2051 (Abell (1958), Abell *et al.* (1989)), and is situated at $z = 0.1198$, which corresponds to an angular scale of 1 arcsec = 0.46294 kpc.
245 sources are detected at $> 5\sigma$ level within 4 Mpc of the cluster centre. These are tabulated in Table C.18.Of the 245 detected sources, **one** is an extended and **eight** are sources.

Source ID	RA	Δ RA	DEC	Δ DEC	total flux	Δ total flux	Peak flux	Δ Peak flux	optical cross-ID	cluster member	comments
0	15:16:41	0.000084	00:03:44	0.000161	0.011629	0.00297	0.00975	0.00175	✗	?	
1	15:16:40	0.000094	00:13:24	0.000087	0.027189	0.008204	0.027666	0.004684	✗	?	
2	15:16:40	0.000112	00:12:40	0.000134	0.026013	0.006788	0.020428	0.004227	✗	?	} double
3	15:16:40	0.000112	00:12:38	0.000105	0.022385	0.006763	0.021824	0.003828	✗	?	
4	15:16:40	0.000096	00:11:55	0.000114	0.023504	0.005292	0.018795	0.003266	✗	?	
5	15:16:37	0.000098	00:07:39	0.000078	0.017622	0.00409	0.015641	0.002447	✗	?	
6	15:16:24	0.000077	00:02:11	0.000071	0.007349	0.002016	0.00791	0.001129	✗	?	
7	15:16:20	0.000156	00:03:38	0.000191	0.028771	0.003713	0.00836	0.001732	✗	?	
7	15:16:21	0.000212	00:03:42	0.000212	0.022811	0.002391	0.007788	0.001843	✗	?	
7	15:16:20	0.000319	00:03:35	0.000253	0.016061	0.002406	0.00593	0.001816	✗	?	

Table 4.20: Positions of radio sources within R_{500} radius of the pointing centre of cluster RXCJ1516.3−0005

Minor artefacts are present around the brighter sources, and there are three minor RFI stripes where the bright sources are located, which we were unable to remove. Fig. 4.37 shows the RMS structure as smooth as expected away from the stripe.
Fig. 4.38 shows the contours from the NVSS overlaid on the GMRT map, demonstrating that seven sources were detected in that survey. These sources and all additionally detected radio sources are listed in Tab. 4.21.
The optical galaxies in the central region of R_{500} which are associated with the cluster are indicated in Fig. 4.38 as green circles the ones not associated are are drawn red. It is shown that the bright source has an optical counterpart not associated with the cluster. Additional radio sources present lack an optical cross-identification, possibly causes by the faintness of the optical source or no associated redshift, making it impossible to determine if it is associated with the cluster. All known positions of optical galaxies are listed in Tab. B.
The redshift range used to identify cluster members was 0.105−0.135 chosen according to Yee (1996). The cluster has a mass of $M_{500} = 2.6\times10^{14}M_{\odot}$ Pratt et al. (2010) and has a low to medium central entropy Pratt et al. (2010). It is classified as a disturbed cluster Pratt et al. (2010).
There are **no** newly confirmed radio sources associated with the cluster and **29** new cluster member candidates.
Further research is needed to verify if a cluster membership is given for these candidates.

Source ID	RA	Δ RA	DEC	Δ DEC	total flux	Δ total flux	Peak flux	Δ Peak flux	optical cross-ID	cluster member	comments
1	15:17:02	0.000234	-01:00:17	0.000076	0.008519	0.000463	0.00168	0.000234	✗	?	
2	15:16:53	0.000137	00:54:41	0.000087	0.001767	0.000409	0.001653	0.000236	✗	?	
3	15:16:52	0.000049	00:54:10	0.000028	0.007026	0.000683	0.00714	0.000387	✗	?	
4	15:16:44	0.000077	00:58:07	0.000037	0.013766	0.000484	0.006702	0.000339	✗	?	
5	15:16:41	0.000204	00:57:60	0.000091	0.001244	0.000408	0.001248	0.000224	✗	?	
6	15:16:40	0.000179	00:57:45	0.00008	0.001536	0.000499	0.001598	0.000274	✗	?	
7	15:16:40	0.000039	00:57:28	0.000023	0.009391	0.000555	0.008159	0.000332	✗	?	
8	15:16:39	0.000315	00:56:35	0.000109	0.00339	0.000393	0.001524	0.000279	✗	?	
9	15:16:32	0.000164	00:54:42	0.000139	0.001303	0.000395	0.001201	0.00023	✗	?	
9	15:16:33	0.000183	00:54:45	0.000138	0.001157	0.000396	0.001065	0.000233	✗	?	
10	15:16:31	0.000121	00:55:55	0.000078	0.003047	0.000624	0.002732	0.000371	✗	?	
11	15:16:31	0.000157	00:53:29	0.000067	0.002245	0.000443	0.001903	0.000262	✗	?	
12	15:16:31	0.000088	00:56:56	0.000053	0.002575	0.000642	0.003172	0.000337	✗	?	
13	15:16:31	0.000159	00:58:08	0.000092	0.0026	0.00045	0.001947	0.000279	✗	?	
14	15:16:31	0.000101	00:56:43	0.000043	0.007786	0.000923	0.006609	0.000538	✗	?	
15	15:16:30	0.000024	00:56:25	0.000015	0.033209	0.001265	0.029011	0.000755			
15	15:16:30	0.000124	00:56:33	0.000042	0.004025	0.001319	0.005327	0.000651	✔	✗	extended
15	15:16:31	0.000173	00:56:20	0.000118	0.003579	0.001284	0.003547	0.000738			
16	15:16:30	0.00012	00:52:16	0.000051	0.001166	0.000401	0.001534	0.000202	✗	?	
17	15:16:30	0.000188	00:53:06	0.000087	0.001515	0.00051	0.001536	0.000284	✗	?	
18	15:16:29	0.000259	00:56:48	0.000102	0.003111	0.000735	0.002269	0.000455	✗	?	
19	15:16:29	0.000169	00:52:42	0.000097	0.001288	0.000411	0.001266	0.000235	✗	?	
20	15:16:28	0.000209	00:57:34	0.000147	0.002849	0.000412	0.001541	0.000284	✗	?	
21	15:16:25	0.000173	00:50:18	0.000111	0.005573	0.001418	0.004673	0.000858	✗	?	
21	15:16:25	0.000258	00:50:21	0.000193	0.003693	0.001414	0.003048	0.000858	✗	?	
23	15:16:24	0.000042	00:49:47	0.000031	0.094981	0.002762	0.050158	0.001922	✗	?	
23	15:16:24	0.000058	00:49:49	0.000043	0.054643	0.002853	0.033268	0.00191	✗	?	
25	15:16:23	0.000188	00:53:01	0.000082	0.005062	0.000676	0.003101	0.000445	✗	?	
26	15:16:23	0.000212	00:58:05	0.000139	0.001786	0.000412	0.001249	0.000264	✗	?	
28	15:16:20	0.000144	-01:01:51	0.000127	0.000954	0.000273	0.000891	0.000159	✗	?	
28	15:16:19	0.000162	-01:01:49	0.000192	0.000571	0.000277	0.000608	0.000154	✗	?	
29	15:16:16	0.000073	00:50:06	0.000045	0.006014	0.000628	0.005024	0.000381	✗	?	

Table 4.21: Positions of radio sources within R_{500} radius of the pointing centre of cluster RXCJ1516.5−0056

4.4.20 RXCJ2014.8−2430

This cluster is situated at $z = 0.1612$, corresponding to an angular scale of 1 arcsec = 0.37463 kpc.

64 sources are detected at $> 5\sigma$ level within 4 Mpc of the cluster centre. These are tabulated in Table C.19.Of the 64 detected sources, none are extended.

Minor artefacts are present around the bright source, and there is a smooth background as expected away from brighter sources, as Fig. 4.39 indicates.

Fig. 4.40 shows the contours from the NVSS overlaid on the GMRT map, demonstrating that only the central source was detected in that survey. This source and all additionally detected radio sources are listed in Tab. 4.22.

The optical galaxies in the central region of R_{500} which are associated with the cluster are indicated in Fig. 4.40 as green circles the ones not associated are indicated by red ones. It is shown that the bright source has an optical counterpart, Additional radio sources present lacking an optical cross-identification, possibly caused by the faintness of the optical source or no associated redshift, making it impossible to determine if it is associated with the cluster. All known optical galaxy positions are listed in Tab. B.20.

The redshift range used to identify cluster members was $0.145 - 0.175$ chosen according to Yee (1996).

There is **one** newly confirmed radio source associated with the cluster and **five** new cluster member candidates.

Further research is needed to verify if a cluster membership is given for these candidates. This cluster is rather interesting, as it shows large scale gas sloshing Walker et al. (2014) and is the strongest cool core cluster in the REXCESS sample Haarsma et al. (2010). It is massive with $M_{500} = 5.4 \times 10^{14} M_{\odot}$ from Pratt et al. (2010) and has a very low central entropy Pratt et al. (2010).

4.4.21 RXCJ2023.0−2056

This cluster is known as S0868 (Abell *et al.* (1989)), an is situated at $z = 0.0564$, corresponding to an angular scale of 1 arcsec = 0.91382 kpc.

Source ID	RA	Δ RA	DEC	Δ DEC	total flux	Δ total flux	Peak flux	Δ Peak flux	optical cross-ID	cluster member	comments
0	20:15:16	0.00014	-24:30:11	0.00011	0.017534	0.002025	0.011534	0.001328	✗	?	} double
0	20:15:16	0.00016	-24:30:02	0.000234	0.00978	0.00205	0.007105	0.001297	✗	?	
1	20:15:03	0.000123	-24:34:01	0.000224	0.005925	0.001939	0.005957	0.001092	✗	?	
2	20:15:02	0.00023	-24:33:05	0.00022	0.00821	0.002339	0.007196	0.001349	✗	?	
3	20:14:54	0.000138	-24:30:28	0.000214	0.019582	0.006819	0.02035	0.003801	✗	?	
4	20:14:52	0.000023	-24:30:23	0.000016	0.49117	0.013374	0.410638	0.00814	✔	✔	BCG

Table 4.22: Positions of radio sources within R_{500} radius of the pointing centre of cluster RXCJ2014.8−2430

346 sources are detected at $> 5\sigma$ level within 4 Mpc of the cluster centre. These are tabulated in Table C.20.Of the 346 detected sources, **two** are extended.
Minor artefacts are present around the brighter sources, and there is a smooth background as expected away from brighter sources, as Fig. 4.41 indicates.
Fig. 4.42 shows the contours from the NVSS overlaid on the GMRT map, demonstrating that three sources were detected in that survey. These sources and all additionally detected radio sources are listed in Tab. 4.23.
The optical galaxies in the central region of R_{500} which are associated with the cluster are indicated in Fig. 4.42 as green circles the ones not associated are indicated by red circles. It is shown that the bright central source and one additional radio source have an optical counterpart. All additional radio sources present lack an optical cross-identification, possibly caused by the faintness of the optical source or no associated redshift, making it impossible to determine if it is associated with the cluster. All optical galaxy positions are provided in Tab. B.21.
The redshift range used to identify cluster members was $0.045-0.075$ chosen according to Yee (1996). The cluster has a mass of $M_{500} = 1.2 \times 10^{14} M_{\odot}$ Pratt et al. (2010) and has a low central entropy Pratt et al. (2010). It is classified as a disturbed cluster and is the least massive cluster in the REXCESS sample Pratt et al. (2010).
There is **one** newly confirmed radio source associated with the cluster and **32** new cluster member candidates.
Further research is needed to verify if a cluster membership is given for these candidates.

4.4.22 RXCJ2048.1−1750

This cluster is known as A2328 (Abell (1958), Abell *et al.* (1989)), an is situated at $z = 0.1475$, corresponding to an angular scale of 1 arcsec = 0.38790 kpc.
88 sources are detected at $> 5\sigma$ level within 4 Mpc of the cluster centre. These are tabulated in Table C.21.Of the 88 detected sources, **five** are extended.
There is a smooth background present throughout the whole map, which is shown in Fig. 4.43.
Fig. 4.44 shows the contours from the NVSS overlaid on the GMRT map, demonstrating that five sources were detected in that survey. The optical galaxies in the central region of R_{500} which are associated with the cluster are indicated in Fig. 4.44 as green circles. It is shown that one source has an optical counterpart. All additional radio sources present have no optical cross-identification, possibly caused by the faintness of the optical source or no associated redshift, making it impossible to

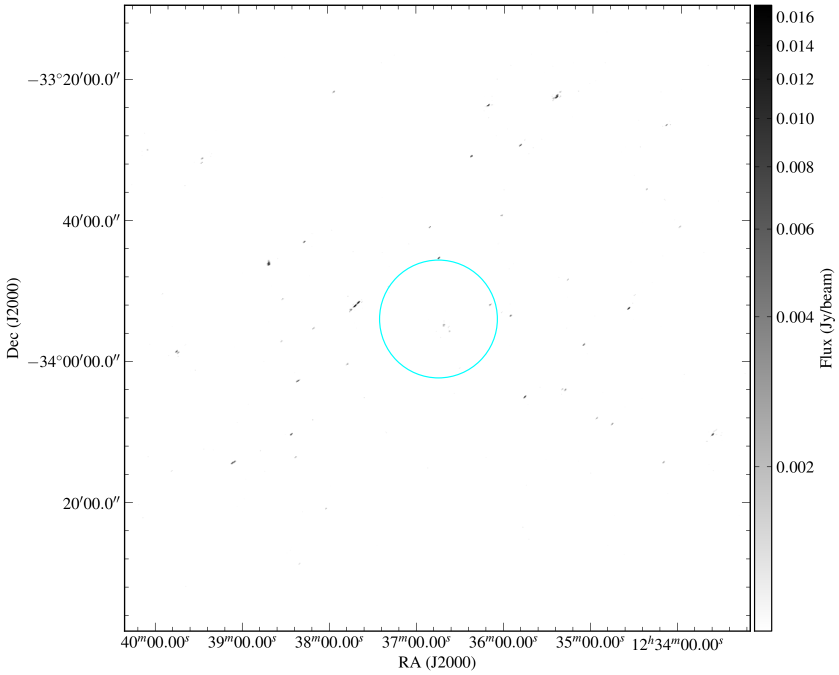

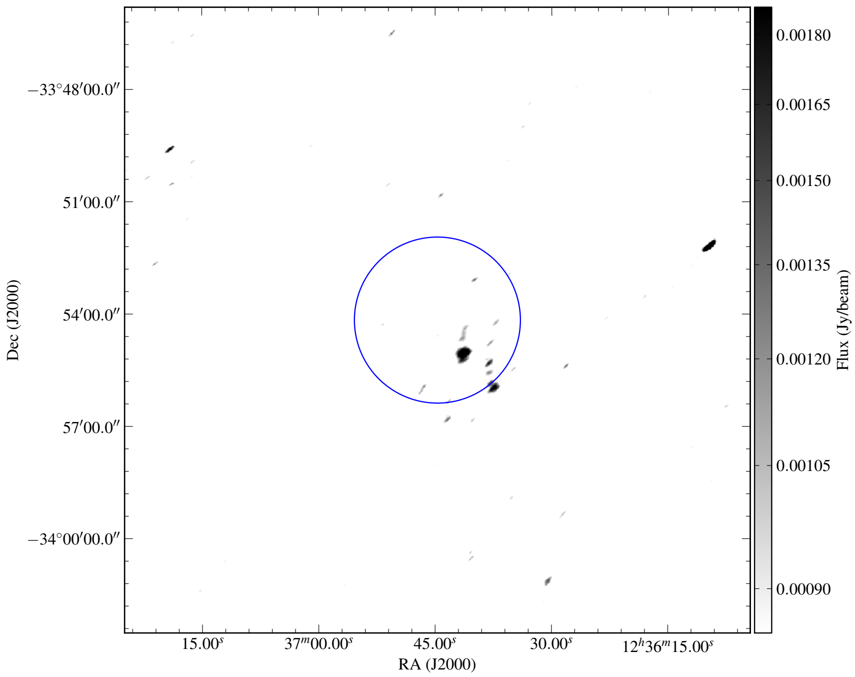

Figure 4.29: 610-MHz GMRT maps of RXCJ1236.7−3354. Top: overview of a region 4 Mpc × 4 Mpc centred on the cluster, R_{500} being indicated by the circle; bottom: central region of the cluster ($R_{500} \times R_{500}$)the circle indicates a region of radius 200kpc around the centre.

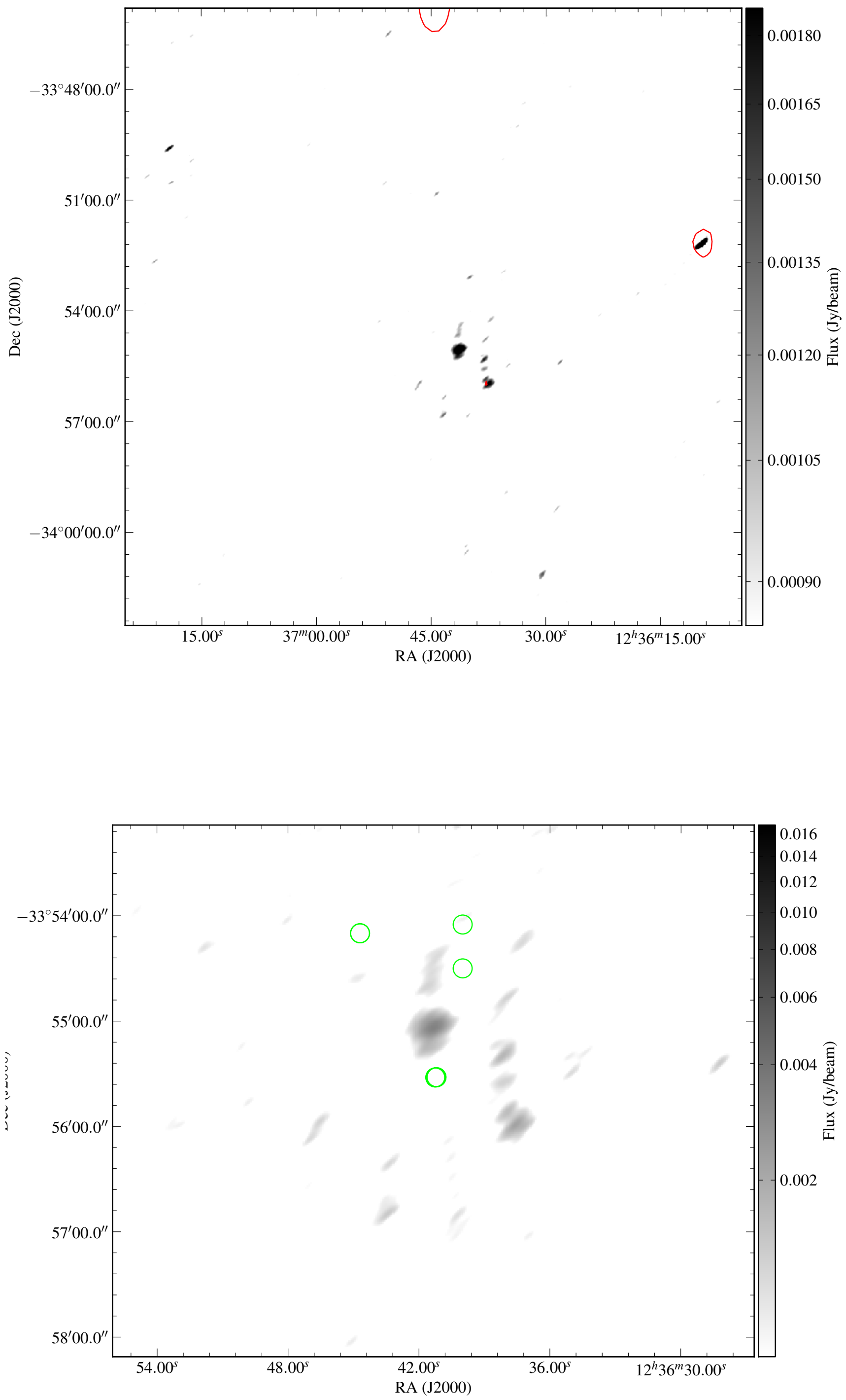

Figure 4.30: 610-MHz GMRT maps of RXCJ1236.7−3354. central region of the cluster ($R_{500} \times R_{500}$); top: contours from SUMSS overlaid; bottom: positions of known cluster member galaxies overlaid in green and known background or foreground sources indicated by red circles.

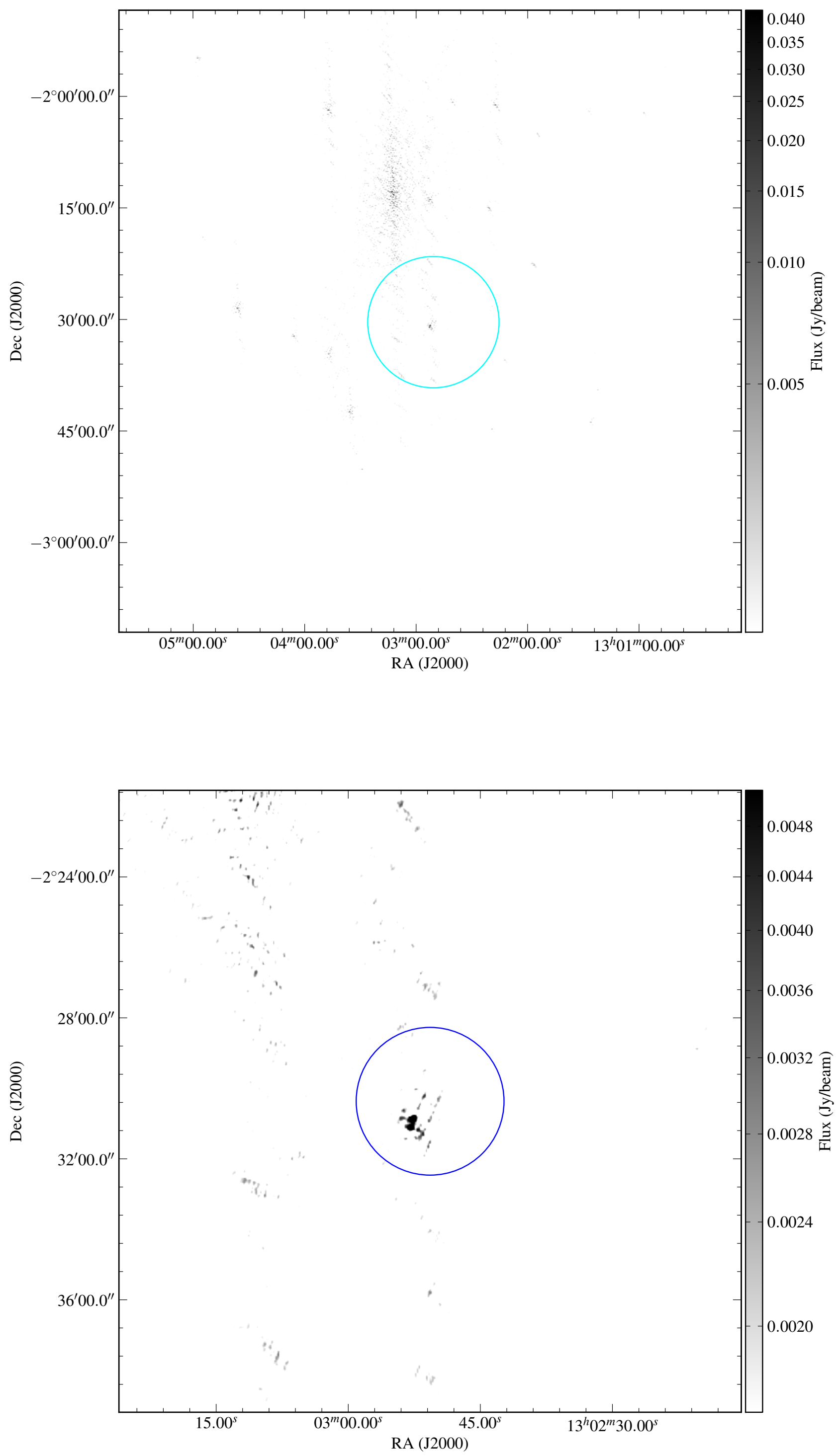

Figure 4.31: 610-MHz GMRT maps of RXCJ1302.8−0230. Top: overview of a region 4 Mpc $\times$ 4 Mpc centred on the cluster, R_{500} being indicated by the circle; bottom: central region of the cluster ($R_{500} \times R_{500}$)the circle indicates a region of radius 200kpc around the centre.

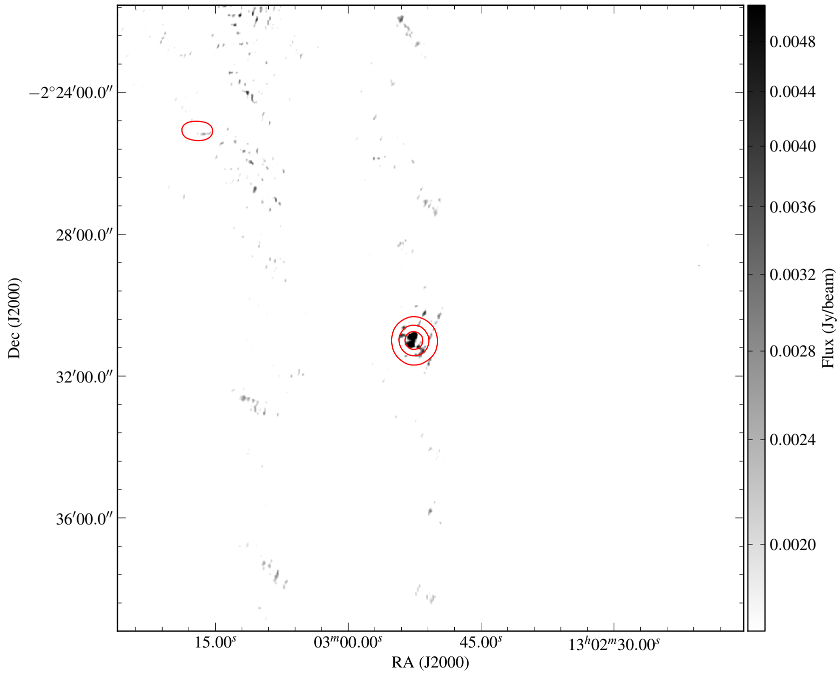

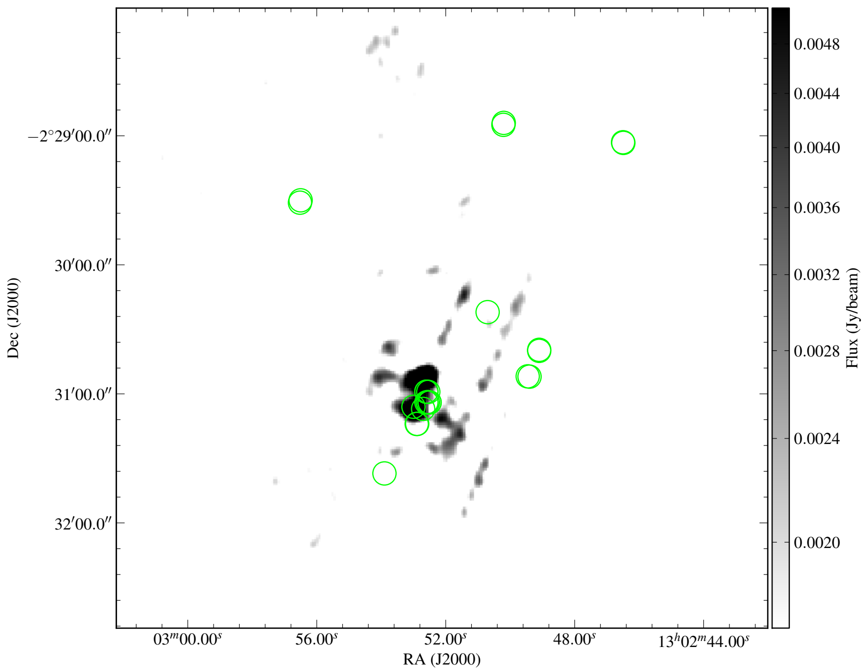

Figure 4.32: 610-MHz GMRT maps of RXCJ1302.8−0230. central region of the cluster ($R_{500} \times R_{500}$); top: contours from NVSS overlaid; bottom: positions of known cluster member galaxies overlaid in green and known background or foreground sources indicated by red circles.

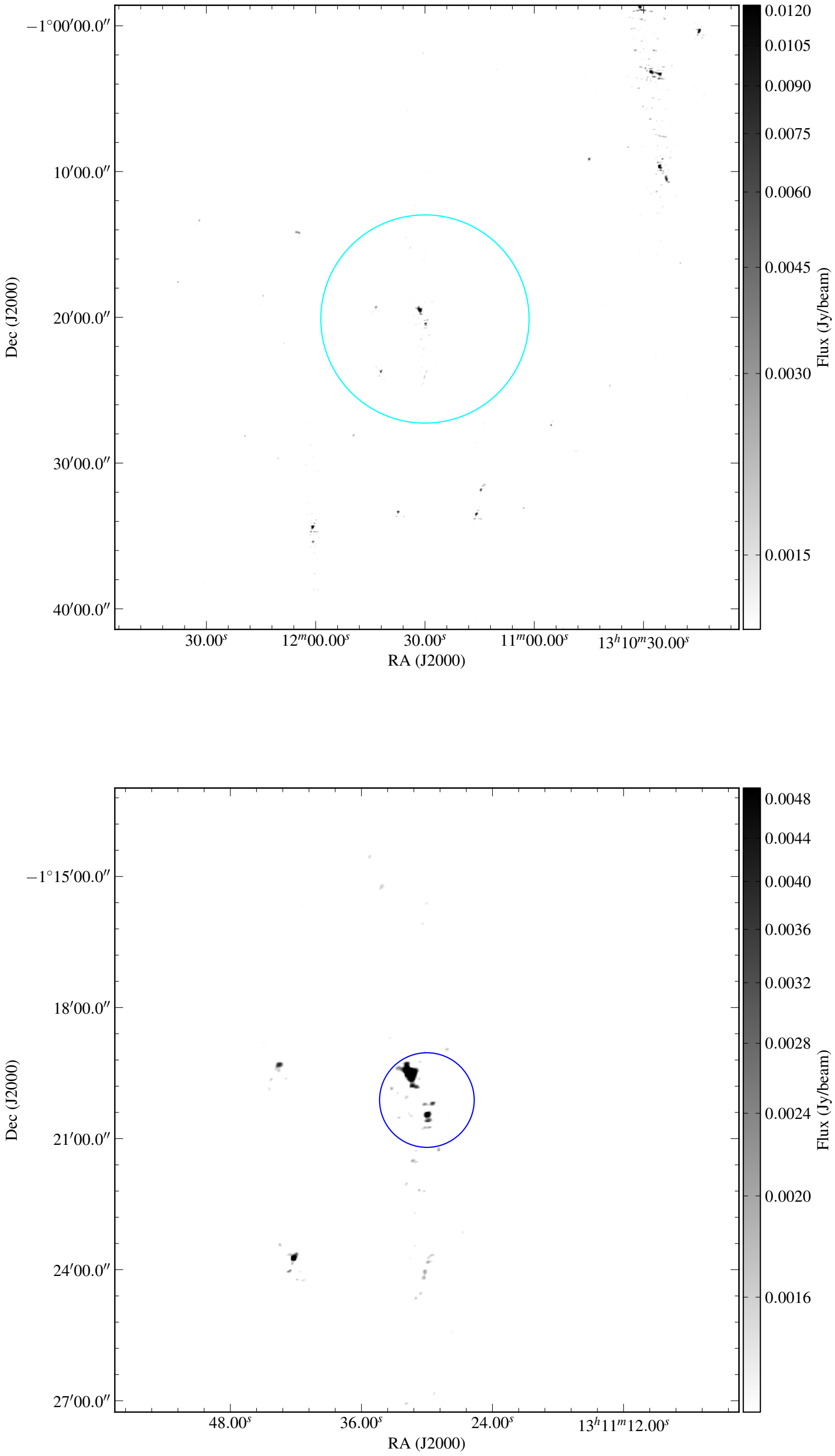

Figure 4.33: 610-MHz GMRT maps of RXCJ1311.4−0120. Top: overview of a region 4 Mpc × 4 Mpc centred on the cluster, R_{500} being indicated by the circle; bottom: central region of the cluster ($R_{500} \times R_{500}$)the circle indicates a region of radius 200kpc around the centre.

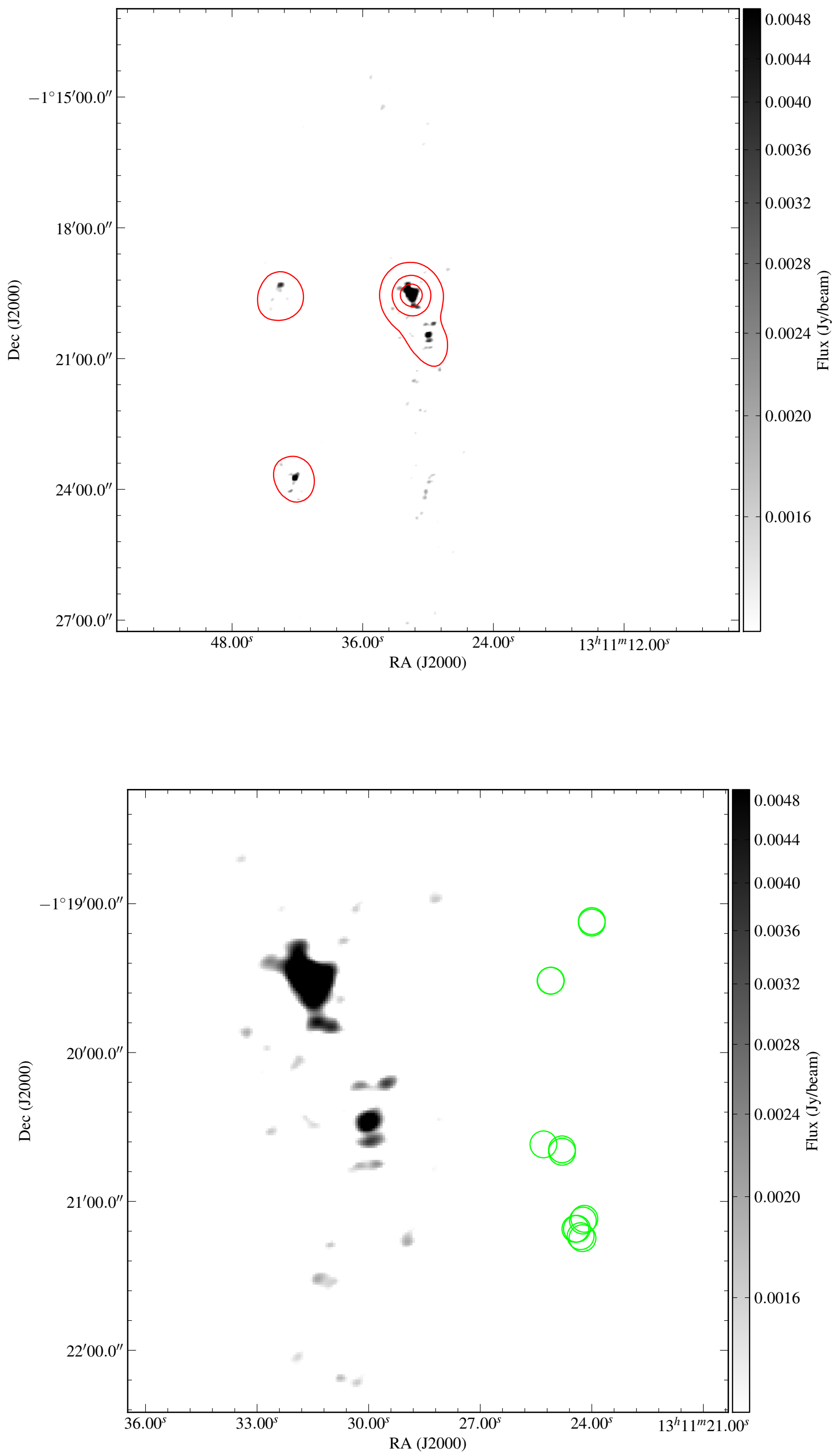

Figure 4.34: 610-MHz GMRT maps of RXCJ1311.4−0120. central region of the cluster ($R_{500} \times R_{500}$); top: contours from NVSS overlaid; bottom: positions of known cluster member galaxies overlaid in green.

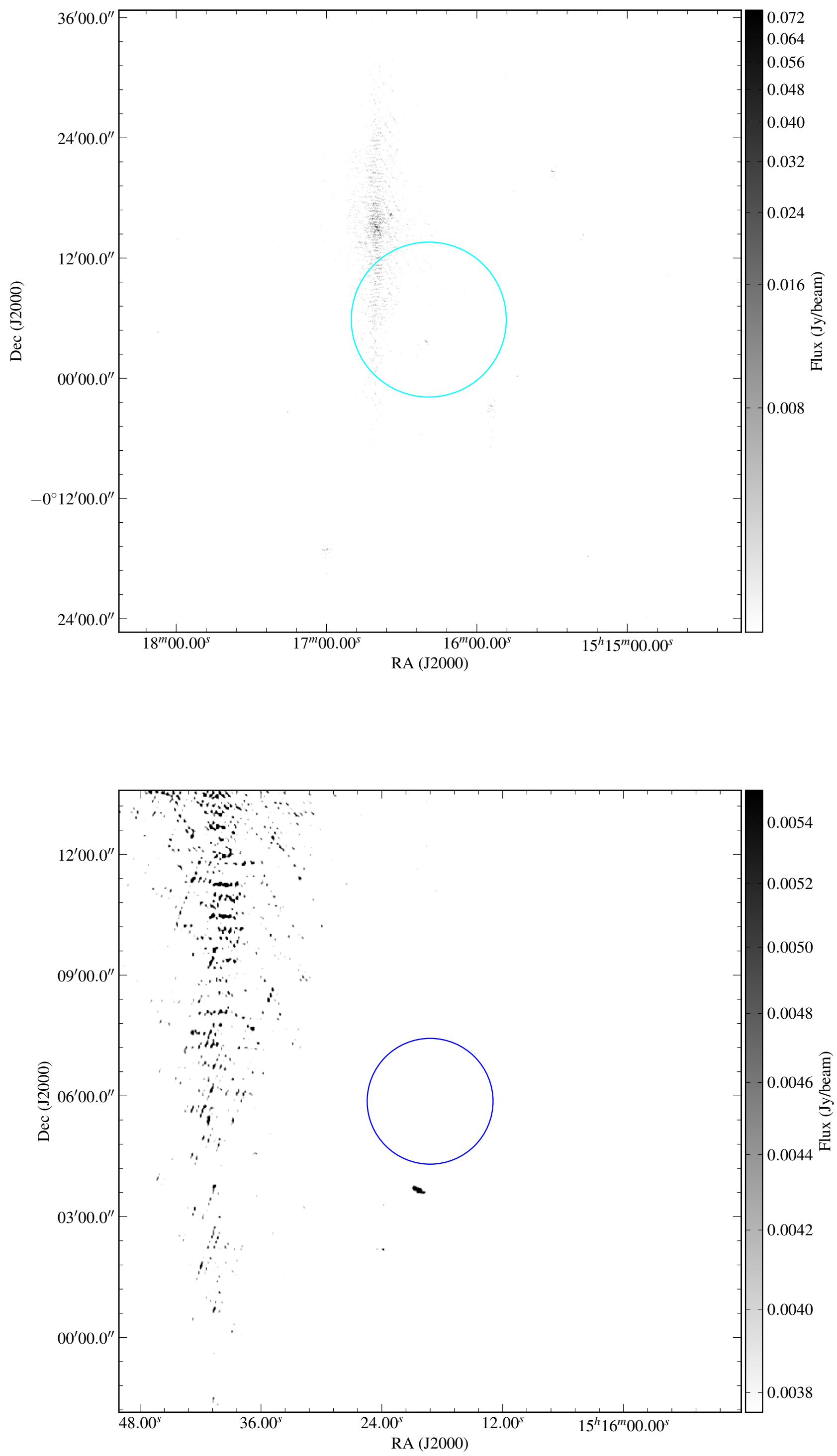

Figure 4.35: 610-MHz GMRT maps of RXCJ1516.3+0005. Top: overview of a region 4 Mpc $\times$ 4 Mpc centred on the cluster, R_{500} being indicated by the circle; bottom: central region of the cluster ($R_{500} \times R_{500}$)the circle indicates a region of radius 200kpc around the centre.

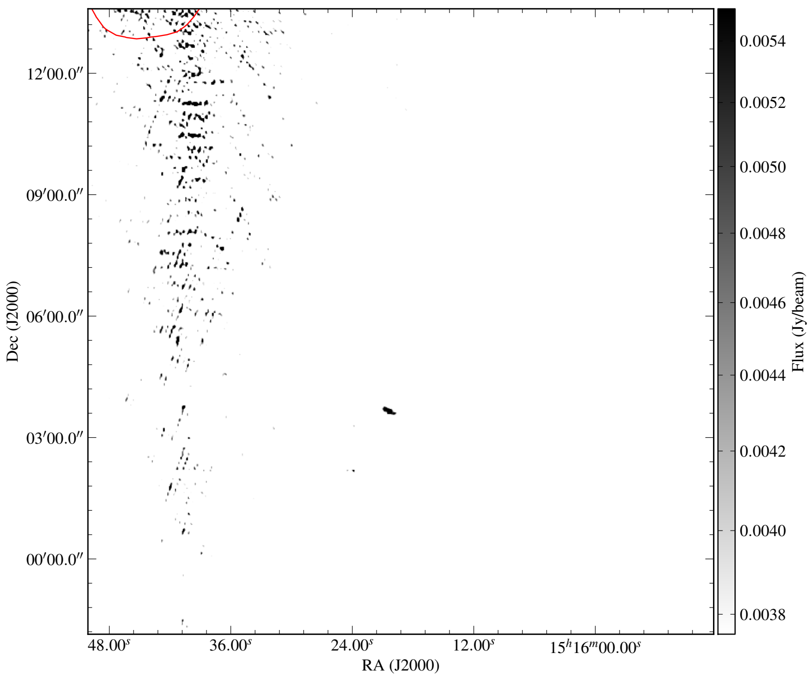

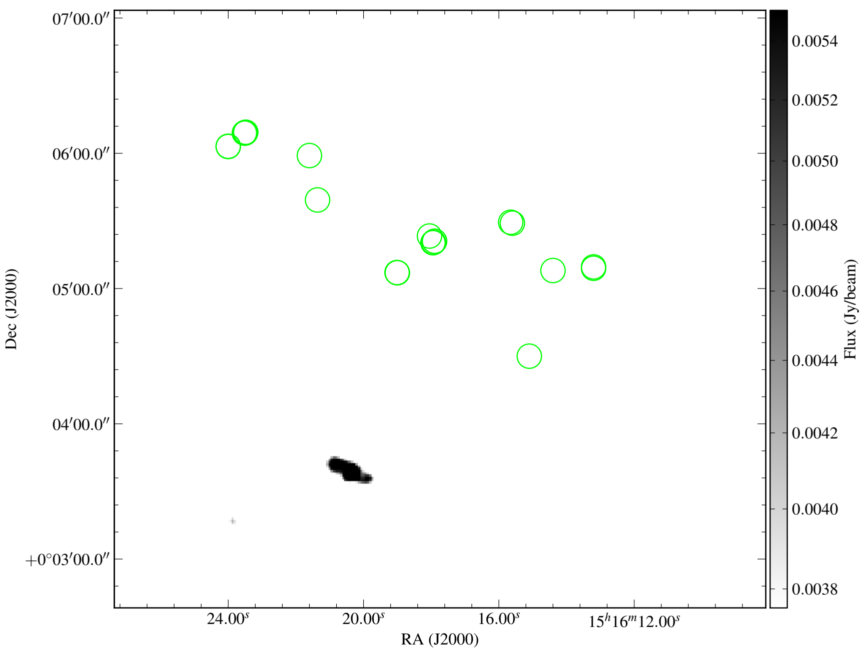

Figure 4.36: 610-MHz GMRT maps of RXCJ1516.3+0005. central region of the cluster ($R_{500} \times R_{500}$); top: contours from NVSS overlaid; bottom: positions of known cluster member galaxies overlaid in green.

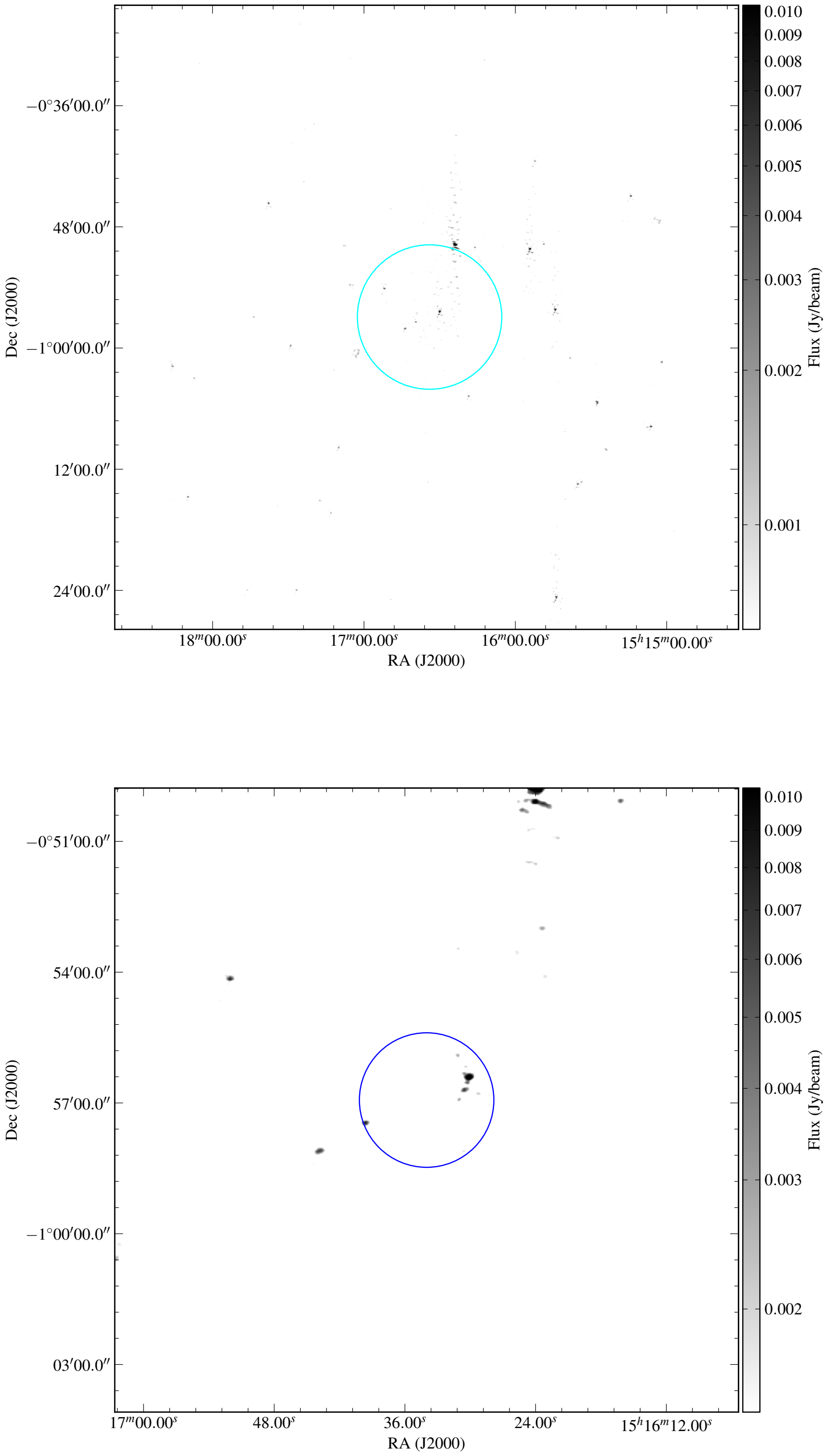

Figure 4.37: 610-MHz GMRT maps of RXCJ1516.5−0056. Top: overview of a region 4 Mpc $\times$ 4 Mpc centred on the cluster, R_{500} being indicated by the circle; bottom: central region of the cluster ($R_{500} \times R_{500}$)the circle indicates a region of radius 200kpc around the centre.

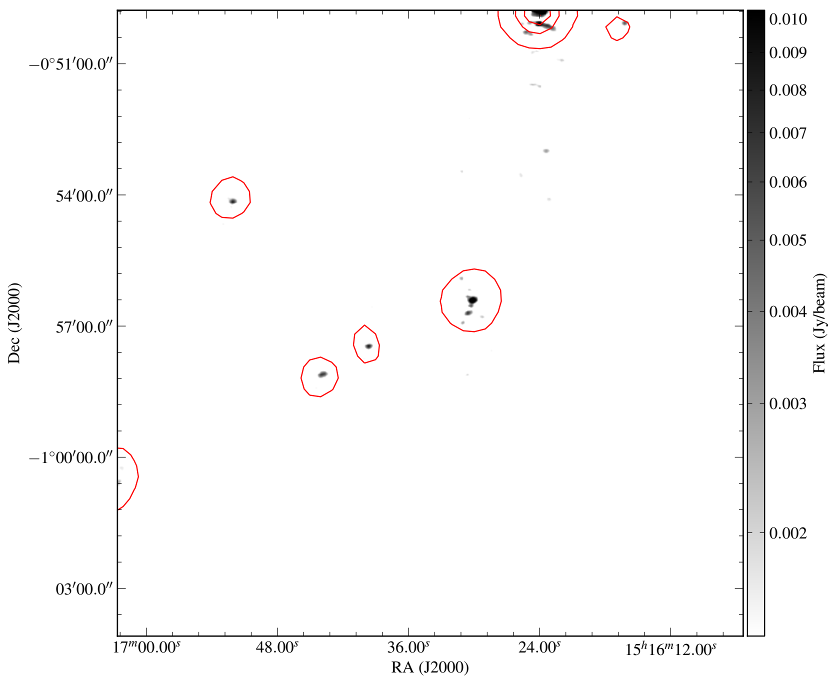

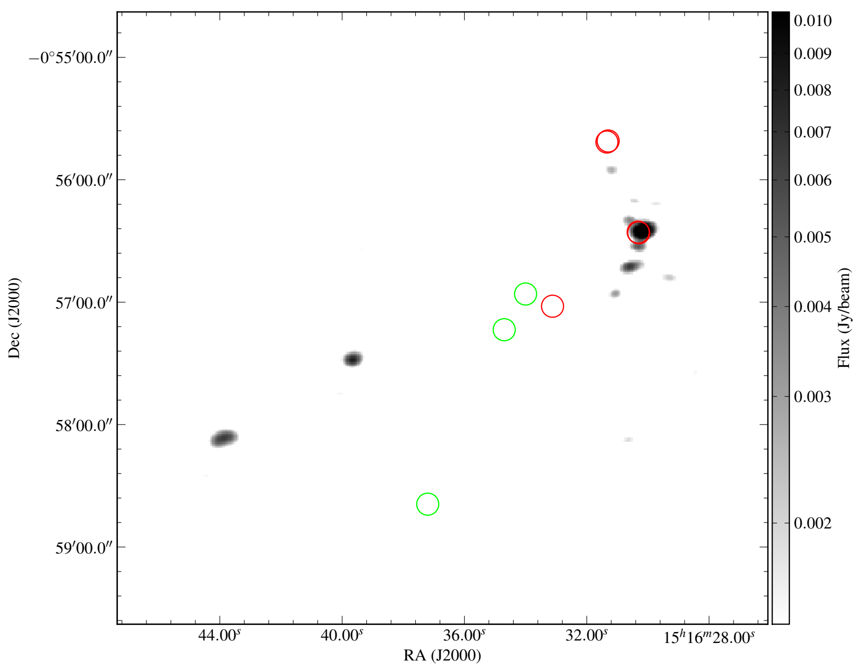

Figure 4.38: 610-MHz GMRT maps of RXCJ1516.5−0056. central region of the cluster ($R_{500} \times R_{500}$); top: contours from NVSS overlaid; bottom: positions of known cluster member galaxies overlaid in green and known background or foreground sources indicated by red circles.

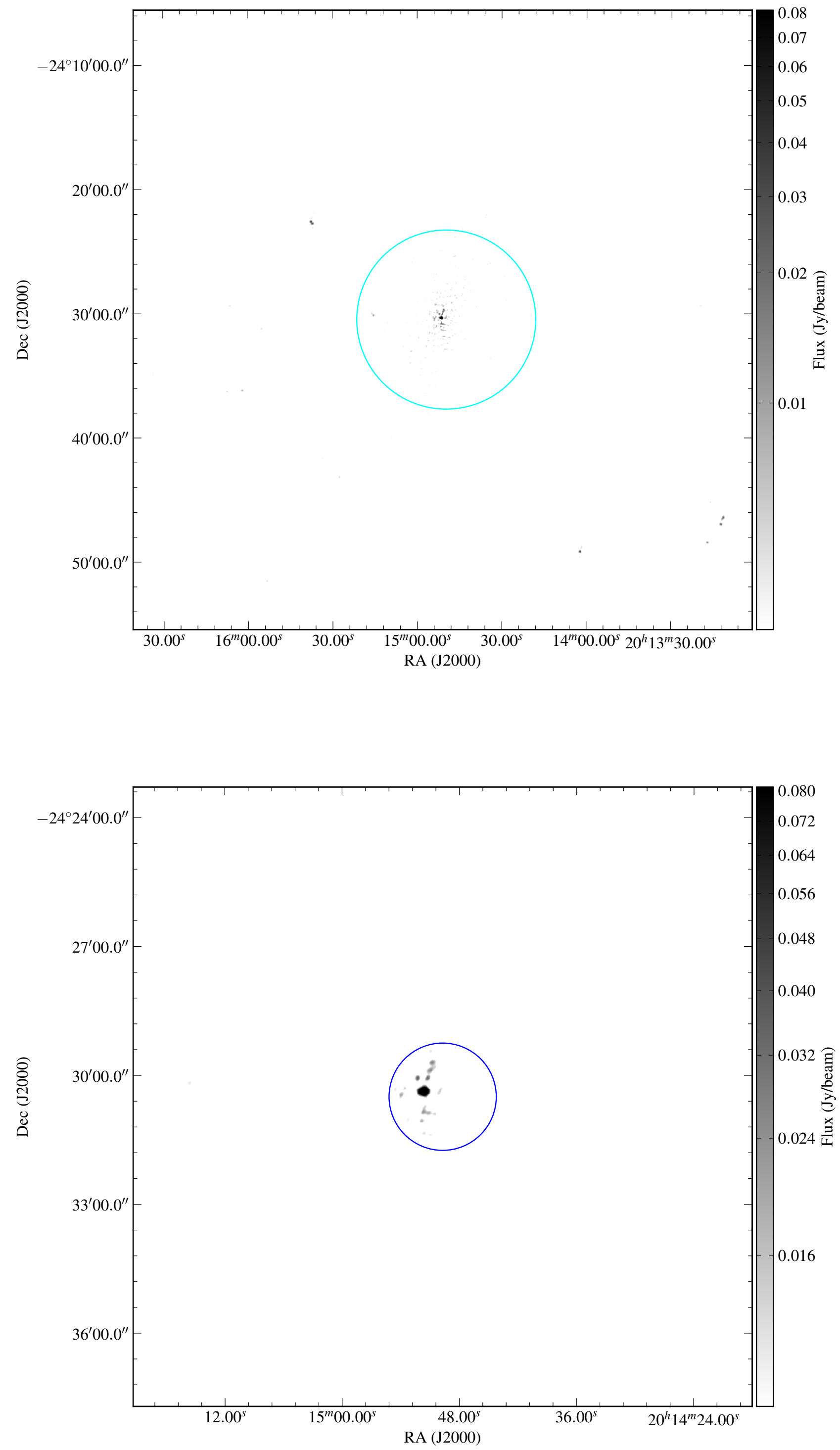

Figure 4.39: 610-MHz GMRT maps of RXCJ2014.8−2430. Top: overview of a region 4 Mpc $\times$ 4 Mpc centred on the cluster, R_{500} being indicated by the circle; bottom: central region of the cluster ($R_{500} \times R_{500}$)the circle indicates a region of radius 200kpc around the centre.

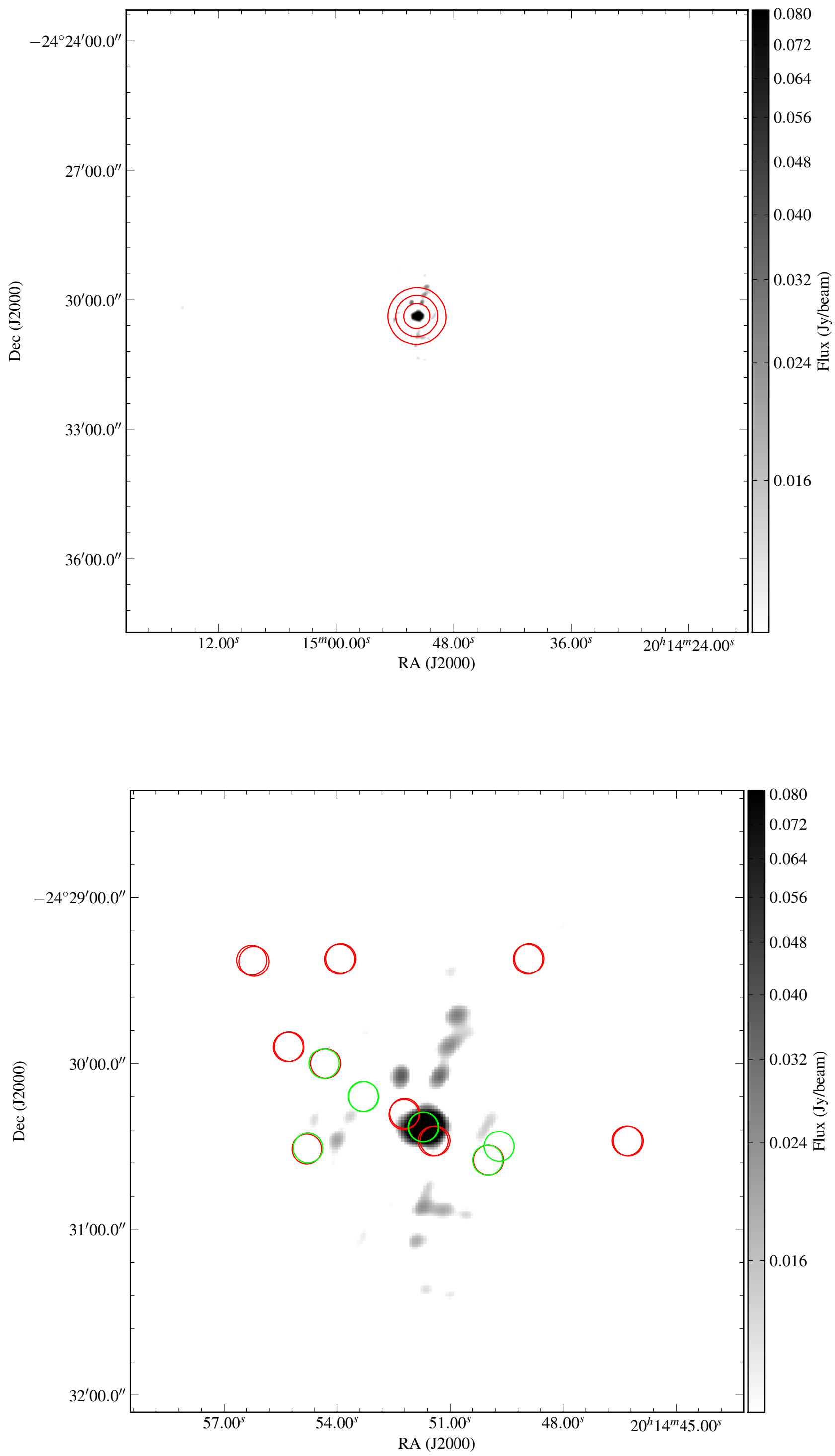

Figure 4.40: 610-MHz GMRT maps of RXCJ2014.8−2430. central region of the cluster ($R_{500} \times R_{500}$); top: contours from NVSS overlaid; bottom: positions of known cluster member galaxies overlaid in green and known background or foreground sources indicated by red circles.

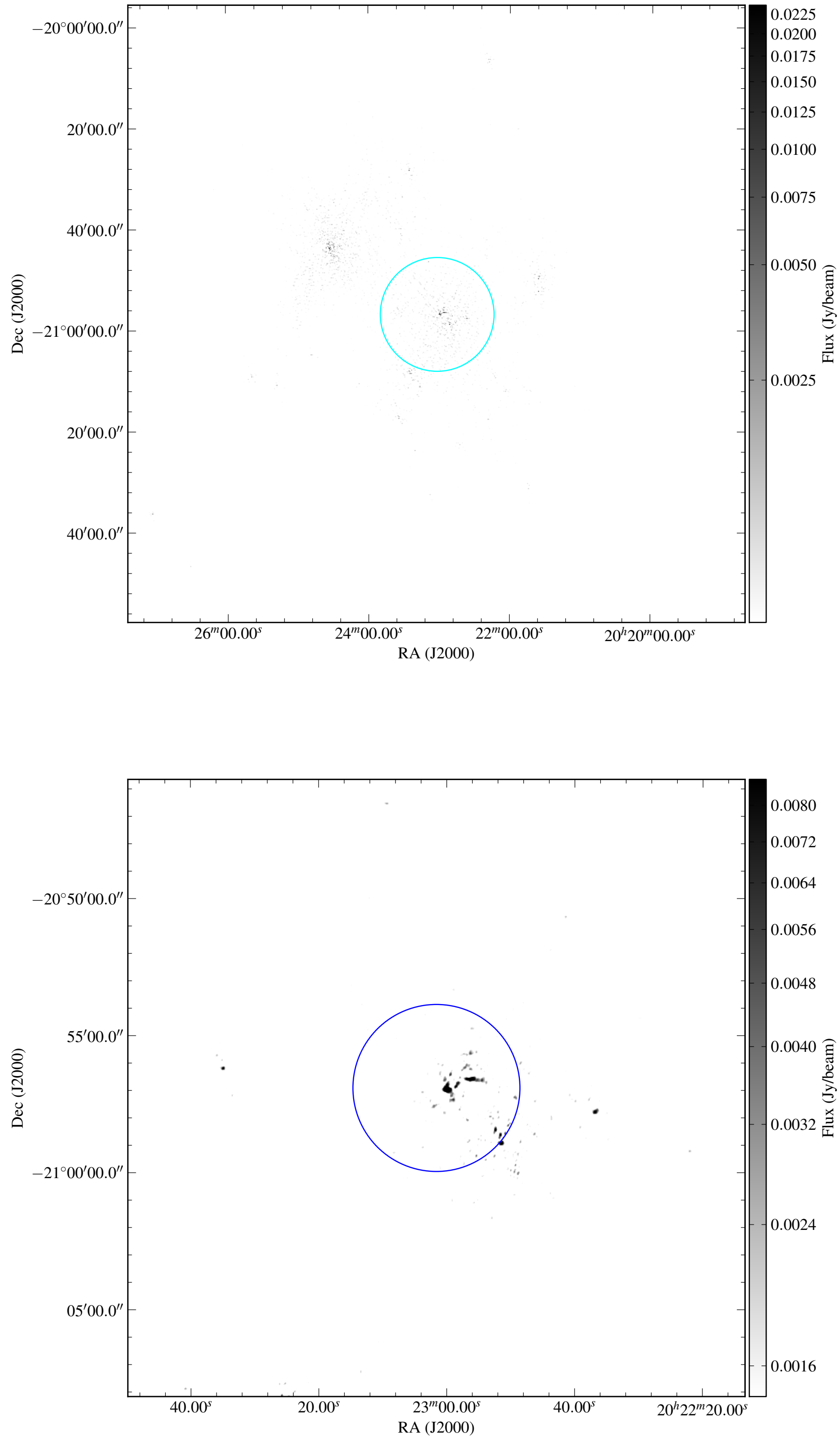

Figure 4.41: 610-MHz GMRT maps of RXCJ2023.0−2056. Top: overview of a region 4 Mpc $\times$ 4 Mpc centred on the cluster, R_{500} being indicated by the circle; bottom: central region of the cluster ($R_{500} \times R_{500}$)the circle indicates a region of radius 200kpc around the centre.

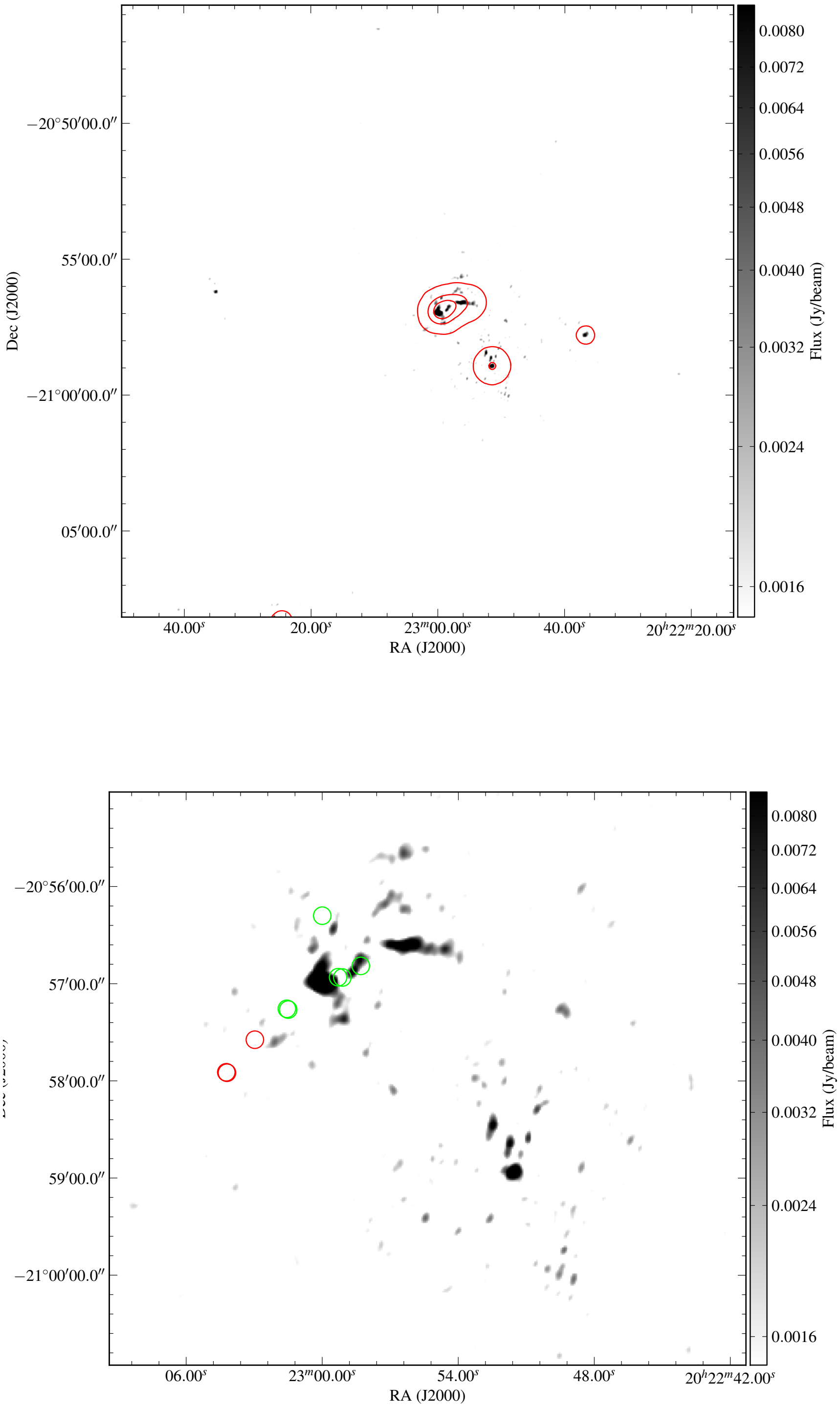

Figure 4.42: 610-MHz GMRT maps of RXCJ2023.0−2056. central region of the cluster ($R_{500} \times R_{500}$); top: contours from NVSS overlaid; bottom: positions of known cluster member galaxies overlaid in green and known background or foreground sources indicated by red circles.

determine if it is associated with the cluster. All known optical galaxy positions are provided in Tab. B.22.
The redshift range used to identify cluster members was 0.125−0.155 chosen according to Yee (1996). The cluster has a mass of $M_{500} = 4.3 \times 10^{14} M_{\odot}$ Pratt et al. (2010) and has a medium to high central entropy Pratt et al. (2010). It is classified as a disturbed cluster Pratt et al. (2010). According to Haarsma et al. (2010) it is one of the most disturbed clusters of the REXCESS sample and has a large offset between BCG and X-ray peak and mazbe therefore be misidentified, unless unlikely. This cluster shows the most diffuse X-ray emission and the longest cooling time, making it possible the gas is not in hydrostatic equilibrium Haarsma et al. (2010).
There is **one** newly confirmed radio source associated with the cluster and **no** new cluster member candidates.
Further research is needed to verify if a cluster membership is given for these candidates.

4.4.23 RXCJ2149.1−3041

This cluster is known as A3814 (Abell (1958), Abell *et al.* (1989)), an is situated at $z = 0.1184$, corresponding to an angular scale of 1 arcsec = 0.46768 kpc.
44 sources are detected at $> 5\sigma$ level within 4 Mpc of the cluster centre. These are

Source ID	RA	Δ RA	DEC	Δ DEC	total flux	Δ total flux	Peak flux	Δ Peak flux	optical cross-ID	cluster member	comments
0	20:23:41	0.000168	-21:07:53	0.000112	0.004866	0.000757	0.002829	0.000512	✗	?	
1	20:23:36	0.000089	-20:55:45	0.000169	0.003038	0.000816	0.002613	0.000482	✗	?	
2	20:23:35	0.00004	-20:56:13	0.000034	0.013345	0.000848	0.00988	0.000538	✗	?	
3	20:23:33	0.000126	-20:57:12	0.000196	0.003033	0.000648	0.002161	0.000401	✗	?	
5	20:23:24	0.000087	-21:07:59	0.000111	0.002203	0.000944	0.002924	0.000469	✗	?	
6	20:23:09	0.000181	-20:46:35	0.000066	0.007176	0.000459	0.002861	0.000337	✗	?	
7	20:23:02	0.000273	-20:57:36	0.000224	0.011896	0.001067	0.003926	0.00082	✗	?	
8	20:22:60	0.000076	-20:56:59	0.000072	0.252156	0.003169	0.036144	0.002183	✔	✔	BCG
9	20:22:60	0.000098	-20:56:27	0.000187	0.008018	0.002225	0.006786	0.00131	✗	?	
10	20:22:59	0.000251	-20:57:22	0.000116	0.018099	0.001449	0.006359	0.001101	✗	?	
11	20:22:59	0.000097	-20:56:53	0.00013	0.014213	0.00297	0.011586	0.001789	✗	?	double
11	20:22:58	0.000158	-20:56:46	0.000181	0.014968	0.002816	0.008826	0.001896	✗	?	
12	20:22:56	0.000219	-20:56:37	0.000049	0.095242	0.001658	0.017956	0.001398	✗	?	ext.
13	20:22:56	0.000155	-20:55:40	0.000178	0.015027	0.001014	0.004835	0.000791	✗	?	
14	20:22:55	0.000078	-20:59:25	0.000134	0.004559	0.001199	0.004286	0.00069	✗	?	
15	20:22:55	0.000147	-20:56:39	0.000135	0.013837	0.001618	0.006763	0.001149	✗	?	
16	20:22:52	0.000052	-20:58:28	0.000147	0.017835	0.001526	0.010146	0.000997	✗	?	
17	20:22:52	0.000014	-20:58:56	0.000017	0.050357	0.00173	0.043271	0.001045	✗	?	
18	20:22:52	0.000052	-20:58:39	0.00011	0.010824	0.002022	0.009822	0.00117	✗	?	
18	20:22:52	0.000107	-20:58:45	0.000162	0.004295	0.002074	0.00477	0.001146	✗	?	
19	20:22:51	0.000058	-20:58:35	0.00014	0.005764	0.001984	0.006553	0.001049	✗	?	double
20	20:22:51	0.000094	-20:58:18	0.000132	0.005148	0.001679	0.005508	0.000905	✗	?	
22	20:22:49	0.000093	-20:57:17	0.000101	0.010135	0.001353	0.004062	0.000582	✗	?	
23	20:22:49	0.000076	-20:59:45	0.00012	0.003611	0.001263	0.004209	0.000668	✗	?	
24	20:22:49	0.000138	-21:00:03	0.000208	0.007458	0.001039	0.004011	0.000703	✗	?	
25	20:22:49	0.000169	-20:56:02	0.000209	0.00506	0.000847	0.002932	0.000558	✗	?	
26	20:22:46	0.000107	-20:58:37	0.000175	0.003682	0.00101	0.003253	0.000577	✗	?	
27	20:22:46	0.000113	-20:57:25	0.000167	0.002881	0.000752	0.002277	0.000463	✗	?	
28	20:22:44	0.000087	-21:02:46	0.000228	0.002408	0.000517	0.001636	0.000327	✗	?	
29	20:22:42	0.000176	-20:50:42	0.000135	0.004774	0.000631	0.002366	0.000447	✗	?	
30	20:22:39	0.000091	-20:58:22	0.000215	0.003883	0.000651	0.002358	0.000427	✗	?	
31	20:22:37	0.000073	-20:57:48	0.000063	0.029965	0.000795	0.010003	0.000612	✗	?	
33	20:22:22	0.00013	-20:59:14	0.000093	0.003993	0.000591	0.002559	0.00039	✗	?	

Table 4.23: Positions of radio sources within R_{500} radius of the pointing centre of cluster RXCJ2023.0−2056

tabulated in Table C.22.Of the 44 detected sources, **eight** are extended and **four** are double sources.

Minor artefacts are present around the brighter sources, and there is a smooth background as expected away from brighter sources, as Fig. 4.45 indicates.

Fig. 4.46 shows the contours from the SUMSS overlaid on the GMRT map, demonstrating that two sources were detected in that survey. These sources and all additionally detected radio sources are listed in Tab. 4.24. One of them being a triple source.

The optical galaxies in the central region of R_{500} which are associated with the cluster are indicated in Fig. 4.46 as green circles the ones not associated are indicates by red circles. It is shown that the central source has an optical counterpart. All additional radio sources present have no optical cross-identification, possibly caused by the faintness of the optical source or no associated redshift, making it impossible to determine if it is associated with the cluster. All known positions of optical galaxies are provided in Tab. B.23.

The redshift range used to identify cluster members was $0.095-0.125$ chosen according to Yee (1996). The cluster has a mass of $M_{500} = 2.3 \times 10^{14} M_{\odot}$ Pratt et al. (2010) and has a very low central entropy Pratt et al. (2010). It is classified as a cool core cluster Pratt et al. (2010).

There are **no** newly confirmed radio sources associated with the cluster and **two** new cluster member candidates.

Further research is needed to verify if a cluster membership is given for these candidates.

4.4.24 RXCJ2152.2−1942

This cluster is known as A2384 (B) (Abell (1958), Abell *et al.* (1989)), an is situated at $z = 0.0963$, corresponding to an angular scale of 1 arcsec = 0.56066 kpc.

64 sources are detected at $> 5\sigma$ level within 4 Mpc of the cluster centre. These are tabulated in Table C.23.Of the 64 detected sources, **none** are extended.

Minor artefacts are present around the brighter sources, and there is a smooth background as expected away from brighter sources, as Fig. 4.47 indicates.

Source ID	RA	Δ RA	DEC	Δ DEC	total flux	Δ total flux	Peak flux	Δ Peak flux	optical cross-ID	cluster member	comments
0	21:49:08	0.000023	-30:42:06	0.000078	0.082396	0.002531	0.058405	0.001535	✔	✔	BCG
1	21:49:04	0.000123	-30:38:53	0.000323	0.013832	0.00108	0.006894	0.000748	✗	?	
3	21:48:40	0.000323	-30:48:48	0.00073	0.007017	0.00056	0.002104	0.00044	✗	?	

Table 4.24: Positions of radio sources within R_{500} radius of the pointing centre of cluster RXCJ2149.1−3041

Fig. 4.48 shows the contours from the NVSS overlaid on the GMRT map, demonstrating that one source was detected in that survey. This source and all additionally detected radio sources are listed in Tab. 4.25.
The optical galaxies in the central region of R_{500} which are associated with the cluster are indicated in Fig. 4.48 as green circles the ones not associated are indicated by red circles. It is shown that no source has an optical counterpart. All additional radio sources present lack an optical cross-identification, possibly caused by the faintness of the optical source or no associated redshift, making it impossible to determine if it is associated with the cluster. All known positions of optical galaxies are listed in Tab. B.24.
The redshift range used to identify cluster members was $0.075-0.105$ chosen according to Yee (1996).
There are **no** newly confirmed radio sources associated with the cluster and **14** new cluster member candidates.
Further research is needed to verify if a cluster membership is given for these candidates.

4.4.25 RXCJ2157.4−0747

This cluster is known as A2399 (Abell (1958), Abell *et al.* (1989)), an is situated at $z = 0.0579$, corresponding to an angular scale of 1 arcsec = 0.89172 kpc.
158 sources are detected at $> 5\sigma$ level within 4 Mpc of the cluster centre. These are tabulated in Table C.22.Of the 158 detected sources, **two** are extended and **one** is a triple source, which might be a jet-like structure.
There is a smooth background present throughout the whole map, which is shown in Fig. 4.49.
Fig. 4.50 shows the contours from the SUMSS overlaid on the GMRT map, demonstrating that two sources were detected in that survey. These sources and all addi-

Source ID	RA	Δ RA	DEC	Δ DEC	total flux	Δ total flux	Peak flux	Δ Peak flux	optical cross-ID	cluster member	comments
0	21:52:51	0.000246	-19:28:49	0.000135	0.097706	0.014472	0.059424	0.009632	✗	?	
1	21:52:10	0.000208	-19:43:22	0.00011	0.106178	0.02016	0.082228	0.012455	✗	?	
2	21:51:55	0.00014	-19:45:44	0.000145	0.063161	0.023037	0.072986	0.01264	✗	?	
3	21:51:54	0.000248	-19:50:41	0.000169	0.085759	0.019497	0.064474	0.012143	✗	?	
4	21:51:54	0.0002	-19:46:00	0.00017	0.13518	0.036493	0.119044	0.021669	✗	?	
5	21:51:52	0.000322	-19:47:16	0.000188	0.129407	0.028367	0.090575	0.017675	✗	?	
6	21:51:52	0.000074	-19:46:43	0.000073	0.439224	0.060536	0.429713	0.035122	✗	?	
7	21:51:51	0.000042	-19:46:05	0.000021	2.397568	0.100983	1.988671	0.060842	✗	?	
8	21:51:52	0.000187	-19:46:27	0.000141	0.328986	0.081779	0.30366	0.047226	✗	?	
10	21:51:50	0.00015	-19:45:31	0.00013	0.212912	0.064936	0.23456	0.035588	✗	?	
11	21:51:50	0.000115	-19:45:19	0.000091	0.157238	0.04604	0.19262	0.024678	✗	?	
12	21:51:49	0.000247	-19:49:16	0.000107	0.077176	0.021144	0.069855	0.012274	✗	?	
13	21:51:48	0.000117	-19:48:32	0.000132	0.025858	0.013738	0.040807	0.006573	✗	?	
14	21:51:43	0.000163	-19:44:35	0.000209	0.042272	0.016032	0.049416	0.008129	✗	?	

Table 4.25: Positions of radio sources within R_{500} radius of the pointing centre of cluster RXCJ2152.2−1942

tionally detected radio sources are listed in Tab. 4.26.
The optical galaxies in the central region of R_{500} which are associated with the cluster are indicated in Fig. 4.50 as green circles the ones not associated are indicated by red circles. It is shown that one radio source has an optical counterpart, The additional radio sources present lack an optical cross-identification, possibly caused by the faintness of the optical source or the lack of an associated redshift, making it impossible to determine if it is associated with the cluster. All known optical galaxy positions are provided in Tab. B.25.
The redshift range used to identify cluster members was $0.045-0.75$ chosen according to Yee (1996). The cluster has a mass of $M_{500} = 1.3 \times 10^{14} M_{\odot}$ Pratt et al. (2010) and has a medium to high central entropy Pratt et al. (2010). RXCJ2157.4$-$0747 has the highest scaled entropy among the REXCESS clusters.Mitsuishi *et al.* (2018) It is one of the least massive clusters in the REXCESS sample and classified as disturbed Pratt et al. (2010). In the X-ray part of the spectrum this cluster shows a bimodal structure and it is classifies as a low surface brightness cluster. It shows a decline in temperature similar to relaxed clusters while there is no significant cool core structure within $0.3r_{200}$. There are no reports for signs of cavities and they conclude the central entropy origin is unlikely to be AGN feedback and a merger is a likely explanation Mitsuishi *et al.* (2018). The Omega WINGS survey identified 234 spectral galaxies as members Moretti*et .al* (2017). This cluster shows a cold front Mitsuishi *et al.* (2018). This cluster is one of the most disturbed ones of the REXCESS sample and shows one of the lowest core gas density and has multiple galaxies of similar brightness, suggesting a young dynamic age Haarsma et al. (2010).
There is **one** newly confirmed radio source associated with the cluster and **29** new cluster member candidates.
Further research is needed to verify if a cluster membership is given for these candidates.

4.4.26 RXCJ2217.7$-$3543

This cluster is known as A3854 (Abell (1958), Abell *et al.* (1989)), an is situated at $z = 0.1486$, corresponding to an angular scale of 1 arcsec = 0.38551 kpc.
69 sources are detected at $> 5\sigma$ level within 4 Mpc of the cluster centre. These are tabulated in Table C.25. Of the 69 detected sources, **one** is extended and **one** is a double source.
There is a smooth background present throughout the whole map, which is shown

in Fig. 4.51.
Fig. 4.52 shows the contours from the SUMSS overlaid on the GMRT map, demonstrating that one source were detected in that survey. This source and all additionally detected radio sources are listed in Tab. 4.27.
The optical galaxies in the central region of R_{500} which are associated with the cluster are indicated in Fig. 4.52 as green circles the ones not associated are indicated by red circles. It is shown that no radio source has an optical counterpart. Additional radio sources, without any optical cross-identification, possibly caused by the faintness of the optical source or no associated redshift, making it impossible to determine if it is associated with the cluster, are present. All known optical galaxy positions are tabulated in Tab. B.26.
The redshift range used to identify cluster members was $0.125-0.155$ chosen according to Yee (1996). The cluster has a mass of $M_{500} = 3.6 \times 10^{14} M_{\odot}$ Pratt et al. (2010) and has a low central entropy Pratt et al. (2010).
There are **no** newly confirmed radio sources associated with the cluster and **two** new cluster member candidates.
Further research is needed to verify if a cluster membership is given for these candidates.

Source ID	RA	Δ RA	DEC	Δ DEC	total flux	Δ total flux	Peak flux	Δ Peak flux	optical cross-ID	cluster member	comments
0	21:58:05	0.000095	-07:41:34	0.000066	0.003173	0.000417	0.002664	0.000252	✗	?	
1	21:57:59	0.000046	-07:57:21	0.000036	0.005308	0.000455	0.005036	0.000267	✗	?	
2	21:57:50	0.000077	-07:52:42	0.000081	0.003765	0.000431	0.002915	0.000269	✗	?	
3	21:57:40	0.000143	-07:41:42	0.000154	0.006598	0.000436	0.002727	0.00032	✗	?	
4	21:57:37	0.000045	-07:44:33	0.000032	0.012151	0.000666	0.009284	0.000417	✗	?	
4	21:57:37	0.000059	-07:44:29	0.000037	0.013201	0.000642	0.00843	0.000423	✗	?	
5	21:57:37	0.000216	-07:38:25	0.000216	0.003624	0.000472	0.001709	0.000339	✗	?	
5	21:57:37	0.000377	-07:38:25	0.000299	0.001988	0.000483	0.001071	0.000332	✗	?	
7	21:57:36	0.000235	-07:45:23	0.000258	0.006998	0.000643	0.002557	0.000487	✗	?	
8	21:57:35	0.000402	-07:48:55	0.00019	0.021682	0.000523	0.003279	0.000457	✗	?	
9	21:57:34	0.000105	-07:41:59	0.000426	0.012945	0.000642	0.001989	0.000364	✗	?	
6	21:57:35	0.000053	-07:47:47	0.000048	0.661724	0.003114	0.050694	0.000487	✔	✔	ext.
6	21:57:34	0.000038	-07:48:14	0.000061	0.036794	0.001115	0.015584	0.000487	✔	✔	ext.
10	21:57:33	0.000102	-07:48:17	0.000067	0.012237	0.000669	0.006435	0.00046	✗	?	ext.
11	21:57:32	0.00042	-07:53:16	0.000383	0.01265	0.000307	0.001509	0.000276	✗	?	
12	21:57:20	0.000042	-07:44:38	0.000027	0.007123	0.000459	0.006646	0.000265	✗	?	
13	21:57:10	0.000275	-07:51:50	0.000293	0.003445	0.000348	0.001215	0.000266	✗	?	
14	21:57:09	0.000146	-07:39:27	0.000089	0.002818	0.00047	0.002232	0.000287	✗	?	
14	21:57:08	0.000363	-07:39:6	0.000311	0.00112	0.000464	0.000883	0.000278	✗	?	
15	21:57:06	0.00026	-07:41:26	0.000273	0.005212	0.000433	0.001671	0.000338	✗	?	
16	21:57:05	0.000377	-07:44:52	0.000234	0.005945	0.000359	0.00152	0.000291	✗	?	
17	21:57:01	0.000038	-07:50:47	0.000054	0.291041	0.002338	0.031359	0.000578	✗	?	ext.
17	21:57:03	0.000051	-07:50:21	0.000032	0.351975	0.002021	0.033063	0.000578	✗	?	ext.
17	21:57:01	0.000164	-07:51:12	0.000097	0.042004	0.000606	0.008977	0.000501	✗	?	ext.
17	21:57:02	0.00008	-07:50:37	0.000148	0.001765	0.001048	0.003038	0.000451	✗	?	ext.
17	21:57:00	0.000158	-07:51:13	0.000157	0.001902	0.001014	0.002366	0.00054	✗	?	ext.
18	21:57:03	0.000253	-07:49:51	0.000176	0.006221	0.00101	0.003474	0.000687	✗	?	ext.
20	21:56:59	0.000344	-07:51:21	0.000163	0.012632	0.000932	0.003303	0.000447	✗	?	ext.
19	21:57:02	0.000192	-07:39:29	0.000144	0.001996	0.000438	0.001505	0.000274	✗	?	
21	21:56:49	0.000041	-07:45:32	0.00004	0.006467	0.000419	0.005288	0.000258	✗	?	
21	21:56:49	0.000374	-07:45:29	0.000135	0.001759	0.000386	0.001071	0.000252	✗	?	

Table 4.26: Positions of radio sources within R_{500} radius of the pointing centre of cluster RXCJ2157.4−0747

4.4.27 RXCJ2218.6−3853

This cluster is known as A3856 (Abell (1958), Abell *et al.* (1989)), an is situated at $z = 0.1411$, corresponding to an angular scale of 1 arcsec = 0.40261 kpc.
50 sources are detected at $> 5\sigma$ level within 4 Mpc of the cluster centre. These are tabulated in Table C.26. Of the 50 detected sources, **none** are extended.
Minor artefacts are present around the brighter sources, and there is a smooth background as expected away from brighter sources, as Fig. 4.53 indicates. The cross-shaped structure around the central bright source might be structure from the dirty beam in conjunction with the brightness of the source, which we were not able to remove. Additionally there might be some emission from a cluster member galaxy.
Fig. 4.54 shows the contours from the SUMSS overlaid on the GMRT map, demonstrating that two sources were detected in that survey. These sources and all additionally detected radio sources are listed in Tab. 4.28.
The optical galaxies in the central region of R_{500} which are associated with the cluster are indicated in Fig. 4.54 as green circles. It is shown that the central source has an optical counterpart. The additional radio sources present have no optical cross-ID, possibly caused by the faintness of the optical source or no associated redshift, making it impossible to determine if it is associated with the cluster. All known positions of optical galaxies are given in Tab. B.27.
The redshift range used to identify cluster members was $0.125-0.155$ chosen according to Yee (1996). The cluster has a mass of $M_{500} = 4.9 \times 10^{14} M_{\odot}$ Pratt et al. (2010) and has a low central entropy Pratt et al. (2010).
There are **two** newly confirmed radio source associated with the cluster and **four** new cluster member candidates.
Further research is needed to verify if a cluster membership is given for these candidates.

Source ID	RA	Δ RA	DEC	Δ DEC	total flux	Δ total flux	Peak flux	Δ Peak flux	optical cross-ID	cluster member	comments
0	22:18:00	0.000515	-35:41:07	0.000276	0.003207	0.000643	0.002211	0.000407	✗	?	
1	22:17:15	0.000058	-35:48:51	0.000128	0.047948	0.001695	0.026113	0.000769	✗	?	ext.

Table 4.27: Positions of radio sources within R_{500} radius of the pointing centre of cluster RXCJ2217.7−3543

Source ID	RA	Δ RA	DEC	Δ DEC	total flux	Δ total flux	Peak flux	Δ Peak flux	optical cross-ID	cluster member	comments
0	22:18:44	0.000273	-38:55:45	0.00007	0.169609	0.011301	0.099115	0.007274	✗	?	
0	22:18:45	0.000352	-38:55:59	0.000224	0.025419	0.013379	0.032656	0.006847	✗	?	
1	22:18:40	0.000065	-38:53:51	0.000018	0.451851	0.006183	0.241518	0.004101	✔	✔	BCG
2	22:18:22	0.000356	-38:51:02	0.000373	0.105143	0.003488	0.023899	0.002888	✔	✔	
3	22:18:04	0.000399	-38:50:23	0.000426	0.087455	0.00299	0.018588	0.002503	✗	?	} double
3	22:18:05	0.000585	-38:50:53	0.000425	0.067733	0.003026	0.015204	0.00251	✗	?	

Table 4.28: Positions of radio sources within R_{500} radius of the pointing centre of cluster RXCJ2218.6−3853

4.4.28 RXCJ2234.5−3744

The cluster, shown in Fig. 4.55 is known as A3888 (Abell (1958), Abell *et al.* (1989)), an is situated at $z = 0.1510$, corresponding to an angular scale of 1 arcsec = 0.38039 kpc. **32** sources are detected at $> 5\sigma$ level within 4 Mpc of the cluster centre. These are tabulated in Table C.27. Of the 32 detected sources, **two** are extended and **one** is a double source. Minor artefacts are present around the brighter sources, and there is a smooth background as expected away from brighter sources, as Fig. 4.55 indicates. Fig. 4.56 shows the contours from the SUMSS overlaid on the GMRT map, demonstrating that two sources were detected in that survey. These sources and all additionally detected radio sources are listed in Tab. 4.29. One of the sources detected by SUMSS is a double source. The optical galaxies in the central region of R_{500} which are associated with the cluster are indicated in Fig. 4.56 as green circles the ones not associated are indicated by red circles. It is shown that both central radio sources have an optical counterpart. There are additional radio sources present lacking an optical cross-identification, possibly caused by the faintness of the optical source or no associated redshift, making it impossible to determine if it is associated with the cluster. All known positions of optical galaxies are provided by Tab. B.28. The redshift range used to identify cluster members was 0.135−0.165 chosen according to Yee (1996). The cluster has a mass of $M_{500} = 7.4 \times 10^{14} M_{\odot}$ Pratt et al. (2010) and has a medium to high central entropy Pratt et al. (2010). This cluster shows a large offset between BCG and X-ray peak and has one of the lowest core gas density of the REXCESS sample. Additionally it has multiple galaxies of similar brightness Haarsma et al. (2010). This cluster has a giant radio halo with a spectral index $\alpha = -1.49$.**?**
There are **two** newly confirmed radio source associated with the cluster and **four** new cluster member candidates. Further research is needed to verify if a cluster membership is given for these candidates.

Source ID	RA	Δ RA	DEC	Δ DEC	total flux	Δ total flux	Peak flux	Δ Peak flux	optical cross-ID	cluster member	comments
0	22:34:25	0.000044	-37:44:37	0.000076	0.065829	0.004603	0.055788	0.00274	✔	✔	BCG
1	22:34:22	0.000026	-37:43:33	0.000049	0.115002	0.005051	0.099932	0.002949	✔	✔	ext.
1	22:34:21	0.000055	-37:43:44	0.000102	0.100964	0.004682	0.056918	0.003181			
2	22:34:17	0.000122	-37:38:28	0.000224	0.006054	0.0015	0.006005	0.000826	✗	?	
3	22:34:15	0.000068	-37:49:11	0.000173	0.008241	0.002932	0.012941	0.001228	✗	?	
4	22:34:01	0.000263	-37:47:58	0.000302	0.005398	0.001235	0.004016	0.000753	✗	?	
5	22:34:00	0.000017	-37:42:54	0.000033	0.044032	0.001453	0.041728	0.000814	✗	?	

Table 4.29: Positions of radio sources within R_{500} radius of the pointing centre of cluster RXCJ2234.5−3744

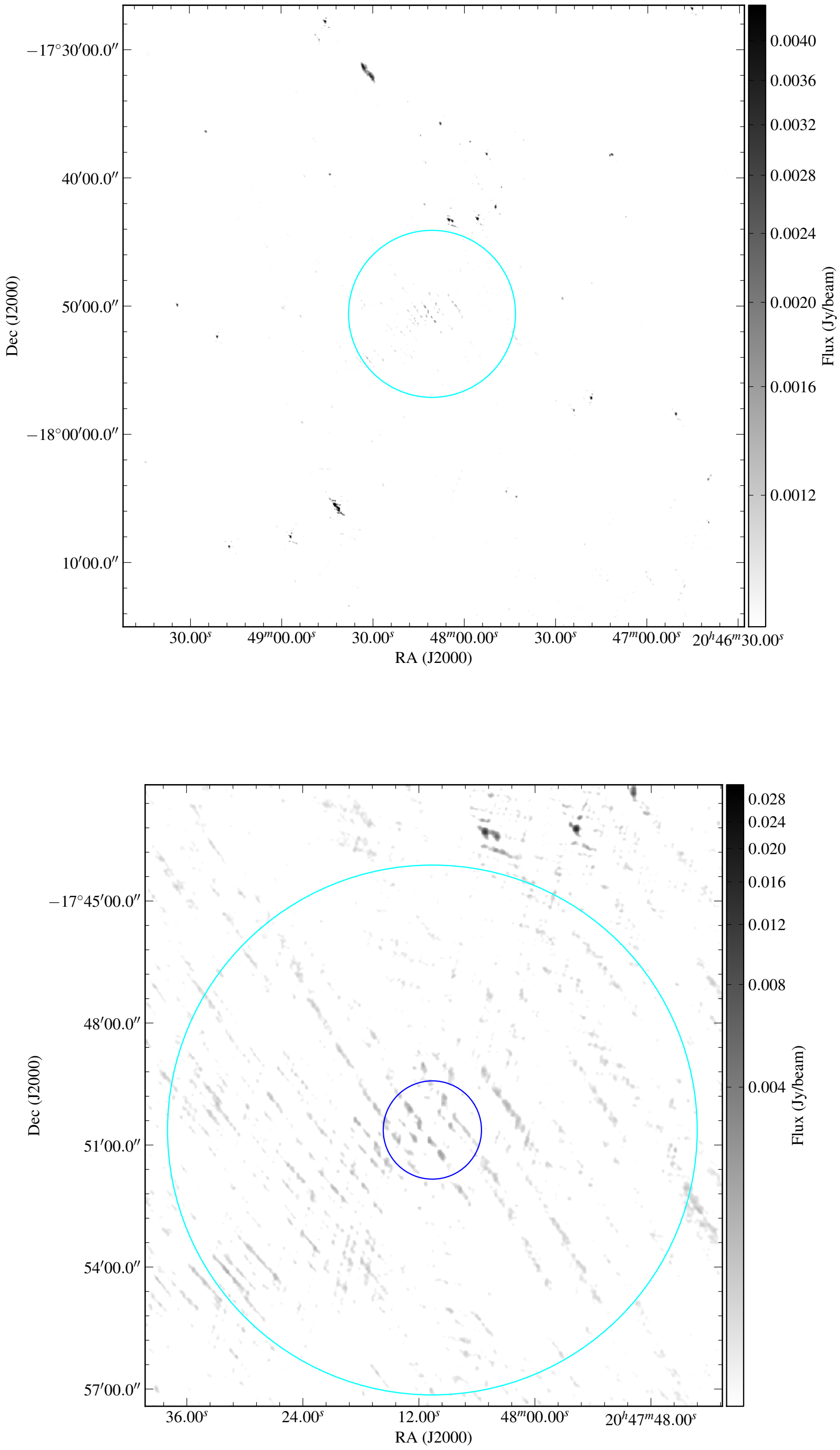

Figure 4.43: 610-MHz GMRT maps of RXCJ2048.1−1750. Top: overview of a region 4 Mpc × 4 Mpc centred on the cluster, R_{500} being indicated by the circle; bottom: central region of the cluster ($R_{500} \times R_{500}$)the circle indicates a region of radius 200kpc around the centre.

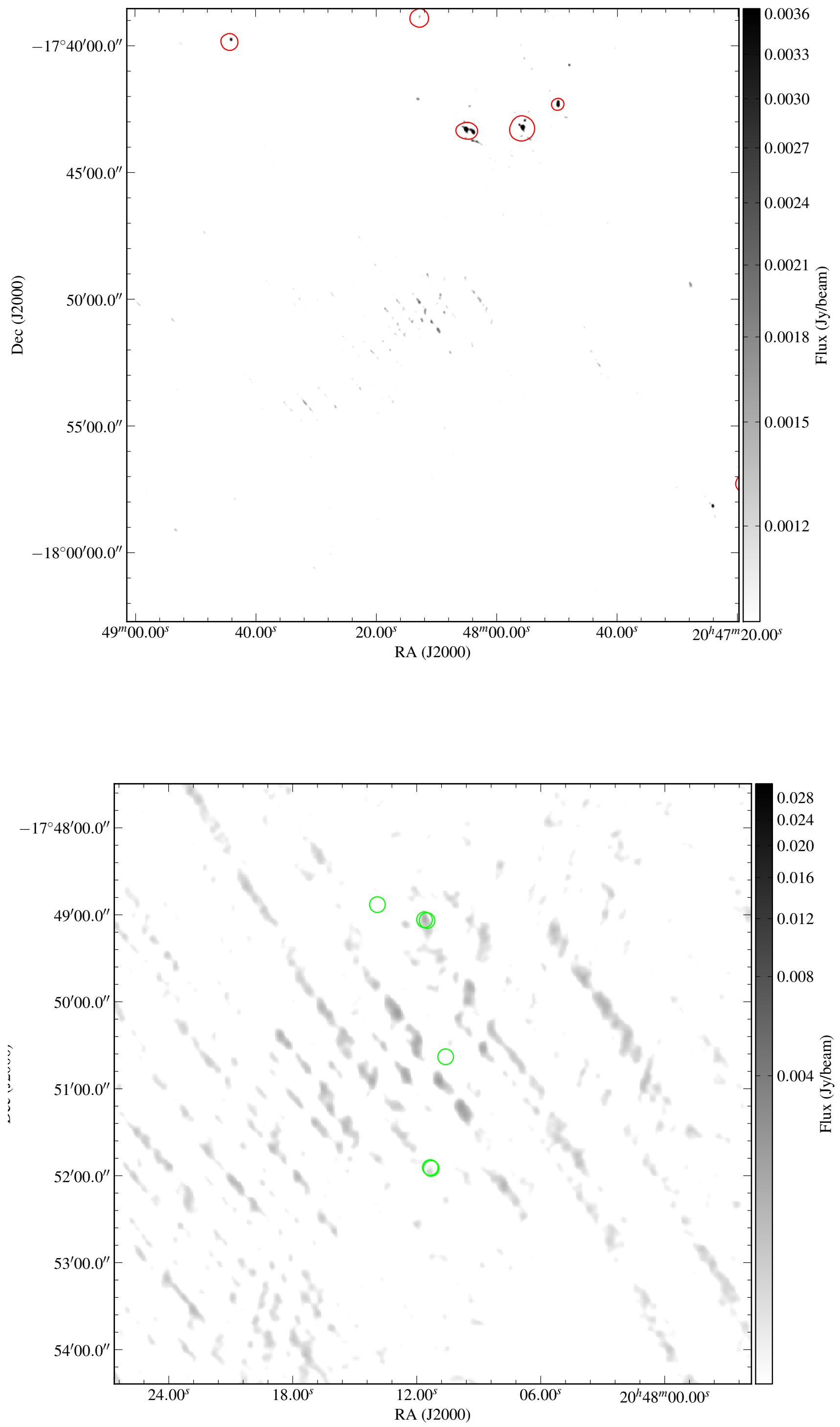

Figure 4.44: 610-MHz GMRT maps of RXCJ2048.1−1750. central region of the cluster ($R_{500} \times R_{500}$); top: contours from NVSS overlaid; bottom: positions of known cluster member galaxies overlaid in green.

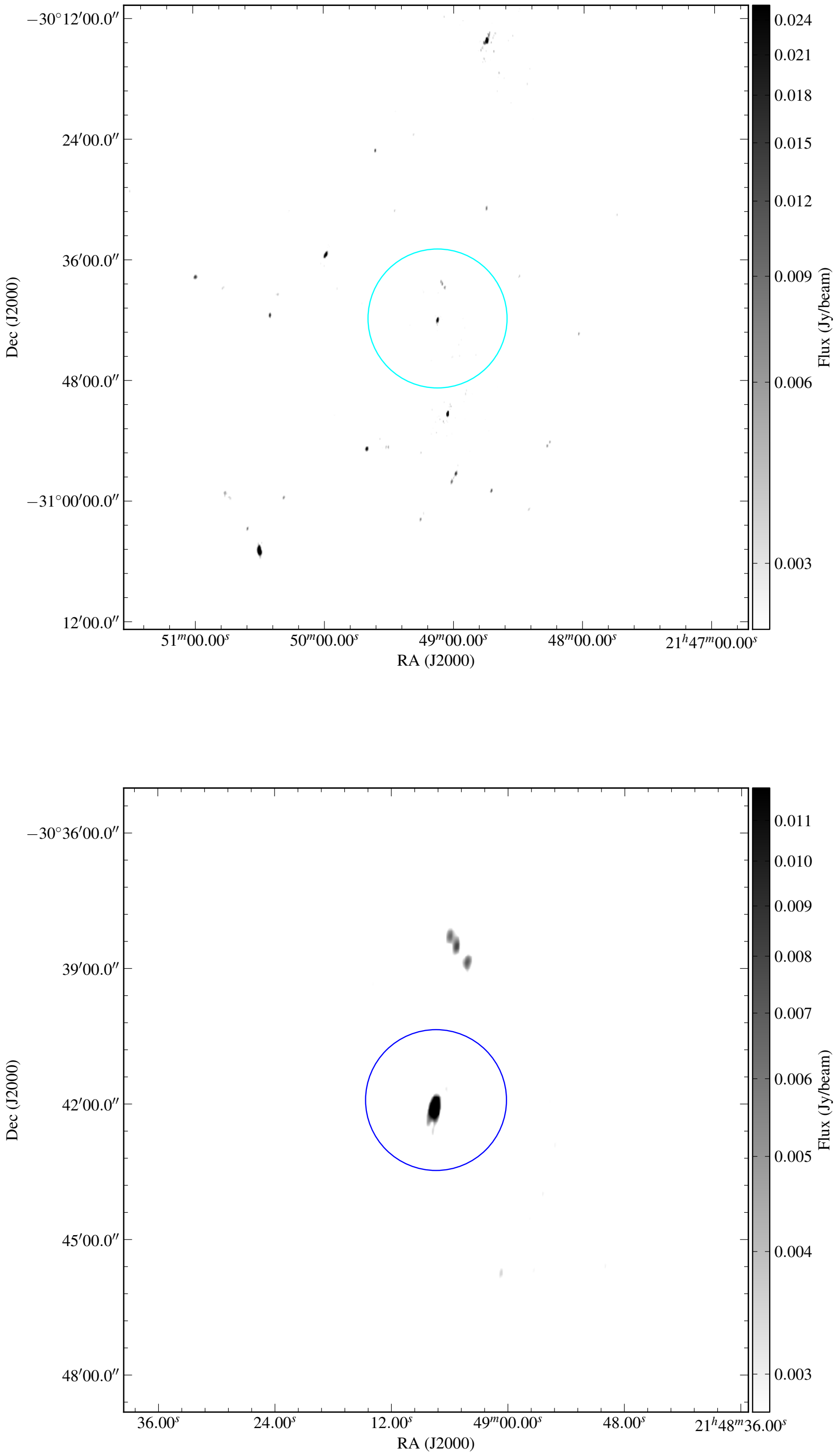

Figure 4.45: 610-MHz GMRT maps of RXCJ2149.1−3041. Top: overview of a region 4 Mpc × 4 Mpc centred on the cluster, R_{500} being indicated by the circle; bottom: central region of the cluster ($R_{500} \times R_{500}$)the circle indicates a region of radius 200kpc around the centre.

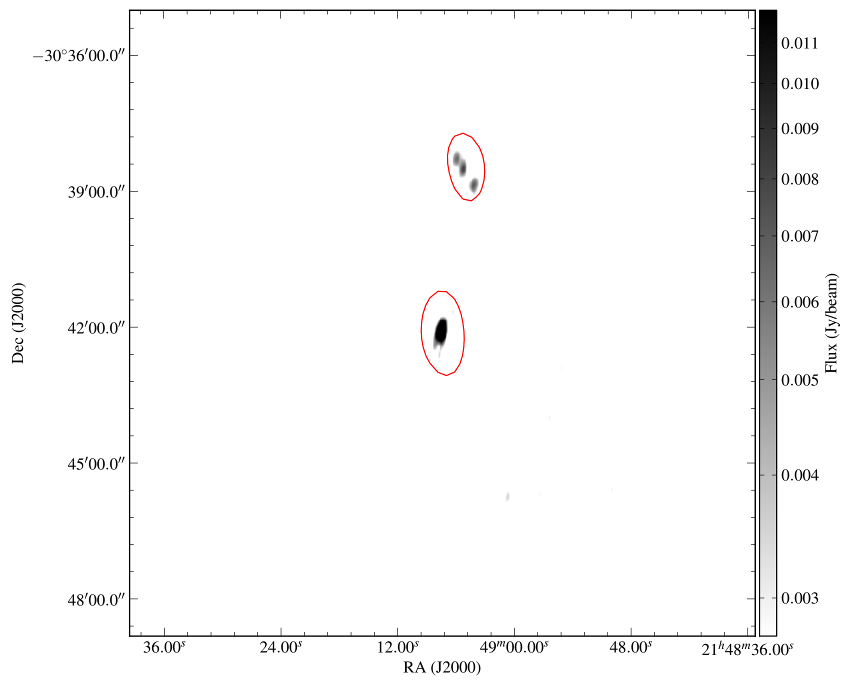

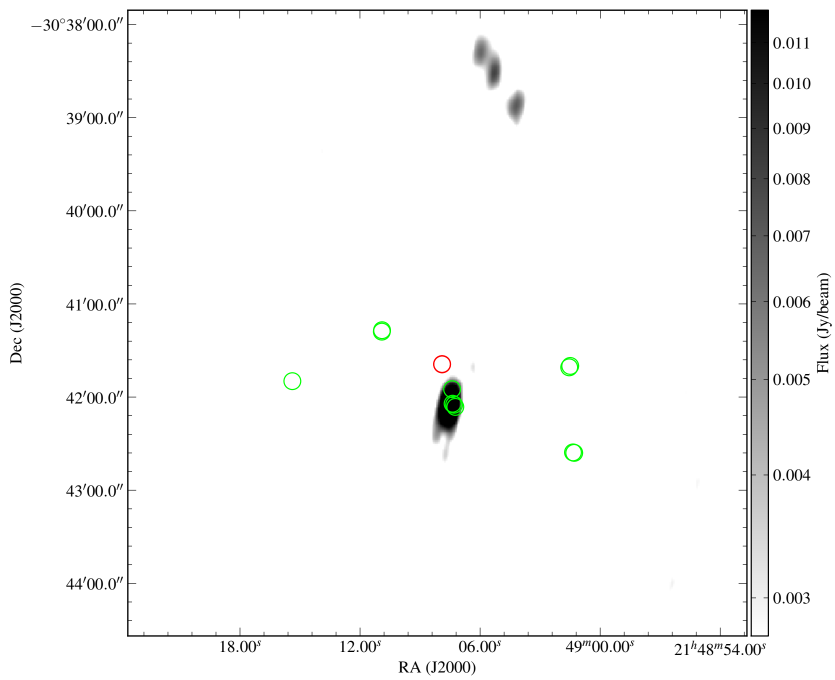

Figure 4.46: 610-MHz GMRT maps of RXCJ2149.1−3041. central region of the cluster ($R_{500} \times R_{500}$); top: contours from SUMSS overlaid; bottom: positions of known cluster member galaxies overlaid in green and known background or foreground sources indicated by red circles.

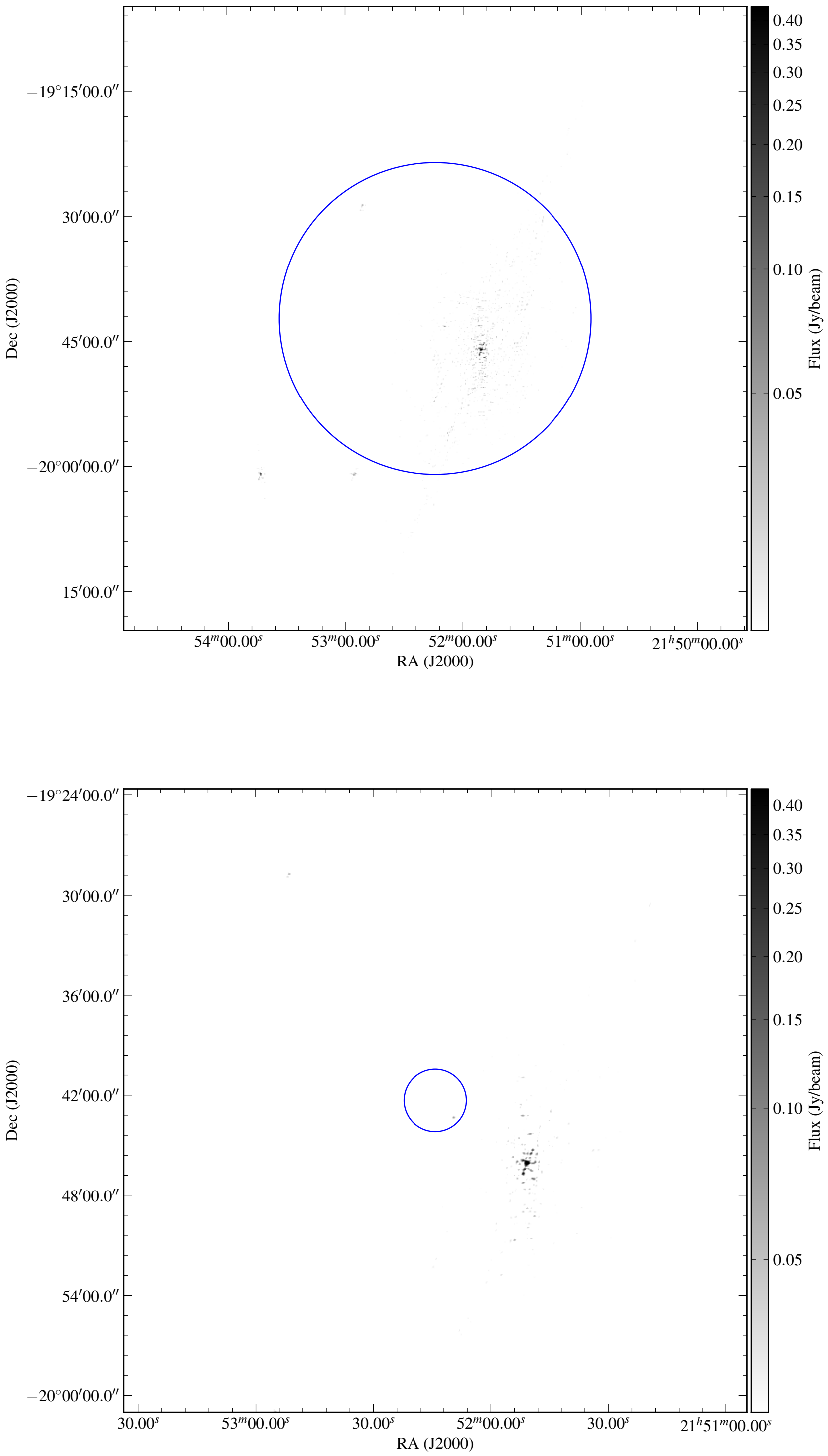

Figure 4.47: 610-MHz GMRT maps of RXCJ2152.2−1942. Top: overview of a region 4 Mpc × 4 Mpc centred on the cluster; bottom: central region of the cluster (2 Mpc × 2 Mpc)the circle indicates a region of radius 200kpc around the centre.

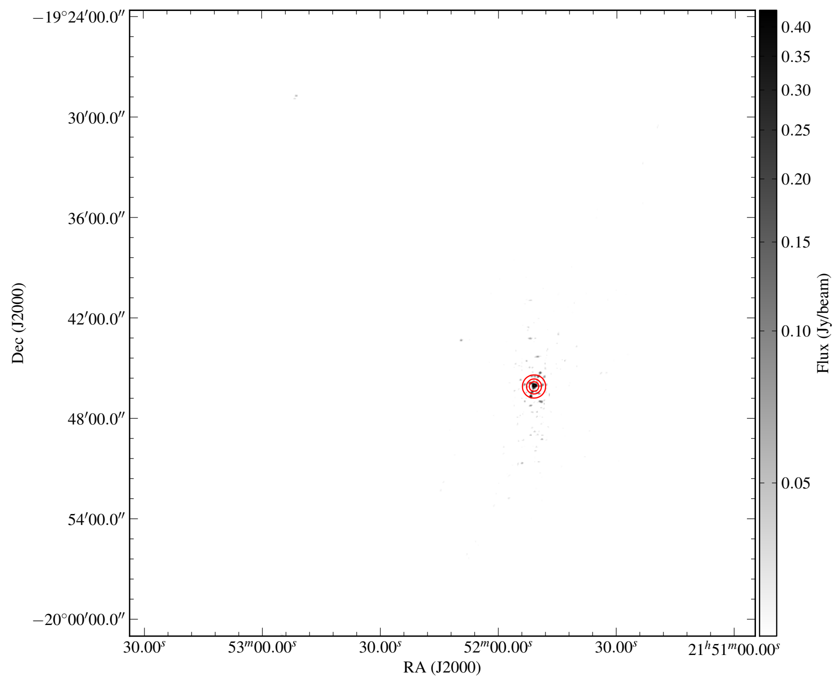

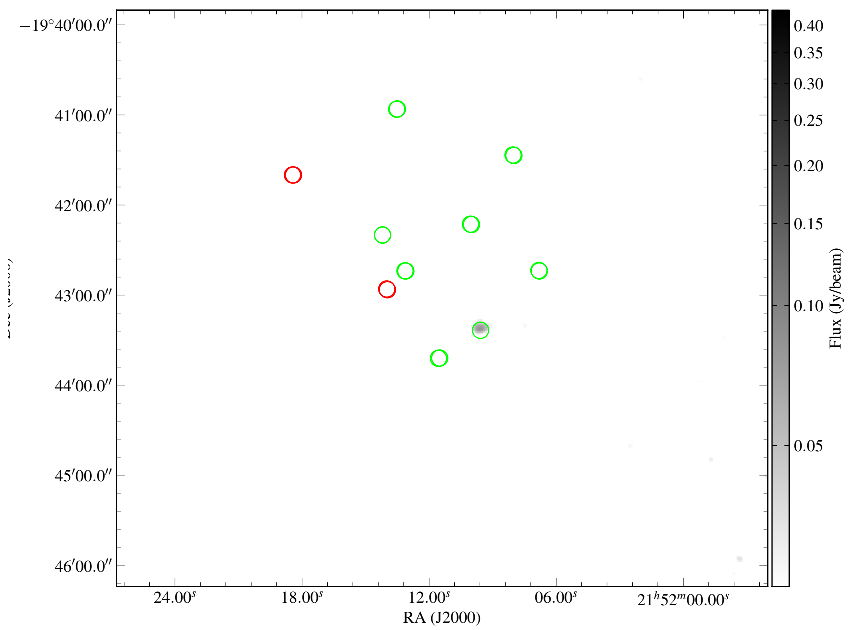

Figure 4.48: 610-MHz GMRT maps of RXCJ2152.2−1942. central region of the cluster (2 Mpc × 2 Mpc); top: contours from NVSS overlaid; bottom: positions of known cluster member galaxies overlaid in green and known background or foreground sources indicated by red circles.

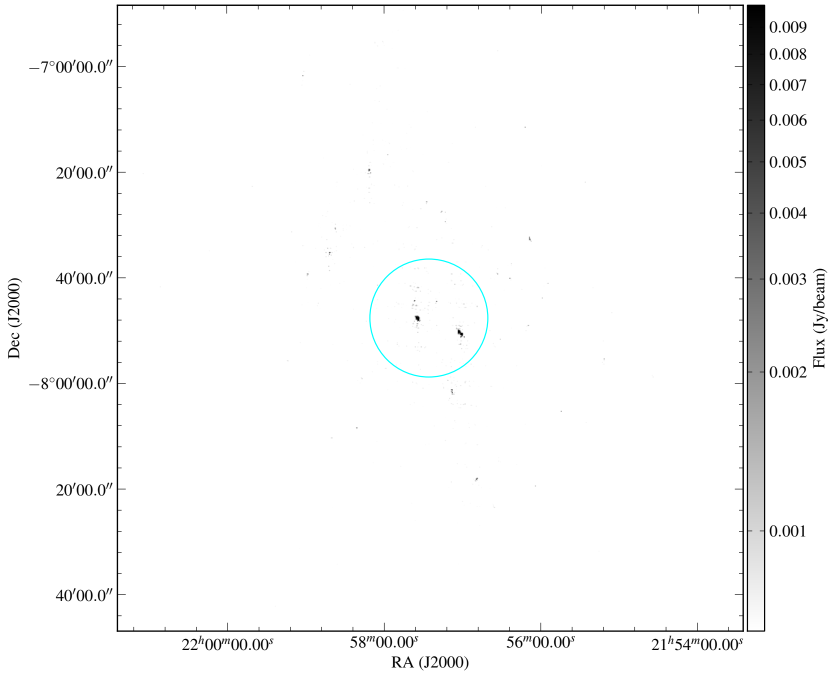

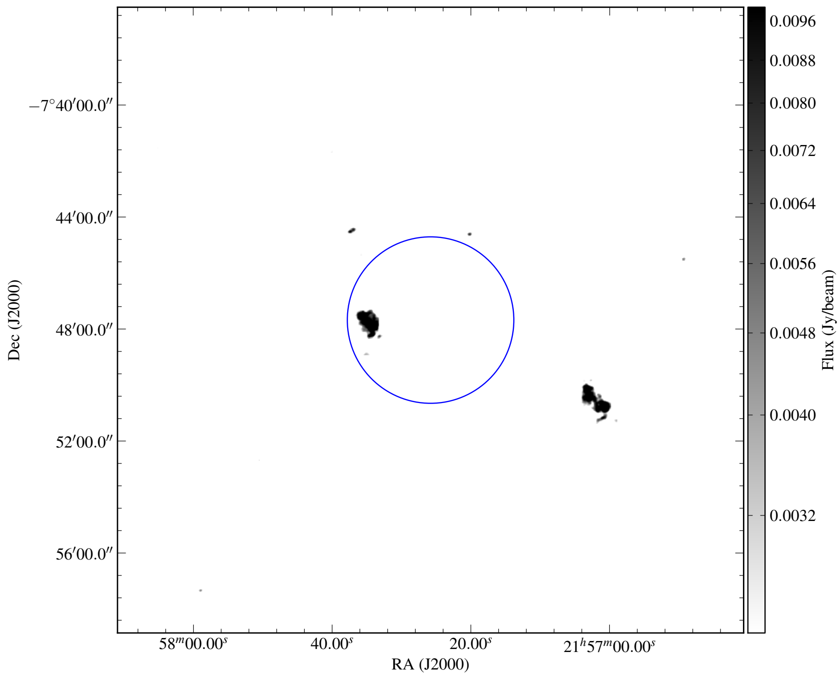

Figure 4.49: 610-MHz GMRT maps of RXCJ2157.4−0747. Top: overview of a region 4 Mpc × 4 Mpc centred on the cluster, R_{500} being indicated by the circle; bottom: central region of the cluster ($R_{500} \times R_{500}$)the circle indicates a region of radius 200kpc around the centre.

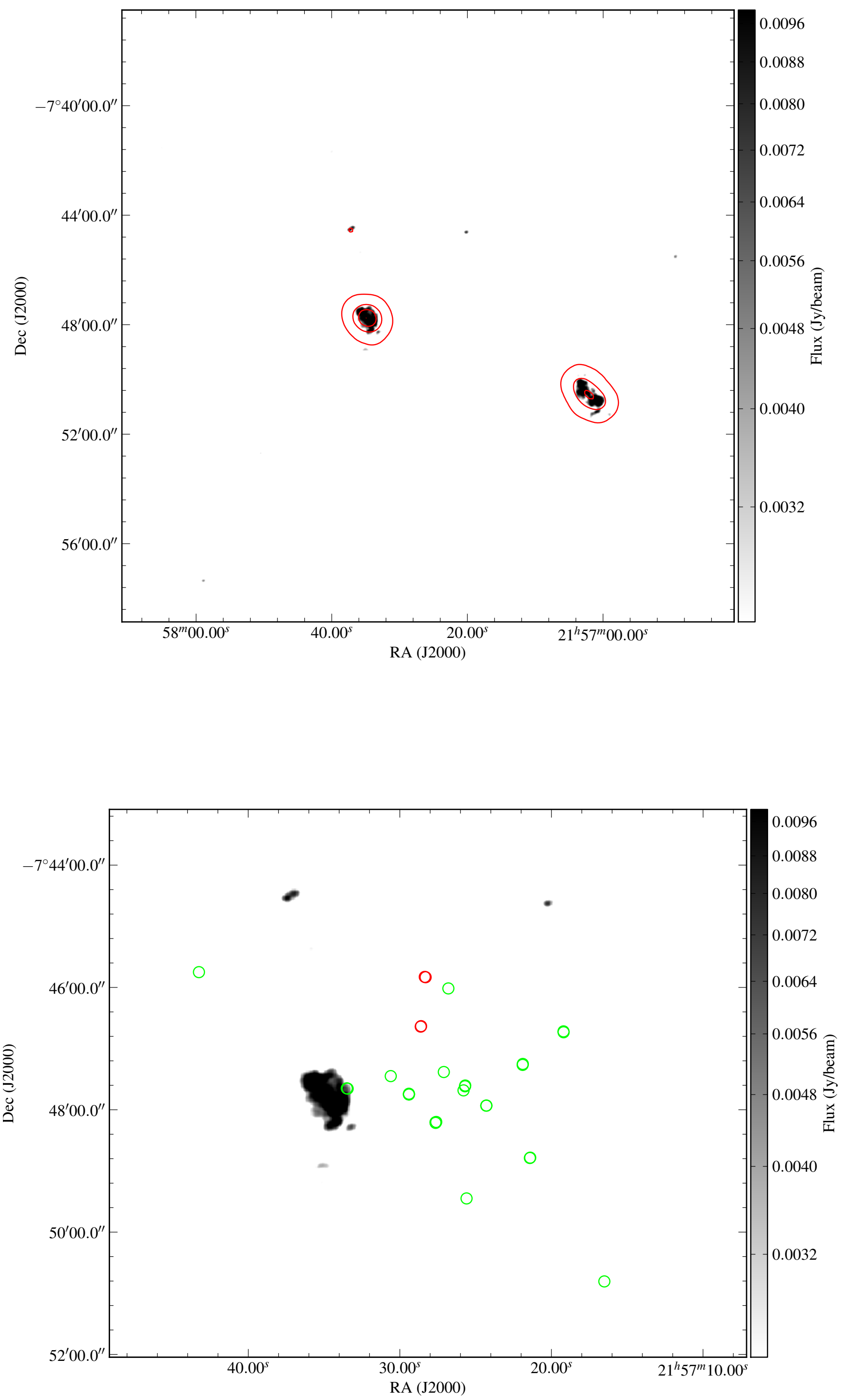

Figure 4.50: 610-MHz GMRT maps of RXCJ2157.4−0747. central region of the cluster ($R_{500} \times R_{500}$); top: contours from NVSS overlaid; bottom: positions of known cluster member galaxies overlaid in green and known background or foreground sources indicated by red circles.

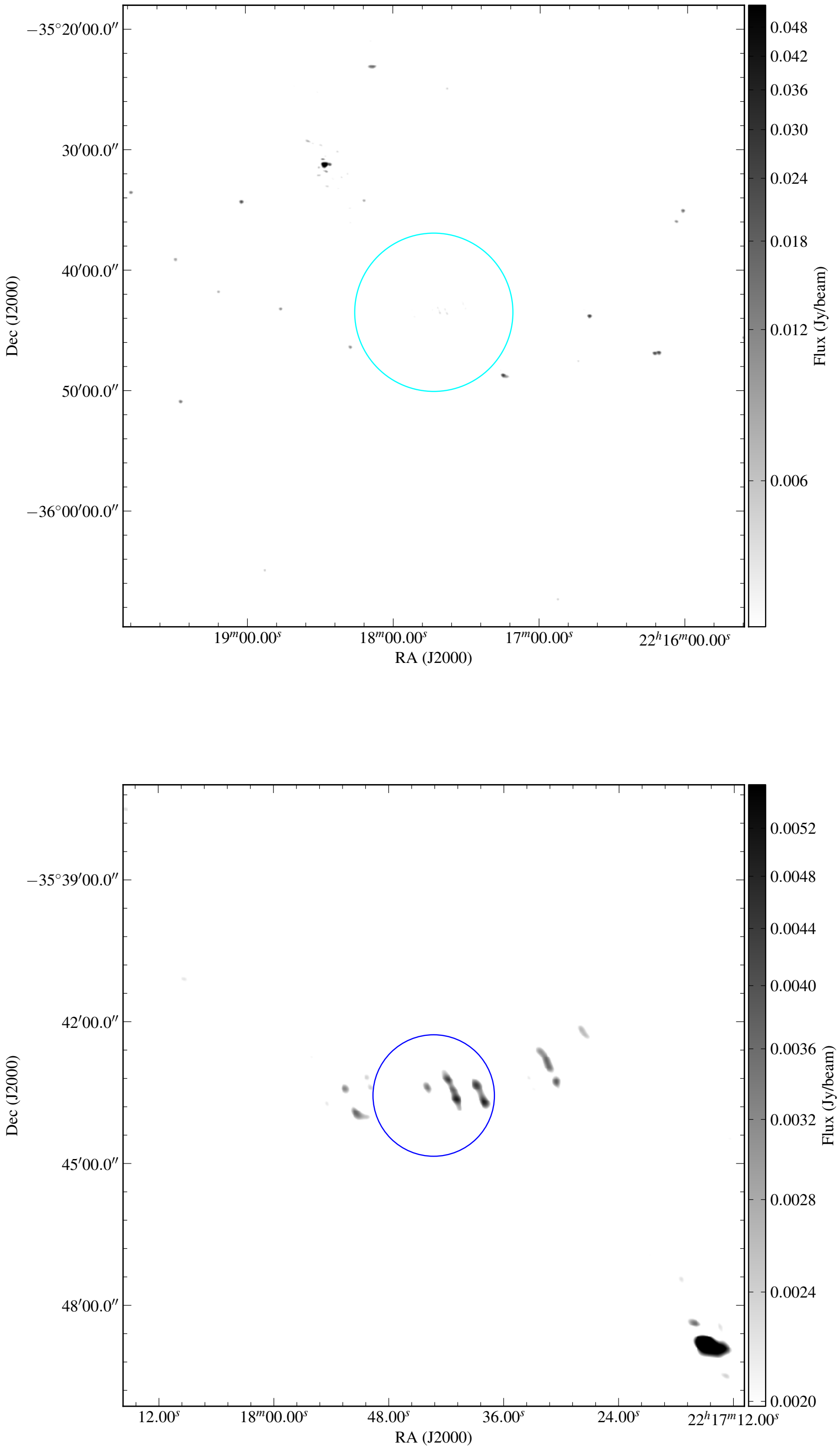

Figure 4.51: 610-MHz GMRT maps of RXCJ2217.7−3543. Top: overview of a region 4 Mpc × 4 Mpc centred on the cluster, R_{500} being indicated by the circle; bottom: central region of the cluster ($R_{500} \times R_{500}$)the circle indicates a region of radius 200kpc around the centre.

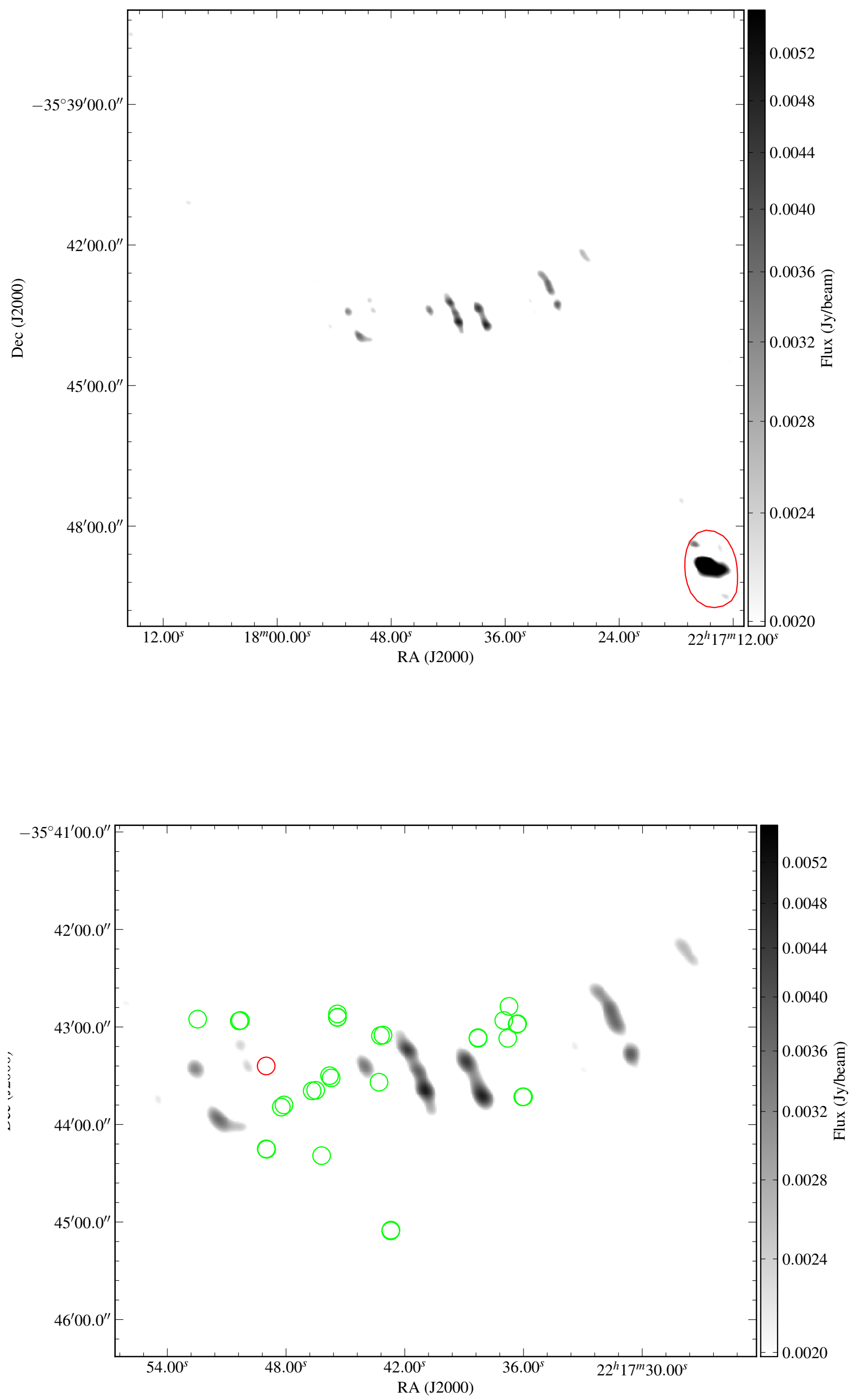

Figure 4.52: 610-MHz GMRT maps of RXCJ2217.7−3543. central region of the cluster ($R_{500} \times R_{500}$); top: contours from SUMSS overlaid; bottom: positions of known cluster member galaxies overlaid in green and known background or foreground sources indicated by red circles.

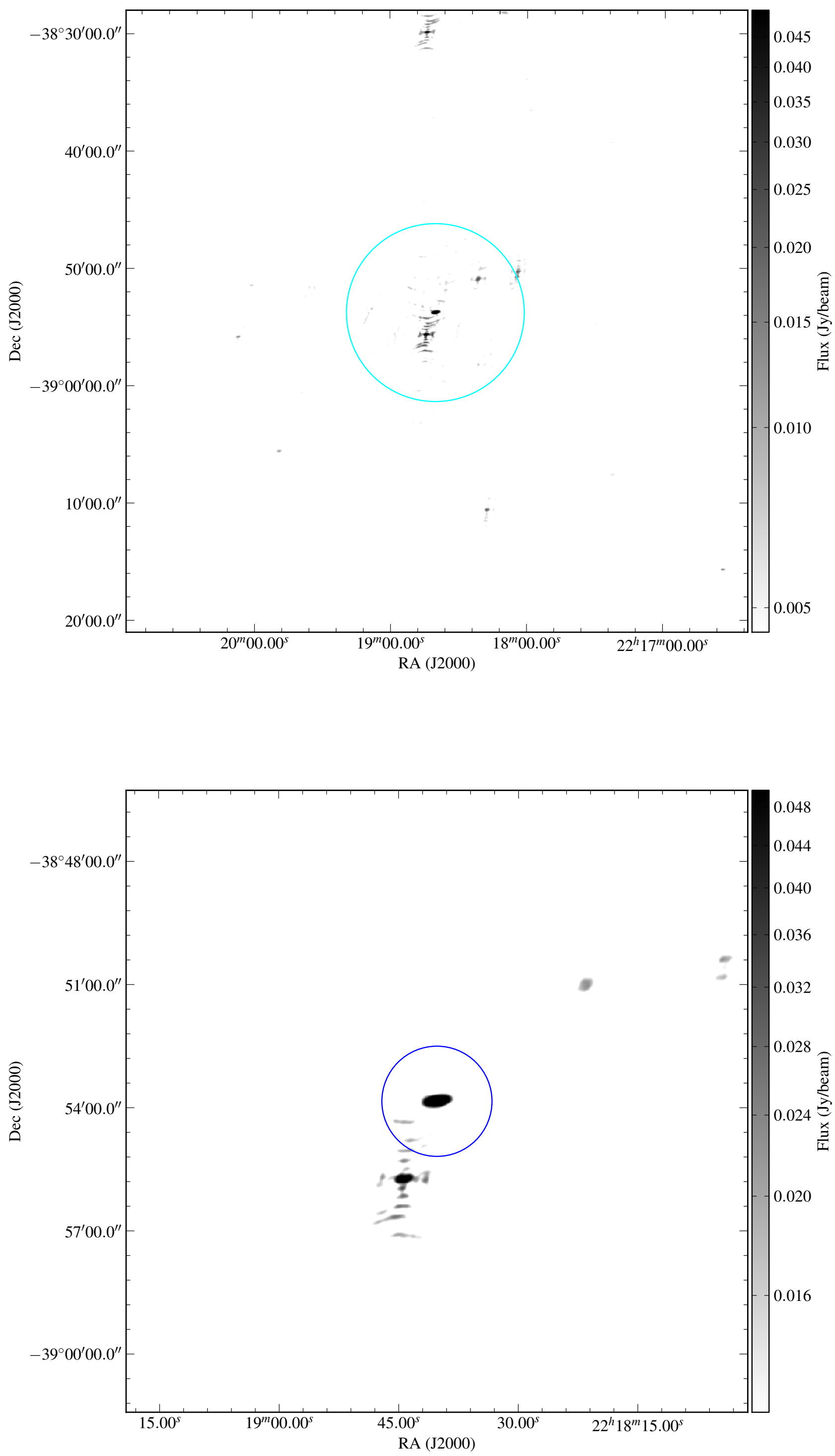

Figure 4.53: 610-MHz GMRT maps of RXCJ2218.6−3853. Top: overview of a region 4 Mpc $\times$ 4 Mpc centred on the cluster, R_{500} being indicated by the circle; bottom: central region of the cluster ($R_{500} \times R_{500}$)the circle indicates a region of radius 200kpc around the centre.

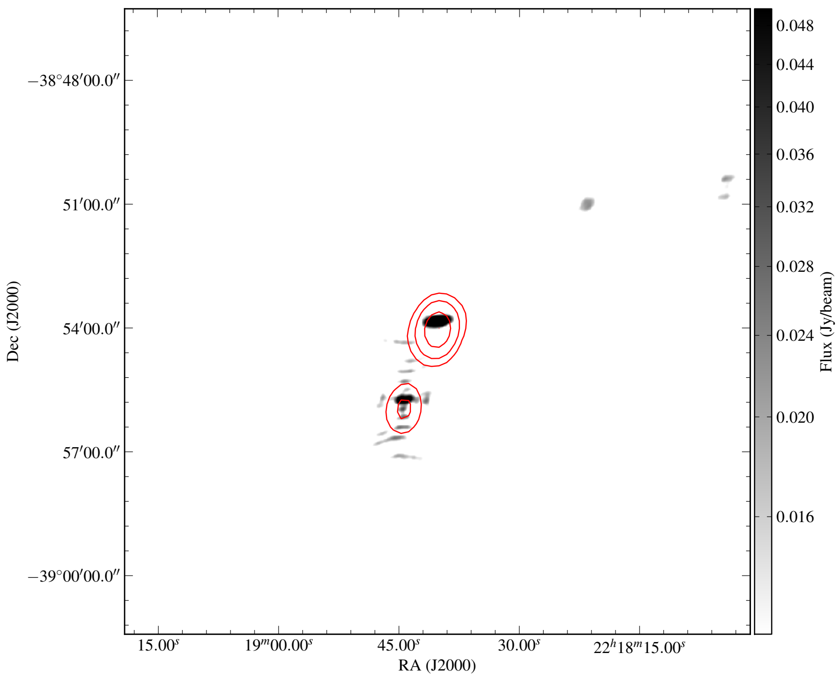

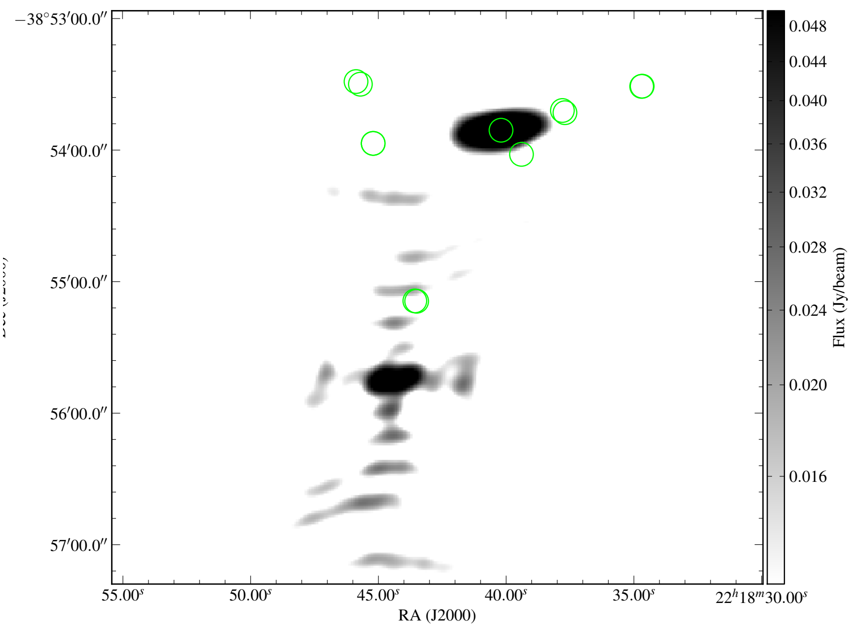

Figure 4.54: 610-MHz GMRT maps of RXCJ2218.6−3853. central region of the cluster ($R_{500} \times R_{500}$); top: contours from SUMSS overlaid; bottom: positions of known cluster member galaxies overlaid in green.

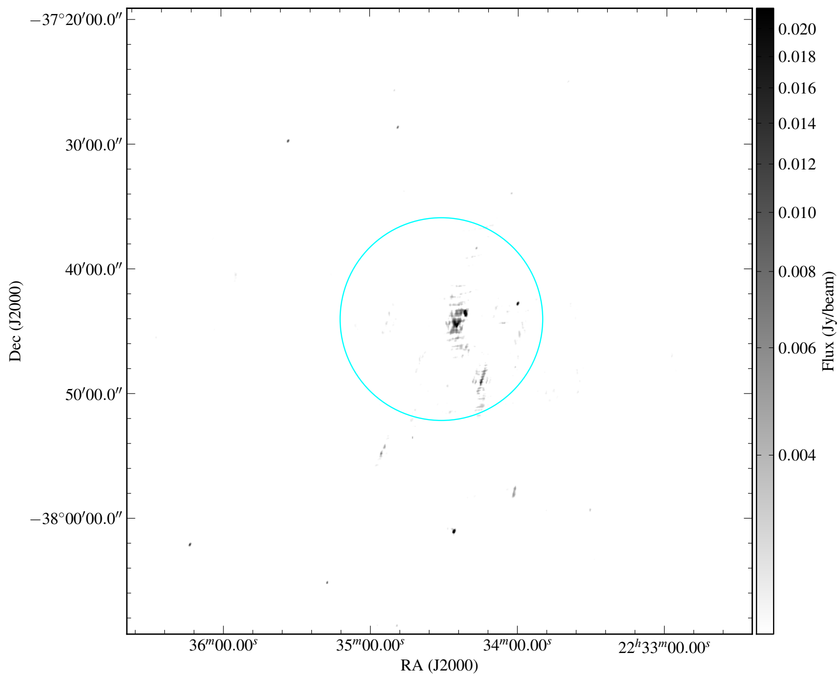

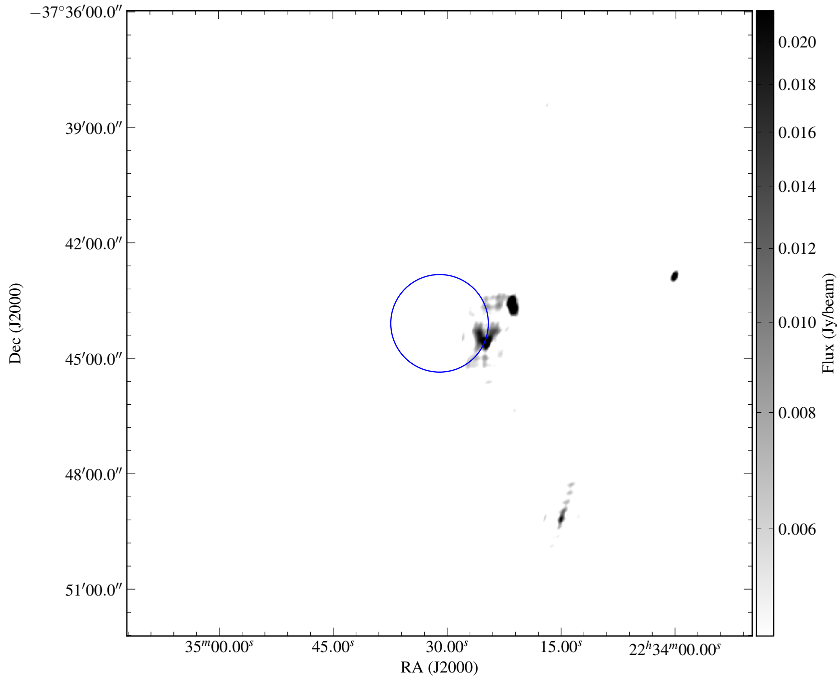

Figure 4.55: 610-MHz GMRT maps of RXCJ2234.5−3744. Top: overview of a region 4 Mpc × 4 Mpc centred on the cluster, R_{500} being indicated by the circle; bottom: central region of the cluster ($R_{500} \times R_{500}$)the circle indicates a region of radius 200kpc around the centre.

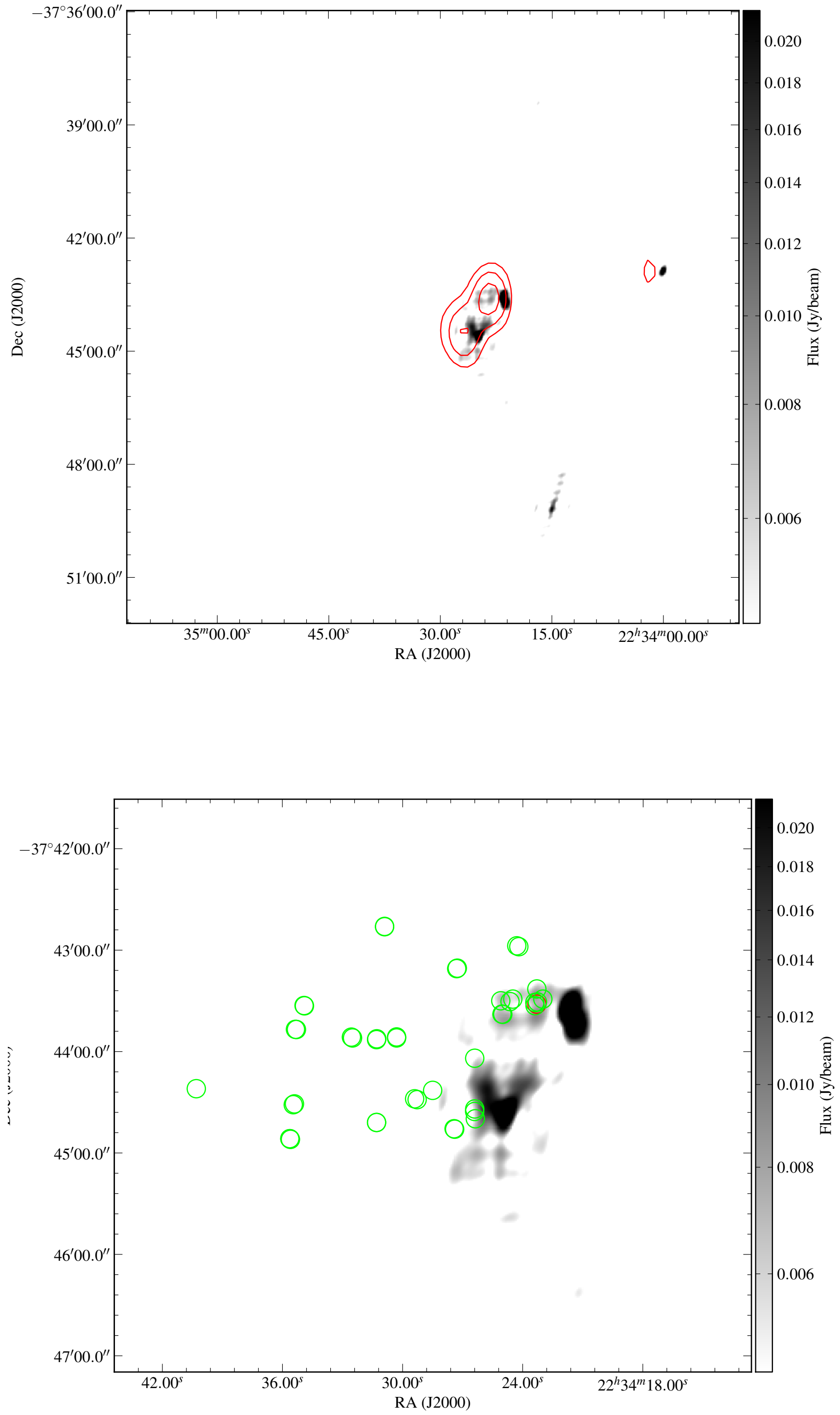

Figure 4.56: 610-MHz GMRT maps of RXCJ2234.5−3744. central region of the cluster ($R_{500} \times R_{500}$); top: contours from SUMSS overlaid; bottom: positions of known cluster member galaxies overlaid in green and known background or foreground sources indicated by red circles.

4.5 Summary

In total 20 radio sources were confirmed as cluster members by matching them with their optical counterparts. 294 detected radio sources are cluster member candidates, requiring further research to confirm their status. This results in 15.7% of all detected radio sources, not associated with background sources, being confirmed as cluster members. This sample of radio sources builds the base for further research in the following chapters.

There are two possible outcomes: If the result confirms the hypothesis, then you made a measurement. If the result is contrary to the hypothesis, then you made a discovery.

E. FERMI (1901 - 1954)

5

240MHz observations and Spectra

This chapter discusses the observations, data quality and optical cross-identification of 13 REXCESS clusters, observed at 240 MHz. It lists observational properties of the radio sources and compares them with the data presented in the previous chapter. It additionally provides a spectral analysis of these clusters, based on this data.

5.1 240 MHz Maps

5.1.1 Motivation

The previous chapter provided in depth information about the radio sources associated with the individual clusters of the REXCESS sample at 610 MHz but the information about the spectral index is still left to be discovered. This chapter tries to fill that gap. Spectral indexes are important to determine whether a radiation is thermally or synchrotron dominated. Additionally it provides information about radio sources detected at 240MHz, but not at 610 MHz.

5.1.2 Data Quality Summary

In this section the overall data quality is discussed. Of the 13 maps in total one has a measured RMS of less than 10 times the theoretical noise, four are between 10 and 20 times the theoretical RMS and eight are between 20 and 100. Only one map has a measured RMS that is more than 100 times higher than the theoretical one. Table 5.1.2 shows this in detail as well as the time spend on each source. The theoretical noises range from 1.96×10^{-4} to 2.38×10^{-4}, while the measured RMS range is from 1.98×10^{-3} to the over one order of magnitude larger 2.97×10^{-2}. A comparison with the 610 MHz maps reveals a overall higher RMS for the 240 MHz radio maps. Due to the small number of sources the one source with high RMS was included in the analysis as well as the on with some phase calibration issues. For source detection a detection limit of 5 σ was chosen, because of the overall high RMS levels.

After this discussion of the overall data quality, the next section is focused on the individual radio maps.

5.1.3 Individual clusters at 240 MHz

In this section the map of each cluster is discussed in its own paragraph.

5.1.3.1 RXCJ0006.0−3443

In Fig.5.1 a region of 4Mpc around the cluster centre of RXCJ0006.0−3443 is shown.

There are **25** sources detected at $> 5\sigma$ level within 4 Mpc of the cluster centre, tabulated in Tab. D.1. There is no central bright source detected at this sensitivity. Of the 25 detected sources **four** are extended and **six** of them are located within a R_{500} radius. There might be additional sources present missed by the source detection as a very conservative detection level was chosen. Some artefacts are present around the brighter sources. Fig. 5.1 indicates the RMS to be as smooth as expected in the overall map. Fig. 5.2 shows the contours from the 610 MHz map as seen in the previous chapter overlaid on the 240 MHz map, demonstrating that the same sources were detected at both frequencies. All sources detected within R_{500} are listed in Tab. 5.6 There are optical galaxies in the central region of R_{500} associated with the cluster as indicated in Fig. 5.2 by the green circles the ones not associated are indicated by red circles. It is shown that no radio source has an optical counterpart. The additional radio sources lack an optical cross-identification, possibly caused by

Observed source	antennae used	Integration time	theoretical noise (Jy)	measured noise (Jy)	measured x times higher than theoretical	dynamic range	Resolution
RXCJ0006.0−3443	29	02:48:53	2.13×10^{-4}	1.98×10^{-3}	9.29	79	$20.4'' \times 8.4''$
RXCJ0020.7−2542	29	03:19:22	1.96×10^{-4}	8.36×10^{-3}	42.64	17	$17.1'' \times 8.8''$
RXCJ0049.4−2931	29	03:05:40	2.03×10^{-4}	9.92×10^{-3}	48.80	64	$24.3'' \times 15.0''$
RXCJ0211.4−4017	29	02:55:53	2.09×10^{-4}	4.22×10^{-3}	20.22	89	$21.0'' \times 9.8''$
RXCJ0225.1−2928	29	02:47:13	2.14×10^{-4}	3.28×10^{-3}	15.31	367	$26.1'' \times 12.8''$
RXCJ0605.8−3518	29	02:15:20	2.38×10^{-4}	8.31×10^{-3}	34.92	22	$21.0'' \times 8.9''$
RXCJ0821.8+0112	29	02:44:25	2.16×10^{-4}	2.69×10^{-3}	12.43	105	$19.1'' \times 11.3''$
RXCJ0958.3−1103	29	02:34:55	2.23×10^{-4}	2.48×10^{-3}	11.13	82	$18.9'' \times 9.7''$
RXCJ1141.4−1216	29	02:50:17	2.12×10^{-4}	6.75×10^{-3}	31.80	19	$11.0'' \times 9.4''$
RXCJ1236.7−3354	29	03:04:33	2.04×10^{-4}	2.97×10^{-2}	145.52	48	$31.6'' \times 12.7''$
RXCJ1311.4−0120	29	02:30:09	2.26×10^{-4}	1.44×10^{-2}	63.69	11	$123.1'' \times 68.0''$
RXCJ1516.5−0056	29	02:48:37	2.13×10^{-4}	1.59×10^{-2}	74.44	11	$50.8'' \times 22.3''$
RXCJ2014.8−2430	29	03:06:47	2.03×10^{-4}	5.09×10^{-3}	25.11	150	$24.6'' \times 9.4''$

Table 5.1: Observation properties for all clusters at observed at 240 MHz

either the faintness of the optical source or no associated redshift, making it impossible to determine if it is associated with the cluster. All known optical sources are provided in Tab. B.2. The redshift range used to identify cluster members was 0.075−0.125, chosen according to Yee (1996).
There are **no** newly confirmed radio sources associated with the cluster and **six** new cluster member candidates. **Two** more sources were detected compared to the 610 MHz map. One of them is a resolved double source. Further research is needed to verify if a cluster membership is given for these candidates.

5.1.3.2 RXCJ0020.7−2542

In Fig.5.3 a region of 4Mpc around the cluster centre of RXCJ0020.7−2542 is shown.
3 sources are detected at $> 5\sigma$ level within 4 Mpc of the cluster centre. These are tabulated in Table D.2. Of the 3 detected sources, **one** is a double source. There might be additional sources present, but due to the high level of background RFI present in this map it was not possible to determine exactly which ones are real and a very conservative level was chosen for source detection. There is RFI present throughout the whole map, especially to the top left, which is shown in Fig. 5.3. It was impossible to remove more RFI in this map without losing information about the real sources. Fig.5.4 shows the contours from the 610 MHz map, as seen in the previous chapter, overlaid on the 240 MHz map, demonstrating that the only one sources was detected at both frequencies, namely the bright central galaxy. The source detected within R_{500} is listed in Tab. 5.3. The optical galaxies in the central region of R_{500} which are associated with the cluster are indicated in Fig. 5.3 as green circles the ones not associated are red. It is shown that only the central bright source has an optical counterpart. All known positions of optical sources are given in Tab. B.3. The redshift range used to identify cluster members was 0.125−0.155, chosen according to Yee (1996).
There is **one** newly confirmed radio source associated with the cluster and **no** cluster member candidates. There were less sources detected compared to the 610 MHz

Source ID	RA	Δ RA	DEC	Δ DEC	total flux	Δ total flux	Peak flux	Δ Peak flux	optical cross-ID	cluster member	comments
11	00:06:41	0.000278	-34:50:28	0.00026	0.12079	0.006118	0.055358	0.004239	✗	?	
12	00:06:41	0.000074	-34:51:23	0.000205	0.062197	0.007252	0.058714	0.003984	✗	?	
14	00:06:15	0.00048	-34:47:31	0.000368	0.105934	0.005161	0.032198	0.004034	✗	?	
15	00:06:16	0.000194	-34:48:32	0.000448	0.079767	0.00583	0.034443	0.004212	✗	?	
15	00:06:16	0.000266	-34:49:04	0.000648	0.041295	0.006173	0.021914	0.004218	✗	?	
24	00:05:54	0.000374	-34:44:34	0.000288	0.09882	0.005049	0.037142	0.003747	✗	?	double
25	00:05:54	0.000142	-34:45:28	0.000321	0.026654	0.006633	0.03165	0.003124	✗	?	

Table 5.2: Positions of radio sources within R_{500} radius of the pointing centre of cluster RXCJ0006.0−3443 detected at a 5σ level.

map. Further research is needed to verify if a cluster membership is given for these candidates.

5.1.3.3 RXCJ0049.4−2931

In Fig.5.5 a region of 4Mpc around the cluster centre of RXCJ0049.4−2931 is shown.

Of the 5 detected sources **one** is extended. The are no sources within R_{500}. There might be additional sources present missed by the source detection as a very conservative detection level was chosen. Minor artefacts are present around the bright sources, and there is a smooth background as expected away from brighter sources, as Fig. 5.5 indicates. Fig. 5.6 shows the contours from the 610 MHz map, as shown in the previous chapter, overlaid on the 240 MHz map, demonstrating that no sources were detected at both frequencies. The optical galaxies in the central region of R_{500} which are associated with the cluster are indicated in Fig. 5.6 as green circles the ones not associated are red. All known positions of optical sources are provided in Tab. B.4. The redshift range used to identify cluster members was 0.085−0.115, chosen according to Yee (1996)

There is **no** newly confirmed radio source associated with the cluster and **no** new cluster member candidates. Further research is needed to verify if cluster members were missed due to lack of sensitivity.

5.1.3.4 RXCJ0211.4−4017

In Fig. 5.7 a region of 4 Mpc around the cluster centre of RXCJ0211.4−4017 is shown.

15 sources are detected at $> 5\sigma$ level within 4 Mpc of the cluster centre. These are tabulated in Table D.4. Of the 15 detected sources, **one** is a double sources and **two** are extended.The is **one** extended source within R_{500}. There might be additional sources present missed by the source detection as a very conservative detection level was chosen. Minor artefacts are present around the bright central source. The overall smooth RMS structure is shown in Fig. 5.7.The sources show a very small elongation which might be caused by some leftover dirty beam structure, which

Source ID	RA	Δ RA	DEC	Δ DEC	total flux	Δ total flux	Peak flux	Δ Peak flux	optical cross-ID	cluster member	comments
3	00:20:43	0.000177	-25.71057	-25:42:38	0.116106	0.020092	0.083105	0.012562	✔	✔	BCG

Table 5.3: Positions of radio sources within R_{500} radius of the pointing centre of cluster RXCJ0020.7−2542 detected at a 5σ level.

we were not able to remove. Fig. 5.8 shows the contours from the 610 MHz map, as seen in the previous chapter, overlaid on the 240 MHz map, demonstrating that more sources were detected in the 240 MHz map. These sources are listed in 5.4.
The optical galaxies in the central region of R_{500} which are associated with the cluster are indicated in Fig. 4.10 as green circles. The central bright extended radio source is the only one with an optical counterpart. The additional radio source lacks an optical cross-identification, possibly caused by the faintness of the optical source or lack of determined redshift, making it impossible to determine if it is associated with the cluster. All optical identified galaxies with known position and redshift in this region of the sky are tabulated in Tab. B.5. The redshift range used to identify cluster members was $0.085-0.115$, chosen according to Yee (1996)
There is **one** newly confirmed radio source associated with the cluster and **one** new cluster member candidate. Further research is needed to verify if a cluster membership is given for this candidate.

5.1.3.5 RXCJ0225.1−2928

In Fig. 5.9 a region of 4Mpc around the cluster centre of RXCJ0225.1−2928 is shown.
50 sources are detected at $> 5\sigma$ level within 4 Mpc of the cluster centre. These are tabulated in Table D.5. Of the 50 detected sources, **five** are extended.The are **two** extended source within R_{500}.There might be additional sources present missed by the source detection as a very conservative detection level was chosen. There is very little RFI present in this map. The overall smooth RMS structure is shown in Fig. 5.9. Fig. 5.10 shows the contours from the 610 MHz map, as provided in the previous chapter, overlaid on the GMRT map, demonstrating that one source was at both frequencies. There is one extended source close to the centre of cluster detected at 240 MHz, but not at 610 MHz. Given its extended structure it would be interesting if this source is present at even lower frequencies. The radio sources detected within R_{500} are listed in Tab.5.5. The optical galaxies in the central region of R_{500} which are associated with the cluster are indicated in Fig. 5.10 as green circles. There are no radio sources with an optical counterpart. The lack of optical counterparts for the radio sources could be caused by either the faintness of the

Source ID	RA	Δ RA	DEC	Δ DEC	total flux	Δ total flux	Peak flux	Δ Peak flux	optical cross-ID	cluster member	comments
17	02:11:25	0.000014	-40:17:25	0.000044	0.459104	0.00816	0.376854	0.004749	✔	✔	BCG
18	02:11:27	0.000213	-40:18:49	0.000703	0.032634	0.008037	0.02474	0.004812	✗	?	

Table 5.4: Positions of radio sources within R_{500} radius of the pointing centre of cluster RXCJ0211.4−4017 detected at a 5σ level.

optical source or no associated redshift, making it impossible to determine its cluster membership. All optical identified galaxies are tabulated in Tab. B.6. The redshift range used to identify cluster members was $0.045-0.75$, chosen according to Yee (1996).

There are **no** newly confirmed radio source associated with the cluster and **four** new cluster member candidates. Further research is needed to verify if a cluster membership is given for these candidates.

5.1.3.6 RXCJ0605.8−35/18

In Fig.5.1 a region of 4Mpc around the cluster centre of RXC0605.8-35/18− is shown.

There are **12** sources detected at $> 5\sigma$ level within 4 Mpc of the cluster centre. These are tabulated in Tab. D.1. There is one central bright source detected at this sensitivity. Of the 12 detected sources, **one** is extended and **four** of them are located within a R_{500} radius. There might be additional sources present missed by the source detection as a very conservative detection level was chosen. Some artefacts are present around the brighter sources, which show a slight elongation, which might be caused by some leftover dirty beam structure, which we were not able to remove. Fig. 5.2 shows the contours from the 610 MHz map as seen in the previous chapter overlaid on the 240 MHz map, demonstrating that the same sources were detected at both frequencies, but slightly shifted, which could be caused by phase calibration issues which we were unable to remove. For analysis of this source this shift was taken into account. All sources detected within R_{500} are listed in Tab. 5.6 The optical galaxies associated with the cluster are indicated in Fig. 5.2 by the green circles the ones not associated are indicated by red circles. It is shown that only the bright central galaxy has an optical counterpart. The additional radio sources lack

Source ID	RA	Δ RA	DEC	Δ DEC	total flux	Δ total flux	Peak flux	Δ Peak flux	optical cross-ID	cluster member	comments
44	02:25:16	0.000452	-29:27:24	0.000633	0.034493	0.007932	0.025187	0.004993	✗	?	}ext.
44	02:25:16	0.000865	-29:27:42	0.000814	0.020608	0.008007	0.017412	0.004642	✗	?	
46	02:25:09	0.000371	-29:27:49	0.000625	0.313555	0.004871	0.04872	0.00425	✗	?	
47	02:24:42	0.000089	-29:34:16	0.000039	0.284302	0.010713	0.204501	0.004698	✗	?	

Table 5.5: Positions of radio sources within R_{500} radius of the pointing centre of cluster RXCJ0225.1−2928 detected at a 5σ level.

Source ID	RA	Δ RA	DEC	Δ DEC	total flux	Δ total flux	Peak flux	Δ Peak flux	optical cross-ID	cluster member	comments
5	06:06:26	0.000199	-35:17:17	0.000272	0.174174	0.015665	0.139492	0.008193	✗	?	
12	06:05:54	0.000014	-35:18:09	0.000009	4.290157	0.041503	3.801031	0.017773	✔	✔	BCG
15	06:05:53	0.000257	-35:16:17	0.000329	0.161033	0.027103	0.161118	0.01266	✗	?	
17	06:05:42	0.000401	-35:22:01	0.000524	0.1007	0.022636	0.097866	0.01013	✗	?	

Table 5.6: Positions of radio sources within R_{500} radius of the pointing centre of cluster RXCJ0605.8-3518 detected at a 5σ level.

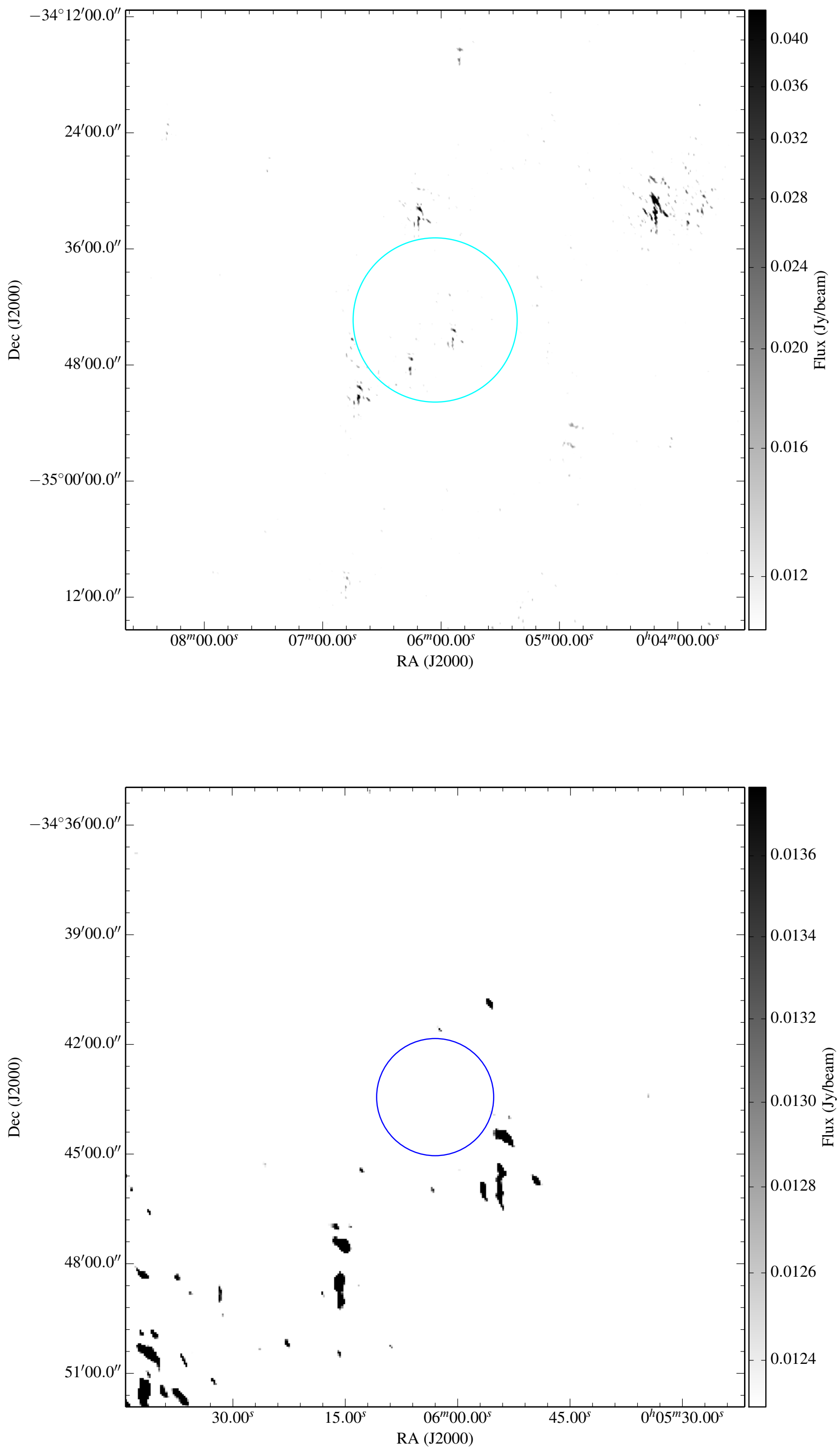

Figure 5.1: 240-MHz GMRT maps of RXCJ0006.0−3443.Top : overview of a region 4 Mpc × 4 Mpc centred on the cluster, R_{500} being indicated by the circle; bottom: central region of the cluster ($R_{500} \times R_{500}$)the circle indicates a region of radius 200kpc around the centre.

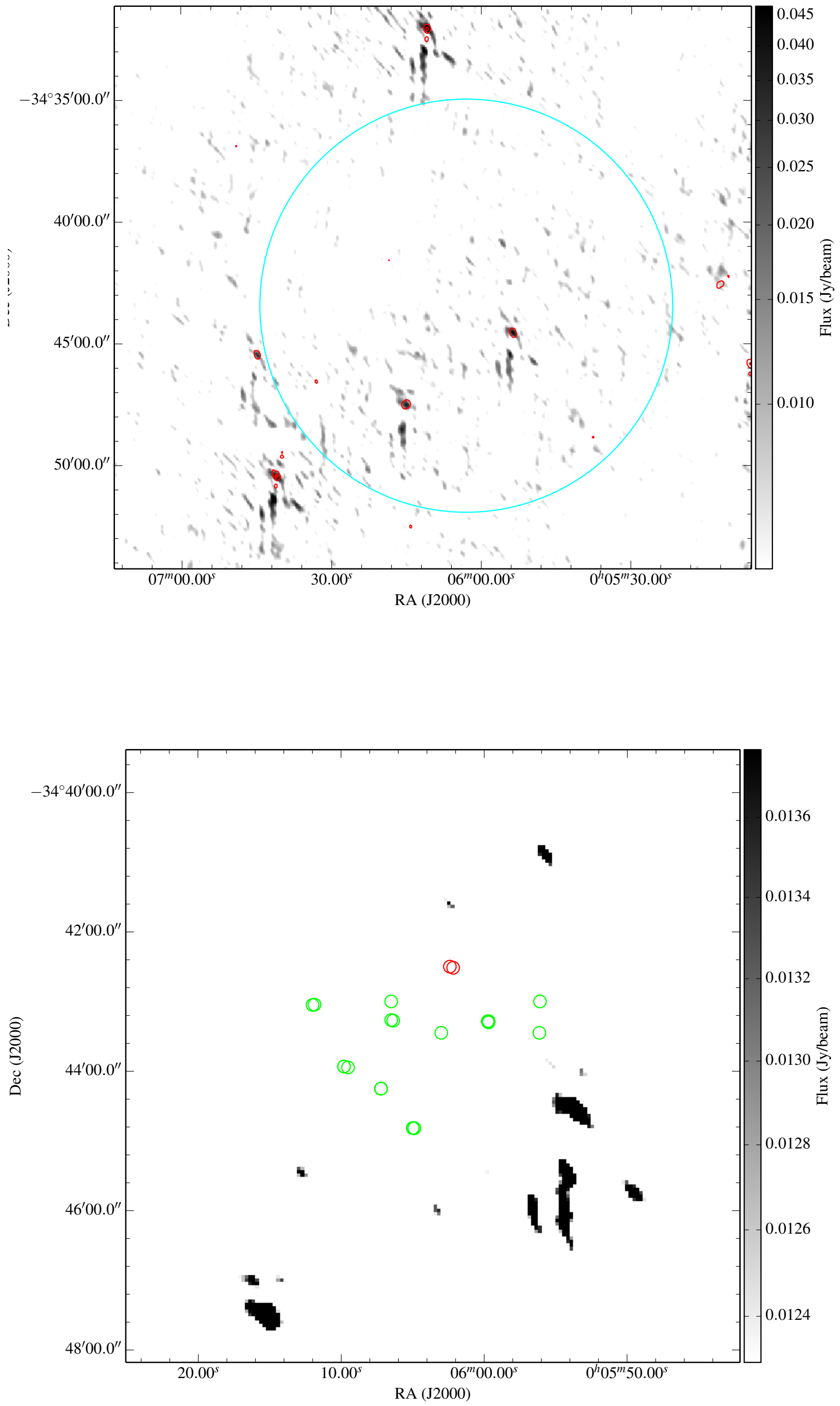

Figure 5.2: 240-MHz GMRT maps of RXCJ0006.0−3443. central region of the cluster ($R_{500} \times R_{500}$); top: contours from 610 MHz map overlaid; bottom: positions of known cluster member galaxies overlaid in green and known background or foreground sources indicated by red circles.

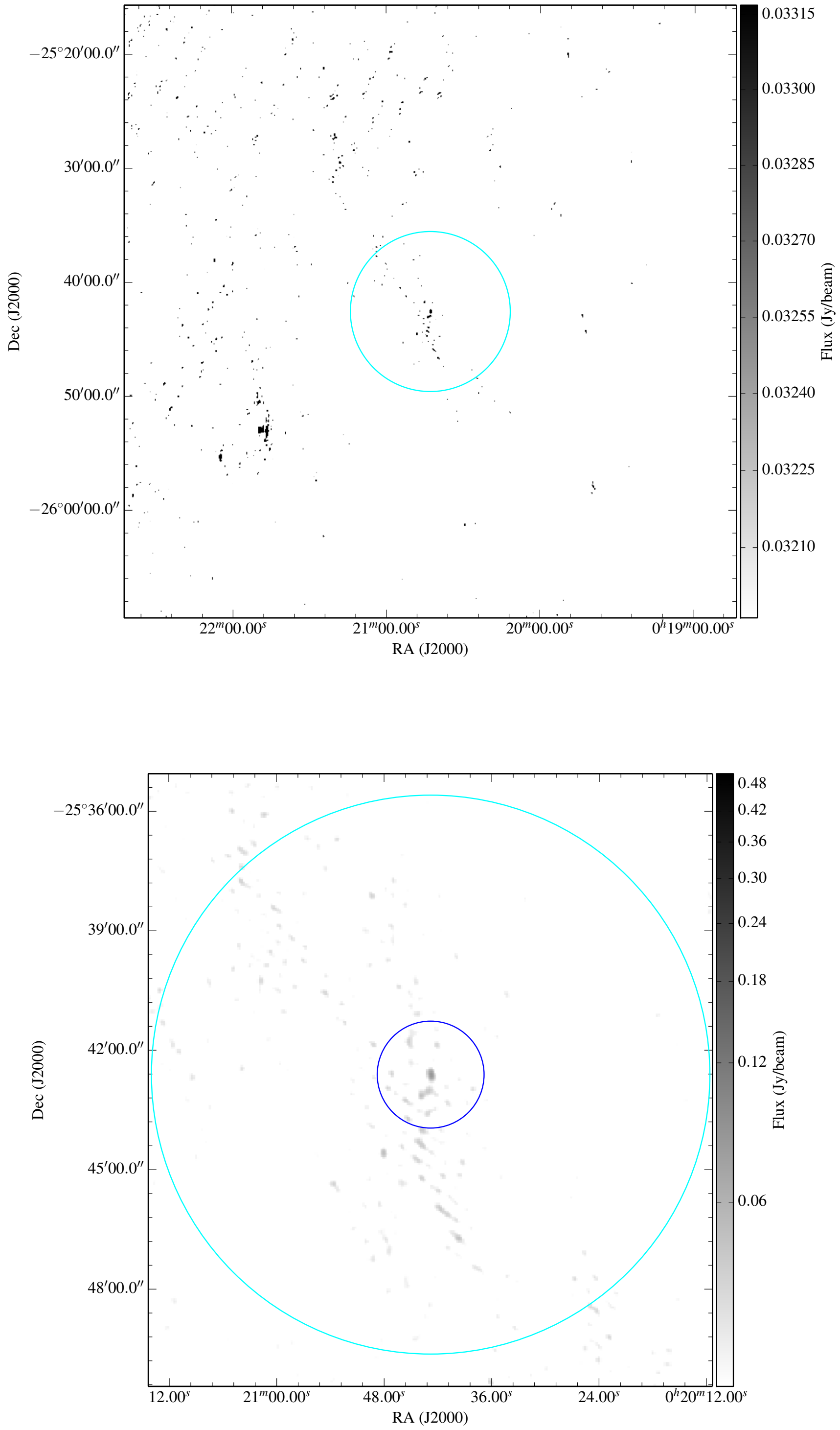

Figure 5.3: 240-MHz GMRT maps of RXCJ0020.7−2542. Top: overview of a region 4 Mpc $\times$ 4 Mpc centred on the cluster, R_{500} being indicated by the circle; bottom: central region of the cluster ($R_{500} \times R_{500}$)the circle indicates a region of radius 200kpc around the centre.

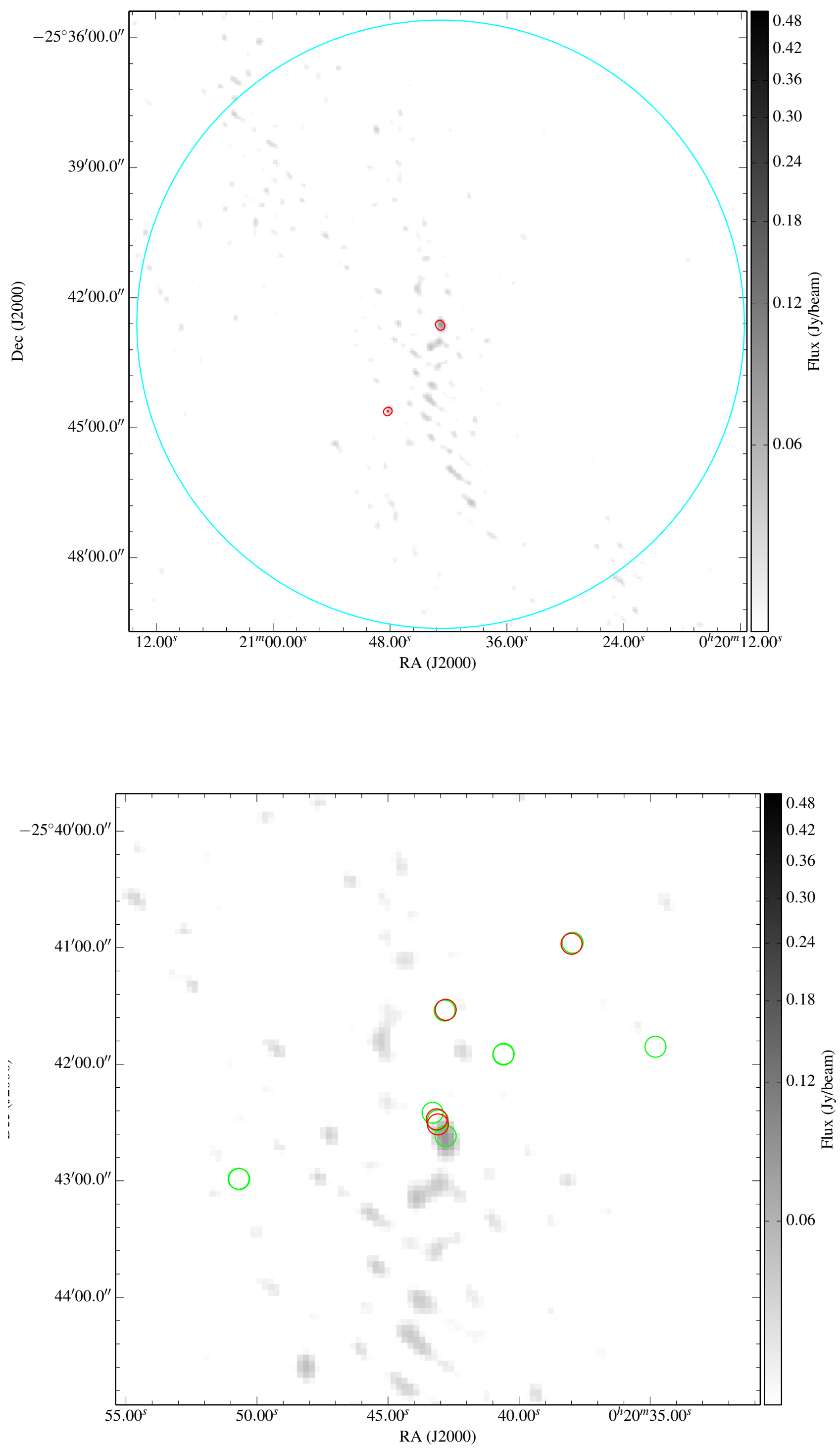

Figure 5.4: 240-MHz GMRT maps of RXCJ0020.7−2542. top: central region of the cluster ($R_{500} \times R_{500}$) contours from 610 MHz map overlaid; bottom: positions of known cluster member galaxies overlaid in green and known background or foreground sources indicated by red circles zoomed in to a region of 200kpc $\times$ 200kpc.

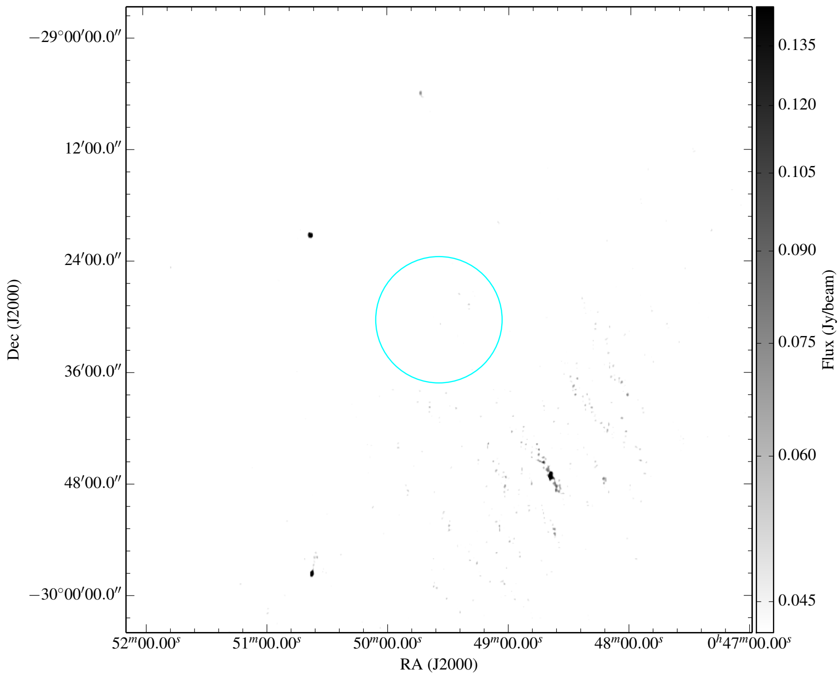

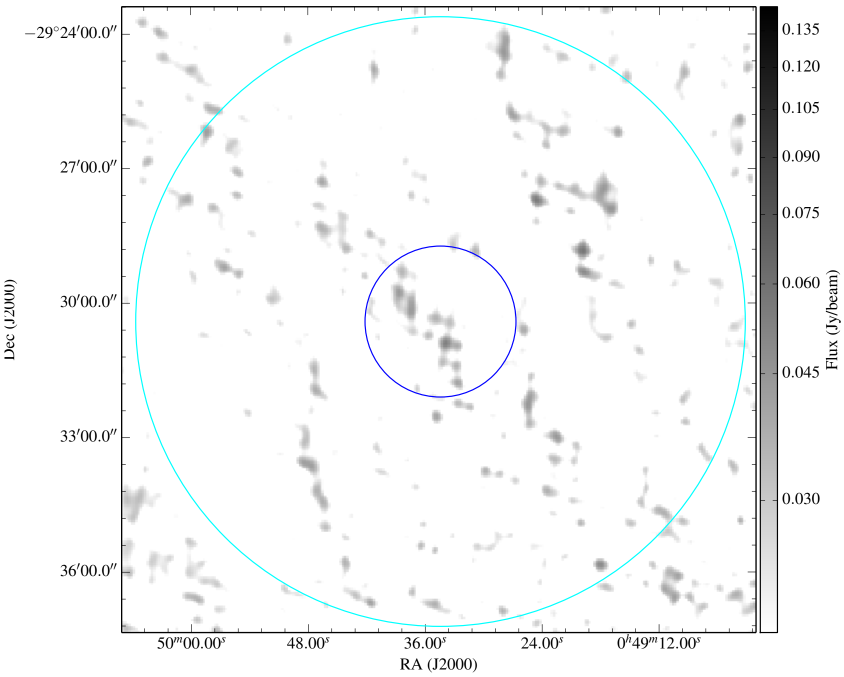

Figure 5.5: 240-MHz GMRT maps of RXCJ0049.4−2931.Top: overview of a region 4 Mpc × 4 Mpc centred on the cluster, R_{500} being indicated by the circle; bottom: central region of the cluster ($R_{500} \times R_{500}$)the circle indicates a region of radius 200kpc around the centre. There are no sources detected within this radius, all structure shown in this map is RFI, which helps in getting an idea of the smoothness of the RFI structure

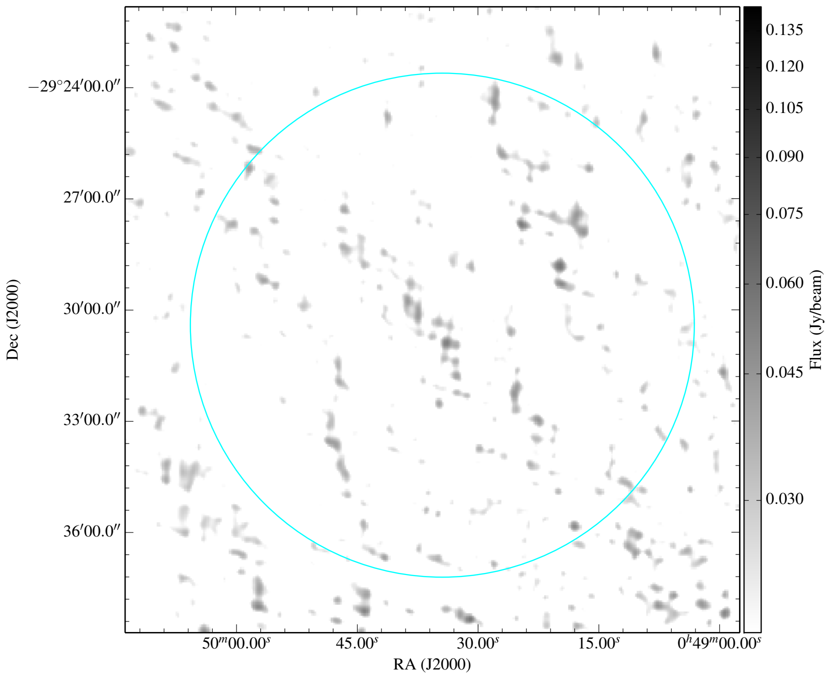

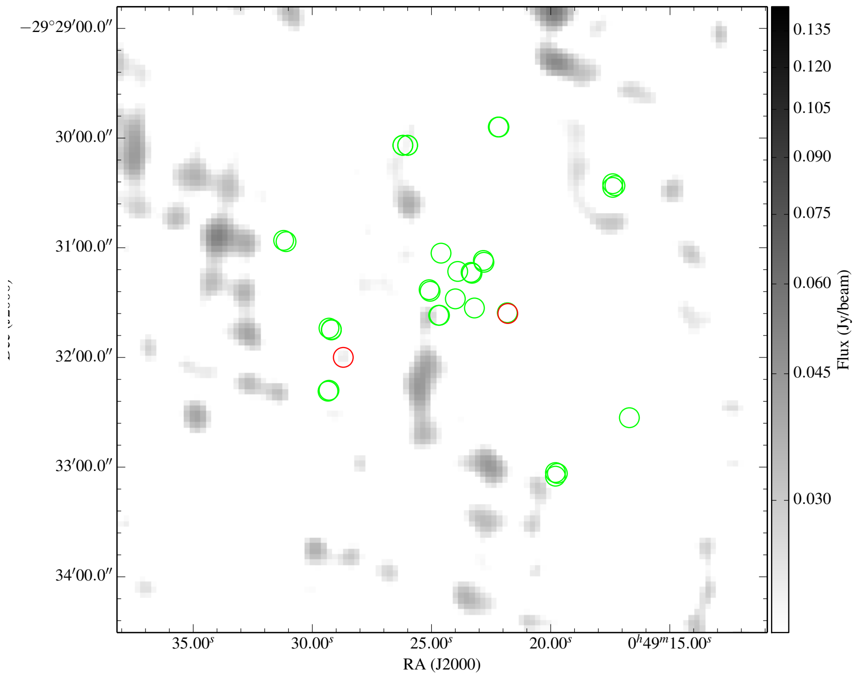

Figure 5.6: 240-MHz GMRT maps of RXCJ0049.4−2931.central region of the cluster ($R_{500} \times R_{500}$); top: contours from 610 MHz map overlaid; bottom: positions of known cluster member galaxies overlaid in green and known background or foreground sources indicated by red circles zoomed in to a region of 200kpc $\times$ 200kpc.

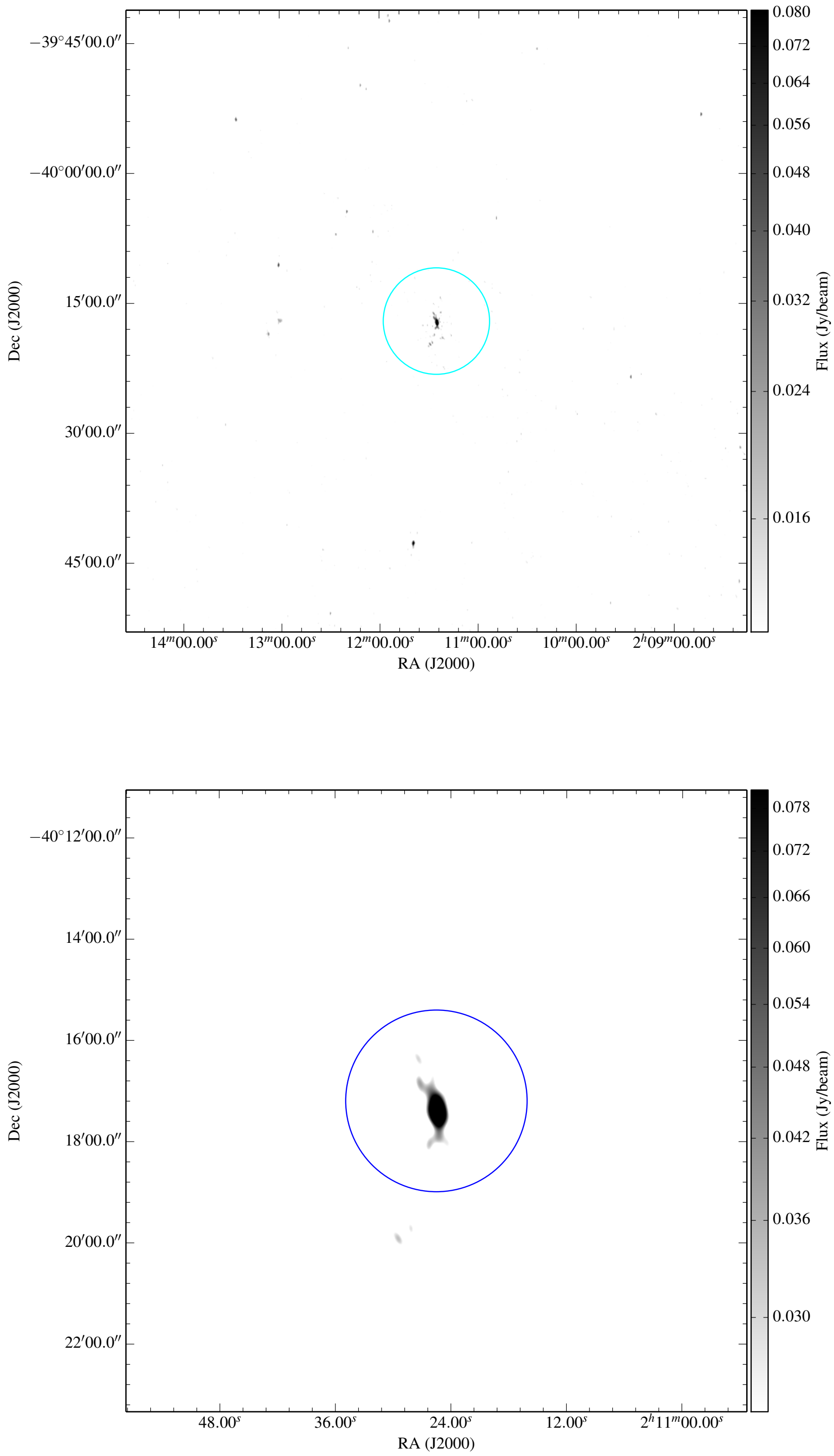

Figure 5.7: 240-MHz GMRT maps of RXCJ0211.4−4017.Top: overview of a region 4 Mpc $\times$ 4 Mpc centred on the cluster, R_{500} being indicated by the circle; bottom: central region of the cluster ($R_{500} \times R_{500}$)the circle indicates a region of radius 200kpc around the centre.

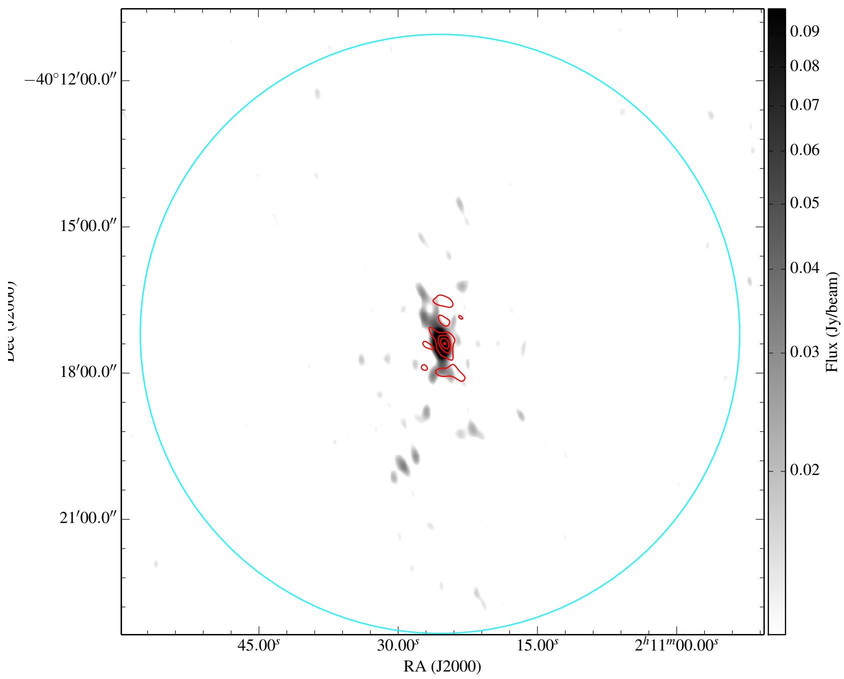

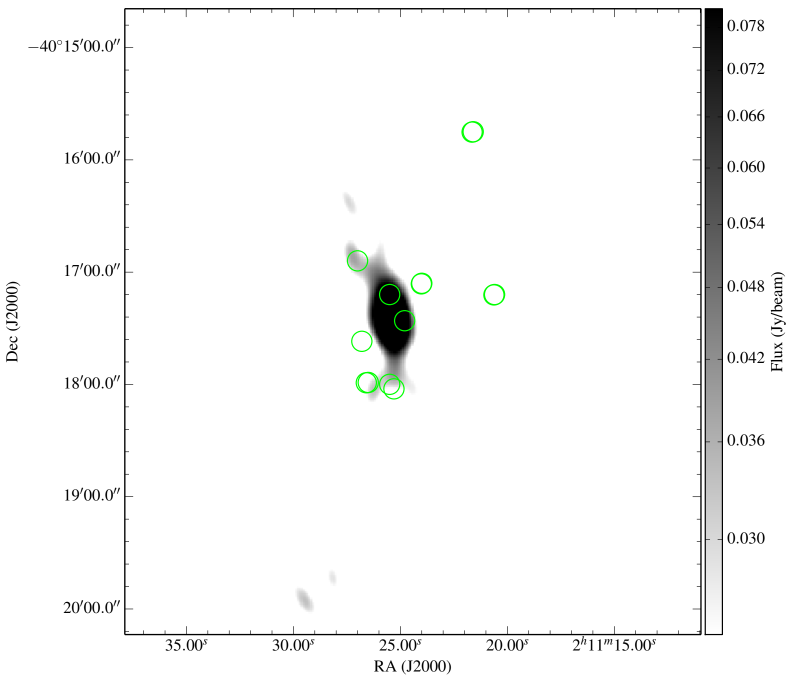

Figure 5.8: 240-MHz GMRT maps of RXCJ0211.4−4017.central region of the cluster ($R_{500} \times R_{500}$); top: contours from 610 MHz map overlaid; bottom: positions of known cluster member galaxies overlaid in green.

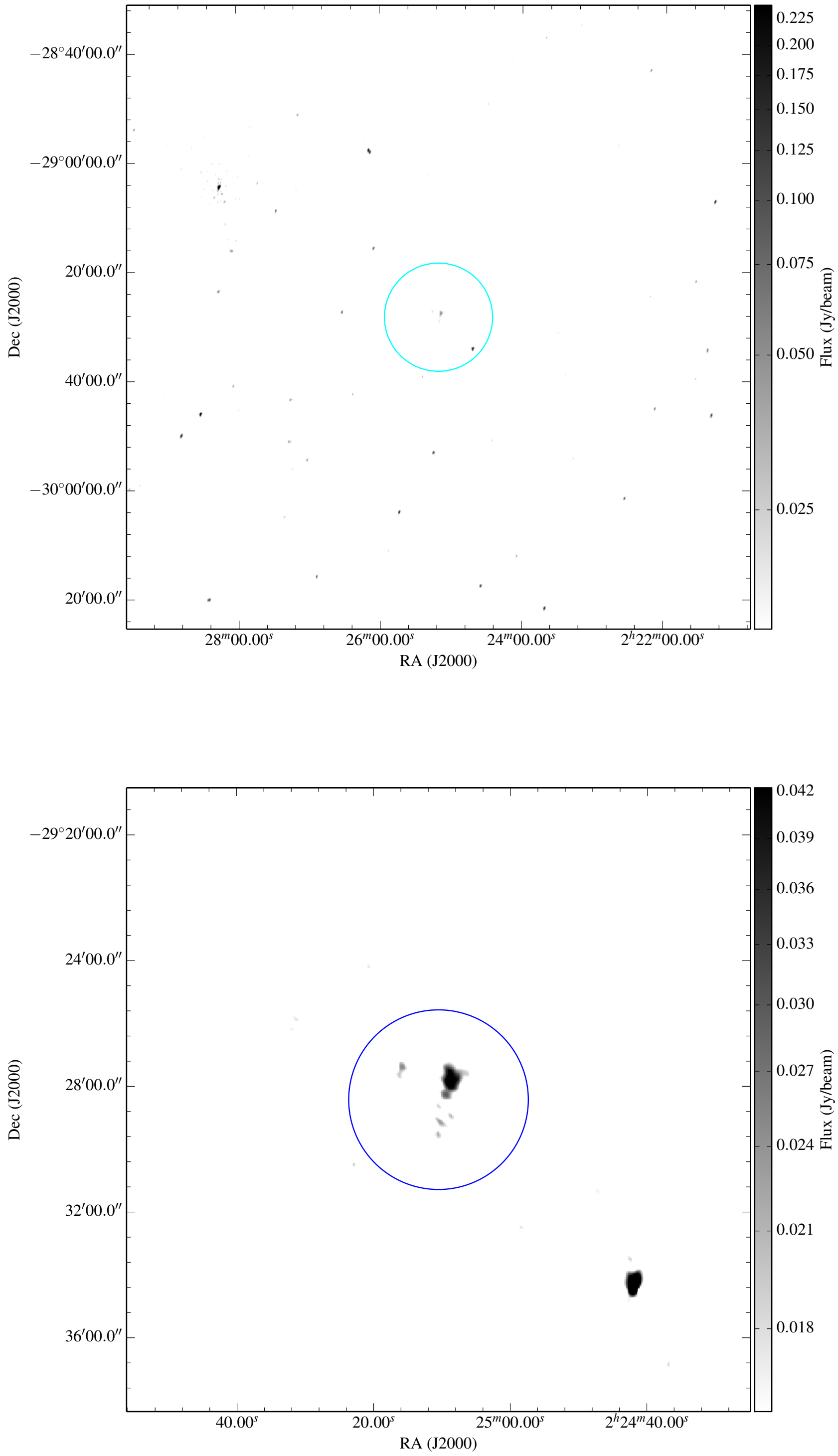

Figure 5.9: 240-MHz GMRT maps of RXCJ0225.1−2928.Top: overview of a region 4 Mpc $\times$ 4 Mpc centred on the cluster, R_{500} being indicated by the circle; bottom: central region of the cluster ($R_{500} \times R_{500}$)the circle indicates a region of radius 200kpc around the centre.

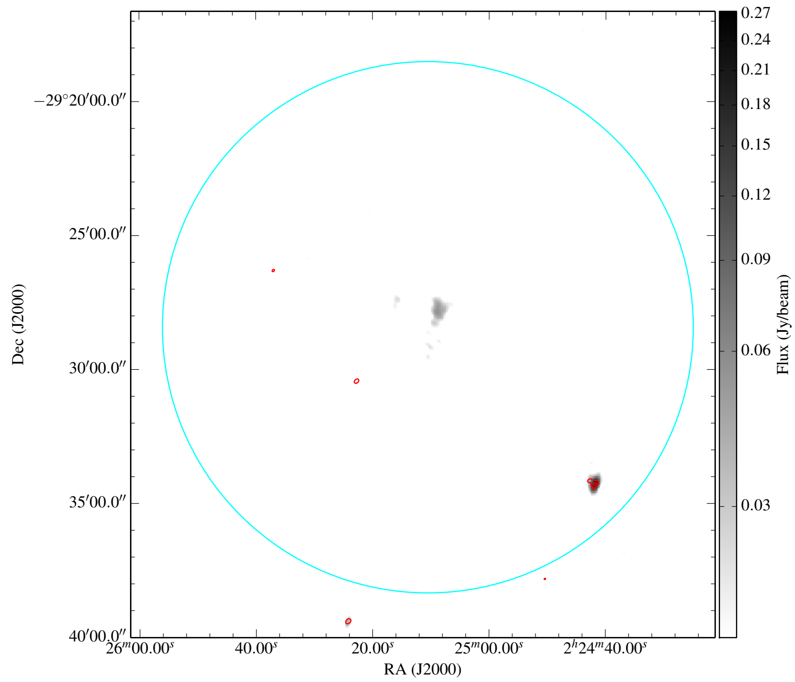

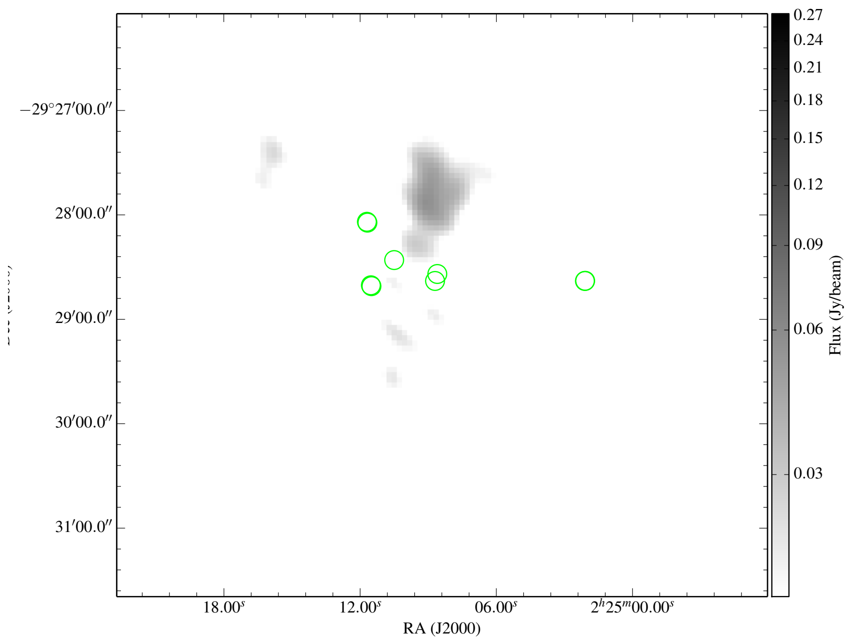

Figure 5.10: 240-MHz GMRT maps of RXCJ0225.1−2928. central region of the cluster ($R_{500} \times R_{500}$)the circle indicates a region of radius 200kpc around the centre; Top: contours from 610 MHz map overlaid; bottom: positions of known cluster member galaxies overlaid in green zoomed in to a region of 200kpc $\times$ 200kpc.

an optical cross-identification, possibly caused by either the faintness of the optical source or no associated redshift, making it impossible to determine if it is associated with the cluster. All known optical sources are provided in Tab. B.2. The redshift range used to identify cluster members was 0.115−0.145, chosen according to Yee (1996).
There is **one** newly confirmed radio source associated with the cluster and **three** new cluster member candidates. There are **no** more radio sources detected at 240MHz than at 610MHz. Further research is needed to verify if a cluster membership is given for these candidates.

5.1.3.7 RXCJ0821.8+0112

In Fig.5.1 a region of 4Mpc around the cluster centre of RXCJ0821.8 + 0112 is shown.
There are **27** sources detected at $> 5\sigma$ level within 4 Mpc of the cluster centre. These are tabulated in Tab. D.1. There is no central bright source detected at this sensitivity. Of the 27 detected sources, **four** are extended and **one** of them is located within a R_{500} radius. There might be additional sources present missed by the source detection as a very conservative detection level was chosen. Some artefacts are present. Fig. 5.1 indicates the RMS structure of the map as a whole. All sources show some elongation possibly caused by some leftover structure from the dirty beam, which we were not able to remove. Fig. 5.2 shows the contours from the 610 MHz map as seen in the previous chapter overlaid on the 240 MHz map, demonstrating that only one source, was detected at both frequencies. The other sources within R500 were missed by the detection, possibly caused by choosing a higher detection limit or by the high RMS. All sources detected within R_{500} are listed in Tab. 5.6 There are no optical galaxies in the central region of R_{500} associated with the cluster as indicated in Fig. 5.2 by the green circles the ones not associated are indicated by red circles. It is shown that no radio sources has an optical counterpart. The additional radio source lacks an optical cross-identification, possibly caused by either the faintness of the optical source or no associated redshift, making it impossible to determine if it is associated with the cluster. All known optical sources are provided in Tab. B.2. The redshift range used to identify cluster members was

Source ID	RA	Δ RA	DEC	Δ DEC	total flux	Δ total flux	Peak flux	Δ Peak flux	optical cross-ID	cluster member	comments
16	08:21:60	0.000092	01:10:55	0.000141	0.075586	0.005567	0.066222	0.003189	✗	?	

Table 5.7: Positions of radio sources within R_{500} radius of the pointing centre of cluster RXCJ0821.8+0112 detected at a 5σ level.

0.065−0.95, chosen according to Yee (1996).
There is no **no** newly confirmed radio source associated with the cluster and **one** new cluster member candidate. There are 11 sources less deteted at 240 MHz than at 610 MHz, It is worth mentioning, that the central source does extend much further at 240 MHz Further research is needed to verify if a cluster membership is given for this candidate.

5.1.3.8 RXCJ0958.3-1103

In Fig.5.15 a region of 4Mpc around the cluster centre of RXCJ0958.3-1103 is shown.
There are **19** sources detected at $> 5\sigma$ level within 4 Mpc of the cluster centre, tabulated in Tab. D.8. Of the 19 detected sources, **three** are extended and **two** of them are located within a R_{500} radius. There might be additional sources present missed by the source detection as a very conservative detection level was chosen. Some artefacts are present around the brighter sources. Fig. 5.15 indicates the RMS to be as smooth as expected in the overall map. Fig. 5.16 shows the contours from the 610 MHz map as seen in the previous chapter overlaid on the 240 MHz map, demonstrating that some sources were detected at both frequencies, with others were only,detected at one frequency. It is worth mentioning, that the central source does extend much further at 240 MHz All sources detected within R_{500} are listed in Tab. 5.8 There is only the bright central galaxy associated with an optical galaxies in the central region of R_{500} as indicated in Fig. 5.16 by the green circles the ones not associated are indicated by red circles. The additional radio sources lack an optical cross-identification, possibly caused by either the faintness of the optical source or no associated redshift, making it impossible to determine if it is associated with the cluster. All known optical sources are provided in Tab. B.12. The redshift range used to identify cluster members was 0.145−0.175, chosen according to Yee (1996).
There is**one** newly confirmed radio source associated with the cluster and seven new cluster member candidates. Further research is needed to verify if a cluster membership is given for these candidates.

5.1.3.9 RXCJ1141.4−1216

In Fig.5.17 a region of 4Mpc around the cluster centre of RXCJ1141.4−1216 is shown.
There are **21** sources detected at $> 5\sigma$ level within 4 Mpc of the cluster centre.

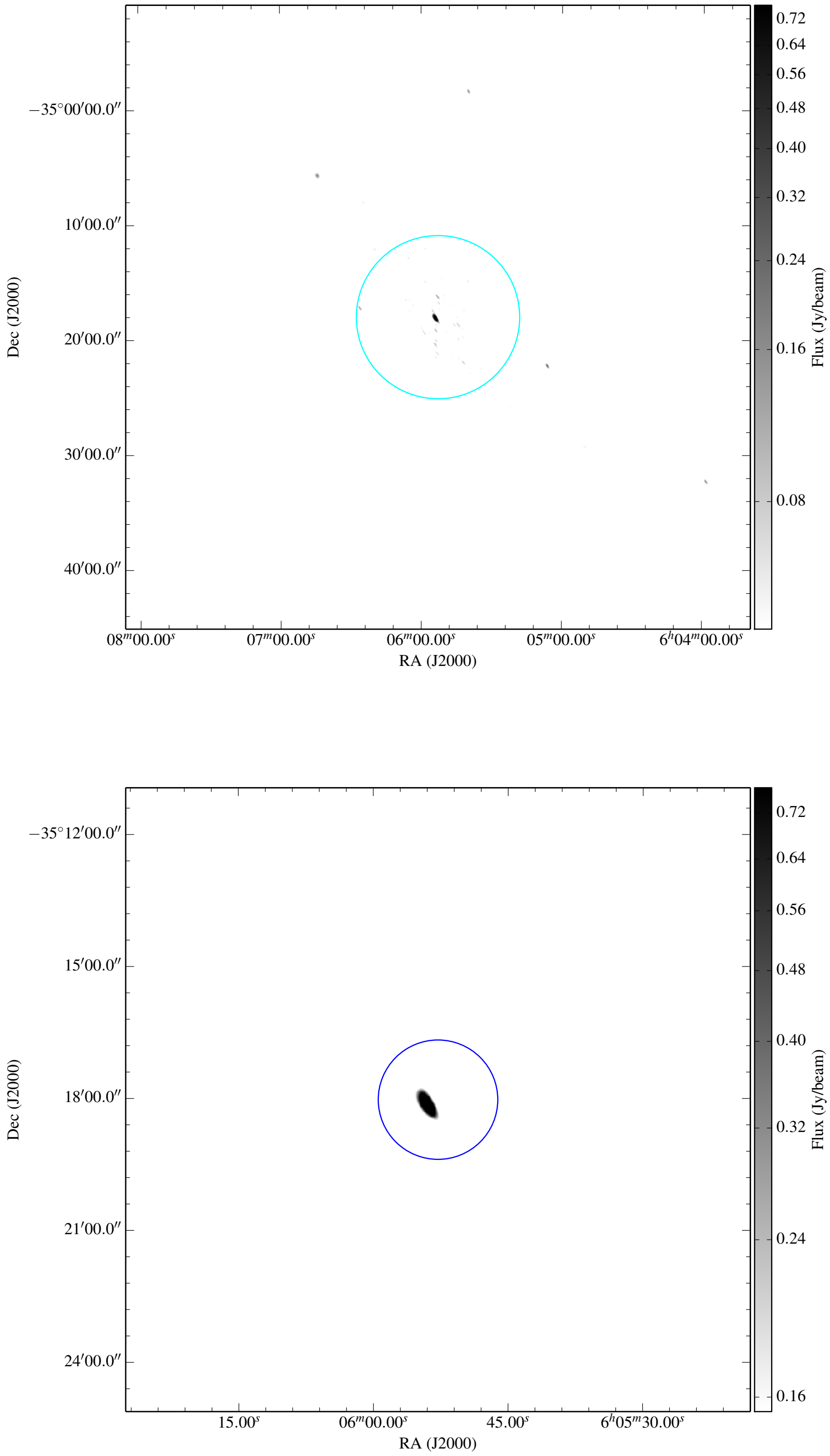

Figure 5.11: 240-MHz GMRT maps of RXCJ0605.8−3518.Top: overview of a region 4 Mpc × 4 Mpc centred on the cluster, R_{500} being indicated by the circle; bottom: central region of the cluster ($R_{500} \times R_{500}$)the circle indicates a region of radius 200kpc around the centre.

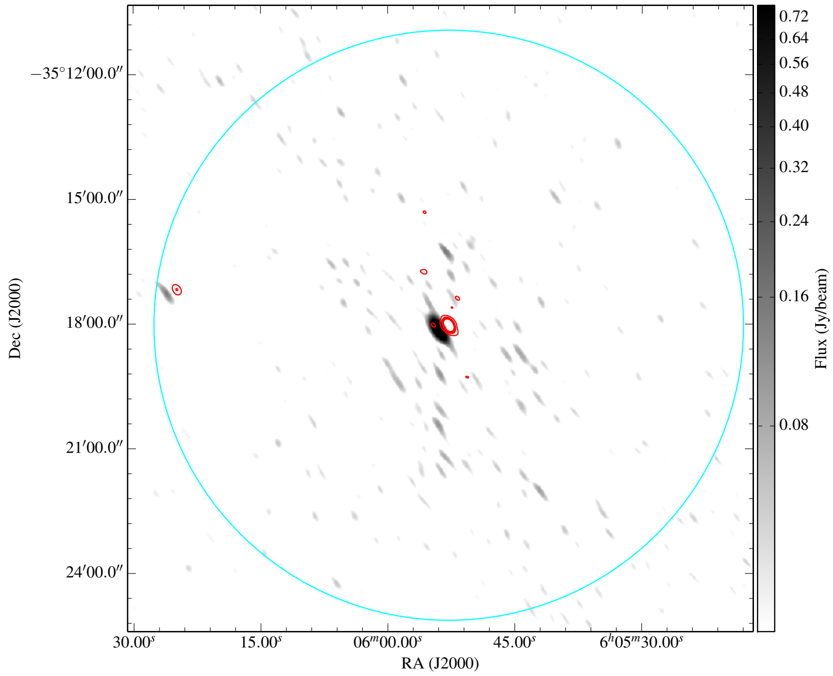

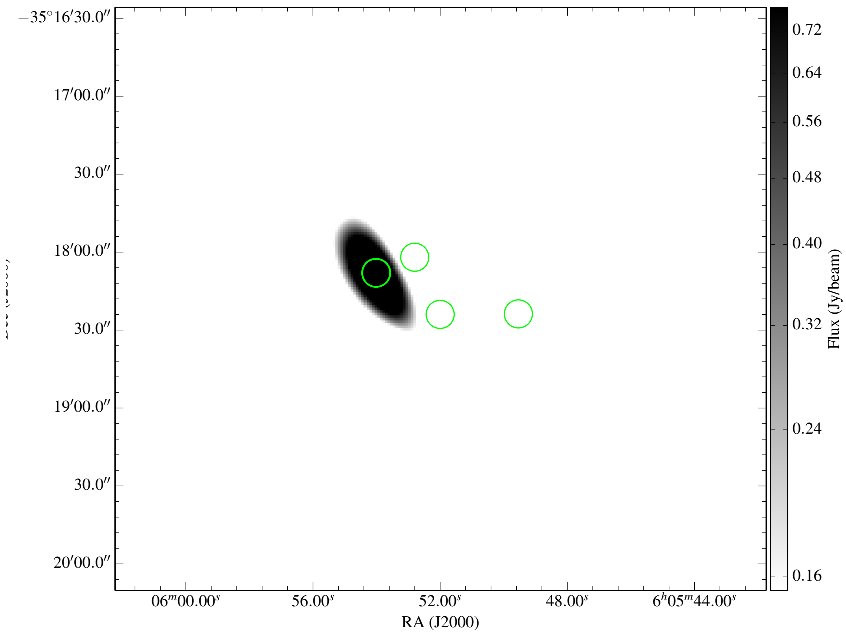

Figure 5.12: 240-MHz GMRT maps of RXCJ0605.8−3518. central region of the cluster ($R_{500} \times R_{500}$); top: contours from 610 MHz map overlaid; bottom: positions of known cluster member galaxies overlaid in green.

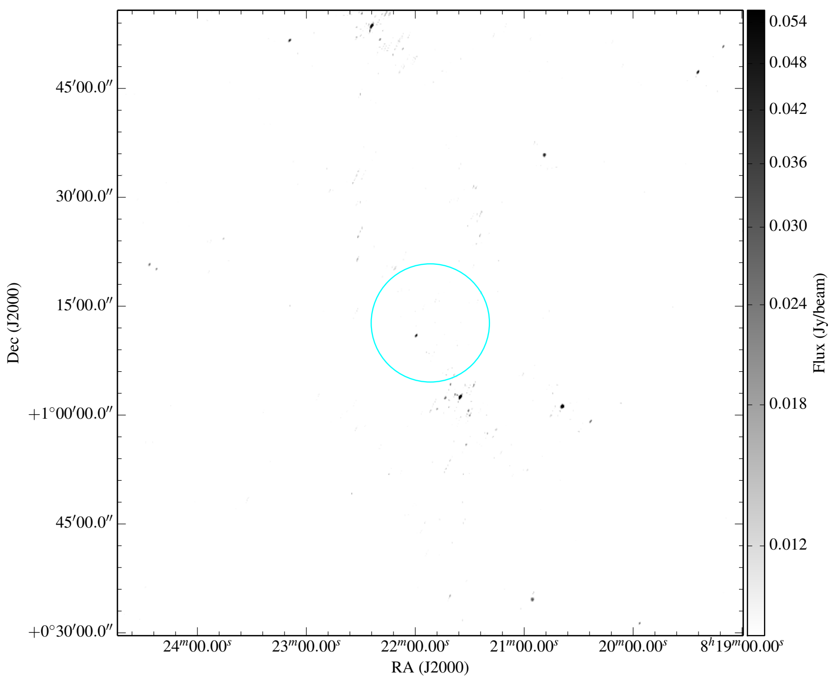

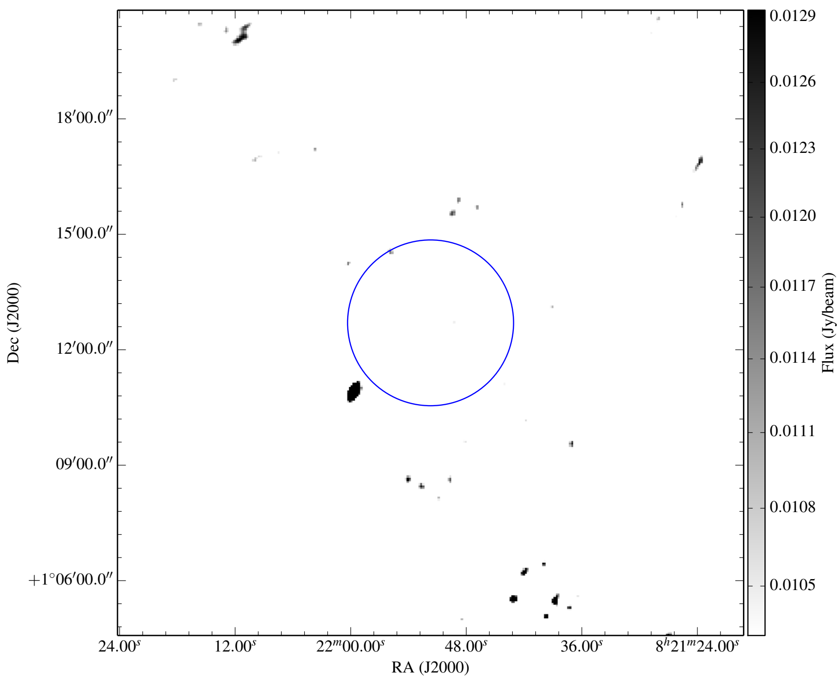

Figure 5.13: 240-MHz GMRT maps of RXCJ0821.8+0112.Top: overview of a region 4 Mpc × 4 Mpc centred on the cluster, R_{500} being indicated by the circle; bottom: central region of the cluster ($R_{500} \times R_{500}$)the circle indicates a region of radius 200kpc around the centre.

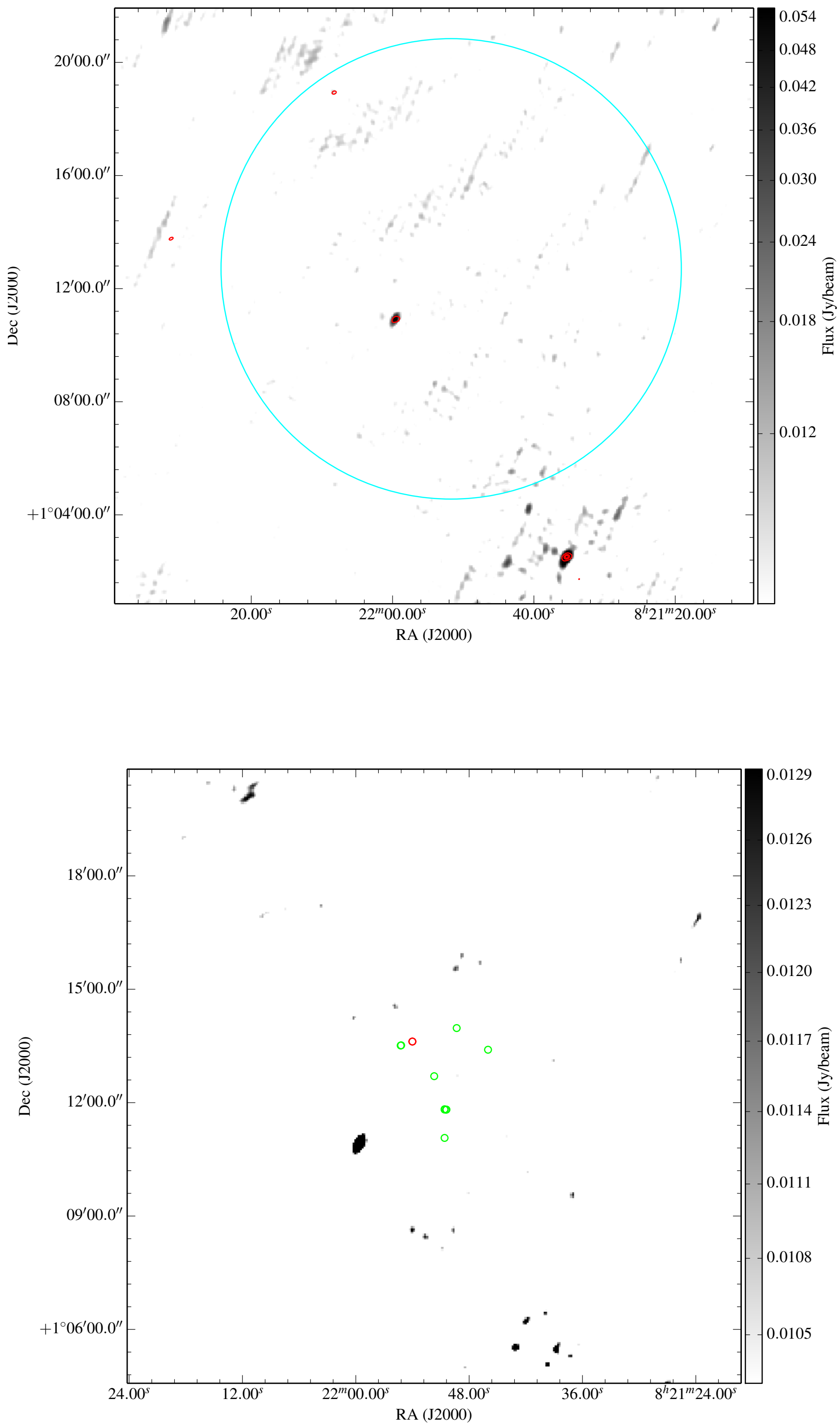

Figure 5.14: 240-MHz GMRT maps of RXCJ0821.8+0112. central region of the cluster ($R_{500} \times R_{500}$); top: contours from 610 MHz map overlaid; bottom: positions of known cluster member galaxies overlaid in green and known background or foreground sources indicated by red circles.

These are tabulated in Tab. D.9. Of the 21 detected sources, **three** are extended and **two** are located within a R_{500} radius. There might be additional sources present missed by the source detection as a very conservative detection level was chosen. Some artefacts are present at the top left comer. Fig. 5.17 indicates the RMS to be as smooth as expected in the overall map. Fig. 5.18 shows the contours from the 610 MHz map as seen in the previous chapter overlaid on the 240 MHz map, demonstrating that same sources were detected at both frequencies. All sources detected within R_{500} are listed in Tab. 5.9 Fig. 5.18 indicates the, optical galaxies associated with this cluster by the green circles the ones not associated by red circles. It is shown that only one radio source, has an optical counterpart, which happens to be the central bright one. The additional radio source lacks an optical cross-identification, possibly caused by either the faintness of the optical source or no associated redshift, making it impossible to determine if it is associated with the cluster. All known optical sources are provided in Tab. B.14. The redshift range used to identify cluster members was 0.095−0.125, chosen according to Yee (1996). There is **one** newly confirmed radio source associated with the cluster and **one** new cluster member candidates. There are more sources detected at 610 MHz, possilby caused by the much lower RMS level. Further research is needed to verify if a cluster membership is given for these candidates.

5.1.3.10 RXCJ1236.7−3354

In Fig.5.19 a region of 4Mpc around the cluster centre of RXCJ1236.7−3354 is shown.

There are **35** sources detected at $> 5\sigma$ level within 4 Mpc of the cluster centre.

Source ID	RA	Δ RA	DEC	Δ DEC	total flux	Δ total flux	Peak flux	Δ Peak flux	optical cross-ID	cluster member	comments
4	09:58:34	0.000199	-11:03:53	0.000496	0.014972	0.004436	0.013911	0.002515	✗	?	
6	09:58:32	0.000117	-10:59:54	0.000457	0.017758	0.00479	0.017719	0.002567	✗	?	
14	09:58:22	0.000011	-11:03:51	0.000044	0.20004	0.005232	0.202105	0.002773	✗	✓	} ext., BCG
14	09:58:23	0.000101	-11:04:14	0.000323	0.018051	0.005388	0.022101	0.002702	✗	✓	
15	09:58:22	0.000109	-11:04:31	0.000379	0.025674	0.005285	0.023929	0.00294	✗	?	
17	09:58:21	0.000058	-11:05:25	0.000234	0.038121	0.005484	0.039274	0.002884	✗	?	
19	09:58:19	0.000153	-11:01:01	0.000457	0.017766	0.005175	0.017408	0.002867	✗	?	
21	09:58:17	0.000071	-11:03:54	0.000348	0.027303	0.005381	0.028266	0.002742	✗	?	
23	09:58:16	0.000108	-11:02:50	0.000382	0.017847	0.005402	0.020427	0.002767	✗	?	

Table 5.8: Positions of radio sources within R_{500} radius of the pointing centre of cluster RXCJ0958.3−1103 detected at a 5σ level.

Source ID	RA	Δ RA	DEC	Δ DEC	total flux	Δ total flux	Peak flux	Δ Peak flux	optical cross-ID	cluster member	comments
17	11:41:49	0.00017	-12:12:02	0.00042	0.047982	0.011619	0.038559	0.006853	✗	?	
19	11:41:24	0.000072	-12:16:39	0.000085	0.273151	0.022927	0.233406	0.013883	✔	✔	BCG

Table 5.9: Positions of radio sources within R_{500} radius of the pointing centre of cluster RXCJ1141.4−1216 detected at a 5σ level.

These are tabulated in Tab. D.10. There is no central bright source detected at this sensitivity. Of the 35 detected sources, **four** seven are extended, but no one is within and within a R_{500} radius. There might be additional sources present missed by the source detection as a very conservative detection level was chosen. Another possible cause for not detecting sources, could be the relatively high RMS.

Fig. 5.20 shows the contours from the 610 MHz map as seen in the previous chapter overlaid on the 240 MHz map, demonstrating that the same sources were detected at both frequencies. All sources detected within R_{500} are listed in Tab. **??** The redshift range used to identify cluster members was 0.055−0.85, chosen according to Yee (1996).
There are **no** newly confirmed radio source associated with the cluster and **six** new cluster member candidates. Further research is needed to verify if a cluster membership is given for these candidates. There were more sources detected at 610 MHz, possibly caused by the overall lower RMS od the map.

5.1.3.11 RXCJ1311.4−0120

In Fig.5.21 a region of 4Mpc around the cluster centre of RXCJ1311.4−0120 is shown.
There are **10** sources detected at $> 5\sigma$ level within 4 Mpc of the cluster centre. These are tabulated in Tab. D.11. There is no central bright source detected at this sensitivity. Of the 10 detected sources, **two** are extended and **none** of them are located within the R_{500} radius. There might be additional sources present missed by the source detection as a very conservative detection level was chosen.

Fig. 5.21 shows the slightly elongated shape of all sources caused by phase calibration issues, we were unable to remove. In Fig.5.21 a region of 4Mpc around the cluster centre of RXCJ1311.4−0120 is shown.
There are 10 sources detected at $> 5\sigma$ level within 4 Mpc of the cluster centre. These are tabulated in Tab. D.11. There is no central bright source detected at this sensitivity. Of the 10 detected sources, **two** are extended and **none** of them are located within the R_{500} radius. There might be additional sources present missed by the source detection as a very conservative detection level was chosen. Fig. 5.21 indicates the RMS to be as smooth as expected in the overall map. All sources have a slightly elongated shape indicating some leftover dirty beam structure, which we were not able to remove. Fig. 5.22 shows the contours from the 610 MHz map as seen in the previous chapter overlaid on the 240 MHz map, demonstrating that no sources were detected at both frequencies. The optical galaxies in the central region

of R_{500} associated with the cluster as indicated in Fig. 5.22 by the green circles. It is shown that no radio source has an optical counterpart. All known optical sources are provided in Tab. B.17. The redshift range used to identify cluster members was $0.165-0.195$, chosen according to Yee (1996).
There are **no** newly confirmed radio source associated with the cluster and **no** new cluster member candidates. There were more sources detected at 610 MHz, possibly caused by the high detection limit chosen. Further research is needed to verify if a cluster membership is given for these candidates.e overall map.

5.1.3.12 RXCJ1516.5-0056

In Fig.5.23 a region of 4Mpc around the cluster centre of RXCJ1516.5−0056 is shown.
There are **four** sources detected at $> 5\sigma$ level within 4 Mpc of the cluster centre. These are tabulated in Tab. 5.10. There is no central bright source detected at this sensitivity. Of the four detected sources, **three** are extended and **none** of them is located within a R_{500} radius. There might be additional sources present missed by the source detection as a very conservative detection level was chosen. Fig. 5.23 indicates the RMS to be as smooth as expected in the overall map. Fig. 5.24 shows the contours from the 610 MHz map as seen in the previous chapter overlaid on the 240 MHz map, demonstrating that only one source was detected at both frequencies. All sources detected within R_{500} are listed in Tab. **??** There are no optical galaxies in the central region of R_{500} associated with the cluster as indicated in Fig. 5.24 by the green circles the ones not associated are indicated by red circles. It is shown that no radio sources has an optical counterpart.Possibly caused by either the faintness of the optical source or no associated redshift, making it impossible to determine if it is associated with the cluster. All known optical sources are provided in Tab. B. The redshift range used to identify cluster members was $0.105-0.135$, chosen according to Yee (1996).
There are **no** newly confirmed radio source associated with the cluster and **two** new cluster member candidates. At 610 MHz a lot more sources where detected. Further research is needed to verify if a cluster membership is given for these candidates.

Source ID	RA	Δ RA	DEC	Δ DEC	total flux	Δ total flux	Peak flux	Δ Peak flux	optical cross-ID	cluster member	comments
1	15:16:54	0.000681	00:43:36	0.001247	0.284318	0.019993	0.114826	0.014623	✗	?	
2	15:16:24	0.000327	00:49:44	0.000664	0.139552	0.034684	0.182316	0.015715	✗	?	

Table 5.10: Positions of radio sources within R_{500} radius of the pointing centre of cluster RXCJ1516.5−0056 detected at a 5σ level.

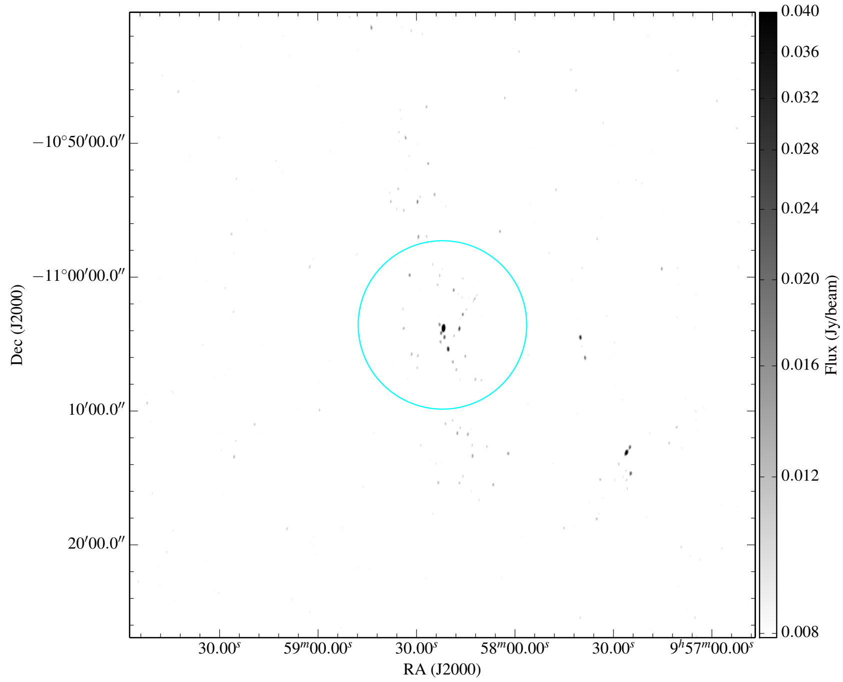

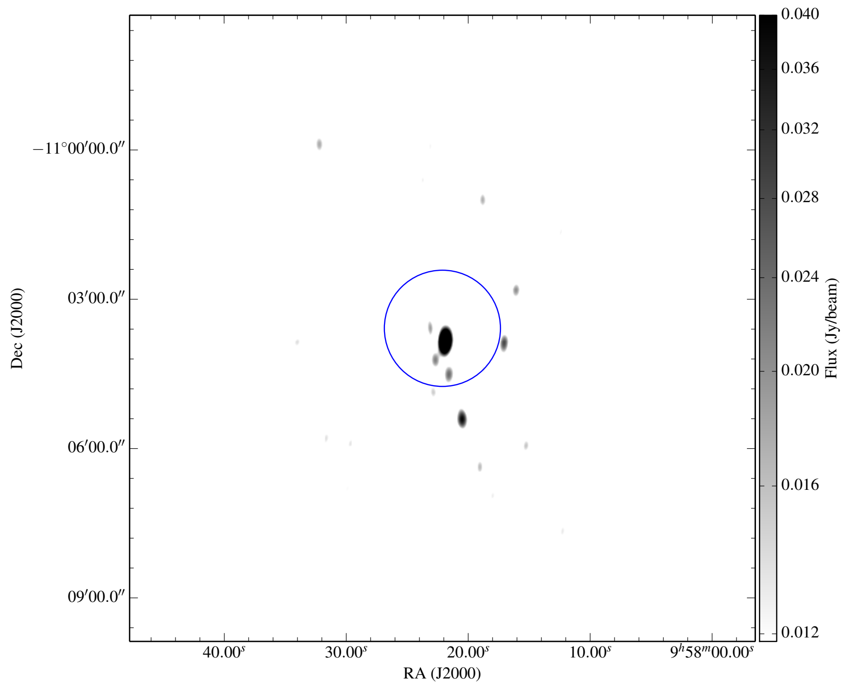

Figure 5.15: 240-MHz GMRT maps of RXCJ0958.3−1103. Top: overview of a region 4 Mpc × 4 Mpc centred on the cluster, R_{500} being indicated by the circle; bottom: central region of the cluster ($R_{500} \times R_{500}$)the circle indicates a region of radius 200kpc around the centre.

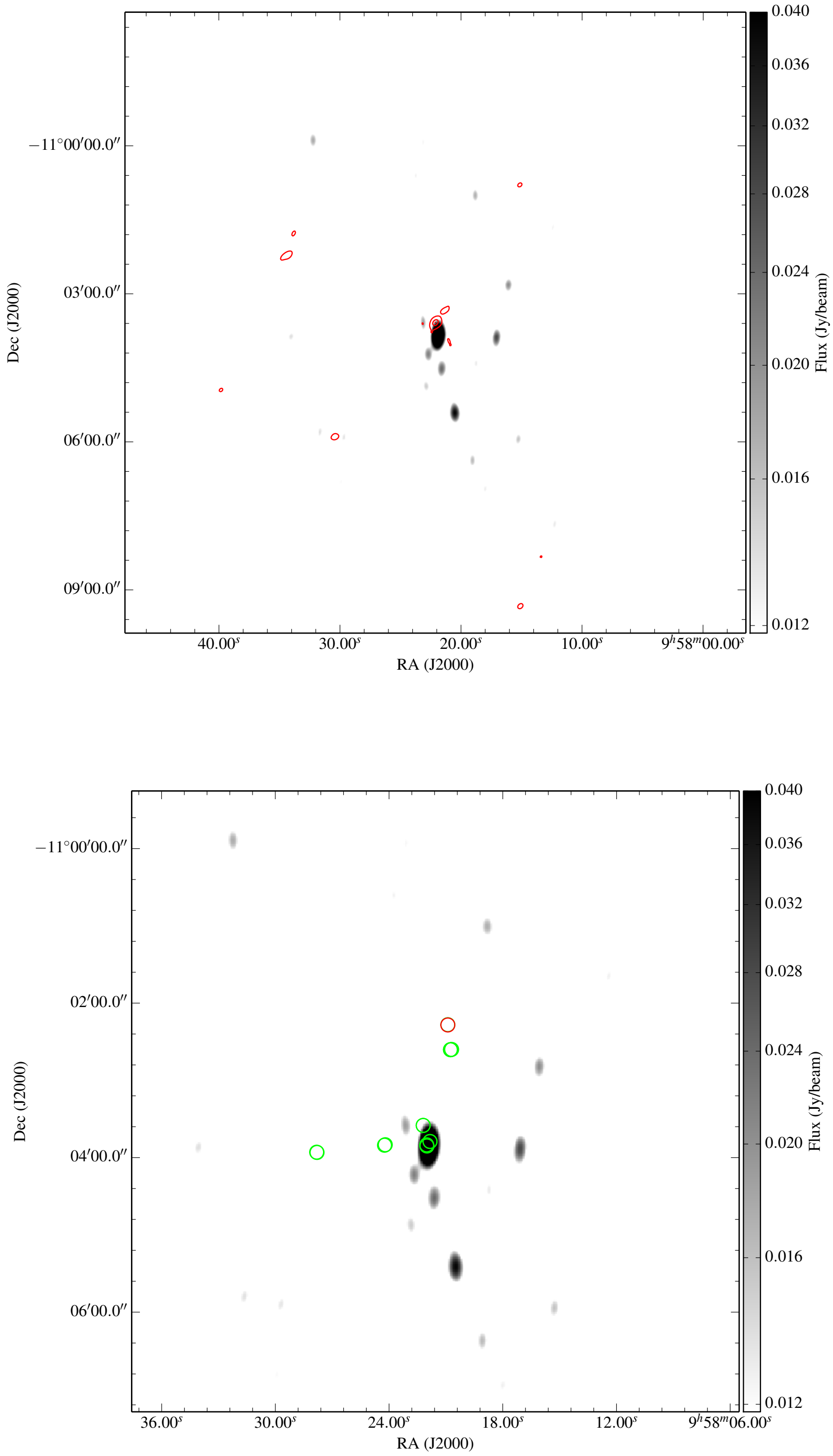

Figure 5.16: 240-MHz GMRT maps of RXCJ0958.3−1103. central region of the cluster ($R_{500} \times R_{500}$); top: contours from 610 MHz map overlaid; bottom: positions of known cluster member galaxies overlaid in green and known background or foreground sources indicated by red circles.

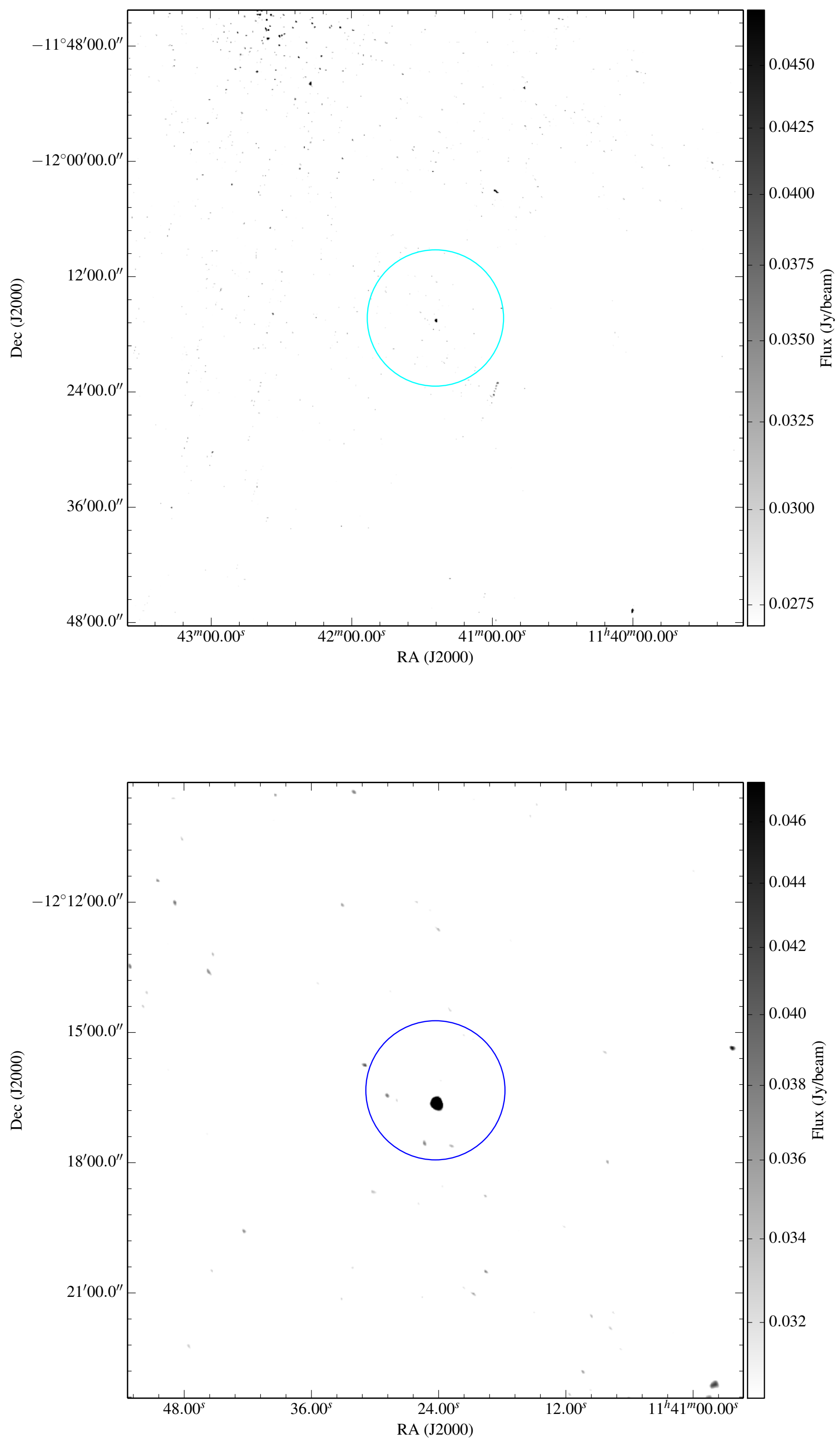

Figure 5.17: 240-MHz GMRT maps of RXCJ1141.4−1216. Top: overview of a region 4 Mpc $\times$ 4 Mpc centred on the cluster, R_{500} being indicated by the circle; bottom: central region of the cluster ($R_{500} \times R_{500}$)the circle indicates a region of radius 200kpc around the centre.

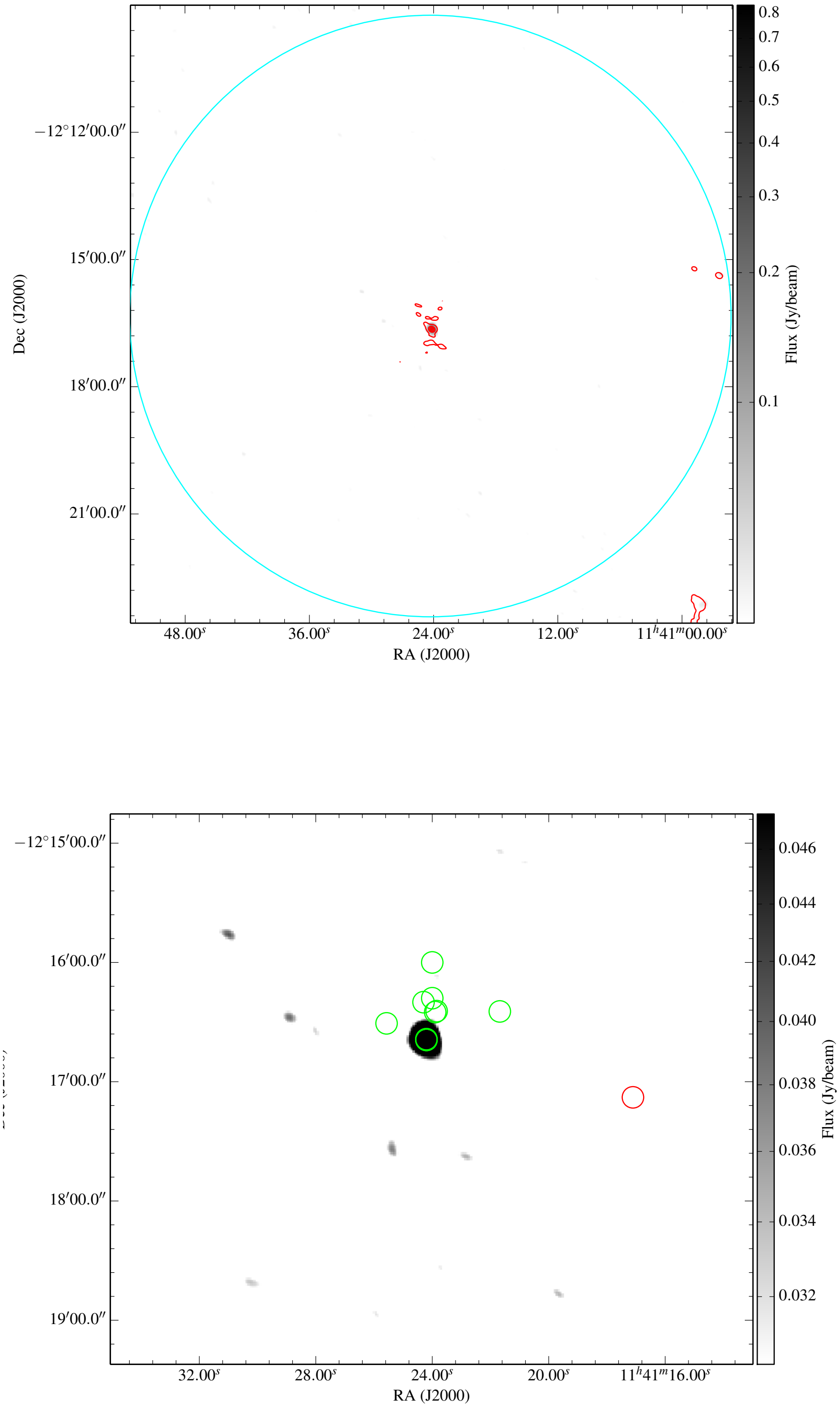

Figure 5.18: 240-MHz GMRT maps of RXCJ1141.4−1216. central region of the cluster ($R_{500} \times R_{500}$); top: contours from 610 MHz map overlaid; bottom: positions of known cluster member galaxies overlaid in green and known background or foreground sources indicated by red circles.

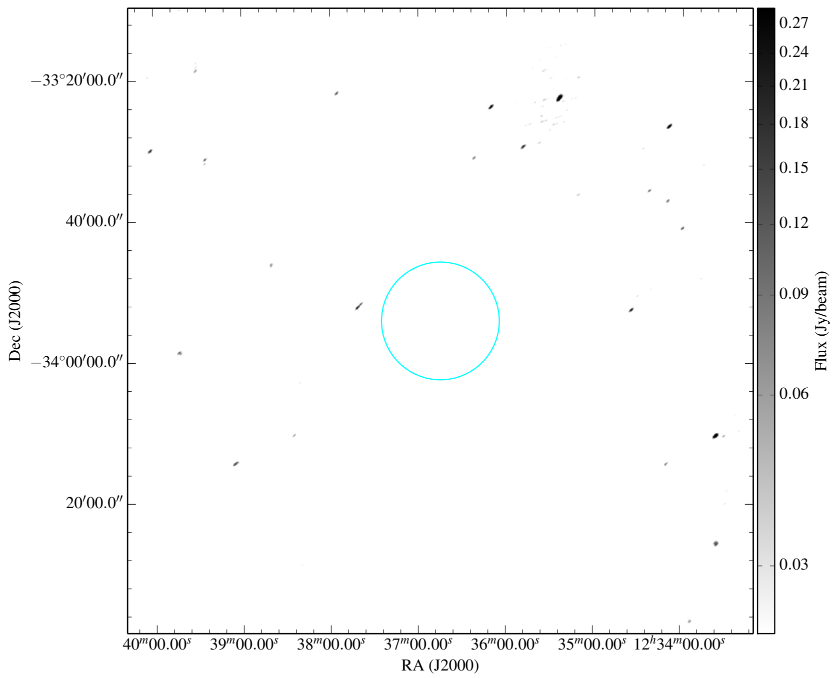

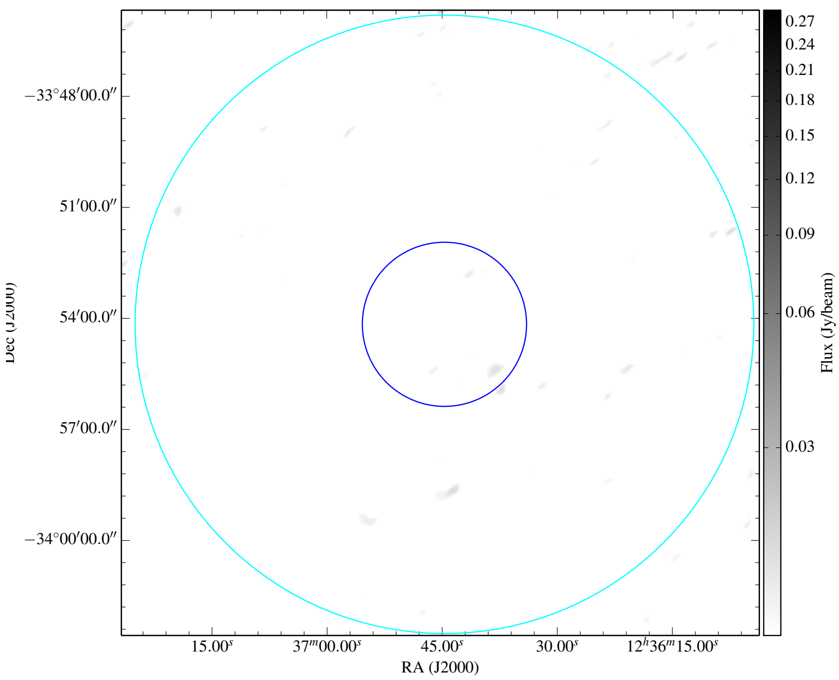

Figure 5.19: 240-MHz GMRT maps of RXCJ1236.7−3354. Top: overview of a region 4 Mpc × 4 Mpc centred on the cluster, R_{500} being indicated by the circle; bottom: central region of the cluster ($R_{500} \times R_{500}$)the circle indicates a region of radius 200kpc around the centre.

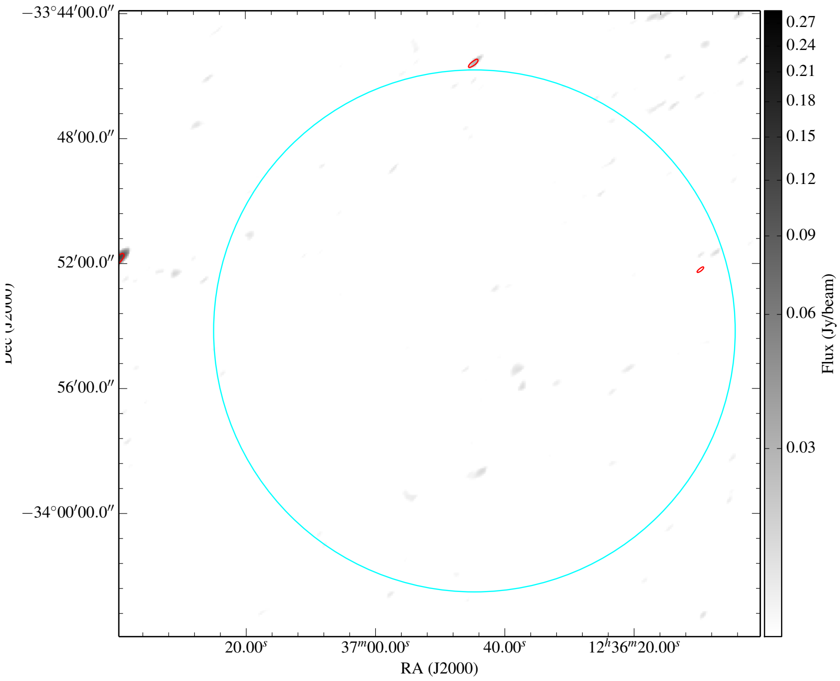

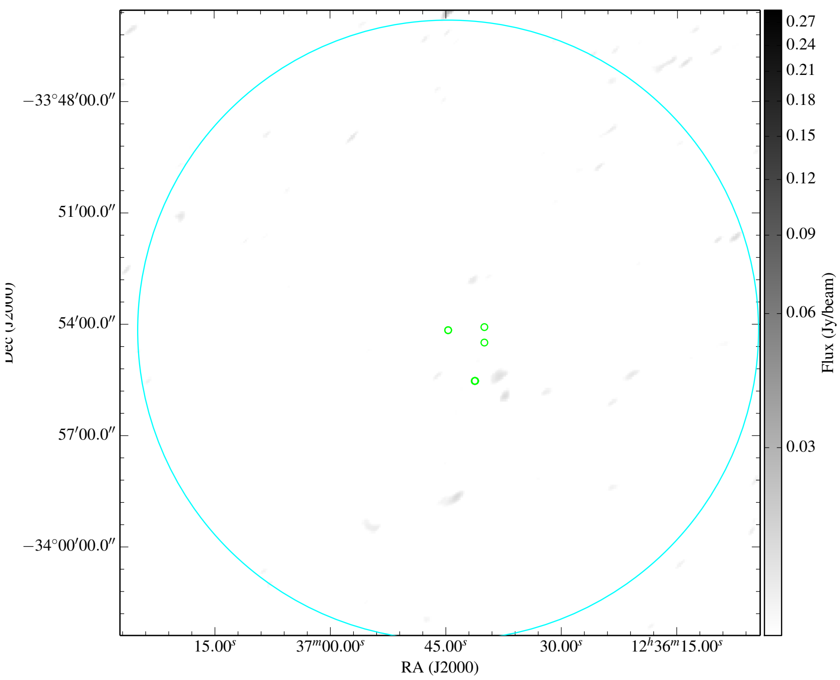

Figure 5.20: 240-MHz GMRT maps of RXCJ1236.7−3354. central region of the cluster ($R_{500} \times R_{500}$); top: contours from 610 MHz map overlaid; bottom: positions of known cluster member galaxies overlaid in green and known background or foreground sources indicated by red circles.

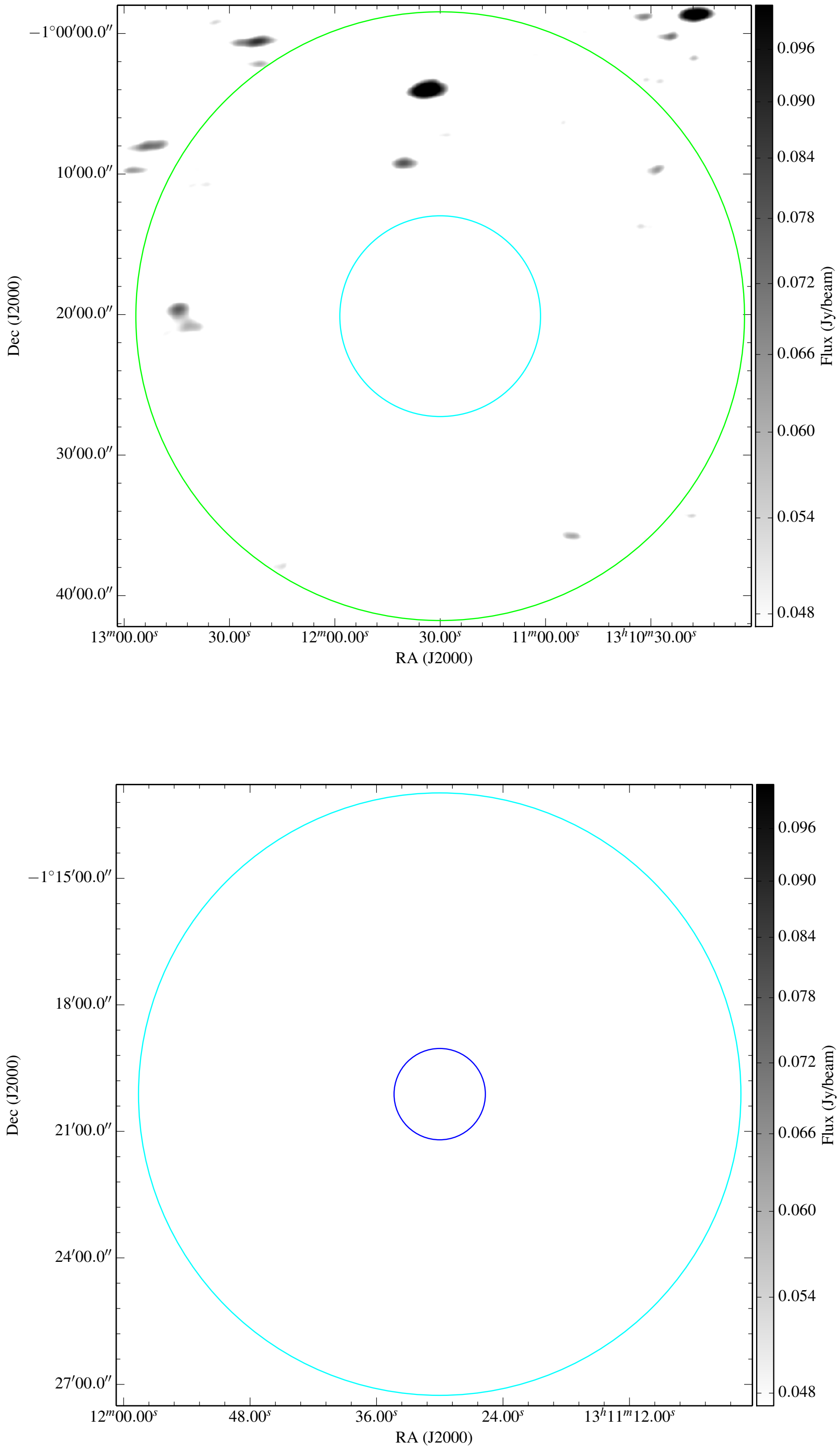

Figure 5.21: 240-MHz GMRT maps of RXCJ1311.4−0120. Top: overview of a region 4 Mpc × 4 Mpc centred on the cluster, R_{500} being indicated by the circle; bottom: central region of the cluster ($R_{500} \times R_{500}$)the circle indicates a region of radius 200kpc around the centre.

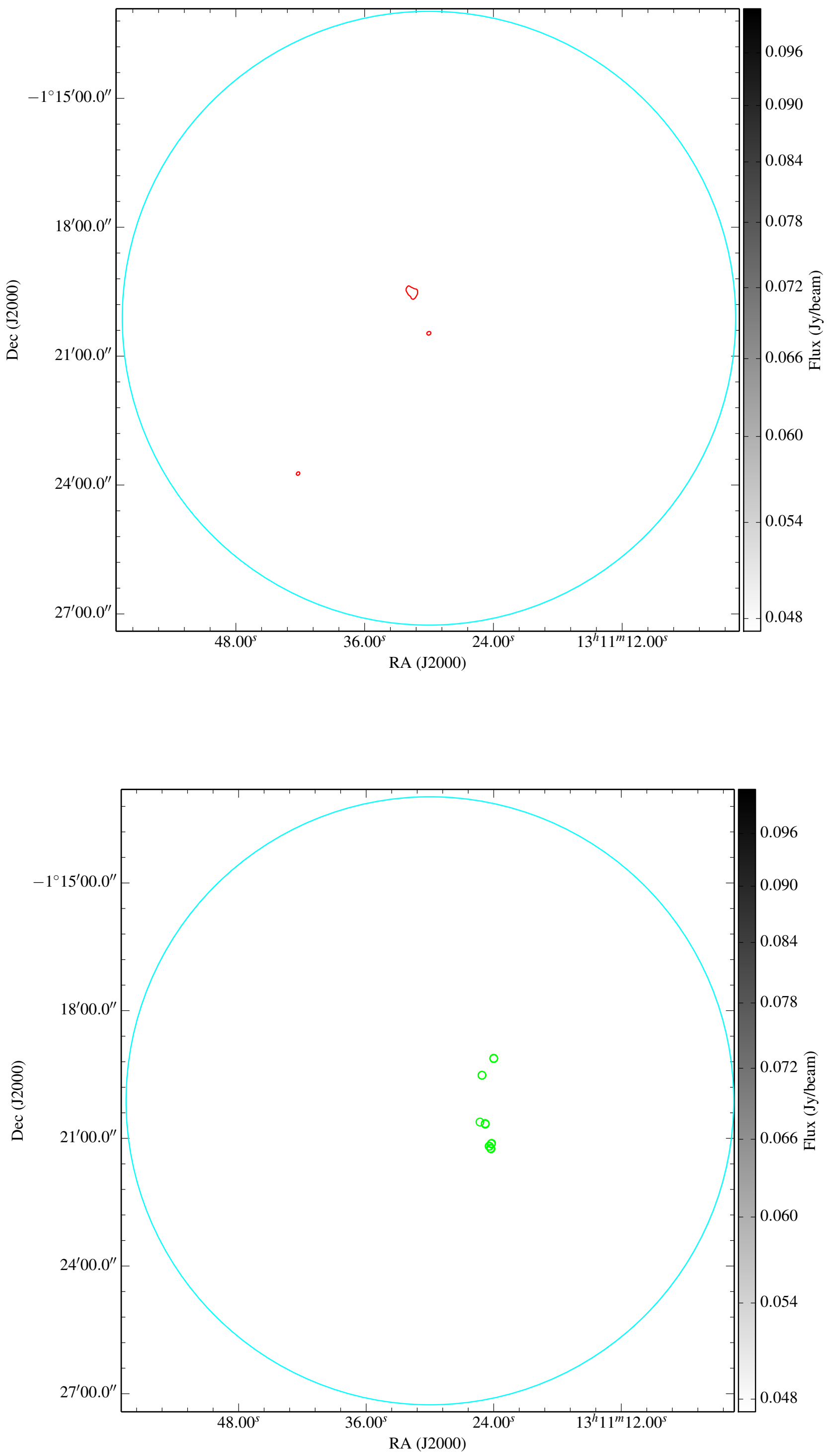

Figure 5.22: 240-MHz GMRT maps of RXCJ1311.4−0120. central region of the cluster ($R_{500} \times R_{500}$); top: contours from 610 MHz map overlaid; bottom: positions of known cluster member galaxies overlaid in green.

5.1.3.13 RXCJ2014.8-2430

In Fig.5.25 a region of 4Mpc around the cluster centre of RXCJ2014.8.0 is shown. There are **4** sources detected at $> 5\sigma$ level within 4 Mpc of the cluster centre. These are tabulated in Tab. 5.11. Of the 4 detected sources, **two** are extended and **one** is located within a R_{500} radius, being the bright central galaxy. There might be additional sources present missed by the source detection as a very conservative detection level was chosen. Some artefacts are present around the bright central source. Fig. 5.25 indicates the RMS to be as smooth as expected in the overall map. Fig. 5.26 shows the contours from the 610 MHz map as seen in the previous chapter overlaid on the 240 MHz map, demonstrating that the bright central source was detected at both frequencies. All sources detected within R_{500} are listed in Tab. 5.11 There optical galaxies in the central region of R_{500} associated with the cluster as indicated in Fig. 5.26 by the green circles the ones not associated are indicated by red circles. It is shown that only one radio source has an optical counterpart. This could be either caused by the faintness of the optical source or no associated redshift, making it impossible to determine, whether it is associated with the cluster. All known optical sources are provided in Tab. B.20. The redshift range used to identify cluster members was 0.145−0.175, chosen according to Yee (1996).
There is **one** newly confirmed radio source associated with the cluster and **no** new cluster member candidates. There are four more sources detected at 610MHz, possibly caused by the RMS around the bright central source. Further research is needed to verify if the sources found at 610 MHz can be detected at 240 MHz with higher sensitivity. This cluster is rather interesting, as it shows large scale gas sloshing Walker et al. (2014) and is the strongest cool core cluster in the REXCESS sample Haarsma et al. (2010). It is massive with $M_{500} = 5.4 \times 10^{14} M_{\odot}$ from Pratt et al. (2010) and has a very low central entropy Pratt et al. (2010).

5.2 Spectral Analysis

This section focuses on the spectral analysis of the previously discussed clusters and gives spectral indices for them.
Of the 13 cluster, observed at both frequencies, 240 MHz and 610MHz, only 10

Source ID	RA	Δ RA	DEC	Δ DEC	total flux	Δ total flux	Peak flux	Δ Peak flux	optical cross-ID	cluster member	comments
1	20:14:52	0.000027	-24:30:23	0.00008	0.769785	0.026974	0.765477	0.013456	✔	✔	BCG

Table 5.11: Positions of radio sources within R_{500} radius of the pointing centre of cluster RXCJ2014.8−243 detected at a 5σ level.

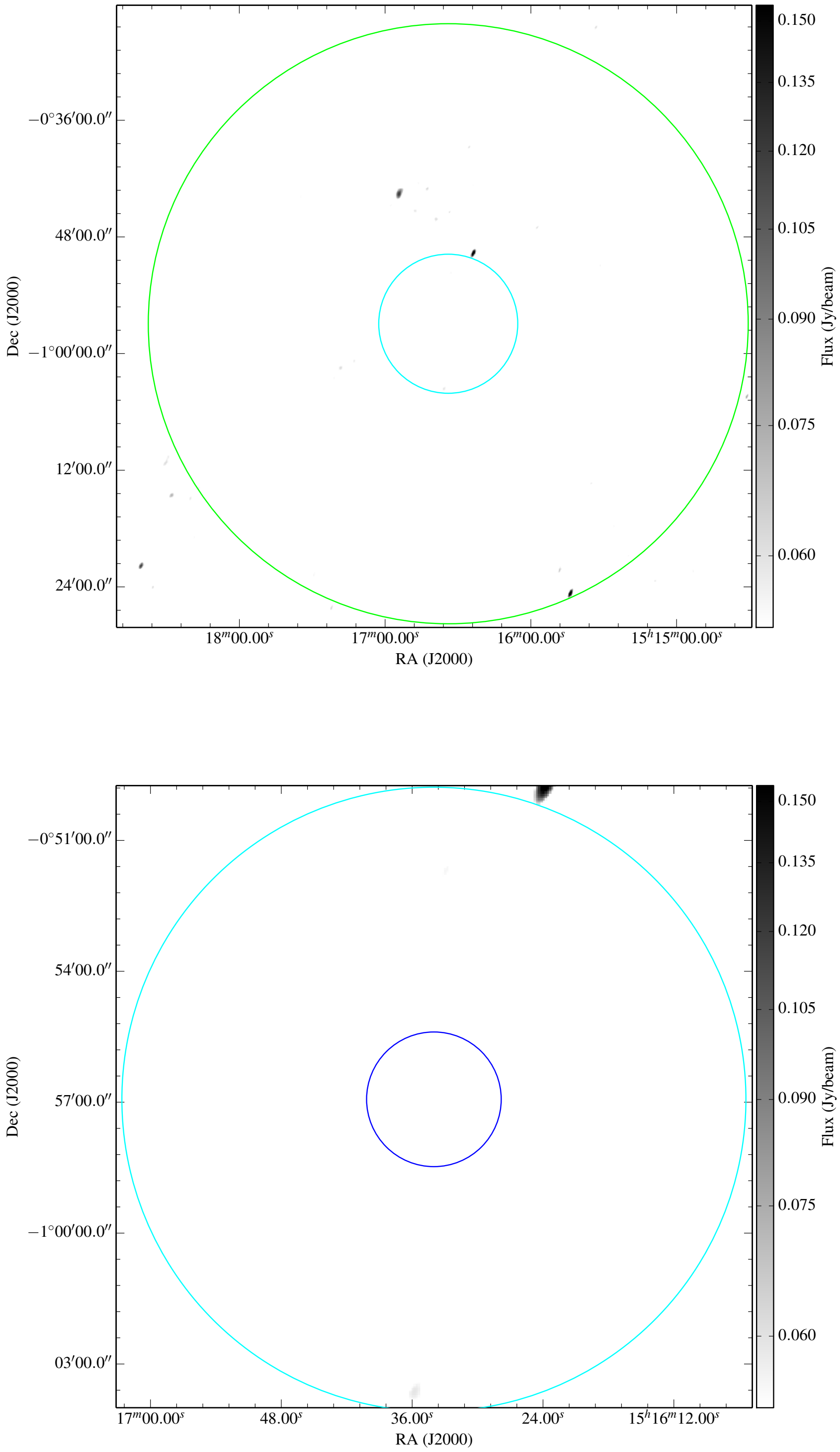

Figure 5.23: 240-MHz GMRT maps of RXCJ1516.5−0056. Top: overview of a region 4 Mpc × 4 Mpc centred on the cluster, R_{500} being indicated by the circle; bottom: central region of the cluster ($R_{500} \times R_{500}$)the circle indicates a region of radius 200kpc around the centre.

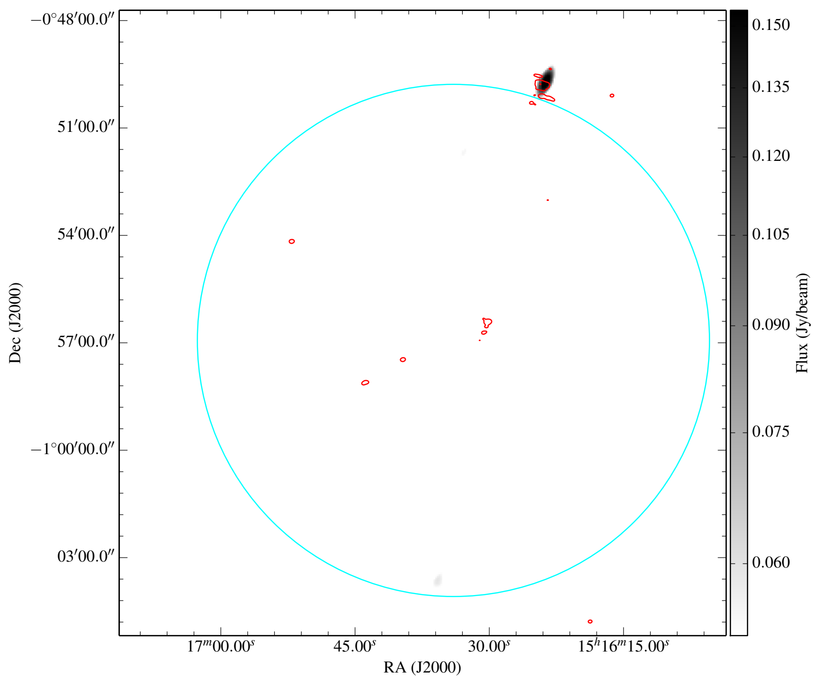

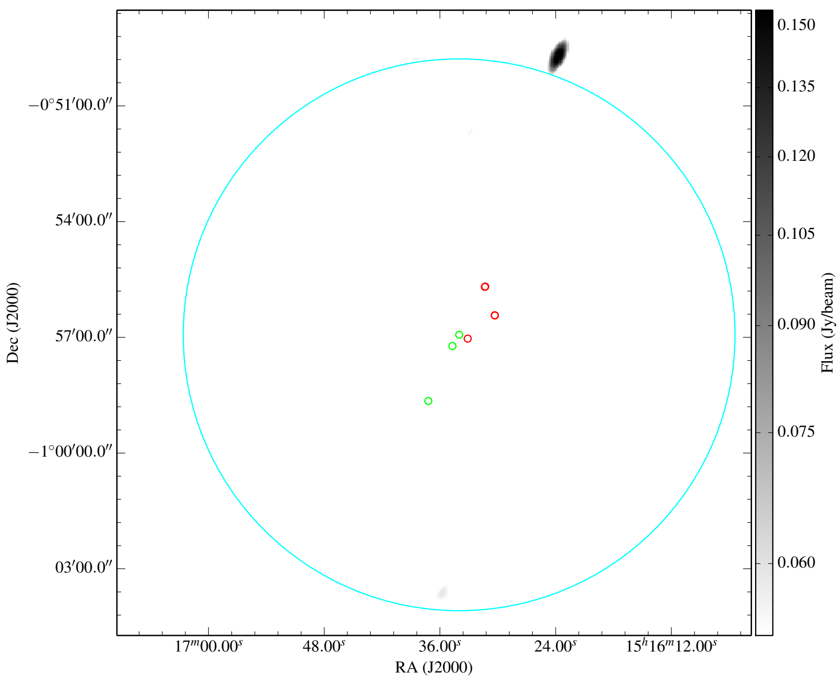

Figure 5.24: 240-MHz GMRT maps of RXCJ1516.5−0056. central region of the cluster ($R_{500} \times R_{500}$); top: contours from 240 MHz map overlaid; bottom: positions of known cluster member galaxies overlaid in green and known background or foreground sources indicated by red circles.

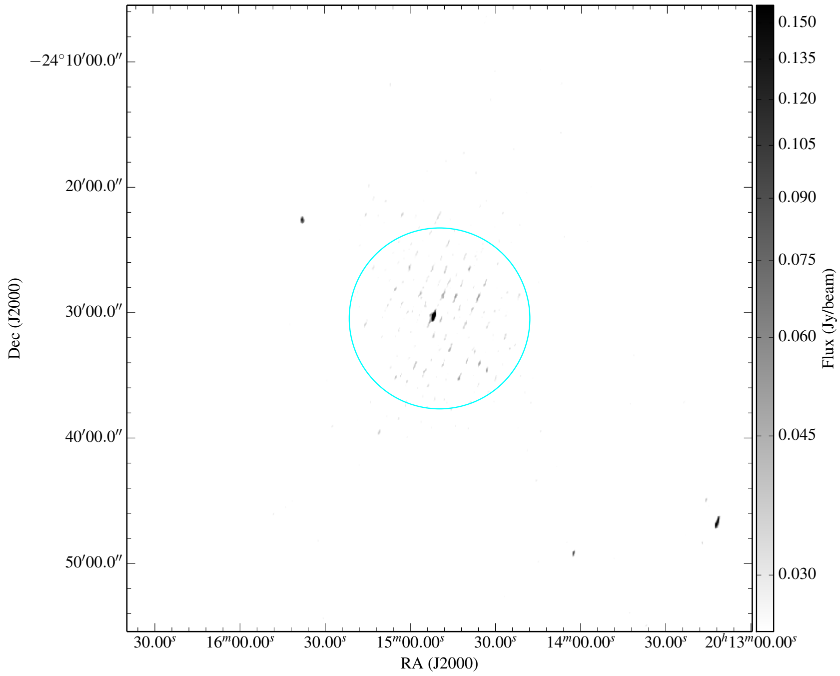

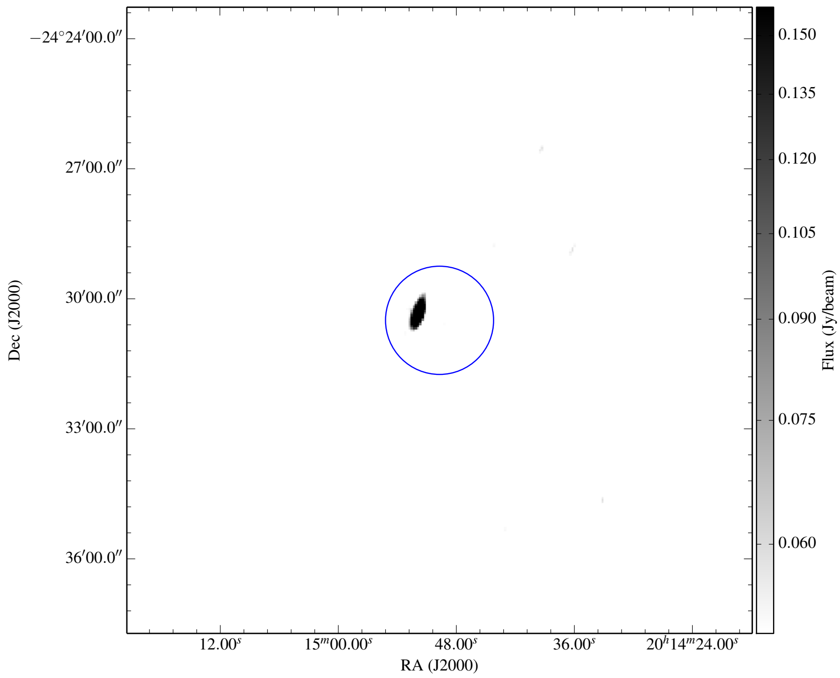

Figure 5.25: 240-MHz GMRT maps of RXCJ2014.8−2430. Top: overview of a region 4 Mpc $\times$ 4 Mpc centred on the cluster, R_{500} being indicated by the circle; bottom: central region of the cluster ($R_{500} \times R_{500}$)the circle indicates a region of radius 200kpc around the centre.

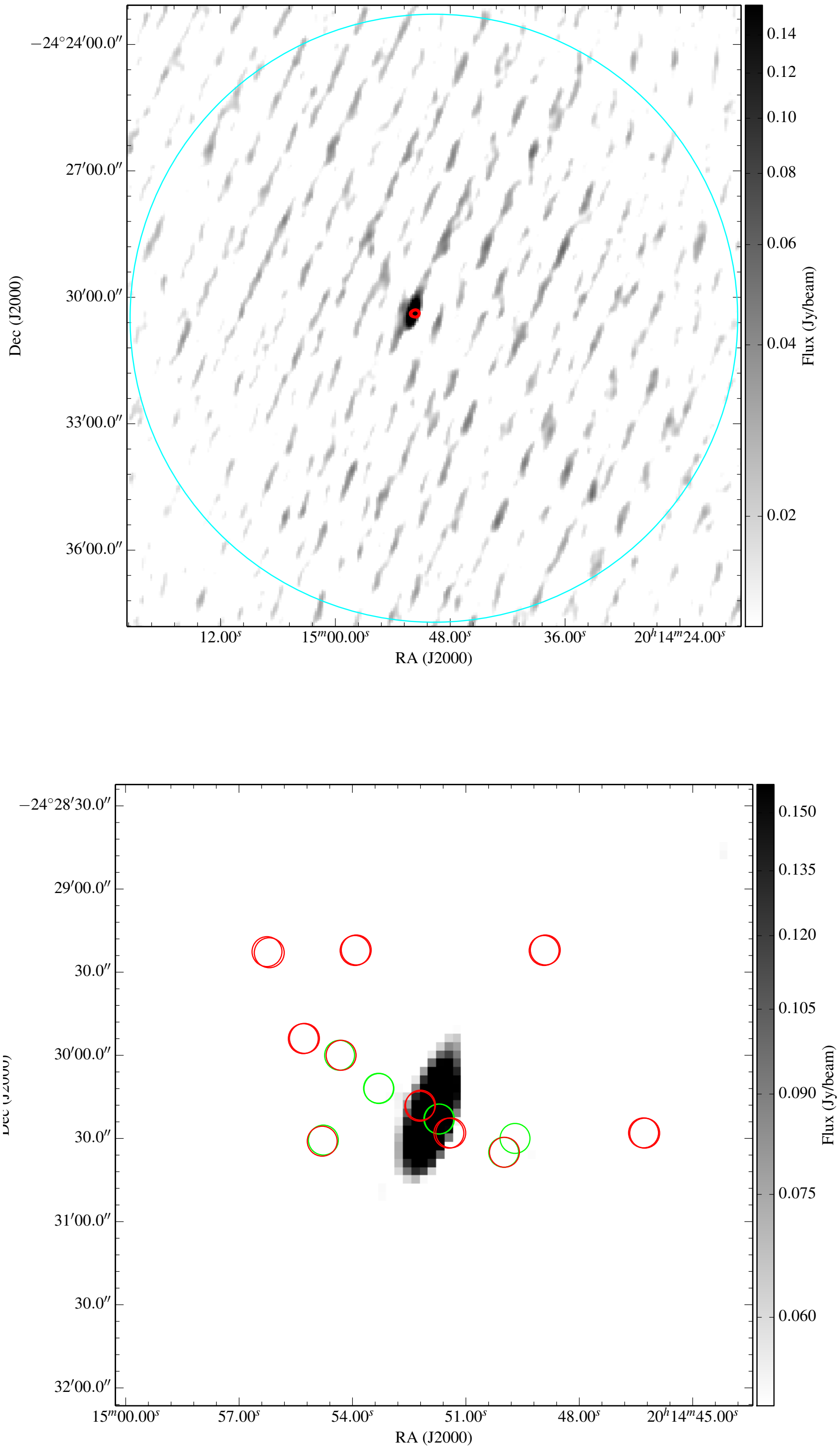

Figure 5.26: 240-MHz GMRT maps of RXCJ2014.8−2430. central region of the cluster ($R_{500} \times R_{500}$); top: contours from 240 MHz map overlaid; bottom: positions of known cluster member galaxies overlaid in green and known background or foreground sources indicated by red circles.

could be analysed regarding their spectral index, as the other clusters lacked sources identified with the cluster. In this analysis all cluster member candidates were included. Additional data points are from NVSS Condon *et al.* (1998), SUMSS Mauch*et al.* (2013) and Hogan et al.Hogan *et al.* (2015a). At the end all sources identified with the bright central galaxy are plotted with their spectral index to give an overview of the sample as a whole.
In Fig. 5.27 the spectral indices of RXCJ0006.0−3443 and RXCJ0020.7−2542 are shown. It is worth mentioning, that not all sources show the same spectral index. For all but one the spectral index of the peak flux is in the same direction as the total flux. The majority of the sources has a larger flux at 240 MHz corresponding to a positive spectral index. Only the source with the ID 11 in Tab. 5.6 shows a lower flux at 240MHz at peak flux, but not at the total flux. In Tab. 5.12 the spectral indices of each source are listed, one calculated from the peak flux and one from the total flux of the individual sources. The spectral indices positive indicate a non-thermal emission.

Another cluster shown in Fig. 5.27 is RXCJ0020.7−2542. This cluster has only one source detected at both frequencies. Its spectral index is also positive and the peak and total one are very close. This again indicates a non-thermal emission process. This source is the bright central galaxy of the cluster.

The bottom left panel in Fig. 5.27 shows the spectral index of R0211.4 where only the central bright source could be matched at both frequencies. Both calculations show a spectral index greater zero, indicating a non- thermal emission process.

The bottom right panel of Fig. 5.27 shows the spectral indices of R0225.1 where two pairs of sources were found. Both have a positive spectral index, indicating

Source ID		Spectral Index	
240 MHz	610 MHz	peak flux	total flux
11	2	1.677	1.074
12	3	1.252	0.625
14	7	1.229	0.966
24+25	8	1.202	0.841

Table 5.12: Spectral indices of RXCJ0006.0−3443

Source ID		Spectral Index	
240 MHz	610 MHz	peak flux	total flux
3	1	0.874	0.891

Table 5.13: Spectral indices of RXCJ0020.7−2542

non-thermal emission processes.

The top left panel of Fig. 5.28 shows the spectral indices of R0605.8−3518, where two pairs of sources were found. In this cluster the matched sources are almost point-like, as seen by comparing peak and total flux at 610 MHz. These sources are resolved at 240 MHz, indicated by the difference between peak and total flux. Both sources show a very similar spectral index, when the one calculated from total and peak flux are compared. All spectral indices are positive, which is a strong evidence for non-thermal emission processes to be the underlying cause for the detected emission.

The top right panel of Fig. 5.28 shows the spectral index of RXCJ0821.8+0112 where only one source was identified at both frequencies. It is worth mentioning, that the spectral index calculated from the total flux is significantly less steep than the one calculated from the peak flux. This could be caused by the source being resolved at 240MHz, but not at 610MHz. The positive spectral index indicates a non-thermal emission process.

Fig. 5.28 shows the spectral indices of RXCJ0958.3−1103 and R1141.4. The bottom left panel shows the four cluster member candidates of RXCJ0958.3−1103, we were able to find at both frequencies. This cluster is a bit special, as the source with ID 11 at 610 MHz is located matching both, ID 14 and 21 at 240 MHz, so it is listed for both as a match. It is worth noting, that three of four matched sources seem to be point-like at 240 MHz, but not at 610 MHz. This is indicated by having an almost identical peak and point flux. The sources seem to have non-thermal emission processes, as indicated by the positive spectral index.

The bottom left panel of Fig 1.4 shows the only match found for cluster R1141.4 − 1216, this source shows a positive spectral index, which provides evidence for non-thermal emission processes. Fig. 5.29 displays the spectral index of R2014.8−2430. The source seems resolved at 610MHz, but point-like at 240 MHz. Nevertheless,

Source ID		Spectral Index	
240 MHz	610 MHz	peak flux	total flux
17	0	0.603	0.834

Table 5.14: Spectral indices of RXCJ0211.4−4017

Source ID		Spectral Index	
240 MHz	610 MHz	peak flux	total flux
46	6	0.634	0.298
47	11	0.765	0.633

Table 5.15: Spectral indices of RXCJ0225.1−2928

the spectral indices remain positive for both, providing evidence for on-thermal emission processes taking place in this source.

Fig. 5.30 displays the spectral index of RXCJ0547.6−3152. The source shows a negative spectral index when the SUMSS Mauch*et al.* (2013) data points are compared to the measurement at 610MHz, but if the NVSS Condon *et al.* (1998) are considered a positive spectral index is given. This is the one of the two sources in the sample, changing the sign of their spectral index. The spectral index of RXCJ1044.5−0704 shows a negative spectral index when compared with NVSS Condon *et al.* (1998), but an overall positive one when compared to the measurement made by Hogan *et al.* (2015a). The spectral index of RXCJ2234.5−3744 is the only negative one in Fig. 5.31. The spectral indices of the other sources in Fig. 5.31 and Fig. 5.30 are all positive. The steep spectral index of RXCJ2149.1−3041 Hogan *et al.* (2015a) is even steeper at lower frequencies (see Fig. 5.31).

5.3 Summary

13 radio maps, with decent signal to noise ration could be produced from the available data. There were in total **230** sources detected, **34** of them were extended. **6** of the total detected sources could be confirmed as cluster members and **31** are cluster member candidates.
The spectral indices of **42** sources could be determined, by using not only the measured data but also data provided by Hogan *et al.* (2015a),Mauch*et al.* (2013) and Condon *et al.* (1998). **36** of them showed a positive spectral index, **one** a neutral one and **four** a negative spectral index. **One** source changed its spectral index from negative to positive.

Source ID		Spectral Index	
240 MHz	610 MHz	peak flux	total flux
5	0	0.794	0.718
12	1	1.220	1.224

Table 5.16: Spectral indices of RXCJ0605.8−3518

Source ID		Spectral Index	
240 MHz	610 MHz	peak flux	total flux
16	4	0.145	1.002

Table 5.17: Spectral indices of RXCJ0821.8+0112

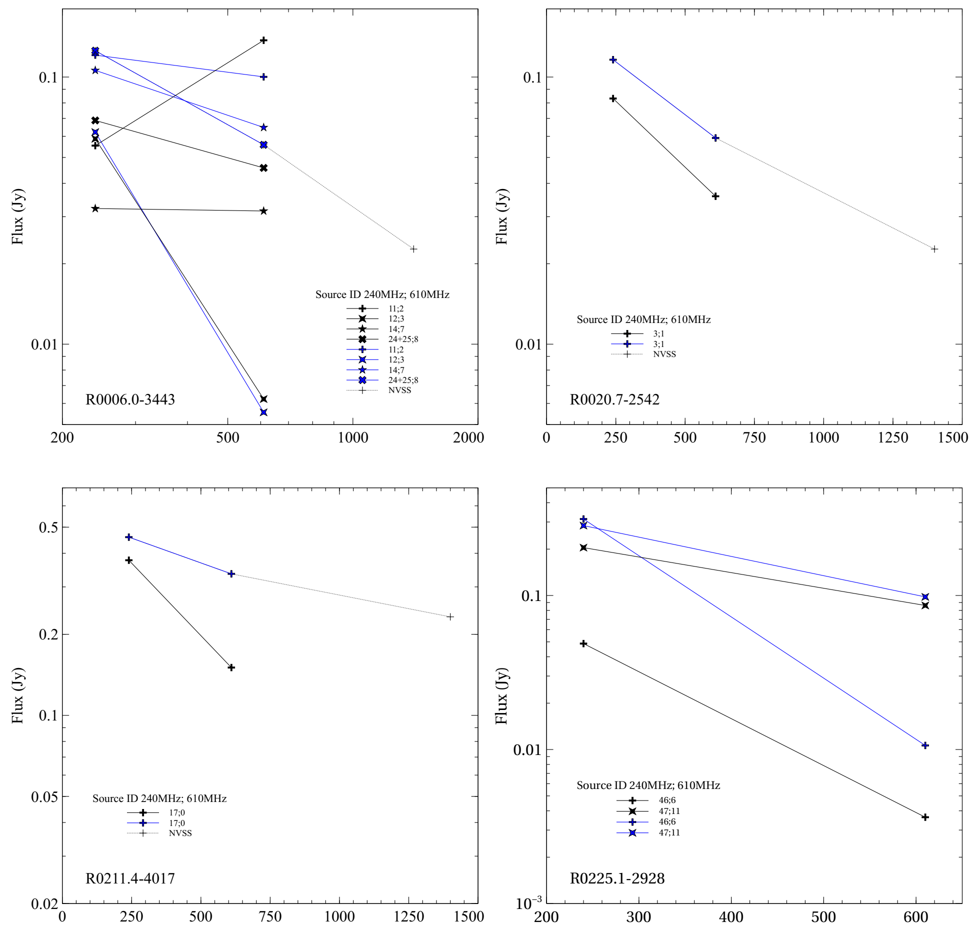

Figure 5.27: Spectral indices of RXCJ0006.0−3443 sources in the top left panel and of RXCJ0020.7−2542 in the top right panel. The numbers are the source IDs from Tab. 5.6 and Tab. 4.5 for cluster RXCJ0006.0−3443 and in Tab. 5.3 and Tab. 4.6 for cluster RXCJ0020.7−2542.The NVSS data points are obtained from Condon *et al.* (1998). Spectral indices of RXCJ0211.4−4017 sources in the bottom left panel and of RXCJ0225.1−2928 in the bottom right panel. The numbers are the source IDs from Tab. 5.4, Tab. 4.7 and from Condon *et al.* (1998) for cluster RXCJ0211.4−4017 and in Tab. 5.4 and Tab. 4.8 for cluster RXCJ0225.1−2928. In all graphs the black lines and markers indicate the peak fluxes while the blue ones correspond to the total flux. Dotted grey lines connect the NVSS data points to the ones measured as part of this thesis.

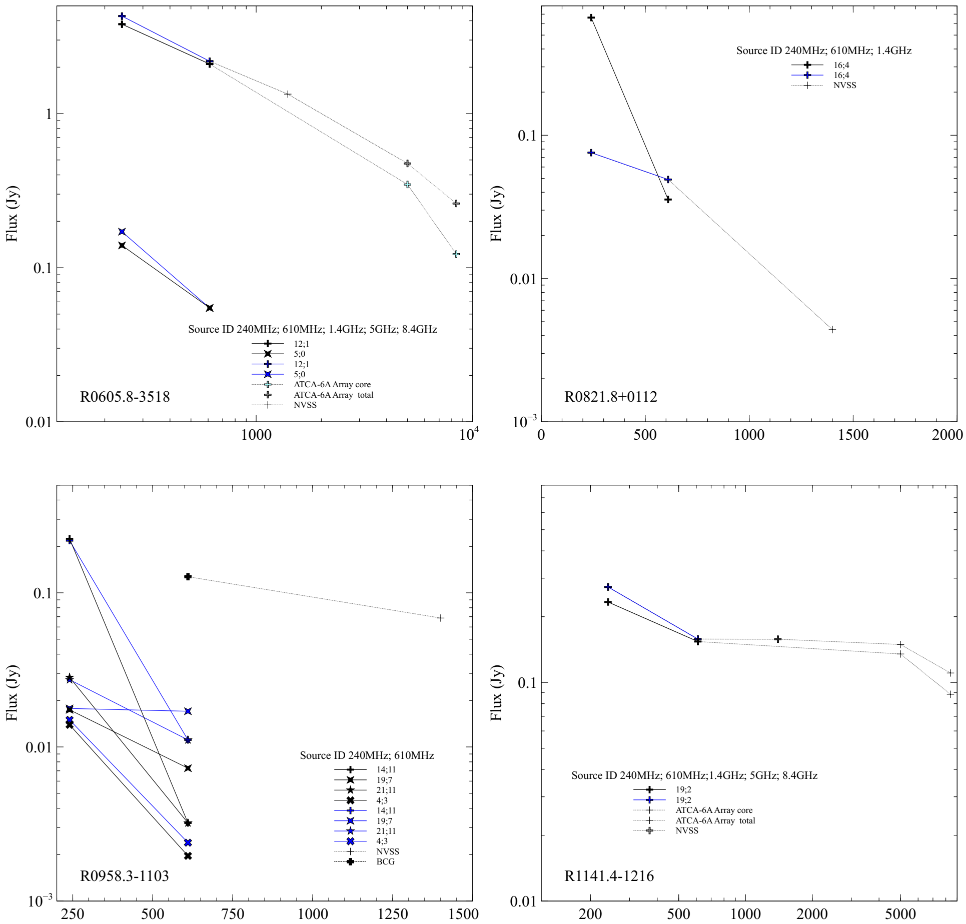

Figure 5.28: Spectral indices of RXCJ0605.8−3518 sources in the top panel and of RXCJ0821.8−0112in the bottom panel. The numbers are the source IDs from Tab. **??** and Tab. 4.11 for cluster RXCJ0605.8−3518 and in Tab. 5.7 and Tab. 4.12 for cluster RXCJ0821.8−0112. Spectral indices of RXCJ0958.3−1103 sources in the top panel and of RXCJ1141.4−1216in the bottom panel. The numbers are the source IDs from Tab. 5.8 and Tab. 4.14 for cluster RXCJ0958.3−1103 and in Tab. 5.9 and Tab. 4.16 for cluster RXCJ1141.4−1216. In all graphs the black lines and markers indicate the peak fluxes while the blue ones correspond to the total flux.The NVSS data points are obtained from Condon *et al.* (1998) and are connected to the measured data points by dotted grey lines. The ATCA data points are cited from Hogan *et al.* (2015a) and also connected by grey dotted lines.

Source ID		Spectral Index	
240 MHz	610 MHz	peak flux	total flux
4	3	0.803	0.815
14	11	0.305	0.396
19	7	0.963	1.16
21	11	0.739	0.943

Table 5.18: Spectral indices of RXCJ0958.3−1103

Source ID		Spectral Index	
240 MHz	610 MHz	peak flux	total flux
19	2	0.910	0.822

Table 5.19: Spectral indices of RXCJ1141.4−1216

Source ID		Spectral Index	
240 MHz	610 MHz	peak flux	total flux
1	4	0.257	0.314

Table 5.20: Spectral indices of RXCJ2014.8−2430

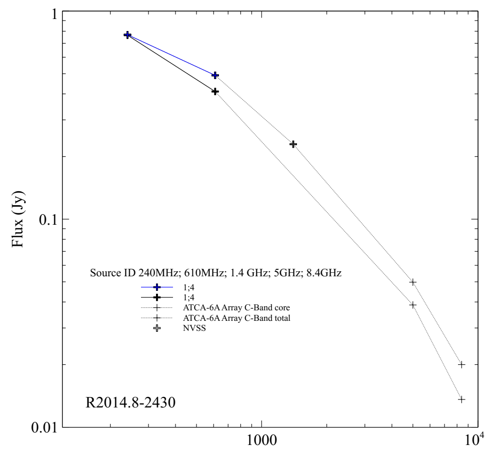

Figure 5.29: Spectral indices of RXCJ2014.8−2430 sources. The black lines and markers indicate the peak fluxes while the blue ones correspond to the total flux. The numbers are the source IDs from Tab. 5.11 and Tab. 4.22.The NVSS data points are obtained from Condon *et al.* (1998) and are connected to the measured data points by dotted grey lines. The ATCA data points are cited from Hogan *et al.* (2015a) and also connected by grey dotted lines.

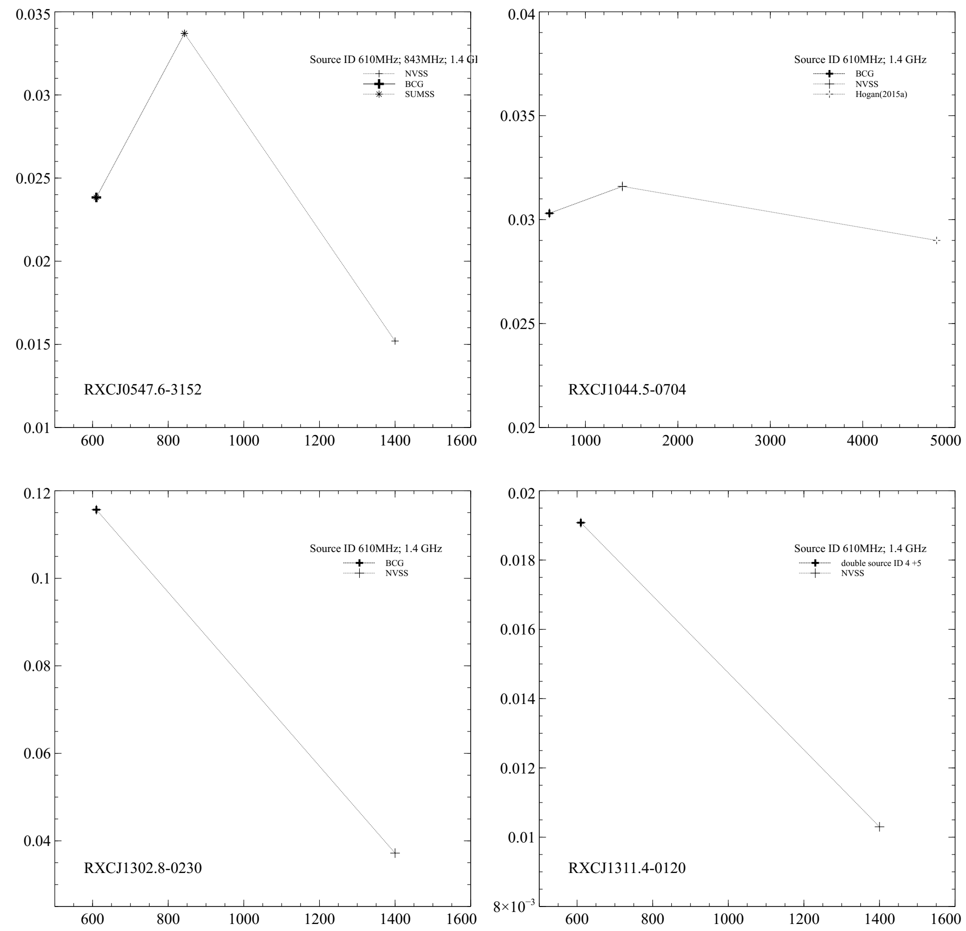

Figure 5.30: Spectral indices of RXCJ0547.6−3152 BCG in the top left panel and of RXCJ1044.5−0704 in the top right panel. Both are the sources labeled as BCG in Tab. 4.10 for cluster RXCJ0547.6−3152 and in Tab. 4.15 for cluster RXCJ1044.5−0704. The NVSS data points are obtained from Condon *et al.* (1998) and are connected to the measured data points by dotted grey lines. The SUMSS data points are provided in Mauch*et al.* (2013) and also connected by grey dotted lines. Spectral indices of RXCJ1302.8−0230 sources in the bottom left panel and of RXCJ1311.4−0120 in the bottom right panel. The sources are both the ones labelled BCG from Tab. 4.18 for cluster RXCJ1302.8−0230 and in Tab. 4.19 for cluster RXCJ1311.4−0120. The NVSS data points are obtained from Condon *et al.* (1998) and are connected to the measured data points by dotted grey lines.

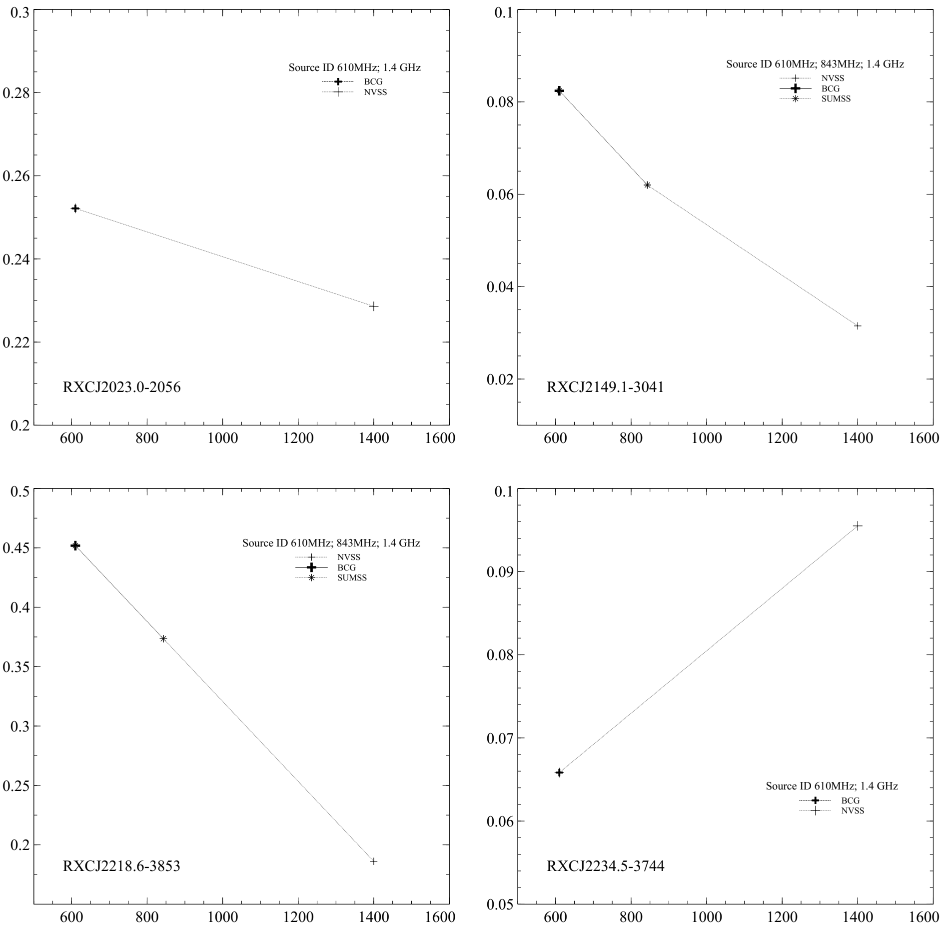

Figure 5.31: Spectral indices of RXCJ2023.0−2056 sources in the top left panel and of RXCJ2218.6−3853 in the bottom left panel. The source is labelled as BCG in Tab. 4.23 for cluster RXCJ2023.0−2056 and in Tab. 4.28 for cluster RXCJ2218.6−3853. Spectral indices of RXCJ2149.1−3041 sources in the top right panel and of RXCJ2234.5−3744 in the bottom right panel. The sources are labelled as BCG in Tab. 4.24 for cluster RXCJ2149.1−3041 and in Tab. 4.29 for cluster RXCJ2234.5−3744 The NVSS data points are obtained from Condon *et al.* (1998) , the SUMSS data points are provided in Mauch*et al.* (2013) and are connected to the measured data points by dotted grey lines.

"Astronomers say the universe is finite, which is a comforting thought for those people who can't remember where they leave things."

WOODY ALLEN

6

Comparison of radio an X-ray positions within R_{500}

In this chapter a detailed overview of the position of radio sources in comparison with the X-ray point source population is given.

It additionally defines a subsample of radio sources having an X-ray counterpart.

6.1 Comparison of the individual REXCESS clusters observed at 610 MHz with their X-Ray observations

This section provides a detailed discussion of the individual cluster maps at 610MHz compared with their X-ray counterparts. It also summarises the overall abundance of a positional coincidence between the radio and X-ray source population inside the clusters.

6.1.1 RXCJ0003.8+0203

In cluster RXCJ0003.8+0203 there are **three** radio sources with X-ray counterparts as shown in Fig.6.1 at the top panel, one is located directly at the centre of the X-ray emission, associated with the bright central galaxy. A possible fourth source was not counted as there are some RFI issues in that area as described in 4.4.1. The radio sources with an X-ray counterpart are listed in Tab.6.1

6.1.2 RXCJ0006.0−3443

This cluster shows **one** radio source associated with an X-ray source. It is located in the bottom left corner of the central region of the cluster. The X-ray source is rather faint as indicated by the contours in Fig.6.1 bottom panel. The radio source with an X-ray counterpart is listed in Tab.6.1

6.1.3 RXCJ0020.7−2542

This cluster shows **no** evidence of a radio source associated with an X-ray source as shown in Fig.6.2. But there is an X-ray peak at the same position as the bright central galaxy and its X-ray counterpart. So this was counted as an coincidence in position an listed in Tab.6.1

6.1.4 RXCJ0225.1−2928

In this cluster there is **one** radio source associated with an X-ray source shown in Fig.6.2. There is no radio source associated with the central peak in X-ray or the optical bright central galaxy. It is listed in Tab.6.1

6.1.5 RXCJ0345.7.8−4112

In cluster RXCJ0345.7.8−4112 there is **one** radio sources with anX-ray counterpart present as shown in Fig.6.3 at the top panel, one is located directly at the centre of the X-ray emission, associated with the bright central galaxy. The radio source with an X-ray counterpart is listed in Tab.6.1

6.1.6 RXCJ0547.6.0−3152

This cluster shows **one** radio source associated with an X-ray source. It is associated with the bright central galaxy as shown in Fig.6.3 bottom panel. The radio source with an X-ray counterpart is listed in Tab.6.1

6.1.7 RXCJ0605.8−3518

This cluster shows evidence of **one** radio source associated with an X-ray source as shown in Fig.6.4. But there is an X-ray peak at the same position as the bright central galaxy and its X-ray counterpart. So this was counted as an association in position an listed in Tab.6.1

6.1.8 RXCJ0821.8+0112

In this cluster there is **one** radio source associated with an X-ray source shown in Fig.6.4. There is no radio source associated with the central peak in X-ray or the optical bright central galaxy. It is listed in Tab.6.1

6.1.9 RXCJ0956.4−1004

In this cluster there are **four** radio source associated with an X-ray counterpart in this cluster, as shown in Fig.6.5. There is no central peak in X-ray, but there are three bright x-ray sources, two of them have an associated radio source. They are listed in Tab.6.1

6.1.10 RXCJ0958.3−1103

In this cluster there are **two** radio sources associated with an X-ray source shown in Fig.6.5. One of them is associated with the central peak in X-ray or the optical bright central galaxy. Both are listed in Tab.6.1

6.1.11 RXCJ1044.5−00704

In this cluster there is **one** radio source associated with an X-ray source shown in Fig.6.6. This radio source is associated with the central peak in X-ray or the optical bright central galaxy. It is listed in Tab.6.1

6.1.12 RXCJ1141.4−1216

In this cluster there are **three** radio sources associated with an X-ray source shown in Fig.6.6. One of them being associated with the central peak in X-ray or the optical bright central galaxy. All are listed in Tab.6.1

6.1.13 RXCJ1236.7−3354

In this cluster there are **two** radio sources associated with an X-ray source shown in Fig.6.7. One of them is associated with the central peak in X-ray or the optical bright central galaxy. Both are listed in Tab.6.1

6.1.14 RXCJ1302.8−0230

In this cluster there are **two** radio sources associated with an X-ray source shown in Fig.6.7. This radio source is a double source, therefore they are both associated with the central peak in X-ray or the optical bright central galaxy. Both are listed in Tab.6.1

6.1.15 RXCJ1311.4−0120

In this cluster there are **four** radio source associated with an X-ray counterpart in this cluster, as shown in Fig.6.8. Three of them coincide with the central peak in X-ray. Details about these are given in Tab.6.1

6.1.16 RXCJ2014.8−2430

In this cluster there is **one** radio source associated with an X-ray source shown in Fig.6.8. This radio source is associated with the central peak in X-ray or the optical bright central galaxy. It is listed in Tab.6.1

6.1.17 RXCJ2023.0−2056

In this cluster there are **three** radio sources associated with an X-ray source shown in Fig.6.9. All three being associated with the central peak in X-ray or the optical bright central galaxy. They are listed in Tab.6.1

6.1.18 RXCJ2149.1−3041

In this cluster there are **two** radio sources associated with an X-ray source shown in Fig.6.9. One of them is associated with the central peak in X-ray or the optical bright central galaxy. The other one is associated with another bright x-ray source at the outer parts of the central region. Both are listed in Tab.6.1

6.1.19 RXCJ2157.4−0747

In this cluster there are **seven** radio sources associated with an X-ray source shown in Fig.6.10. This map lacks a central peak in X-ray or the optical bright central galaxy. There is also just one bright x-ray source, but this one is lacking an radio counterpart. All of the radio-x-ray pairs are listed in Tab.6.1

6.1.20 RXCJ2217.7−3543

This cluster shows **one** radio source associated with an X-ray source. It is located in the bottom right corner of the central region of the cluster. The X-ray source is rather faint as indicated by the contours in Fig.6.10 bottom panel. The radio source with an X-ray counterpart is listed in Tab.6.1

6.1.21 RXCJ2218.6−3853

In this cluster there is **one** radio source associated with an X-ray source shown in Fig.6.11. This radio source is associated with the central peak in X-ray or the optical bright central galaxy. It is listed in Tab.6.1

6.1.22 RXCJ2234.5−3744

In this cluster there are **two** radio sources associated with an X-ray source shown in Fig.6.11. One of them is associated with the central peak in X-ray or the optical bright central galaxy. Both are listed in Tab.6.1

6.2 Radio sources with an X-ray counterpart

This sample is constructed of all radio sources having an X-ray counterpart. The individual sources are listed by cluster and source ID in Tab.6.1 These sources form the subsample of the radio sources with an X-ray counterpart.

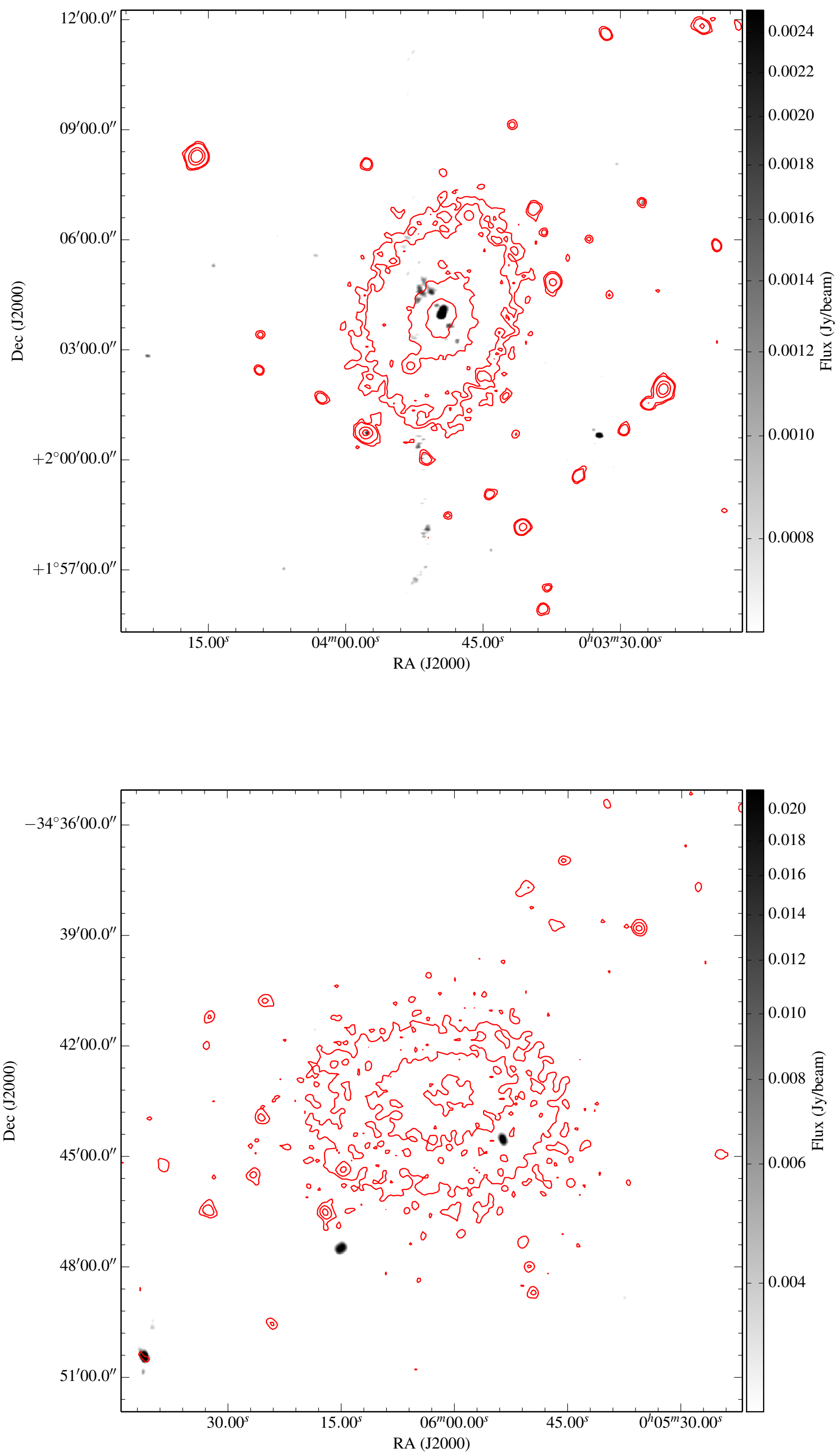

Figure 6.1: 610-MHz GMRT maps overlaid with X-ray observation, central region of the cluster ($R_{500} \times R_{500}$). Top: RXCJ0003.8+0203 revealing three source radio and X-ray matches; bottom: RXCJ0006.0−3443 showing the one source associated with an X-ray source.

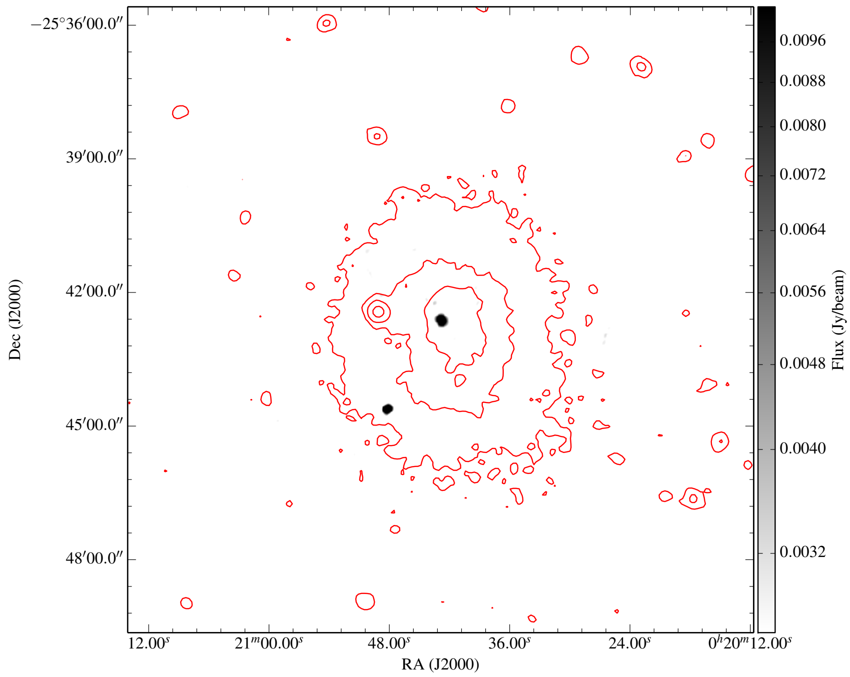

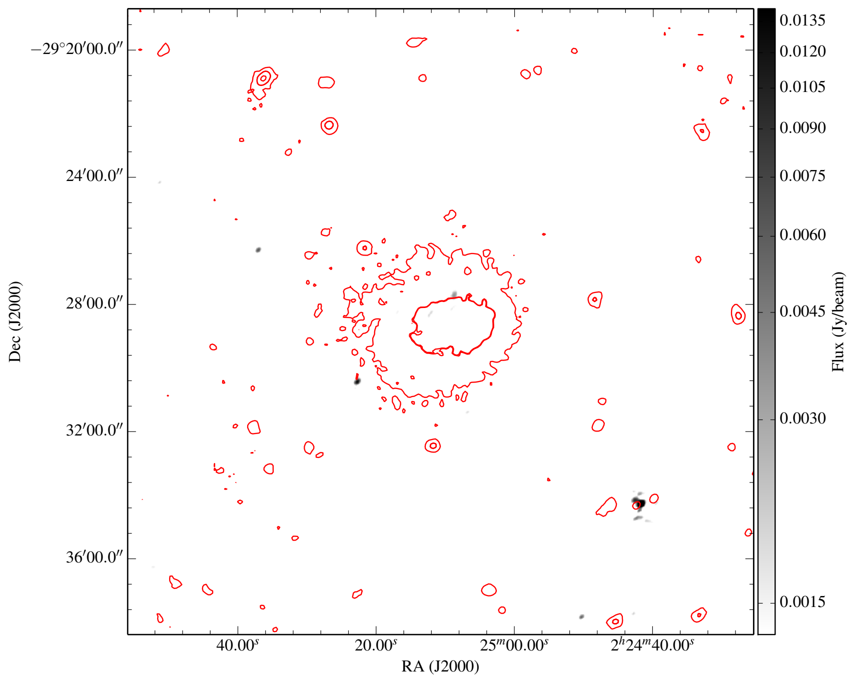

Figure 6.2: 610-MHz GMRT maps overlaid with X-ray observation, central region of the cluster ($R_{500} \times R_{500}$) revealing three source radio and X-ray matches. Top: RXCJ0020.7−2542; bottom: RXCJ0225.1−2928

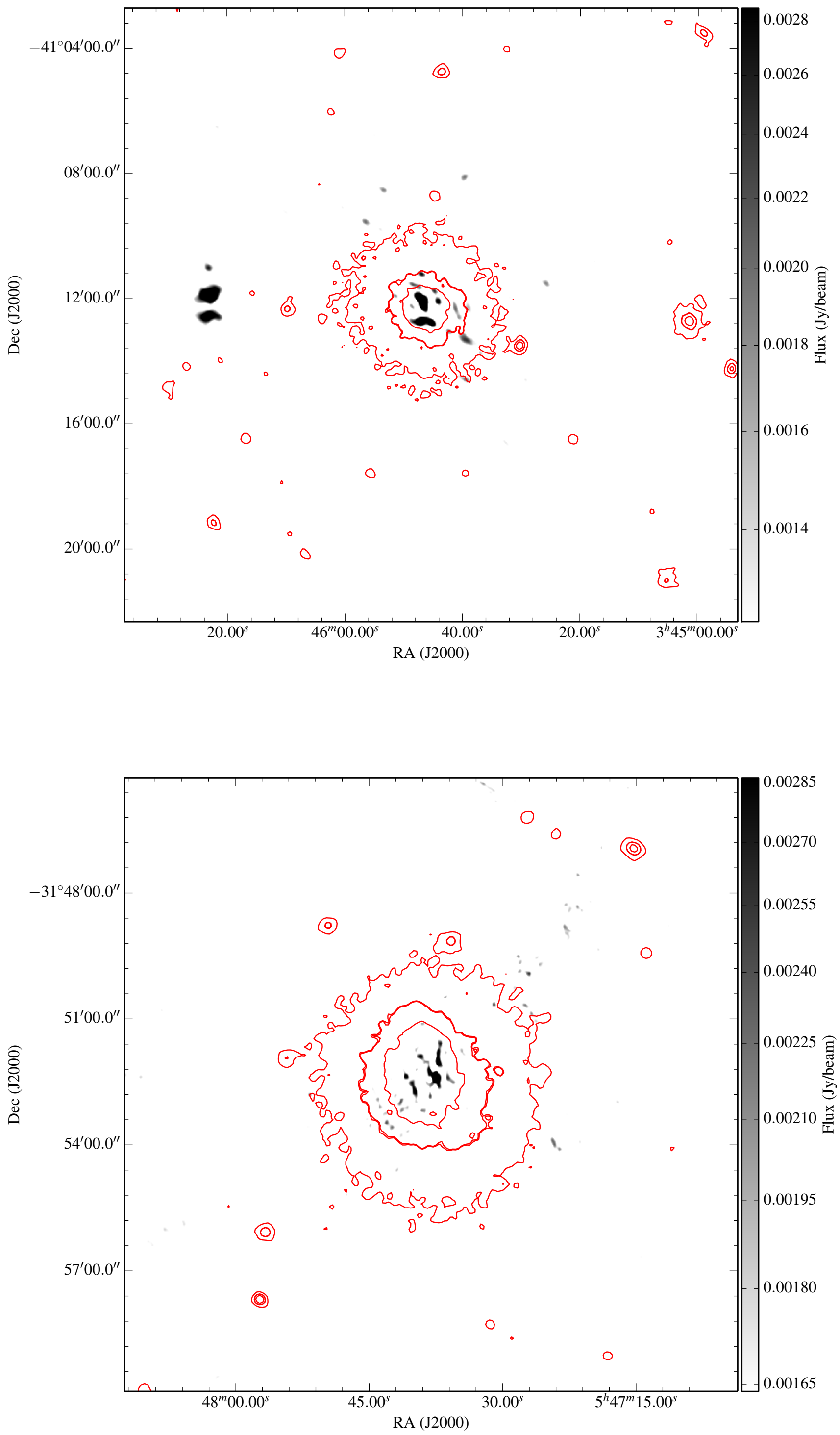

Figure 6.3: 610-MHz GMRT maps overlaid with X-ray observation, central region of the cluster ($R_{500} \times R_{500}$). Top: RXCJ0345.7.8−4112 showing the coincidence of the radio and x-ray peak at the bright central galaxy, bottom: RXCJ0547.6.0−3152 showing the one source associated with an X-ray source.

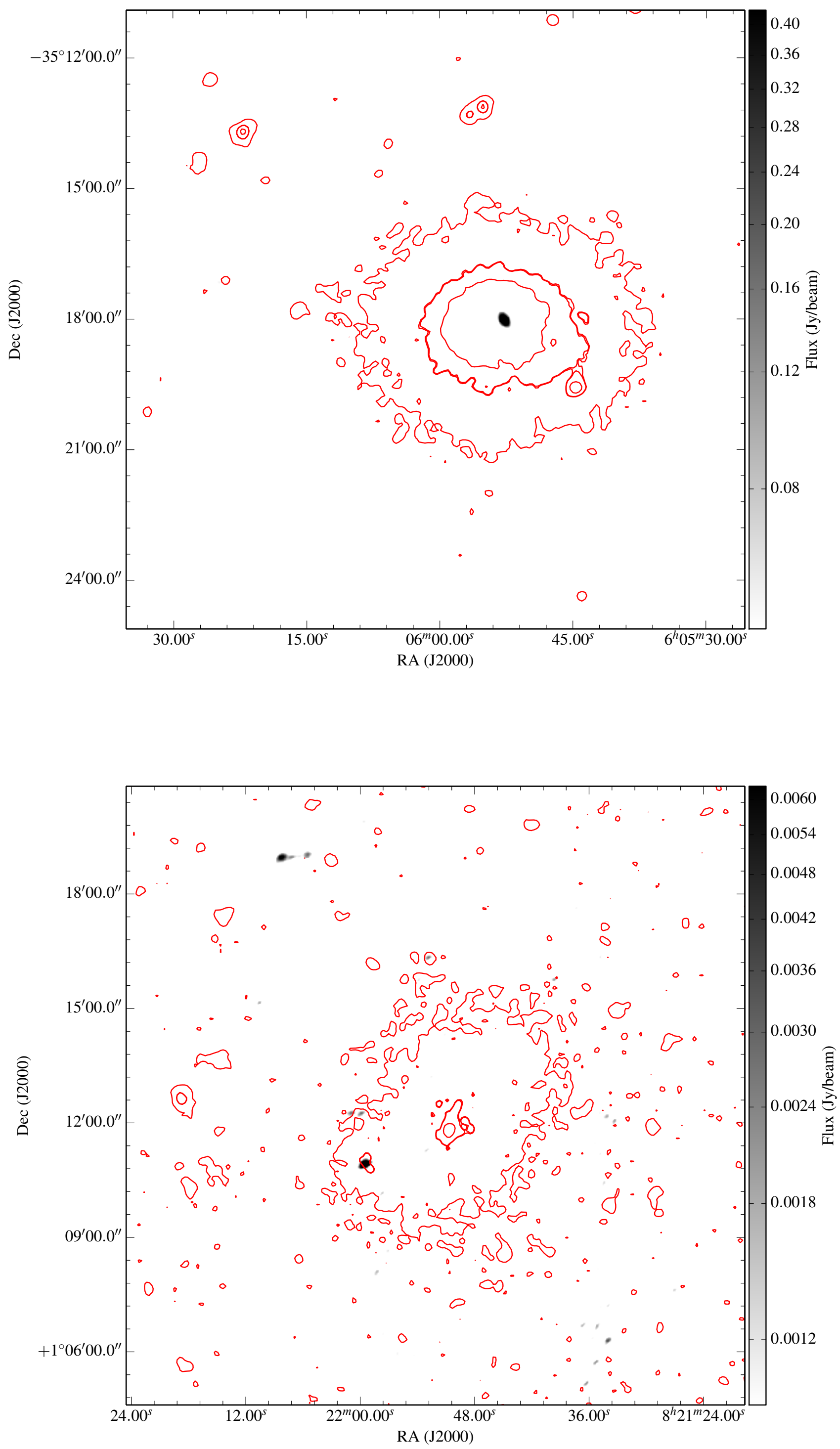

Figure 6.4: 610-MHz GMRT maps overlaid with X-ray observation, central region of the cluster ($R_{500} \times R_{500}$) Top: RXCJ0605.8−3518 revealing one source of radio and X-ray match; bottom: RXCJ0821.8+0112 with its source not associated with the bright central galaxy.

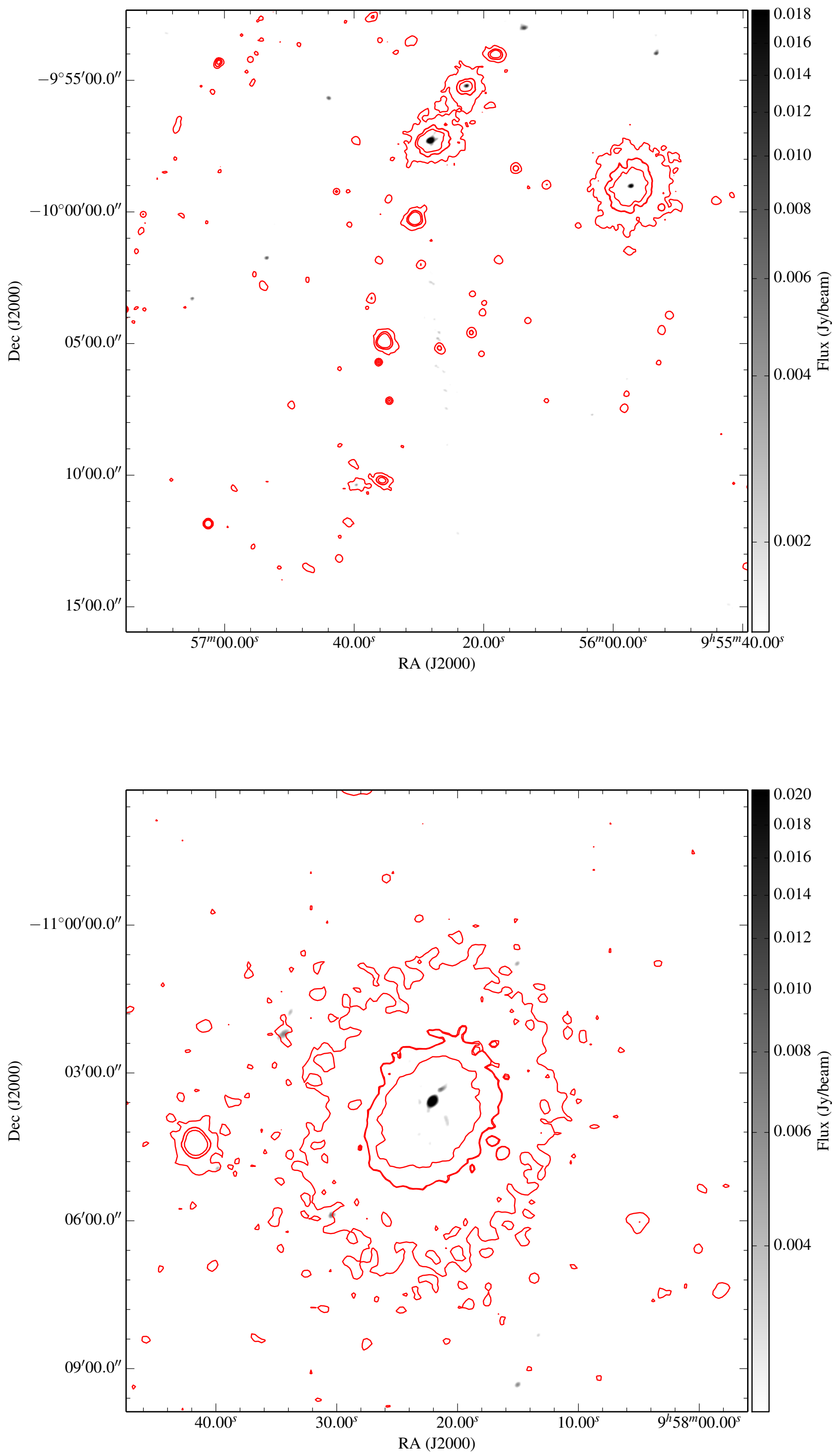

Figure 6.5: 610-MHz GMRT maps overlaid with X-ray observation, central region of the cluster ($R_{500} \times R_{500}$). Top: RXCJ0956.4−1004 revealing four source radio and X-ray matches; bottom: RXCJ0958.3−1103 showing the one source associated with the central bright galaxy and another one with an X-ray source.

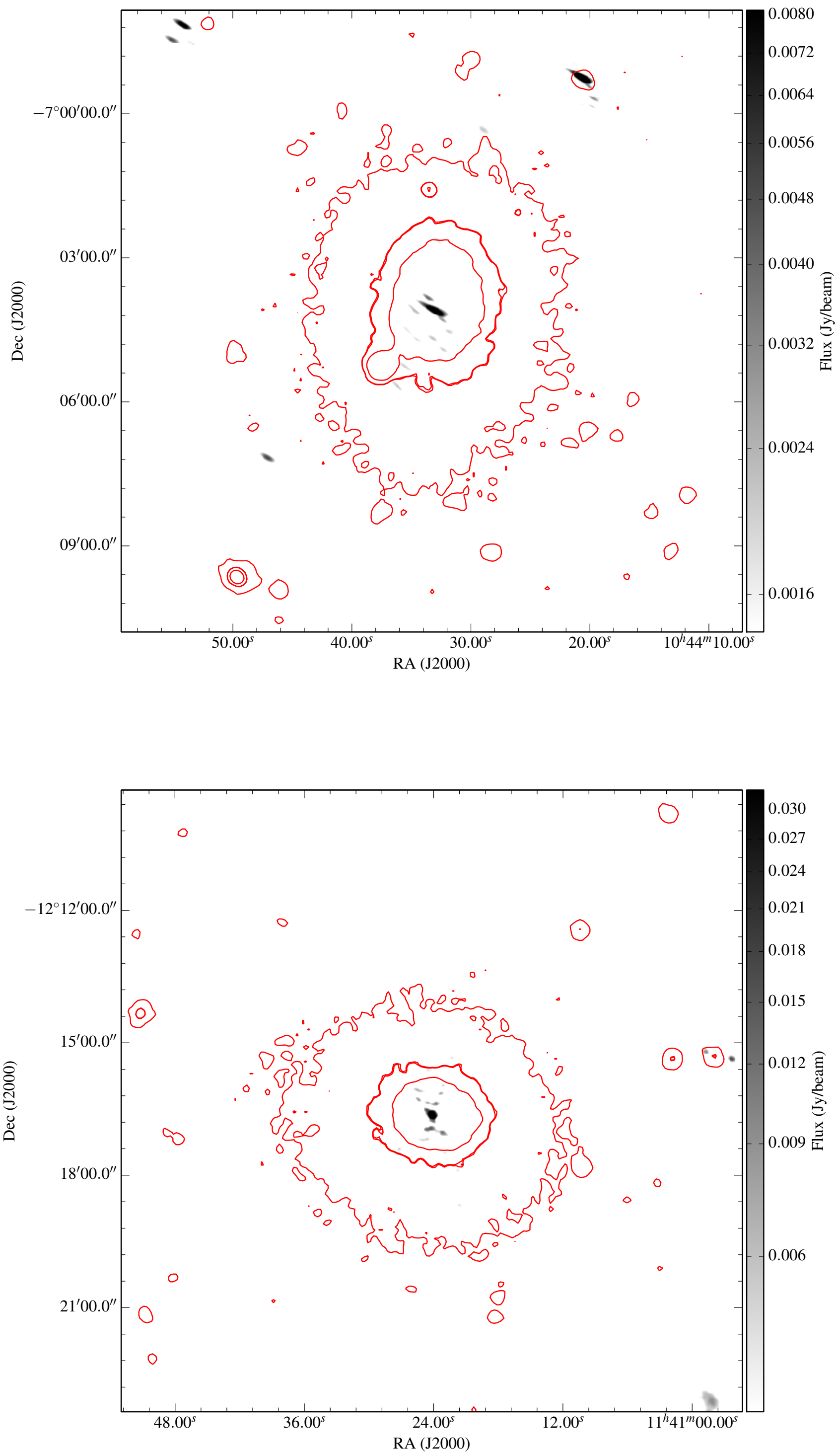

Figure 6.6: 610-MHz GMRT maps overlaid with X-ray observation, central region of the cluster ($R_{500} \times R_{500}$) Top: RXCJ1044.5−00704 revealing one source radio and X-ray match; bottom: RXCJ1141.4−1216 showing the radio sources with their x-ray counterparts

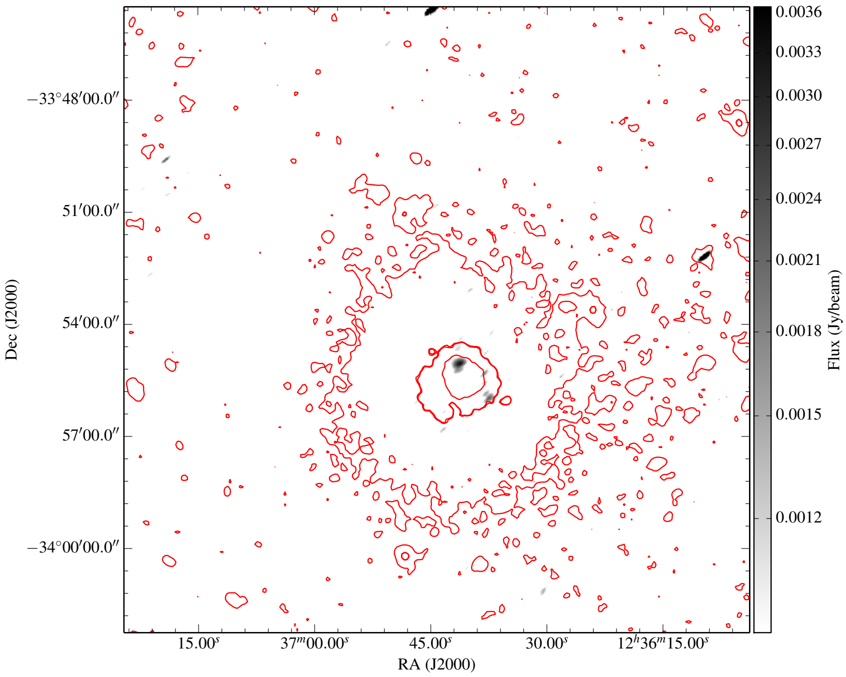

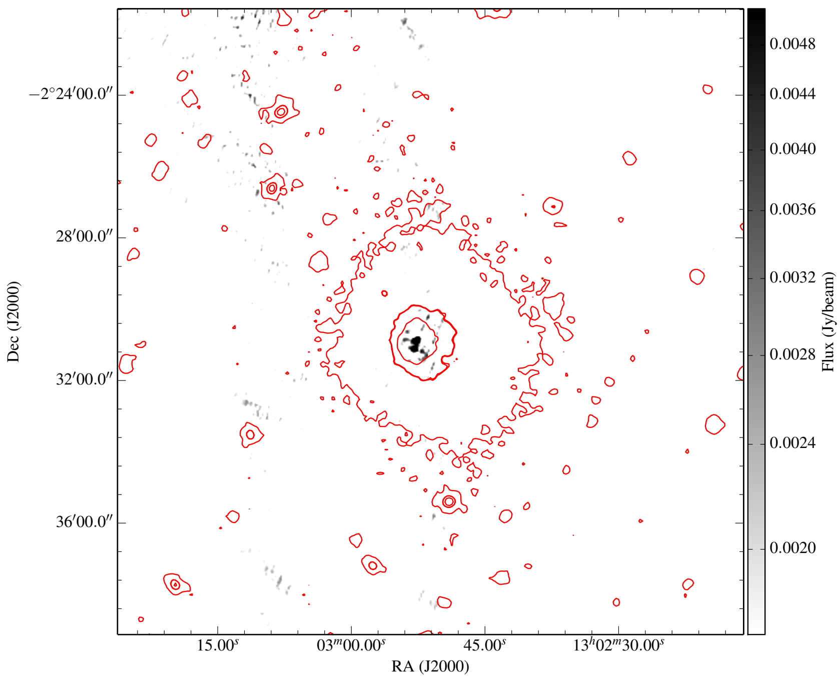

Figure 6.7: 610-MHz GMRT maps overlaid with X-ray observation, central region of the cluster ($R_{500} \times R_{500}$). Top: RXCJ1236.7−3354 with its two radio x-ray matches; bottom: RXCJ1302.8−0230 with two radio x-ray pairs

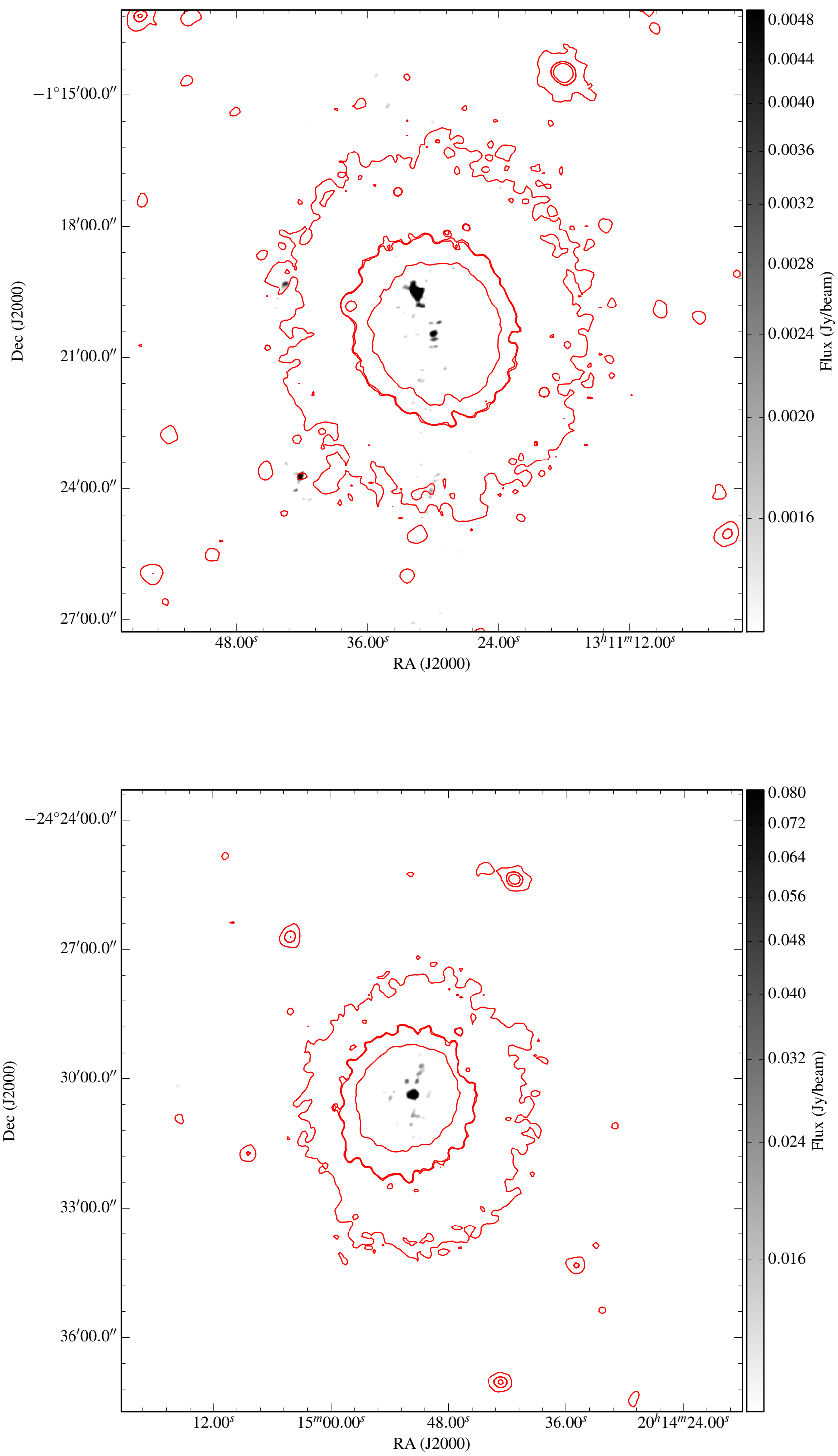

Figure 6.8: 610-MHz GMRT maps overlaid with X-ray observation, central region of the cluster ($R_{500} \times R_{500}$) Top: RXCJ1311.4−0120 another cluster with four coinciding radio and x-ray sources; bottom: RXCJ2014.8−2430 revealing its radio and x-ray match

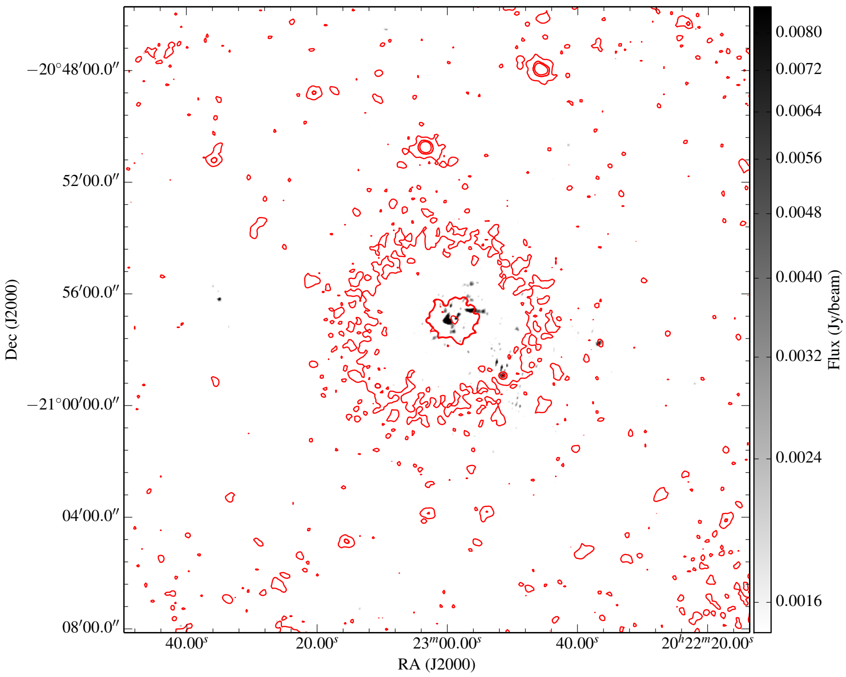

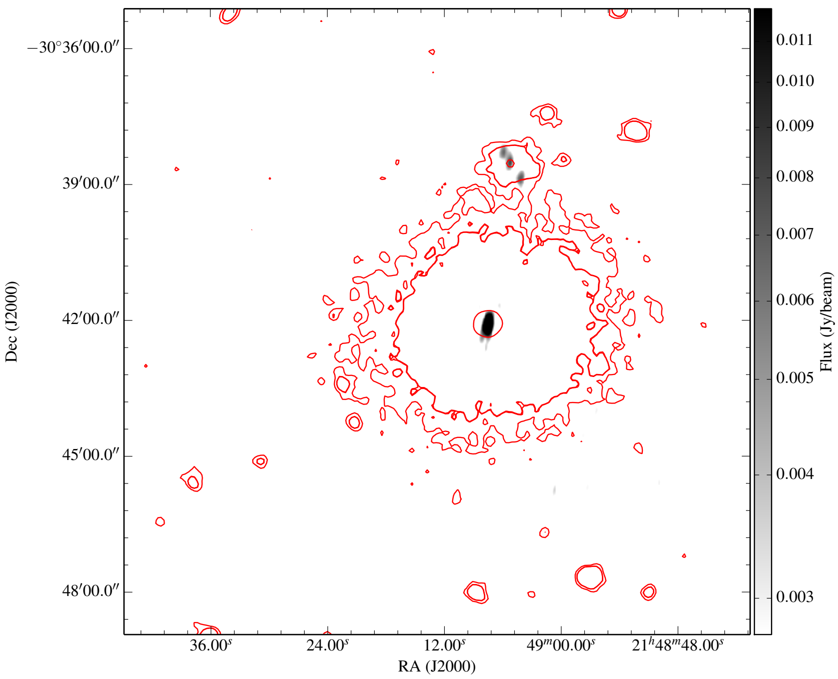

Figure 6.9: 610-MHz GMRT maps overlaid with X-ray observation, central region of the cluster ($R_{500} \times R_{500}$) Top: RXCJ2023.0−2056 showing its three x-ray radio matches associated with its central bright galaxy; bottom: RXCJ2149.1−3041 revealing its match for the central galaxy and another bright x-ray source.

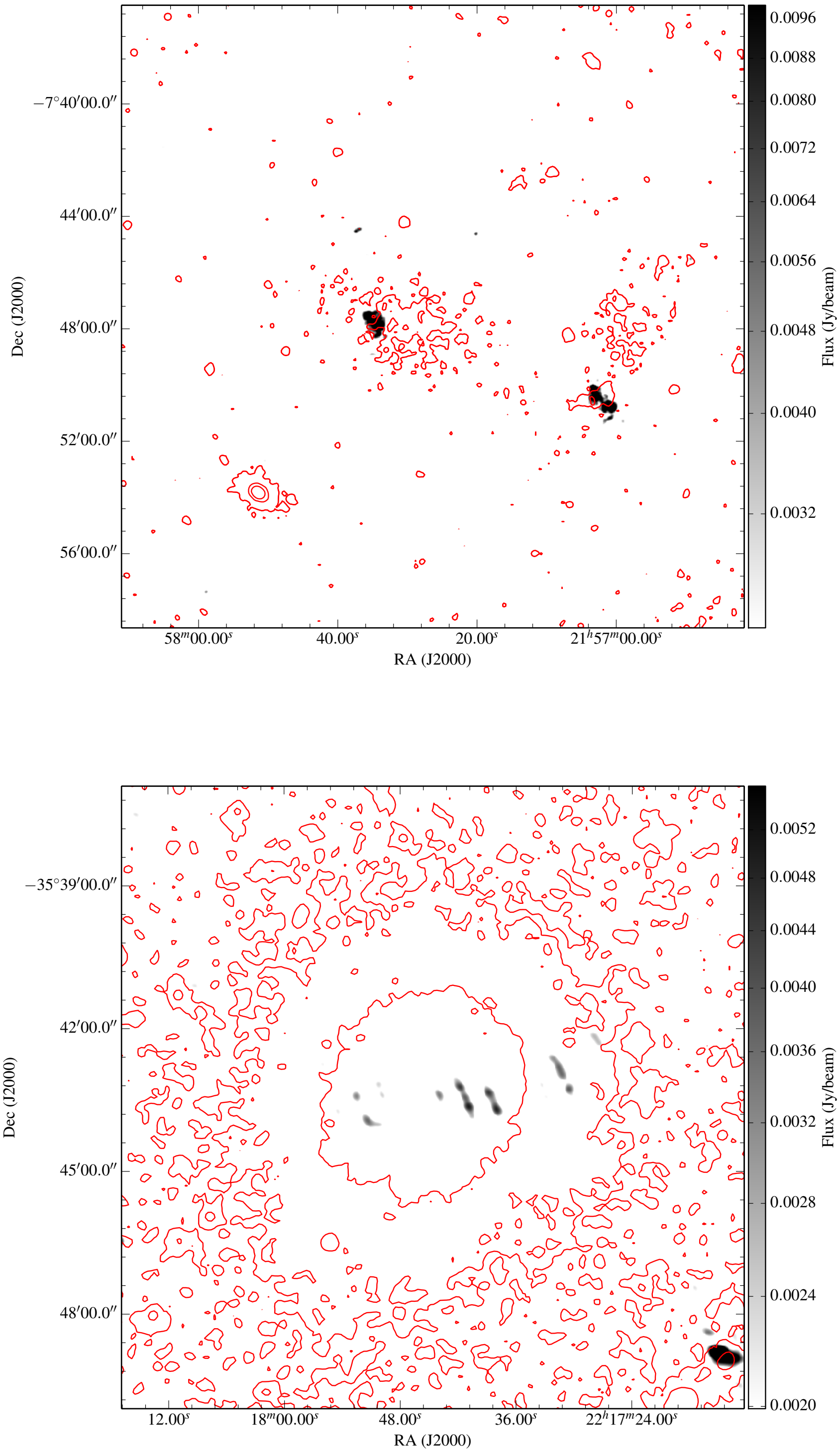

Figure 6.10: 610-MHz GMRT maps overlaid with X-ray observation, central region of the cluster ($R_{500} \times R_{500}$) Top: RXCJ2157.4−0747 having the highest number, seven, of radio x-ray assiciate pairs; bottom: RXCJ2217.7−3543 revealing a match with a faint x-ray source.

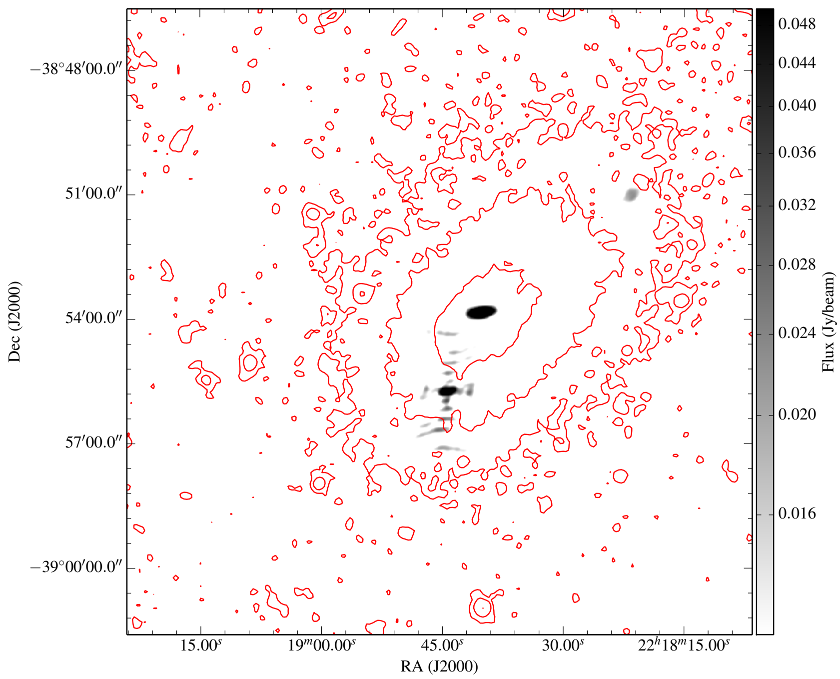

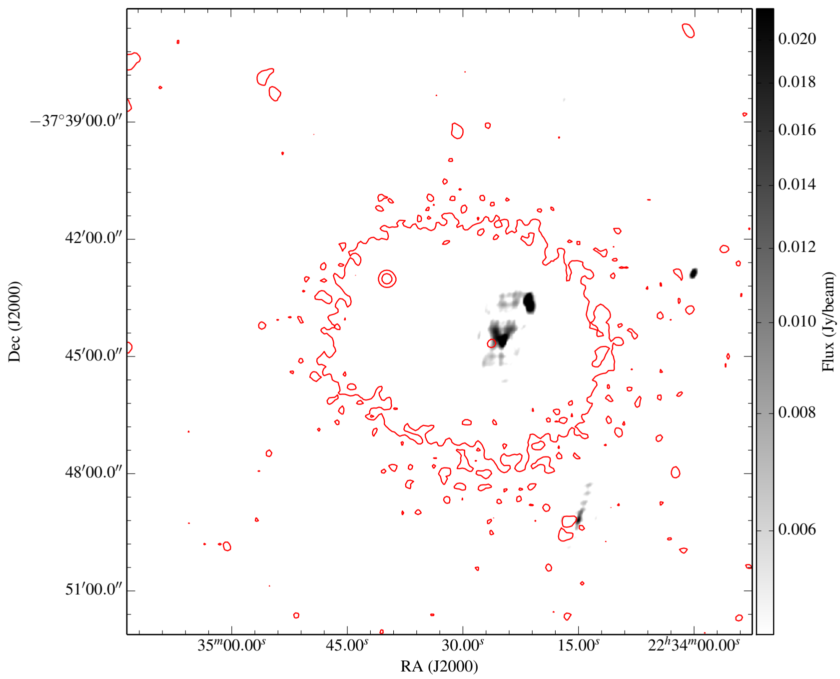

Figure 6.11: 610-MHz GMRT maps overlaid with X-ray observation, central region of the cluster ($R_{500} \times R_{500}$) Top: RXCJ2218.6−3853 showing its radio and x-ray match; bottom: RXCJ2234.5−3744 with its two matched sources.

6.3 Summary

Of the 49 radio sources with an X-ray counterpart 19 can be associated with the bright central galaxy. There are 20 x-ray peaks coinciding with the central bright galaxy. It is expected that a large fraction of the central bright galaxies have a radio counterpart. The two disturbed clusters show very different behaviour, as in one of them the bright x-ray sources all have a radio counterpart and in the other one the bright x-ray source lacks a radio partner.

Source ID	RA	Δ RA	DEC	Δ DEC	total flux	Δ total flux	Peak flux	Δ Peak flux	associated with cluster
3	00:03:058	0.000078	02:00:044	0.000048	0.002207	0.000282	0.002195	0.000161	RXCJ0003.8+0203
10	00:03:050	0.000051	02:03:060	0.00003	0.029397	0.000641	0.012193	0.000285	
10	00:03:050	0.0002	02:04:012	0.000146	0.001471	0.000493	0.00144	0.000283	
16	00:03:028	0.000194	02:06:060	0.00023	0.003781	0.000219	0.001303	0.000167	
2	00:06:041	0.000005	-34:50:027	0.000008	0.100146	0.00114	0.103272	0.000641	RXCJ0006.0−3443
1	00:20:043	0.00003	-25:42:038	0.000034	0.059145	0.001438	0.035786	0.000965	RXCJ0020.7−2542
11	02:24:042	0.000007	-29:34:017	0.000006	0.075696	0.000763	0.070395	0.000444	RXCJ0225.1−2928
11	02:24:042	0.00006	-29:34:029	0.000047	0.003381	0.000793	0.005722	0.000359	
11	02:24:043	0.000085	-29:34:010	0.000042	0.018852	0.000681	0.01002	0.000469	
12	02:24:043	0.000208	-29:33:053	0.000125	0.001812	0.000635	0.001941	0.000354	
6	03:45:047	0.000404	-41:11:015	0.000277	0.002768	0.000901	0.002784	0.0005	RXCJ0345.7−4112
0	05:47:038	0.000078	-31:52:025	0.000132	0.023835	0.00174	0.013861	0.00117	RXCJ0547.6−3152
1	06:05:053	0.000002	-35:18:002	0.000002	2.186014	0.008317	2.095744	0.003403	RXCJ0605.8−3518
4	08:21:060	0.000009	01:10:055	0.000013	0.049081	0.000736	0.031561	0.000315	RXCJ0821.8+0112
13	09:56:051	0.000281	-10:10:022	0.000272	0.003312	0.000175	0.000794	0.000143	RXCJ0956.4−1004
21	09:56:028	0.000003	-09:57:019	0.000004	0.149655	0.001072	0.090002	0.000291	
31	09:56:023	0.000007	-09:55:015	0.000013	0.018076	0.000491	0.016327	0.000201	
43	09:55:057	0.000004	-09:59:003	0.000007	0.035353	0.000577	0.030881	0.000202	
2	09:58:034	0.000087	-11:02:013	0.000064	0.017053	0.000494	0.006584	0.000367	RXCJ0958.3−1103
9	09:58:022	0.000008	-11:03:035	0.00001	0.127187	0.001734	0.101351	0.001062	
8	10:44:021	0.000027	-06:59:017	0.000015	0.036973	0.00085	0.038777	0.00039	RXCJ1044.5−0704
2	11:41:024	0.000022	-12:16:039	0.000017	0.157953	0.006608	0.153916	0.003823	RXCJ1141.4−1216
6	11:40:059	0.000062	-12:15:013	0.000042	0.010175	0.001013	0.009566	0.000588	
7	11:40:056	0.000041	-12:15:023	0.000031	0.018728	0.001369	0.018119	0.000791	
3	12:36:041	0.000216	-33:55:005	0.000233	0.014475	0.000306	0.002891	0.000259	RXCJ1236.7−3354
7	12:36:010	0.000063	-33:52:012	0.000051	0.009797	0.000447	0.009348	0.000216	
0	13:02:053	0.000053	-02:30:053	0.000035	0.069922	0.001366	0.025382	0.001036	RXCJ1302.8−0230
0	13:02:053	0.000083	-02:31:007	0.000069	0.045747	0.001334	0.014892	0.001037	
0	13:11:044	0.000155	-01:19:020	0.000169	0.013744	0.000463	0.003398	0.000377	RXCJ1311.4−0120
2	13:11:042	0.000028	-01:23:044	0.000024	0.011314	0.000693	0.011081	0.000397	
2	13:11:042	0.000243	-01:23:052	0.000154	0.002057	0.000674	0.001752	0.000394	
4	13:11:030	0.000037	-01:20:028	0.000029	0.0147	0.000845	0.011908	0.000518	
4	20:14:052	0.000023	-24:30:023	0.000016	0.49117	0.013374	0.410638	0.00814	RXCJ2014.8−2430
8	20:22:060	0.000076	-20:56:059	0.000072	0.252156	0.003169	0.036144	0.002183	RXCJ2023.0−2056
24	20:22:049	0.000138	-21:00:003	0.000208	0.007458	0.001039	0.004011	0.000703	
31	20:22:037	0.000073	-20:57:048	0.000063	0.029965	0.000795	0.010003	0.000612	
0	21:49:008	0.000023	-30:42:006	0.000078	0.082396	0.002531	0.058405	0.001535	RXCJ2149.1−3041
1	21:49:004	0.000123	-30:38:053	0.000323	0.013832	0.00108	0.006894	0.000748	
17	21:57:001	0.000038	-07:50:047	0.000054	0.291041	0.002338	0.031359	0.000578	RXCJ2157.4−0747
17	21:57:003	0.000051	-07:50:021	0.000032	0.351975	0.002021	0.033063	0.000578	
17	21:57:001	0.000164	-07:51:012	0.000097	0.042004	0.000606	0.008977	0.000501	
17	21:57:002	0.00008	-07:50:037	0.000148	0.001765	0.001048	0.003038	0.000451	
17	21:57:00	0.000158	-07:51:013	0.000157	0.001902	0.001014	0.002366	0.00054	
18	21:57:003	0.000253	-07:49:051	0.000176	0.006221	0.00101	0.003474	0.000687	
20	21:56:059	0.000344	-07:51:021	0.000163	0.012632	0.000932	0.003303	0.000447	
1	22:17:015	0.000058	-35:48:051	0.000128	0.047948	0.001695	0.026113	0.000769	RXCJ2217.7−3543
1	22:18:040	0.000065	-38:53:051	0.000018	0.451851	0.006183	0.241518	0.004101	RXCJ2218.6−3853
0	22:34:025	0.000044	-37:44:037	0.000076	0.065829	0.004603	0.055788	0.00274	RXCJ2234.5−3744
3	22:34:015	0.000068	-37:49:011	0.000173	0.008241	0.002932	0.012941	0.001228	

Table 6.1: Positions of radio sources within R_{500} radius of the pointing centre and associated with X-ray counterparts

Nothing shocks me. I'm a scientist.

HARRISON FORD (1942 -), AS INDIANA JONES

7

Conclusion and Future Work

7.1 Reflection

The REXCESS sample is a well constructed sample for probing the local population of galaxy clusters. It provided the base for the cluster selection made previous to this thesis and the data available for being used within this work. The main focus of this work is providing information about the radio structure of the members of the REXCESS sample and a short comparison to its x-ray properties. The theoretical background from a history of radio astronomy to galaxies, the observational properties of radio galaxies was given as well as an explanation of the term galactic cluster. This chapter was closed by a section about radio emission mechanisms. The third chapter focused on the Data calibration and analysis process, starting with a description of radio interferometry it describes the Data calibration process followed by a section on data analysis. In chapter four the individual sources observed at 610MHz are the main concern, but it also provides the reader with information about the REXCESS sample and a summary of the quality of the produced maps. Chapter five presents the 240MHz maps as well as spectral indices for cluster members and cluster member candidates. In chapter six the radio sources are compared to the x-ray observations and a sample of all radio sources with an x-ray counterpart is constructed. One of the main issues of the this thesis was the low raw data quality, especially for the 240MHz maps, resulting in a significantly lower number of maps at that frequency.

7.2 Results

In this section the results of this thesis are brought together for an overview. First the detections at the different wave lengths are summarised. Then the radio emitting BCGs are compared to the general poulation of detected radio sources. Thirdly the spectral slopes are examined and finally the radio emitting BCG are compared to a more general sample.

7.2.1 Radio detections

The cluster RXCJ0003.8+0203 has 2 confirmed cluster members and 16 cluster member candidates emitting at 610MHz. This cluster was not mapped at 240MHz. The cluster RXCJ0006.0−3443 has no confirmed cluster members and 13 cluster member candidates emitting at 610MHz. At 240MHz are no confirmed cluster members and 6 new cluster member candidates. Additionally detected were 2 sources, compared to the 610MHz map. The cluster RXCJ0020.7−2542 has one confirmed cluster member and one cluster member candidates emitting at 610MHz. At 240MHz are one confirmed cluster member and no new cluster member candidates. Less sources were detected, compared to the 610MHz map. The cluster RXCJ0049.4−2931 has no confirmed cluster members and no cluster member candidates emitting at 610MHz. At 240MHz are no confirmed cluster members and no new cluster member candidates. The cluster RXCJ0211.4−4017 has one confirmed cluster member and one cluster member candidate emitting at 610MHz. At 240MHz is one confirmed cluster member and one new cluster member candidate. Less sources were detected, compared to the 610MHz map. The cluster RXCJ0225.1−2928 has no confirmed cluster members and 19 cluster member candidates emitting at 610MHz. At 240MHz are no confirmed cluster members and 4 new cluster member candidates. Less sources were detected, compared to the 610MHz map. The cluster RXCJ0345.7−4112 has one confirmed cluster member and 6 cluster member candidates emitting at 610MHz. This cluster was not mapped at 240MHz. The cluster RXCJ0547.6−3152 has no confirmed cluster members and no cluster member candidates emitting at 610MHz. This cluster was also not mapped at 240MHz. The cluster RXCJ0605.8−3518 has one confirmed cluster member and one cluster member candidate emitting at 610MHz. At 240MHz are one confirmed cluster member and the new cluster member candidates. More sources were detected, compared to the 610MHz map. The cluster RXCJ0821.8+0112 has one confirmed cluster member and 13 cluster member candidates emitting at 610MHz. At 240MHz are no confirmed cluster members and one new cluster member candidate. Less sources were detected, compared to the 610MHz map. The cluster RXCJ0956.4−1004 has one confirmed cluster member and 54 cluster member candidates emitting at 610MHz. This cluster was not mapped at 240MHz. The cluster RXCJ0958.3−1103 has one confirmed cluster member and no cluster member candidates emitting at 610MHz. At 240MHz is one confirmed cluster members and 7 new cluster member candidates. More sources were detected, compared to the 610MHz map. The cluster RXCJ1044.5−0704 has one confirmed cluster member and 5 cluster member candidates emitting at 610MHz. This cluster was not mapped at 240MHz. The cluster RXCJ1141.4−1216 has no confirmed cluster member and 8 cluster member candidates emitting at 610MHz. At 240MHz is one confirmed cluster member and one new cluster member candidate. Less sources were detected, but more confirmed as cluster members, compared to the 610MHz map. The cluster RXCJ1236.7−3354 has no confirmed cluster member and 7 cluster member candidates emitting at 610MHz. At 240MHz are no confirmed cluster members and 6 new cluster member candidates. Less sources were detected, compared to the 610MHz map. The cluster RXCJ1302.8−0230 has no confirmed cluster member and 4 cluster member candidates emitting at 610MHz. This cluster was not mapped at 240MHz. The cluster RXCJ1311.4−0120 has no confirmed cluster members and 7 cluster member candidates emitting at 610MHz. At 240MHz are no confirmed cluster members and no new cluster member candidates. Less sources were detected, compared to the 610MHz map. The cluster RXCJ1516.3+0005 has no confirmed cluster member and 9 cluster member candidates emitting at 610MHz. This cluster was not mapped at 240MHz. The cluster RXCJ1516.5−0056 has no confirmed cluster members and 29 cluster member candidates emitting at 610MHz. At 240MHz are no confirmed cluster members and two new cluster member candidates. Less sources were detected, compared to the 610MHz map. The cluster RXCJ2014.8−2430 has one confirmed cluster members and 5 cluster member candidates emitting at 610MHz. At 240MHz is one confirmed cluster member and no new cluster member candidates. Less sources were detected, compared to the 610MHz map. The cluster RXCJ2023.0−2056 has one confirmed cluster member and 32 cluster member candidates emitting at 610MHz. This cluster and all of the following clusters were

not mapped at 240MHz. The cluster RXCJ2048.1−1750 has one confirmed cluster member and no cluster member candidates emitting at 610MHz. The cluster RXCJ2149.1−3041 has no confirmed cluster members and 2 cluster member candidates emitting at 610MHz. The cluster RXCJ2152.2−1942 has no confirmed cluster members and 14 cluster member candidates emitting at 610MHz. The cluster RXCJ2157.4−0747 has one confirmed cluster member and 29 cluster member candidates emitting at 610MHz. The cluster RXCJ2217.7−3543 has no confirmed cluster members and 2 cluster member candidates emitting at 610MHz. The cluster RXCJ2218.6−3853 has 2 confirmed cluster members and 4 cluster member candidates emitting at 610MHz. The cluster RXCJ2234.5−3744 has 2 confirmed cluster members and 4 cluster member candidates emitting at 610MHz.
In total were 18 cluster members detected at 610MHz and 3 at 240MHz. The detected cluster member candidates were 285 at 610 MHz and 31 at 240MHz. 28 clusters were mapped at 610MHz and only 13 were mapped at 240MHz. Even if this is taken into consideration less cluster members and cluster member candidates were detected at 240MHz. This could well be caused by the significant lower quality of the 240MHz maps.

7.2.2 Radio emitting BCGs

This section is split into two subsections, the first one investigates the flux of the radio emitting BCGs at 610MHz and compares them to to non-BCG cluster member candidates, while the second one does the same for the much smaller sample at 240MHz.

7.2.2.1 610MHz

12 maps exist where one radio source could be identified as the BCG. Eight other radio sources have a flux comparable to the one of the BCG and 44 of the other sources have a flux, which is a power of 10 fainter than the BCG flux in the same map. There are 25 sources 100 times fainter than the BCG in the same cluster. In one cluster there is a source 4 times brighter than the BCG . This extended source is in the cluster RXCJ2234.5−3744, where the position of the BCG has a huge offset to the X-ray peak and therefore is not entirely confirmed Haarsma et al. (2010). The same cluster also has another source of similar brightness than the BCG. The three other clusters containing sources of similar brightness as the BCG are RXCJ0020.7−2542, RXCJ1044.5−0704 and RXCJ0345.7−4112. The last one

contains 4 sources of similar brightness as the BCG. RXCJ1044.5−0704 has two sources of a brightness comparable to the BCG.

7.2.2.2 240MHz

Only 5 maps of the 13 maps have a radio source identified as the BCG. 2 of them have only the BCG as a radio source associated with the cluster. So 3 BCG radio sources can be compared to other sources. All 11 of these are roughly ten times fainter than the BCG.

7.2.2.3 Summary

In total there are 60 sources with a 10 times fainter flux than the BCG, 11 of them are at 240MHz and 49 are at 610MHz. 8 sources are of comparable brightness as the BCG and all of them are measured at 610MHz. 25 sources are 100 times fainter than the BCG and all of these are measured at 610 MHz. One source is 4 times brighter than the BCG and this one is located in RXCJ2234.5−3744 at 610 MHz. It would be interesting to find out it the source is also detected at 240MHz and if it is considerably brighter as the BCG as well.

7.2.3 Spectral slopes

This section focuses on the seven sources where reasonable spectral slopes could be calculated and briefly mentions the other ten sources were either only two data points were available or the spectral indices were changing.
All spectral slopes calculated are positive. The lowest spectral slope was calculated for RXCJ0211.4−4017. It has a calculated $\alpha = 0.38$. The two sources with a medium spectral slopes are RXCJ0605.8−3518 and RXCJ2014.8−2430. Their spectral indices are $\alpha = 0.77$ and $\alpha = 0.68$ respectively. The other four sources have a higher spectral index. RXCJ0020.7−2542 has the lowest spectral index in this group with $\alpha = 0.92$. The second lowest spectral index $\alpha = 0.97$ is associated with RXCJ0006.0−3443. The two sources with the highest spectral index are RXCJ2149.1−3041 and RXCJ2218.6−3853. They both have spectral indices larger than one, $\alpha = 1.17$ and $\alpha = 1.09$ respectively. These are still smaller than the ones calculated by Hogan *et al.* (2015a), $\alpha = 1.41$ and $\alpha = 1.36$ respectively.

7.2.4 Radio BCGs comparison

Since the flux and luminosity are direct proportional to each other it can be easily compared to Hogan *et al.* (2015a). As the sample size of the number of clusters with a BCG observed is rather small, 12 at 610MHz and 5 at 240MHz. Only a qualitative comparison can be done. Fig.7.1 shows the same trend as Hogan *et al.* (2015a), higher luminosities are less often observed than lower ones. The samples from the measured BSGs here show not a smooth curve, but this might well be caused by the size of the sample. It is obvious though, the highest flux is only reached by one BCG and the difference to the next higher one is significant, a feature shared with the way larger sample presented by Hogan *et al.* (2015a).
In a nutshell the measured fluxes show the same features as the fluxes of a larger sample, when the sample size is taken into consideration.

7.3 BCG activity in the radio regime

Brightest cluster galaxies (BCG) are located in the center of the gravitational potential well of a galaxy cluster.Best *et al.* (2007) They are very luminous objects and have large radii. Schombert (1986) The environment inside their cluster influence the properties of the BCG located within. Edge (1991),Lin, & Mohr (2004),Brough et al. (2005). The likelihood of a BCG to be radio-loud is higher than of a non-dominant cluster ellipticals Burns et al. (1981), Valentijn, & Bijleveld (1983),Burns (1990). This radio-loud AGN activity of the BCG is thought to be a potential solution of the cooling-flow problem Best *et al.* (2007). It is shown that radio lobes coincide with the bubbles and cavities in the X-ray waveband Boehringer et al.

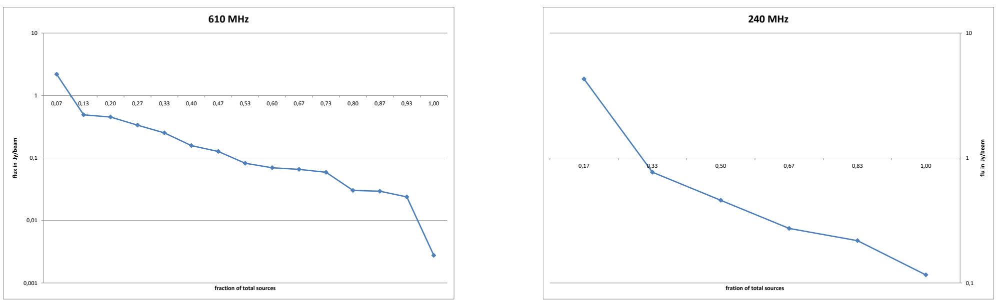

(a) flux of BCGs at 610MHz **(b)** flux of BCGs at 240MHz

Figure 7.1: The flux of BCGs compared to the fraction of the total sample that exceeded that flux

(1993), Carilli et al. (1994), **?**, Fabian et al. (2000), Blanton et al. (2001), McNamara, & Nulsen (2012). In these regions the relativistic radio plasma has replaced the intracluster gas. The radio activity is recurrent and sufficient to balance radio losses Best *et al.* (2007), Dalla Vecchia et al. (2004), Brüggen et al. (2005), Nusser et al. (2006). The radio-loud AGN fraction of the total population is strongly dependent on mass Best et al. (2005). The sample used by Best *et al.* (2007) consists of 625 galaxy clusters and was constructed from NVSS Condon *et al.* (1998) and FIRST Becker et al. (1995). Optical properties were used to distinguish radio-loud AGN from radio-emitting star-forming galaxies Best *et al.* (2007) . The distribution of radio-luminosities of the galaxies inside of a cluster or field galaxies is the same Ledlow, & Owen (1996).

The findings that the likelihood of a BCG to be radio-loud is not influenced by its surroundings is confirmed with the results of the radio-loud BCGs in this thesis. 6 of them are hosted by cool core clusters and 6 are hosted by non-cool core clusters. If the non-BCG radio-loud sources are examined only 3 of them are located in cool core clusters.

Richer clusters show a stronger incidence of AGN activity in BCGs McNamara, & Nulsen (2012). In the sample of this thesis 60% of the most massive clusters have a radio-loud BCG, which coincides nicely with the results of McNamara, & Nulsen (2012). Instead of the 75% of the clusters containing an BCG found by Mittal et al. (2009), only 40% of this sample have a radio-loud AGN. This value is approximately constant for both radio wavelengths. This could be partially explained by the small sample size in this work, compared to the 5 times larger sample used by Mittal et al. (2009). Both samples were constructed based on their X-ray flux Böhringer *et al.* (2007) and Reiprich, & Böhringer (2002).

In conclusion the findings of this thesis coincide with the findings of previous studies and verify them, only the predicted number of radio-loud AGN is lower than expected but this could be explained by the small size of the sample and the over-representation of less-massive clusters.

7.4 Research questions - answered.

The properties of the observed clusters are, as expected, quite variable, as the sample contains relaxed and disturbed clusters. There are small clusters with only a few detected sources and large ones with many sources either confirmed members or member candidates. How the radio sources and the optical sources matched was used, for the optical sources of known redshift, to determine the cluster membership of a radio source. How the radio and the x-ray observations compared to each other was answered by another chapter. To put it in a nutshell, there seems to be a correlation between radio sources and x-ray point sources.

7.5 Outlook

There are always things to be improved. For the 610MHz maps further in depth research would be needed to confirm if the cluster member candidates are cluster members or sources not associated with the cluster. Additionally even more careful flagging on some of the maps might be resulting in lower rms and a higher signal to noise ratio. It could also possibly remove the phase artefacts still present in some maps. The same issues apply to the 240MHz maps. in this case even complete manual flagging might give better results, but this was refused by time constraints. As for the spectra, additional data could verify the findings further and even extend it to other frequencies resulting in even more valid findings. The comparison with the x-ray could be carried out even more deeply by making sure all artefacts are removed from the radio maps and therefore false detections are minimised.

Nevertheless a base for future research was created with the findings of this thesis. It would be interesting to obtain data for these sources at different frequencies in order to get better spectral indices and evaluating them in respect to known emission mechanisms to get a better insight on the astrophysical properties of the sources. Another interesting question could be answered by searching for halos and relics. Answering these questions could have a great impact on the understanding of galaxy clusters and how the radio and the x-ray observations are related.

BIBLIOGRAPHY

G.O. Abell, 1958 *ApJS* 3, 211.

G.O. Abell, H.G. Corwin, R.P. Olowin 1989 *ApJS* 70, 1.

Becker, R. H., White, R. L., & Helfand, D. J. 1995, Astrophys. J., 450, 559.

Best, P. N., Kauffmann, G., Heckman, T. M., et al. 2005, Mon. Not. R. Astron. Soc., 362, 25.

P. N. Best, A. Von Der Linden, G. Kauffmann, T. M. Heckman, C. R. Kaiser; On the prevalence of radio-loud active galactic nuclei in brightest cluster galaxies: implications for AGN heating of cooling flows, Monthly Notices of the Royal Astronomical Society, Volume 379, Issue 3, 11 August 2007, Pages 894908

Blandford R. D., Konigl A., 1979, Astrophys. J., 232, 34

Blanton, E. L., Sarazin, C. L., McNamara, B. R., et al. 2001, Astrophys. J., 558, L15.

Boehringer, H., Voges, W., Fabian, A. C., et al. 1993, Mon. Not. R. Astron. Soc., 264, L25.

H. Böhringer, P. Schuecker,G. W. Pratt, M. Arnaud, T.J. Ponman, J.H. Croston, S. Borgani, R.G. Bower, U.G. Briel, C.A. Collins, M. Donahue, W.R. Forman, A. Finoguenov, M.J. Geller, L. Guzzo, J.P. Henry, R. Kneissl, J.J. Mohr, K. Matsushita, C.R. Mullis, T. Ohashi, K. Pedersen, D. Pierini, H. Quintana, S. Raychaudhury, T.H. Reiprich, A.K. Romer, P. Rosati, K. Sabirli, R.F. Temple, P.T.P. Viana, A. Vikhlinin, G.M. Voit, Y.-Y. Zhang 2007 *A & A* 469, 363.

H. Bridle, D. H. Hough, C. J. Lonsdale, J. O. Burns, and R. A. Laing. Deep VLA imaging of twelve extended 3CR quasars. AJ, 108:766820, Sept. 1994.

A. H. Bridle and R. A. Perley. Extragalactic Radio Jets. ARA&A , 22:319358, 1984.

Brough, S., Collins, C. A., Burke, D. J., et al. 2005, Mon. Not. R. Astron. Soc., 364, 1354.

Brüggen, M., Ruszkowski, M., & Hallman, E. 2005, Astrophys. J., 630, 740.

Burns, J. O., White, R. A., & Hough, D. H. 1981, Astron. J., 86, 1.

Burns, J. O. 1990, Astron. J., 99, 14.

Carilli, C. L., Perley, R. A., & Harris, D. E. 1994, Mon. Not. R. Astron. Soc., 270, 173.

Caroll, B.W., Ostlie, D.A., 2007, An Introduction to Modern Astrophysics, 2nd edn. , Pearson as Addison-Wesley, San Francisco

A. S. Cohen, W. M. Lane, W. D. Cotton, N. E. Kassim, T. J. W. Lazio, R. A. Perley, J. J. Condon, W. C. Erickson, Astron.J.134:1245-1262,2007

Condon, J. J., Cotton, W. D., Greisen, E. W., Yin, Q. F., Perley, R. A., Taylor, G. B.,

& Broderick, J. J. 1998, AJ, 115, 1693

Dalla Vecchia, C., Bower, R. G., Theuns, T., et al. 2004, Mon. Not. R. Astron. Soc., 355, 995.

Donahue, M. 2009, American Institute of Physics Conference Series, 177.

Edge, A. C. 1991, Mon. Not. R. Astron. Soc., 250, 103.

Fabian, A. C., Sanders, J. S., Ettori, S., et al. 2000, Mon. Not. R. Astron. Soc., 318, L65.

Gribbin, J. ,2008,Galaxies, *Oxford University Press* Oxford

Haarsma, D. B., Leisman, L., Donahue, M., et al. 2010, Astrophys. J., 713, 1037.

Herschel, W. 1785, Royal Society of London Philosophical Transactions Series I, 75, 213

Herzog, E., Wild, P., & Zwicky, F. 1957, PASP, 69, 409

Hey,J.S., 1984, Das Radiouniversum. Einfhrung in die Radioastronomie,Translated from the English edition by Scheffler, H., Weinheim (F.R. Germany): Verlag Chemie, 8 + 280

M. T. Hogan, A. C. Edge, J. Hlavacek-Larrondo, K. J. B. Grainge, S. L. Hamer, E. K. Mahony, H. R. Russell, A. C. Fabian, B. R. McNamara, R. J. Wilman; A comprehensive study of the radio properties of brightest cluster galaxies, Monthly Notices of the Royal Astronomical Society, Volume 453, Issue 2, 21 October 2015, Pages 12011222

M. T. Hogan, A. C. Edge, J. E. Geach, K. J. B. Grainge, J. Hlavacek-Larrondo, T. Hovatta, A. Karim, B. R. McNamara, C. Rumsey, H. R. Russell, P. Salom, H. D. Aller, M. F. Aller, D. J. Benford, A. C. Fabian, A. C. S. Readhead, E. M. Sadler, R. D. E. Saunders; High radio-frequency properties and variability of brightest cluster galaxies, Monthly Notices of the Royal Astronomical Society, Volume 453, Issue 2, 21 October 2015, Pages 12231240

Hubble, E. P., 1925, ApJ, 62, 409

Hubble, E. P., 1926, ApJ, 64, 321

Jansky, K.G.: 1933 *Nature* 132, 66.

Jennison, R. C. and Das Gupta, M. K.: 1953 *Nature* 172, 996.

Ledlow, M. J., & Owen, F. N. 1996, Astron. J., 112, 9.

Lin, Y.-T., & Mohr, J. J. 2004, Astrophys. J., 617, 879.

Longair M. S., 2010, High Energy Astrophysics

Maciel W.J., 2013, Astrophysics of the Interstellar Medium, Springer, New York

T. Mauch, T. Murphy, H.J. Buttery, J. Curran, R.W. Hunstead, B. Piestrzynska, J.G. Robertson and E.M. Sadler (2003), MNRAS, 342, 1117-1130

McNamara, B. R., Wise, M., Nulsen, P. E. J., et al. 2000, Astrophys. J., 534, L135.

McNamara, B. R., & Nulsen, P. E. J. 2012, New Journal of Physics, 14, 55023.

Messier, C. 1781, Catalogue des Nebuleuses et des amas detoiles (Catalog of Nebulae and Star Clusters), Tech. rep

Mittal, R., Hudson, D. S., Reiprich, T. H., et al. 2009, Astron. Astrophys., 501, 835.

Mitsuishi, I., Babazaki, Y., Ota, N., et al. 2018, Publications of the Astronomical Society of Japan, 70, 112.

A. Moretti, M. Gullieuszik, B. Poggianti, A. Paccagnella, W. J. Couch, B. Vulcani, D. Bettoni, J. Fritz, A. Cava, G. Fasano, M. DOnofrio and A. Omizzolo A&A, 599 (2017) A81

Tara Murphy, Elaine M. Sadler, Ronald D. Ekers, Marcella Massardi, Paul J. Hancock, Elizabeth Mahony, Roberto Ricci, Sarah Burke-Spolaor, Mark Calabretta, Rajan Chhetri, Gianfranco De Zotti, Philip G. Edwards, Jennifer A. Ekers, Carole A. Jackson, Michael J. Kesteven, Emma Lindley, Katherine Newton-McGee, Chris Phillips, Paul Roberts, Robert J. Sault, Lister Staveley-Smith, Ravi Subrahmanyan, Mark A. Walker, Warwick E. Wilson; The Australia Telescope 20 GHz Survey: the source catalogue, Monthly Notices of the Royal Astronomical Society, Volume 402, Issue 4, 11 March 2010, Pages 24032423,

Nusser, A., Silk, J., & Babul, A. 2006, Mon. Not. R. Astron. Soc., 373, 739.

Perley R., 2003, Synthesis Imaging in Radio Astronomy II

Peterson B. M., 1997,An Introduction to Active Galactic Nuclei

G.W. Pratt, J.H. Croston, M. Arnaud, 2009, Galaxy cluster X-ray luminosity scaling relations from a representative local sample (REXCESS) *A & A* 498,361-378.

Pratt, G. W., Arnaud, M., Piffaretti, R., et al. 2010, Astron. Astrophys., 511, A85.

Reiprich, T. H., & Böhringer, H. 2002, Astrophys. J., 567, 716.

Ryle M., Hewish A., 1960, Mon. Not. R. Astron. Soc., 120, 220

Ryle M., Vonberg D. D., 1948, Royal Society of London Proceedings Series A, 193, 98

Schombert, J. M. 1986, The Astrophysical Journal Supplement Series, 60, 603.

Shakouri, S., Johnston-Hollitt, M., & Pratt, G. W. 2016, Mon. Not. R. Astron. Soc., 459, 2525.

http://skatelescope.org/ accessed 20.August 2017

https://www.skatelescope.org/cosmicdawn/ accessed 11.November 2018

Smith F. G., 1974, Radio astronomy

Stoughton, C., Lupton, R. H., Bernardi, M., et al. 2002, Astron. J., 123, 485.

http://www.phy.cam.ac.uk/history/years/radioast accessed 31.July 2017

Valentijn, E. A., & Bijleveld, W. 1983, Astron. Astrophys., 125, 223.

Walker, S. A., Fabian, A. C., & Sanders, J. S. 2014, Mon. Not. R. Astron. Soc., 441, L31.

Wilson A. S., Heckman T. M., 1985, in J. S. Miller (ed.), Astrophysics of Active Galaxies and Quasi-Stellar Objects

H. K. C. Yee, E. Ellingson, R.G.Carlberg, 1996, The CNOC cluster redshift survey catalogue: 1 Observational strategy and data reduction techniques *ApJS* 102,269-287.

York, D. G., Adelman, J., Anderson, J. E., et al. 2000, Astron. J., 120, 1579.

Zwicky, F., 1933, Helvetica Physica Acta, 6, 110

APPENDICES

It is a good morning exercise for a research scientist to discard a pet hypothesis every day before breakfast. It keeps him young.

KONRAD LORENZ (1903 - 1989)

GMRT calibration Pipeline

In the following lines the original python script used to calibrate the data is provided.

```
import time
import os

print "Low Fequency GMRT-Data Calibration"
print "Using AOFlagger and CASA"
print "Version 2010-10-26 (CASA-Version 3.0.2)"
print ""

# please note, that the fitsfile has to be imorted to use the script
#======================================================================
#
# This script has some interactive commands: scriptmode = True
# if you are running it and want it to stop during interactive parts.

scriptmode = True

#======================================================================
#Set up variables
#======================================================================
# edit wprojectplanes in Line 866 if neccesary default =90, imsize=10000
# default cellsize= 1 arcsec
# Set up the MS filename and save as new global variable
msfile = '4.DEC.USB.240.ms'
#Flux calibrator
calflux ='3C48'
#flux density of flux calibrator and model image if available
calfluxden= -1
calfluxmodimage =''
#phase calibrator
calphase ='0025-260'
#source
caltarget='RXCJ0020'
#reference antenna
calrefant = '6'
#phase and flux calibrator
calfluxphase = '3C48,0025-260'
#phase calibrator and source
calphasetarget = '0025-260,RXCJ0020'
#averaged file
avgmsfile= msfile+caltarget+'.avg'
#splited output file
splitmsfile = caltarget+'.LSB.610.split.ms'
calimage=caltarget+'.LSB.610'


#======================================================================
# Data Import and List
#======================================================================
#
# List a summary of the MS
#
print '--Listobs--'
vis=msfile
inp importgmrt

#=====================================================================
print "Use listobs to print summary to logger"

# You may wish to see more detailed information, in this case
# use the verbose = True option
listobs()


# Auf Logfile wechseln

# Pause script if you are running in scriptmode
#if scriptmode:
 #  user_check=raw_input('Return to continue script\n')


#======================================================================
# Data Examination and Flagging
```

```
#======================================================================
#
# flag the edges of the data
#
default ('flagdata')
vis=msfile
spw                 =         '0:0~1;105~127'
field =calflux
flagdata()

default ('flagdata')
vis=msfile
spw                 =         '0:0~1;105~127'
field =calphase
flagdata()

default ('flagdata')
vis=msfile
spw                 =         '0:0~1;105~127'
field =caltarget
flagdata()

default ('split')
vis=msfile
outputvis           =       msfile+calflux+'a.firstflagging.ms'
field               = calflux
datacolumn          = 'all'
split ()
default ('split')
vis=msfile
outputvis           =       msfile+calphase+'a.firstflagging.ms'
field               = calphase
datacolumn          = 'all'
split ()
default ('split')
vis=msfile
outputvis           =       msfile+caltarget+'a.firstflagging.ms'
field               = caltarget
datacolumn          = 'all'
split ()
print "Use the AO Flagger to do the rough flagging on the Flux calibrator"
print "If that is finished, press return to continue"
# Pause script if you are running in scriptmode
if scriptmode:
    user_check=raw_input('Return to continue script\n')

#===============================================================================
print "Now we use plotxy to check the flagging of the flux calibrator"
print "by channel, by uvdistance and time"
default('plotxy')
vis = msfile +calflux+'firstflagging.ms'
field = calflux
xaxis = 'chan'
datacolumn= 'corrected'
plotxy()

# Pause script if you are running in scriptmode
if scriptmode:
    user_check=raw_input('Return to continue script\n')

xaxis = 'uvdist'
plotxy()
# Pause script if you are running in scriptmode
if scriptmode:
    user_check=raw_input('Return to continue script\n')

xaxis = 'time'
plotxy()
# Pause script if you are running in scriptmode
if scriptmode:
    user_check=raw_input('Return to continue script\n')
#===================================================================================
```

```
print "Produce an uv-fits-file with the flagged data"

default ('exportuvfits')

vis          =        msfile+calflux+'a.firstflagging.ms'
fitsfile= calflux+'roughflagged.uv.fits'
field              =       calflux

exportuvfits ()



print "combine files for calibration"
default ('concat')
vis          =    [msfile+calflux+'a.firstflagging.ms', msfile+caltarget+'a.firstflagging.ms', msfile
+calphase+'a.firstflagging.ms']
concatvis          = msfile+'a.firstflag.ms'
concat()
#===================================================================================
print "Now we are doing a first calibration run for one channel of the flux calibrator"

print "Bandpass calibration"

#Now do bandpass calibration
#Setjy
default ('setjy')
vis=msfile +'a.firstflag.ms'
field = calflux
fluxdensity = calfluxden
modimage= calfluxmodimage
setjy()

#bandpass
default ('bandpass')

vis=msfile +'a.firstflag.ms'
field = calflux
spw='0:37~37'
caltable           =       msfile+ '.a.flux.0channel37.bcal'
refant             = calrefant
solnorm=True

bandpass()

#check with plotcal
default ('plotcal')
caltable           =       msfile+ '.a.flux.0channel37.bcal'
xaxis              =        'antenna'
yaxis='amp'
plotcal()

# Pause script if you are running in scriptmode
if scriptmode:
    user_check=raw_input('Return to continue script\n')

print "Gains calibration"

default ('gaincal')
vis=msfile +'a.firstflag.ms'
field = calflux
spw='0:37~37'
caltable           =       msfile+ '.a.flux.0channel37.gcal'
solint             =     '30.0s'
combine            =        ''
refant             = calrefant
gaintable          =      [msfile+ '.a.flux.0channel37.bcal']
gainfield          =      [calflux]
interp             =      ['linear']
gaincal()

#check with plotcal
default ('plotcal')
```

```
caltable            =        msfile+ '.a.flux.0channel37.gcal'
xaxis               =         'antenna'
yaxis='amp'
plotcal()
# Pause script if you are running in scriptmode
if scriptmode:
    user_check=raw_input('Return to continue script\n')

print "apply calibration to all channels and fields"

default ('applycal')
vis=msfile +'a.firstflag.ms'
selectdata          = False
gaintable           =       [msfile+ '.a.flux.0channel37.gcal',msfile+ '.a.flux.0channel37.bcal']
gainfield           =       ['*',calflux]
interp              =       ['linear']
applycal()

#check with plotxy
default ('plotxy')
vis=msfile +'a.firstflag.ms'
xaxis               =     'chan'
datacolumn     =     'corrected'
selectdata          = False
field               = calflux
plotxy ()

if scriptmode:
    user_check=raw_input('Return to continue script\n')
#=================================================================================
print "Produce an uv-fits-file with the data after the calibration with one channel"

default ('exportuvfits')

vis          =        msfile +'a.firstflag.ms'
fitsfile= calflux+'after1chancalib.uv.fits'
field               =       calflux

exportuvfits()
default ('exportuvfits')

vis          =        msfile +'a.firstflag.ms'
fitsfile= calphase+'after1chancalib.uv.fits'
field               =       calphase

exportuvfits()
default ('exportuvfits')

vis          =        msfile +'a.firstflag.ms'
fitsfile= caltarget+'after1chancalib.uv.fits'
field               =       caltarget

exportuvfits()

#=========================================================================================
print "Now we are doing a first calibration run for the flux calibrator"

print "Bandpass calibration"

#Now do bandpass calibration
#Setjy
default ('setjy')
vis=msfile +'a.firstflag.ms'
field = calflux
fluxdensity = calfluxden
modimage= calfluxmodimage
setjy()

#bandpass
default ('bandpass')

vis=msfile +'a.firstflag.ms'
```

```
field = calflux
caltable            =        msfile+ '.a.flux.RFI.bcal'
refant              = calrefant
solnorm=True

bandpass()

#check with plotcal
default ('plotcal')
caltable            =        msfile+ '.a.flux.RFI.bcal'
xaxis               =         'antenna'
yaxis='amp'
plotcal()

# Pause script if you are running in scriptmode
if scriptmode:
    user_check=raw_input('Return to continue script\n')

print "Gains calibration"

default ('gaincal')
vis=msfile +'a.firstflag.ms'
field = calflux
caltable            =        msfile+ '.a.flux.RFI.gcal'
solint              =      '30.0s'
combine             =         ''
refant              = calrefant
gaintable           =       [msfile+ '.a.flux.RFI.bcal']
gainfield           =       [calflux]
interp              =       ['linear']
gaincal()

#check with plotcal
default ('plotcal')
caltable            =        msfile+ '.a.flux.RFI.gcal'
xaxis               =         'antenna'
yaxis='amp'
plotcal()

# Pause script if you are running in scriptmode
if scriptmode:
    user_check=raw_input('Return to continue script\n')

print "apply calibration"

default ('applycal')
vis=msfile +'a.firstflag.ms'
selectdata          = False
gaintable           =       [msfile+ '.a.flux.RFI.gcal',msfile+ '.a.flux.RFI.bcal']
gainfield           =       ['*',calflux]
interp              =       ['linear']
applycal()

#check with plotxy
default ('plotxy')
vis=msfile +'a.firstflag.ms'
xaxis               =     'chan'
datacolumn     =     'corrected'
selectdata          = False
field               = calflux
plotxy()
#==================================================================================
print "Produce an uv-fits-file with the data after the calibration with the unflagged Fluxcalibrator"

default ('exportuvfits')

vis          =         msfile +'a.firstflag.ms'
fitsfile= calflux+'.afterfluxRFI.uv.fits'
field               =        calflux

exportuvfits()
default ('exportuvfits')
```

```
vis           =        msfile +'a.firstflag.ms'
fitsfile= calphase+'.afterfluxRFI.uv.fits'
field               =       calphase

exportuvfits()
default ('exportuvfits')

vis           =        msfile +'a.firstflag.ms'
fitsfile= caltarget+'.afterfluxRFI.uv.fits'
field               =       caltarget

exportuvfits()

# Pause script if you are running in scriptmode
if scriptmode:
    user_check=raw_input('Return to continue script\n')

#======================================================================
print "Flagging bad data using automated flaggers"
default ('split')
vis=msfile+'a.firstflag.ms'
outputvis           =       msfile+calflux+'a.secondflagging.ms'
field               = calflux
datacolumn          = 'all'
split ()
default ('split')
vis=msfile+'a.firstflag.ms'
outputvis           =       msfile+calphase+'a.secondflagging.ms'
field               = calphase
datacolumn          = 'all'
split ()
default ('split')
vis=msfile+'a.firstflag.ms'
outputvis           =       msfile+caltarget+'a.secondflagging.ms'
field               = caltarget
datacolumn          = 'all'
split ()


print "Use the AO Flagger to do the rough flagging on the Flux calibrator"
print "If that is finished, press return to continue"

# Pause script if you are running in scriptmode
if scriptmode:
    user_check=raw_input('Return to continue script\n')

print "check calibration"
#check with plotxy
default ('plotxy')
vis=msfile +calflux+'a.secondflagging.ms'
xaxis               =     'chan'
datacolumn     =     'corrected'
selectdata          = False
field               = calflux
plotxy()
# Pause script if you are running in scriptmode
if scriptmode:
    user_check=raw_input('Return to continue script\n')
print "Flagging in rfi mode"

default ('flagdata')
vis=msfile+calflux+'a.secondflagging.ms'
mode                = 'rfi'

field               = calflux
selectdata          = False

flagdata ()

print "combine files for calibration"
default ('concat')
```

```
vis           =    [msfile+calflux+'a.secondflagging.ms', msfile+caltarget+'a.secondflagging.ms',
msfile+calphase+'a.secondflagging.ms']
concatvis           = msfile+'.a.secondflag.ms'
concat()



#===================================================================================
print "Produce an uv-fits-file with the flagged flux calibrator data"

default ('exportuvfits')

vis           =         msfile +'.a.secondflag.ms'
fitsfile= calflux+'.a.fluxflagged.uv.fits'
field               =        calflux

exportuvfits()
# Pause script if you are running in scriptmode
if scriptmode:
    user_check=raw_input('Return to continue script\n')

#==============================================================================
print "redo calibration with flagged data for the flux calibrator"

print "Bandpass calibration"

#Now do bandpass calibration

#bandpass
default ('bandpass')

vis=msfile +'.a.secondflag.ms'
field = calflux
caltable            =        msfile+ '.a.flux.bcal'
refant              = calrefant
solnorm=True

bandpass()

#check with plotcal
default ('plotcal')
caltable            =        msfile+ '.a.flux.bcal'
xaxis               =         'chan'
iteration ='antenna'
yaxis='amp'
plotcal()

# Pause script if you are running in scriptmode
if scriptmode:
    user_check=raw_input('Return to continue script\n')

print "Gains calibration"

default ('gaincal')
vis=msfile +'.a.secondflag.ms'
field = calflux
caltable            =        msfile+ '.a.flux.gcal'
solint              =      '30.0s'
combine             =         ''
refant              = calrefant
gaintable           =       [msfile+ '.a.flux.bcal']
gainfield           =       [calflux]
interp              =       ['linear']
gaincal()

#check with plotcal
default ('plotcal')
caltable            =        msfile+ '.a.flux.gcal'
xaxis               =         'antenna'
yaxis='amp'
plotcal()
```

```
# Pause script if you are running in scriptmode
if scriptmode:
    user_check=raw_input('Return to continue script\n')

print "apply calibration"

default ('applycal')
vis=msfile +'.a.secondflag.ms'
selectdata          = False
gaintable           =       [msfile+ '.a.flux.bcal',msfile+ '.a.flux.gcal']
gainfield           =       [calflux, '*']
interp              =       ['linear']
applycal()

#check with plotxy
default ('plotxy')
vis=msfile +'.a.secondflag.ms'
xaxis               =     'chan'
datacolumn     =     'corrected'
selectdata          = False
iteration ='antenna'
field               = calflux
plotxy()
#==============================================================================
print "Produce an uv-fits-file with the data after the calibration with the flagged Fluxcalibrator"

default ('exportuvfits')

vis           =         msfile +'.a.secondflag.ms'
fitsfile= calflux+'.afterflux.uv.fits'
field               =       calflux

exportuvfits()
default ('exportuvfits')

vis           =         msfile +'.a.secondflag.ms'
fitsfile= calphase+'.afterflux.uv.fits'
field               =       calphase

exportuvfits()
default ('exportuvfits')

vis           =         msfile +'.a.secondflag.ms'
fitsfile= caltarget+'.afterflux.uv.fits'
field               =       caltarget

exportuvfits()
# Pause script if you are running in scriptmode
if scriptmode:
    user_check=raw_input('Return to continue script\n')
#=====================================================================
print "First calibration run with unflagged phase calibrator"
print "Gains calibration"

default ('gaincal')
vis=msfile +'.a.secondflag.ms'
field = calfluxphase
caltable            =       msfile+caltarget+'.a.phase.RFI.gcal'
solint              =      '30.0s'
combine             =         ''
refant              = calrefant
gaintable           =       [msfile+ '.flux.bcal']
gainfield           =       [calflux]
interp              =       ['linear']
gaincal()

#check with plotcal
default ('plotcal')
caltable            =    msfile+ caltarget+'.a.phase.RFI.gcal'
xaxis               =         'antenna'
yaxis='amp'
plotcal()
```

```
# Pause script if you are running in scriptmode
if scriptmode:
    user_check=raw_input('Return to continue script\n')

print "Flux scaling"

default ('fluxscale')

vis=msfile +'.a.secondflag.ms'
caltable           =       msfile+caltarget+'.a.phase.RFI.gcal'
fluxtable          =       msfile+caltarget+'.a.phase.RFI.fcal'
reference          =      [calflux]

fluxscale ()
#check with plotcal
default ('plotcal')
caltable           =   msfile+ caltarget+'.a.phase.RFI.fcal'
xaxis              =        'antenna'
yaxis='amp'
plotcal()

# Pause script if you are running in scriptmode
if scriptmode:
    user_check=raw_input('Return to continue script\n')

print "apply calibration"

default ('applycal')
vis=msfile +'.a.secondflag.ms'
field= calphasetarget
selectdata         = False
gaintable          =      [msfile+ caltarget+'.a.phase.RFI.fcal',msfile+ '.a.flux.bcal']
gainfield          =      [calfluxphase, calflux]
interp             =      ['linear']
applycal()

#check with plotxy
default ('plotxy')
vis=msfile +'.a.secondflag.ms'
xaxis              =     'chan'
datacolumn     =     'corrected'
selectdata         = False
field              = calphase
plotxy()
#==================================================================================
print "Produce an uv-fits-file with the data after the calibration with the unflagged phase calibrator"

default ('exportuvfits')

vis          =        msfile +'.a.secondflag.ms'
fitsfile= calflux+'.afterphaseRFI.uv.fits'
field              =       calflux

exportuvfits ()
default ('exportuvfits')

vis          =        msfile +'.a.secondflag.ms'
fitsfile= calphase+'.afterphaseRFI.uv.fits'
field              =       calphase

exportuvfits ()
default ('exportuvfits')

vis          =        msfile +'.a.secondflag.ms'
fitsfile= caltarget+'.afterphaseRFI.uv.fits'
field              =       caltarget

exportuvfits ()

# Pause script if you are running in scriptmode
if scriptmode:
```

```
    user_check=raw_input('Return to continue script\n')
#=====================================================================================
print "flag bad data in phase calibrator using automated flagger"
print "Flagging bad data using automated flaggers"
default ('split')
vis=msfile+'.a.secondflag.ms'
outputvis           =       msfile+calflux+'thirdflagging.ms'
field               = calflux
datacolumn          = 'all'
split ()
default ('split')
vis=msfile+'.a.secondflag.ms'
outputvis           =       msfile+calphase+'thirdflagging.ms'
field               = calphase
datacolumn          = 'all'
split ()
default ('split')
vis=msfile+'.a.secondflag.ms'
outputvis           =       msfile+caltarget+'thirdflagging.ms'
field               = caltarget
datacolumn          = 'all'
split ()

print "Use the AO Flagger to do the rough flagging on the Phase calibrator"
print "If that is finished, press return to continue"
# Pause script if you are running in scriptmode
if scriptmode:
    user_check=raw_input('Return to continue script\n')

print "check calibration"
#check with plotxy
default ('plotxy')
vis=msfile +calphase+'thirdflagging.ms'
xaxis               =     'chan'
datacolumn     =     'corrected'
selectdata          = False
field               = calphase
plotxy()
# Pause script if you are running in scriptmode
if scriptmode:
    user_check=raw_input('Return to continue script\n')
print "Flagging in rfi mode"

default ('flagdata')
vis=msfile +calphase+'thirdflagging.ms'
mode                = 'rfi'

field               = calphase
selectdata          = False

flagdata ()

print "combine files for calibration"
default ('concat')
vis           =    [msfile+calflux+'thirdflagging.ms', msfile+caltarget+'thirdflagging.ms', msfile
+calphase+'thirdflagging.ms']
concatvis           = msfile+'.a.thirdflag.ms'
concat()


#==================================================================================
print "Produce an uv-fits-file with the flagged phase calibrator data"

default ('exportuvfits')

vis           =         msfile +'.a.thirdflag.ms'
fitsfile= calphase+'.phaseflagged.uv.fits'
field               =        calphase

exportuvfits ()
# Pause script if you are running in scriptmode
if scriptmode:
```

```
    user_check=raw_input('Return to continue script\n')
#=======================================================================
print "redo calibration with flagged phase calibrator"

print "Gains calibration"

default ('gaincal')
vis=msfile +'.a.thirdflag.ms'
field = calfluxphase
caltable            =       msfile+caltarget+'.phase.gcal'
solint              =      '30.0s'
combine             =         ''
refant              = calrefant
gaintable           =      [msfile+ '.flux.bcal']
gainfield           =      [calflux]
interp              =      ['linear']
gaincal()

#check with plotcal
default ('plotcal')
caltable            =   msfile+ caltarget+'.phase.gcal'
xaxis               =        'antenna'
yaxis='amp'
plotcal()

# Pause script if you are running in scriptmode
if scriptmode:
    user_check=raw_input('Return to continue script\n')

print "Flux scaling"

default ('fluxscale')

vis=msfile +'.a.thirdflag.ms'
caltable            =       msfile+caltarget+'.phase.gcal'
fluxtable           =       msfile+caltarget+'.phase.fcal'
reference           =      [calflux]
fluxscale ()
#check with plotcal
default ('plotcal')
caltable            =   msfile+ caltarget+'.phase.fcal'
xaxis               =        'antenna'
yaxis='amp'
plotcal()

# Pause script if you are running in scriptmode
if scriptmode:
    user_check=raw_input('Return to continue script\n')

print "apply calibration"

default ('applycal')
vis=msfile +'.a.thirdflag.ms'
field = calphasetarget
selectdata          = False
gaintable           =      [msfile+ caltarget+'.phase.fcal',msfile+ '.flux.bcal' ]
gainfield           =      [calfluxphase, calflux]
interp              =      ['linear']
applycal()

#check with plotxy
default ('plotxy')
vis=msfile +'.a.thirdflag.ms'
xaxis               =     'chan'
datacolumn     =     'corrected'
selectdata          = False
field               = calphase
plotxy()
#=================================================================================
print "Produce an uv-fits-file with the data after the calibration with theflagged phase calibrator"

default ('exportuvfits')
```

```
vis           =         msfile +'.a.thirdflag.ms'
fitsfile= calflux+'.afterphase.uv.fits'
field               =       calflux

exportuvfits ()
default ('exportuvfits')

vis           =         msfile +'.a.thirdflag.ms'
fitsfile= calphase+'.afterphase.uv.fits'
field               =       calphase

exportuvfits ()
default ('exportuvfits')

vis           =         msfile +'.a.thirdflag.ms'
fitsfile= caltarget+'.afterphase.uv.fits'
field               =       caltarget

exportuvfits ()
# Pause script if you are running in scriptmode
if scriptmode:
    user_check=raw_input('Return to continue script\n')
#==============================================================================

print "flag bad data in source using automated flagger"
default ('split')
vis=msfile+'.a.thirdflag.ms'
outputvis           =       msfile+calflux+'fourthflagging.ms'
field               = calflux
datacolumn          = 'all'
split ()
default ('split')
vis=msfile+'.a.thirdflag.ms'
outputvis           =       msfile+calphase+'fourthflagging.ms'
field               = calphase
datacolumn          = 'all'
split ()
default ('split')
vis=msfile+'.a.thirdflag.ms'
outputvis           =       msfile+caltarget+'fourthflagging.ms'
field               = caltarget
datacolumn          = 'all'
split ()

print "Use the AO Flagger to do the rough flagging on the Source"
print "If that is finished, press return to continue"
# Pause script if you are running in scriptmode
if scriptmode:
    user_check=raw_input('Return to continue script\n')

print "check calibration"
#check with plotxy
default ('plotxy')
vis=msfile +calphase+'fourthflagging.ms'
xaxis               =     'chan'
datacolumn     =     'corrected'
selectdata          = False
field               = caltarget
plotxy()

# Pause script if you are running in scriptmode
if scriptmode:
    user_check=raw_input('Return to continue script\n
print "Flagging in rfi mode"

default ('flagdata')
vis=msfile+caltarget+'fourthflagging.ms'
mode                = 'rfi'
field               = caltarget
selectdata          = False
```

```
flagdata ()

default ('concat')
vis           =    [msfile+calflux+'fourthflagging.ms', msfile+caltarget+'fourthflagging.ms', msfile
+calphase+'fourthflagging.ms']
concatvis           = msfile+'.a.fourthflag.ms'

concat()

#=================================================================================
print "Produce an uv-fits-file with the flagged source data"

default ('exportuvfits')

vis           =         msfile +'.a.fourthflag.ms'
fitsfile= caltarget+'.sourceflagged.uv.fits'
field               =        caltarget

exportuvfits ()
# Pause script if you are running in scriptmode
if scriptmode:
    user_check=raw_input('Return to continue script\n')
#===================================================================
print "average channels together"

default ('split')
vis=msfile +'.a.fourthflag.ms'
outputvis           =         avgmsfile
datacolumn          = 'all'
width               =          11
split()
#=================================================================================
print "Produce an uv-fits-file with the data after averaging"
default ('exportuvfits')

vis           =         avgmsfile
fitsfile= calflux+'.averaged.uv.fits'
field               =        calflux

exportuvfits ()
default ('exportuvfits')

vis           =         avgmsfile
fitsfile= calphase+'.averavged.uv.fits'
field               =        calphase

exportuvfits ()
default ('exportuvfits')

vis           =         avgmsfile
fitsfile= caltarget+'.averaged.uv.fits'
field               =        caltarget

exportuvfits ()
# Pause script if you are running in scriptmode
if scriptmode:
    user_check=raw_input('Return to continue script\n')
default ('split')
vis=avgmsfile
outputvis           =       avgmsfile+calflux+'fifthflagging.ms'
field               = calflux
datacolumn          = 'all'
split ()
default ('split')
vis=avgmsfile
outputvis           =       avgmsfile+calphase+'fifthflagging.ms'
field               = calphase
datacolumn          = 'all'
split ()
default ('split')
vis=avgmsfile
outputvis           =       avgmsfile+caltarget+'fifthflagging.ms'
```

```
field               = caltarget
datacolumn          = 'all'
split ()

print "Use the AO Flagger to do the rough flagging on the Phase calibrator"
print "If that is finished, press return to continue"
# Pause script if you are running in scriptmode
if scriptmode:
    user_check=raw_input('Return to continue script\n')
default ('flagdata')
vis= avgmsfile+caltarget+'fifthflagging.ms'
mode                = 'rfi'

field               = caltarget
selectdata          = False

flagdata ()
print "combine files for calibration"
default ('concat')
vis           =    [avgmsfile+calflux+'fifthflagging.ms', avgmsfile+caltarget+'fifthflagging.ms',
avgmsfile+calphase+'fifthflagging.ms']
concatvis           = avgmsfile+'flag.ms'
concat()
print "Flagging in rfi mode"


#=================================================================
print "redo calibration"
#Setjy
default ('setjy')
vis=avgmsfile +'flag.ms'
field = calflux
fluxdensity = calfluxden
modimage=calfluxmodimage
setjy()

#bandpass
default ('bandpass')

vis=avgmsfile +'flag.ms'
field = calflux
caltable            =       msfile+caltarget+ '.avg.bcal'
refant              = calrefant
solnorm=True

bandpass()

#check with plotcal
default ('plotcal')
caltable            =       msfile+caltarget+ '.avg.bcal'
xaxis               =        'chan'
iteration ='antenna'
yaxis='amp'
plotcal()

# Pause script if you are running in scriptmode
if scriptmode:
    user_check=raw_input('Return to continue script\n')

print "Gains calibration"

default ('gaincal')
vis=avgmsfile +'flag.ms'
field = calfluxphase
caltable            =       msfile+caltarget+'.avg.gcal'
solint              =     '30.0s'
combine             =        ''
refant              = calrefant
gaintable           =      [msfile+ caltarget+'.avg.bcal']
gainfield           =      [calflux]
interp              =      ['linear']
gaincal()
```

```
#check with plotcal
default ('plotcal')
caltable            =    msfile+ caltarget+'.avg.gcal'
xaxis               =         'time'
iteration='antenna'
yaxis='amp'
plotcal()

# Pause script if you are running in scriptmode
if scriptmode:
    user_check=raw_input('Return to continue script\n')

print "Flux scaling"

default ('fluxscale')

vis=avgmsfile +'flag.ms'
caltable            =        msfile+caltarget+'.avg.gcal'
fluxtable           =        msfile+caltarget+'.avg.fcal'
reference           =       [calflux]

fluxscale ()
#check with plotcal
default ('plotcal')
caltable            =    msfile+ caltarget+'.avg.fcal'
xaxis               =         'antenna'
yaxis='amp'
plotcal()

# Pause script if you are running in scriptmode
if scriptmode:
    user_check=raw_input('Return to continue script\n')

print "apply calibration"

default ('applycal')
vis=avgmsfile +'flag.ms'
field = calphasetarget
selectdata          = False
gaintable           =       [msfile+ caltarget+'.avg.fcal',msfile+ '.avg.bcal' ]
gainfield           =       [calfluxphase, calflux]
interp              =       ['linear']
applycal()

#check with plotxy
default ('plotxy')
vis=avgmsfile +'flag.ms'
xaxis               =      'chan'
datacolumn     =     'corrected'
selectdata          = False
field               = calphase
plotxy()
# Pause script if you are running in scriptmode
if scriptmode:
    user_check=raw_input('Return to continue script\n')
#=====================================================================
print "average channels together"

default ('split')
vis=msfile +'.a.fourthflag.ms'
outputvis           =         avgmsfile
datacolumn          = 'all'
width               =          11
split()
#===================================================================================
print "Produce an uv-fits-file with the data after averaging"
default ('exportuvfits')

vis           =         avgmsfile
fitsfile= calflux+'.averaged.uv.fits'
field               =        calflux
```

```
exportuvfits ()
default ('exportuvfits')

vis          =        avgmsfile
fitsfile= calphase+'.averavged.uv.fits'
field              =       calphase

exportuvfits ()
default ('exportuvfits')

vis          =        avgmsfile
fitsfile= caltarget+'.averaged.uv.fits'
field              =       caltarget

exportuvfits ()
# Pause script if you are running in scriptmode
if scriptmode:
    user_check=raw_input('Return to continue script\n')
default ('split')
vis=avgmsfile
outputvis          =      avgmsfile+calflux+'fifthflagging.ms'
field              = calflux
datacolumn         = 'all'
split ()
default ('split')
vis=avgmsfile
outputvis          =      avgmsfile+calphase+'fifthflagging.ms'
field              = calphase
datacolumn         = 'all'
split ()
default ('split')
vis=avgmsfile
outputvis          =      avgmsfile+caltarget+'fifthflagging.ms'
field              = caltarget
datacolumn         = 'all'
split ()

print "Use the AO Flagger to do the rough flagging on the Phase calibrator"
print "If that is finished, press return to continue"
# Pause script if you are running in scriptmode
if scriptmode:
    user_check=raw_input('Return to continue script\n')

print "Flagging in rfi mode"

default ('flagdata')
vis=avgmsfile+caltarget+'fifthflagging.ms'
mode               = 'rfi'

field              = caltarget
selectdata         = False

flagdata ()

print "combine files for calibration"
default ('concat')
vis          =    [avgmsfile+calflux+'fifthflagging.ms', avgmsfile+caltarget+'fifthflagging.ms',
avgmsfile+calphase+'fifthflagging.ms']
concatvis          = avgmsfile+'flag.ms'
concat()

#===============================================================================

print "redo calibration"
#Setjy
default ('setjy')
vis=avgmsfile +'flag.ms'
field = calflux
fluxdensity = calfluxden
modimage=calfluxmodimage
setjy()
```

```
#bandpass
default ('bandpass')

vis=avgmsfile +'flag.ms'
field = calflux
caltable            =       msfile+caltarget+ '.avg.bcal'
refant              = calrefant
solnorm=True

bandpass()

#check with plotcal
default ('plotcal')
caltable            =       msfile+caltarget+ '.avg.bcal'
xaxis               =        'antenna'
yaxis='amp'
plotcal()

# Pause script if you are running in scriptmode
if scriptmode:
    user_check=raw_input('Return to continue script\n')

print "Gains calibration"

default ('gaincal')
vis=avgmsfile +'flag.ms'
field = calfluxphase
caltable            =       msfile+caltarget+'.avg.gcal'
solint              =     '30.0s'
combine             =        ''
refant              = calrefant
gaintable           =      [msfile+ caltarget+'.avg.bcal']
gainfield           =      [calflux]
interp              =      ['linear']
gaincal()

#check with plotcal
default ('plotcal')
caltable            =   msfile+ caltarget+'.avg.gcal'
xaxis               =        'antenna'
yaxis='amp'
plotcal()

# Pause script if you are running in scriptmode
if scriptmode:
    user_check=raw_input('Return to continue script\n')

print "Flux scaling"

default ('fluxscale')

vis=avgmsfile +'flag.ms'
caltable            =       msfile+caltarget+'.avg.gcal'
fluxtable           =       msfile+caltarget+'.avg.fcal'
reference           =      [calflux]
fluxscale ()

#check with plotcal
default ('plotcal')
caltable            =   msfile+ caltarget+'.avg.fcal'
xaxis               =        'antenna'
yaxis='amp'
plotcal()

# Pause script if you are running in scriptmode
if scriptmode:
    user_check=raw_input('Return to continue script\n')
print "apply calibration"

default ('applycal')
vis=avgmsfile +'flag.ms'
```

```
field = calphasetarget
selectdata          = False
gaintable           =       [msfile+ caltarget+'.avg.fcal', msfile+caltarget+ '.avg.bcal']
gainfield           =       [calfluxphase, calflux]
interp              =       ['linear']
applycal()

#check with plotxy
default ('plotxy')
vis=avgmsfile +'flag.ms'
xaxis               =     'chan'
datacolumn     =     'corrected'
selectdata          = False
field               = caltarget
plotxy()

# Pause script if you are running in scriptmode
if scriptmode:
    user_check=raw_input('Return to continue script\n')
#==================================================================================
print "Produce an uv-fits-file with the data after averaged calibration "

default ('exportuvfits')

vis           =         avgmsfile +'flag.ms'
fitsfile= calflux+'.afteravg.uv.fits'
field               =        calflux

exportuvfits()
default ('exportuvfits')

vis           =         avgmsfile +'flag.ms'
fitsfile= calphase+'.afteravg.uv.fits'
field               =        calphase

exportuvfits  ()
default ('exportuvfits')

vis           =         avgmsfile +'flag.ms'
fitsfile= caltarget+'.afteravg.uv.fits'
field               =        caltarget

exportuvfits ()
# Pause script if you are running in scriptmode
if scriptmode:
    user_check=raw_input('Return to continue script\n')
#==============================================================================
print "Split calibrated data off into separate file"

default ('split')
vis=avgmsfile +'flag.ms'
outputvis           =         splitmsfile
field               =         caltarget
width               =          1
split()

print "make an image using clean and widefield"
default ('clean')
vis           =         splitmsfile
imagename           =       [calimage+'.calibrated']
gridmode            =         'widefield'
wprojplanes    =          90
niter               = 10000
threshold           =   '0.01mJy'
imsize              = [10000,10000]
cell                = ['1.0arcsec']
weighting           =  'briggs'
robust         =        0.5
clean()
```

```
viewer()

#==============================================================================
print "Produce an uv-fits-file with the calibrated data"

default ('exportuvfits')

vis           =         splitmsfile
fitsfile= calimage+'calibrated.uv.fits'

exportuvfits()

default ('exportfits')
imagename= calimage+'.calibrated.image'

fitsimage          =calimage+'calibrated.fits'
exportfits ()

print "End of script"
```

```
import time
import os

print "Low Fequency GMRT-Data Calibration - Self Calibration"
print "Version 2010-06-17 (CASA-Version 3.0.2)"
print ""
#
#======================================================================
#
# This script has some interactive commands: scriptmode = True
# if you are running it and want it to stop during interactive parts.

scriptmode = True

#======================================================================
#Set up variables
#======================================================================

# Set up the MS filename and save as new global variable

#source
caltarget = 'RXCJ2234'
#sideband
calband = caltarget+'USB.610.'
caltabrun = calband+'scal1'
#splited output file
splitmsfile = caltarget+'USB.610.scal1.ms'
#reference antenna
calrefant = '6'
#projection planes
calproj = 90
#number of iterations
#suggestion 10000*self-calibration run
caliter = 100000
#======================================================================
default ('gaincal')

vis         = splitmsfile
caltable = caltabrun+'.gcal'
selectdata          = True
uvrange        =         '>0klambda'
solint          =     '60.0s'
refant          = calrefant
solnorm         =         False
calmode         =             'p'

gaincal ()
#======================================================================
#check with plotcal
default ('plotcal')
caltable            =     caltabrun+'.gcal'
xaxis               =         'time'
yaxis='amp'
plotcal()
# Pause script if you are running in scriptmode
if scriptmode:
    user_check=raw_input('Return to continue script\n')
#======================================================================
#check with plotxy
default ('plotxy')
vis=splitmsfile
xaxis               =     'uvdist'
datacolumn     =     'model'
selectdata          = False
plotxy()
# Pause script if you are running in scriptmode
if scriptmode:
    user_check=raw_input('Return to continue script\n')
#======================================================================
default ('applycal')
vis         =splitmsfile
```

```
selectdata          =        False
gaintable           =       [caltabrun+'.gcal']
gainfield           =          ['']
interp    =  ['linear']
spwmap    =    []

applycal ()

#======================================================================
#check with plotxy
default ('plotxy')
vis=splitmsfile
xaxis               =     'uvdist'
datacolumn     =     'corrected'
selectdata          = False
plotxy()
# Pause script if you are running in scriptmode
if scriptmode:
    user_check=raw_input('Return to continue script\n')
#======================================================================
default ('clean')
vis  = splitmsfile
imagename           =         [caltabrun]
selectdata          =        False
gridmode            = 'widefield'
wprojplanes   =   calproj
interactive         =       True
gain=0.001
niter               = caliter
threshold           =   '0.0001mJy'
imsize              = [10000,10000]
cell                = ['1 arcsec']
weighting           =   'briggs'
robust        =            0.5

clean ()

#======================================================================

default ('viewer')
infile              =         caltabrun+'.image'

viewer ()

#======================================================================

print "export fitsfile"
default ('exportfits')
imagename           = caltabrun+'.image'
fitsimage           = caltabrun+'.image.fits'
exportfits ()
#======================================================================
print "export uvfitsfile"

default ('exportuvfits')

vis                 =splitmsfile
fitsfile            = caltabrun+'.uv.fits'

exportuvfits ()
#======================================================================
#check with plotxy
default ('plotxy')
vis=splitmsfile
xaxis               =     'uvdist'
datacolumn     =     'corrected'
selectdata          = False
plotxy()
# Pause script if you are running in scriptmode
if scriptmode:
    user_check=raw_input('Return to continue script\n')
#======================================================================
```

```
print "end of script"
```

The great tragedy of Science - the slaying of a beautiful hypothesis by an ugly fact.

THOMAS H. HUXLEY (1825 - 1895)

optical REXCESS table

RA	DEC	cluster member
00:03:019	02:11:058	✔
00:03:028	02:07:001	✔
00:03:030	01:57:010	✔
00:03:030	02:06:003	✔
00:03:034	02:08:015	✔
00:03:037	02:03:042	✔
00:03:047	02:00:054	✔
00:03:056	02:13:033	✔
00:04:005	02:07:012	✔
00:04:011	02:09:025	✔
00:04:021	02:04:034	✔
00:04:024	02:02:026	✔
00:04:035	02:14:013	✔
03:49.7	+02:03:59	✔
03:50.6	+02:03:48	✔
03:49.6	+02:04:00	✔

Table B.1: Positions of optical galaxies associated with the cluster RXCJ0003.8+0203

RA	DEC	cluster member
00:06:06.5	-34:43	✔
00:06:05.0	-34:44:49	✔
00:06:06.36	-34:43:16.5	✔
00:06:04.89	-34:44:49.2	✔
00:05:59.7	-34:43:17	✔
00:06:07.2	-34:44:15	✔
00:06:07.221	-34:44:15.12	✔
00:05:59.7	-34:43:17	✔
00:05:59.756	-34:43:17.17	✔
00:06:03.0	-34:43:27	✔
00:06:11.86	-34:43:02.7	✔
00:05:59.7	-34:43:18	✔
00:06:06.5	-34:43:16	✔
00:05:56.14	-34:43:27.0	✔
00:06:04.9	-34:44:49	✔
00:06:09.52	-34:43:56.8	✔
00:06:12.0	-34:43:03	✔
00:06:09.8	-34:43:56	✔
00:06:09.8	-34:43:56	✔
00:05:56.1	-34:43	✔
00:06:02.4	-34:42:30	✗
00:06:02.17	-34:42:31.0	✗

Table B.2: Positions of optical galaxies associated with the cluster RXCJ0006.0−3443

RA	DEC	cluster member
00:20:43.3	-25:42:25	✔
00:20:37.960	-25:40:57.44	✔
00:20:42.843	-25:41:32.41	✔
00:20:43.1	-25:42:29	✔
00:20:42.8	-25:42:37	✔
00:20:34.8	-25:41:51	✔
00:20:50.68	-25:42:59.1	✔
00:20:40.59	-25:41:54.7	✔
00:20:50.7	-25:42:59	✔
00:20:40.6	-25:41:55	✔
00:20:38.0	-25:40:58	✗
00:20:42.8	-25:41:32	✗
00:20:43.142	-25:42:28.40	✗
00:20:43.1	-25:42:31	✗

Table B.3: Positions of optical galaxies associated with the cluster RXCJ0020.7−2542

RA	DEC	cluster member
00:49:29.2	-29:31:45	✔
00:49:19.8	-29:33:05	✔
00:49:17.4	-29:30:27	✔
00:49:29.3	-29:32:18	✔
00:49:22.2	-29:29:54	✔
00:49:24.7	-29:31:37	✔
00:49:29.20	-29:31:44.7	✔
00:49:19.72	-29:33:03.5	✔
00:49:23.34	-29:31:13.5	✔
00:49:17.307	-29:30:26.05	✔
00:49:29.34	-29:32:18.5	✔
00:49:22.17	-29:29:54.0	✔
00:49:22.8	-29:31:08	✔
00:49:24.665	-29:31:36.98	✔
00:49:25.059	-29:31:23.86	✔
00:49:22.825	-29:31:07.00	✔
00:49:24.0	-29:31:28	✔
00:49:23.2	-29:31:33	✔
00:49:16.7	-29:32:33	✔
00:49:23.9	-29:31:13	✔
00:49:24.6	-29:31:3	✔
00:49:26.0	-29:30:04	✔
00:49:26.2	-29:30:04	✔
00:49:21.82	-29:31:35.6	✔
00:49:26.0	-29:30:04	✔
00:49:26.2	-29:30:04	✔
00:49:31.10	-29:30:56.7	✔
00:49:23.3	-29:31:14	✔
00:49:31.2	-29:30:56	✔
00:49:29.3	-29:31:44	✔
00:49:25.1	-29:31:23	✔
00:49:19.8	-29:33:03	✔
00:49:17.4	-29:30:25	✔
00:49:21.8	-29:31:36	✗
00:49:28.7	-29:32	✗

Table B.4: Positions of optical galaxies associated with the cluster RXCJ0049.4−2931

RA	DEC	cluster member
02:11:26.5	-40:17:59	✔
02:11:26.591	-40:17:59.15	✔
02:11:25.5	-40:17:12	✔
02:11:27.0	-40:16.9	✔
02:11:25.5	-40:18:00	✔
02:11:20.6	-40:17:12	✔
02:11:24.0	-40:17:06	✔
02:11:26.8	-40:17:37	✔
02:11:20.63	-40:17:12.2	✔
02:11:21.65	-40:15:45.2	✔
02:11:24.02	-40:17:06.3	✔
02:11:25.30	-40:18:02.4	✔
02:11:24.8	-40:17:26	✔
02:11:21.6	-40:15:45	✔

Table B.5: Positions of optical galaxies associated with the cluster RXCJ0211.4−4017

RA	DEC	cluster member
02:25:11.5	-29:28:41	✔
02:25:11.7	-29:28:04	✔
02:25:11.678	-29:28:04.49	✔
02:25:10.5	-29:28:26	✔
02:25:08.6	-29:28:34	✔
02:25:02.1	-29:28:38	✔
02:25:11.525	-29:28:40.49	✔
02:25:02.09	-29:28:37.9	✔
02:25:08.7	-29:28:38	✔

Table B.6: Positions of optical galaxies associated with the cluster RXCJ0225.1−29283

RA	DEC	cluster member
03:45:046	-41:12:016	✔
03:45:052	-41:10:042	✔
03:46:024	-41:10:002	✔
03:45:045	-41:10:042	✔
03:45:046	-41:12:016	✔
03:45:052	-41:10:042	✔
45:45.7	-41:43:001	✔
45:45.0	-41:10:42	✔
45:46.3	-41:43:001	✔
45:46.4	-41:12:14.94	✔

Table B.7: Positions of optical galaxies associated with the cluster RXCJ0345.7−4112

RA	DEC	cluster member
05:47:31.4	-31:52:01	✔
05:47:31.39	-31:52:00.8	✔
05:47:39.4	-31:51:32	✔
05:47:39.41	-31:51:31.7	✔
05:47:39.8	-31:52:56.0	✔
05:47:39.86	-31:52:55.9	✔
05:47:40.1	-31:50:56	✔
05:47:40.10	-31:50:56.0	✔
05:47:40.6	-31:52:11	✔
05:47:40.66	-31:52:10.9	✔
05:47:40.8	-31:52:25	✔
05:47:40.80	-31:52:24.6	✔
05:47:38.2	-31:52:31	✔
05:47:37.42	-31:53:08.2	✔
05:47:38.35	-31:51:39.2	✔
05:47:39.50	-31:50:39.1	✔
05:47:37.4	-31:53:08	✔
05:47:38.3	-31:51:39	✔
05:47:34.0	-31:53.0	✔
05:47:37.7	-31:52:24	✗
05:47:33.6	-31:53:24	✗
05:47:33.60	-31:53:24.0	✗
05:47:35.4	-31:53:08	✗
05:47:35.42	-31:53:07.8	✗
05:47:39.5	-31:50:39	✗
05:47:37.734	-31:52:23.74	✗

Table B.8: Positions of optical galaxies associated with the cluster RXCJ0547.6−3152

RA	DEC	cluster member
06:05:49.540	-35:18:23.80	✔
06:05:54.020	-35:18:07.90	✔
06:05:54.018	-35:18:08.13	✔
06:05:52.8	-35:18:02	✔
06:05:52.0	-35:18.4	✔
06:05:54.0	-35:18:08	✔

Table B.9: Positions of optical galaxies associated with the cluster RXCJ0605.8−3518

RA	DEC	cluster member
08:21:49.32	+01:13:58.4	✔
08:21:50.45	+01:11:48.8	✔
08:21:55.25	+01:13:30.7	✔
08:21:50.6	+01:11:4	✔
08:21:50.6	+01:11:49.55	✔
08:21:55.2	+01:13:31	✔
08:21:51.7	+01:12:42	✔
08:21:46.0	+01:13:24	✔
08:21:50.4	+01:11:49	✔
08:21:50.6	+01:11:49	✔
08:21:54.02	+01:13:37	✗
08:21:54.0	+01:13:37	✗

Table B.10: Positions of optical galaxies associated with the cluster RXCJ0821.8+0112

RA	DEC	cluster member
09:56:26.4	-10:04:12	✔
09:56:27.0	-10:03:26.0	✔
09:56:20.3	-10:05:24	✗
09:56:21.8	-10:04:36	✗
09:56:20.3	-10:05:24	✗
09:56:21.7	-10:03:06	✗
09:56:20.1	-10:03:49	✗
09:56:19.8	-10:03:27	✗
09:56:19.8	-10:03:27	✗
09:56:20.1	-10:03:48	✗
09:56:20.3	-10:05:24	✗
09:56:21.6	-10:03:05	✗
09:56:26.7	-10:03:26	✗
09:56:26.5	-10:03:22	✗
09:56:21.8	-10:04:35	✗
09:56:26.8	-10:05:09	✗

Table B.11: Positions of optical galaxies associated with the cluster RXCJ0956.4−1004

RA	DEC	cluster member
09:58:22.010	-11:03:50.80	✔
09:58:20.760	-11:02:36.20	✔
09:58:22.200	-11:03:35.00	✔
09:58:21.840	-11:03:47.50	✔
09:58:22.0	-11:03:51	✔
09:58:20.76	-11:02:36.2	✔
09:58:20.90	-11:02:16.8	✔
09:58:24.2	-11:03:50	✔
09:58:24.24	-11:03:50.4	✔
09:58:27.82	-11:03:55.8	✔
09:58:27.8	-11:03:56	✔
09:58:20.7	-11:02:36	✔
09:58:22.013	-11:03:50.09	✔
09:58:22.2	-11:03:35	✔
09:58:21.84	-11:03:47.5	✔
09:58:20.9	-11:02:17	✗

Table B.12: Positions of optical galaxies associated with the cluster RXCJ0958.3−1103

RA	DEC	cluster member
10:44:30.3	-07:05:21	✔
10:44:32.8	-07:04:08	✔
10:44:32.878	-07:04:07.42	✔
10:44:34.1	-07:03:27	✔
10:44:33.0	-07:04:22	✔
10:44:31.7	-07:05:43	✔
10:44:30.9	-07:03:47	✔
10:44:37.1	-07:04:47	✔
10:44:34.6	-07:04:23	✔
10:44:34.65	-07:04:23.2	✔
10:44:30.91	-07:03:47.1	✔
10:44:31.73	-07:05:42.5	✔
10:44:31.73	-07:05:42.5	✔
10:44:34.08	-07:03:27.1	✔
10:44:37.5	-07:04:33	✔
10:44:37.56	-07:04:33.0	✔
10:44:37.5	-07:05:16	✗
10:44:37.49	-07:05:15.9	✗

Table B.13: Positions of optical galaxies associated with the cluster RXCJ1044.5−0704

RA	DEC	cluster member
11:41:24.300	-12:16:20.00	✔
11:41:24.203	-12:16:38.66	✔
11:41:24.200	-12:16:38.60	✔
11:41:24.000	-12:16:00.00	✔
11:41:21.680	-12:16:24.66	✔
11:41:25.569	-12:16:30.66	✔
11:41:23.9	-12:16:25	✔
11:41:23.85	-12:16:24.5	✔
11:41:24.2	-12:16:39	✔
11:41:24.2	-12:16:39	✔
11:41:24.0	-12:16:18	✔
11:41:17.108	-12:17:07.87	✗

Table B.14: Positions of optical galaxies associated with the cluster RXCJ1141.4−1216

RA	DEC	cluster member
12:36:40.000	-33:54:05.00	✔
12:36:41.250	-33:55:32.11	✔
12:36:44.700	-33:54:10.00	✔
12:36:41.200	-33:55:32.00	✔
12:36:40.0	-33:54.5	✔
12:36:41.250	-33:55:32.11	✔
12:36:44.7	-33:54:10	✔
12:36:41.2	-33:55:32	✔

Table B.15: Positions of optical galaxies associated with the cluster RXCJ1236.7−3354

RA	DEC	cluster member
13:08:11.829	-03:53:43.59	✔
13:02:52.600	-02:31:04.00	✔
13:02:52.700	-02:31:07.00	✔
13:02:52.500	-02:31:04.00	✔
13:02:52.560	-02:31:03.80	✔
13:02:56.520	-02:29:31.10	✔
13:02:50.210	-02:28:54.90	✔
13:02:46.490	-02:29:03.30	✔
13:02:52.600	-02:30:59.00	✔
13:02:52.540	-02:30:59.07	✔
13:02:56.500	-02:29:30.00	✔
13:02:50.700	-02:30:22.00	✔
13:02:53.900	-02:31:37.00	✔
13:02:52.550	-02:31:04.00	✔
13:02:46.500	-02:29:03.00	✔
13:02:49.100	-02:30:40.00	✔
13:02:50.200	-02:28:54.00	✔
13:02:52.900	-02:31:14.00	✔
13:02:52.884	-02:31:13.97	✔
13:02:52.600	-02:30:59.00	✔
13:02:49.100	-02:30:39.52	✔
13:02:53.000	-02:31:06.00	✗
13:02:49.457	-02:30:51.85	✗
13:02:52.500	-02:31:04.00	✗
13:02:49.400	-02:30:52.00	✗

Table B.16: Positions of optical galaxies associated with the cluster RXCJ1302.8−0230

RA	DEC	cluster member
13:11:24.0	-01:19:07	✔
13:11:24.00	-01:19:07.6	✔
13:11:24.2	-01:21:07	✔
13:11:24.24	-01:21:07.7	✔
13:11:24.25	-01:21:14.8	✔
13:11:24.3	-01:21:14	✔
13:11:24.4	-01:21:11	✔
13:11:24.441	-01:21:11.06	✔
13:11:24.8	-01:20:40.0	✔
13:11:24.8	-01:20:39	✔
13:11:25.1	-01:19:31	✔
13:11:25.110	-01:19:31.07	✔
13:11:25.3	-01:20:37	✔

Table B.17: Positions of optical galaxies associated with the cluster RXCJ1311.4−0120

RA	DEC	cluster member
15:16:13.2	+00:05:09	✔
15:16:13.20	+00:05:09.6	✔
15:16:14.4	+00:05:08	✔
15:16:14.45	+00:05:08.9	✔
15:16:15.1	+00:04:30	✔
15:16:15.6	+00:05:29	✔
15:16:15.65	+00:05:29.4	✔
15:16:17.9	+00:05:21	✔
15:16:17.93	+00:05:20.5	✔
15:16:17.948	+00:05:20.33	✔
15:16:18.05	+00:05:23.3	✔
15:16:19.0	+00:05:07	✔
15:16:19.01	+00:05:07.1	✔
15:16:21.36	+00:05:39.3	✔
15:16:21.6	+00:05:59	✔
15:16:23.481	+00:06:09.34	✔
15:16:23.5	+00:06:09	✔
15:16:23.5	+00:06:09	✔
15:16:23.522	+00:06:09.00	✔
15:16:24.0	+00:06:03	✔
15:16:24.000	+00:06:03.12	✔

Table B.18: Positions of optical galaxies associated with the cluster RXCJ1516.3+0005

RA	DEC	cluster member
15:16:34.0	-00:56:56	✔
15:16:34.699	-00:57:13.50	✔
15:16:37.2	-00:58:39	✔
15:16:30.319	-00:56:25.66	✗
15:16:31.34	-00:55:41.5	✗
15:16:30.3	-00:56:26	✗
15:16:31.3	-00:55:41	✗
15:16:33.119	-00:57:01.99	✗

Table B.19: Positions of optical galaxies associated with the cluster RXCJ1516.5−0056

RA	DEC	cluster member
20:14:49.7	-24:30:30	✔
20:14:49.7	-24:30:30	✔
20:14:51.7	-24:30:23	✔
20:14:51.716	-24:30:22.99	✔
20:14:53.3	-24:30:12	✔
20:14:53.31	-24:30:11.9	✔
20:14:50.0	-24:30:35	✔
20:14:54.34	-24:30:00.0	✔
20:14:54.77	-24:30:30.6	✔
20:14:46.27	-24:30:28.1	✗
20:14:46.3	-24:30:28	✗
20:14:48.9	-24:29:22	✗
20:14:48.93	-24:29:22.2	✗
20:14:49.98	-24:30:35.0	✗
20:14:51.4	-24:30:28	✗
20:14:51.45	-24:30:28.1	✗
20:14:52.2	-24:30:18	✗
20:14:52.22	-24:30:18.4	✗
20:14:53.9	-24:29:22	✗
20:14:53.93	-24:29:22.2	✗
20:14:54.3	-24:30:00	✗
20:14:54.8	-24:30:31	✗
20:14:55.27	-24:29:53.9	✗
20:14:55.3	-24:29:54	✗
20:14:56.2	-24:29:23	✗
20:14:56.26	-24:29:22.6	✗

Table B.20: Positions of optical galaxies associated with the cluster RXCJ2014.8−2430

RA	DEC	cluster member
20:22:58.3	-20:56:49	✔
20:22:59.114	-20:56:56.18	✔
20:22:59.3	-20:56:56	✔
20:23:00	-20:56.3	✔
20:23:01.5	-20:57:16	✔
20:23:01.56	-20:57:15.5	✔
20:23:01.6	-20:56:55	✔
20:23:02.97	-20:57:34.6	✗
20:23:03.0	-20:57:35	✗
20:23:04.2	-20:57:55	✗
20:23:04.23	-20:57:54.7	✗

Table B.21: Positions of optical galaxies associated with the cluster RXCJ2023.0−2056

RA	DEC	cluster member
20:48:11.3	-17:51:55	✔
20:48:11.5	-17:49:04	✔
20:48:11.623	-17:49:03.41	✔
20:48:11.345	-17:51:54.41	✔
20:48:10.6	-17:50:38	✔
20:48:13.9	-17:48:53	✔

Table B.22: Positions of optical galaxies associated with the cluster RXCJ2048.1−1750

RA	DEC	cluster member
21:52:14.2	-19:42:20	✔
21:52:06.82	-19:42:43.6	✔
21:52:08.04	-19:41:26.7	✔
21:52:10.05	-19:42:12.8	✔
21:52:11.56	-19:43:42.2	✔
21:52:13.14	-19:42:43.9	✔
21:52:13.53	-19:40:56.2	✔
21:52:06.8	-19:42:44	✔
21:52:08.0	-19:41:27	✔
21:52:11.5	-19:43:42	✔
21:52:13.5	-19:40:56	✔
21:52:10.0	-19:42:13	✔
21:52:09.6	-19:43:25	✔
21:52:09.573	-19:43:23.52	✔
21:52:13.1	-19:42:44	✔
21:52:14.2	-19:42:20	✔
21:49:07.9	-30:41:39	✗
21:49:07.90	-30:41:38.8	✗

Table B.23: Positions of optical galaxies associated with the cluster RXCJ2149.1−3041

RA	DEC	cluster member
21:52:14.2	-19:42:20	✔
21:52:06.82	-19:42:43.6	✔
21:52:08.04	-19:41:26.7	✔
21:52:10.05	-19:42:12.8	✔
21:52:11.56	-19:43:42.2	✔
21:52:13.14	-19:42:43.9	✔
21:52:13.53	-19:40:56.2	✔
21:52:06.8	-19:42:44	✔
21:52:08.0	-19:41:27	✔
21:52:11.5	-19:43:42	✔
21:52:13.5	-19:40:56	✔
21:52:10.0	-19:42:13	✔
21:52:09.6	-19:43:25	✔
21:52:09.573	-19:43:23.52	✔
21:52:13.1	-19:42:44	✔
21:52:14.2	-19:42:20	✔
21:52:14.0	-19:42:56	✗
21:52:13.97	-19:42:56.5	✗
21:52:18.45	-19:41:40.0	✗
21:52:18.4	-19:41:40	✗

Table B.24: Positions of optical galaxies associated with the cluster RXCJ2152.2−1942

RA	DEC	cluster member
21:57:21.4	-07:48:47	✔
21:57:25.7	-07:47:37	✔
21:57:27.1	-07:47:23	✔
21:57:27.6	-07:48:12	✔
21:57:29.4	-07:47:45	✔
21:57:30.6	-07:47:27	✔
21:57:33.5	-07:47:39	✔
21:57:33.442	-07:47:39.31	✔
21:57:24.3	-07:47:56	✔
21:57:29.400	-07:47:44.31	✔
21:57:21.423	-07:48:47.33	✔
21:57:27.649	-07:48:12.32	✔
21:57:25.8	-07:47:41	✔
21:57:27.64	-07:48:12.9	✔
21:57:26.8	-07:46:01	✔
21:57:24.289	-07:47:55.91	✔
21:57:19.2	-07:46:44	✔
21:57:21.9	-07:47:16	✔
21:57:25.6	-07:49:27	✔
21:57:29.4	-07:47:45	✔
21:57:19.205	-07:46:43.13	✔
21:57:21.890	-07:47:15.09	✔
21:57:25.689	-07:47:36.26	✔
21:56:47.82	-07:45:04.4	✔
21:57:12.82	-07:39:45.6	✔
21:57:16.51	-07:50:48.4	✔
21:57:43.25	-07:45:45	✔
21:58:00.60	-07:53:24.1	✔
21:57:28.6	-07:46:38	✗
21:57:28.3	-07:45:50	✗
21:57:28.622	-07:46:38.46	✗
21:57:28.356	-07:45:49.70	✗

Table B.25: Positions of optical galaxies associated with the cluster RXCJ2157.4−0747

RA	DEC	cluster member
22:17:36.0	-35:43:43	✔
22:17:36.04	-35:43:43.0	✔
22:17:36.3	-35:42:58	✔
22:17:36.328	-35:42:58.3	✔
22:17:36.738	-35:42:47.35	✔
22:17:36.8	-35:43:07	✔
22:17:37.0	-35:42:56	✔
22:17:38.3	-35:43:07	✔
22:17:38.30	-35:43:06.6	✔
22:17:42.7	-35:45:05	✔
22:17:42.71	-35:45:05.5	✔
22:17:43.1	-35:43:05	✔
22:17:43.228	-35:43:05.36	✔
22:17:43.3	-35:43:34	✔
22:17:45.4	-35:42:54	✔
22:17:45.4	-35:42:52	✔
22:17:45.40	-35:42:54.2	✔
22:17:45.72	-35:43:31.4	✔
22:17:45.8	-35:43:30	✔
22:17:46.20	-35:44:19.2	✔
22:17:46.5	-35:43:39	✔
22:17:46.677	-35:43:39.35	✔
22:17:48.1	-35:43:48	✔
22:17:48.237	-35:43:49.34	✔
22:17:48.98	-35:44:15.3	✔
22:17:49.0	-35:44:15	✔
22:17:50.3	-35:42:56	✔
22:17:50.36	-35:42:56.3	✔
22:17:52.46	-35:42:55.2	✔
22:17:49	-35:43:24	✗

Table B.26: Positions of optical galaxies associated with the cluster RXCJ2217.7−3543

RA	DEC	cluster member
22:18:39.4	-38:54:02	✔
22:18:40.2	-38:53:51	✔
22:18:43.572	-38:55:08.85	✔
22:18:45.2	-38:53:57	✔
22:18:45.2	-38:53:57	✔
22:18:37.8	-38:53:42	✔
22:18:34.7	-38:53:31	✔
22:18:34.68	-38:53:30.9	✔
22:18:37.7	-38:53:43	✔
22:18:43.5	-38:55:09	✔
22:18:45.7	-38:53:30	✔
22:18:45.87	-38:53:28.8	✔

Table B.27: Positions of optical galaxies associated with the cluster RXCJ2218.6−3853

RA	DEC	cluster member
22:34:26.4	-37:44:4	✔
22:34:23.3	-37:43:23	✔
2:34:23.33	-37:43:22.7	✔
22:34:25.0	-37:43:38	✔
22:34:24.2	-37:42:58	✔
22:34:24.302	-37:42:57.47	✔
22:34:24.5	-37:43:29	✔
22:34:26.4	-37:44:34	✔
22:34:29.4	-37:44:28	✔
22:34:29.275	-37:44:28.50	✔
22:34:32.5	-37:43:52	✔
22:34:32.556	-37:43:51.50	✔
22:34:23.39	-37:43:32.9	✔
22:34:24.639	-37:43:30.47	✔
22:34:26.404	-37:44:35.49	✔
2:34:31.0	-37:44:06	✔
22:34:28.5	-37:44:23	✔
22:34:27.4	-37:44:46	✔
22:34:23.0	-37:43:29	✔
22:34:23.27	-37:43:30.7	✔
22:34:23.4	-37:43:31	✔
22:34:27.3	-37:43:11	✔
22:34:30.9	-37:42:46	✔
22:34:31.3	-37:43:53	✔
22:34:31.3	-37:44:42	✔
22:34:34.9	-37:43:33	✔
22:34:35.3	-37:43:47	✔
22:34:40.3	-37:44:22	✔
22:34:35.4	-37:44:31	✔
22:34:35.6	-37:44:52	✔
22:34:34.92	-37:43:32.8	✔
22:34:25.04	-37:43:37.9	✔
22:34:35.35	-37:43:46.9	✔
22:34:31.29	-37:43:52.5	✔
22:34:35.46	-37:44:31.5	✔
22:34:31.30	-37:44:42.0	✔
22:34:26.37	-37:44:39.8	✔
22:34:27.43	-37:44:45.7	✔
22:34:25.1	-37:43:30	✔
22:34:30.3	-37:43:52	✔
22:34:27.27	-37:43:10.7	✔
22:34:30.30	-37:43:51.4	✔
22:34:35.63	-37:44:51.6	✔
22:34:35.63	-37:44:51.6	✔
22:34:30.90	-37:42:46.2	✔
22:34:23.3	-37:43:32	✗

Table B.28: Positions of optical galaxies associated with the cluster RXCJ2234.5−3744

No amount of experimentation can ever prove me right; a single experiment can prove me wrong.

ALBERT EINSTEIN (1879 - 1955)

Source Catalogue 610 MHz maps

Table C.1: Positions of radio sources within 4MPc radius of the pointing centre of cluster RXCJ0006.0−3443

Source ID	RA	δ RA	DEC	δ DEC	total flux	δ total flux	Peak flux	δ Peak flux
1	00:08:040	0.000139	-34:47:006	0.000147	0.000463	0.000129	0.000492	0.000073
3	00:08:020	0.000189	-34:27:008	0.000467	0.000615	0.000166	0.000424	0.000105
3	00:08:020	0.000471	-34:26:055	0.000356	0.000542	0.000165	0.000376	0.000103
3	00:08:020	0.000208	-34:27:006	0.000196	0.000193	0.000179	0.000325	0.000086
4	00:08:019	0.000186	-34:30:045	0.000275	0.000665	0.000204	0.000579	0.000122
4	00:08:019	0.000249	-34:30:033	0.000271	0.000459	0.000207	0.00046	0.000119
5	00:08:017	0.000055	-34:23:015	0.000071	0.004877	0.000535	0.004918	0.000307
6	00:08:012	0.000179	-34:15:037	0.000308	0.000746	0.000206	0.0006	0.000126
7	00:08:006	0.00009	-34:58:028	0.000163	0.002801	0.000515	0.002598	0.0003
8	00:07:055	0.000161	-35:08:027	0.000172	0.006023	0.00063	0.003419	0.000431
9	00:07:052	0.000176	-35:08:002	0.000205	0.003747	0.000624	0.002576	0.000404
11	00:07:039	0.000181	-34:32:036	0.000153	0.000508	0.000183	0.000573	0.000101
12	00:07:036	0.000132	-34:58:001	0.000217	0.001269	0.000359	0.001237	0.000207
13	00:07:032	0.00018	-34:39:044	0.000495	0.002525	0.00032	0.001156	0.000226
14	00:07:030	0.000116	-34:40:006	0.000199	0.003007	0.000603	0.002573	0.000362
15	00:07:027	0.000138	-34:27:038	0.000346	0.00194	0.000421	0.001408	0.000262
16	00:07:027	0.000045	-34:27:014	0.000074	0.007651	0.000591	0.006623	0.000354
17	00:07:027	0.000141	-34:47:005	0.000172	0.0014	0.000421	0.001482	0.000238
18	00:07:026	0.000079	-34:26:046	0.000199	0.002948	0.000392	0.002234	0.00024
20	00:07:021	0.000474	-35:02:037	0.000374	0.003545	0.000195	0.000803	0.000162
21	00:07:018	0.000574	-34:36:032	0.000237	0.001338	0.000156	0.000511	0.000116
23	00:07:001	0.000679	-34:28:022	0.000698	0.013043	0.000133	0.000772	0.000126
24	00:06:053	0.000197	-34:41:003	0.0002	0.005036	0.000653	0.002939	0.000443
25	00:06:053	0.000082	-34:40:030	0.000207	0.003515	0.0005	0.002696	0.000305
26	00:06:051	0.000158	-35:03:016	0.000251	0.003167	0.000405	0.001828	0.000274
27	00:06:049	0.000111	-34:36:053	0.000193	0.003483	0.000782	0.003237	0.000456
28	00:06:048	0.000029	-35:10:004	0.000053	0.021394	0.001197	0.019086	0.000706
29	00:06:045	0.000023	-34:45:028	0.000013	0.046322	0.001442	0.038789	0.000641
30	00:06:042	0.000139	-34:48:012	0.000182	0.001571	0.000574	0.001825	0.000313
31	00:06:041	0.000012	-34:50:026	0.00002	0.111174	0.002696	0.105996	0.001558
32	00:06:040	0.000092	-34:29:045	0.000143	0.003121	0.00042	0.002562	0.000255
33	00:06:033	0.000097	-34:46:034	0.000186	0.005265	0.000852	0.004371	0.000511
34	00:06:030	0.000049	-34:59:055	0.0001	0.003516	0.0005	0.003798	0.000274
35	00:06:029	0.00016	-35:03:025	0.000303	0.0044	0.000941	0.003247	0.000586
37	00:06:027	0.000041	-35:09:037	0.000071	0.005913	0.000477	0.005447	0.000279
39	00:06:018	0.000055	-34:41:035	0.000144	0.003193	0.000478	0.003098	0.000268
40	00:06:015	0.00009	-34:47:030	0.000106	0.065003	0.004792	0.031448	0.002025
41	00:06:014	0.000063	-34:52:031	0.000135	0.004316	0.000645	0.004139	0.000368
42	00:06:011	0.000011	-34:32:005	0.000018	0.084599	0.001699	0.07574	0.001009
43	00:06:011	0.000095	-34:32:030	0.00018	0.007927	0.001646	0.007482	0.000953
44	00:06:002	0.000082	-34:54:045	0.000199	0.002009	0.000568	0.002253	0.000304

Continued on next page

Table C.1: Positions of radio sources within 4MPc radius of the pointing centre of cluster RXCJ0006.0−3443

Source ID	RA	δ RA	DEC	δ DEC	total flux	δ total flux	Peak flux	δ Peak flux
45	00:05:058	0.000141	-35:08:009	0.000277	0.000797	0.000279	0.000835	0.000152
46	00:05:057	0.000135	-35:10:025	0.000279	0.002447	0.000466	0.001774	0.000292
47	00:05:055	0.000134	-34:34:026	0.000184	0.002335	0.000606	0.002264	0.000352
48	00:05:054	0.000022	-34:44:033	0.000035	0.059644	0.001709	0.046102	0.001051
49	00:05:040	0.000491	-34:52:051	0.000575	0.006963	0.000183	0.000885	0.000164
50	00:05:038	0.000226	-34:48:051	0.000226	0.006404	0.000701	0.003221	0.000493
51	00:05:034	0.000484	-34:21:007	0.000775	0.016458	0.000087	0.000685	0.000083
52	00:05:028	0.00011	-34:56:044	0.000209	0.002612	0.0007	0.002626	0.000395
53	00:05:021	0.000041	-34:58:059	0.000082	0.006201	0.000513	0.00554	0.000301
54	00:05:021	0.000445	-34:12:009	0.000298	0.000964	0.000153	0.000464	0.000108
56	00:05:018	0.000185	-34:29:043	0.00041	0.002267	0.000241	0.000971	0.000175
57	00:05:017	0.000032	-34:27:006	0.000062	0.004576	0.000409	0.00494	0.000225
59	00:05:006	0.000011	-34:45:049	0.00002	0.063479	0.001491	0.059358	0.000867
60	00:05:006	0.000242	-34:49:024	0.000187	0.00159	0.000303	0.001118	0.000194
61	00:05:003	0.000046	-35:08:034	0.000092	0.006731	0.00061	0.005959	0.000359
62	00:05:001	0.000244	-35:10:057	0.000173	0.016545	0.001203	0.006765	0.000891
63	00:05:001	0.000198	-34:13:008	0.000238	0.00072	0.000219	0.000638	0.000131
64	00:04:052	0.00015	-34:53:031	0.000183	0.012835	0.002426	0.010314	0.001494
65	00:04:049	0.000064	-35:00:023	0.000112	0.006643	0.000785	0.005911	0.000463
67	00:04:045	0.0003	-34:11:058	0.000344	0.00072	0.000169	0.000486	0.000108
68	00:04:039	0.000117	-35:04:021	0.000263	0.000659	0.000199	0.000659	0.000111
69	00:04:036	0.000065	-35:03:033	0.00012	0.003517	0.000441	0.003146	0.00026
71	00:04:013	0.000036	-34:30:060	0.000057	0.053243	0.002931	0.043477	0.001792
72	00:04:012	0.00015	-35:01:026	0.000273	0.002616	0.000588	0.002066	0.00036
73	00:04:012	0.000017	-34:31:023	0.00003	0.114223	0.003053	0.093872	0.001845
74	00:04:012	0.000121	-34:31:048	0.000218	0.008942	0.002216	0.008283	0.001294
75	00:04:006	0.0002	-34:32:055	0.000219	0.001947	0.000532	0.001754	0.000312
76	00:04:004	0.000024	-34:55:036	0.00004	0.035838	0.001542	0.032005	0.00091
77	00:03:056	0.000017	-34:32:028	0.000031	0.029765	0.000986	0.026845	0.00058
78	00:03:049	0.000016	-34:30:040	0.000028	0.027651	0.000804	0.02427	0.000479
79	00:03:045	0.000152	-35:14:044	0.00019	0.006401	0.000661	0.003565	0.000454
80	00:03:035	0.000196	-34:39:003	0.000311	0.001274	0.000258	0.000844	0.000168

Table C.2: Positions of radio sources within 4MPc radius of the pointing centre of cluster RXCJ0020.7−2542

Source ID	RA	δ RA	DEC	δ DEC	total flux	δ total flux	Peak flux	δ Peak flux
0	00:22:023	0.000105	-25:26:043	0.000091	0.008296	0.001188	0.007138	0.000719
1	00:22:005	0.000151	-25:55:031	0.000081	0.04179	0.001882	0.015425	0.000865

Continued on next page

Table C.2: Positions of radio sources within 4MPc radius of the pointing centre of cluster RXCJ0020.7−2542

Source ID	RA	δ RA	DEC	δ DEC	total flux	δ total flux	Peak flux	δ Peak flux
1	00:22:004	0.000119	-25:54:024	0.000289	0.025112	0.001097	0.007765	0.000854
1	00:22:004	0.000147	-25:54:043	0.000244	0.005904	0.001456	0.004791	0.000887
2	00:21:048	0.000125	-25:53:004	0.000435	0.286245	0.003542	0.114273	0.000988
3	00:21:051	0.000173	-25:52:033	0.000428	0.011515	0.001424	0.005142	0.001018
4	00:21:049	0.000266	-25:52:038	0.000302	0.009084	0.001529	0.005035	0.001039
5	00:21:047	0.000295	-25:52:048	0.000166	0.01185	0.001494	0.005985	0.001046
5	00:21:048	0.000256	-25:52:042	0.000267	0.00798	0.001571	0.00475	0.001061
6	00:21:042	0.000148	-25:40:023	0.000152	0.003378	0.001303	0.003986	0.000708
7	00:21:039	0.000071	-25:44:022	0.00006	0.009863	0.001431	0.010798	0.000795
8	00:21:038	0.000076	-25:44:042	0.000055	0.011869	0.001426	0.011706	0.00082
9	00:21:034	0.000023	-25:38:011	0.000019	0.030446	0.001197	0.02987	0.000693
10	00:21:033	0.000095	-25:53:022	0.000097	0.006754	0.001405	0.007391	0.000778
11	00:21:033	0.000036	-25:50:049	0.00004	0.027332	0.001352	0.022268	0.00083
12	00:21:032	0.000077	-26:08:016	0.000079	0.006786	0.00113	0.007356	0.000628
13	00:21:030	0.000399	-25:16:008	0.000258	0.009271	0.000935	0.003352	0.00071
13	00:21:030	0.000428	-25:15:059	0.000241	0.002393	0.001145	0.002092	0.000679
14	00:21:029	0.000327	-25:16:057	0.000593	0.021363	0.000663	0.003183	0.000581
15	00:21:011	0.00017	-25:58:046	0.000287	0.006266	0.001137	0.003901	0.000753
16	00:20:054	0.000212	-25:28:003	0.000343	0.01094	0.000864	0.004085	0.000645
17	00:20:048	0.000015	-25:44:038	0.000015	0.051957	0.001495	0.052167	0.000859
18	00:20:043	0.000031	-25:42:038	0.000035	0.059146	0.001486	0.035806	0.000997
19	00:20:042	0.000271	-25:29:022	0.000379	0.011816	0.000878	0.003837	0.000678
20	00:20:039	0.000101	-25:35:030	0.00011	0.008462	0.001102	0.006636	0.000687
21	00:20:032	0.000095	-25:55:028	0.000089	0.004583	0.001182	0.005652	0.000632
22	00:20:026	0.00036	-25:17:001	0.000304	0.006852	0.000733	0.002569	0.000552
23	00:20:026	0.000171	-25:17:022	0.000155	0.010018	0.000794	0.00478	0.000565
24	00:20:020	0.000027	-25:28:032	0.000047	0.05562	0.001521	0.031843	0.000713
24	00:20:018	0.000057	-25:28:022	0.000049	0.02248	0.001175	0.015727	0.000755
25	00:20:019	0.000354	-25:27:059	0.000485	0.019622	0.000753	0.003473	0.000646
26	00:19:057	0.000502	-26:02:057	0.000246	0.025175	0.000509	0.00329	0.000453
27	00:19:052	0.000014	-25:34:009	0.000013	0.050158	0.00123	0.049097	0.000714
28	00:19:051	0.00006	-25:43:056	0.000057	0.011917	0.001104	0.010739	0.000658
29	00:19:050	0.000029	-25:20:009	0.000028	0.022469	0.000812	0.017936	0.000503
30	00:19:044	0.00013	-25:44:016	0.000093	0.010921	0.000967	0.006747	0.000644
31	00:19:043	0.000034	-25:44:021	0.000031	0.020215	0.001032	0.018161	0.000617
32	00:19:040	0.000219	-25:35:023	0.00022	0.009749	0.001022	0.004466	0.000738
33	00:19:021	0.000236	-25:38:026	0.000214	0.02025	0.000771	0.005046	0.000629
35	00:19:001	0.000195	-26:03:042	0.000383	0.010054	0.00075	0.003323	0.000579
36	00:18:049	0.000023	-25:45:033	0.000021	0.025854	0.000906	0.023407	0.000539

Table C.3: Positions of radio sources within 4MPc radius of the pointing centre of cluster RXCJ0049.4−2931

Source ID	RA	δ RA	DEC	δ DEC	total flux	δ total flux	Peak flux	δ Peak flux
0	00:51:001	0.000046	-29:39:054	0.000067	0.006005	0.0006	0.005668	0.000344
1	00:50:053	0.000146	-29:42:045	0.000177	0.002112	0.000589	0.001949	0.000343
1	00:50:053	0.000175	-29:42:053	0.000225	0.004068	0.00078	0.001472	0.000345
2	00:50:050	0.00012	-29:14:027	0.000128	0.005406	0.000742	0.003927	0.000467
3	00:50:047	0.000024	-29:37:039	0.000018	0.01841	0.00104	0.017091	0.000431
3	00:50:047	0.00013	-29:37:036	0.000131	0.002372	0.00075	0.002504	0.000425
4	00:50:043	0.000216	-29:20:00	0.000163	0.003912	0.001265	0.003805	0.000702
5	00:50:041	0.000098	-29:22:002	0.000205	0.003182	0.001384	0.003988	0.000696
6	00:50:040	0.000129	-29:58:022	0.000257	0.005216	0.000915	0.003313	0.000598
7	00:50:040	0.000134	-29:22:027	0.000182	0.004682	0.001337	0.00465	0.00074
8	00:50:038	0.000019	-29:21:024	0.00001	0.192197	0.00293	0.103437	0.00082
8	00:50:037	0.000006	-29:21:031	0.000009	0.109761	0.001404	0.103597	0.0008
9	00:50:037	0.000008	-29:57:047	0.000006	0.101496	0.00172	0.082906	0.000589
9	00:50:038	0.000032	-29:57:042	0.00006	0.009854	0.001021	0.010189	0.000573
9	00:50:037	0.000039	-29:57:030	0.000198	0.009355	0.000894	0.006363	0.000529
9	00:50:037	0.000075	-29:57:015	0.000096	0.00604	0.001014	0.00569	0.000595
10	00:50:038	0.000076	-29:20:043	0.000143	0.004339	0.001432	0.005242	0.00076
11	00:50:038	0.000075	-29:21:052	0.000204	0.010142	0.001291	0.006734	0.000816
12	00:50:038	0.000141	-29:58:009	0.000251	0.005119	0.000938	0.003396	0.000602
13	00:50:038	0.000089	-29:58:029	0.000107	0.003275	0.001025	0.004124	0.000539
14	00:50:037	0.000101	-29:56:045	0.000126	0.005177	0.001437	0.003043	0.000592
15	00:50:037	0.000095	-29:20:048	0.000205	0.007087	0.001365	0.005439	0.000841
16	00:50:037	0.000099	-29:57:003	0.000186	0.005594	0.000984	0.004163	0.000616
17	00:50:037	0.000133	-29:58:020	0.000362	0.008664	0.000807	0.003415	0.000595
18	00:50:035	0.000148	-29:20:056	0.000182	0.005471	0.001401	0.004534	0.000858
19	00:50:034	0.000133	-29:57:017	0.000137	0.00555	0.000991	0.004194	0.000625
20	00:50:034	0.000194	-29:21:003	0.000121	0.004402	0.001424	0.004466	0.000796
21	00:50:031	0.000018	-29:35:058	0.000019	0.040135	0.000813	0.02795	0.000522
23	00:50:022	0.000029	-29:07:035	0.00005	0.009248	0.000592	0.008254	0.000345
24	00:50:010	0.000079	-29:25:047	0.000077	0.009232	0.000895	0.00692	0.000563
25	00:50:011	0.00014	-29:26:002	0.000235	0.003996	0.000891	0.002967	0.000557
25	00:50:011	0.000274	-29:25:054	0.000265	0.002656	0.000898	0.002213	0.000526
26	00:50:005	0.000033	-29:50:031	0.000034	0.025336	0.000655	0.014836	0.00044
28	00:50:004	0.000518	-29:51:002	0.000366	0.04825	0.000236	0.002088	0.000226
29	00:50:003	0.000059	-29:50:032	0.000084	0.030511	0.000858	0.009579	0.000412
30	00:50:003	0.000162	-29:41:039	0.000188	0.002329	0.000735	0.002158	0.00043
31	00:49:050	0.000333	-29:25:051	0.000496	0.017446	0.000442	0.002303	0.000393
32	00:49:050	0.000036	-29:16:055	0.000053	0.008002	0.000715	0.007925	0.000405
33	00:49:047	0.000021	-29:12:053	0.000017	0.059459	0.001204	0.030707	0.000437
34	00:49:046	0.00017	-29:12:018	0.000153	0.00165	0.000784	0.002262	0.000367
35	00:49:044	0.000134	-29:06:011	0.000083	0.061785	0.000675	0.008227	0.000423

Continued on next page

Table C.3: Positions of radio sources within 4MPc radius of the pointing centre of cluster RXCJ0049.4−2931

Source ID	RA	δ RA	DEC	δ DEC	total flux	δ total flux	Peak flux	δ Peak flux
35	00:49:044	0.000701	-29:06:050	0.000588	0.027696	0.000266	0.00148	0.000252
36	00:49:032	0.000239	-29:18:035	0.000227	0.006999	0.000499	0.002409	0.000382
37	00:49:019	0.000066	-29:15:055	0.000118	0.00369	0.000689	0.003714	0.000386
38	00:49:007	0.000032	-29:40:046	0.000045	0.015059	0.001014	0.014304	0.000577
39	00:48:053	0.000195	-29:13:006	0.000113	0.001807	0.000859	0.002465	0.000407
40	00:48:053	0.000012	-29:12:001	0.000007	0.047054	0.001207	0.046655	0.000483
41	00:48:053	0.00012	-29:12:023	0.00023	0.00236	0.00084	0.002439	0.000459
42	00:48:045	0.000146	-29:52:052	0.000406	0.010394	0.001144	0.0043	0.000831
43	00:48:044	0.000216	-29:45:051	0.000254	0.01235	0.002023	0.006672	0.001396
44	00:48:044	0.000155	-29:46:053	0.000186	0.00639	0.002538	0.007633	0.001271
44	00:48:044	0.00017	-29:47:002	0.000274	0.006122	0.002476	0.006091	0.001365
46	00:48:042	0.000106	-29:48:036	0.000161	0.006348	0.00255	0.007656	0.001363
49	00:48:041	0.000161	-29:46:043	0.000176	0.009973	0.002549	0.008162	0.001568
50	00:48:039	0.000005	-29:47:018	0.000005	0.57434	0.005611	0.441517	0.001534
50	00:48:040	0.000045	-29:46:055	0.000113	0.022956	0.002564	0.019626	0.001484
50	00:48:039	0.000167	-29:46:060	0.000026	0.040719	0.003564	0.023118	0.001534
50	00:48:039	0.000065	-29:46:047	0.000077	0.009401	0.002699	0.013307	0.001364
50	00:48:039	0.000043	-29:46:035	0.000135	0.024097	0.002498	0.018448	0.001495
51	00:48:040	0.000073	-29:48:024	0.000073	0.015395	0.002608	0.017265	0.001391
53	00:48:040	0.000106	-29:46:019	0.000096	0.011739	0.002548	0.011628	0.001475
53	00:48:039	0.000079	-29:46:014	0.000091	0.007232	0.002591	0.01047	0.0013
55	00:48:038	0.000238	-29:17:028	0.000248	0.018194	0.000467	0.003176	0.000402
56	00:48:038	0.000213	-29:48:043	0.000396	0.026636	0.001821	0.007541	0.001449
57	00:48:038	0.000089	-29:46:008	0.000189	0.006575	0.002562	0.007721	0.001361
59	00:48:037	0.000049	-29:46:008	0.000102	0.007606	0.002598	0.011624	0.001238
60	00:48:036	0.000022	-29:17:035	0.000025	0.044521	0.001223	0.024979	0.000433
61	00:48:036	0.000086	-29:46:030	0.000177	0.005944	0.002651	0.007744	0.001353
62	00:48:036	0.00008	-29:46:050	0.000106	0.025367	0.002483	0.017273	0.001605
63	00:48:034	0.000113	-29:46:056	0.000178	0.007314	0.00261	0.008687	0.001331
64	00:48:034	0.000047	-29:26:001	0.000105	0.018009	0.000594	0.007598	0.000432
66	00:48:031	0.000075	-29:32:039	0.000159	0.007645	0.000948	0.005545	0.000585
67	00:48:030	0.000224	-29:43:047	0.000297	0.016347	0.001404	0.006189	0.001047
68	00:48:030	0.000121	-29:22:059	0.000245	0.002461	0.000688	0.002197	0.000394
71	00:48:018	0.000101	-29:16:038	0.000215	0.00301	0.000562	0.002251	0.000347
72	00:47:060	0.000053	-29:44:046	0.00008	0.010711	0.000886	0.00832	0.000543
73	00:47:051	0.000033	-29:41:018	0.000046	0.014845	0.000699	0.011502	0.000425

Table C.4: Positions of radio sources within 4MPc radius of the pointing centre of cluster RXCJ0211.4−4017

Source ID	RA	δ RA	DEC	δ DEC	total flux	δ total flux	Peak flux	δ Peak flux
0	02:13:033	0.00028	-40:29:00	0.000409	0.009232	0.000394	0.002383	0.000318
2	02:13:007	0.000175	-40:18:036	0.000191	0.013557	0.000755	0.005521	0.00056
3	02:12:060	0.00039	-40:17:010	0.000277	0.024405	0.0006	0.004289	0.000516
4	02:13:001	0.000084	-40:10:045	0.000207	0.025712	0.000724	0.008487	0.000557
5	02:12:034	0.000099	-40:43:032	0.000397	0.006845	0.000509	0.003217	0.000348
6	02:12:033	0.000136	-40:18:047	0.000344	0.013065	0.000836	0.005198	0.000616
8	02:12:026	0.000151	-40:07:016	0.000284	0.011273	0.000971	0.005651	0.000677
9	02:12:019	0.000087	-40:04:036	0.000226	0.012021	0.000997	0.007071	0.000661
9	02:12:021	0.000438	-40:04:034	0.000328	0.017142	0.000773	0.004031	0.000637
10	02:12:018	0.000095	-39:45:046	0.000383	0.00436	0.000525	0.00271	0.000329
11	02:12:011	0.000183	-39:50:002	0.000515	0.005384	0.000512	0.002219	0.000372
12	02:12:003	0.000076	-40:06:054	0.000192	0.009339	0.001235	0.007885	0.000723
13	02:11:044	0.000371	-40:35:034	0.000625	0.014694	0.00065	0.00303	0.000545
14	02:11:038	0.000165	-40:43:025	0.000438	0.024187	0.000943	0.003273	0.000484
14	02:11:041	0.000216	-40:43:024	0.000556	0.011449	0.00103	0.002838	0.000484
14	02:11:040	0.000344	-40:43:027	0.000316	0.003628	0.000784	0.002294	0.000521
15	02:11:039	0.00007	-40:42:049	0.000045	0.052786	0.001346	0.018666	0.000492
17	02:11:034	0.000564	-40:30:013	0.000567	0.018423	0.000727	0.00312	0.000629
18	02:11:032	0.000211	-40:15:011	0.000496	0.02124	0.003261	0.007875	0.001136
20	02:11:025	0.000019	-40:17:024	0.000012	0.305235	0.005375	0.148674	0.001154
20	02:11:027	0.00018	-40:17:026	0.000108	0.009174	0.00208	0.012018	0.000906
20	02:11:025	0.000126	-40:17:059	0.000029	0.022939	0.001941	0.021327	0.00105
20	02:11:024	0.00008	-40:18:00	0.00008	0.034982	0.002542	0.026853	0.001154
20	02:11:027	0.000099	-40:17:054	0.000121	0.005489	0.00203	0.008631	0.000984
22	02:11:027	0.00023	-40:16:046	0.000176	0.010313	0.00196	0.009888	0.001028
24	02:11:025	0.000035	-40:16:032	0.000084	0.06569	0.003244	0.035849	0.001163
25	02:11:025	0.000419	-40:18:025	0.000133	0.017538	0.001625	0.00942	0.001048
26	02:11:025	0.000049	-40:16:056	0.000044	0.03177	0.002023	0.034441	0.001067
28	02:11:021	0.000168	-40:15:046	0.000182	0.009773	0.001956	0.009209	0.00111
31	02:10:049	0.000082	-40:05:023	0.000271	0.011321	0.000958	0.00665	0.000621
32	02:10:037	0.000053	-40:51:056	0.000202	0.01446	0.000534	0.006527	0.000372
32	02:10:038	0.000131	-40:51:042	0.000291	0.001257	0.000709	0.001957	0.000309
33	02:10:037	0.000214	-40:51:028	0.000205	0.001717	0.000686	0.00213	0.000351
35	02:10:018	0.000419	-40:09:046	0.000546	0.007653	0.000637	0.002354	0.000499
37	02:09:056	0.00008	-40:18:008	0.000279	0.009848	0.000705	0.005342	0.000465
39	02:09:042	0.000223	-40:50:009	0.000454	0.002476	0.000543	0.001704	0.00034
40	02:09:039	0.000081	-40:49:039	0.00031	0.001999	0.000597	0.002316	0.000287
41	02:09:030	0.000222	-40:24:001	0.000263	0.003285	0.000807	0.002939	0.000463
43	02:09:028	0.000118	-40:23:036	0.000038	0.018863	0.001097	0.010609	0.000469
44	02:09:012	0.000186	-40:27:050	0.000247	0.008873	0.000674	0.003978	0.000488
45	02:08:046	0.000084	-39:53:018	0.000277	0.004269	0.000374	0.002476	0.000245

Continued on next page

Table C.4: Positions of radio sources within 4MPc radius of the pointing centre of cluster RXCJ0211.4−4017

Source ID	RA	δ RA	DEC	δ DEC	total flux	δ total flux	Peak flux	δ Peak flux
46	02:08:042	0.000438	-40:42:017	0.000574	0.008837	0.000422	0.001936	0.000351

Table C.5: Positions of radio sources within 4MPc radius of the pointing centre of cluster RXCJ0225.1−2928

Source ID	RA	δ RA	DEC	δ DEC	total flux	δ total flux	Peak flux	δ Peak flux
0	02:28:048	0.000254	-29:50:003	0.00025	0.001744	0.000295	0.001008	0.0002
1	02:28:031	0.000091	-29:46:007	0.00007	0.004804	0.000495	0.003938	0.000302
2	02:28:015	0.000055	-29:04:038	0.000045	0.025886	0.001585	0.020559	0.000981
3	02:28:014	0.000243	-30:16:012	0.000251	0.000493	0.000114	0.000359	0.000071
4	02:28:004	0.000221	-29:16:022	0.000132	0.003829	0.000646	0.002688	0.000412
5	02:28:004	0.000127	-29:41:001	0.000115	0.002678	0.000401	0.002217	0.000243
6	02:27:027	0.000054	-29:08:059	0.000047	0.007572	0.000509	0.00638	0.000309
8	02:27:018	0.000135	-29:33:018	0.000067	0.002521	0.000239	0.001757	0.000152
9	02:27:016	0.000134	-29:24:019	0.000114	0.002416	0.000465	0.002257	0.00027
10	02:27:016	0.000071	-29:43:038	0.000061	0.010154	0.0004	0.005533	0.000275
11	02:27:004	0.000209	-29:10:054	0.000246	0.001758	0.000397	0.001276	0.000251
12	02:27:003	0.000176	-29:23:024	0.000234	0.004627	0.00056	0.002602	0.000378
13	02:27:002	0.000084	-29:54:033	0.00008	0.005191	0.00054	0.004295	0.000328
14	02:26:058	0.000201	-29:25:020	0.000183	0.004417	0.000465	0.002254	0.000326
15	02:26:052	0.00011	-29:28:046	0.000094	0.001693	0.000343	0.001809	0.00019
16	02:26:041	0.000261	-29:28:031	0.000168	0.001171	0.000266	0.000957	0.000156
17	02:26:036	0.000163	-29:17:052	0.000121	0.001829	0.000328	0.001518	0.000198
18	02:26:032	0.000043	-29:27:031	0.000039	0.030886	0.001468	0.024311	0.000908
19	02:26:029	0.000169	-29:27:012	0.000137	0.003947	0.000728	0.003305	0.000434
20	02:26:028	0.000107	-29:32:003	0.000103	0.002972	0.000364	0.002436	0.000219
21	02:26:023	0.000089	-29:42:031	0.000091	0.014594	0.000921	0.009355	0.000593
22	02:26:011	0.00017	-29:23:020	0.000172	0.003114	0.000463	0.002093	0.0003
23	02:26:009	0.000092	-28:57:057	0.000101	0.025888	0.001721	0.014911	0.001171
24	02:26:008	0.000182	-28:58:020	0.000191	0.019976	0.001511	0.008674	0.001101
25	02:26:008	0.000098	-29:05:034	0.000122	0.002198	0.000373	0.00211	0.000212
26	02:26:005	0.000072	-29:15:055	0.00005	0.033124	0.001373	0.020314	0.000901
27	02:26:005	0.000114	-29:57:040	0.000104	0.002055	0.000374	0.002024	0.000213
28	02:25:055	0.000204	-29:19:023	0.000257	0.001605	0.000386	0.001204	0.000241
29	02:25:053	0.000149	-30:11:009	0.000148	0.001772	0.000408	0.001656	0.000238
30	02:25:052	0.000304	-29:36:015	0.000212	0.004036	0.000363	0.001574	0.000271
31	02:25:051	0.000111	-29:24:011	0.000088	0.001981	0.000398	0.0022	0.000215
32	02:25:046	0.000132	-29:46:054	0.000166	0.002204	0.000501	0.002084	0.000287
33	02:25:044	0.000057	-30:04:008	0.000055	0.015294	0.001154	0.012955	0.000699

Continued on next page

Table C.5: Positions of radio sources within 4MPc radius of the pointing centre of cluster RXCJ0225.1−2928

Source ID	RA	δ RA	DEC	δ DEC	total flux	δ total flux	Peak flux	δ Peak flux
34	02:25:037	0.000061	-29:26:019	0.000059	0.006819	0.000683	0.006688	0.000389
35	02:25:025	0.000126	-28:58:018	0.00011	0.003186	0.000372	0.002359	0.000232
36	02:25:024	0.000033	-29:39:024	0.000033	0.020666	0.001054	0.019424	0.000609
37	02:25:023	0.000043	-29:30:027	0.000043	0.014493	0.000945	0.013473	0.000548
38	02:25:021	0.000148	-29:41:018	0.00016	0.001124	0.000344	0.001234	0.000187
39	02:25:021	0.000225	-29:31:002	0.000189	0.001087	0.000356	0.001052	0.000202
40	02:25:019	0.000163	-29:02:028	0.00026	0.004646	0.000488	0.002228	0.000347
41	02:25:016	0.000149	-29:16:044	0.000146	0.001599	0.000309	0.00141	0.000181
42	02:25:015	0.000047	-29:53:015	0.000085	0.039627	0.001367	0.020936	0.000934
43	02:25:014	0.00011	-29:53:021	0.000108	0.009867	0.001428	0.008519	0.000851
45	02:25:002	0.000182	-29:06:034	0.00035	0.003965	0.000624	0.002193	0.000423
46	02:24:055	0.000233	-29:05:002	0.000131	0.000921	0.000284	0.000885	0.000164
47	02:24:054	0.000101	-29:04:002	0.000135	0.003395	0.000377	0.002457	0.000237
48	02:24:050	0.000047	-29:37:049	0.00004	0.005331	0.000433	0.005602	0.00024
49	02:24:048	0.000133	-29:16:056	0.000113	0.000986	0.000271	0.001117	0.000147
50	02:24:044	0.000131	-29:17:023	0.000119	0.003483	0.000534	0.002902	0.000321
51	02:24:043	0.000145	-29:37:043	0.000135	0.002303	0.000522	0.002185	0.000302
52	02:24:042	0.00004	-29:34:017	0.000038	0.079433	0.004488	0.070357	0.002667
53	02:24:041	0.000294	-29:15:030	0.000192	0.00352	0.000459	0.001773	0.000322
54	02:24:041	0.000165	-29:56:058	0.000101	0.000634	0.000258	0.000866	0.000129
55	02:24:035	0.000082	-29:51:048	0.000091	0.003192	0.000439	0.003009	0.000255
56	02:24:026	0.000061	-29:50:060	0.000064	0.007879	0.000684	0.006908	0.000407
57	02:24:024	0.000168	-29:32:042	0.000217	0.001949	0.000437	0.001512	0.000272
58	02:24:020	0.000189	-28:55:004	0.000235	0.00103	0.000293	0.000903	0.000173
59	02:24:018	0.000168	-29:10:009	0.000167	0.001453	0.000375	0.001379	0.000215
60	02:24:018	0.000123	-28:57:003	0.000114	0.001421	0.000328	0.001555	0.000177
61	02:24:014	0.000058	-29:49:046	0.000065	0.005879	0.000516	0.005238	0.000305
62	02:24:005	0.000199	-30:12:007	0.000172	0.000902	0.000303	0.000925	0.00017
63	02:24:001	0.000234	-30:16:024	0.000229	0.00037	0.000116	0.000345	0.000066
64	02:23:059	0.000176	-29:21:055	0.00025	0.001409	0.000415	0.001269	0.000241
65	02:23:058	0.000209	-29:30:059	0.000158	0.001115	0.000365	0.001139	0.000204
66	02:23:044	0.000187	-29:33:025	0.000211	0.001334	0.00034	0.001157	0.0002
67	02:23:036	0.000165	-29:15:013	0.000199	0.001859	0.000429	0.001582	0.000256
68	02:23:030	0.000104	-29:31:025	0.000078	0.004435	0.000611	0.004083	0.000356
68	02:23:030	0.000126	-29:31:016	0.00012	0.005269	0.000584	0.003669	0.000373
69	02:23:030	0.000082	-29:18:011	0.000101	0.00341	0.000364	0.00275	0.000222
70	02:23:024	0.000331	-29:38:055	0.000292	0.002987	0.000398	0.001402	0.000282
71	02:23:023	0.000228	-29:39:023	0.0002	0.002586	0.000305	0.001337	0.000213
72	02:23:017	0.000142	-29:54:019	0.000132	0.002842	0.000389	0.002046	0.000248
73	02:23:013	0.000071	-29:34:016	0.000076	0.003792	0.00041	0.003432	0.000241
74	02:23:002	0.000204	-29:46:010	0.000142	0.001426	0.000319	0.001171	0.000195

Continued on next page

Table C.5: Positions of radio sources within 4MPc radius of the pointing centre of cluster RXCJ0225.1−2928

Source ID	RA	δ RA	DEC	δ DEC	total flux	δ total flux	Peak flux	δ Peak flux
75	02:23:00	0.00017	-29:47:020	0.000224	0.001106	0.000278	0.000945	0.000165
76	02:22:033	0.00022	-29:09:025	0.000241	0.001702	0.000366	0.001259	0.000226
77	02:22:030	0.000189	-29:22:059	0.000256	0.001832	0.000381	0.001312	0.00024
78	02:22:014	0.000147	-29:19:053	0.000136	0.001786	0.000274	0.001419	0.000166
79	02:21:050	0.000416	-29:18:019	0.000262	0.000608	0.000091	0.000272	0.000066
80	02:21:044	0.000208	-28:35:010	0.000164	0.000323	0.000116	0.000364	0.000061
81	02:21:019	0.00016	-29:07:015	0.000194	0.002323	0.000326	0.001575	0.000207
82	02:20:050	0.000296	-28:33:041	0.000169	0.000449	0.000128	0.00039	0.000074
83	02:20:048	0.000279	-28:40:035	0.000265	0.000696	0.000126	0.0004	0.000086

Table C.6: Positions of radio sources within 4MPc radius of the pointing centre of cluster RXCJ0345.7−4112

Source ID	RA	δ RA	DEC	δ DEC	total flux	δ total flux	Peak flux	δ Peak flux
0	03:48:052	0.000256	-41:20:017	0.000314	0.005629	0.000353	0.002294	0.000262
1	03:48:050	0.000461	-41:20:059	0.000223	0.001736	0.000407	0.001399	0.000246
1	03:48:052	0.000548	-41:20:056	0.000328	0.001376	0.000408	0.00108	0.000251
2	03:48:049	0.000574	-41:11:058	0.000555	0.005231	0.000287	0.001479	0.000228
3	03:48:047	0.001078	-41:46:028	0.000656	0.00721	0.000235	0.001057	0.000207
4	03:48:038	0.000542	-41:33:057	0.000483	0.00235	0.00037	0.00129	0.00025
5	03:48:020	0.000096	-41:43:047	0.000071	0.024255	0.000635	0.010452	0.000289
5	03:48:022	0.000434	-41:43:057	0.000308	0.004096	0.000435	0.002087	0.000302
5	03:48:019	0.000304	-41:44:028	0.000132	0.009948	0.000388	0.004433	0.000269
5	03:48:022	0.000131	-41:44:020	0.000234	0.003159	0.000493	0.002817	0.000291
5	03:48:021	0.000289	-41:44:043	0.000506	0.009298	0.000353	0.002449	0.000285
5	03:48:017	0.000191	-41:43:049	0.000161	0.002073	0.000507	0.002453	0.000271
7	03:48:020	0.000461	-41:42:053	0.000153	0.003221	0.000461	0.002311	0.000276
10	03:47:055	0.00022	-41:25:003	0.000262	0.007673	0.000356	0.003174	0.00026
11	03:47:055	0.000368	-41:25:041	0.000168	0.001493	0.000434	0.001612	0.000231
12	03:47:053	0.000272	-41:25:007	0.000215	0.001107	0.000444	0.00141	0.000233
13	03:47:053	0.000608	-41:41:008	0.000127	0.003534	0.000624	0.001591	0.00027
14	03:47:046	0.000982	-40:28:015	0.000755	0.005119	0.00021	0.000899	0.00018
16	03:47:025	0.000255	-41:16:009	0.000142	0.002121	0.000529	0.002447	0.000279
17	03:47:023	0.000067	-41:16:034	0.00005	0.005135	0.000528	0.006659	0.000277
17	03:47:022	0.000117	-41:16:040	0.000072	0.006609	0.000512	0.006082	0.000293
17	03:47:025	0.000148	-41:16:034	0.00013	0.006247	0.000495	0.004968	0.000294
18	03:47:023	0.000045	-41:15:059	0.000037	0.026154	0.001028	0.01584	0.000303
18	03:47:020	0.00012	-41:15:059	0.000095	0.00407	0.000527	0.004347	0.000296
19	03:47:023	0.000281	-41:15:006	0.000102	0.003365	0.000517	0.003315	0.000271

Continued on next page

Table C.6: Positions of radio sources within 4MPc radius of the pointing centre of cluster RXCJ0345.7−4112

Source ID	RA	δ RA	DEC	δ DEC	total flux	δ total flux	Peak flux	δ Peak flux
20	03:47:018	0.000258	-41:07:028	0.000095	0.004788	0.000634	0.002623	0.000267
23	03:46:057	0.000391	-40:54:057	0.000499	0.003781	0.000334	0.001457	0.000251
24	03:46:055	0.000429	-41:36:025	0.000312	0.002665	0.000364	0.001619	0.000238
25	03:46:051	0.000333	-40:37:044	0.000432	0.001396	0.000348	0.001125	0.00021
26	03:46:023	0.000215	-41:12:035	0.000116	0.008955	0.000473	0.004773	0.000324
26	03:46:023	0.000061	-41:11:054	0.000088	0.02401	0.00067	0.010653	0.000311
26	03:46:021	0.000257	-41:12:037	0.000229	0.001652	0.000543	0.001892	0.000297
27	03:46:023	0.000443	-41:11:001	0.00032	0.005316	0.000456	0.002228	0.000336
28	03:46:009	0.000478	-41:48:024	0.000077	0.002883	0.000552	0.001397	0.000232
29	03:45:056	0.000475	-41:09:034	0.000426	0.003374	0.000553	0.001978	0.000369
30	03:45:054	0.000557	-41:08:033	0.000411	0.003263	0.000525	0.001839	0.000353
31	03:45:047	0.00023	-41:12:044	0.000077	0.012148	0.000528	0.00624	0.00036
31	03:45:045	0.000106	-41:12:049	0.000082	0.003277	0.000637	0.004879	0.000309
32	03:45:047	0.000077	-41:12:007	0.000045	0.023738	0.000854	0.014222	0.000362
33	03:45:049	0.000324	-41:12:017	0.000371	0.001535	0.00064	0.001874	0.000317
34	03:45:047	0.000269	-41:11:015	0.000181	0.002615	0.000629	0.002799	0.000341
35	03:45:044	0.000125	-41:12:007	0.000178	0.002558	0.000635	0.003305	0.000328
35	03:45:045	0.000216	-41:11:047	0.000229	0.00206	0.000635	0.002538	0.000328
36	03:45:044	0.000352	-41:58:015	0.000259	0.001033	0.000361	0.001122	0.000197
36	03:45:044	0.000331	-41:58:029	0.000456	0.000767	0.000361	0.000855	0.000195
37	03:45:042	0.000529	-41:13:005	0.000385	0.003091	0.000562	0.001818	0.000378
41	03:45:040	0.000412	-41:08:009	0.000375	0.003163	0.000531	0.001922	0.000355
42	03:45:031	0.000071	-40:49:013	0.000061	0.010635	0.000554	0.006804	0.000242
43	03:45:031	0.000155	-40:49:048	0.000097	0.00247	0.000424	0.002828	0.000231
43	03:45:029	0.000465	-40:49:052	0.000258	0.000781	0.000432	0.001043	0.000209
44	03:45:031	0.000343	-40:48:020	0.000174	0.001064	0.000429	0.001434	0.000206
45	03:45:029	0.000585	-41:33:057	0.000804	0.00513	0.000299	0.00131	0.000242
46	03:45:026	0.000438	-41:11:033	0.000493	0.003004	0.000551	0.001839	0.000363
47	03:45:020	0.00021	-40:56:039	0.000415	0.002964	0.000377	0.001772	0.000251
48	03:44:053	0.000134	-40:45:034	0.000138	0.006222	0.000375	0.003773	0.000252
49	03:44:053	0.000211	-40:46:008	0.000178	0.001194	0.000409	0.001567	0.000213
49	03:44:051	0.000403	-40:46:013	0.000236	0.001178	0.000404	0.001254	0.000219
50	03:44:048	0.0001	-41:26:023	0.000044	0.153637	0.001001	0.022676	0.000285
50	03:44:046	0.000482	-41:27:011	0.000369	0.003355	0.000431	0.00184	0.00029
50	03:44:051	0.00051	-41:26:026	0.000661	0.005513	0.000351	0.001911	0.000261
51	03:44:051	0.000284	-41:48:020	0.000461	0.001379	0.000394	0.001171	0.000236
52	03:44:049	0.000131	-41:47:055	0.000383	0.005534	0.00033	0.002651	0.000227
53	03:44:045	0.000433	-41:18:002	0.000126	0.002725	0.0007	0.001688	0.000287
53	03:44:044	0.000312	-41:17:050	0.000411	0.000646	0.000511	0.001009	0.000239
53	03:44:046	0.000485	-41:17:045	0.000458	0.001168	0.000491	0.001048	0.000294
54	03:44:022	0.000306	-41:09:002	0.000299	0.001474	0.000501	0.00158	0.000276

Continued on next page

Table C.6: Positions of radio sources within 4MPc radius of the pointing centre of cluster RXCJ0345.7−4112

Source ID	RA	δ RA	DEC	δ DEC	total flux	δ total flux	Peak flux	δ Peak flux
56	03:44:017	0.000062	-41:11:045	0.000046	0.006542	0.000517	0.007721	0.00028
56	03:44:015	0.000174	-41:11:051	0.000135	0.00494	0.000493	0.004264	0.000282
56	03:44:019	0.000114	-41:11:043	0.000195	0.004397	0.000497	0.003852	0.000288
57	03:44:017	0.000046	-41:11:010	0.000033	0.025142	0.000684	0.016211	0.000294
58	03:44:017	0.000174	-41:10:017	0.000115	0.00428	0.000495	0.003941	0.000283
59	03:44:016	0.000314	-41:10:045	0.000118	0.001856	0.000514	0.0022	0.000261
60	03:44:014	0.000146	-41:11:013	0.000161	0.001724	0.000514	0.002356	0.000266
61	03:44:012	0.000626	-41:21:035	0.000362	0.00188	0.000449	0.001368	0.000273
62	03:44:010	0.000106	-41:07:017	0.000146	0.008425	0.000441	0.005069	0.000295
63	03:44:010	0.000286	-41:08:014	0.000192	0.001171	0.000496	0.001549	0.000256
65	03:44:010	0.000193	-41:07:049	0.000141	0.00207	0.000489	0.002396	0.000267
65	03:44:008	0.000405	-41:07:056	0.000193	0.001789	0.000478	0.001715	0.000269
66	03:44:002	0.000211	-40:52:021	0.000675	0.003417	0.000551	0.001477	0.000238
66	03:44:004	0.000864	-40:52:022	0.000616	0.002889	0.000321	0.000992	0.000246
67	03:44:003	0.000328	-40:51:044	0.000177	0.007125	0.000332	0.002682	0.000249
68	03:44:004	0.000289	-41:03:025	0.000295	0.00171	0.000434	0.001513	0.000261
69	03:44:001	0.000403	-41:10:038	0.000319	0.001566	0.000489	0.001472	0.00028
71	03:43:059	0.000133	-41:24:036	0.00007	0.010118	0.000574	0.005371	0.000258
72	03:43:059	0.000377	-41:23:041	0.000191	0.001917	0.000443	0.001902	0.000235
73	03:43:058	0.000387	-41:25:013	0.000754	0.004799	0.000556	0.001951	0.000256
74	03:43:051	0.000202	-40:48:060	0.000366	0.001437	0.000402	0.001393	0.00023
75	03:43:038	0.000436	-42:03:019	0.000138	0.002515	0.000529	0.001414	0.000217
76	03:43:031	0.000448	-40:54:009	0.000611	0.005232	0.0003	0.001524	0.000237
77	03:43:031	0.000387	-40:54:041	0.000346	0.002023	0.000389	0.00142	0.000247
78	03:43:002	0.000151	-41:29:051	0.000333	0.002956	0.000434	0.002297	0.000262
79	03:42:060	0.000099	-41:29:023	0.000062	0.012476	0.000606	0.007731	0.000264
80	03:42:059	0.000285	-41:29:056	0.000149	0.001722	0.000458	0.001902	0.000248
81	03:42:057	0.000226	-41:29:025	0.000289	0.001455	0.000458	0.001562	0.000257
82	03:42:029	0.000793	-40:49:051	0.00094	0.013382	0.000176	0.001101	0.000163
83	03:42:028	0.00016	-40:49:016	0.000282	0.006156	0.000332	0.002894	0.000234

Table C.7: Positions of radio sources within 4MPc radius of the pointing centre of cluster RXCJ0547.6−3152

Source ID	RA	δ RA	DEC	δ DEC	total flux	δ total flux	Peak flux	δ Peak flux
0	05:49:033	0.000265	-31:51:055	0.000324	0.006456	0.000596	0.00237	0.000451
1	05:49:033	0.00016	-32:15:032	0.000298	0.003882	0.000891	0.002773	0.000563
1	05:49:033	0.00012	-32:15:043	0.000333	0.003874	0.000884	0.002841	0.000544
1	05:49:034	0.000221	-32:15:055	0.00028	0.002737	0.000919	0.002336	0.000549

Continued on next page

Table C.7: Positions of radio sources within 4MPc radius of the pointing centre of cluster RXCJ0547.6−3152

Source ID	RA	δ RA	DEC	δ DEC	total flux	δ total flux	Peak flux	δ Peak flux
2	05:49:032	0.00008	-31:52:030	0.000139	0.009741	0.000675	0.0053	0.000464
3	05:49:031	0.00002	-32:15:012	0.000017	0.059974	0.001302	0.035979	0.000546
3	05:49:029	0.000036	-32:15:001	0.000049	0.016384	0.000923	0.013304	0.000568
3	05:49:032	0.000025	-32:15:004	0.000116	0.00357	0.001	0.005704	0.000426
3	05:49:029	0.000093	-32:15:015	0.000092	0.005034	0.000948	0.005146	0.000543
3	05:49:030	0.000171	-32:15:028	0.00009	0.001939	0.00098	0.003048	0.000448
5	05:49:032	0.000115	-31:52:009	0.000249	0.002783	0.000725	0.002442	0.000425
5	05:49:031	0.000179	-31:51:058	0.000239	0.002955	0.000715	0.002253	0.000447
6	05:49:032	0.000142	-32:15:041	0.000302	0.005891	0.000841	0.003339	0.000566
7	05:49:031	0.000069	-32:14:052	0.000074	0.006291	0.000953	0.006616	0.00054
8	05:49:030	0.000073	-32:14:036	0.000172	0.002243	0.000977	0.003246	0.000469
9	05:49:030	0.000249	-32:15:047	0.000303	0.017366	0.000633	0.003945	0.000523
11	05:49:028	0.000224	-32:15:004	0.000179	0.003395	0.000921	0.002778	0.000566
12	05:49:017	0.000113	-31:53:006	0.000328	0.003907	0.000811	0.002759	0.000505
14	05:49:013	0.000013	-31:53:010	0.000021	0.033704	0.000848	0.029233	0.000508
14	05:49:014	0.000022	-31:53:002	0.000161	0.007598	0.000814	0.00679	0.000421
14	05:49:013	0.000031	-31:52:050	0.000065	0.004015	0.000883	0.006489	0.000415
17	05:49:012	0.000024	-31:41:037	0.000038	0.021913	0.000656	0.015038	0.000423
17	05:49:012	0.000045	-31:41:016	0.000118	0.001674	0.000714	0.002931	0.000318
19	05:49:012	0.000339	-31:53:013	0.000196	0.006842	0.000699	0.003078	0.000496
20	05:49:012	0.000118	-31:54:020	0.000192	0.003026	0.000827	0.002927	0.000476
20	05:49:011	0.000228	-31:54:023	0.000206	0.00181	0.000835	0.001902	0.000473
21	05:49:011	0.000335	-31:41:039	0.000297	0.004638	0.000582	0.001985	0.000425
22	05:49:011	0.000064	-31:52:025	0.000194	0.001929	0.000871	0.00281	0.000408
23	05:49:011	0.000084	-31:53:018	0.00031	0.003192	0.000808	0.002741	0.000461
24	05:48:053	0.000045	-32:00:058	0.000069	0.004718	0.000701	0.005554	0.000379
25	05:48:053	0.000105	-32:00:036	0.000224	0.002809	0.000685	0.002481	0.000403
26	05:48:040	0.000082	-32:02:017	0.000116	0.007481	0.00065	0.004876	0.000426
27	05:48:035	0.000238	-31:40:040	0.000185	0.009648	0.000516	0.003158	0.0004
28	05:48:025	0.00016	-31:37:024	0.000275	0.011908	0.000486	0.003199	0.000391
30	05:48:012	0.000134	-31:30:040	0.000115	0.078428	0.001197	0.013245	0.000576
30	05:48:014	0.000145	-31:30:027	0.000151	0.03601	0.000662	0.007374	0.000558
31	05:48:014	0.000149	-31:52:044	0.000328	0.003333	0.000761	0.002325	0.000483
31	05:48:014	0.000381	-31:53:001	0.000448	0.015116	0.000475	0.002295	0.000416
32	05:48:013	0.000052	-31:52:018	0.00006	0.014895	0.000751	0.00982	0.000492
33	05:48:013	0.000103	-32:11:048	0.000293	0.003829	0.001002	0.00336	0.000571
33	05:48:013	0.000144	-32:12:001	0.000461	0.004438	0.00092	0.002664	0.000599
34	05:48:012	0.000014	-32:07:023	0.000028	0.031524	0.001072	0.029003	0.000624
34	05:48:013	0.000023	-32:07:014	0.00025	0.008486	0.000954	0.006621	0.000498
35	05:48:012	0.000024	-32:06:021	0.000065	0.014331	0.001056	0.013759	0.000592
35	05:48:012	0.000043	-32:07:003	0.000085	0.004092	0.001097	0.006427	0.000516

Continued on next page

Table C.7: Positions of radio sources within 4MPc radius of the pointing centre of cluster RXCJ0547.6−3152

Source ID	RA	δ RA	DEC	δ DEC	total flux	δ total flux	Peak flux	δ Peak flux
36	05:48:012	0.000072	-32:06:00	0.0002	0.003188	0.001073	0.00394	0.000532
37	05:48:011	0.000011	-32:11:028	0.000022	0.061648	0.001013	0.044036	0.00064
37	05:48:012	0.00002	-32:11:020	0.000104	0.011139	0.001048	0.011009	0.00054
37	05:48:012	0.000103	-32:11:006	0.000266	0.001251	0.001131	0.002268	0.000467
40	05:48:011	0.000153	-32:07:026	0.000216	0.004545	0.001059	0.003698	0.000645
41	05:48:011	0.000029	-32:11:008	0.000088	0.006178	0.001129	0.008341	0.000551
43	05:48:010	0.000176	-32:11:032	0.000241	0.004204	0.001026	0.003387	0.00062
44	05:47:038	0.000042	-31:52:025	0.000079	0.020652	0.001185	0.014118	0.000761
47	05:47:036	0.000014	-31:31:004	0.000028	0.044045	0.000875	0.030629	0.000557
47	05:47:036	0.000047	-31:30:057	0.000209	0.007218	0.000852	0.005401	0.000498
48	05:47:036	0.000025	-31:30:042	0.000174	0.006139	0.000887	0.006059	0.000443
49	05:47:034	0.000218	-31:31:006	0.000248	0.006309	0.00081	0.003264	0.000563
51	05:47:029	0.000028	-32:04:055	0.000053	0.015352	0.000873	0.012961	0.000525
52	05:47:029	0.000051	-32:04:035	0.00012	0.003632	0.00089	0.004598	0.000457
52	05:47:029	0.000087	-32:04:022	0.000172	0.003002	0.000882	0.003399	0.000473
52	05:47:029	0.000225	-32:04:011	0.00026	0.005797	0.000773	0.00291	0.000544
52	05:47:029	0.000212	-32:04:001	0.000407	0.0024	0.000837	0.001881	0.000508
53	05:47:028	0.000139	-32:04:023	0.000218	0.00204	0.000891	0.002339	0.000485
53	05:47:028	0.000134	-32:04:014	0.000322	0.003028	0.000849	0.00244	0.000512
54	05:47:018	0.000081	-32:06:025	0.000242	0.002201	0.000975	0.00282	0.000481
55	05:47:017	0.000046	-32:06:033	0.000015	0.020075	0.001324	0.01708	0.000539
55	05:47:017	0.00004	-32:06:036	0.000035	0.031999	0.000857	0.018402	0.000584
56	05:47:017	0.000049	-32:06:014	0.000107	0.003027	0.000975	0.004645	0.000467
57	05:47:016	0.000073	-32:06:016	0.000105	0.002834	0.00096	0.004104	0.000481
58	05:47:016	0.000333	-32:05:058	0.000037	0.006705	0.001324	0.004134	0.000548
59	05:46:055	0.000021	-31:51:011	0.000029	0.035426	0.001018	0.026574	0.000641
59	05:46:055	0.000083	-31:51:024	0.000133	0.002332	0.001073	0.003582	0.000525
61	05:46:055	0.000045	-31:50:051	0.000089	0.007061	0.001056	0.007733	0.000579
61	05:46:055	0.000306	-31:50:034	0.000063	0.011189	0.001348	0.005584	0.000606
63	05:46:051	0.000046	-31:28:017	0.000026	0.015875	0.001014	0.011396	0.000452
63	05:46:051	0.000093	-31:28:029	0.000251	0.001402	0.000803	0.001941	0.000392
64	05:46:051	0.000072	-31:27:056	0.000156	0.002626	0.000793	0.003189	0.000415
64	05:46:051	0.000088	-31:27:045	0.000219	0.001439	0.000804	0.002105	0.000384
65	05:46:044	0.000068	-32:00:010	0.000065	0.047179	0.001191	0.016095	0.000594
65	05:46:046	0.00006	-31:59:052	0.000061	0.070263	0.001178	0.020692	0.000594
66	05:46:047	0.000442	-32:00:035	0.000396	0.014413	0.000635	0.002949	0.000533
67	05:46:035	0.00006	-31:37:058	0.000056	0.020482	0.000742	0.010902	0.000516
68	05:46:035	0.000223	-31:37:038	0.000129	0.00285	0.000796	0.002599	0.000467
69	05:46:035	0.000295	-31:37:013	0.000311	0.008433	0.000599	0.00253	0.000474
70	05:46:028	0.000071	-31:57:034	0.000126	0.009374	0.000845	0.006274	0.000548
71	05:46:028	0.000113	-31:57:014	0.000208	0.002842	0.000903	0.00291	0.000509

Continued on next page

Table C.7: Positions of radio sources within 4MPc radius of the pointing centre of cluster RXCJ0547.6−3152

Source ID	RA	δ RA	DEC	δ DEC	total flux	δ total flux	Peak flux	δ Peak flux
72	05:46:012	0.000108	-32:08:049	0.000169	0.003914	0.000908	0.003625	0.000533
73	05:46:006	0.000041	-31:31:060	0.000114	0.002709	0.000597	0.003464	0.000301
74	05:46:001	0.000062	-32:04:015	0.000103	0.012572	0.001068	0.009013	0.000677
75	05:46:001	0.000132	-31:58:018	0.000204	0.004974	0.001062	0.003991	0.000652

Table C.8: Positions of radio sources within 4MPc radius of the pointing centre of cluster RXCJ0605.8−3518

Source ID	RA	δ RA	DEC	δ DEC	total flux	δ total flux	Peak flux	δ Peak flux
0	06:07:035	0.000302	-35:00:011	0.000374	0.014293	0.000917	0.004269	0.000724
1	06:07:032	0.000317	-34:59:050	0.000283	0.014655	0.000977	0.004639	0.000764
2	06:06:054	0.000166	-35:25:050	0.000145	0.015005	0.001826	0.010531	0.001154
3	06:06:043	0.000019	-35:05:037	0.000024	0.055379	0.001777	0.054145	0.001016
3	06:06:043	0.000025	-35:05:041	0.000031	0.04701	0.001764	0.043267	0.001029
5	06:06:038	0.000158	-35:06:011	0.000159	0.004911	0.001871	0.006256	0.000967
6	06:06:025	0.000025	-35:17:010	0.000031	0.055321	0.002345	0.054954	0.001328
8	06:05:053	0.000002	-35:18:002	0.000001	2.19345	0.006817	2.095798	0.002815
9	06:05:039	0.000022	-34:58:021	0.000026	0.043403	0.001367	0.039517	0.000798
10	06:05:033	0.000088	-35:33:002	0.000088	0.020485	0.001676	0.015632	0.001036
11	06:05:031	0.000124	-34:57:015	0.00018	0.005145	0.00133	0.005445	0.000733
12	06:05:005	0.000004	-35:22:012	0.000005	0.290425	0.001817	0.284329	0.001027
13	06:04:059	0.000029	-35:21:006	0.000052	0.049786	0.0018	0.038792	0.00108
14	06:04:043	0.000155	-35:16:010	0.000231	0.00547	0.001989	0.006241	0.001055
15	06:04:025	0.000173	-35:35:014	0.000299	0.019291	0.001144	0.006864	0.000869
16	06:04:012	0.000042	-35:41:005	0.000056	0.01937	0.001198	0.017767	0.00069
17	06:04:002	0.000212	-35:00:008	0.00028	0.008495	0.001328	0.005305	0.000869
18	06:03:058	0.000017	-35:32:011	0.000009	0.109991	0.001826	0.092257	0.000808

Table C.9: Positions of radio sources within 4MPc radius of the pointing centre of cluster RXCJ0821.8+0112

Source ID	RA	δ RA	DEC	δ DEC	total flux	δ total flux	Peak flux	δ Peak flux
0	08:24:022	0.000156	01:20:003	0.000089	0.002942	0.000286	0.00183	0.000187
1	08:24:017	0.000247	01:14:001	0.000101	0.001782	0.000231	0.0011	0.000148
2	08:24:003	0.000265	01:27:015	0.000129	0.001252	0.000293	0.001024	0.000171

Continued on next page

Table C.9: Positions of radio sources within 4MPc radius of the pointing centre of cluster RXCJ0821.8+0112

Source ID	RA	δ RA	DEC	δ DEC	total flux	δ total flux	Peak flux	δ Peak flux
3	08:23:056	0.00025	01:25:031	0.000131	0.000763	0.000241	0.00075	0.000131
4	08:23:045	0.000204	01:24:014	0.000069	0.002537	0.000288	0.00174	0.000175
6	08:23:025	0.000195	01:11:006	0.000106	0.001432	0.000299	0.001256	0.000171
8	08:23:016	0.000234	01:54:043	0.00024	0.000396	0.000113	0.000332	0.000066
9	08:23:015	0.000231	01:18:012	0.000129	0.001164	0.000391	0.001212	0.000209
10	08:23:014	0.000113	00:44:038	0.000068	0.002981	0.000322	0.002462	0.000187
11	08:23:014	0.000123	01:15:024	0.000063	0.004401	0.000484	0.003693	0.000276
12	08:23:012	0.00034	01:14:040	0.000158	0.005883	0.000482	0.002174	0.000362
13	08:23:009	0.000224	01:14:060	0.00008	0.016791	0.000755	0.007169	0.000521
15	08:23:002	0.000149	00:54:003	0.000097	0.001425	0.000323	0.001466	0.000175
16	08:22:052	0.000113	00:44:032	0.000085	0.00241	0.000329	0.002126	0.000189
17	08:22:050	0.0002	00:53:031	0.000172	0.000995	0.000336	0.001041	0.000179
18	08:22:046	0.000122	00:50:046	0.000073	0.001902	0.000294	0.001822	0.000162
19	08:22:045	0.000126	01:25:025	0.000065	0.002364	0.000306	0.002034	0.000177
20	08:22:044	0.000078	01:20:032	0.000041	0.004367	0.000359	0.003897	0.000202
21	08:22:042	0.000378	01:17:060	0.000101	0.003117	0.000264	0.001319	0.000186
22	08:22:035	0.000063	00:49:013	0.000037	0.007895	0.000516	0.006792	0.000297
23	08:22:031	0.000044	01:13:046	0.000024	0.009725	0.000509	0.009169	0.000282
24	08:22:027	0.000387	01:45:048	0.000402	0.001504	0.000142	0.000462	0.000111
25	08:22:026	0.000168	01:35:053	0.000119	0.001796	0.000324	0.001495	0.00019
26	08:22:026	0.000161	01:13:018	0.000091	0.001855	0.000386	0.001786	0.000214
27	08:22:025	0.000242	01:01:016	0.000156	0.003054	0.000474	0.001917	0.000307
28	08:22:024	0.000058	01:53:028	0.000035	0.016604	0.001059	0.013882	0.00063
29	08:22:023	0.000175	01:50:039	0.000179	0.001689	0.0004	0.001406	0.000239
31	08:22:011	0.000175	01:15:007	0.000131	0.001885	0.000459	0.001778	0.000258
32	08:22:009	0.000117	01:44:051	0.000067	0.004564	0.000365	0.002895	0.000239
33	08:22:008	0.000084	01:18:056	0.000057	0.011558	0.000709	0.007412	0.000462
34	08:22:007	0.000075	01:50:018	0.00005	0.005058	0.000448	0.00435	0.000263
35	08:22:006	0.000202	01:18:060	0.000171	0.006093	0.000581	0.002788	0.000418
36	08:22:003	0.000201	01:25:043	0.000093	0.001616	0.000378	0.001556	0.000206
37	08:22:002	0.00013	00:53:006	0.000075	0.001991	0.000365	0.002014	0.000198
38	08:22:001	0.000288	01:12:015	0.000152	0.00484	0.0007	0.002648	0.000476
39	08:22:001	0.000061	01:31:034	0.000037	0.004627	0.000369	0.00445	0.000205
40	08:21:060	0.000009	01:10:055	0.000013	0.049059	0.000722	0.03157	0.000309
41	08:21:060	0.000274	01:12:014	0.00018	0.004078	0.000778	0.002788	0.000484
42	08:21:053	0.000214	01:16:019	0.000104	0.002991	0.000695	0.00271	0.000391
44	08:21:041	0.000074	01:25:016	0.000044	0.003827	0.000387	0.003809	0.000211
45	08:21:040	0.000178	01:15:045	0.000089	0.002214	0.000445	0.001999	0.000254
46	08:21:036	0.000186	01:03:059	0.000155	0.001249	0.00041	0.001219	0.000236
47	08:21:035	0.000004	01:02:031	0.000006	0.211411	0.001574	0.142879	0.000664
49	08:21:035	0.000141	00:54:009	0.00022	0.008916	0.000817	0.004527	0.00056

Continued on next page

Table C.9: Positions of radio sources within 4MPc radius of the pointing centre of cluster RXCJ0821.8+0112

Source ID	RA	δ RA	DEC	δ DEC	total flux	δ total flux	Peak flux	δ Peak flux
50	08:21:034	0.000181	00:59:041	0.00022	0.007428	0.00113	0.004737	0.000724
51	08:21:034	0.000211	01:06:018	0.000176	0.004291	0.001033	0.003474	0.00062
52	08:21:034	0.000087	01:01:044	0.000083	0.005575	0.000752	0.005233	0.000426
53	08:21:032	0.000178	01:03:011	0.000101	0.002236	0.000514	0.002007	0.000301
54	08:21:030	0.000222	01:44:051	0.000156	0.00247	0.000551	0.001931	0.000335
55	08:21:021	0.000103	01:00:009	0.000072	0.003102	0.000389	0.002833	0.000219
56	08:21:012	0.000049	01:29:011	0.000029	0.007169	0.000463	0.006946	0.000255
57	08:21:012	0.000239	01:25:056	0.000192	0.001223	0.000286	0.000922	0.000175
58	08:21:004	0.000158	01:20:049	0.000077	0.002393	0.000369	0.002105	0.000207
59	08:21:001	0.000258	01:26:006	0.00014	0.001238	0.000297	0.00097	0.00018
60	08:20:056	0.000267	00:34:033	0.000231	0.002593	0.000261	0.001064	0.000192
61	08:20:051	0.00025	00:46:059	0.00018	0.001775	0.000352	0.001218	0.000223
62	08:20:049	0.00031	01:07:012	0.000422	0.004283	0.000254	0.001091	0.000205
63	08:20:040	0.000424	01:53:042	0.000519	0.004727	0.000124	0.000567	0.000112
64	08:20:040	0.000104	01:01:018	0.00006	0.030083	0.003058	0.024027	0.001841
64	08:20:039	0.000155	01:01:009	0.0001	0.072609	0.002428	0.022332	0.001907
65	08:20:038	0.00016	01:38:046	0.000121	0.0023	0.000495	0.002111	0.000282
66	08:20:034	0.000143	01:14:026	0.00009	0.002093	0.000366	0.001954	0.000204
67	08:20:033	0.000227	01:07:019	0.000118	0.001473	0.000382	0.00138	0.000211
68	08:20:024	0.000052	00:59:008	0.000037	0.007919	0.000366	0.00588	0.000224
69	08:20:010	0.000175	01:07:039	0.000094	0.002305	0.000351	0.001808	0.000209
71	08:19:055	0.000233	01:20:014	0.000124	0.004824	0.000473	0.002451	0.000326
72	08:19:055	0.000172	01:01:003	0.000115	0.001446	0.000292	0.001322	0.000163
73	08:19:055	0.000279	01:20:038	0.000242	0.003475	0.000543	0.001866	0.000371
74	08:19:052	0.000191	00:54:060	0.000117	0.001235	0.000329	0.001247	0.000178
75	08:19:039	0.000103	01:14:048	0.000072	0.005323	0.000332	0.003068	0.000223
76	08:19:037	0.000228	01:18:023	0.000341	0.004137	0.00039	0.001565	0.000291
77	08:19:011	0.000237	01:50:036	0.000185	0.001298	0.000299	0.001014	0.000179

Table C.10: Positions of radio sources within 4MPc radius of the pointing centre of cluster RXCJ0956.4−1004

Source ID	RA	δ RA	DEC	δ DEC	total flux	δ total flux	Peak flux	δ Peak flux
0	09:58:036	0.000505	-09:55:032	0.000236	0.00187	0.000091	0.000378	0.000077
1	09:58:035	0.000064	-10:11:022	0.000029	0.003078	0.000156	0.0021	0.000099
2	09:58:019	0.000079	-09:41:048	0.000036	0.001578	0.000185	0.001518	0.000105
3	09:58:011	0.000049	-09:42:014	0.000023	0.003328	0.000184	0.002737	0.000111
3	09:58:010	0.00014	-09:42:013	0.000174	0.00033	0.000193	0.000438	0.0001
4	09:58:007	0.000132	-09:53:030	0.000046	0.001519	0.000183	0.001212	0.000109

Continued on next page

Table C.10: Positions of radio sources within 4MPc radius of the pointing centre of cluster RXCJ0956.4−1004

Source ID	RA	δ RA	DEC	δ DEC	total flux	δ total flux	Peak flux	δ Peak flux
4	09:58:007	0.000131	-09:53:025	0.000051	0.001382	0.000185	0.001148	0.000109
5	09:57:051	0.000108	-09:54:034	0.000061	0.001007	0.000196	0.001047	0.000109
6	09:57:047	0.000189	-10:07:045	0.000212	0.000897	0.00017	0.000572	0.000112
7	09:57:033	0.000035	-10:24:010	0.000024	0.007568	0.000187	0.00442	0.000126
8	09:57:032	0.000123	-09:50:038	0.000094	0.000444	0.000218	0.000656	0.000108
9	09:57:030	0.000094	-09:40:025	0.000001	0.000575	0.000375	0.001987	0.000056
10	09:57:027	0.000032	-10:15:047	0.000018	0.010015	0.000202	0.005668	0.000137
10	09:57:029	0.000084	-10:15:022	0.000114	0.008265	0.000317	0.002637	0.000129
11	09:57:027	0.0001	-10:00:018	0.000047	0.001584	0.000223	0.001463	0.000129
12	09:57:023	0.000078	-09:53:035	0.000042	0.001737	0.000251	0.00181	0.00014
13	09:57:020	0.000171	-10:20:040	0.000099	0.000837	0.000194	0.00073	0.000115
14	09:57:020	0.000134	-09:46:007	0.000096	0.001095	0.000267	0.001132	0.000147
15	09:57:019	0.000003	-09:45:041	0.000007	0.025314	0.000379	0.023871	0.000156
15	09:57:018	0.000217	-09:45:039	0.000147	0.001	0.000262	0.000952	0.000138
17	09:57:018	0.000041	-10:01:053	0.000024	0.004045	0.00025	0.003684	0.000147
18	09:57:017	0.000165	-10:04:022	0.000116	0.001667	0.000226	0.001031	0.000151
19	09:57:016	0.000225	-10:10:036	0.00011	0.00243	0.000202	0.001099	0.000144
20	09:57:012	0.000186	-09:52:021	0.000107	0.001485	0.000256	0.001066	0.000161
21	09:57:009	0.000164	-09:53:016	0.000071	0.004796	0.000208	0.001839	0.000154
22	09:57:008	0.000253	-10:13:055	0.000321	0.002302	0.000204	0.000747	0.000159
23	09:57:006	0.000175	-10:24:053	0.000181	0.000921	0.000273	0.000825	0.000159
24	09:57:004	0.000006	-10:23:046	0.000005	0.069501	0.000642	0.035882	0.000162
25	09:57:005	0.000029	-10:03:019	0.000015	0.006525	0.000267	0.005913	0.000157
27	09:57:003	0.000113	-09:58:016	0.000077	0.001265	0.000247	0.001241	0.00014
27	09:57:003	0.000277	-09:58:016	0.000193	0.000617	0.000243	0.000527	0.000146
29	09:57:001	0.000169	-10:05:038	0.000084	0.000644	0.000276	0.000814	0.000143
30	09:56:054	0.000102	-10:02:018	0.000116	0.001469	0.000266	0.001252	0.00016
31	09:56:054	0.000011	-10:01:046	0.000024	0.008323	0.000384	0.007321	0.000158
32	09:56:052	0.000145	-10:00:030	0.000114	0.002718	0.000252	0.001463	0.000174
33	09:56:052	0.000122	-09:52:054	0.00008	0.001162	0.000272	0.001172	0.000155
34	09:56:051	0.000281	-10:10:022	0.000269	0.003459	0.000168	0.000791	0.000139
35	09:56:044	0.000028	-09:55:043	0.00002	0.010578	0.000284	0.007164	0.000184
36	09:56:042	0.000116	-10:22:047	0.000114	0.000771	0.000238	0.000837	0.000133
37	09:56:040	0.000246	-09:53:001	0.000084	0.001144	0.000313	0.00103	0.000177
38	09:56:040	0.000037	-10:10:022	0.000023	0.004337	0.000269	0.004136	0.000156
39	09:56:037	0.000143	-10:07:052	0.000085	0.000737	0.000308	0.000966	0.000158
40	09:56:035	0.00022	-09:53:029	0.000107	0.001546	0.000326	0.001157	0.000203
41	09:56:029	0.000292	-10:01:011	0.000172	0.002767	0.000399	0.001386	0.000279
41	09:56:030	0.000268	-10:01:003	0.000224	0.001637	0.000431	0.001075	0.000283
42	09:56:029	0.000181	-10:04:002	0.000183	0.00272	0.000422	0.001566	0.000287
43	09:56:028	0.000005	-09:57:019	0.000004	0.171757	0.00077	0.090567	0.000235

Continued on next page

Table C.10: Positions of radio sources within 4MPc radius of the pointing centre of cluster RXCJ0956.4−1004

Source ID	RA	δ RA	DEC	δ DEC	total flux	δ total flux	Peak flux	δ Peak flux
45	09:56:028	0.000131	-10:02:021	0.000181	0.003082	0.000631	0.001435	0.000266
46	09:56:027	0.00015	-10:04:036	0.000137	0.004979	0.000407	0.00235	0.00029
46	09:56:028	0.000198	-10:04:029	0.000174	0.002109	0.000446	0.00143	0.00029
47	09:56:028	0.000115	-10:04:006	0.000101	0.002121	0.000463	0.001967	0.000274
48	09:56:027	0.00013	-10:05:054	0.000217	0.004925	0.000653	0.001958	0.000284
48	09:56:026	0.000224	-10:06:004	0.000206	0.004519	0.0004	0.001918	0.00029
49	09:56:027	0.000127	-10:04:051	0.000128	0.006439	0.000633	0.002497	0.000274
50	09:56:027	0.000212	-09:57:043	0.000138	0.002611	0.000378	0.001495	0.000257
51	09:56:026	0.000205	-10:07:029	0.000167	0.004441	0.000426	0.002042	0.000305
51	09:56:027	0.000286	-10:07:021	0.00031	0.004104	0.000394	0.001364	0.000305
52	09:56:027	0.000237	-09:58:004	0.000222	0.003755	0.000342	0.001505	0.000252
54	09:56:026	0.000275	-10:08:051	0.000242	0.003401	0.000403	0.00147	0.000292
54	09:56:025	0.000365	-10:08:059	0.000306	0.003854	0.000368	0.0013	0.000281
57	09:56:023	0.000257	-10:15:028	0.000316	0.002351	0.000325	0.000994	0.000239
57	09:56:024	0.000288	-10:15:022	0.000246	0.002997	0.000313	0.001148	0.000235
58	09:56:024	0.000205	-10:06:052	0.000265	0.00275	0.000458	0.001539	0.000309
59	09:56:023	0.000007	-09:55:015	0.000013	0.018187	0.000505	0.016337	0.000207
60	09:56:020	0.00004	-09:43:057	0.000034	0.011591	0.000311	0.005018	0.000152
61	09:56:019	0.000111	-09:55:059	0.00008	0.002629	0.000324	0.001926	0.000205
62	09:56:019	0.000318	-09:43:026	0.000306	0.005051	0.000157	0.000868	0.000135
63	09:56:017	0.000183	-09:54:032	0.0001	0.001194	0.000325	0.001094	0.00019
65	09:56:014	0.000023	-09:53:002	0.00003	0.028647	0.000329	0.009333	0.000173
66	09:56:008	0.000152	-09:54:008	0.000072	0.001764	0.000284	0.001424	0.000171
67	09:56:005	0.000149	-09:48:006	0.000154	0.001458	0.000223	0.000924	0.000148
68	09:56:003	0.000093	-10:07:042	0.000039	0.003068	0.000286	0.002431	0.000173
69	09:56:003	0.000131	-10:02:035	0.000172	0.001041	0.000284	0.000929	0.000169
70	09:56:002	0.000314	-10:15:042	0.000268	0.0054	0.000193	0.000989	0.000165
71	09:56:00	0.000228	-10:06:017	0.000109	0.001025	0.000287	0.000877	0.000171
72	09:55:058	0.000064	-09:43:019	0.000038	0.002708	0.000248	0.002456	0.000144
73	09:55:057	0.000003	-09:59:003	0.000005	0.031677	0.000401	0.03067	0.000163
73	09:55:057	0.000116	-09:58:046	0.000105	0.000286	0.000325	0.000809	0.000092
74	09:55:058	0.000093	-10:06:022	0.000057	0.002197	0.00028	0.001874	0.000169
75	09:55:058	0.00018	-10:19:042	0.000078	0.000883	0.000281	0.000951	0.000153
76	09:55:058	0.000131	-09:59:020	0.000116	0.000826	0.000289	0.000998	0.00015
76	09:55:058	0.000164	-09:59:027	0.000297	0.000923	0.000271	0.000686	0.000169
77	09:55:058	0.000048	-09:48:041	0.000026	0.002661	0.000231	0.002766	0.000129
79	09:55:054	0.000016	-09:54:00	0.000016	0.013694	0.000349	0.009511	0.000147
80	09:55:054	0.000119	-09:53:022	0.000081	0.004509	0.000338	0.001637	0.000147
81	09:55:052	0.00015	-10:26:032	0.00011	0.001194	0.00026	0.001032	0.000155
82	09:55:050	0.000171	-09:58:011	0.00007	0.002562	0.000239	0.001464	0.00016
83	09:55:042	0.000172	-10:14:054	0.000083	0.005632	0.000184	0.001675	0.000145

Continued on next page

Table C.10: Positions of radio sources within 4MPc radius of the pointing centre of cluster RXCJ0956.4−1004

Source ID	RA	δ RA	DEC	δ DEC	total flux	δ total flux	Peak flux	δ Peak flux
83	09:55:042	0.000131	-10:15:002	0.000082	0.00194	0.000236	0.001346	0.000151
84	09:55:041	0.000491	-10:13:057	0.000416	0.012681	0.000083	0.000598	0.000079
85	09:55:039	0.000003	-09:41:028	0.00001	0.077354	0.000541	0.044845	0.000166
85	09:55:038	0.000095	-09:41:011	0.000067	0.000684	0.000304	0.001245	0.000126
86	09:55:039	0.000147	-10:10:021	0.000088	0.006297	0.000183	0.001806	0.000146
86	09:55:038	0.000132	-10:10:017	0.000144	0.003444	0.000205	0.001336	0.000154
86	09:55:040	0.000149	-10:10:028	0.000099	0.001722	0.000233	0.001146	0.000152
87	09:55:039	0.000141	-09:41:014	0.000101	0.000959	0.000289	0.001012	0.000162
88	09:55:038	0.000096	-10:09:034	0.000113	0.002582	0.000232	0.001491	0.000158
89	09:55:037	0.000371	-10:09:050	0.000346	0.00428	0.000151	0.000707	0.000131
90	09:55:038	0.000164	-09:41:051	0.000106	0.001957	0.000265	0.001259	0.000174
91	09:55:035	0.000149	-10:01:054	0.000057	0.000867	0.000239	0.000983	0.000126
92	09:55:033	0.000217	-10:10:035	0.000142	0.001835	0.00022	0.000932	0.000154
93	09:55:033	0.000075	-10:10:004	0.000049	0.001893	0.00025	0.001814	0.000145
94	09:55:025	0.000173	-10:11:030	0.000105	0.000916	0.000242	0.000853	0.00014

Table C.11: Positions of radio sources within 4MPc radius of the pointing centre of cluster RXCJ0958.3−1103

Source ID	RA	δ RA	DEC	δ DEC	total flux	δ total flux	Peak flux	δ Peak flux
0	09:59:048	0.000081	-11:00:029	0.000057	0.001283	0.000194	0.001266	0.00011
1	09:59:044	0.000316	-10:47:034	0.000543	0.014211	0.00008	0.000641	0.000077
2	09:59:037	0.000074	-11:06:009	0.000057	0.002541	0.000216	0.001873	0.000135
3	09:59:035	0.000272	-10:46:026	0.000135	0.001554	0.000228	0.000836	0.000155
4	09:59:030	0.000047	-11:14:031	0.000038	0.002771	0.000227	0.00256	0.000132
5	09:59:029	0.000175	-11:06:046	0.000136	0.000597	0.000226	0.000651	0.000121
6	09:59:026	0.000061	-10:55:028	0.000058	0.002795	0.00025	0.002211	0.000154
6	09:59:026	0.000179	-10:55:028	0.000266	0.000531	0.000256	0.000505	0.000149
7	09:59:024	0.00004	-10:43:036	0.000031	0.002631	0.000226	0.002709	0.000127
8	09:59:022	0.000137	-11:13:030	0.000104	0.000911	0.000213	0.000865	0.000122
9	09:59:022	0.000132	-10:50:034	0.000112	0.00078	0.00026	0.000871	0.000141
10	09:59:020	0.000038	-11:07:036	0.00003	0.002693	0.000222	0.002872	0.000122
11	09:59:019	0.000134	-11:04:001	0.000143	0.000822	0.000236	0.000758	0.00014
12	09:59:016	0.00003	-10:41:007	0.000024	0.0042	0.000256	0.004138	0.000147
13	09:59:012	0.000085	-10:47:058	0.00008	0.002392	0.00026	0.001877	0.000157
14	09:59:007	0.000036	-10:42:039	0.000028	0.004587	0.00027	0.004064	0.00016
15	09:59:008	0.000134	-10:46:010	0.000118	0.001145	0.000281	0.001064	0.000163
16	09:59:006	0.000107	-11:02:030	0.00012	0.0025	0.000278	0.001556	0.000184
16	09:59:005	0.000149	-11:02:025	0.000108	0.003113	0.000263	0.00151	0.000187

Continued on next page

Table C.11: Positions of radio sources within 4MPc radius of the pointing centre of cluster RXCJ0958.3−1103

Source ID	RA	δ RA	DEC	δ DEC	total flux	δ total flux	Peak flux	δ Peak flux
17	09:59:004	0.000515	-11:02:056	0.000248	0.0098	0.000134	0.000841	0.000124
18	09:59:004	0.000321	-10:47:019	0.000138	0.007487	0.000173	0.00124	0.000149
19	09:58:060	0.000064	-10:47:056	0.000049	0.001938	0.000287	0.00209	0.000159
20	09:58:056	0.000074	-10:42:055	0.000057	0.001563	0.000295	0.001785	0.000159
21	09:58:055	0.000126	-10:57:008	0.000086	0.001133	0.000305	0.001208	0.000168
22	09:58:053	0.000178	-10:52:048	0.000146	0.001334	0.000291	0.001005	0.000181
23	09:58:042	0.000053	-11:23:020	0.000046	0.002843	0.000236	0.002417	0.000142
24	09:58:040	0.000111	-11:10:059	0.000115	0.001642	0.000299	0.001362	0.000181
25	09:58:040	0.000038	-11:04:057	0.000032	0.003915	0.000329	0.004077	0.000184
27	09:58:034	0.000062	-11:02:013	0.000046	0.016728	0.000347	0.006572	0.000256
27	09:58:034	0.000278	-11:01:051	0.00013	0.010402	0.000502	0.003839	0.000252
28	09:58:034	0.000081	-11:01:023	0.000156	0.002459	0.000437	0.00198	0.000264
29	09:58:031	0.000133	-10:57:031	0.000138	0.001672	0.00042	0.001564	0.00024
30	09:58:030	0.000041	-11:05:054	0.000028	0.010587	0.000429	0.00721	0.000277
31	09:58:030	0.000193	-10:56:057	0.000245	0.002742	0.000368	0.001272	0.000264
33	09:58:028	0.00011	-11:13:020	0.000095	0.001801	0.000362	0.001676	0.00021
34	09:58:027	0.000014	-10:51:020	0.000013	0.014691	0.0004	0.014073	0.00023
35	09:58:025	0.000188	-11:01:034	0.000212	0.010037	0.000348	0.002413	0.000285
36	09:58:025	0.000116	-11:02:012	0.000312	0.004077	0.000434	0.001781	0.000311
37	09:58:025	0.000189	-11:00:053	0.000186	0.003182	0.000441	0.001688	0.000306
38	09:58:024	0.000067	-11:02:046	0.000126	0.002611	0.000532	0.002476	0.000307
39	09:58:023	0.000143	-11:02:031	0.000176	0.004369	0.000462	0.00219	0.000324
40	09:58:023	0.000115	-11:04:015	0.000128	0.004241	0.000508	0.00257	0.000342
41	09:58:023	0.00006	-11:03:036	0.000142	0.004664	0.000505	0.003118	0.000322
42	09:58:023	0.000068	-11:03:017	0.000125	0.002344	0.000539	0.002355	0.000306
42	09:58:023	0.000188	-11:03:009	0.000161	0.001524	0.000534	0.001371	0.000319
43	09:58:022	0.000004	-11:03:035	0.000003	0.13084	0.000892	0.10153	0.000309
43	09:58:021	0.000045	-11:03:021	0.000035	0.007608	0.000526	0.007124	0.000294
44	09:58:022	0.00012	-11:03:022	0.000094	0.001206	0.000547	0.001638	0.000282
45	09:58:022	0.000087	-11:04:027	0.000128	0.003479	0.000524	0.002595	0.00033
46	09:58:022	0.000103	-11:03:060	0.000282	0.003632	0.000471	0.001874	0.000323
47	09:58:021	0.000163	-11:04:025	0.000252	0.00248	0.000501	0.001625	0.000321
48	09:58:021	0.000183	-11:03:059	0.000061	0.011295	0.000656	0.003192	0.000313
49	09:58:021	0.000092	-10:51:005	0.000137	0.002323	0.000351	0.001771	0.000216
50	09:58:019	0.000116	-11:06:036	0.000129	0.001273	0.000543	0.001591	0.000286
51	09:58:018	0.000179	-11:10:049	0.000366	0.003821	0.000378	0.001373	0.000286
52	09:58:015	0.000036	-11:09:020	0.000034	0.00623	0.000494	0.006192	0.000282
53	09:58:015	0.000036	-11:00:048	0.000034	0.00475	0.000364	0.004696	0.000207
54	09:58:013	0.000059	-11:08:020	0.00006	0.003127	0.000486	0.003338	0.000271
55	09:58:009	0.000115	-10:43:022	0.000123	0.000815	0.000228	0.000812	0.000131
56	09:57:059	0.000048	-10:43:002	0.000025	0.008266	0.000203	0.004151	0.000142

Continued on next page

Table C.11: Positions of radio sources within 4MPc radius of the pointing centre of cluster RXCJ0958.3−1103

Source ID	RA	δ RA	DEC	δ DEC	total flux	δ total flux	Peak flux	δ Peak flux
56	09:57:058	0.000049	-10:43:003	0.000027	0.005772	0.000214	0.003573	0.000142
57	09:57:050	0.000111	-10:53:043	0.000135	0.00085	0.000244	0.000877	0.000136
58	09:57:049	0.000028	-10:48:003	0.000025	0.003654	0.000217	0.003639	0.000123
59	09:57:048	0.000135	-11:15:019	0.00013	0.000791	0.000262	0.000848	0.000144
60	09:57:043	0.000023	-10:44:018	0.000013	0.008515	0.000206	0.006362	0.000128
61	09:57:043	0.000097	-10:57:031	0.000076	0.002286	0.000251	0.001616	0.000161
61	09:57:042	0.000339	-10:57:019	0.000361	0.002474	0.000188	0.00065	0.000152
62	09:57:042	0.000057	-11:19:007	0.00005	0.002318	0.000266	0.002217	0.000154
63	09:57:042	0.00036	-10:57:045	0.000497	0.008701	0.000112	0.000652	0.000104
64	09:57:041	0.000006	-11:04:015	0.000007	0.026998	0.000288	0.02197	0.000177
65	09:57:040	0.000044	-10:55:023	0.000039	0.002607	0.000245	0.00267	0.000137
66	09:57:039	0.000052	-11:20:041	0.000049	0.003396	0.000238	0.002585	0.000149
67	09:57:038	0.000492	-10:47:059	0.00036	0.012751	0.000082	0.000608	0.000079
68	09:57:037	0.000227	-10:48:021	0.000285	0.007381	0.000273	0.000643	0.000139
69	09:57:036	0.000378	-10:46:060	0.000333	0.003482	0.000141	0.000593	0.000122
70	09:57:035	0.00004	-11:17:026	0.000037	0.006855	0.00024	0.003994	0.000163
71	09:57:027	0.000014	-11:12:052	0.000013	0.031044	0.000382	0.018209	0.00017
72	09:57:027	0.000016	-11:14:010	0.000014	0.00902	0.000289	0.008777	0.000166
73	09:57:025	0.000085	-11:12:019	0.000101	0.004817	0.000241	0.002456	0.000164
73	09:57:025	0.000118	-11:12:030	0.000091	0.006299	0.000226	0.002156	0.000173
74	09:57:026	0.000228	-11:13:016	0.000231	0.00285	0.000227	0.000956	0.000176
74	09:57:026	0.000376	-11:13:007	0.000193	0.000867	0.000268	0.000569	0.000174
75	09:57:025	0.000407	-11:12:043	0.000367	0.006717	0.000146	0.000784	0.000132
76	09:57:024	0.0001	-11:23:024	0.000116	0.001148	0.000225	0.000993	0.000135
77	09:57:024	0.000046	-10:53:042	0.000042	0.001655	0.000207	0.001865	0.000113
78	09:57:019	0.000086	-10:46:005	0.000093	0.001258	0.000192	0.001075	0.000115
79	09:57:016	0.000015	-10:59:008	0.000022	0.010117	0.000199	0.00644	0.000131
80	09:57:015	0.000136	-11:17:022	0.000104	0.001133	0.000229	0.000949	0.000139
81	09:57:013	0.000151	-11:03:043	0.000165	0.00323	0.000205	0.00117	0.000156
82	09:57:007	0.000126	-10:50:035	0.000162	0.001982	0.000174	0.001013	0.00012
83	09:57:00	0.00005	-10:54:042	0.000038	0.001876	0.000183	0.001865	0.000103
84	09:56:053	0.000041	-10:40:036	0.000035	0.002007	0.000155	0.001925	0.000089

Table C.12: Positions of radio sources within 4MPc radius of the pointing centre of cluster RXCJ1044.5−0704

Source ID	RA	δ RA	DEC	δ DEC	total flux	δ total flux	Peak flux	δ Peak flux
0	10:46:012	0.000272	-07:11:013	0.000159	0.001845	0.0002	0.001167	0.000122
1	10:46:001	0.00008	-07:05:037	0.000051	0.005733	0.00023	0.003941	0.000138

Continued on next page

Table C.12: Positions of radio sources within 4MPc radius of the pointing centre of cluster RXCJ1044.5−0704

Source ID	RA	δ RA	DEC	δ DEC	total flux	δ total flux	Peak flux	δ Peak flux
2	10:46:00	0.000006	-06:50:011	0.000011	0.028076	0.00041	0.029115	0.000164
3	10:46:00	0.00023	-06:49:056	0.000117	0.001071	0.000295	0.001364	0.000121
3	10:46:001	0.000142	-06:49:054	0.000084	0.000967	0.000328	0.00179	0.000103
5	10:45:060	0.000125	-06:50:045	0.000069	0.002265	0.000284	0.002649	0.00012
5	10:46:00	0.000192	-06:50:044	0.000123	0.00158	0.000277	0.00169	0.000125
6	10:45:059	0.000192	-06:50:036	0.000137	0.001404	0.000284	0.001614	0.000122
6	10:45:060	0.000201	-06:50:035	0.000126	0.001509	0.00028	0.00167	0.000121
9	10:45:051	0.00008	-07:11:006	0.000064	0.013708	0.000221	0.005243	0.000162
9	10:45:051	0.000042	-07:11:011	0.000021	0.011929	0.000267	0.009304	0.000147
9	10:45:051	0.000037	-07:11:027	0.000193	0.010447	0.000315	0.003159	0.00017
9	10:45:049	0.000194	-07:11:018	0.000104	0.002639	0.000265	0.002076	0.000143
9	10:45:050	0.000011	-07:10:054	0.000017	0.037708	0.000444	0.02328	0.00017
10	10:45:051	0.000391	-07:10:037	0.000126	0.002275	0.000236	0.001341	0.000142
12	10:45:047	0.000069	-07:12:046	0.000037	0.005663	0.000281	0.00536	0.000137
17	10:45:028	0.000025	-06:58:019	0.000015	0.016473	0.000253	0.013372	0.000139
18	10:45:027	0.000254	-06:58:044	0.000133	0.002557	0.000228	0.001597	0.000138
20	10:45:014	0.000072	-07:14:007	0.000069	0.018465	0.000341	0.006031	0.000167
20	10:45:013	0.000089	-07:15:012	0.000122	0.007374	0.000352	0.003398	0.000167
20	10:45:013	0.000216	-07:14:027	0.00011	0.004146	0.000224	0.002377	0.000133
20	10:45:014	0.000183	-07:15:001	0.000098	0.001775	0.000284	0.001852	0.000134
20	10:45:014	0.000321	-07:14:040	0.000135	0.001795	0.000254	0.001428	0.000129
20	10:45:013	0.000471	-07:14:039	0.000234	0.003061	0.000193	0.00129	0.000127
20	10:45:015	0.000263	-07:14:036	0.000183	0.000451	0.000305	0.000707	0.000132
22	10:45:012	0.000192	-07:00:053	0.000117	0.002127	0.000233	0.00175	0.000122
24	10:45:006	0.000139	-07:14:005	0.000075	0.003525	0.000252	0.002828	0.000133
25	10:45:003	0.000172	-07:12:005	0.000085	0.001914	0.000272	0.00199	0.000126
27	10:44:055	0.000086	-06:58:029	0.000043	0.005901	0.00028	0.004806	0.000149
27	10:44:054	0.000409	-06:58:033	0.000182	0.004497	0.000199	0.001615	0.000141
28	10:44:054	0.000031	-06:58:010	0.000017	0.01387	0.000288	0.012883	0.00014
31	10:44:052	0.000045	-06:48:050	0.000025	0.009122	0.000245	0.007762	0.000127
33	10:44:047	0.000093	-07:07:010	0.000053	0.006853	0.00033	0.00506	0.000189
42	10:44:034	0.00037	-07:04:044	0.000265	0.00184	0.000409	0.001546	0.000209
42	10:44:035	0.000426	-07:04:030	0.000406	0.003503	0.000318	0.001699	0.000198
43	10:44:035	0.000316	-07:04:005	0.000267	0.004403	0.000323	0.002323	0.000194
44	10:44:033	0.000016	-07:04:006	0.00003	0.035405	0.000664	0.025497	0.000256
44	10:44:032	0.000336	-07:04:033	0.000168	0.004329	0.000359	0.001862	0.000258
44	10:44:032	0.000181	-07:04:018	0.00012	0.002092	0.000462	0.002715	0.000178
45	10:44:034	0.000133	-07:03:050	0.000086	0.004112	0.000423	0.004069	0.000197
47	10:44:033	0.000367	-07:02:040	0.000306	0.003643	0.000323	0.001856	0.000202
48	10:44:030	0.000026	-07:19:029	0.000048	0.008652	0.00038	0.007652	0.000163
50	10:44:029	0.000035	-07:11:024	0.000072	0.009734	0.000424	0.007234	0.000204

Continued on next page

Table C.12: Positions of radio sources within 4MPc radius of the pointing centre of cluster RXCJ1044.5−0704

Source ID	RA	δ RA	DEC	δ DEC	total flux	δ total flux	Peak flux	δ Peak flux
51	10:44:024	0.000076	-07:24:056	0.000041	0.004951	0.000244	0.004591	0.000117
52	10:44:023	0.000353	-07:18:025	0.000151	0.002262	0.000213	0.001036	0.00015
53	10:44:021	0.000007	-06:59:016	0.000012	0.045561	0.000514	0.04026	0.000195
53	10:44:020	0.000099	-06:59:027	0.000062	0.002051	0.000386	0.003513	0.000117
54	10:44:021	0.000189	-06:58:059	0.00011	0.000916	0.000406	0.001778	0.000112
56	10:44:021	0.000194	-06:59:050	0.000112	0.000943	0.000384	0.001657	0.000122
56	10:44:020	0.000188	-06:59:052	0.000089	0.001332	0.000371	0.002045	0.000124
57	10:44:019	0.000256	-06:59:041	0.000202	0.001552	0.000314	0.001446	0.000156
57	10:44:020	0.000122	-06:59:042	0.000076	0.002596	0.000336	0.003069	0.000141
58	10:44:009	0.00005	-06:43:017	0.000027	0.009042	0.000262	0.007504	0.000138
60	10:43:059	0.000197	-06:55:002	0.000073	0.006597	0.000223	0.002983	0.000148
61	10:43:058	0.000172	-07:31:049	0.000092	0.004801	0.000212	0.002702	0.000128
63	10:43:058	0.000151	-06:56:050	0.000092	0.001102	0.000312	0.001497	0.000144
64	10:43:057	0.000008	-06:56:017	0.000015	0.049701	0.000538	0.031901	0.000174
65	10:43:057	0.000324	-06:55:030	0.000179	0.008438	0.00017	0.002198	0.000131
67	10:43:057	0.000206	-06:56:040	0.000125	0.002417	0.000268	0.002101	0.000127
67	10:43:056	0.000218	-06:56:044	0.000151	0.002427	0.000262	0.001814	0.000143
71	10:43:039	0.000073	-07:21:025	0.000041	0.006248	0.000245	0.005203	0.000125
72	10:43:038	0.000326	-07:16:014	0.000219	0.001703	0.000218	0.001133	0.000125
73	10:43:036	0.000086	-07:22:016	0.000058	0.00698	0.000236	0.004224	0.000148
73	10:43:037	0.000129	-07:22:005	0.000082	0.004327	0.00024	0.002867	0.000143
75	10:43:032	0.000023	-07:00:021	0.000054	0.035326	0.000539	0.016121	0.000158
78	10:43:030	0.000244	-07:00:046	0.00014	0.000571	0.000311	0.000997	0.000105
79	10:43:026	0.000016	-07:24:044	0.000031	0.0191	0.000348	0.014566	0.000163
81	10:43:027	0.000169	-06:59:046	0.000092	0.002103	0.000258	0.002026	0.000124
83	10:43:025	0.000362	-07:25:012	0.000132	0.003326	0.000206	0.001429	0.000142
85	10:43:019	0.000236	-06:58:054	0.000138	0.00233	0.000218	0.00153	0.000129
87	10:43:014	0.000017	-07:16:045	0.00003	0.013537	0.000336	0.012207	0.00015
90	10:43:006	0.000016	-07:09:006	0.000032	0.021295	0.00032	0.01352	0.000148
93	10:43:005	0.000322	-07:09:033	0.00016	0.002896	0.000193	0.001411	0.000125
94	10:42:056	0.000203	-07:22:019	0.0001	0.001407	0.000218	0.001445	0.000099
95	10:42:055	0.000186	-07:25:032	0.000105	0.001372	0.000232	0.001542	0.000099
96	10:42:050	0.00015	-06:52:018	0.000081	0.002776	0.000206	0.002179	0.000109
97	10:42:048	0.00034	-06:47:044	0.000225	0.002042	0.000144	0.000901	0.000099
98	10:42:042	0.000084	-06:55:059	0.00005	0.005582	0.000219	0.003501	0.000139

Table C.13: Positions of radio sources within 4MPc radius of the pointing centre of cluster RXCJJ1141.4−1216

Source ID	RA	δ RA	DEC	δ DEC	total flux	δ total flux	Peak flux	δ Peak flux
0	11:43:021	0.000144	-11:50:019	0.00009	0.003263	0.000605	0.002711	0.000368
1	11:43:017	0.000089	-12:36:004	0.000069	0.003661	0.000518	0.003323	0.000305
3	11:43:001	0.000251	-11:48:037	0.000302	0.006991	0.00068	0.002489	0.000518
4	11:42:051	0.000079	-12:37:010	0.000064	0.00431	0.000409	0.003242	0.000258
5	11:42:049	0.000194	-11:44:034	0.00023	0.004891	0.000981	0.003071	0.00065
6	11:42:041	0.000139	-11:46:012	0.000285	0.009376	0.001107	0.004431	0.000785
7	11:42:039	0.000248	-11:44:018	0.000173	0.005448	0.001254	0.00394	0.000782
8	11:42:038	0.000174	-11:45:007	0.000057	0.006054	0.001321	0.005803	0.000735
9	11:42:036	0.000177	-11:44:029	0.000088	0.009537	0.001243	0.006276	0.000802
10	11:42:036	0.000254	-11:48:001	0.000086	0.006476	0.001012	0.004179	0.000648
11	11:42:036	0.000096	-11:44:014	0.00006	0.010672	0.001307	0.00922	0.000772
12	11:42:036	0.000291	-11:43:041	0.000041	0.015784	0.000989	0.007145	0.000664
15	11:42:034	0.000232	-11:43:044	0.000135	0.005257	0.001271	0.003961	0.000795
16	11:42:034	0.000162	-12:12:056	0.00007	0.001647	0.000579	0.002022	0.000297
17	11:42:034	0.000333	-11:46:058	0.000123	0.005674	0.001078	0.003554	0.000692
18	11:42:033	0.000161	-11:44:042	0.0001	0.004485	0.001301	0.005082	0.000665
18	11:42:032	0.000343	-11:44:042	0.000176	0.004264	0.001207	0.003225	0.000723
18	11:42:033	0.000382	-11:44:041	0.000162	0.005312	0.001157	0.003176	0.000762
19	11:42:032	0.000102	-11:43:051	0.000064	0.007239	0.001287	0.007528	0.000707
20	11:42:032	0.000253	-12:40:005	0.000094	0.001868	0.00043	0.001471	0.000259
22	11:42:030	0.000149	-11:44:048	0.000115	0.003336	0.001235	0.003984	0.000649
23	11:42:027	0.000206	-11:43:031	0.000196	0.004699	0.001076	0.003628	0.000648
24	11:42:025	0.000184	-12:28:038	0.000133	0.001441	0.000472	0.001431	0.000268
25	11:42:024	0.000271	-11:45:008	0.000328	0.005718	0.000835	0.002762	0.000581
26	11:42:023	0.000203	-12:12:051	0.000206	0.002505	0.000568	0.001709	0.000368
27	11:42:022	0.000177	-11:45:046	0.000206	0.003789	0.000915	0.00282	0.000576
28	11:42:021	0.000218	-11:44:023	0.000193	0.004128	0.000858	0.002808	0.000549
29	11:42:020	0.000159	-12:46:048	0.000139	0.00392	0.000374	0.001944	0.000264
30	11:42:019	0.000151	-12:08:033	0.000084	0.003729	0.000619	0.002952	0.000379
31	11:42:019	0.000081	-12:12:033	0.000047	0.02229	0.000795	0.00808	0.000355
32	11:42:018	0.000041	-11:52:004	0.000027	0.035945	0.001059	0.018239	0.000493
33	11:42:018	0.000256	-12:12:056	0.000211	0.00957	0.000435	0.002525	0.00035
34	11:42:017	0.000095	-12:03:040	0.000058	0.005838	0.000674	0.004731	0.000413
35	11:42:016	0.000147	-11:43:035	0.000286	0.00478	0.00075	0.002611	0.000513
36	11:42:008	0.000032	-12:31:006	0.000023	0.008398	0.000546	0.008765	0.000308
36	11:42:008	0.000208	-12:31:014	0.000092	0.000937	0.000557	0.001303	0.000276
37	11:41:060	0.000301	-12:15:049	0.000102	0.00347	0.000637	0.002223	0.000409
38	11:41:059	0.000043	-12:15:016	0.000033	0.011776	0.000683	0.00966	0.000418
39	11:41:059	0.000155	-12:15:001	0.000089	0.001541	0.000714	0.002083	0.000363
40	11:41:058	0.000549	-11:54:031	0.000252	0.015078	0.000389	0.001976	0.000346
41	11:41:057	0.00008	-12:00:021	0.000038	0.007248	0.000624	0.005904	0.000376

Continued on next page

Table C.13: Positions of radio sources within 4MPc radius of the pointing centre of cluster RXCJJ1141.4−1216

Source ID	RA	δ RA	DEC	δ DEC	total flux	δ total flux	Peak flux	δ Peak flux
42	11:41:057	0.000207	-12:00:005	0.000092	0.00348	0.000612	0.002509	0.000384
43	11:41:051	0.000142	-11:47:049	0.000302	0.003723	0.000612	0.002072	0.000415
44	11:41:047	0.000215	-11:58:018	0.000203	0.003595	0.00066	0.002161	0.000443
45	11:41:041	0.000039	-11:49:043	0.000034	0.008627	0.00067	0.008418	0.000389
46	11:41:037	0.000179	-12:43:003	0.000168	0.004617	0.000374	0.002014	0.000271
47	11:41:035	0.000123	-11:48:057	0.000058	0.003594	0.000644	0.003414	0.00037
47	11:41:035	0.000291	-11:49:003	0.000179	0.001961	0.000626	0.001514	0.000388
48	11:41:035	0.000183	-11:48:038	0.000242	0.003175	0.000601	0.001899	0.000405
49	11:41:032	0.000105	-12:27:009	0.000076	0.003798	0.000751	0.003788	0.00043
50	11:41:027	0.000102	-12:17:025	0.000113	0.004966	0.001234	0.005015	0.00071
51	11:41:026	0.000181	-12:17:035	0.000169	0.004861	0.001197	0.003821	0.000742
52	11:41:025	0.000298	-12:16:005	0.000067	0.011959	0.000921	0.006587	0.000549
53	11:41:025	0.000082	-12:16:018	0.000057	0.007274	0.00126	0.008842	0.000623
53	11:41:024	0.000071	-12:16:024	0.000028	0.010658	0.001241	0.011517	0.000665
55	11:41:024	0.00002	-12:16:058	0.00009	0.023147	0.001758	0.014192	0.000716
55	11:41:023	0.000134	-12:17:003	0.000054	0.017572	0.001062	0.010403	0.000676
56	11:41:024	0.000005	-12:16:039	0.000005	0.193066	0.002504	0.158534	0.000717
57	11:41:024	0.000045	-12:15:039	0.00014	0.006434	0.00172	0.004504	0.000694
58	11:41:024	0.000068	-11:47:040	0.000082	0.010081	0.000572	0.00553	0.000394
59	11:41:024	0.000198	-12:15:003	0.00008	0.003051	0.00117	0.003525	0.000618
61	11:41:023	0.000079	-12:15:059	0.000109	0.00429	0.001224	0.005057	0.000664
61	11:41:023	0.000101	-12:15:054	0.0001	0.001211	0.001207	0.002769	0.000496
61	11:41:024	0.000247	-12:15:048	0.00019	0.003144	0.001193	0.002818	0.000704
62	11:41:023	0.0001	-12:16:010	0.00005	0.006974	0.001229	0.007568	0.000662
63	11:41:023	0.000179	-12:17:030	0.000097	0.004339	0.001218	0.004429	0.000667
64	11:41:022	0.000101	-12:15:021	0.000077	0.003738	0.001191	0.005061	0.000599
65	11:41:022	0.000347	-12:22:015	0.000172	0.006211	0.000754	0.002674	0.000547
66	11:41:022	0.000169	-12:17:054	0.000127	0.004851	0.00116	0.004385	0.000669
66	11:41:021	0.00008	-12:17:058	0.000198	0.000935	0.001201	0.002028	0.000493
67	11:41:022	0.000193	-12:18:041	0.000117	0.005204	0.001084	0.004463	0.000621
68	11:41:018	0.000025	-12:43:028	0.000019	0.010893	0.000458	0.010177	0.000268
69	11:41:019	0.000156	-12:43:011	0.000071	0.001125	0.000478	0.001589	0.000229
70	11:41:018	0.000092	-12:08:034	0.000069	0.00539	0.000863	0.005211	0.000495
71	11:41:018	0.000137	-12:43:012	0.000068	0.001366	0.000472	0.001731	0.000244
73	11:41:015	0.000057	-11:45:001	0.000047	0.007365	0.000548	0.005826	0.000339
74	11:41:007	0.000128	-11:43:051	0.000108	0.002758	0.000534	0.002356	0.000322
75	11:40:060	0.000087	-12:23:059	0.000072	0.012847	0.001177	0.007267	0.000487
75	11:40:058	0.00014	-12:23:004	0.00013	0.072928	0.000406	0.00742	0.00037
75	11:40:060	0.000076	-12:24:018	0.00023	0.029141	0.000511	0.005844	0.000429
75	11:41:00	0.000221	-12:24:036	0.000192	0.019624	0.000929	0.00484	0.000487
75	11:40:059	0.000142	-12:23:033	0.000363	0.043957	0.000377	0.004836	0.00034

Continued on next page

Table C.13: Positions of radio sources within 4MPc radius of the pointing centre of cluster RXCJJ1141.4−1216

Source ID	RA	δ RA	DEC	δ DEC	total flux	δ total flux	Peak flux	δ Peak flux
75	11:40:060	0.000377	-12:25:001	0.000497	0.00584	0.000625	0.001778	0.00049
75	11:41:00	0.000124	-12:23:054	0.000302	0.001311	0.000868	0.001733	0.000414
77	11:40:058	0.000028	-12:03:021	0.000033	0.049628	0.001095	0.024485	0.000478
77	11:40:059	0.000023	-12:03:009	0.000027	0.057939	0.001084	0.027206	0.000478
77	11:40:058	0.000175	-12:03:032	0.000089	0.002995	0.000827	0.003113	0.000448
78	11:40:059	0.000052	-12:15:013	0.000034	0.010313	0.000826	0.009518	0.000482
79	11:40:056	0.000023	-12:15:023	0.000017	0.017297	0.000808	0.018146	0.000453
80	11:40:056	0.000149	-12:15:007	0.00008	0.001756	0.000819	0.002484	0.000406
81	11:40:049	0.000051	-12:30:059	0.000041	0.008616	0.000616	0.007026	0.000379
82	11:40:047	0.000021	-11:52:031	0.000015	0.024534	0.000657	0.019901	0.000402
83	11:40:046	0.000213	-11:52:015	0.000091	0.002096	0.000665	0.002072	0.000374
84	11:40:046	0.000058	-11:58:013	0.000044	0.007376	0.000634	0.006446	0.000378
85	11:40:038	0.000162	-12:17:026	0.000122	0.001922	0.000653	0.002037	0.000364
86	11:40:026	0.000166	-12:29:049	0.000136	0.00174	0.000486	0.001629	0.000282
88	11:40:001	0.000066	-12:46:052	0.000161	0.010932	0.000407	0.003859	0.000308
88	11:40:001	0.000121	-12:46:041	0.000095	0.005366	0.000481	0.003079	0.000328
89	11:39:059	0.00011	-12:33:051	0.000084	0.00165	0.000418	0.001864	0.000226
90	11:39:057	0.000108	-12:17:021	0.000086	0.00426	0.000425	0.002873	0.000274
91	11:39:054	0.000047	-12:15:045	0.000035	0.005166	0.000424	0.004946	0.000245
93	11:39:023	0.000044	-12:20:023	0.000027	0.008744	0.000426	0.006792	0.000264
93	11:39:022	0.000317	-12:20:032	0.000093	0.001052	0.000439	0.001061	0.000237
94	11:39:022	0.000189	-12:09:034	0.000092	0.00149	0.000408	0.001414	0.000234

Table C.14: Positions of radio sources within 4MPc radius of the pointing centre of cluster RXCJ1236.7−3354

Source ID	RA	δ RA	DEC	δ DEC	total flux	δ total flux	Peak flux	δ Peak flux
0	12:40:003	0.000295	-33:30:008	0.000511	0.010585	0.0003	0.001778	0.000259
2	12:39:048	0.000317	-34:15:035	0.000252	0.001939	0.000442	0.001864	0.000212
3	12:39:044	0.000067	-33:58:040	0.000048	0.013934	0.000463	0.010464	0.000261
4	12:39:043	0.000131	-33:58:051	0.000103	0.009369	0.000434	0.005667	0.000268
7	12:39:026	0.000184	-33:31:060	0.000142	0.003611	0.000493	0.003627	0.000227
8	12:39:026	0.000138	-33:31:023	0.00009	0.008132	0.000446	0.005598	0.000259
9	12:39:006	0.000069	-34:14:031	0.000055	0.019951	0.000412	0.010457	0.000273
9	12:39:005	0.000072	-34:14:020	0.000058	0.012841	0.000446	0.009179	0.000258
12	12:38:041	0.00005	-33:46:027	0.000037	0.024241	0.000438	0.013715	0.000286
12	12:38:041	0.000219	-33:45:059	0.000237	0.008602	0.000393	0.002655	0.000309
12	12:38:041	0.000059	-33:46:016	0.00005	0.023059	0.000426	0.011331	0.000294
13	12:38:032	0.000258	-33:57:020	0.000175	0.005487	0.000403	0.003206	0.000246

Continued on next page

Table C.14: Positions of radio sources within 4MPc radius of the pointing centre of cluster RXCJ1236.7−3354

Source ID	RA	δ RA	DEC	δ DEC	total flux	δ total flux	Peak flux	δ Peak flux
14	12:38:031	0.00023	-33:51:022	0.000134	0.004191	0.000441	0.003248	0.000239
15	12:38:026	0.00004	-34:10:029	0.000046	0.022083	0.000627	0.014106	0.000296
16	12:38:023	0.000186	-34:13:044	0.000138	0.004926	0.000467	0.003881	0.000252
17	12:38:021	0.000051	-34:02:056	0.000083	0.019677	0.000574	0.010215	0.000267
18	12:38:021	0.000268	-34:28:048	0.000234	0.002633	0.000467	0.002388	0.000229
19	12:38:016	0.000049	-33:43:017	0.000037	0.014182	0.000444	0.012971	0.000219
21	12:38:010	0.000115	-33:55:032	0.000083	0.005942	0.000467	0.005638	0.000226
22	12:38:002	0.000322	-34:21:00	0.000292	0.006761	0.000339	0.002372	0.000252
23	12:37:056	0.000077	-33:22:005	0.000058	0.009386	0.000435	0.008142	0.000223
24	12:37:047	0.000108	-34:00:036	0.00009	0.006703	0.000426	0.00556	0.000225
26	12:37:042	0.000008	-33:52:023	0.000009	0.09852	0.000884	0.08491	0.000326
26	12:37:040	0.000018	-33:51:053	0.000017	0.063592	0.000783	0.043549	0.000326
26	12:37:045	0.000063	-33:52:054	0.000107	0.012737	0.00071	0.007266	0.000326
26	12:37:046	0.000254	-33:53:010	0.000257	0.002391	0.000554	0.002632	0.000231
31	12:37:037	0.000339	-33:51:049	0.000257	0.002026	0.000537	0.002094	0.000244
33	12:37:021	0.000375	-34:10:013	0.000695	0.005472	0.000276	0.001166	0.00023
34	12:37:019	0.000274	-33:49:037	0.000212	0.002324	0.000432	0.002242	0.000201
35	12:36:051	0.000064	-33:41:014	0.000053	0.008323	0.00044	0.00856	0.000203
36	12:36:045	0.000032	-33:45:036	0.000026	0.018782	0.000431	0.017778	0.00021
37	12:36:041	0.00026	-33:55:005	0.000277	0.014448	0.000366	0.002897	0.000309
38	12:36:038	0.000433	-33:55:019	0.000488	0.004478	0.000429	0.001522	0.000329
39	12:36:038	0.000427	-33:55:059	0.000445	0.012002	0.000322	0.001811	0.000283
40	12:36:023	0.000052	-33:31:012	0.000038	0.021282	0.000408	0.011611	0.000274
41	12:36:011	0.000022	-33:23:059	0.000018	0.031895	0.000504	0.030715	0.000239
42	12:36:010	0.000063	-33:52:012	0.000052	0.009783	0.000451	0.009344	0.000218
43	12:36:009	0.000341	-33:23:057	0.000286	0.002795	0.000479	0.002278	0.000242
47	12:36:002	0.000271	-33:39:034	0.000142	0.009235	0.000376	0.003163	0.000286
49	12:35:056	0.000059	-33:53:045	0.00005	0.009371	0.000479	0.010028	0.000213
50	12:35:049	0.000023	-33:29:038	0.000028	0.018698	0.00071	0.019645	0.000278
50	12:35:051	0.000338	-33:29:043	0.000257	0.001551	0.000486	0.001828	0.000195
52	12:35:046	0.000038	-34:05:014	0.000038	0.02341	0.000619	0.015239	0.000282
56	12:35:025	0.000014	-33:22:048	0.000016	0.045899	0.00071	0.040954	0.000301
56	12:35:025	0.000076	-33:22:034	0.000049	0.013304	0.000466	0.009793	0.000265
57	12:35:028	0.000248	-33:22:042	0.000274	0.002502	0.000485	0.001897	0.000292
60	12:35:022	0.00026	-33:22:006	0.000239	0.003106	0.000485	0.002882	0.000217
60	12:35:023	0.000303	-33:22:005	0.00022	0.003083	0.000479	0.002451	0.000257
61	12:35:022	0.000278	-33:22:046	0.000226	0.003082	0.000482	0.002552	0.000251
62	12:35:020	0.000207	-34:04:007	0.000157	0.005334	0.000406	0.00328	0.000251
63	12:35:018	0.000147	-34:04:012	0.000156	0.009507	0.00037	0.004415	0.000253
64	12:35:017	0.000177	-33:48:038	0.000177	0.004809	0.000417	0.003822	0.000208
67	12:35:006	0.000066	-33:57:049	0.00006	0.012634	0.000436	0.009737	0.000236

Continued on next page

Table C.14: Positions of radio sources within 4MPc radius of the pointing centre of cluster RXCJ1236.7−3354

Source ID	RA	δ RA	DEC	δ DEC	total flux	δ total flux	Peak flux	δ Peak flux
68	12:34:057	0.000145	-34:08:012	0.000135	0.006085	0.00043	0.004424	0.000241
69	12:34:046	0.000086	-34:09:001	0.000074	0.0095	0.000429	0.007451	0.00023
70	12:34:035	0.000019	-33:52:039	0.000022	0.029401	0.000667	0.026462	0.000279
74	12:34:023	0.000158	-33:35:048	0.00014	0.006791	0.000455	0.0038	0.000304
75	12:34:011	0.000152	-34:14:023	0.000139	0.007482	0.000403	0.004333	0.000254
77	12:34:010	0.000059	-33:26:041	0.000049	0.010954	0.000469	0.010651	0.000221
79	12:34:001	0.000159	-33:41:005	0.00013	0.004131	0.000442	0.003605	0.000232
81	12:33:037	0.00005	-34:10:025	0.000053	0.024992	0.000636	0.012576	0.000315

Table C.15: Positions of radio sources within 4MPc radius of the pointing centre of cluster RXCJ1302.8−0230

Source ID	RA	δ RA	DEC	δ DEC	total flux	δ total flux	Peak flux	δ Peak flux
3	13:04:057	0.000177	-01:54:048	0.000087	0.002154	0.000543	0.001804	0.000326
3	13:04:058	0.000202	-01:54:048	0.00005	0.001367	0.000569	0.001637	0.000279
5	13:04:058	0.000022	-01:55:00	0.00012	0.006173	0.000813	0.00489	0.000328
6	13:04:058	0.000195	-01:54:015	0.000076	0.002017	0.000514	0.001704	0.000302
6	13:04:058	0.000161	-01:54:016	0.000116	0.001542	0.000527	0.001459	0.000308
7	13:04:058	0.00014	-01:50:037	0.000202	0.001922	0.000373	0.001182	0.000248
8	13:04:058	0.000059	-01:57:024	0.000177	0.002052	0.000626	0.001327	0.000256
8	13:04:057	0.000227	-01:57:026	0.000145	0.002293	0.0004	0.001263	0.000275
8	13:04:058	0.000169	-01:57:025	0.000179	0.001018	0.00044	0.000958	0.000259
10	13:04:057	0.000112	-01:52:023	0.000072	0.00125	0.000427	0.001475	0.000231
10	13:04:058	0.000237	-01:52:022	0.000126	0.001938	0.000386	0.001265	0.000247
11	13:04:057	0.000075	-01:55:012	0.000074	0.003285	0.000564	0.002947	0.000337
11	13:04:057	0.000166	-01:55:014	0.000073	0.002041	0.000564	0.001976	0.000314
11	13:04:057	0.000091	-01:55:021	0.000082	0.003496	0.000555	0.002909	0.000335
13	13:04:056	0.000348	-01:59:038	0.000156	0.004606	0.000313	0.001268	0.00025
13	13:04:057	0.000237	-01:59:039	0.000444	0.001041	0.000402	0.000689	0.000256
14	13:04:056	0.000274	-01:59:013	0.000303	0.00411	0.000319	0.0012	0.000251
15	13:04:056	0.000243	-01:55:046	0.000174	0.005419	0.000428	0.001762	0.000333
16	13:04:056	0.000117	-01:55:033	0.000179	0.002554	0.000532	0.001781	0.000342
17	13:04:055	0.000514	-02:18:049	0.000263	0.018747	0.000139	0.000975	0.000132
18	13:04:055	0.000166	-02:19:003	0.000034	0.003075	0.000358	0.002137	0.000215
19	13:04:055	0.000445	-02:06:013	0.000219	0.008265	0.000153	0.000876	0.000139
22	13:04:054	0.00011	-02:19:023	0.000095	0.001945	0.000395	0.001614	0.000242
22	13:04:053	0.000223	-02:19:024	0.000121	0.005622	0.00048	0.001427	0.000233
22	13:04:054	0.0002	-02:19:017	0.000128	0.001626	0.000383	0.001188	0.00024
23	13:04:054	0.000152	-02:19:015	0.000159	0.001894	0.000382	0.001251	0.00025

Continued on next page

Table C.15: Positions of radio sources within 4MPc radius of the pointing centre of cluster RXCJ1302.8−0230

Source ID	RA	δ RA	DEC	δ DEC	total flux	δ total flux	Peak flux	δ Peak flux
24	13:04:053	0.000144	-02:19:048	0.000191	0.001922	0.000373	0.00124	0.000244
24	13:04:053	0.000153	-02:19:040	0.000251	0.001823	0.000366	0.001042	0.000248
25	13:04:038	0.000055	-02:23:049	0.00011	0.001441	0.000601	0.00202	0.000301
26	13:04:038	0.000364	-02:15:023	0.000276	0.011144	0.000222	0.001214	0.000201
29	13:04:037	0.000072	-02:21:027	0.000192	0.001831	0.000549	0.00172	0.000311
30	13:04:037	0.000267	-02:29:007	0.000142	0.011457	0.000741	0.003402	0.000584
31	13:04:036	0.000011	-02:28:034	0.000036	0.034304	0.001453	0.023267	0.000602
31	13:04:036	0.000095	-02:28:031	0.000045	0.00288	0.001068	0.004197	0.00052
31	13:04:037	0.00015	-02:28:034	0.000078	0.001658	0.001064	0.002457	0.000522
32	13:04:037	0.000079	-02:21:020	0.000215	0.001916	0.000542	0.001635	0.000318
33	13:04:037	0.00013	-02:23:056	0.000221	0.002142	0.000572	0.001741	0.000335
35	13:04:037	0.000139	-02:19:055	0.000249	0.003602	0.000466	0.001718	0.000329
36	13:04:037	0.000157	-02:28:019	0.000106	0.004225	0.001003	0.003489	0.000604
37	13:04:037	0.000124	-02:24:028	0.000147	0.002388	0.000596	0.002193	0.000333
38	13:04:037	0.000141	-02:27:049	0.000091	0.002969	0.000986	0.003089	0.000553
40	13:04:036	0.000189	-02:28:048	0.000136	0.003877	0.000995	0.003266	0.000574
41	13:04:036	0.000055	-02:25:027	0.000123	0.002218	0.000661	0.002517	0.000354
42	13:04:036	0.000042	-02:25:042	0.00008	0.001399	0.000686	0.002508	0.000312
43	13:04:036	0.000064	-02:25:021	0.000055	0.002285	0.000656	0.003097	0.000339
44	13:04:036	0.000121	-02:25:055	0.00013	0.00304	0.000676	0.002615	0.000395
45	13:04:036	0.000166	-02:29:017	0.000077	0.003031	0.000983	0.003135	0.000539
47	13:04:036	0.00008	-02:28:053	0.000062	0.007402	0.001008	0.006662	0.000578
49	13:04:036	0.000135	-02:29:006	0.000094	0.004436	0.00099	0.003871	0.000583
50	13:04:035	0.000193	-02:24:028	0.000175	0.005247	0.000502	0.002134	0.000371
51	13:04:035	0.00008	-02:28:045	0.000116	0.002727	0.001058	0.003351	0.000562
52	13:04:035	0.00013	-02:33:010	0.000138	0.002586	0.000585	0.001958	0.000369
53	13:04:035	0.000055	-02:27:057	0.000113	0.004309	0.00101	0.004736	0.00053
54	13:04:035	0.000075	-02:32:045	0.000136	0.002391	0.000613	0.002278	0.000353
57	13:04:035	0.000085	-02:33:001	0.000154	0.002356	0.0006	0.002068	0.000357
58	13:04:035	0.00005	-02:29:021	0.000094	0.003106	0.000992	0.004045	0.000512
58	13:04:034	0.000098	-02:29:014	0.000268	0.003858	0.000897	0.003051	0.000503
59	13:04:035	0.000077	-02:32:052	0.000209	0.0033	0.000566	0.002172	0.000362
60	13:04:035	0.000064	-02:28:003	0.000114	0.001978	0.001023	0.002968	0.000502
62	13:04:034	0.000111	-02:28:032	0.000177	0.003166	0.001022	0.003112	0.000564
63	13:04:034	0.000109	-02:33:037	0.000164	0.001925	0.000588	0.001812	0.000336
64	13:04:034	0.000107	-02:33:015	0.000166	0.003017	0.000574	0.002075	0.00037
64	13:04:034	0.000135	-02:33:006	0.000204	0.002418	0.000574	0.001692	0.000367
65	13:04:033	0.000098	-02:33:051	0.000161	0.003186	0.00055	0.002174	0.000354
65	13:04:033	0.000122	-02:33:059	0.000272	0.002011	0.000549	0.001427	0.000345
68	13:04:024	0.000151	-02:17:036	0.000083	0.001426	0.000392	0.001334	0.000227
68	13:04:024	0.000206	-02:17:036	0.000162	0.001523	0.000372	0.001128	0.000228

Continued on next page

Table C.15: Positions of radio sources within 4MPc radius of the pointing centre of cluster RXCJ1302.8−0230

Source ID	RA	δ RA	DEC	δ DEC	total flux	δ total flux	Peak flux	δ Peak flux
69	13:04:023	0.000178	-02:17:056	0.000142	0.001872	0.000387	0.001224	0.000255
71	13:04:006	0.000016	-02:32:018	0.000056	0.024228	0.001382	0.013789	0.000469
71	13:04:007	0.00018	-02:32:018	0.000134	0.002487	0.000798	0.002258	0.000461
74	13:04:005	0.000048	-02:32:037	0.000035	0.001435	0.000811	0.003515	0.000317
75	13:04:006	0.000153	-02:29:054	0.00021	0.002695	0.000571	0.001877	0.000355
77	13:04:006	0.000058	-02:29:026	0.000105	0.001954	0.000606	0.002375	0.000319
78	13:04:005	0.000099	-02:29:004	0.000094	0.001967	0.000592	0.002211	0.00032
79	13:04:005	0.000063	-02:31:042	0.000092	0.002183	0.000838	0.003277	0.000391
80	13:04:005	0.000073	-02:32:015	0.000049	0.002589	0.000836	0.003679	0.000423
81	13:04:005	0.000135	-02:32:050	0.000118	0.002515	0.0008	0.002504	0.000452
82	13:04:005	0.000061	-02:32:030	0.000093	0.002047	0.000833	0.002921	0.000419
83	13:04:005	0.000096	-02:33:006	0.000123	0.002116	0.000789	0.002388	0.000434
86	13:04:004	0.000071	-02:31:047	0.000153	0.002006	0.00082	0.002376	0.000435
91	13:03:048	0.000215	-02:35:012	0.000193	0.006532	0.000931	0.003355	0.00064
92	13:03:047	0.000017	-02:34:039	0.000053	0.028597	0.001481	0.016915	0.000648
93	13:03:048	0.000098	-02:02:032	0.000108	0.006961	0.00134	0.005631	0.000826
94	13:03:047	0.00001	-02:01:057	0.000035	0.058152	0.001937	0.035349	0.000824
94	13:03:047	0.000079	-02:01:055	0.00005	0.002552	0.001438	0.004736	0.000652
96	13:03:047	0.000167	-01:59:018	0.000089	0.003703	0.000962	0.003438	0.00054
96	13:03:047	0.000081	-01:59:019	0.00008	0.002383	0.000994	0.003332	0.00051
98	13:03:047	0.000043	-01:59:007	0.000106	0.001863	0.000975	0.003147	0.000444
99	13:03:047	0.000048	-01:58:044	0.000049	0.002987	0.00091	0.004625	0.000449
100	13:03:047	0.000255	-01:56:008	0.000112	0.007135	0.000644	0.002804	0.000477
101	13:03:047	0.000181	-01:53:046	0.00022	0.005463	0.00068	0.002394	0.000495
102	13:03:047	0.000124	-02:04:023	0.00011	0.004341	0.001008	0.003594	0.000618
103	13:03:047	0.000105	-02:33:049	0.000085	0.003247	0.001144	0.003787	0.000625
104	13:03:047	0.000115	-02:34:058	0.000083	0.006038	0.001102	0.005435	0.000625
105	13:03:047	0.000087	-02:34:021	0.000061	0.002103	0.001162	0.003575	0.00055
105	13:03:046	0.000059	-02:34:002	0.000121	0.001885	0.001198	0.003362	0.000516
106	13:03:047	0.000074	-02:02:017	0.000052	0.010119	0.001387	0.009689	0.00078
106	13:03:046	0.000106	-02:02:021	0.000196	0.010298	0.001221	0.00568	0.000818
107	13:03:046	0.000185	-01:57:053	0.000185	0.009372	0.00065	0.003036	0.000506
108	13:03:047	0.000101	-02:34:036	0.000068	0.00236	0.001165	0.003525	0.000578
109	13:03:047	0.00012	-02:02:030	0.00007	0.00483	0.001393	0.005152	0.000774
110	13:03:047	0.000102	-01:59:051	0.000115	0.002669	0.001093	0.003186	0.000589
111	13:03:046	0.000073	-02:02:008	0.000095	0.004249	0.001438	0.005219	0.000769
112	13:03:046	0.000124	-02:08:059	0.000191	0.006561	0.000766	0.003238	0.000539
113	13:03:046	0.000068	-02:35:004	0.000116	0.004091	0.001141	0.004323	0.000638
113	13:03:046	0.000115	-02:34:056	0.000204	0.003701	0.001106	0.003318	0.000628
114	13:03:046	0.000095	-02:06:034	0.000135	0.006103	0.000884	0.004007	0.000577
115	13:03:046	0.000039	-02:01:021	0.000087	0.003433	0.001408	0.005612	0.00065

Continued on next page

Table C.15: Positions of radio sources within 4MPc radius of the pointing centre of cluster RXCJ1302.8−0230

Source ID	RA	δ RA	DEC	δ DEC	total flux	δ total flux	Peak flux	δ Peak flux
116	13:03:046	0.000072	-02:06:008	0.000139	0.002975	0.000946	0.003207	0.000518
117	13:03:046	0.000069	-02:01:011	0.000102	0.002638	0.001361	0.00403	0.000668
118	13:03:046	0.000083	-02:06:023	0.000172	0.003374	0.000927	0.003025	0.000542
121	13:03:045	0.000092	-02:06:055	0.00025	0.005861	0.000825	0.003131	0.000562
121	13:03:045	0.000085	-02:06:047	0.000181	0.002811	0.00094	0.002721	0.000536
122	13:03:045	0.00008	-02:06:038	0.000133	0.004646	0.000919	0.003847	0.000554
122	13:03:045	0.000092	-02:06:030	0.000177	0.003522	0.000921	0.002995	0.000549
123	13:03:037	0.000141	-02:42:059	0.000168	0.005576	0.001126	0.00412	0.000689
124	13:03:036	0.000016	-02:42:025	0.000044	0.034327	0.00175	0.02235	0.00073
127	13:03:036	0.000071	-02:39:018	0.000187	0.002469	0.000972	0.002859	0.000492
129	13:03:036	0.000128	-02:39:012	0.000112	0.002851	0.000954	0.003101	0.000514
130	13:03:036	0.000098	-02:41:035	0.000078	0.003194	0.00124	0.004083	0.000656
131	13:03:035	0.000065	-02:42:008	0.000085	0.003286	0.001279	0.00476	0.000633
132	13:03:035	0.000088	-02:42:044	0.000063	0.006939	0.001206	0.006483	0.000699
132	13:03:035	0.000063	-02:42:050	0.000128	0.00582	0.001197	0.005181	0.000704
132	13:03:035	0.0001	-02:42:043	0.000197	0.005635	0.001141	0.0047	0.00063
133	13:03:035	0.000083	-02:46:037	0.000155	0.004007	0.000739	0.002962	0.000463
134	13:03:035	0.000093	-02:43:029	0.000201	0.005612	0.001011	0.003839	0.000637
139	13:03:032	0.000076	-02:48:003	0.000197	0.002961	0.000702	0.002539	0.000401
140	13:03:029	0.000199	-02:50:009	0.000056	0.010611	0.000506	0.003783	0.000378
141	13:03:029	0.000128	-02:46:033	0.000092	0.00326	0.000673	0.002673	0.000411
142	13:03:028	0.000141	-02:50:028	0.000152	0.002882	0.000624	0.002101	0.000394
143	13:03:028	0.000124	-02:50:007	0.000111	0.001655	0.000676	0.001967	0.000358
144	13:03:024	0.000235	-03:04:036	0.00022	0.003784	0.000271	0.001108	0.000215
145	13:03:015	0.00016	-02:12:051	0.000081	0.013206	0.003797	0.01234	0.002202
146	13:03:013	0.000005	-02:12:058	0.000014	0.299074	0.005784	0.208719	0.002373
148	13:03:014	0.000077	-02:13:032	0.000058	0.013382	0.004147	0.017615	0.002163
149	13:03:014	0.000092	-02:12:034	0.000084	0.00853	0.004096	0.012618	0.002023
150	13:03:014	0.000077	-02:05:016	0.000195	0.01018	0.001921	0.007236	0.001202
151	13:03:014	0.000066	-02:04:039	0.00017	0.006335	0.001941	0.006357	0.001076
152	13:03:013	0.000074	-02:08:012	0.000164	0.015478	0.002449	0.010659	0.001557
153	13:03:013	0.000123	-02:13:010	0.000153	0.013861	0.004138	0.012813	0.002393
154	13:03:013	0.000053	-02:09:045	0.000057	0.022199	0.002831	0.020579	0.00166
155	13:03:013	0.000156	-02:10:049	0.000135	0.01219	0.003133	0.01001	0.001892
157	13:03:013	0.000103	-02:10:019	0.000077	0.008022	0.003057	0.010119	0.001619
158	13:03:013	0.000059	-02:11:034	0.000075	0.009766	0.003675	0.014367	0.001838
159	13:03:013	0.000062	-02:13:041	0.000053	0.017931	0.004224	0.023081	0.002176
160	13:03:013	0.000088	-02:14:026	0.000098	0.008767	0.003828	0.011747	0.001982
161	13:03:013	0.000108	-02:12:010	0.000094	0.012269	0.003959	0.013969	0.002127
164	13:03:013	0.000037	-02:13:018	0.000026	0.031993	0.004273	0.041983	0.002181
164	13:03:012	0.000044	-02:13:023	0.00005	0.044252	0.004108	0.036567	0.002521

Continued on next page

Table C.15: Positions of radio sources within 4MPc radius of the pointing centre of cluster RXCJ1302.8−0230

Source ID	RA	δ RA	DEC	δ DEC	total flux	δ total flux	Peak flux	δ Peak flux
165	13:03:013	0.000078	-02:11:001	0.000056	0.011465	0.003373	0.014748	0.001771
166	13:03:012	0.000047	-02:13:008	0.000069	0.034084	0.00412	0.02936	0.002477
167	13:03:012	0.000119	-02:11:014	0.000151	0.012116	0.003372	0.011062	0.001946
168	13:03:012	0.000049	-02:15:027	0.000085	0.01829	0.003144	0.017641	0.001815
169	13:03:012	0.000083	-02:12:022	0.00009	0.051258	0.003488	0.028034	0.002359
170	13:03:012	0.00005	-02:17:009	0.000094	0.008752	0.002825	0.011498	0.00145
172	13:03:012	0.000078	-02:13:045	0.000085	0.008735	0.004164	0.013435	0.002021
173	13:03:011	0.000091	-02:17:015	0.00018	0.009797	0.002689	0.008557	0.001582
174	13:03:011	0.000447	-02:13:037	0.000215	0.061911	0.002414	0.010566	0.002079
175	13:02:054	0.00024	-02:21:058	0.000312	0.025068	0.000598	0.003385	0.000531
176	13:02:053	0.000035	-02:30:053	0.000024	0.054723	0.001042	0.02459	0.000752
176	13:02:053	0.000047	-02:31:007	0.000043	0.022016	0.001134	0.013486	0.00076
177	13:02:054	0.000194	-02:30:039	0.0002	0.010669	0.001011	0.003958	0.000766
178	13:02:054	0.000376	-02:13:044	0.000267	0.0297	0.000856	0.004038	0.000759
179	13:02:053	0.000159	-02:14:013	0.000175	0.021217	0.001136	0.006238	0.000901
180	13:02:053	0.000145	-02:13:059	0.000081	0.043837	0.001015	0.010262	0.000835
181	13:02:052	0.000204	-02:13:040	0.000259	0.009424	0.00123	0.004279	0.000874
182	13:02:051	0.000135	-02:30:014	0.000246	0.010245	0.000966	0.004465	0.000687
183	13:02:051	0.000096	-02:31:040	0.000224	0.005083	0.001064	0.003468	0.000678
183	13:02:051	0.000111	-02:31:032	0.000193	0.004075	0.001104	0.003321	0.000668
184	13:02:051	0.000283	-02:18:054	0.000219	0.012726	0.000746	0.003143	0.000609
185	13:02:051	0.000234	-02:35:049	0.000367	0.01757	0.000592	0.0029	0.000513
186	13:02:051	0.000113	-02:30:056	0.000188	0.004986	0.001123	0.003597	0.000712
186	13:02:051	0.000132	-02:30:050	0.00034	0.00432	0.001064	0.002674	0.000691
187	13:02:044	0.000286	-02:16:033	0.000203	0.006615	0.000642	0.002385	0.000485
189	13:02:042	0.000239	-02:00:036	0.000374	0.024563	0.000446	0.002602	0.000405
190	13:02:041	0.000032	-02:00:055	0.000156	0.02294	0.00104	0.006975	0.000511
190	13:02:040	0.000151	-02:00:052	0.000101	0.002035	0.000893	0.002312	0.00049
192	13:02:040	0.000102	-02:01:006	0.000195	0.003135	0.000834	0.002568	0.000502
193	13:02:021	0.000072	-02:15:007	0.000038	0.014046	0.0008	0.008979	0.000512
193	13:02:022	0.000092	-02:14:060	0.000043	0.00678	0.000856	0.005603	0.000515
193	13:02:021	0.000078	-02:15:019	0.000053	0.002249	0.000898	0.003508	0.000434
193	13:02:020	0.000202	-02:15:026	0.000164	0.003238	0.000836	0.002879	0.000443
194	13:02:022	0.000305	-02:14:046	0.000167	0.008159	0.000674	0.002644	0.000521
195	13:02:021	0.000071	-02:18:017	0.000232	0.010083	0.000788	0.002412	0.000379
196	13:02:021	0.000126	-02:28:054	0.000098	0.002981	0.000601	0.002361	0.000373
198	13:02:020	0.000086	-02:14:031	0.000143	0.003579	0.000882	0.003173	0.000522
199	13:02:020	0.000124	-02:42:008	0.000144	0.00175	0.000466	0.001512	0.000278
200	13:02:020	0.000272	-02:28:021	0.000377	0.012076	0.000348	0.00165	0.000309
203	13:02:019	0.000087	-02:45:006	0.000091	0.00206	0.000524	0.002182	0.000291
204	13:02:019	0.000063	-02:44:029	0.000107	0.001056	0.00055	0.001636	0.000267

Continued on next page

Table C.15: Positions of radio sources within 4MPc radius of the pointing centre of cluster RXCJ1302.8−0230

Source ID	RA	δ RA	DEC	δ DEC	total flux	δ total flux	Peak flux	δ Peak flux
205	13:02:018	0.000146	-01:52:040	0.000223	0.004269	0.000602	0.0021	0.000425
205	13:02:019	0.000134	-01:52:035	0.000375	0.002213	0.000622	0.001434	0.000395
206	13:02:019	0.000091	-02:44:044	0.000074	0.001381	0.000542	0.001851	0.000281
208	13:02:018	0.000017	-02:01:018	0.000032	0.039172	0.001509	0.02447	0.000646
210	13:02:019	0.00007	-02:44:058	0.000129	0.001338	0.000534	0.00166	0.00028
212	13:02:018	0.000079	-02:44:010	0.000148	0.00186	0.000541	0.001896	0.000299
213	13:02:018	0.000112	-02:44:044	0.000176	0.001721	0.000522	0.001594	0.000298
215	13:02:018	0.000124	-01:58:052	0.000168	0.002494	0.000815	0.002455	0.000451
216	13:02:018	0.000041	-01:58:028	0.000101	0.002043	0.000796	0.003024	0.000383
217	13:02:017	0.000066	-01:58:005	0.000081	0.003827	0.000755	0.003964	0.00042
218	13:02:017	0.000059	-01:58:041	0.00009	0.001763	0.000812	0.002796	0.000387
219	13:02:017	0.000101	-02:01:039	0.000153	0.047592	0.001267	0.007956	0.000635
222	13:02:017	0.000063	-02:01:016	0.000065	0.003034	0.001138	0.004547	0.000568
223	13:02:017	0.00011	-02:08:019	0.000195	0.005149	0.000699	0.002775	0.000481
224	13:02:016	0.000119	-02:05:054	0.00024	0.004878	0.000778	0.002743	0.000524
225	13:02:016	0.000036	-02:00:042	0.000082	0.004518	0.00113	0.005931	0.000567
226	13:02:016	0.000084	-02:05:030	0.000144	0.00419	0.000837	0.003428	0.000503
227	13:02:016	0.000087	-02:01:017	0.000132	0.002279	0.001158	0.003367	0.000535
228	13:02:016	0.000095	-02:05:044	0.000171	0.003105	0.000853	0.00268	0.00051
229	13:02:016	0.000073	-02:01:051	0.000221	0.003198	0.001056	0.002999	0.000593
230	13:02:016	0.000051	-02:00:048	0.000169	0.003553	0.001112	0.003921	0.000572
232	13:02:016	0.000086	-02:06:015	0.00023	0.003342	0.000817	0.002607	0.000489
232	13:02:015	0.000076	-02:06:008	0.000222	0.002369	0.000854	0.002315	0.000473
233	13:02:016	0.000078	-02:05:053	0.000178	0.0027	0.000859	0.002648	0.000482
234	13:02:015	0.000176	-02:05:058	0.000283	0.010459	0.000608	0.002913	0.000484
235	13:02:013	0.000152	-02:35:030	0.000048	0.001982	0.000547	0.002187	0.000279
236	13:02:006	0.000087	-02:02:023	0.000052	0.003064	0.000608	0.00314	0.000344
237	13:01:058	0.000285	-02:22:032	0.000262	0.048335	0.00019	0.002039	0.000183
237	13:01:057	0.000174	-02:22:046	0.000174	0.017932	0.000341	0.002749	0.000298
238	13:01:055	0.000185	-02:05:009	0.000208	0.022393	0.000262	0.002336	0.000239
238	13:01:054	0.000187	-02:05:029	0.00026	0.028124	0.00023	0.002257	0.000213
239	13:01:053	0.000285	-02:39:022	0.000095	0.003088	0.000314	0.001312	0.000226
240	13:01:047	0.000072	-02:02:029	0.000034	0.001281	0.000464	0.002114	0.000216
242	13:01:046	0.0001	-02:02:041	0.000129	0.001267	0.000444	0.00134	0.00025
243	13:01:046	0.000205	-02:01:054	0.000201	0.001924	0.000399	0.001249	0.000254
244	13:01:042	0.000156	-02:19:032	0.000073	0.002438	0.000345	0.001602	0.000223
245	13:01:028	0.000072	-02:02:009	0.00002	0.007808	0.000445	0.005457	0.000273
249	13:01:028	0.000232	-01:59:031	0.000126	0.002062	0.000336	0.001215	0.000222
250	13:01:027	0.000365	-02:43:032	0.000316	0.023873	0.000205	0.001486	0.000193
251	13:01:027	0.000066	-02:43:049	0.000029	0.008231	0.000495	0.005511	0.000317
253	13:01:027	0.000259	-01:56:020	0.000119	0.001906	0.000315	0.001033	0.000215

Continued on next page

Table C.15: Positions of radio sources within 4MPc radius of the pointing centre of cluster RXCJ1302.8−0230

Source ID	RA	δ RA	DEC	δ DEC	total flux	δ total flux	Peak flux	δ Peak flux
254	13:01:027	0.000379	-02:06:015	0.000163	0.004217	0.000288	0.001144	0.00023
254	13:01:026	0.00022	-02:06:021	0.000255	0.002516	0.000543	0.000939	0.000237
255	13:01:027	0.000288	-02:02:030	0.000154	0.015179	0.000257	0.001906	0.000229
256	13:01:027	0.000179	-02:01:045	0.000141	0.002272	0.000442	0.001567	0.000279
257	13:01:027	0.000095	-02:41:011	0.000095	0.001219	0.000464	0.001566	0.000239
258	13:01:027	0.000141	-02:02:021	0.000099	0.002103	0.000472	0.001767	0.000283
259	13:01:027	0.000109	-02:41:025	0.000132	0.001247	0.00046	0.001311	0.00026
260	13:01:026	0.000145	-02:01:033	0.000133	0.00229	0.000437	0.001607	0.00028
260	13:01:026	0.000232	-02:01:038	0.00024	0.002233	0.000405	0.001184	0.000277
262	13:01:026	0.000249	-02:44:008	0.000219	0.004332	0.00038	0.002303	0.000223
264	13:01:025	0.000072	-02:43:012	0.000106	0.002269	0.000533	0.002252	0.000304
264	13:01:026	0.000483	-02:43:025	0.000243	0.007553	0.000637	0.002151	0.000308
264	13:01:025	0.000079	-02:43:017	0.000125	0.001946	0.000533	0.001936	0.000305
265	13:01:026	0.000105	-02:43:046	0.000073	0.001772	0.000548	0.002092	0.000291
267	13:01:025	0.000149	-02:43:046	0.000258	0.004112	0.000441	0.001795	0.000316
268	13:01:025	0.000454	-02:34:035	0.000307	0.017747	0.000146	0.000999	0.000139
269	13:01:025	0.000294	-02:48:046	0.000256	0.006024	0.000256	0.001242	0.000215
271	13:01:023	0.000109	-02:39:029	0.000033	0.003435	0.000447	0.002966	0.000255
272	13:01:023	0.00012	-02:36:051	0.000151	0.001165	0.000379	0.001176	0.000209
273	13:01:022	0.000087	-02:39:049	0.000082	0.002365	0.000449	0.00215	0.000266
273	13:01:021	0.0001	-02:39:048	0.000183	0.001897	0.000436	0.001511	0.000262
273	13:01:022	0.000073	-02:39:042	0.00016	0.001432	0.000453	0.001446	0.000254
273	13:01:022	0.000113	-02:39:044	0.000139	0.000897	0.000461	0.001133	0.000242
273	13:01:022	0.000121	-02:39:055	0.000284	0.001124	0.000442	0.001007	0.000251
274	13:01:022	0.00009	-02:39:012	0.000118	0.001475	0.000461	0.001542	0.000261
274	13:01:022	0.000106	-02:39:005	0.000266	0.001208	0.000448	0.001063	0.000259
279	13:01:00	0.000249	-01:55:007	0.000336	0.00583	0.00018	0.000902	0.000157
280	13:00:057	0.000064	-02:02:021	0.000065	0.002071	0.000462	0.002449	0.000246
280	13:00:058	0.000019	-02:02:023	0.000079	0.00939	0.000625	0.005947	0.000263
280	13:00:058	0.000074	-02:02:027	0.000135	0.001931	0.00045	0.001811	0.000257
281	13:00:059	0.000377	-01:53:045	0.00025	0.005051	0.000186	0.000831	0.000161
282	13:00:059	0.000153	-02:02:002	0.000159	0.002275	0.000429	0.00155	0.000273
282	13:00:059	0.000364	-02:02:010	0.000257	0.001544	0.000407	0.000901	0.000268
283	13:00:059	0.000129	-02:02:057	0.00012	0.001996	0.000414	0.001656	0.000245
284	13:00:058	0.000107	-01:59:045	0.00012	0.001537	0.000361	0.001473	0.0002
285	13:00:058	0.000093	-01:59:010	0.000113	0.001253	0.000353	0.001283	0.000199
286	13:00:058	0.000126	-01:59:045	0.000105	0.001258	0.000367	0.001324	0.000198
287	13:00:058	0.00011	-02:02:036	0.000077	0.001423	0.000458	0.00163	0.000249
289	13:00:057	0.000099	-02:01:058	0.00014	0.00129	0.000476	0.001533	0.000242
289	13:00:058	0.000077	-02:02:005	0.000147	0.001169	0.000477	0.001426	0.000246
290	13:00:057	0.000087	-02:02:043	0.000078	0.002541	0.000439	0.002273	0.000258

Continued on next page

Table C.15: Positions of radio sources within 4MPc radius of the pointing centre of cluster RXCJ1302.8−0230

Source ID	RA	δ RA	DEC	δ DEC	total flux	δ total flux	Peak flux	δ Peak flux
292	13:00:057	0.000059	-02:02:034	0.00008	0.001801	0.00046	0.002095	0.000251
294	13:00:057	0.000232	-02:06:060	0.000171	0.002846	0.0003	0.001154	0.000222
295	13:00:057	0.000086	-02:01:046	0.000103	0.00208	0.000465	0.002143	0.000251
297	13:00:056	0.000084	-02:03:003	0.000199	0.001543	0.00041	0.001374	0.000232
297	13:00:056	0.000071	-02:03:009	0.000138	0.000927	0.00043	0.001216	0.00022
298	13:00:056	0.000091	-02:07:012	0.000184	0.001693	0.000345	0.001282	0.000211
298	13:00:056	0.000086	-02:07:019	0.000221	0.001488	0.000345	0.001105	0.000213
299	13:00:056	0.000089	-02:07:003	0.000236	0.001824	0.000331	0.001152	0.000214
303	13:00:005	0.000443	-02:40:009	0.000239	0.009188	0.000088	0.000616	0.000083
305	13:00:005	0.000176	-02:40:026	0.000077	0.006962	0.000137	0.001412	0.000115
306	13:00:004	0.000137	-02:40:005	0.00028	0.001137	0.000192	0.000618	0.00013

Table C.16: Positions of radio sources within 4MPc radius of the pointing centre of cluster RXCJ1311.4−0120

Source ID	RA	δ RA	DEC	δ DEC	total flux	δ total flux	Peak flux	δ Peak flux
0	13:12:055	0.000203	-01:08:058	0.000313	0.003932	0.000181	0.000899	0.000149
2	13:12:049	0.000141	-01:26:046	0.000152	0.000887	0.000274	0.000793	0.000163
2	13:12:049	0.00022	-01:26:042	0.000257	0.000798	0.000265	0.000563	0.00017
3	13:12:046	0.000161	-01:16:056	0.000108	0.001206	0.000294	0.001039	0.000174
5	13:12:038	0.000058	-01:17:036	0.000063	0.00446	0.000306	0.00302	0.000196
6	13:12:032	0.000203	-01:13:043	0.000121	0.002158	0.000293	0.001417	0.000179
7	13:12:033	0.000214	-01:09:003	0.000131	0.00162	0.000277	0.001004	0.000182
8	13:12:032	0.000056	-01:13:023	0.000042	0.005615	0.000435	0.003483	0.000192
8	13:12:032	0.000145	-01:13:033	0.000228	0.000812	0.000328	0.000753	0.000191
10	13:12:031	0.000116	-01:38:005	0.000163	0.002317	0.000284	0.001361	0.000189
11	13:12:028	0.000127	-01:39:054	0.000128	0.001344	0.000297	0.001152	0.000176
13	13:12:019	0.000064	-01:28:008	0.000072	0.005216	0.000318	0.003097	0.000211
15	13:12:015	0.000147	-01:15:039	0.000163	0.001381	0.000287	0.000975	0.000184
16	13:12:015	0.000213	-01:18:052	0.000134	0.002377	0.000355	0.001293	0.000244
17	13:12:014	0.000051	-01:18:033	0.000036	0.004556	0.000524	0.003593	0.000225
18	13:12:014	0.000149	-01:18:018	0.000082	0.000904	0.000393	0.001162	0.000199
19	13:12:010	0.000109	-01:29:041	0.000121	0.003483	0.000419	0.002245	0.000272
20	13:12:009	0.000077	-01:21:048	0.000085	0.002285	0.000424	0.002192	0.000245
21	13:12:005	0.000057	-01:14:015	0.000062	0.009224	0.000501	0.003738	0.000247
21	13:12:005	0.000099	-01:14:013	0.000045	0.011376	0.000338	0.004154	0.000255
24	13:12:002	0.000159	-01:19:037	0.000121	0.001999	0.000419	0.001473	0.000265
24	13:12:002	0.000271	-01:19:031	0.000261	0.000888	0.000425	0.000742	0.000258
26	13:12:001	0.000011	-01:34:023	0.000011	0.046656	0.001132	0.031049	0.000375

Continued on next page

Table C.16: Positions of radio sources within 4MPc radius of the pointing centre of cluster RXCJ1311.4−0120

Source ID	RA	δ RA	DEC	δ DEC	total flux	δ total flux	Peak flux	δ Peak flux
27	13:12:001	0.000236	-01:28:048	0.000167	0.00336	0.000469	0.00163	0.000333
28	13:12:001	0.000076	-01:34:042	0.000038	0.006196	0.000634	0.005441	0.000367
30	13:12:001	0.000036	-01:35:024	0.000034	0.008876	0.000628	0.007892	0.000374
32	13:12:001	0.000365	-01:29:032	0.000134	0.004051	0.000436	0.001554	0.000324
34	13:12:001	0.000265	-01:38:037	0.000137	0.003537	0.000454	0.001684	0.000321
36	13:11:060	0.000236	-01:34:043	0.000104	0.005092	0.000556	0.002467	0.00039
36	13:12:00	0.000149	-01:34:042	0.000043	0.004785	0.000609	0.003772	0.00035
37	13:12:00	0.00031	-01:36:007	0.000349	0.005911	0.000425	0.001518	0.000344
38	13:12:00	0.000076	-01:34:007	0.000035	0.003788	0.000652	0.004369	0.000343
39	13:12:00	0.000149	-01:33:054	0.000122	0.002732	0.000614	0.002212	0.000374
41	13:11:050	0.000092	-01:28:006	0.000145	0.007774	0.000384	0.003024	0.000284
42	13:11:044	0.000367	-01:19:040	0.000185	0.005316	0.000398	0.001569	0.000313
43	13:11:044	0.000103	-01:19:019	0.000056	0.007741	0.000494	0.004136	0.00034
44	13:11:043	0.000212	-01:23:026	0.000185	0.003563	0.0005	0.001738	0.000355
45	13:11:042	0.000024	-01:23:044	0.00002	0.011314	0.000587	0.011062	0.000336
45	13:11:042	0.000206	-01:23:052	0.000133	0.00199	0.000573	0.00174	0.00033
46	13:11:043	0.000138	-01:24:002	0.000087	0.003312	0.000562	0.00275	0.000329
48	13:11:038	0.000036	-01:33:020	0.000029	0.017942	0.000551	0.010163	0.000377
49	13:11:032	0.000031	-01:19:031	0.000022	0.099474	0.000961	0.023279	0.000417
49	13:11:031	0.000166	-01:19:050	0.000046	0.006671	0.000632	0.004211	0.000394
50	13:11:031	0.000073	-01:01:058	0.000069	0.00198	0.000531	0.002469	0.000281
52	13:11:030	0.000124	-01:20:013	0.000073	0.004191	0.000695	0.003514	0.000412
52	13:11:030	0.000223	-01:20:014	0.000065	0.003033	0.000682	0.00245	0.0004
53	13:11:030	0.000031	-01:20:028	0.000024	0.014753	0.000698	0.01185	0.000429
54	13:11:017	0.000097	-01:33:048	0.000049	0.004894	0.000592	0.004258	0.000338
55	13:11:016	0.000018	-01:33:029	0.000016	0.026319	0.000842	0.018858	0.000355
55	13:11:016	0.000161	-01:33:038	0.00008	0.003583	0.00058	0.002645	0.000358
56	13:11:016	0.000232	-01:28:039	0.000142	0.002767	0.000491	0.001591	0.000333
58	13:11:016	0.000102	-01:33:014	0.000046	0.003546	0.00061	0.003607	0.000332
59	13:11:015	0.000038	-01:31:049	0.00004	0.015545	0.00052	0.008659	0.000355
60	13:11:014	0.000298	-01:31:028	0.000145	0.009586	0.000368	0.002085	0.000306
61	13:11:010	0.000186	-01:03:004	0.000192	0.002551	0.000387	0.001451	0.00026
62	13:11:003	0.000055	-01:33:005	0.000052	0.003012	0.00044	0.003081	0.000252
62	13:11:003	0.000119	-01:32:059	0.000184	0.00182	0.000422	0.00137	0.000265
63	13:10:056	0.000188	-01:27:043	0.000119	0.00213	0.000454	0.001665	0.000273
64	13:10:056	0.000049	-01:27:024	0.000033	0.007511	0.000633	0.005252	0.000274
65	13:10:055	0.000106	-01:27:009	0.000071	0.001788	0.000475	0.00204	0.000254
66	13:10:052	0.000124	-01:41:020	0.000107	0.005019	0.000303	0.002115	0.000222
67	13:10:049	0.000064	-01:29:011	0.000065	0.002305	0.000441	0.002479	0.000248
68	13:10:045	0.000045	-01:09:012	0.000035	0.018467	0.000682	0.007936	0.000337
70	13:10:041	0.00018	-01:29:037	0.000105	0.002158	0.000385	0.001466	0.000248

Continued on next page

Table C.16: Positions of radio sources within 4MPc radius of the pointing centre of cluster RXCJ1311.4−0120

Source ID	RA	δ RA	DEC	δ DEC	total flux	δ total flux	Peak flux	δ Peak flux
71	13:10:039	0.000082	-01:24:043	0.000121	0.004245	0.000402	0.002682	0.000259
72	13:10:035	0.000105	-01:08:023	0.000106	0.003987	0.000606	0.003082	0.000371
73	13:10:033	0.000311	-00:59:006	0.000113	0.007555	0.000754	0.003055	0.000552
75	13:10:031	0.000008	-00:58:041	0.000012	0.129133	0.001314	0.061449	0.000573
75	13:10:031	0.000056	-00:58:050	0.000021	0.019657	0.00092	0.013699	0.000575
75	13:10:030	0.000158	-00:59:002	0.000058	0.01127	0.000847	0.00592	0.000573
75	13:10:031	0.000136	-00:58:060	0.000041	0.02207	0.000756	0.008318	0.000558
76	13:10:032	0.000303	-01:04:021	0.000126	0.006975	0.000725	0.00288	0.000529
77	13:10:031	0.000183	-01:02:054	0.000205	0.004101	0.000911	0.002691	0.000594
77	13:10:031	0.000189	-01:02:053	0.000137	0.003809	0.000937	0.002824	0.000593
78	13:10:031	0.000252	-00:59:038	0.000089	0.009269	0.000816	0.003955	0.000589
79	13:10:030	0.000195	-01:05:036	0.000174	0.004783	0.000762	0.002764	0.000511
80	13:10:030	0.000135	-01:02:059	0.000101	0.006939	0.000951	0.004463	0.000626
81	13:10:029	0.000159	-01:03:009	0.000153	0.004672	0.000975	0.003282	0.000626
82	13:10:028	0.000233	-01:06:028	0.000095	0.007163	0.000718	0.003344	0.000508
83	13:10:028	0.00002	-01:03:014	0.000025	0.081943	0.001157	0.033225	0.000581
83	13:10:026	0.000037	-01:03:022	0.000099	0.076948	0.001348	0.020582	0.000581
85	13:10:028	0.000211	-00:59:006	0.000131	0.005187	0.000924	0.003391	0.000593
85	13:10:029	0.00032	-00:59:005	0.000144	0.003749	0.00092	0.002478	0.000583
86	13:10:027	0.000118	-01:03:034	0.000048	0.010893	0.000928	0.006746	0.000607
86	13:10:028	0.000103	-01:03:033	0.000081	0.003441	0.001029	0.00389	0.000567
87	13:10:027	0.000236	-01:01:046	0.000113	0.007108	0.000809	0.003373	0.000573
87	13:10:027	0.000253	-01:01:048	0.000152	0.003654	0.000884	0.002401	0.000577
88	13:10:027	0.000128	-01:22:039	0.000148	0.001987	0.000505	0.001746	0.000297
89	13:10:027	0.000177	-01:11:026	0.0001	0.005774	0.000738	0.003515	0.000483
90	13:10:026	0.00001	-01:09:040	0.00001	0.060908	0.001289	0.045565	0.000525
90	13:10:026	0.00002	-01:09:048	0.000067	0.02756	0.00123	0.012814	0.000525
91	13:10:026	0.000123	-01:09:026	0.000051	0.005286	0.000898	0.004646	0.000526
92	13:10:026	0.000104	-01:09:059	0.000044	0.00862	0.000844	0.006258	0.000523
92	13:10:025	0.000169	-01:10:002	0.000113	0.004162	0.000859	0.003116	0.000537
93	13:10:025	0.000309	-01:03:042	0.000087	0.00945	0.00073	0.003611	0.000536
93	13:10:026	0.000103	-01:03:041	0.000047	0.011831	0.000871	0.007456	0.000562
95	13:10:026	0.00022	-01:11:047	0.000067	0.002738	0.000774	0.002485	0.000438
96	13:10:026	0.000176	-01:09:025	0.000081	0.002529	0.000932	0.003007	0.000464
97	13:10:025	0.000104	-01:09:011	0.000093	0.00632	0.000874	0.004809	0.000539
99	13:10:025	0.000142	-01:10:011	0.000086	0.003822	0.000871	0.003413	0.000512
100	13:10:025	0.000188	-00:59:036	0.000204	0.00743	0.00073	0.002924	0.000546
101	13:10:023	0.000132	-01:10:046	0.000115	0.007617	0.000755	0.00404	0.000524
101	13:10:024	0.000066	-01:10:030	0.000068	0.013937	0.000753	0.00784	0.000508
101	13:10:024	0.000101	-01:10:023	0.000074	0.009536	0.000766	0.005659	0.00051
101	13:10:024	0.000027	-01:10:037	0.000053	0.021829	0.000758	0.012142	0.000516

Continued on next page

Table C.16: Positions of radio sources within 4MPc radius of the pointing centre of cluster RXCJ1311.4−0120

Source ID	RA	δ RA	DEC	δ DEC	total flux	δ total flux	Peak flux	δ Peak flux
102	13:10:020	0.00012	-01:16:019	0.000181	0.004362	0.000516	0.002339	0.000354
103	13:10:015	0.000026	-01:00:025	0.000017	0.068638	0.000983	0.025371	0.000391
105	13:10:014	0.000236	-01:00:054	0.00012	0.004262	0.000589	0.002222	0.000408
105	13:10:015	0.000222	-01:00:055	0.000176	0.000994	0.000676	0.001191	0.000359
106	13:10:014	0.000243	-01:00:044	0.000166	0.002947	0.00061	0.001781	0.000408
106	13:10:014	0.000261	-01:00:044	0.000133	0.002509	0.000623	0.00176	0.000393
107	13:10:007	0.000069	-01:24:015	0.000088	0.003122	0.000396	0.002463	0.000244
107	13:10:007	0.000212	-01:24:023	0.000111	0.000721	0.000414	0.000865	0.00022

Table C.17: Positions of radio sources within 4MPc radius of the pointing centre of cluster RXCJ1516.3+0005

Source ID	RA	δ RA	DEC	δ DEC	total flux	δ total flux	Peak flux	δ Peak flux
0	15:18:011	0.000134	00:23:015	0.000098	0.00223	0.000663	0.002041	0.000386
5	15:17:048	0.000109	-00:08:012	0.00008	0.006957	0.001213	0.005088	0.000769
6	15:17:016	0.000131	-00:03:024	0.000098	0.007622	0.002069	0.006431	0.001254
6	15:17:015	0.000361	-00:03:030	0.000237	0.019471	0.001444	0.004808	0.001175
7	15:17:001	0.000104	-00:19:038	0.000111	0.007048	0.001694	0.005732	0.001043
9	15:16:042	0.000104	00:15:051	0.000132	0.057499	0.013668	0.044701	0.008487
10	15:16:041	0.000085	00:14:032	0.000076	0.069646	0.016087	0.065038	0.009461
11	15:16:041	0.000087	00:03:044	0.000169	0.011604	0.003109	0.009741	0.001831
12	15:16:040	0.000024	00:15:001	0.000021	0.435973	0.025322	0.385799	0.01514
12	15:16:041	0.000086	00:15:006	0.000105	0.102181	0.025317	0.090297	0.015142
13	15:16:040	0.000099	00:13:024	0.000094	0.025596	0.0091	0.027642	0.005082
14	15:16:040	0.000124	00:12:038	0.000115	0.023262	0.007401	0.02221	0.004216
15	15:16:040	0.000099	00:11:055	0.000122	0.022439	0.005511	0.018379	0.003371
16	15:16:037	0.000105	00:07:039	0.000084	0.017772	0.004371	0.015694	0.00262
17	15:16:035	0.000112	00:16:012	0.00011	0.054677	0.00623	0.03031	0.004238
17	15:16:034	0.000137	00:16:018	0.000337	0.091522	0.004516	0.019768	0.003757
18	15:16:024	0.000085	00:02:011	0.000077	0.007557	0.002201	0.007998	0.00124
19	15:16:011	0.00009	-00:19:046	0.000114	0.001915	0.000526	0.001732	0.000312
20	15:15:055	0.000112	-00:08:015	0.000171	0.006122	0.000897	0.003355	0.000613
21	15:15:055	0.000243	-00:04:026	0.000114	0.009841	0.001248	0.004352	0.000898
23	15:15:055	0.000056	-00:02:049	0.000046	0.032545	0.004346	0.029165	0.002582
24	15:15:053	0.000097	00:25:023	0.000095	0.00286	0.000723	0.002519	0.000435
25	15:15:049	0.000124	00:27:009	0.000085	0.002609	0.000713	0.002305	0.000427
26	15:15:049	0.000085	00:30:015	0.000072	0.009436	0.001778	0.008004	0.001078
27	15:15:048	0.000201	00:27:008	0.000122	0.004691	0.000738	0.002589	0.000498
28	15:15:046	0.000223	00:18:035	0.000167	0.020409	0.001078	0.005072	0.000879

Continued on next page

Table C.17: Positions of radio sources within 4MPc radius of the pointing centre of cluster RXCJ1516.3+0005

Source ID	RA	δ RA	DEC	δ DEC	total flux	δ total flux	Peak flux	δ Peak flux
29	15:15:044	0.000231	-00:02:012	0.00011	0.006382	0.000737	0.002863	0.000525
29	15:15:044	0.00015	-00:02:011	0.00014	0.003047	0.000861	0.002397	0.000528
30	15:15:044	0.000086	00:00:009	0.000064	0.016089	0.00229	0.012231	0.001427
32	15:15:030	0.000195	00:20:035	0.000089	0.053226	0.002455	0.016531	0.001893
34	15:15:019	0.000106	00:12:016	0.000099	0.002045	0.000675	0.00202	0.000391
35	15:15:018	0.000054	00:10:012	0.0001	0.002739	0.000743	0.002878	0.000415
36	15:15:018	0.000137	00:11:008	0.000097	0.003542	0.000799	0.002876	0.000478
37	15:15:018	0.000163	00:11:053	0.00008	0.004211	0.000956	0.003162	0.000594
37	15:15:018	0.000118	00:11:054	0.000094	0.002485	0.001006	0.002696	0.000564
38	15:15:018	0.00006	00:14:014	0.000049	0.015737	0.002346	0.014337	0.00139
39	15:15:017	0.000122	-00:19:019	0.000137	0.003499	0.000682	0.002416	0.000434
41	15:15:017	0.000129	-00:20:006	0.000137	0.002906	0.000687	0.002102	0.000437
42	15:15:016	0.000132	-00:23:013	0.00017	0.004354	0.000526	0.001977	0.000381
44	15:15:016	0.000072	-00:17:046	0.000061	0.01554	0.002243	0.012732	0.001365
46	15:14:052	0.000107	-00:23:046	0.000097	0.004963	0.00076	0.003254	0.000498
47	15:14:048	0.000085	00:36:015	0.000083	0.002833	0.000574	0.002378	0.000351
48	15:14:045	0.000074	00:06:027	0.00011	0.002258	0.000547	0.002011	0.000326
49	15:14:045	0.000145	00:07:023	0.000114	0.002907	0.000635	0.002092	0.000402
50	15:14:045	0.000138	00:08:009	0.000085	0.002013	0.000677	0.001937	0.000392
50	15:14:045	0.000206	00:08:007	0.00012	0.002591	0.000636	0.001742	0.00041
51	15:14:045	0.000106	00:10:030	0.000082	0.010204	0.002054	0.008146	0.001268
52	15:14:044	0.000166	00:07:023	0.000112	0.003415	0.000657	0.002191	0.00043
53	15:14:027	0.00022	00:28:024	0.000094	0.002008	0.00029	0.001034	0.0002
54	15:14:018	0.000126	00:02:022	0.000092	0.002719	0.000515	0.001918	0.00033

Table C.18: Positions of radio sources within 4MPc radius of the pointing centre of cluster RXCJ1516.5−0056

Source ID	RA	δ RA	DEC	δ DEC	total flux	δ total flux	Peak flux	δ Peak flux
0	15:18:016	0.000232	-01:01:051	0.00009	0.00923	0.000778	0.004098	0.000555
1	15:18:016	0.000151	-01:15:003	0.000077	0.000814	0.000241	0.000842	0.000135
2	15:18:010	0.000127	-01:14:044	0.000073	0.008606	0.000661	0.004587	0.000455
3	15:18:007	0.000117	-01:03:001	0.00007	0.003643	0.00053	0.002813	0.000329
4	15:17:046	0.000117	-01:23:055	0.000084	0.002504	0.000373	0.001883	0.000234
5	15:17:044	0.000119	-00:56:059	0.000062	0.004387	0.000602	0.003376	0.000372
6	15:17:038	0.000059	-00:45:044	0.000059	0.013247	0.000637	0.007049	0.000443
7	15:17:038	0.000144	-01:04:006	0.000109	0.000357	0.000127	0.000377	0.000072
8	15:17:033	0.000128	-01:02:045	0.000093	0.001394	0.000311	0.001239	0.000186
9	15:17:029	0.000093	-00:59:047	0.000057	0.005973	0.000687	0.004604	0.000426

Continued on next page

Table C.18: Positions of radio sources within 4MPc radius of the pointing centre of cluster RXCJ1516.5−0056

Source ID	RA	δ RA	DEC	δ DEC	total flux	δ total flux	Peak flux	δ Peak flux
10	15:17:028	0.000169	-00:39:053	0.000147	0.001493	0.000323	0.001059	0.000207
11	15:17:027	0.000205	-01:24:014	0.000104	0.00175	0.000498	0.001529	0.000293
12	15:17:027	0.000076	-01:23:056	0.000057	0.005621	0.000614	0.004478	0.000379
13	15:17:024	0.000157	-00:43:035	0.000101	0.00178	0.000397	0.001459	0.000242
14	15:17:020	0.000122	-00:37:057	0.000086	0.001543	0.000349	0.00143	0.000205
15	15:17:018	0.000054	-01:15:006	0.0002	0.004358	0.000874	0.001806	0.000371
16	15:17:013	0.000087	-01:16:020	0.000061	0.003844	0.000553	0.003361	0.000331
17	15:17:013	0.00014	-00:57:045	0.000079	0.00078	0.000323	0.00098	0.000169
18	15:17:012	0.000276	-01:14:013	0.000307	0.001088	0.000122	0.000376	0.000094
19	15:17:010	0.000101	-01:09:052	0.000064	0.005269	0.000718	0.004219	0.00044
20	15:17:006	0.000248	-00:53:050	0.000109	0.002392	0.000539	0.00168	0.00034
20	15:17:006	0.000244	-00:53:044	0.000158	0.002243	0.00054	0.001493	0.000351
21	15:17:006	0.00012	-00:31:024	0.000101	0.001321	0.000279	0.00113	0.000169
22	15:17:002	0.000193	-01:00:034	0.000257	0.006891	0.000686	0.002613	0.000516
23	15:16:053	0.000128	-00:54:041	0.00008	0.001755	0.000379	0.001652	0.000218
24	15:16:052	0.000075	-00:54:010	0.000046	0.010367	0.000865	0.007451	0.00055
25	15:16:044	0.000094	-00:58:007	0.000044	0.013708	0.000588	0.006714	0.00041
26	15:16:041	0.000158	-00:56:058	0.000075	0.000807	0.000354	0.001017	0.000183
27	15:16:040	0.00005	-00:57:028	0.000029	0.009259	0.000734	0.008219	0.000435
28	15:16:031	0.00012	-00:55:055	0.000078	0.003039	0.00062	0.00273	0.000368
29	15:16:031	0.000168	-00:53:029	0.00007	0.002266	0.000465	0.001895	0.000277
30	15:16:031	0.000092	-00:56:056	0.000056	0.002569	0.000682	0.003171	0.000358
31	15:16:031	0.000205	-00:58:008	0.000064	0.001988	0.000575	0.001962	0.000312
32	15:16:031	0.000125	-00:56:043	0.000064	0.007673	0.001307	0.006697	0.000765
33	15:16:030	0.000138	-00:52:016	0.00006	0.001143	0.000475	0.001538	0.000239
34	15:16:030	0.000048	-00:56:025	0.000031	0.033847	0.002471	0.028882	0.001489
35	15:16:025	0.000142	-00:46:053	0.000105	0.003269	0.000599	0.002443	0.000378
36	15:16:024	0.000043	-00:49:047	0.00003	0.094794	0.00282	0.050396	0.001957
36	15:16:024	0.000059	-00:49:049	0.000043	0.052982	0.002929	0.033043	0.001949
37	15:16:024	0.00029	-00:44:058	0.000119	0.003672	0.000487	0.0018	0.00034
38	15:16:023	0.000232	-00:53:001	0.000101	0.005029	0.000838	0.003105	0.000551
39	15:16:019	0.000067	-01:04:047	0.000042	0.006242	0.00064	0.005338	0.000386
40	15:16:016	0.000093	-00:50:006	0.000058	0.005931	0.000831	0.005064	0.0005
41	15:16:013	0.000165	-00:31:036	0.000113	0.00166	0.00029	0.001151	0.000186
42	15:16:004	0.000227	-00:55:039	0.000132	0.001383	0.000314	0.000993	0.000197
43	15:15:056	0.000224	-00:49:044	0.000109	0.005152	0.000596	0.002654	0.000411
44	15:15:055	0.000071	-00:50:045	0.000044	0.004615	0.000661	0.004743	0.00037
45	15:15:055	0.000244	-00:51:057	0.000142	0.00425	0.000577	0.002295	0.00039
46	15:15:055	0.000139	-00:50:032	0.000072	0.008965	0.001658	0.007792	0.000969
47	15:15:055	0.000038	-00:50:014	0.000025	0.043452	0.00259	0.037568	0.001556
48	15:15:055	0.000125	-00:46:006	0.000085	0.001679	0.000528	0.001872	0.00029

Continued on next page

Table C.18: Positions of radio sources within 4MPc radius of the pointing centre of cluster RXCJ1516.5−0056

Source ID	RA	δ RA	DEC	δ DEC	total flux	δ total flux	Peak flux	δ Peak flux
49	15:15:054	0.000258	-00:50:037	0.000101	0.006187	0.001153	0.00407	0.000732
50	15:15:053	0.000093	-00:41:034	0.000055	0.006083	0.000742	0.004861	0.000456
51	15:15:051	0.000233	-01:03:010	0.000155	0.000773	0.000177	0.000525	0.000114
52	15:15:049	0.000081	-00:49:046	0.000052	0.005893	0.000786	0.00523	0.000467
53	15:15:046	0.000115	-01:26:051	0.00014	0.001345	0.000412	0.001304	0.00024
54	15:15:045	0.000214	-00:55:043	0.000116	0.003136	0.000591	0.002127	0.000377
55	15:15:045	0.000102	-00:56:044	0.000068	0.00281	0.000712	0.003188	0.000385
56	15:15:045	0.000173	-01:21:040	0.000097	0.001487	0.000543	0.001623	0.000294
57	15:15:045	0.00013	-01:25:007	0.000062	0.002781	0.000634	0.002852	0.000348
58	15:15:045	0.000127	-00:56:031	0.000071	0.005336	0.001382	0.005668	0.000758
59	15:15:045	0.000126	-00:52:005	0.000073	0.001491	0.000505	0.001768	0.000271
60	15:15:044	0.000046	-00:56:013	0.000029	0.034235	0.0022	0.028032	0.001341
61	15:15:044	0.000089	-01:24:055	0.000051	0.006448	0.001015	0.006279	0.000576
62	15:15:044	0.000116	-01:20:028	0.000064	0.002145	0.0005	0.002193	0.000282
63	15:15:044	0.000034	-01:24:037	0.000024	0.029777	0.001567	0.024891	0.000953
63	15:15:044	0.000176	-01:24:045	0.00007	0.002587	0.001647	0.003926	0.000778
64	15:15:041	0.000158	-01:14:060	0.000091	0.002282	0.000402	0.001674	0.000253
65	15:15:039	0.000094	-01:01:002	0.00008	0.004033	0.000536	0.003045	0.000338
66	15:15:036	0.000068	-01:13:028	0.000042	0.011927	0.000776	0.008033	0.0005
67	15:15:034	0.000099	-01:13:015	0.000083	0.0044	0.000765	0.003811	0.00046
68	15:15:028	0.000144	-01:05:028	0.000099	0.008736	0.001641	0.006743	0.001021
68	15:15:028	0.000174	-01:05:021	0.000395	0.012527	0.00223	0.004577	0.000981
69	15:15:024	0.000217	-01:10:004	0.000173	0.005579	0.000597	0.002487	0.000431
69	15:15:025	0.000331	-01:09:058	0.000211	0.002209	0.000659	0.001405	0.000434
70	15:15:024	0.000241	-01:08:029	0.000183	0.001398	0.000305	0.000887	0.0002
71	15:15:022	0.000406	-00:44:032	0.000156	0.002071	0.000148	0.000591	0.000117
73	15:15:019	0.000603	-00:34:023	0.000365	0.008533	0.000057	0.000379	0.000055
74	15:15:015	0.000057	-00:45:001	0.000037	0.011307	0.00084	0.008833	0.00052
77	15:15:008	0.000271	-01:07:051	0.000106	0.004107	0.000721	0.002468	0.000475
78	15:15:007	0.000082	-01:07:048	0.000049	0.016404	0.00108	0.009921	0.000722
79	15:15:002	0.000139	-01:01:025	0.000088	0.009831	0.00042	0.003634	0.000315
80	15:14:057	0.000438	-00:36:023	0.000434	0.003535	0.000076	0.000347	0.00007
81	15:14:058	0.000171	-01:18:004	0.000111	0.001676	0.000409	0.001366	0.00025

Table C.19: Positions of radio sources within 4MPc radius of the pointing centre of cluster RXCJ2014.8−2430

Source ID	RA	δ RA	DEC	δ DEC	total flux	δ total flux	Peak flux	δ Peak flux
0	20:16:039	0.000126	-24:24:057	0.000097	0.006013	0.000473	0.00339	0.000324
1	20:16:036	0.000186	-24:33:006	0.000082	0.003251	0.000547	0.00261	0.000331
1	20:16:036	0.000232	-24:33:016	0.000428	0.001733	0.000532	0.001172	0.000342
2	20:16:034	0.000281	-24:34:050	0.000089	0.009375	0.000441	0.003491	0.000322
3	20:16:027	0.000195	-24:19:020	0.000071	0.004188	0.000462	0.002728	0.000296
4	20:16:025	0.000249	-24:36:007	0.000204	0.00357	0.000534	0.001949	0.000368
5	20:16:008	0.000142	-24:36:019	0.000077	0.00847	0.000693	0.005061	0.000462
6	20:16:007	0.000158	-24:36:034	0.000327	0.003789	0.000691	0.002282	0.000459
7	20:16:006	0.000136	-24:29:025	0.000091	0.010471	0.000623	0.005043	0.000443
8	20:16:002	0.000088	-24:36:013	0.000044	0.011409	0.000752	0.008008	0.000477
8	20:16:003	0.000201	-24:35:059	0.000421	0.007883	0.000601	0.002557	0.000464
10	20:15:060	0.000235	-24:14:011	0.000126	0.001478	0.000472	0.001411	0.000272
11	20:15:055	0.000155	-24:31:014	0.000071	0.010136	0.000685	0.005372	0.000471
12	20:15:054	0.00018	-24:30:033	0.000249	0.00444	0.000718	0.002606	0.000486
13	20:15:053	0.00008	-24:51:031	0.000061	0.007186	0.000782	0.006313	0.000469
16	20:15:037	0.000026	-24:22:049	0.000017	0.036112	0.001073	0.02985	0.000653
16	20:15:038	0.000012	-24:22:040	0.000013	0.058502	0.001543	0.048244	0.000635
18	20:15:037	0.000125	-24:23:011	0.000401	0.006002	0.000949	0.004358	0.000502
19	20:15:037	0.000261	-24:21:057	0.000172	0.005574	0.000994	0.003804	0.000626
19	20:15:036	0.000189	-24:22:007	0.000303	0.004554	0.001006	0.003128	0.000639
21	20:15:028	0.000148	-24:43:011	0.000136	0.009309	0.001239	0.006197	0.000809
22	20:15:016	0.000094	-24:30:011	0.000079	0.017565	0.001419	0.011567	0.000931
22	20:15:016	0.000113	-24:30:002	0.000171	0.01016	0.001423	0.007097	0.000909
23	20:15:014	0.000278	-24:12:041	0.000134	0.002609	0.000582	0.001916	0.000364
24	20:15:002	0.000218	-24:33:005	0.000212	0.008369	0.002241	0.007243	0.0013
25	20:14:055	0.000071	-24:30:021	0.000215	0.011918	0.003204	0.012794	0.001662
26	20:14:054	0.000063	-24:30:028	0.000075	0.01626	0.00329	0.020528	0.001731
26	20:14:054	0.000121	-24:30:019	0.000104	0.012403	0.00327	0.013882	0.001796
26	20:14:054	0.000119	-24:30:037	0.00018	0.008645	0.003274	0.009922	0.001789
29	20:14:053	0.000142	-24:29:049	0.000139	0.008982	0.003262	0.010348	0.001794
29	20:14:053	0.000305	-24:30:00	0.000148	0.010999	0.003119	0.008877	0.001885
29	20:14:053	0.00012	-24:29:052	0.000358	0.005045	0.003323	0.006564	0.001604
30	20:14:053	0.000374	-24:30:034	0.00016	0.014393	0.002994	0.009159	0.001932
31	20:14:053	0.000088	-24:30:051	0.000109	0.005644	0.003285	0.010131	0.001529
32	20:14:052	0.000004	-24:30:023	0.000005	0.487623	0.005682	0.412378	0.001893
32	20:14:051	0.00004	-24:30:005	0.000058	0.026877	0.003343	0.033591	0.001697
32	20:14:051	0.000066	-24:29:043	0.000047	0.02579	0.003302	0.028433	0.001817
32	20:14:051	0.000081	-24:29:054	0.000063	0.025804	0.003266	0.025727	0.001837
32	20:14:051	0.000209	-24:29:049	0.00011	0.01087	0.003268	0.010746	0.001862
33	20:14:052	0.000023	-24:30:005	0.000038	0.026277	0.003334	0.039647	0.001637
34	20:14:052	0.000112	-24:31:004	0.000059	0.01646	0.003279	0.018467	0.001777

Continued on next page

Table C.19: Positions of radio sources within 4MPc radius of the pointing centre of cluster RXCJ2014.8−2430

Source ID	RA	δ RA	DEC	δ DEC	total flux	δ total flux	Peak flux	δ Peak flux
35	20:14:052	0.000127	-24:30:050	0.000052	0.025747	0.004778	0.020877	0.001896
35	20:14:051	0.000097	-24:30:053	0.00006	0.016922	0.003318	0.019537	0.001795
35	20:14:051	0.000141	-24:30:055	0.000072	0.009908	0.003341	0.012962	0.001718
36	20:14:052	0.000117	-24:31:022	0.000085	0.009616	0.003237	0.012812	0.001678
36	20:14:051	0.00017	-24:31:024	0.000066	0.008619	0.003271	0.011701	0.001608
37	20:14:051	0.000137	-24:29:027	0.000132	0.011989	0.003189	0.012176	0.001819
40	20:14:048	0.0001	-24:29:011	0.000195	0.008331	0.003113	0.010065	0.001613
41	20:14:045	0.00042	-24:47:027	0.000543	0.014297	0.000249	0.001353	0.000228
42	20:14:035	0.000284	-24:15:005	0.00013	0.003804	0.000766	0.002666	0.000484
45	20:14:004	0.000098	-24:48:046	0.0003	0.003758	0.000764	0.002827	0.00046
46	20:14:002	0.00001	-24:49:010	0.000011	0.04514	0.001171	0.039724	0.000474
47	20:14:003	0.000026	-24:48:053	0.000165	0.003385	0.000871	0.004744	0.000356
49	20:14:002	0.000039	-24:48:049	0.000169	0.009303	0.000739	0.006198	0.000452
50	20:14:002	0.000091	-24:48:015	0.000174	0.002217	0.000835	0.002791	0.000431
51	20:14:002	0.000331	-24:48:030	0.000413	0.009896	0.000578	0.002421	0.000472
54	20:13:028	0.000174	-24:30:017	0.00015	0.004401	0.000503	0.002511	0.000343
55	20:13:020	0.000106	-24:29:025	0.000047	0.004862	0.000498	0.00406	0.000297
57	20:13:019	0.000106	-24:39:00	0.000214	0.008116	0.000422	0.003016	0.000317
58	20:13:017	0.000041	-24:48:024	0.000027	0.0205	0.000899	0.016264	0.000555
59	20:13:016	0.000113	-24:45:009	0.000073	0.005889	0.000821	0.005124	0.000492
60	20:13:016	0.000185	-24:47:044	0.000236	0.003787	0.000962	0.002922	0.0006
61	20:13:013	0.000021	-24:46:057	0.000022	0.034356	0.000944	0.027173	0.000587
61	20:13:012	0.000053	-24:46:026	0.000035	0.040218	0.001546	0.021148	0.00056

Table C.20: Positions of radio sources within 4MPc radius of the pointing centre of cluster RXCJ2023.0−2056

Source ID	RA	δ RA	DEC	δ DEC	total flux	δ total flux	Peak flux	δ Peak flux
0	20:27:004	0.000123	-21:36:014	0.000101	0.007745	0.000979	0.004694	0.000651
1	20:26:046	0.000107	-21:36:015	0.00015	0.000447	0.000148	0.000453	0.000081
2	20:26:033	0.000149	-21:53:042	0.000176	0.000685	0.000158	0.0005	0.000097
3	20:25:039	0.000128	-21:09:012	0.000111	0.013065	0.001217	0.006242	0.000868
4	20:25:029	0.000162	-21:20:050	0.000131	0.000842	0.000198	0.000598	0.000127
5	20:25:028	0.000119	-21:29:046	0.000155	0.00054	0.000173	0.00051	0.000098
6	20:25:017	0.000064	-21:10:059	0.000039	0.015484	0.000974	0.009631	0.000645
7	20:24:049	0.000124	-21:04:057	0.000076	0.006201	0.000707	0.003671	0.000475
8	20:24:040	0.000184	-21:22:031	0.000166	0.001098	0.000176	0.000579	0.000122
9	20:24:036	0.000093	-20:44:037	0.000106	0.011197	0.001278	0.007882	0.000776

Continued on next page

Table C.20: Positions of radio sources within 4MPc radius of the pointing centre of cluster RXCJ2023.0−2056

Source ID	RA	δ RA	DEC	δ DEC	total flux	δ total flux	Peak flux	δ Peak flux
10	20:24:034	0.000039	-20:43:030	0.000081	0.02621	0.003112	0.022038	0.001843
11	20:24:034	0.000084	-20:42:040	0.000201	0.007969	0.001933	0.00619	0.00117
12	20:24:033	0.000012	-20:43:059	0.000023	0.234316	0.004882	0.113395	0.002403
13	20:24:034	0.000092	-20:43:004	0.000094	0.014732	0.003444	0.013829	0.002003
14	20:24:034	0.000077	-20:43:041	0.00019	0.03072	0.004832	0.019888	0.003079
15	20:24:033	0.000098	-20:42:046	0.000112	0.006288	0.001454	0.005952	0.000814
16	20:24:033	0.00003	-20:43:040	0.000035	0.10355	0.006076	0.057259	0.00254
17	20:24:032	0.000071	-20:44:018	0.000194	0.007794	0.001767	0.0062	0.001048
18	20:24:032	0.000101	-20:44:055	0.000125	0.005843	0.001508	0.005095	0.000905
19	20:24:032	0.000072	-20:43:017	0.000119	0.014276	0.003397	0.013057	0.001996
20	20:24:031	0.000091	-20:45:003	0.000167	0.010803	0.002792	0.009609	0.001593
21	20:24:030	0.000101	-20:34:051	0.000092	0.005738	0.00088	0.004038	0.000567
22	20:24:029	0.000099	-20:43:046	0.000133	0.006543	0.001913	0.006322	0.001088
23	20:24:026	0.000093	-20:45:005	0.000154	0.004077	0.001	0.003638	0.00057
24	20:24:024	0.00006	-20:43:035	0.000164	0.002547	0.00086	0.002786	0.000449
25	20:24:022	0.000083	-20:42:028	0.000169	0.003572	0.001114	0.003489	0.000618
27	20:24:021	0.000103	-20:40:023	0.000143	0.003401	0.000937	0.003024	0.000552
28	20:24:010	0.000052	-20:41:009	0.000046	0.013764	0.001188	0.01033	0.00075
29	20:23:041	0.000161	-21:07:053	0.000114	0.004473	0.000822	0.002886	0.000541
30	20:23:036	0.000085	-20:55:045	0.00016	0.003106	0.000747	0.002596	0.000445
31	20:23:035	0.000048	-20:56:013	0.000042	0.013126	0.001068	0.009999	0.000671
32	20:23:034	0.000069	-21:17:030	0.000048	0.011418	0.000934	0.007577	0.000609
33	20:23:034	0.000126	-20:57:012	0.000189	0.002931	0.000684	0.002172	0.000421
34	20:23:027	0.000063	-20:28:004	0.000185	0.003241	0.000892	0.002917	0.000508
35	20:23:026	0.000046	-20:28:032	0.000039	0.016836	0.001183	0.012092	0.000757
36	20:23:026	0.000051	-21:08:009	0.000114	0.008058	0.001079	0.006276	0.000647
37	20:23:025	0.000028	-21:08:038	0.000026	0.03178	0.00162	0.024938	0.001007
38	20:23:025	0.000073	-21:08:020	0.000161	0.005296	0.001821	0.00557	0.000987
39	20:23:024	0.000054	-21:08:016	0.000133	0.004554	0.001336	0.004937	0.000716
40	20:23:021	0.000082	-20:37:046	0.00008	0.003354	0.000743	0.003219	0.000433
41	20:23:021	0.000084	-21:23:053	0.000091	0.002621	0.000514	0.002242	0.000312
42	20:23:017	0.000196	-21:11:015	0.000175	0.018982	0.000988	0.00491	0.000802
43	20:23:009	0.00022	-20:46:035	0.000077	0.006683	0.000594	0.002911	0.000425
44	20:22:060	0.000156	-20:57:00	0.000144	0.265918	0.003028	0.030803	0.002728
45	20:22:059	0.000209	-20:57:022	0.000143	0.013624	0.002032	0.0068	0.001433
46	20:22:059	0.000073	-20:56:053	0.000097	0.014262	0.00222	0.011599	0.001339
46	20:22:058	0.000117	-20:56:046	0.000133	0.01467	0.002117	0.008854	0.001417
48	20:22:056	0.000201	-20:55:040	0.000172	0.014069	0.001268	0.005028	0.000968
49	20:22:055	0.000066	-20:59:025	0.000113	0.004587	0.000998	0.004275	0.000575
50	20:22:052	0.000047	-20:58:028	0.000138	0.017474	0.001509	0.010224	0.00098
51	20:22:052	0.000017	-20:58:056	0.00002	0.050374	0.002112	0.043315	0.001275

Continued on next page

Table C.20: Positions of radio sources within 4MPc radius of the pointing centre of cluster RXCJ2023.0−2056

Source ID	RA	δ RA	DEC	δ DEC	total flux	δ total flux	Peak flux	δ Peak flux
52	20:22:049	0.000091	-20:57:017	0.000127	0.009868	0.001711	0.004033	0.000731
53	20:22:049	0.000081	-20:59:045	0.000138	0.003767	0.001321	0.004174	0.000708
54	20:22:046	0.000112	-20:57:025	0.000173	0.003025	0.000711	0.00225	0.000444
55	20:22:044	0.000073	-21:23:020	0.000062	0.006495	0.000873	0.005177	0.000541
56	20:22:037	0.000092	-20:57:048	0.000081	0.029404	0.001034	0.010104	0.000791
57	20:22:026	0.000185	-20:43:032	0.000093	0.003475	0.000635	0.00225	0.000414
58	20:22:022	0.000159	-20:59:014	0.000129	0.003866	0.000802	0.002581	0.000524
59	20:22:018	0.000104	-20:07:005	0.000109	0.008074	0.001653	0.006428	0.001021
60	20:22:017	0.00014	-20:19:028	0.000169	0.003603	0.000534	0.001968	0.000367
61	20:22:004	0.000146	-21:12:009	0.000128	0.00329	0.000823	0.00251	0.000517
62	20:21:045	0.000188	-21:31:019	0.000088	0.010695	0.000924	0.004601	0.000671
63	20:21:037	0.000052	-20:49:025	0.000117	0.005011	0.001019	0.004707	0.000578
64	20:21:037	0.000016	-20:49:053	0.000031	0.039811	0.001558	0.023177	0.000742
65	20:21:036	0.000052	-20:52:025	0.000048	0.014766	0.001179	0.010546	0.000754
66	20:21:037	0.000061	-20:49:035	0.000127	0.004447	0.001484	0.005106	0.000786
70	20:21:010	0.000108	-20:33:002	0.000121	0.001994	0.000445	0.001597	0.000275
71	20:20:033	0.000084	-20:50:047	0.000184	0.000417	0.000134	0.000394	0.000076
72	20:20:011	0.000155	-19:59:042	0.000226	0.000735	0.000149	0.000474	0.000094
73	20:18:054	0.000126	-20:54:053	0.000169	0.000558	0.000153	0.000462	0.000092

Table C.21: Positions of radio sources within 4MPc radius of the pointing centre of cluster RXCJ2048.1−1750

Source ID	RA	δ RA	DEC	δ DEC	total flux	δ total flux	Peak flux	δ Peak flux
0	20:49:044	0.000184	-18:02:011	0.000207	0.004269	0.000333	0.001517	0.000255
1	20:49:034	0.000037	-17:49:057	0.000099	0.008806	0.000329	0.004019	0.000233
2	20:49:025	0.00009	-17:36:027	0.000107	0.008134	0.000356	0.00322	0.000264
3	20:49:021	0.000055	-17:52:025	0.000025	0.009162	0.000582	0.00555	0.000243
3	20:49:022	0.000099	-17:52:019	0.000143	0.00124	0.000424	0.001326	0.000237
4	20:49:021	0.000165	-17:52:008	0.000134	0.002103	0.000403	0.001486	0.000257
5	20:49:018	0.000295	-18:08:022	0.000208	0.003822	0.000304	0.00128	0.000233
6	20:49:017	0.00003	-18:08:045	0.000044	0.006221	0.0004	0.005127	0.000244
6	20:49:017	0.000257	-18:08:054	0.000168	0.002308	0.000362	0.001205	0.000251
6	20:49:018	0.000155	-18:08:038	0.000192	0.000874	0.000412	0.00094	0.000228
7	20:49:016	0.000091	-18:08:023	0.000266	0.001838	0.000378	0.00126	0.000237
7	20:49:017	0.000167	-18:08:029	0.000127	0.001239	0.000406	0.001159	0.000239
7	20:49:017	0.000221	-18:08:017	0.000227	0.000878	0.000407	0.00088	0.000223
8	20:48:057	0.000021	-18:08:00	0.000011	0.017247	0.00072	0.014401	0.000296
8	20:48:058	0.000076	-18:07:054	0.000088	0.002024	0.00052	0.002402	0.000275

Continued on next page

Table C.21: Positions of radio sources within 4MPc radius of the pointing centre of cluster RXCJ2048.1−1750

Source ID	RA	δ RA	DEC	δ DEC	total flux	δ total flux	Peak flux	δ Peak flux
9	20:48:057	0.000156	-18:08:022	0.000138	0.002623	0.000481	0.001916	0.0003
10	20:48:057	0.00006	-18:07:044	0.000046	0.003123	0.000523	0.003512	0.000289
12	20:48:056	0.000236	-18:11:027	0.000301	0.003554	0.000363	0.001292	0.000274
13	20:48:053	0.000416	-17:59:006	0.000333	0.010392	0.00026	0.00131	0.000232
14	20:48:049	0.000203	-17:28:058	0.000228	0.005188	0.000359	0.00178	0.000274
15	20:48:048	0.000078	-17:29:020	0.000089	0.003284	0.000455	0.002607	0.000282
15	20:48:048	0.0002	-17:29:013	0.000163	0.002228	0.000435	0.00141	0.000288
15	20:48:048	0.000343	-17:29:028	0.000155	0.003301	0.000379	0.001313	0.00028
16	20:48:047	0.000126	-17:28:026	0.000107	0.001089	0.000472	0.001358	0.00025
17	20:48:046	0.00001	-17:27:054	0.000016	0.018448	0.000454	0.015945	0.000273
17	20:48:046	0.000053	-17:27:049	0.000064	0.002087	0.000472	0.002771	0.000239
17	20:48:045	0.000112	-17:28:003	0.00008	0.001936	0.000462	0.001972	0.000261
18	20:48:046	0.000222	-17:28:016	0.000088	0.002566	0.000424	0.001718	0.000267
19	20:48:045	0.00005	-17:27:038	0.000051	0.002395	0.000468	0.00306	0.000246
22	20:48:044	0.000042	-17:39:048	0.000061	0.005354	0.000443	0.004175	0.000276
23	20:48:042	0.000059	-18:05:045	0.000075	0.036241	0.000939	0.018756	0.00036
23	20:48:042	0.000055	-18:05:013	0.000047	0.002043	0.000631	0.003314	0.000303
23	20:48:043	0.000021	-18:05:029	0.00002	0.036259	0.001003	0.019964	0.00036
23	20:48:043	0.000115	-18:05:012	0.000098	0.002018	0.000628	0.00224	0.000345
23	20:48:041	0.000135	-18:05:057	0.000043	0.003749	0.000606	0.003319	0.000346
23	20:48:041	0.000063	-18:05:032	0.000075	0.001016	0.000623	0.002018	0.000277
23	20:48:040	0.000377	-18:06:012	0.000326	0.001563	0.000574	0.001432	0.000268
24	20:48:038	0.000371	-18:13:023	0.000364	0.011763	0.000225	0.001208	0.000204
25	20:48:033	0.000106	-17:31:024	0.000186	0.031537	0.000227	0.003937	0.000202
25	20:48:030	0.000401	-17:32:016	0.000203	0.036374	0.000343	0.002056	0.000269
27	20:48:019	0.000113	-17:34:009	0.000215	0.00179	0.000436	0.001359	0.000271
28	20:48:015	0.000074	-17:36:047	0.000119	0.002889	0.000473	0.002343	0.000289
29	20:48:013	0.00021	-17:42:009	0.00014	0.004369	0.000457	0.001975	0.00033
32	20:48:011	0.000199	-17:50:055	0.000302	0.005441	0.000676	0.002316	0.000492
33	20:48:008	0.000072	-17:35:052	0.000122	0.01173	0.000346	0.00379	0.000267
34	20:48:005	0.000029	-17:43:020	0.000017	0.020853	0.000851	0.014044	0.000354
34	20:48:004	0.000111	-17:43:024	0.000143	0.015101	0.000767	0.005472	0.000354
34	20:48:006	0.00012	-17:43:014	0.000093	0.002292	0.000614	0.00231	0.000351
35	20:48:006	0.00016	-17:43:003	0.000093	0.002392	0.0006	0.002168	0.000351
35	20:48:005	0.000155	-17:43:004	0.000128	0.001852	0.000608	0.001841	0.000345
36	20:48:004	0.000197	-17:43:049	0.000495	0.014383	0.000703	0.002629	0.000358
37	20:48:002	0.000067	-17:37:027	0.000151	0.002076	0.000482	0.001939	0.000278
38	20:47:058	0.000046	-17:37:016	0.000086	0.004069	0.00048	0.003419	0.000289
39	20:47:056	0.000021	-17:43:016	0.000012	0.024957	0.000886	0.018586	0.000364
39	20:47:056	0.000055	-17:43:009	0.000065	0.002903	0.000639	0.003594	0.00034
40	20:47:056	0.000066	-17:42:059	0.000056	0.003178	0.000632	0.003713	0.000343

Continued on next page

Table C.21: Positions of radio sources within 4MPc radius of the pointing centre of cluster RXCJ2048.1−1750

Source ID	RA	δ RA	DEC	δ DEC	total flux	δ total flux	Peak flux	δ Peak flux
42	20:47:053	0.00005	-17:38:014	0.000023	0.011095	0.000687	0.007539	0.00029
42	20:47:053	0.000076	-17:38:007	0.000146	0.00137	0.000509	0.001635	0.00027
43	20:47:052	0.00008	-17:37:057	0.000131	0.001138	0.000507	0.001511	0.000262
44	20:47:050	0.000027	-17:42:023	0.000039	0.006718	0.000588	0.006989	0.000332
44	20:47:050	0.000041	-17:42:016	0.000061	0.00411	0.00059	0.00439	0.00033
45	20:47:048	0.000075	-17:40:048	0.000085	0.002963	0.000539	0.002809	0.000316
46	20:47:046	0.000083	-18:04:029	0.000259	0.005944	0.000365	0.002133	0.000274
47	20:47:043	0.000057	-18:04:054	0.000078	0.002702	0.000478	0.002764	0.000273
48	20:47:041	0.000098	-17:37:007	0.000187	0.002057	0.000442	0.001577	0.000274
49	20:47:028	0.000262	-17:49:027	0.00033	0.014928	0.000227	0.001547	0.000207
50	20:47:024	0.000041	-17:58:010	0.000065	0.005599	0.000488	0.004487	0.0003
50	20:47:025	0.000142	-17:58:003	0.00015	0.001547	0.000499	0.001432	0.000296
50	20:47:024	0.000228	-17:58:019	0.000168	0.000987	0.000504	0.001043	0.000279
51	20:47:025	0.000088	-17:32:038	0.000181	0.001444	0.000329	0.001188	0.000199
52	20:47:019	0.000031	-17:57:012	0.000053	0.016119	0.000455	0.00784	0.000322
52	20:47:019	0.000124	-17:57:005	0.000145	0.001101	0.000528	0.001335	0.000284
53	20:47:018	0.000167	-17:56:055	0.000101	0.002917	0.00049	0.002003	0.000316
54	20:47:018	0.00009	-17:48:017	0.000117	0.001385	0.000405	0.001491	0.000226
55	20:47:013	0.000057	-17:38:020	0.000092	0.005857	0.000375	0.003247	0.000257
55	20:47:012	0.00008	-17:38:016	0.000084	0.010878	0.000327	0.003888	0.000248
56	20:47:008	0.000122	-17:38:039	0.000182	0.001631	0.000374	0.001246	0.000233
57	20:47:007	0.000049	-17:43:006	0.000081	0.002122	0.000353	0.002149	0.000201
58	20:46:051	0.000048	-17:58:027	0.000017	0.014337	0.00056	0.007904	0.000251
58	20:46:051	0.000188	-17:58:019	0.000165	0.001663	0.000417	0.001225	0.000264
60	20:46:046	0.000012	-17:26:053	0.000019	0.015019	0.000411	0.012499	0.00025
60	20:46:046	0.000062	-17:26:047	0.000063	0.002268	0.000423	0.002528	0.000234
60	20:46:046	0.000238	-17:27:002	0.000092	0.001713	0.000398	0.001359	0.000235
62	20:46:045	0.000064	-17:26:036	0.000048	0.001838	0.000432	0.002498	0.00022
63	20:46:045	0.000126	-17:26:025	0.000177	0.001389	0.000422	0.001318	0.00024
64	20:46:040	0.000087	-18:03:031	0.000137	0.002563	0.000427	0.001928	0.000268
65	20:46:040	0.000046	-18:06:051	0.000071	0.004172	0.000491	0.003799	0.000287
66	20:46:039	0.000478	-18:03:013	0.00031	0.025944	0.000148	0.00119	0.000141

Table C.22: Positions of radio sources within 4MPc radius of the pointing centre of cluster RXCJ2149.1−3041

Source ID	RA	δ RA	DEC	δ DEC	total flux	δ total flux	Peak flux	δ Peak flux
0	21:51:029	0.00022	-30:29:015	0.000488	0.009338	0.000711	0.003572	0.000527
1	21:50:059	0.000058	-30:37:048	0.000047	0.044986	0.000818	0.016322	0.000423

Continued on next page

Table C.22: Positions of radio sources within 4MPc radius of the pointing centre of cluster RXCJ2149.1−3041

Source ID	RA	δ RA	DEC	δ DEC	total flux	δ total flux	Peak flux	δ Peak flux
3	21:50:046	0.000275	-30:59:016	0.000475	0.039425	0.000537	0.004873	0.000481
4	21:50:044	0.000207	-30:59:039	0.000461	0.005156	0.000933	0.003282	0.000603
4	21:50:043	0.000182	-30:59:047	0.000676	0.011186	0.000732	0.003566	0.000561
5	21:50:044	0.000284	-30:33:005	0.000741	0.007294	0.000501	0.002061	0.000398
6	21:50:036	0.000079	-31:02:047	0.000203	0.015945	0.00096	0.009795	0.000606
7	21:50:030	0.000045	-31:04:058	0.000014	0.333152	0.001439	0.071709	0.000613
9	21:50:025	0.000022	-30:41:037	0.000073	0.035953	0.000773	0.020993	0.000507
10	21:50:021	0.000235	-30:39:032	0.000262	0.019635	0.000947	0.003945	0.000506
11	21:50:019	0.00007	-30:59:042	0.00016	0.014137	0.000706	0.008156	0.000467
13	21:49:059	0.000041	-30:35:037	0.000023	0.121401	0.001578	0.05164	0.000597
18	21:49:040	0.00002	-30:54:053	0.000041	0.056505	0.000775	0.031496	0.000525
19	21:49:036	0.00003	-30:25:017	0.000101	0.019793	0.000862	0.01474	0.000514
20	21:49:034	0.000171	-30:53:054	0.000427	0.006551	0.000762	0.003558	0.000512
21	21:49:030	0.000072	-30:54:043	0.000324	0.010233	0.000766	0.005773	0.000493
21	21:49:031	0.000103	-30:54:042	0.000408	0.009688	0.00074	0.004726	0.000503
23	21:49:019	0.00011	-30:23:042	0.000353	0.006744	0.00091	0.00459	0.000565
24	21:49:015	0.000056	-31:01:054	0.000194	0.012295	0.000783	0.008224	0.000477
25	21:49:015	0.000111	-30:55:017	0.000401	0.005324	0.001007	0.004514	0.000548
27	21:49:008	0.00001	-30:42:006	0.000033	0.076562	0.001156	0.05866	0.000682
28	21:49:005	0.000052	-30:38:032	0.000232	0.009392	0.000908	0.007179	0.000528
28	21:49:006	0.000079	-30:38:018	0.000278	0.010335	0.000866	0.006342	0.000552
31	21:49:005	0.000177	-30:12:002	0.000463	0.00681	0.000898	0.003822	0.000597
32	21:49:004	0.000103	-30:38:053	0.000255	0.013781	0.000882	0.006885	0.000612
33	21:49:003	0.000019	-30:51:025	0.000005	0.143232	0.002015	0.114572	0.00082
35	21:48:059	0.000037	-30:57:020	0.000093	0.027501	0.000968	0.017463	0.000625
35	21:49:001	0.000053	-30:58:009	0.000212	0.011313	0.000978	0.008586	0.000568
38	21:48:045	0.000016	-30:14:022	0.000005	0.205116	0.001692	0.126944	0.000738
38	21:48:046	0.000114	-30:14:037	0.000162	0.028653	0.001065	0.011552	0.000791
38	21:48:044	0.000031	-30:13:052	0.000174	0.004709	0.001365	0.007687	0.000559
38	21:48:044	0.000044	-30:13:036	0.000286	0.006061	0.001288	0.006933	0.000589
40	21:48:045	0.000034	-30:31:001	0.000152	0.018428	0.000582	0.009713	0.000384
41	21:48:043	0.000032	-30:59:002	0.000109	0.020024	0.00084	0.01438	0.000502
44	21:48:042	0.000111	-30:15:026	0.000385	0.007539	0.001194	0.005327	0.000734
45	21:48:041	0.000126	-30:13:040	0.000408	0.005562	0.001197	0.004451	0.000707
49	21:48:030	0.000131	-30:37:046	0.000336	0.008869	0.000575	0.004531	0.000379
50	21:48:026	0.00022	-30:18:041	0.000663	0.007284	0.00094	0.003283	0.000667
51	21:48:025	0.000201	-31:00:053	0.000377	0.012007	0.000541	0.004299	0.000401
53	21:48:017	0.000037	-30:54:035	0.000153	0.011497	0.000638	0.008124	0.000382
53	21:48:016	0.000047	-30:54:012	0.000176	0.008517	0.000656	0.006547	0.000383
54	21:48:002	0.000053	-30:43:028	0.000195	0.009555	0.000704	0.006794	0.000423
55	21:47:045	0.000177	-30:31:040	0.000411	0.011306	0.000531	0.003507	0.000414

Continued on next page

Table C.22: Positions of radio sources within 4MPc radius of the pointing centre of cluster RXCJ2149.1−3041

Source ID	RA	δ RA	DEC	δ DEC	total flux	δ total flux	Peak flux	δ Peak flux
59	21:46:043	0.000166	-30:57:025	0.000345	0.010506	0.000457	0.003348	0.000355

Table C.23: Positions of radio sources within 4MPc radius of the pointing centre of cluster RXCJ2152.2−1942

Source ID	RA	δ RA	DEC	δ DEC	total flux	δ total flux	Peak flux	δ Peak flux
0	21:54:050	0.000616	-19:47:055	0.000316	0.056616	0.000941	0.005492	0.000861
2	21:54:044	0.000687	-19:16:057	0.000347	0.01923	0.000644	0.002716	0.000568
5	21:53:044	0.000095	-20:01:035	0.000173	0.09426	0.014216	0.070622	0.008887
6	21:53:043	0.00008	-20:00:057	0.000042	0.323456	0.023768	0.251814	0.014652
7	21:53:036	0.000493	-19:38:058	0.000211	0.021703	0.002956	0.009188	0.002146
9	21:53:027	0.000393	-20:09:033	0.000283	0.021982	0.002272	0.007914	0.001726
11	21:52:051	0.00025	-19:28:049	0.000139	0.100172	0.014304	0.058988	0.009612
12	21:52:010	0.000208	-19:43:022	0.00011	0.106063	0.02015	0.082193	0.012446
13	21:51:055	0.000136	-19:45:044	0.000145	0.063876	0.022376	0.072769	0.012338
14	21:51:054	0.000254	-19:50:041	0.000171	0.086649	0.019676	0.064329	0.012304
15	21:51:054	0.000194	-19:46:00	0.000169	0.137509	0.034716	0.118441	0.020733
16	21:51:051	0.00004	-19:46:005	0.00002	2.340278	0.095177	1.957279	0.057209
17	21:51:052	0.000309	-19:47:016	0.000177	0.128772	0.027017	0.09059	0.016785
18	21:51:052	0.000076	-19:46:043	0.000073	0.433884	0.062863	0.432256	0.036239
19	21:51:052	0.000185	-19:46:027	0.000138	0.33355	0.079123	0.30248	0.045959
21	21:51:050	0.000143	-19:45:031	0.000124	0.212988	0.061411	0.23433	0.033622
22	21:51:050	0.000112	-19:45:019	0.000089	0.156685	0.044975	0.192756	0.024065
23	21:51:049	0.000249	-19:49:016	0.00011	0.076348	0.021761	0.069958	0.012598
24	21:51:048	0.000116	-19:48:032	0.000135	0.025181	0.014111	0.040973	0.006636
25	21:51:043	0.000166	-19:44:035	0.000214	0.042077	0.0164	0.04941	0.008294
26	21:50:035	0.000399	-20:05:016	0.0004	0.01679	0.001347	0.005067	0.001055
28	21:49:037	0.000749	-19:08:020	0.000395	0.033449	0.000568	0.002883	0.000524
29	21:49:035	0.000625	-19:50:057	0.000354	0.024977	0.00078	0.003623	0.000685

Table C.24: Positions of radio sources within 4MPc radius of the pointing centre of cluster RXCJ2157.4−0747

Source ID	RA	δ RA	DEC	δ DEC	total flux	δ total flux	Peak flux	δ Peak flux
0	22:01:004	0.00014	-07:20:027	0.000176	0.000821	0.000202	0.000664	0.000125

Continued on next page

Table C.24: Positions of radio sources within 4MPc radius of the pointing centre of cluster RXCJ2157.4−0747

Source ID	RA	δ RA	DEC	δ DEC	total flux	δ total flux	Peak flux	δ Peak flux
1	22:00:051	0.000266	-07:41:046	0.000183	0.0051	0.000136	0.000928	0.000117
2	22:00:050	0.000295	-07:41:032	0.000115	0.000967	0.000199	0.000652	0.000126
3	22:00:013	0.000201	-07:35:003	0.000077	0.002489	0.000219	0.001268	0.000151
4	22:00:003	0.000255	-07:48:004	0.000091	0.001201	0.000238	0.00086	0.000148
5	21:59:040	0.000133	-07:22:051	0.000156	0.001501	0.000282	0.001099	0.000179
6	21:59:024	0.000075	-08:42:015	0.000135	0.001177	0.000246	0.001163	0.000137
7	21:59:023	0.00022	-08:42:035	0.00043	0.00476	0.000276	0.000691	0.000143
7	21:59:023	0.00014	-08:42:025	0.000362	0.000585	0.000241	0.000504	0.000142
7	21:59:024	0.000349	-08:42:035	0.000382	0.001056	0.000214	0.000474	0.000156
8	21:59:014	0.000247	-07:55:052	0.000287	0.014981	0.000148	0.0013	0.000137
9	21:59:011	0.000144	-07:31:026	0.000083	0.002614	0.000345	0.001831	0.00022
10	21:59:006	0.000213	-07:42:043	0.000094	0.001174	0.000353	0.001138	0.000198
11	21:59:004	0.000229	-07:52:024	0.000107	0.001253	0.000332	0.001039	0.000199
12	21:59:003	0.000266	-07:02:033	0.000104	0.003474	0.000254	0.001363	0.000188
13	21:59:002	0.00003	-07:01:045	0.000217	0.002784	0.000444	0.001406	0.000184
14	21:59:002	0.000045	-07:01:059	0.000028	0.00582	0.000309	0.004561	0.000192
15	21:59:001	0.000189	-07:01:009	0.000137	0.00117	0.000311	0.000975	0.000189
16	21:59:001	0.000258	-07:02:023	0.0001	0.002197	0.000281	0.001223	0.000188
18	21:58:058	0.000143	-07:39:046	0.00009	0.001931	0.000384	0.001731	0.000223
18	21:58:059	0.000132	-07:39:047	0.000059	0.001202	0.000399	0.001553	0.000202
19	21:58:058	0.000018	-07:39:028	0.000011	0.012107	0.000393	0.012099	0.000224
20	21:58:059	0.000107	-07:39:012	0.000034	0.002151	0.000398	0.002419	0.000209
20	21:58:058	0.000165	-07:39:013	0.000062	0.001057	0.000407	0.00142	0.000194
21	21:58:049	0.000231	-07:11:025	0.000122	0.001155	0.000318	0.000975	0.000189
22	21:58:044	0.000069	-07:35:025	0.000034	0.005311	0.000421	0.004402	0.000252
24	21:58:043	0.000115	-07:34:034	0.000085	0.00133	0.000441	0.001625	0.000236
24	21:58:043	0.000157	-07:34:029	0.000067	0.000893	0.000448	0.001325	0.000214
26	21:58:042	0.000169	-07:35:058	0.000053	0.00168	0.000438	0.001875	0.000222
27	21:58:042	0.00002	-07:35:045	0.000097	0.006626	0.000615	0.004386	0.000252
27	21:58:041	0.000194	-07:35:048	0.000064	0.005901	0.00035	0.002729	0.000243
28	21:58:042	0.000007	-07:35:025	0.000011	0.035106	0.000717	0.028177	0.000252
28	21:58:042	0.000084	-07:35:034	0.000025	0.002274	0.000449	0.003056	0.000217
29	21:58:042	0.000263	-07:34:056	0.000086	0.001601	0.00042	0.001351	0.000244
29	21:58:042	0.000141	-07:34:057	0.000059	0.000497	0.000456	0.001131	0.000172
30	21:58:042	0.000058	-07:35:010	0.000016	0.003175	0.000452	0.004446	0.000212
30	21:58:041	0.000105	-07:35:011	0.000035	0.001906	0.00045	0.00255	0.000214
31	21:58:042	0.000249	-07:38:048	0.000137	0.002226	0.000391	0.001364	0.000259
33	21:58:042	0.000133	-07:34:030	0.000091	0.001364	0.000441	0.00157	0.000239
36	21:58:041	0.000224	-07:34:057	0.000099	0.002014	0.000415	0.00157	0.000249
39	21:58:039	0.000185	-07:34:052	0.000162	0.001668	0.000425	0.001425	0.00025
41	21:58:037	0.000029	-07:30:055	0.00002	0.010362	0.000423	0.008698	0.000256

Continued on next page

Table C.24: Positions of radio sources within 4MPc radius of the pointing centre of cluster RXCJ2157.4−0747

Source ID	RA	δ RA	DEC	δ DEC	total flux	δ total flux	Peak flux	δ Peak flux
41	21:58:037	0.000167	-07:31:004	0.000042	0.001102	0.00045	0.001574	0.000206
43	21:58:038	0.000188	-07:30:040	0.000053	0.001801	0.000426	0.001781	0.00023
43	21:58:037	0.000235	-07:30:040	0.000067	0.001265	0.000431	0.001338	0.000228
44	21:58:023	0.00022	-07:46:022	0.000107	0.001731	0.00037	0.001346	0.000225
45	21:58:021	0.000046	-08:08:030	0.00007	0.01119	0.000292	0.004674	0.000213
46	21:58:017	0.000047	-07:59:009	0.000033	0.00537	0.000363	0.004581	0.000219
47	21:58:014	0.000229	-07:19:052	0.000118	0.001677	0.000431	0.001349	0.000262
47	21:58:013	0.000245	-07:19:052	0.000152	0.001058	0.000443	0.001021	0.000256
50	21:58:012	0.000239	-07:21:042	0.000057	0.005257	0.000349	0.002466	0.000237
51	21:58:012	0.000088	-07:20:027	0.000033	0.001172	0.000463	0.002124	0.000202
52	21:58:012	0.000092	-07:19:039	0.000026	0.001298	0.000471	0.002308	0.0002
53	21:58:012	0.000125	-07:20:013	0.000037	0.007243	0.000378	0.004395	0.000233
53	21:58:011	0.000171	-07:20:016	0.000038	0.009235	0.000336	0.003723	0.000239
55	21:58:011	0.000006	-07:19:053	0.000011	0.038646	0.000635	0.028453	0.00026
58	21:58:011	0.000323	-07:21:006	0.000115	0.00265	0.000388	0.001416	0.000263
59	21:58:011	0.000103	-07:19:026	0.000064	0.00152	0.00046	0.001998	0.000236
59	21:58:010	0.000094	-07:19:023	0.00008	0.001555	0.000457	0.001902	0.000246
60	21:58:006	0.000099	-07:04:030	0.000062	0.00329	0.000393	0.002616	0.000242
61	21:58:005	0.000097	-07:41:034	0.000068	0.003166	0.000427	0.002668	0.000258
62	21:57:059	0.000043	-07:57:021	0.000034	0.005344	0.000423	0.005027	0.000248
63	21:57:058	0.00007	-07:16:055	0.000048	0.003935	0.000467	0.003671	0.000274
64	21:57:057	0.000171	-08:03:011	0.00008	0.001388	0.000405	0.001436	0.000225
65	21:57:050	0.000082	-07:52:042	0.000084	0.003711	0.000458	0.002927	0.000285
66	21:57:048	0.0002	-08:15:046	0.000248	0.002042	0.000307	0.001032	0.000216
67	21:57:040	0.000136	-07:41:042	0.000146	0.006471	0.00042	0.002722	0.000308
68	21:57:038	0.000193	-07:45:020	0.000239	0.00564	0.000671	0.001834	0.000307
68	21:57:039	0.00037	-07:45:026	0.000314	0.002744	0.000447	0.001168	0.000327
68	21:57:039	0.000236	-07:45:017	0.000121	0.000864	0.000541	0.001099	0.000281
69	21:57:037	0.000043	-07:44:031	0.000062	0.029022	0.000807	0.009461	0.000307
70	21:57:037	0.00019	-07:38:025	0.000215	0.003762	0.000406	0.001652	0.000296
70	21:57:037	0.000365	-07:38:025	0.000251	0.002084	0.000417	0.001065	0.00029
71	21:57:037	0.000304	-07:48:018	0.000282	0.005688	0.000396	0.001603	0.000316
72	21:57:035	0.000033	-07:47:048	0.000027	0.705057	0.002528	0.050691	0.000315
72	21:57:033	0.000044	-07:48:017	0.000074	0.011271	0.000748	0.006214	0.000315
74	21:57:036	0.000214	-07:45:023	0.00019	0.008682	0.000393	0.002311	0.000317
76	21:57:035	0.000093	-07:48:054	0.000167	0.024689	0.000512	0.003524	0.000313
77	21:57:035	0.000438	-07:49:042	0.000299	0.023014	0.000226	0.001662	0.000211
79	21:57:034	0.000278	-07:50:027	0.000197	0.003552	0.00046	0.001586	0.000333
80	21:57:034	0.000226	-07:38:025	0.000348	0.002575	0.000408	0.001182	0.000293
80	21:57:034	0.000452	-07:38:021	0.000358	0.005156	0.000317	0.001083	0.000266
81	21:57:033	0.000325	-07:46:020	0.000407	0.007488	0.000354	0.001456	0.0003

Continued on next page

Table C.24: Positions of radio sources within 4MPc radius of the pointing centre of cluster RXCJ2157.4−0747

Source ID	RA	δ RA	DEC	δ DEC	total flux	δ total flux	Peak flux	δ Peak flux
82	21:57:033	0.000249	-07:49:044	0.000348	0.004248	0.00043	0.001499	0.000327
83	21:57:032	0.000436	-07:53:016	0.000301	0.013312	0.000263	0.001482	0.000238
84	21:57:028	0.000127	-07:25:047	0.000038	0.011014	0.000327	0.004292	0.000239
86	21:57:020	0.000045	-07:44:039	0.000026	0.008568	0.000543	0.007568	0.000322
87	21:57:016	0.000071	-07:27:038	0.000069	0.00494	0.000388	0.00335	0.000252
87	21:57:017	0.000101	-07:27:045	0.000067	0.004916	0.000377	0.003002	0.000251
88	21:57:014	0.000132	-07:29:032	0.000098	0.003575	0.00038	0.002174	0.000254
89	21:57:014	0.000161	-07:27:045	0.000083	0.001127	0.000407	0.001325	0.000216
91	21:57:009	0.000106	-08:01:055	0.000075	0.001243	0.000506	0.001978	0.000229
92	21:57:009	0.000148	-08:02:047	0.000125	0.002381	0.000469	0.00199	0.000278
93	21:57:008	0.000022	-08:01:050	0.000017	0.025998	0.000625	0.016963	0.000282
93	21:57:009	0.00008	-08:01:041	0.000061	0.010651	0.000421	0.004928	0.000302
94	21:57:008	0.000155	-08:00:053	0.000028	0.002142	0.000498	0.002509	0.000239
94	21:57:009	0.000298	-08:00:053	0.000049	0.004346	0.000374	0.002586	0.000212
95	21:57:008	0.000006	-08:01:021	0.00001	0.056419	0.000817	0.039887	0.000282
96	21:57:009	0.000306	-08:02:021	0.000124	0.005785	0.000364	0.001935	0.000278
98	21:57:009	0.000142	-07:39:027	0.000086	0.002807	0.000458	0.002229	0.00028
98	21:57:008	0.000347	-07:39:026	0.000386	0.001288	0.000436	0.000877	0.000274
99	21:57:008	0.000214	-08:02:010	0.000056	0.004257	0.000419	0.002609	0.000262
100	21:57:008	0.000163	-08:00:026	0.000156	0.001501	0.000489	0.001463	0.00028
103	21:57:007	0.000139	-08:02:009	0.000147	0.002227	0.000473	0.001938	0.000275
104	21:57:007	0.000292	-08:00:018	0.000208	0.00283	0.000428	0.001389	0.000302
105	21:57:006	0.000272	-07:41:026	0.000243	0.005981	0.000361	0.001616	0.00029
106	21:57:002	0.000066	-07:50:032	0.000068	0.667811	0.002242	0.033183	0.000299
106	21:57:001	0.000048	-07:51:012	0.000074	0.041897	0.000571	0.009889	0.000299
106	21:57:002	0.000054	-07:50:026	0.000104	0.013763	0.000405	0.005865	0.000288
106	21:57:002	0.000042	-07:50:037	0.000083	0.002017	0.000542	0.003177	0.00024
106	21:57:00	0.0001	-07:51:013	0.00007	0.002107	0.000523	0.002423	0.000285
106	21:57:003	0.000127	-07:49:051	0.000101	0.006952	0.000447	0.003245	0.00032
106	21:56:059	0.000099	-07:51:016	0.00008	0.001328	0.000527	0.001929	0.000263
107	21:57:005	0.000376	-07:44:052	0.000235	0.006028	0.000362	0.001532	0.000294
108	21:57:005	0.000483	-07:49:013	0.000394	0.014474	0.000245	0.001298	0.000225
109	21:57:005	0.000162	-08:03:056	0.000178	0.001297	0.000481	0.001364	0.000263
109	21:57:004	0.000276	-08:04:002	0.000167	0.001056	0.000477	0.00103	0.000271
110	21:57:003	0.000075	-07:44:014	0.000302	0.005332	0.00063	0.001448	0.000293
113	21:57:002	0.000192	-07:39:029	0.000147	0.001964	0.000452	0.001511	0.000281
114	21:57:002	0.000108	-07:50:012	0.0001	0.001779	0.000522	0.001973	0.000291
116	21:56:050	0.000143	-08:18:030	0.000094	0.007638	0.00036	0.002848	0.000272
117	21:56:050	0.000018	-08:18:011	0.000011	0.017632	0.000435	0.015085	0.000262
117	21:56:049	0.000017	-08:18:003	0.00002	0.02317	0.000596	0.01483	0.000256
118	21:56:049	0.000046	-07:45:032	0.000043	0.006312	0.000474	0.005308	0.000289

Continued on next page

Table C.24: Positions of radio sources within 4MPc radius of the pointing centre of cluster RXCJ2157.4−0747

Source ID	RA	δ RA	DEC	δ DEC	total flux	δ total flux	Peak flux	δ Peak flux
118	21:56:049	0.000479	-07:45:029	0.000167	0.002103	0.000411	0.00106	0.000283
119	21:56:049	0.000282	-08:18:023	0.000119	0.003189	0.000371	0.001806	0.000238
120	21:56:048	0.00017	-08:18:057	0.000172	0.002243	0.000415	0.001599	0.000261
121	21:56:048	0.000228	-08:18:050	0.000181	0.00193	0.000413	0.001377	0.000257
123	21:56:041	0.000207	-07:16:021	0.000088	0.002429	0.000321	0.00149	0.000211
124	21:56:034	0.000037	-07:39:023	0.000028	0.007522	0.000409	0.006511	0.000244
125	21:56:034	0.000189	-06:57:021	0.0003	0.003803	0.000198	0.001014	0.00016
126	21:56:032	0.000117	-07:51:048	0.000095	0.001836	0.000405	0.001752	0.000236
128	21:56:024	0.000093	-07:40:013	0.00005	0.008863	0.00033	0.003933	0.000239
129	21:56:023	0.000096	-07:37:028	0.000067	0.004059	0.000366	0.002764	0.000236
130	21:56:013	0.000058	-07:11:043	0.000102	0.007338	0.000253	0.002911	0.000188
131	21:56:010	0.000118	-07:49:011	0.000096	0.005935	0.000302	0.00245	0.000223
131	21:56:011	0.000239	-07:49:016	0.000112	0.00448	0.000281	0.001679	0.00021
132	21:56:009	0.000091	-07:32:054	0.00004	0.024941	0.000419	0.005639	0.000204
132	21:56:009	0.000045	-07:32:033	0.000034	0.013909	0.000441	0.006348	0.000204
133	21:56:005	0.000075	-08:19:029	0.000072	0.004677	0.000277	0.002597	0.000191
133	21:56:004	0.000257	-08:19:037	0.000088	0.000493	0.000313	0.000669	0.000151
134	21:55:060	0.00012	-07:43:058	0.000136	0.003497	0.000311	0.001889	0.000213
135	21:55:056	0.00027	-07:40:044	0.000184	0.001613	0.000314	0.000971	0.000209
135	21:55:057	0.000495	-07:40:047	0.000365	0.002208	0.00026	0.000682	0.000204
136	21:55:055	0.000063	-07:41:015	0.000055	0.002687	0.000341	0.002625	0.000197
137	21:55:045	0.000031	-08:05:024	0.000025	0.005977	0.000304	0.005283	0.000182
137	21:55:046	0.000134	-08:05:019	0.000133	0.000984	0.000308	0.000993	0.000177
138	21:55:027	0.000105	-07:22:001	0.00006	0.00172	0.000285	0.001621	0.000165
139	21:55:026	0.000098	-08:07:025	0.000101	0.00234	0.000273	0.00161	0.000177
140	21:55:016	0.000369	-08:31:047	0.000266	0.005573	0.000369	0.000652	0.000154
142	21:55:012	0.000033	-07:55:030	0.000019	0.005672	0.000296	0.005322	0.000172
144	21:55:007	0.000134	-07:46:058	0.000188	0.003181	0.00025	0.001395	0.000181
144	21:55:007	0.000214	-07:46:043	0.000246	0.001623	0.000267	0.000841	0.000187
145	21:54:036	0.000506	-07:58:033	0.000384	0.010882	0.000087	0.00061	0.000083
146	21:54:035	0.000475	-07:58:053	0.000296	0.009032	0.0001	0.000693	0.000093
147	21:54:020	0.000198	-07:48:042	0.000072	0.000946	0.0002	0.000798	0.000117
148	21:53:026	0.000225	-06:59:023	0.000495	0.002015	0.000128	0.00049	0.000104
148	21:53:025	0.000283	-06:59:024	0.000141	0.000315	0.000191	0.000371	0.0001

Table C.25: Positions of radio sources within 4MPc radius of the pointing centre of cluster RXCJ2217.7−3543

Source ID	RA	δ RA	DEC	δ DEC	total flux	δ total flux	Peak flux	δ Peak flux
0	22:19:047	0.000052	-35:33:037	0.000041	0.013721	0.000673	0.013442	0.00039
1	22:19:029	0.000081	-35:39:011	0.000083	0.010542	0.000647	0.008517	0.0004
1	22:19:030	0.000432	-35:38:051	0.00036	0.002845	0.000631	0.00196	0.000409
2	22:19:029	0.000228	-35:34:058	0.000143	0.002775	0.000614	0.002926	0.000345
3	22:19:027	0.000034	-35:50:058	0.000042	0.017939	0.000845	0.014667	0.000349
4	22:19:024	0.000495	-35:26:010	0.000213	0.002399	0.000629	0.002009	0.000374
5	22:19:012	0.000262	-35:41:027	0.00031	0.001879	0.00061	0.00191	0.00035
6	22:19:011	0.000083	-35:41:053	0.000057	0.007945	0.000611	0.007963	0.000351
7	22:19:011	0.000405	-35:58:009	0.000263	0.003038	0.00056	0.002104	0.000361
8	22:19:003	0.000376	-35:34:001	0.000106	0.001967	0.000701	0.002479	0.000343
10	22:19:002	0.000023	-35:34:026	0.00003	0.025348	0.000981	0.023454	0.000404
10	22:18:060	0.00024	-35:34:026	0.00012	0.003541	0.000698	0.003605	0.000393
11	22:19:002	0.000604	-35:28:033	0.000673	0.005219	0.000537	0.001983	0.000399
11	22:19:002	0.000342	-35:28:016	0.000334	0.001173	0.000695	0.00155	0.000359
13	22:18:053	0.000087	-36:04:057	0.000125	0.00813	0.000489	0.005689	0.000314
14	22:18:046	0.000058	-35:43:018	0.000046	0.012363	0.000616	0.011479	0.000364
18	22:18:035	0.000316	-35:29:025	0.000139	0.012417	0.000958	0.007617	0.000606
18	22:18:033	0.000371	-35:29:037	0.000205	0.004427	0.001079	0.003892	0.000641
19	22:18:035	0.00044	-35:34:001	0.000372	0.004336	0.000918	0.00287	0.000602
20	22:18:031	0.000335	-35:25:022	0.00017	0.003657	0.000911	0.003569	0.000517
21	22:18:030	0.000415	-35:32:015	0.000133	0.009849	0.001093	0.006075	0.000706
22	22:18:030	0.000168	-35:31:036	0.000143	0.006403	0.001231	0.006818	0.000695
23	22:18:029	0.000479	-35:29:045	0.000198	0.007662	0.001023	0.005079	0.00063
25	22:18:029	0.000141	-35:30:055	0.000042	0.011044	0.001225	0.012384	0.000636
26	22:18:028	0.000004	-35:31:022	0.000006	0.310679	0.002496	0.260809	0.000711
26	22:18:026	0.000057	-35:31:021	0.000037	0.020361	0.001242	0.022676	0.000682
27	22:18:027	0.000249	-35:31:055	0.00008	0.012109	0.001177	0.010006	0.000661
29	22:18:028	0.000352	-35:30:038	0.000089	0.003126	0.001241	0.004358	0.000579
31	22:18:023	0.0003	-35:30:018	0.000126	0.005554	0.00107	0.005183	0.000612
32	22:18:022	0.000529	-35:33:021	0.000315	0.00481	0.001093	0.003596	0.000665
33	22:18:021	0.000331	-35:32:025	0.000229	0.004902	0.001145	0.004474	0.000664
34	22:18:019	0.000274	-35:32:008	0.00018	0.004422	0.001078	0.004409	0.000617
35	22:18:018	0.000074	-35:46:029	0.000066	0.014554	0.000644	0.010831	0.000407
36	22:18:018	0.000431	-35:36:010	0.000216	0.005151	0.000866	0.003703	0.000536
37	22:18:018	0.000294	-35:34:059	0.00013	0.00379	0.000967	0.004119	0.000525
38	22:18:012	0.000102	-35:34:021	0.000091	0.009516	0.000828	0.008533	0.000495
39	22:18:009	0.000024	-35:23:015	0.000104	0.037055	0.000886	0.016506	0.000398
40	22:18:009	0.000565	-35:41:007	0.000303	0.003222	0.000705	0.002208	0.000448
41	22:18:009	0.000179	-35:21:008	0.000149	0.00377	0.000671	0.00374	0.000388
42	22:18:009	0.000489	-35:24:005	0.000186	0.00281	0.000671	0.002299	0.0004
43	22:18:007	0.000262	-35:30:031	0.000244	0.001795	0.000746	0.002228	0.000399

Continued on next page

Table C.25: Positions of radio sources within 4MPc radius of the pointing centre of cluster RXCJ2217.7−3543

Source ID	RA	δ RA	DEC	δ DEC	total flux	δ total flux	Peak flux	δ Peak flux
44	22:17:053	0.00024	-35:43:026	0.000319	0.003649	0.000892	0.003272	0.000529
46	22:17:044	0.000286	-35:43:025	0.000428	0.004189	0.001006	0.003451	0.0006
48	22:17:039	0.000482	-35:35:006	0.000988	0.007251	0.000408	0.001653	0.000337
49	22:17:038	0.000202	-35:43:043	0.000283	0.005463	0.001042	0.004859	0.000608
49	22:17:039	0.000268	-35:43:022	0.000349	0.005403	0.001018	0.004297	0.000611
50	22:17:038	0.000125	-35:25:005	0.000076	0.005412	0.000634	0.005651	0.000357
51	22:17:037	0.00031	-35:22:006	0.000434	0.002553	0.00061	0.001909	0.000385
52	22:17:031	0.000223	-35:43:018	0.000405	0.00507	0.000867	0.003612	0.000546
52	22:17:031	0.000338	-35:42:054	0.000165	0.004916	0.001313	0.003878	0.000531
52	22:17:032	0.000355	-35:42:038	0.000325	0.003149	0.000908	0.002928	0.000522
54	22:17:022	0.000602	-35:23:002	0.00032	0.002874	0.000534	0.00168	0.000359
55	22:17:016	0.000387	-35:48:023	0.000206	0.004274	0.000816	0.003505	0.000481
56	22:17:015	0.00004	-35:48:051	0.00009	0.047522	0.001112	0.026244	0.000503
57	22:16:053	0.000134	-36:07:021	0.000079	0.00409	0.000681	0.005018	0.000361
58	22:16:052	0.000288	-35:34:049	0.00023	0.00337	0.00059	0.002588	0.00037
59	22:16:044	0.000133	-35:47:039	0.000138	0.003737	0.000677	0.004182	0.000375
60	22:16:042	0.000346	-35:43:023	0.00027	0.005305	0.000606	0.003318	0.000389
61	22:16:040	0.000017	-35:43:054	0.000021	0.031774	0.000943	0.030195	0.000389
62	22:16:040	0.000353	-35:44:046	0.000154	0.002123	0.000686	0.002399	0.000365
63	22:16:038	0.000223	-35:43:057	0.000247	0.001659	0.000676	0.002122	0.000358
65	22:16:012	0.000023	-35:46:055	0.00003	0.030073	0.000983	0.025738	0.000404
65	22:16:013	0.000021	-35:46:058	0.000031	0.026252	0.00097	0.024312	0.000404
65	22:16:010	0.000359	-35:46:055	0.000286	0.001595	0.000715	0.00202	0.000357
66	22:16:005	0.000068	-35:36:002	0.000038	0.01308	0.000654	0.012296	0.000379
67	22:16:002	0.000037	-35:35:010	0.000045	0.020262	0.000921	0.015695	0.000383
67	22:15:060	0.000361	-35:35:012	0.000187	0.00098	0.000682	0.00161	0.000314
68	22:16:002	0.000359	-35:36:001	0.000415	0.003415	0.000621	0.002141	0.000413
69	22:15:037	0.000061	-35:45:038	0.000045	0.010603	0.000596	0.010437	0.000344

Table C.26: Positions of radio sources within 4MPc radius of the pointing centre of cluster RXCJ2218.6−3853

Source ID	RA	δ RA	DEC	δ DEC	total flux	δ total flux	Peak flux	δ Peak flux
0	22:20:007	0.000369	-38:55:054	0.000072	0.013137	0.001803	0.0108	0.000967
1	22:20:001	0.000591	-38:51:032	0.000255	0.026821	0.001314	0.0073	0.00105
2	22:19:049	0.000356	-39:05:038	0.00013	0.013029	0.001667	0.0085	0.001065
4	22:19:035	0.000487	-38:51:044	0.000767	0.030725	0.001313	0.005884	0.001115
5	22:19:033	0.00046	-38:51:045	0.000851	0.031511	0.001307	0.005781	0.001116
7	22:19:007	0.000533	-38:27:033	0.000331	0.015945	0.001738	0.006551	0.001282

Continued on next page

Table C.26: Positions of radio sources within 4MPc radius of the pointing centre of cluster RXCJ2218.6−3853

Source ID	RA	δ RA	DEC	δ DEC	total flux	δ total flux	Peak flux	δ Peak flux
7	22:19:008	0.000674	-38:27:053	0.000422	0.017909	0.001598	0.005943	0.001231
8	22:18:044	0.000532	-38:30:043	0.000056	0.010353	0.002595	0.011464	0.001013
9	22:18:047	0.000593	-38:56:034	0.000165	0.02475	0.003694	0.017599	0.00201
9	22:18:045	0.00043	-38:56:025	0.000043	0.040857	0.003565	0.025929	0.00206
9	22:18:045	0.000506	-38:56:040	0.00008	0.018104	0.004178	0.018603	0.001818
10	22:18:045	0.000093	-38:55:059	0.000071	0.012274	0.004539	0.025334	0.001934
10	22:18:044	0.000022	-38:55:045	0.000099	0.120493	0.007765	0.093774	0.002595
10	22:18:044	0.000306	-38:55:019	0.000042	0.007905	0.0051	0.016356	0.001679
10	22:18:044	0.000233	-38:56:010	0.000054	0.014087	0.004768	0.022008	0.002013
10	22:18:044	0.000219	-38:55:031	0.000086	0.002762	0.004871	0.010349	0.001276
10	22:18:042	0.000114	-38:55:044	0.000436	0.018679	0.004325	0.016317	0.002433
10	22:18:047	0.000334	-38:55:046	0.000773	0.009178	0.004466	0.01013	0.001987
11	22:18:043	0.000863	-38:57:009	0.000104	0.055661	0.002474	0.018071	0.001767
12	22:18:044	0.000091	-38:30:003	0.000022	0.099866	0.002369	0.06253	0.001472
12	22:18:044	0.000345	-38:29:037	0.000075	0.006576	0.003028	0.011026	0.001073
12	22:18:044	0.000323	-38:30:028	0.000067	0.019844	0.00253	0.017184	0.001304
12	22:18:044	0.000196	-38:30:017	0.000085	0.014311	0.002771	0.016772	0.001394
12	22:18:041	0.000307	-38:30:001	0.000392	0.051937	0.001926	0.012862	0.001573
12	22:18:044	0.000301	-38:29:049	0.000108	0.009154	0.002879	0.012694	0.001198
12	22:18:047	0.000311	-38:30:006	0.000422	0.047027	0.001943	0.012874	0.001552
13	22:18:044	0.000044	-38:31:026	0.000886	0.053402	0.002242	0.01305	0.001506
15	22:18:044	0.000894	-38:28:040	0.00007	0.034582	0.001648	0.012035	0.001131
16	22:18:044	0.000565	-38:55:004	0.000039	0.027119	0.003873	0.020787	0.001951
17	22:18:042	0.000254	-38:29:016	0.000876	0.072738	0.002726	0.016504	0.001604
17	22:18:042	0.000594	-38:29:007	0.000115	0.024744	0.002022	0.014797	0.001081
19	22:18:040	0.00004	-38:53:051	0.000011	0.424687	0.003851	0.239561	0.002508
22	22:18:036	0.00086	-39:17:055	0.000592	0.061661	0.00055	0.003927	0.000518
23	22:18:022	0.000508	-38:51:002	0.000293	0.190417	0.00184	0.018995	0.001679
24	22:18:018	0.000165	-39:10:038	0.000094	0.032483	0.001865	0.018489	0.001265
25	22:18:017	0.000796	-39:10:00	0.00075	0.013325	0.001688	0.00427	0.001315
25	22:18:014	0.000762	-39:09:045	0.000777	0.021298	0.001488	0.00473	0.001238
25	22:18:016	0.000201	-39:09:043	0.001004	0.019678	0.002664	0.005811	0.001259
26	22:18:015	0.000282	-39:10:038	0.000781	0.019916	0.001563	0.006278	0.001211
27	22:18:010	0.000596	-38:28:024	0.000137	0.038971	0.001295	0.010271	0.001025
27	22:18:013	0.000557	-38:28:022	0.000491	0.019297	0.001548	0.005912	0.001218
28	22:18:004	0.000416	-38:50:028	0.000174	0.05518	0.005232	0.01778	0.001757
28	22:18:005	0.000462	-38:51:005	0.000306	0.017522	0.002733	0.009428	0.001888
28	22:18:005	0.0004	-38:50:051	0.000098	0.029117	0.002565	0.016646	0.001645
30	22:18:001	0.000523	-38:34:003	0.000256	0.01084	0.00151	0.005754	0.001031
32	22:17:023	0.000852	-39:07:037	0.000549	0.078307	0.000694	0.005104	0.000653
33	22:17:024	0.000203	-38:39:025	0.000149	0.003315	0.001476	0.005091	0.000703

Continued on next page

Table C.26: Positions of radio sources within 4MPc radius of the pointing centre of cluster RXCJ2218.6−3853

Source ID	RA	δ RA	DEC	δ DEC	total flux	δ total flux	Peak flux	δ Peak flux
33	22:17:023	0.000286	-38:39:024	0.000179	0.003979	0.001478	0.005122	0.00072
35	22:16:034	0.000208	-39:15:043	0.00014	0.060088	0.001393	0.014579	0.000786
37	22:16:033	0.000958	-39:14:043	0.000481	0.031827	0.000733	0.003857	0.000657

Table C.27: Positions of radio sources within 4MPc radius of the pointing centre of cluster RXCJ2234.5-3744

Source ID	RA	δ RA	DEC	δ DEC	total flux	δ total flux	Peak flux	δ Peak flux
0	22:36:027	0.000196	-37:45:032	0.000422	0.005361	0.000637	0.002556	0.000445
0	22:36:027	0.000264	-37:45:046	0.000214	0.000458	0.000781	0.001073	0.000301
1	22:36:013	0.000022	-38:02:007	0.000035	0.020349	0.000602	0.017242	0.00035
2	22:35:033	0.000037	-37:29:052	0.000055	0.015962	0.00079	0.01345	0.000466
3	22:35:018	0.000036	-38:05:012	0.000066	0.011112	0.000682	0.010254	0.000382
4	22:34:057	0.000135	-38:08:037	0.000579	0.00607	0.000483	0.00241	0.000341
5	22:34:054	0.000182	-37:54:020	0.000431	0.006189	0.000912	0.00345	0.000603
5	22:34:056	0.000098	-37:54:053	0.000277	0.006699	0.000973	0.005082	0.000565
6	22:34:054	0.000198	-37:26:018	0.00032	0.002967	0.000574	0.001971	0.00037
9	22:34:049	0.000029	-37:28:047	0.000054	0.010825	0.00068	0.01133	0.000362
15	22:34:025	0.000093	-37:44:032	0.000058	0.111503	0.003528	0.060122	0.001288
15	22:34:026	0.00009	-37:44:026	0.000267	0.059861	0.001517	0.015838	0.001214
15	22:34:025	0.000117	-37:45:003	0.000548	0.002942	0.002307	0.003859	0.001068
16	22:34:026	0.00001	-38:01:006	0.000005	0.11208	0.001163	0.10141	0.000557
17	22:34:021	0.000021	-37:43:044	0.000044	0.092194	0.00194	0.055132	0.001292
17	22:34:022	0.00001	-37:43:033	0.000019	0.094267	0.002122	0.095676	0.001166
19	22:34:017	0.0001	-37:38:028	0.000189	0.00593	0.001225	0.005884	0.000674
20	22:34:016	0.000485	-37:49:055	0.000705	0.072097	0.00067	0.004405	0.000633
21	22:34:016	0.000143	-37:49:039	0.000364	0.011527	0.002345	0.005348	0.001005
21	22:34:014	0.000221	-37:49:040	0.000359	0.004938	0.002427	0.00351	0.001005
21	22:34:014	0.000627	-37:49:049	0.000283	0.007396	0.001499	0.003608	0.001053
22	22:34:015	0.000044	-37:49:011	0.000109	0.01353	0.001882	0.016304	0.000903
22	22:34:015	0.000155	-37:48:059	0.000168	0.003991	0.001947	0.006422	0.000833
24	22:34:003	0.000173	-37:34:004	0.000253	0.006901	0.000754	0.003729	0.000516
25	22:34:002	0.000594	-37:57:056	0.000162	0.077694	0.001035	0.005526	0.00056
26	22:34:00	0.000016	-37:42:054	0.000031	0.044026	0.001371	0.041725	0.000768
27	22:33:040	0.000092	-37:25:007	0.000215	0.001535	0.000614	0.002241	0.00027
29	22:33:031	0.000109	-37:59:022	0.000306	0.009528	0.000698	0.004279	0.000495
30	22:33:029	0.00012	-38:03:022	0.000253	0.00224	0.000689	0.002474	0.000356
31	22:33:017	0.000282	-37:19:004	0.000308	0.001566	0.000557	0.001338	0.000334
31	22:33:016	0.00051	-37:19:002	0.000248	0.003667	0.000467	0.001587	0.000336
31	22:33:018	0.000442	-37:19:007	0.000324	0.002151	0.00052	0.001298	0.000346

Things should be made as simple as possible, but not any simpler.

ALBERT EINSTEIN (1879 - 1955)

Source Catalogue 240 MHz maps

Table D.1: Positions of radio sources within 4MPc radius of the pointing centre of cluster RXCJ0006.0−3443

Source ID	RA	δ RA	DEC	δ DEC	total flux	δ total flux	Peak flux	δ Peak flux
3	00:07:055	0.000336	-35:09:027	0.000591	0.02226	0.004372	0.014751	0.00275
4	00:07:027	0.000207	-34:28:007	0.000587	0.036782	0.003631	0.017159	0.00255
5	00:07:026	0.0004	-34:26:046	0.000423	0.02451	0.004015	0.014763	0.002664
7	00:06:048	0.000298	-35:10:005	0.000568	0.051274	0.005071	0.021809	0.003696
9	00:06:045	0.000247	-34:45:030	0.000335	0.042593	0.006699	0.032809	0.003998
11	00:06:041	0.000278	-34:50:028	0.00026	0.12079	0.006118	0.055358	0.004239
12	00:06:041	0.000074	-34:51:023	0.000205	0.062197	0.007252	0.058714	0.003984
14	00:06:015	0.00048	-34:47:031	0.000368	0.105934	0.005161	0.032198	0.004034
15	00:06:016	0.000194	-34:48:032	0.000448	0.079767	0.00583	0.034443	0.004212
15	00:06:016	0.000266	-34:49:004	0.000648	0.041295	0.006173	0.021914	0.004218
16	00:06:014	0.000127	-34:33:036	0.00071	0.052337	0.005397	0.028768	0.003347
17	00:06:011	0.000106	-34:32:006	0.000131	0.061675	0.006973	0.066237	0.003619
18	00:06:012	0.00078	-34:29:059	0.000464	0.060614	0.004977	0.020048	0.003815
19	00:06:011	0.000077	-34:33:001	0.000174	0.040363	0.007146	0.053064	0.003327
24	00:05:054	0.000374	-34:44:034	0.000288	0.09882	0.005049	0.037142	0.003747
25	00:05:054	0.000142	-34:45:028	0.000321	0.026654	0.006633	0.03165	0.003124
26	00:05:051	0.0006	-34:15:037	0.000405	0.135877	0.00302	0.021556	0.002629
33	00:04:013	0.000335	-34:31:011	0.000244	0.495739	0.018485	0.155695	0.00587
35	00:04:015	0.000197	-34:34:014	0.000588	0.037584	0.008753	0.028174	0.005322
36	00:04:012	0.000056	-34:32:017	0.000119	0.1016	0.010195	0.117738	0.005095
36	00:04:013	0.000113	-34:31:058	0.000258	0.066605	0.009955	0.070581	0.004786
37	00:04:008	0.000343	-34:32:032	0.000408	0.180885	0.007214	0.066036	0.005209
38	00:04:008	0.000319	-34:29:020	0.000432	0.046746	0.009177	0.031356	0.005956
42	00:03:056	0.000233	-34:33:022	0.000588	0.094929	0.007572	0.037488	0.005585
43	00:03:051	0.000387	-34:21:015	0.00053	0.030901	0.00495	0.017211	0.003357
45	00:03:049	0.000372	-34:30:039	0.000384	0.074775	0.007242	0.034644	0.005173
47	00:03:045	0.000611	-35:14:046	0.00038	0.055103	0.003624	0.017855	0.002798

Table D.2: Positions of radio sources within 4MPc radius of the pointing centre of cluster RXCJ0020.7−2542

Source ID	RA	δ RA	DEC	δ DEC	total flux	δ total flux	Peak flux	δ Peak flux
1	00:21:049	0.000235	-25:53:00	0.000227	0.642442	0.025258	0.144706	0.013691
2	00:21:047	0.000162	-25:53:009	0.000496	0.368062	0.017578	0.120566	0.013472
3	00:20:043	0.000177	-25:42:038	0.000405	0.116106	0.020092	0.083105	0.012562

Table D.3: Positions of radio sources within 4MPc radius of the pointing centre of cluster RXCJ0049.4−2931

Source ID	RA	δ RA	DEC	δ DEC	total flux	δ total flux	Peak flux	δ Peak flux
0	00:51:047	0.000201	-29:24:046	0.000741	0.048752	0.018386	0.054291	0.009391
1	00:50:038	0.000207	-29:21:023	0.000147	0.421091	0.034458	0.224917	0.014438
2	00:50:038	0.000067	-29:57:041	0.000223	0.420495	0.026797	0.340278	0.015574
4	00:48:043	0.000561	-29:45:046	0.000447	0.147798	0.042923	0.126464	0.026016
5	00:48:039	0.000052	-29:47:012	0.000214	0.862321	0.039453	0.632644	0.023198

Table D.4: Positions of radio sources within 4MPc radius of the pointing centre of cluster RXCJ0211.4−4017

Source ID	RA	δ RA	DEC	δ DEC	total flux	δ total flux	Peak flux	δ Peak flux
2	02:13:026	0.000062	-39:53:058	0.000277	0.056962	0.005246	0.045252	0.002995
3	02:13:007	0.000468	-40:18:042	0.00098	0.155377	0.00339	0.020996	0.003003
4	02:13:001	0.00076	-40:17:010	0.000703	0.221723	0.002931	0.020401	0.002694
5	02:13:001	0.000049	-40:10:045	0.000249	0.072932	0.005317	0.054472	0.003101
9	02:12:020	0.000087	-40:04:038	0.000359	0.040691	0.005975	0.034898	0.003367
11	02:12:011	0.000075	-39:50:005	0.000368	0.03256	0.005239	0.029863	0.002831
12	02:12:008	0.00014	-39:50:032	0.000402	0.023871	0.005291	0.022466	0.002958
13	02:12:004	0.000094	-40:06:056	0.000488	0.030621	0.006466	0.02829	0.003459
14	02:11:040	0.000046	-40:42:048	0.000151	0.133979	0.006197	0.093642	0.003828
17	02:11:025	0.000014	-40:17:025	0.000044	0.459104	0.00816	0.376854	0.004749
18	02:11:027	0.000213	-40:18:049	0.000703	0.032634	0.008037	0.02474	0.004812
19	02:10:050	0.000086	-40:05:022	0.000552	0.035296	0.0054	0.026853	0.003053
20	02:10:025	0.000212	-39:45:052	0.000363	0.030001	0.005666	0.02374	0.00349
22	02:09:028	0.000066	-40:23:036	0.000334	0.049493	0.006296	0.042528	0.003477
23	02:08:047	0.000053	-39:53:019	0.000251	0.050867	0.005053	0.04437	0.002781

Table D.5: Positions of radio sources within 4MPc radius of the pointing centre of cluster RXCJ0225.1−2928

Source ID	RA	δ RA	DEC	δ DEC	total flux	δ total flux	Peak flux	δ Peak flux
0	02:29:025	0.000202	-28:54:003	0.000377	0.072822	0.006046	0.043206	0.004023
2	02:28:048	0.000082	-29:50:003	0.00004	0.277355	0.008638	0.19697	0.00383
3	02:28:031	0.000045	-29:46:007	0.000019	0.41129	0.009477	0.355014	0.00401
4	02:28:025	0.000065	-30:20:003	0.000136	0.119329	0.006255	0.105533	0.003543
4	02:28:026	0.000081	-30:20:004	0.000181	0.105244	0.00614	0.084392	0.003618

Continued on next page

Table D.5: Positions of radio sources within 4MPc radius of the pointing centre of cluster RXCJ0225.1−2928

Source ID	RA	δ RA	DEC	δ DEC	total flux	δ total flux	Peak flux	δ Peak flux
6	02:28:020	0.000382	-29:00:022	0.000498	0.02674	0.009287	0.026568	0.005356
7	02:28:018	0.000258	-29:06:032	0.000459	0.049408	0.00949	0.045319	0.005274
8	02:28:015	0.000181	-29:23:042	0.000248	0.118997	0.006061	0.065227	0.004116
9	02:28:015	0.000018	-29:04:038	0.000009	1.345179	0.013446	1.204205	0.00561
11	02:28:015	0.000302	-29:03:009	0.000629	0.046151	0.009046	0.03366	0.00565
12	02:28:014	0.000223	-29:00:026	0.000511	0.022512	0.009333	0.028534	0.004726
15	02:28:012	0.000255	-29:03:004	0.000477	0.027688	0.009732	0.034887	0.004722
16	02:28:010	0.000255	-29:07:019	0.000506	0.059016	0.009094	0.048006	0.005187
17	02:28:009	0.000325	-29:11:026	0.000536	0.023136	0.008744	0.024933	0.004833
17	02:28:010	0.000396	-29:11:012	0.000514	0.015698	0.008814	0.019889	0.004668
18	02:28:007	0.000188	-29:14:012	0.00055	0.019515	0.008177	0.024728	0.0041
19	02:28:004	0.000531	-29:16:019	0.000415	0.170713	0.005329	0.041942	0.004357
20	02:28:004	0.000166	-29:41:001	0.000364	0.06905	0.005653	0.049632	0.003331
21	02:28:00	0.00027	-29:14:026	0.000554	0.028585	0.007821	0.026773	0.004493
24	02:27:054	0.000261	-29:24:001	0.000869	0.028175	0.00599	0.020097	0.003667
28	02:27:027	0.000067	-29:09:00	0.000172	0.106858	0.007444	0.099126	0.004137
29	02:27:021	0.00016	-30:04:058	0.000486	0.041308	0.00597	0.032968	0.003498
30	02:27:017	0.000233	-29:51:014	0.000463	0.086433	0.005177	0.038654	0.003712
30	02:27:015	0.000261	-29:51:015	0.000602	0.04546	0.005569	0.027038	0.00368
31	02:27:016	0.000124	-29:43:035	0.000267	0.081754	0.005944	0.062414	0.003493
31	02:27:014	0.000433	-29:43:032	0.000601	0.038033	0.005845	0.023434	0.003845
33	02:27:008	0.000316	-28:51:030	0.000359	0.090066	0.005592	0.040263	0.004051
34	02:27:002	0.000092	-29:54:034	0.00023	0.077641	0.005862	0.065767	0.003331
35	02:26:054	0.000051	-30:15:055	0.000145	0.127008	0.006575	0.115384	0.003603
36	02:26:032	0.000056	-29:27:033	0.000138	0.102319	0.006042	0.100979	0.003212
36	02:26:030	0.001878	-29:27:020	0.000754	0.065959	0.003856	0.013176	0.003247
37	02:26:023	0.000156	-29:42:035	0.000372	0.050828	0.005948	0.039351	0.003589
38	02:26:009	0.000026	-28:57:059	0.000067	0.289074	0.006195	0.229959	0.003688
38	02:26:008	0.000051	-28:58:019	0.000117	0.204492	0.006003	0.13968	0.003773
39	02:26:005	0.00009	-29:15:055	0.000182	0.134433	0.005752	0.089545	0.003617
41	02:25:044	0.000087	-30:04:008	0.000037	0.200737	0.008798	0.168601	0.003813
42	02:25:024	0.000132	-29:39:025	0.000333	0.04154	0.006097	0.040959	0.003276
43	02:25:019	0.000193	-29:02:031	0.000628	0.01766	0.006561	0.02043	0.003329
44	02:25:016	0.000452	-29:27:024	0.000633	0.034493	0.007932	0.025187	0.004993
44	02:25:016	0.000865	-29:27:042	0.000814	0.020608	0.008007	0.017412	0.004642
45	02:25:015	0.000097	-29:53:017	0.000059	0.210537	0.008649	0.14524	0.0038
46	02:25:009	0.000371	-29:27:049	0.000625	0.313555	0.004871	0.04872	0.00425
47	02:24:042	0.000089	-29:34:016	0.000039	0.284302	0.010713	0.204501	0.004698
48	02:24:035	0.000088	-30:17:037	0.000052	0.196283	0.00805	0.131767	0.00357
50	02:24:026	0.00018	-29:51:001	0.000418	0.026152	0.006202	0.029433	0.003148
51	02:24:005	0.000108	-30:12:009	0.000293	0.046866	0.006137	0.046475	0.003303

Continued on next page

Table D.5: Positions of radio sources within 4MPc radius of the pointing centre of cluster RXCJ0225.1−2928

Source ID	RA	δ RA	DEC	δ DEC	total flux	δ total flux	Peak flux	δ Peak flux
52	02:23:041	0.000026	-30:21:041	0.000067	0.193706	0.005944	0.196016	0.003149
55	02:23:017	0.000241	-29:54:020	0.000572	0.032641	0.005115	0.025708	0.002942
57	02:22:034	0.000043	-30:01:032	0.000115	0.111726	0.006	0.113957	0.003183
59	02:22:013	0.00028	-29:24:036	0.000672	0.043002	0.005439	0.024996	0.003602
60	02:22:013	0.000118	-28:43:017	0.000287	0.075626	0.006173	0.06007	0.003566
61	02:22:009	0.000094	-29:45:010	0.000213	0.087782	0.005579	0.069242	0.003272
63	02:21:035	0.000162	-29:39:039	0.000359	0.040076	0.00633	0.038632	0.003454
64	02:21:035	0.000193	-29:21:050	0.000371	0.069778	0.006111	0.044961	0.003921
65	02:21:025	0.000096	-29:34:022	0.000302	0.142105	0.005308	0.069609	0.003654
66	02:21:021	0.000047	-29:46:016	0.000129	0.200854	0.005464	0.139334	0.003293
67	02:21:019	0.000068	-29:07:015	0.000034	0.296603	0.008439	0.227083	0.00406
67	02:21:020	0.000517	-29:07:049	0.000412	0.012216	0.007182	0.016585	0.003599
68	02:20:048	0.000273	-29:58:022	0.000619	0.019664	0.005894	0.019991	0.00315

Table D.6: Positions of radio sources within 4MPc radius of the pointing centre of cluster RXCJ0605.8−3518

Source ID	RA	δ RA	DEC	δ DEC	total flux	δ total flux	Peak flux	δ Peak flux
0	06:07:033	0.000472	-34:59:059	0.000893	0.136753	0.010507	0.038984	0.008354
4	06:06:044	0.000139	-35:05:043	0.000195	0.152981	0.016365	0.146713	0.008442
4	06:06:044	0.000171	-35:05:050	0.000224	0.184368	0.015406	0.144285	0.008584
5	06:06:026	0.000199	-35:17:017	0.000272	0.174174	0.015665	0.139492	0.008193
12	06:05:054	0.000014	-35:18:009	0.000009	4.290157	0.041503	3.801031	0.017773
15	06:05:053	0.000257	-35:16:017	0.000329	0.161033	0.027103	0.161118	0.01266
17	06:05:042	0.000401	-35:22:001	0.000524	0.1007	0.022636	0.097866	0.01013
19	06:05:040	0.000072	-34:58:028	0.000128	0.188466	0.011859	0.16901	0.006476
21	06:05:006	0.000074	-35:22:018	0.000112	0.261395	0.017657	0.258885	0.009174
23	06:04:051	0.000578	-35:29:019	0.000566	0.08429	0.014018	0.065674	0.006783
26	06:04:017	0.000404	-35:17:008	0.000369	0.040216	0.010197	0.035937	0.005723
27	06:04:013	0.000262	-35:41:012	0.000386	0.050735	0.010444	0.04799	0.00545
28	06:03:059	0.000093	-35:32:018	0.000131	0.196753	0.012693	0.179398	0.006666

Table D.7: Positions of radio sources within 4MPc radius of the pointing centre of cluster RXCJ0821.8+0112

Source ID	RA	δ RA	DEC	δ DEC	total flux	δ total flux	Peak flux	δ Peak flux
0	08:24:041	0.000336	01:32:057	0.000434	0.021302	0.003905	0.015082	0.002465
1	08:24:026	0.000243	01:20:042	0.000359	0.052863	0.004369	0.02793	0.002993
2	08:24:022	0.000216	01:20:003	0.000387	0.03381	0.004552	0.024509	0.002778
3	08:23:051	0.000428	01:55:055	0.000344	0.128328	0.003452	0.028828	0.002862
4	08:23:009	0.000122	01:51:029	0.000132	0.088254	0.004847	0.060193	0.003083
5	08:23:009	0.000328	01:15:00	0.000408	0.016265	0.004666	0.01491	0.002719
6	08:22:035	0.000241	00:49:014	0.00038	0.018958	0.005269	0.0203	0.002772
9	08:22:030	0.000747	01:44:004	0.000627	0.069977	0.00365	0.017887	0.002949
11	08:22:024	0.000046	01:53:028	0.000067	0.22731	0.007587	0.19311	0.004385
14	08:22:015	0.000436	00:51:051	0.000432	0.020622	0.00517	0.016241	0.003159
15	08:22:007	0.000295	01:50:018	0.000441	0.021915	0.007821	0.023585	0.004202
16	08:21:060	0.000092	01:10:055	0.000141	0.075586	0.005567	0.066222	0.003189
17	08:21:048	0.000498	01:00:049	0.00049	0.029017	0.006373	0.019927	0.004057
18	08:21:044	0.00028	01:02:020	0.000422	0.052817	0.006233	0.031764	0.004094
19	08:21:041	0.000142	01:04:013	0.000343	0.03912	0.006537	0.03503	0.003703
20	08:21:038	0.000239	01:02:049	0.000615	0.032101	0.006641	0.023058	0.004106
21	08:21:037	0.000221	01:02:044	0.000314	0.022665	0.007198	0.025015	0.003997
22	08:21:035	0.000045	01:02:030	0.000028	0.355028	0.009659	0.280925	0.004143
23	08:21:032	0.000226	00:55:056	0.00055	0.027781	0.006713	0.023258	0.003919
24	08:21:031	0.000185	01:00:035	0.000368	0.045013	0.006986	0.03543	0.004202
25	08:21:030	0.000459	00:59:055	0.000625	0.040732	0.006466	0.022811	0.004338
29	08:20:049	0.00016	01:35:043	0.000224	0.122148	0.00485	0.050869	0.003575
30	08:20:039	0.000082	01:01:011	0.000096	0.259659	0.005285	0.114109	0.003852
32	08:19:025	0.000083	01:47:008	0.000128	0.099848	0.004606	0.07216	0.002815
33	08:19:011	0.000144	01:50:036	0.000216	0.047742	0.00429	0.038281	0.002494

Table D.8: Positions of radio sources within 4MPc radius of the pointing centre of cluster RXCJ0958.3−1103

Source ID	RA	δ RA	DEC	δ DEC	total flux	δ total flux	Peak flux	δ Peak flux
4	09:58:034	0.000199	-11:03:053	0.000496	0.014972	0.004436	0.013911	0.002515
6	09:58:032	0.000117	-10:59:054	0.000457	0.017758	0.00479	0.017719	0.002567
7	09:58:030	0.000064	-10:54:027	0.000393	0.01684	0.005059	0.021172	0.002298
10	09:58:027	0.000161	-10:51:035	0.000471	0.016561	0.004585	0.015471	0.002589
14	09:58:022	0.000011	-11:03:051	0.000044	0.20004	0.005232	0.202105	0.002773
14	09:58:023	0.000101	-11:04:014	0.000323	0.018051	0.005388	0.022101	0.002702
15	09:58:022	0.000109	-11:04:031	0.000379	0.025674	0.005285	0.023929	0.00294
16	09:58:021	0.000126	-11:10:059	0.000504	0.012467	0.00432	0.013531	0.002235

Continued on next page

Table D.8: Positions of radio sources within 4MPc radius of the pointing centre of cluster RXCJ0958.3−1103

Source ID	RA	δ RA	DEC	δ DEC	total flux	δ total flux	Peak flux	δ Peak flux
17	09:58:021	0.000058	-11:05:025	0.000234	0.038121	0.005484	0.039274	0.002884
19	09:58:019	0.000153	-11:01:001	0.000457	0.017766	0.005175	0.017408	0.002867
21	09:58:017	0.000071	-11:03:054	0.000348	0.027303	0.005381	0.028266	0.002742
23	09:58:016	0.000108	-11:02:050	0.000382	0.017847	0.005402	0.020427	0.002767
30	09:58:002	0.000153	-11:13:012	0.000455	0.018597	0.004223	0.015963	0.002455
31	09:57:040	0.000051	-11:04:032	0.000206	0.030025	0.004589	0.034128	0.002322
32	09:57:039	0.00009	-11:06:003	0.000382	0.021859	0.004339	0.021589	0.002255
33	09:57:035	0.000208	-11:18:004	0.000525	0.015717	0.004112	0.013062	0.00244
34	09:57:034	0.000176	-11:15:008	0.000479	0.013763	0.004344	0.013492	0.00242
35	09:57:026	0.000067	-11:13:008	0.00016	0.064148	0.004703	0.054097	0.002698
35	09:57:025	0.000087	-11:12:043	0.000287	0.024194	0.004925	0.025992	0.002591
36	09:57:025	0.000137	-11:14:041	0.000306	0.028419	0.004704	0.024224	0.002778
37	09:57:016	0.00011	-10:59:026	0.000423	0.015928	0.004522	0.016958	0.002365

Table D.9: Positions of radio sources within 4MPc radius of the pointing centre of cluster RXCJJ1141.4−1216

Source ID	RA	δ RA	DEC	δ DEC	total flux	δ total flux	Peak flux	δ Peak flux
0	11:43:017	0.000251	-12:36:002	0.000261	0.078199	0.015068	0.054744	0.009716
1	11:43:001	0.000251	-11:53:042	0.000272	0.050099	0.015512	0.045272	0.009235
2	11:42:048	0.000249	-11:46:044	0.000307	0.062055	0.018344	0.058143	0.010366
3	11:42:040	0.000315	-11:50:049	0.000267	0.113091	0.019456	0.069019	0.013046
5	11:42:036	0.000171	-11:45:025	0.000199	0.088692	0.027058	0.095487	0.015207
6	11:42:036	0.00019	-11:47:022	0.000094	0.179153	0.017943	0.126365	0.011316
7	11:42:035	0.000224	-11:46:028	0.000236	0.111392	0.038334	0.114714	0.021829
8	11:42:034	0.000196	-11:44:055	0.000214	0.089877	0.021566	0.080249	0.012907
9	11:42:031	0.00014	-11:47:007	0.000157	0.119545	0.022567	0.112588	0.013234
10	11:42:024	0.00017	-11:45:038	0.000145	0.083217	0.016165	0.078246	0.009436
11	11:42:023	0.000145	-11:49:019	0.000185	0.065089	0.016902	0.071223	0.009274
12	11:42:020	0.000221	-11:58:039	0.000319	0.06008	0.017429	0.053741	0.010215
13	11:42:019	0.000223	-11:47:047	0.000276	0.057408	0.019993	0.058668	0.011259
14	11:42:013	0.000232	-11:49:012	0.000261	0.079586	0.019192	0.064524	0.011835
15	11:42:005	0.000346	-11:46:012	0.000261	0.121996	0.017363	0.070361	0.011632
16	11:42:004	0.000396	-11:59:049	0.000445	0.100319	0.012143	0.0422	0.008902
17	11:41:049	0.00017	-12:12:002	0.00042	0.047982	0.011619	0.038559	0.006853
18	11:41:038	0.000319	-11:51:004	0.000246	0.049069	0.01682	0.050257	0.009105
19	11:41:024	0.000072	-12:16:039	0.000085	0.273151	0.022927	0.233406	0.013883
21	11:40:047	0.000179	-11:52:030	0.000172	0.149211	0.02299	0.11516	0.014349
22	11:40:001	0.000301	-12:46:046	0.000099	0.233598	0.024983	0.092443	0.010862

Table D.10: Positions of radio sources within 4MPc radius of the pointing centre of cluster RXCJ1236.7−3354

Source ID	RA	δ RA	DEC	δ DEC	total flux	δ total flux	Peak flux	δ Peak flux
0	12:40:004	0.000509	-33:19:041	0.00043	0.043262	0.007908	0.035143	0.004635
1	12:40:002	0.000079	-33:30:004	0.000077	0.243715	0.006867	0.201394	0.003898
5	12:39:043	0.000134	-33:58:037	0.000126	0.112577	0.007454	0.116572	0.00374
5	12:39:042	0.000215	-33:58:046	0.0002	0.071035	0.007403	0.068974	0.003973
6	12:39:031	0.000227	-33:18:047	0.000222	0.039356	0.008192	0.054254	0.003704
7	12:39:025	0.000288	-33:31:056	0.000279	0.042961	0.007382	0.050239	0.003422
8	12:39:025	0.00015	-33:31:020	0.000132	0.121616	0.007044	0.111361	0.003757
9	12:39:005	0.000164	-34:14:023	0.00012	0.261204	0.006529	0.158242	0.003998
10	12:38:040	0.000232	-33:46:017	0.000325	0.133531	0.00753	0.068457	0.005238
11	12:38:025	0.000322	-34:10:024	0.000306	0.081426	0.007208	0.061452	0.004138
14	12:37:056	0.000102	-33:21:060	0.000096	0.150644	0.006428	0.14132	0.003394
15	12:37:042	0.000103	-33:52:021	0.000101	0.262269	0.011236	0.22395	0.004807
15	12:37:039	0.000139	-33:51:049	0.000128	0.114283	0.008303	0.123211	0.004083
17	12:36:022	0.000172	-33:31:009	0.000178	0.106284	0.008535	0.098429	0.004665
18	12:36:011	0.000049	-33:23:055	0.000047	0.428544	0.009745	0.431878	0.004907
19	12:35:049	0.000137	-33:29:033	0.000123	0.271852	0.014069	0.245973	0.007508
21	12:35:024	0.000034	-33:22:039	0.000028	1.960982	0.025782	1.42611	0.011101
23	12:35:012	0.000733	-33:36:021	0.000409	0.087026	0.006406	0.039822	0.004447
24	12:35:005	0.000539	-33:57:045	0.000499	0.027712	0.007023	0.031195	0.003082
25	12:35:004	0.000527	-33:47:010	0.000603	0.034745	0.006439	0.024862	0.003997
26	12:35:002	0.000617	-33:44:008	0.000544	0.018735	0.006874	0.020165	0.003579
28	12:34:035	0.000066	-33:52:036	0.000061	0.265094	0.007771	0.258723	0.004028
30	12:34:027	0.000568	-33:29:045	0.000559	0.040881	0.007985	0.034224	0.004416
31	12:34:023	0.000171	-33:35:043	0.000164	0.110059	0.007542	0.101704	0.003976
33	12:34:011	0.000136	-34:14:023	0.000125	0.096857	0.00661	0.104982	0.003171
34	12:34:010	0.000156	-33:37:009	0.000178	0.116736	0.007689	0.095368	0.004501
35	12:34:010	0.000032	-33:26:035	0.00003	0.60229	0.008894	0.60021	0.004552
38	12:34:00	0.000126	-33:41:001	0.000123	0.146596	0.007483	0.123074	0.004326
39	12:33:054	0.000353	-34:36:032	0.000263	0.190478	0.008478	0.055808	0.004222
40	12:33:057	0.000865	-33:40:024	0.000481	0.029231	0.007312	0.023008	0.004311
43	12:33:047	0.00044	-33:48:006	0.000412	0.037802	0.00657	0.030576	0.003908
45	12:33:037	0.00002	-34:10:021	0.000023	0.955212	0.011043	0.763897	0.004727
46	12:33:036	0.000128	-34:25:035	0.000117	0.328458	0.009873	0.140121	0.004365
47	12:33:031	0.000369	-34:10:022	0.000259	0.087448	0.007568	0.055897	0.004885
48	12:33:030	0.000464	-34:19:057	0.000417	0.048056	0.007446	0.034377	0.004682
50	12:33:024	0.00105	-34:07:023	0.000338	0.058526	0.006729	0.027415	0.004719
52	12:33:018	0.000897	-34:09:039	0.000462	0.03558	0.00764	0.025108	0.004709

Table D.11: Positions of radio sources within 4MPc radius of the pointing centre of cluster RXCJ1311.4−0120

Source ID	RA	δ RA	DEC	δ DEC	total flux	δ total flux	Peak flux	δ Peak flux
1	13:11:034	0.002291	-01:04:005	0.00064	0.17303	0.029979	0.161516	0.016391

Table D.12: Positions of radio sources within 4MPc radius of the pointing centre of cluster RXCJ1516.5−0056

Source ID	RA	δ RA	DEC	δ DEC	total flux	δ total flux	Peak flux	δ Peak flux
0	15:18:040	0.000447	-01:21:048	0.000602	0.129029	0.020832	0.119191	0.011768
1	15:16:054	0.000681	00:43:036	0.001247	0.284318	0.019993	0.114826	0.014623
2	15:16:024	0.000327	00:49:044	0.000664	0.139552	0.034684	0.182316	0.015715
4	15:15:044	0.000277	-01:24:039	0.000563	0.154032	0.023713	0.177466	0.011008

Table D.13: Positions of radio sources within 4MPc radius of the pointing centre of cluster RXCJ2014.8−2430

Source ID	RA	δ RA	DEC	δ DEC	total flux	δ total flux	Peak flux	δ Peak flux
0	20:15:038	0.000095	-24:22:042	0.000257	0.219438	0.011828	0.122385	0.007943
1	20:14:052	0.000027	-24:30:023	0.00008	0.769785	0.026974	0.765477	0.013456
2	20:14:003	0.000095	-24:49:012	0.000309	0.114294	0.011545	0.098013	0.006155
4	20:13:012	0.000266	-24:46:043	0.000088	0.429356	0.016853	0.180664	0.007569